University of Zagreb **Faculty of Metallurgy** **Sisak, Croatia**	
University of Ljubljana **Faculty of Natural Sciences and Engineering** **Ljubljana, Slovenia**	
University North **Koprivnica, Croatia**	Sveučilište Sjever
ELKEM AS **Norway**	Elkem

PROCEEDINGS BOOK

15th INTERNATIONAL FOUNDRYMEN CONFERENCE

INNOVATION –
The Foundation of Competitive Casting Production

Opatija, May 11th – 13th 2016

ORGANIZERS
University of Zagreb Faculty of Metallurgy, Sisak, Croatia
University of Ljubljana Faculty of Natural Sciences and Engineering, Ljubljana, Slovenia
University North, Koprivnica, Croatia
ELKEM AS, Norway

PROCEEDINGS BOOK
15th INTERNATIONAL FOUNDRYMEN CONFERENCE
INNOVATION – The Foundation of Competitive Casting Production

EDITORS
Natalija Dolić, Zdenka Zovko Brodarac

TECHNICAL EDITORS
Natalija Dolić

PUBLISHER
University of Zagreb
Faculty of Metallurgy
Aleja narodnih heroja 3
44103 Sisak
Croatia

PRINT
University North
Trg dr. Žarka Dolinara 1
48000 Koprivnica
Croatia

ISSUE
250 copies

ISBN
978-953-7082-22-2

A CIP record is available in computer catalogue of the National and University Library in Zagreb under the number 000932381.

PREFACE

Scientific organizations in Croatia possess good scientific and research potential and represent a solid basis for the development of a competitive innovation based economy. Croatian medium and large enterprises invest more than 90% of all private investment in research and development, of which large companies invest the largest share (over 60%), as opposed to micro and small enterprises (just under 8%). Due to the lack of public support for scientific and research activities and relatively low interest of companies, investments in the development of research and innovation in recent years has stagnated. Research and development activities, among other activities associated with the introduction of innovation in enterprises, are essential to the Croatian economy in order to become more competitive through companies' productivity growth, access to new markets with higher value added, and finally bringing to sustainable employment in the context of a sharp global competition.

Founding as important industry branch represents the important factor contributing the economic potential of each country. Current market development as well as technical and economic objective, the production of high-quality, low-cost and environmentally friendly casting, requires application of modern advanced materials and manufacturing technologies, as well as an understanding of the production process. Prerequisite to achieve competitiveness on global market is to introduce innovation and R&D attainments transfer from HEIs' to SMEs' and industry. The Conference topics were designed as presentations of the current "state of the art" research in the collaboration with industry, and production innovation with the aim to improve the competitiveness.

The scope of the Conference covers scientific, technological and practical aspects concerning research, development and realization of casting technology with the common foundation - Innovation. Special attention will be focused towards the competitiveness ability of foundries, environmental protection as well as subjects connected to properties and application of castings.

During this Conference 32 paper will be presented. Book of Abstract of the 15th International Foundrymen Conference includes summaries of the papers. The Proceedings book consists of papers *in extenso* published in electronic format (CD). Full length papers have undergone the international review procedure, done by eminent experts from corresponding fields, but have not undergone linguistic proof reading. Sequence of papers in Proceedings book has been done by category of papers in following order: plenary lectures, invited lectures, oral and poster presentation, and inside the category alphabetically by the first author's surname.

This occasion represents the opportunity to discus and increase the mutual collaboration between HEIs' and industry with the aim of information exchange related to advanced experience in foundry processes and technologies, gaining the new experience in presentation and / or teaching process within lifelong learning process.

The organizers of the Conference would like to thank all participants, reviewers, sponsors, auspices, media coverage and all those who have contributed to this Conference in any way.

President of Organizing Board

Z. Z. Brodarac

Assoc.Prof. Zdenka Zovko Brodarac, PhD

THE HEAD OF ORIENTAL GOD (ATIS?)
bronza
2nd century AD
SISCIA (modern Sisak, Croatia)

ILLYRIAN HELMET
iron
6th century BC

UNDER THE HIGH AUSPICES

President of Croatia Kolinda Grabar – Kitarović

UNDER THE PATRONAGE

Ministry of Science, Education and Sports of Republic of Croatia
University of Zagreb
Croatian Foundry Association
AD KLASTER
Mittel Europäische Giesserei Initiative (MEGI)
Chamber of Commerce of Republic of Croatia
Sisak – Moslavina County
City of Sisak

SPONSORED BY

GOLDEN SPONSOR
Comet d.o.o., Novi Marof (HR)

SILVER SPONSOR
Analysis d.o.o., Beograd (RS)
Bentoproduct d.o.o., Šipovo (BiH)
Ferro-Preis d.o.o., Čakovec (HR)
HAGI GmbH, Pyhra (AT)
Instrumentalia Adria d.o.o., Zagreb (HR)

BRONZE SPONSOR
Belloi & Romagnoli s.r.l., Modena (IT)
Chemets d.o.o., Šenčur (SI)
EDC d.o.o., Zagreb (HR)
EKW - KREMEN d.o.o., Šentjerej (SI)
Eurotehnika d.o.o., Zagreb (HR)
Faprosid s.r.l., Adro (IT)
IDEF d.o.o., Zagreb (HR)
KEFO d.o.o., Sisak (HR)¸
Kontroltest International d.o.o., Zagreb (HR)
MECAS ESI s.r.o., Plzen (CZ)
MIKROLUX d.o.o., Zaprešić (HR)
PLINOSERVIS KUZMAN d.o.o., Zagreb (HR)
SCAN d.o.o., Kranj (SI)
TC LIVARSTVO d.o.o., Ljubljana (Sl)
Termit d.o.o., Moravče (SI)
Topomatika d.o.o., Zagreb (HR)
Werner Metal d.o.o., Zlatar Bistrica (HR)

ORGANIZING COMMITTEE

Zdenka Zovko Brodarac
Ladislav Lazić
Primož Mrvar
Jožef Medved
Marin Milković
Mario Tomiša
Anita Begić Hadžipašić
Natalija Dolić
Ljerka Slokar
Gordana Gojsević Marić

PROGRAM COMMITTEE

Željko Alar (HR)
Hasan Avdušinović (BiH)
Branko Bauer (HR)
Anita Begić Hadžipašić (HR)
Ana Beroš (BiH)
Ivan Budić (HR)
Ivica Buljeta (BiH)
Jaka Burja (SI)
Franjo Cajner (HR)
Peter Cvahte (SI)
Lidija Ćurković (HR)
Mile Djurdjević (AT)
Natalija Dolić (HR)
Regina Godec – Fuchs (SI)
Matjaž Godec (SI)
Mirko Gojić (HR)
Dario Iljkić (HR)
Željko Kamberović (RS)
Sebastjan Kastelic (SI)
Varužan Kevorkijan (SI)
Ivica Kladarić (HR)
Borut Kosec (SI)
Dražan Kozak (HR)
Stjepan Kožuh (HR)
Zoran Kožuh (HR)
Milisav Lalović (HR)
Ladislav Lazić (HR)
Martina Lovrenić – Jugović (HR)
Srećko Manasijević (RS)
Srđan Marković (RS)
Jožef Medved (SI)
Daniel Novoselović (HR)
Mitja Petrič (SI)
Bojan Podgornik (SI)
Žarko Radović (ME)
Karlo T. Raić (RS)
Vera Rede (HR)
Milenko Rimac (BiH)
Zdravko Schauperl (HR)
Ljerka Slokar (HR)
Božo Smoljan (HR)
Tahir Sofilić (HR)
Davor Stanić (HR)
Iveta Vaskova (SK)
Maja Vončina (SI)
Franc Zupanič (SI)
Zdenka Zovko Brodarac (HR)
Dragana Živković (RS)

REVIEW COMMITTEE

Hasan Avdušinović (BiH)
Branko Bauer (HR)
Anita Begić Hadžipašić (HR)
Ivan Brnardić (HR)
Natalija Dolić (HR)
Tomislav Galeta (HR)
Stanislaw Gil (PL)
Mirko Gojić (HR)
Lidija Gomidželović (RS)
Tamara Holjevac Grgurić (HR)
Dario Iljkić (HR)
Suzana Jakovljević (HR)
Sebastijan Kastelic (SI)
Varužan Kevorkijan (SI)
Borut Kosec (SI)
Stjepan Kožuh (HR)
Zoran Kožuh (HR)
Witold K. Krajewski (PL)
Ladislav Lazić (HR)
Vesna Maksimović (RS)
Srećko Manasijević (RS)
Srđan Marković (RS)
Daniel Novoselović (HR)
Mitja Petrič (SI)
Alena Pribulova (SK)
Martina Radoš (HR)
Vera Rede (HR)
Zdravko Schauperl (HR)
Davor Stanić (HR)
Sanja Šolić (HR)
Katarina Terzić (HR)
Zdenka Zovko Brodarac (HR)
Dragana Živković (RS)

CONTENTS

15th INTERNATIONAL FOUNDRYMEN CONFERENCE

INNOVATION – The foundation of competitive casting production

Opatija, May 11th-13th, 2016

http://www.simet.hr/~foundry/

EFFECT OF ELEMENTS IN TREATMENT ALLOYS FOR CAST IRON INCLUDING CASE STUDIES

O. Knustad[1], A. Plowman[2] and T. Liu[3]

[1]Elkem Foundry Products R&D, Kristiansand, Norway
[2]Elkem South East Asia, Singapore, Singapore
[3]Elkem Shanghai Ltd, Shanghai, China

Plenary lecture
Subject review

Abstract

The paper gives an overview of the effect of different elements in inoculants and nodularisers. Three case studies show how optimising the alloys can improve microstructure and mechanical properties in thick section castings for wind generators.

Keywords: *grey iron, ductile iron, nodularisation, inoculation*

*Corresponding author (e-mail address): *oddvar.knustad@elkem.no*

INTRODUCTION

Cast iron is an alloy mainly containing carbon, silicon and iron. The properties of cast iron are very much dependent on whether the carbon precipitates as graphite or as other carbon containing phases e.g. iron carbide, and which form the graphite has. Figure 1 [1] shows standard graphite forms as described in EN-ISO 945-1:2008. Form I is ideal grey iron structure, form III ideal compacted graphite structure and form VI shows an ideal ductile iron structure.

The form and distribution of graphite in cast iron is very dependent on the chemistry of raw materials used and of the added alloys such as nodularisers and inoculants.

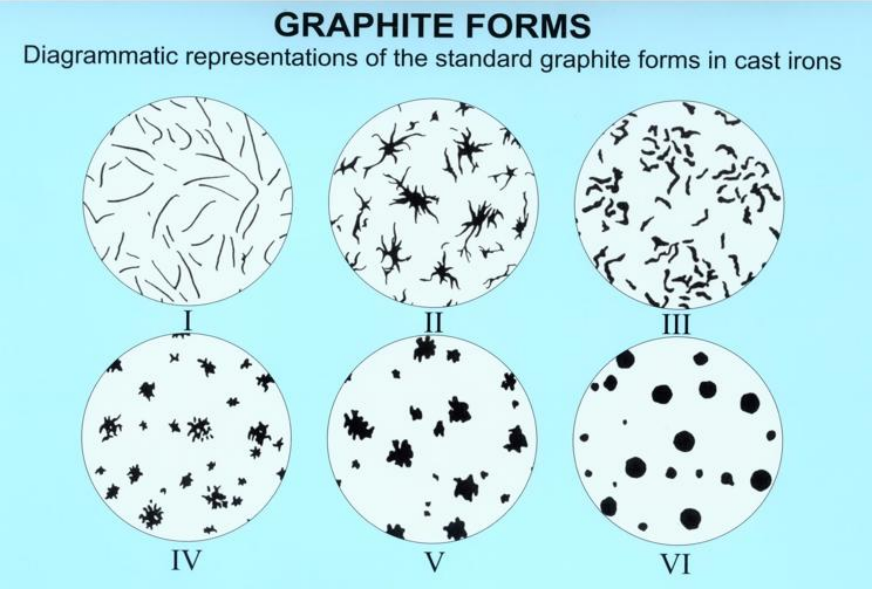

Figure 1. Graphite forms in cast iron

NODULARISATION

To form compacted graphite and nodules as shown in figure 1, it is essential to add alloys containing magnesium and/ or rare earth metals (cerium and lanthanum) to deoxidize and desulphurize the iron. Both the chemistry of, and the process where adding the nodularisation alloy influence the form and distribution of graphite in the finished casting. The main elements in nodularisers are normally Mg, RE, Ca and Al, see Figure 2. The main effects of Mg and RE is to deoxidize and desulphurize, in addition RE is important to neutralise the negative effect of subversive elements such as lead, antimony, arsenic, etc. The main effect of Ca is to reduce reactivity and to give inoculation effect. The effect of Al is to improve dissolution rate and give inoculation effect. Both Ca and Al in excess increase the tendency to slag formation due to their high affinity to oxygen [2].

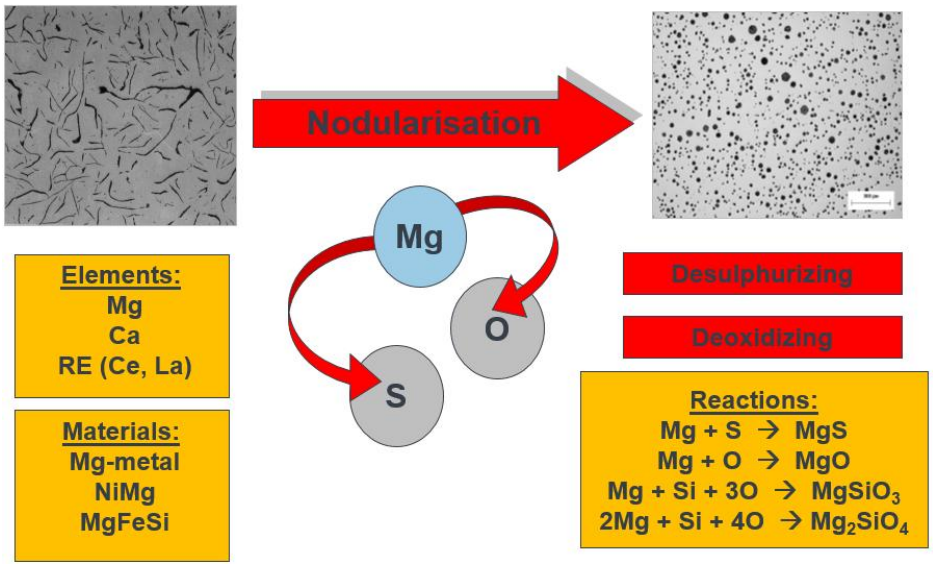

Figure 2. Nodularisation of graphite

NUCLEATION OF GRAPHITE

There are different mechanisms for the nucleation of graphite in grey and in ductile iron. In grey iron, graphite starts to grow from (Mn,X)S [3] containing particles while in ductile iron the graphite starts to grow from Mg-sulphide particles [4]. In grey iron, Figure 3, the main effect of inoculants is to nucleate the precipitation of MnS containing particles that then act as nuclei for graphite growth. In ductile iron, Figure 4, the main effect of the inoculants it to modify the surface of Mg-silicate particles to make them more suitable as nucleation sites for graphite.

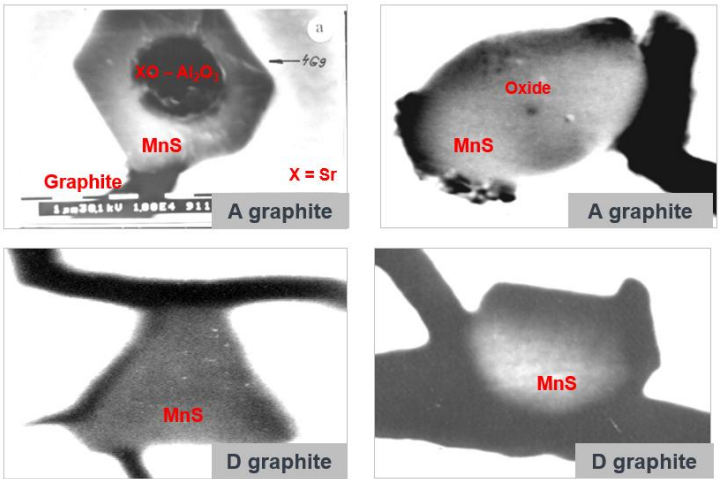

Figure 3. Nucleation of MnS in grey iron

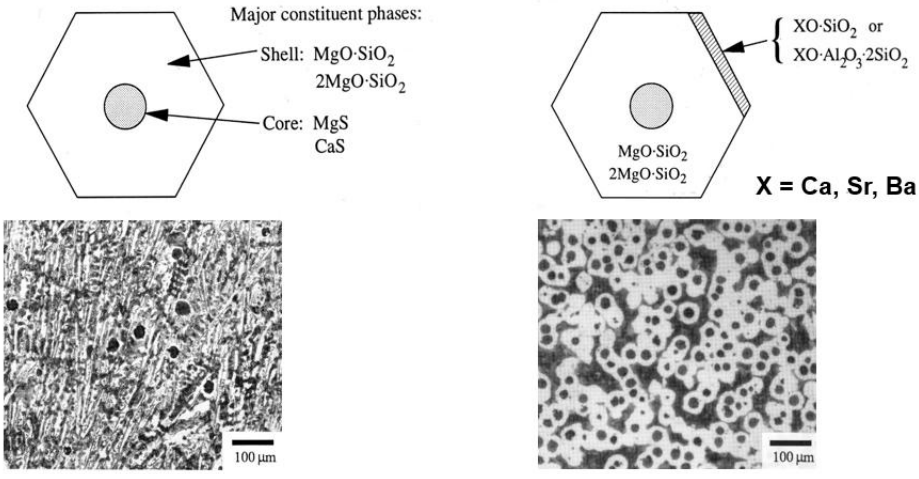

a) b)

Figure 4. Nucleation mechanisms in ductile iron where a sulphide nucleates the growth of a silicate that during inoculation is modified to become a suitable site for graphite growth

Despite the different mechanisms in grey and ductile iron, the inoculants for both grey and ductile iron contain the same elements. The active elements in inoculants are normally Ca, Ba and Sr [3], which are the elements that gives the main nucleation effect. Other important elements in inoculants are Al, Zr, RE and Mn [5]. Those elements can give both nucleation and other effects in the iron. Al is essential in the nucleation of MnS particles in grey iron and is important in formation of the modified silicates in ductile iron, Zr gives inoculation

effect and can neutralise nitrogen, RE increase nucleation and neutralise subversive elements and Mn reduce the alloys melting point and improve dissolution rate.

Figure 5 shows trial results [6] from testing inoculants with different content of active elements in grey iron with different content of sulphur. It shows very clearly that the low sulphur grey iron is more difficult to inoculate, but also that the different inoculants perform differently at different sulphur contents.

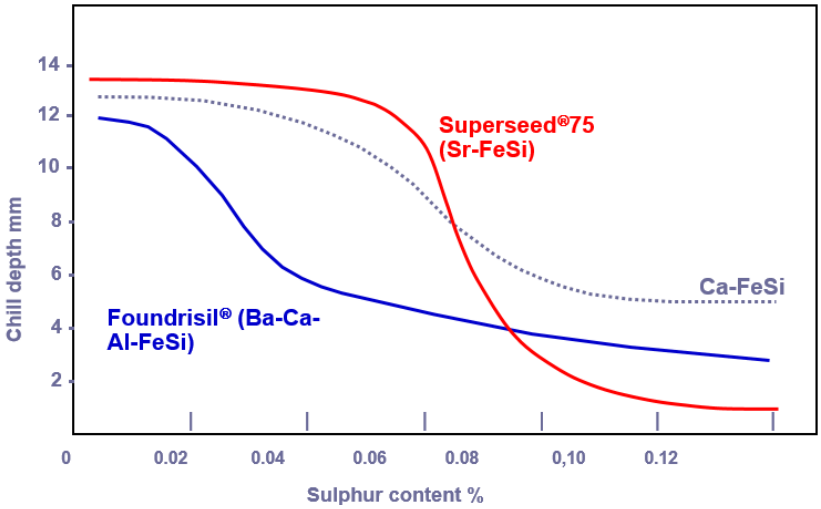

Figure 5. Chill vs. inoculant and sulphur content in grey iron

Figure 6 [7] shows the effect of different inoculants on nodule density and shrinkage tendency in ductile iron with the same composition.

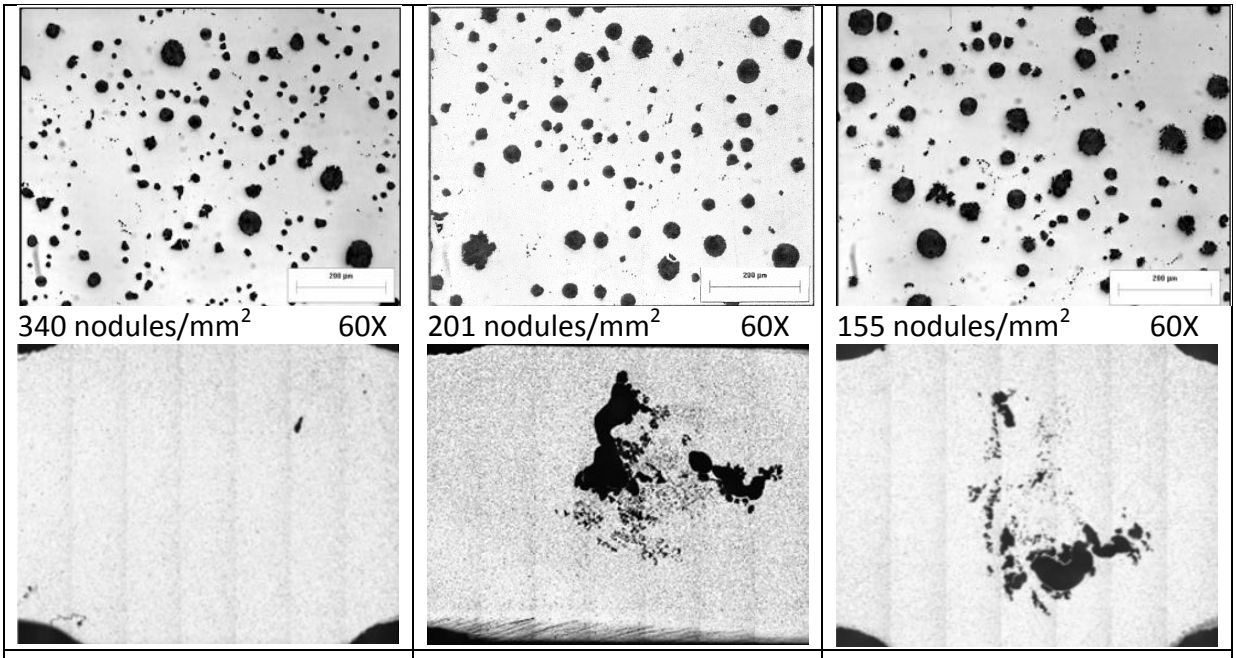

a)Ca, Ce, Al, S, O based inoculant	b) Ca, Ba, Al based inoculant	c) Sr based inoculant

Figure 6. Effect of different inoculants used in ductile iron

CASE STUDIES

Case 1 [8] is a 20.5 tonnes bed plate casting for wind generator, Figure 7.
Originally, the charge contained a high ratio of pig iron and very little steel. The nodularisation was ladle treatment with MgFeSi. Inoculation was 0.64% Ca/Ba containing inoculant plus 0.1% Bi/RE containing inoculant. The main problem was that the casting did not meet the required impact properties. The revised method, see Table 1, was to increase the steel ratio in the charge and to reduce the pig iron. As nodulariser MgFeSi with considerably lower content of Mg and RE was used. In addition, 0.1% of an Al/Zr based preconditioner plus 40 ppm Sb were applied with the charge and finally the inoculation was reduced to 0.2% Ca/Ba containing ladle inoculation plus 0.1% Ce containing inoculation during pouring. The result was improved graphite structure, Figure 8, and considerable improved impact properties, see Table 2.

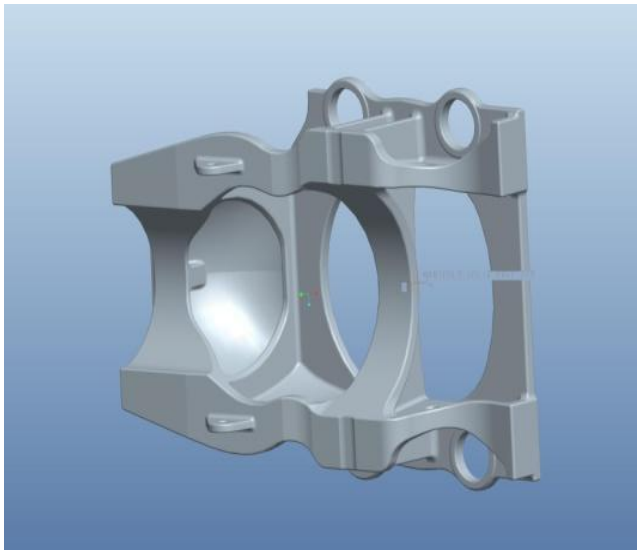

Figure 7. Case 1, bed plate casting for wind generator

Table 1. Method overview, case 1

		Original method	Revise method
Charge materials	Pig iron	60 %	10 %
	CRC Steel	5 %	55 %
	Returns	35 %	35%
Mg-treatment	MgFeSi chemistry	6.8%Mg + 2.3%RE	5.28%Mg + 0.5%RE
	Addition rate	1.38 %	1.1 %
Preconditioner		-	0.1% + 40 ppm Sb
Inoculation	1st step, ladle	0.64 % Ba/Ca based	0.2% Ca/Ba based
	2nd step, pouring	0.1% Bi/RE based	0.1% Ce based

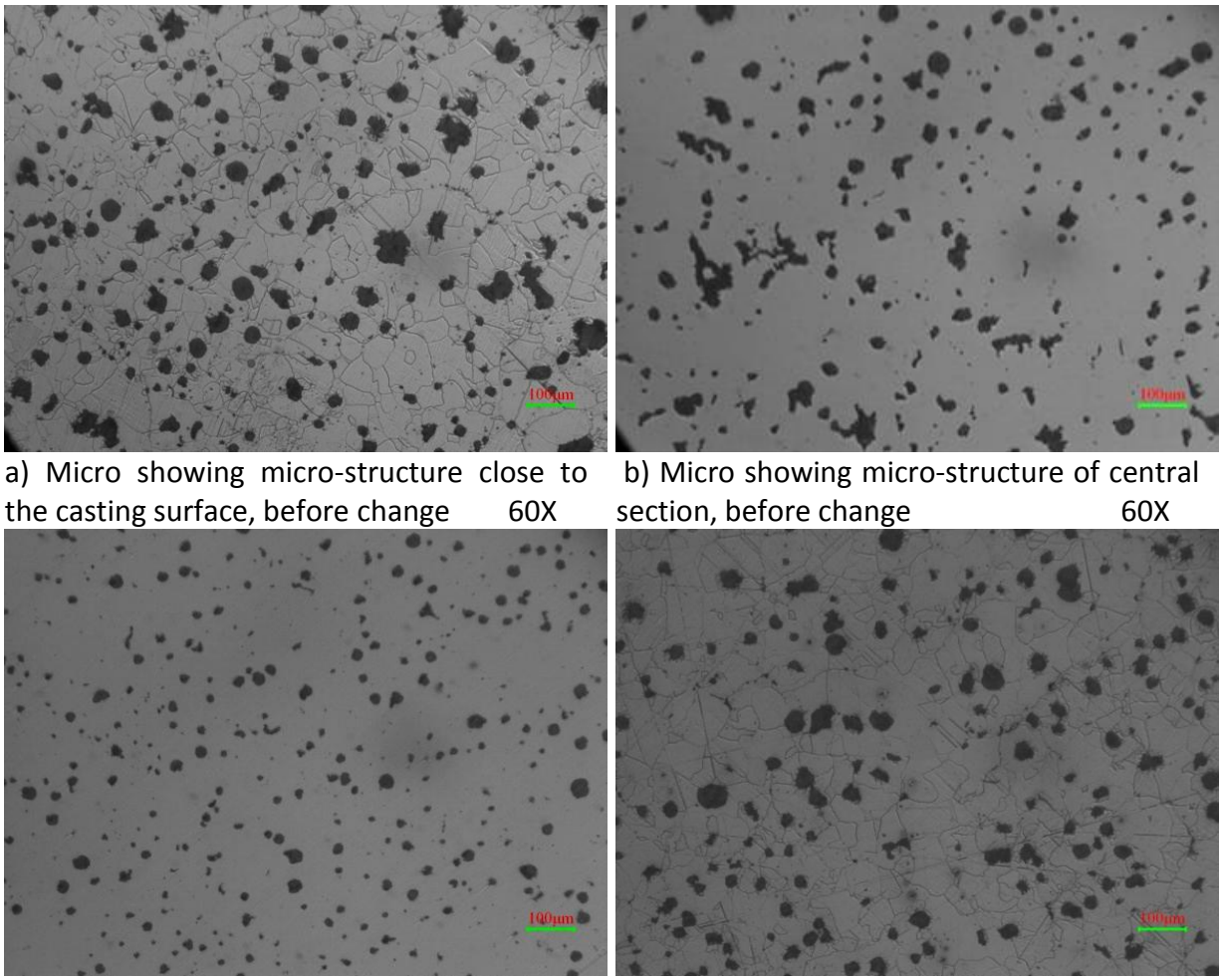

a) Micro showing micro-structure close to the casting surface, before change 60X

b) Micro showing micro-structure of central section, before change 60X

c) Micro showing micro-structure close to the casting surface, after change 60X

d) Micro showing micro-structure of central section, after change 60X

Figure 8. Case study 1, microstructures from samples before and after changing the raw-materials and treatment process

Table 2. Mechanical properties, case 1. Requirements (min) and results before and after changing the process on 70 mm cast on samples and on samples from the castings

	Tensile strength R_m N/mm^2	**0,2 % proof stress** $R_{p0,2}$ N/mm^2	**Elongation** A *%*	**Hardness** BHN	**Impact resistance** *J*
Required	370	220	12	130-175	10
Old, cast on	379	250	24.7	134	11
Old, casting	360	245	22	128	9.3
New, cast on	392	265	23	137	16
New, casting	380	255	22	130	14.7

Case 2 and 3 [9, 10] are from the production of two different wind generator hubs. Casting weight for the hubs including risers and gating systems are 10 and 15 tonnes respectively. Originally, both foundries faced problems meeting tensile and impact requirements.

The revised method is using ladle treatment with MgFeSi containing 5.8 – 5.9%Mg, 0.5-1%RE and 0.1% preconditioner with addition of 30 – 40 ppm Sb. In case 2, first step inoculation is 0.4 – 0.5% Ca/Ba containing ladle inoculation, second step 0.2% Ce containing inoculation during pouring. Microstructures for two different castings produced by the revised treatment method is shown in Figure 9 and mechanical properties are given in Table 3.

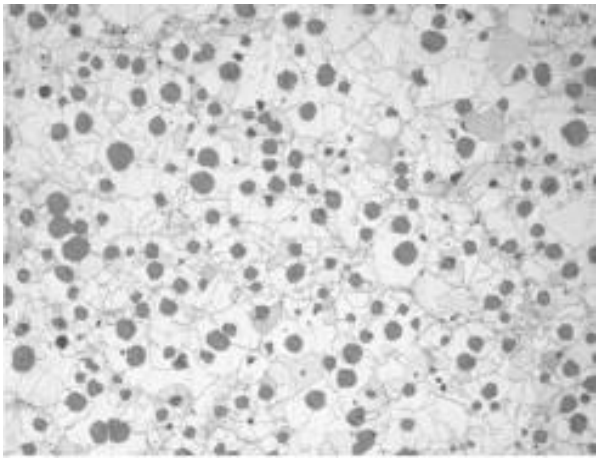

a) Microstructure casting 1 X100

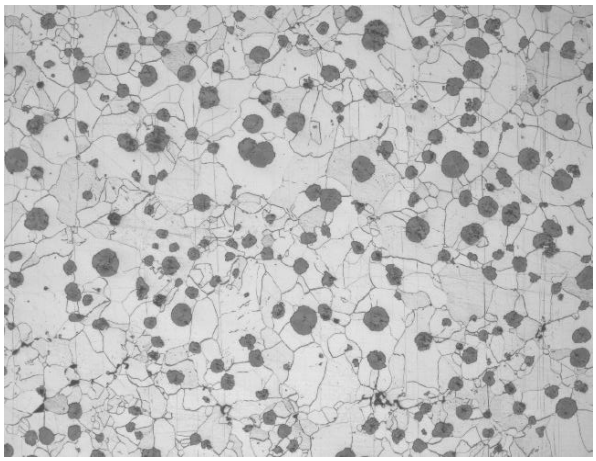

b) Microstructure casting 2 X100

Figure 9. Case 2, microstructure, 70 mm cast on samples

Table 3. Mechanical properties, case 2. Results for revised process on 70 mm cast on samples

	Tensile strength R_m N/mm^2	**0,2 % proof stress** $R_{p0,2}$ N/mm^2	**Elongation** A *%*	**Impact resistance** *J*
Required	370	220	12	10
Casting 1	373	243	27.1	15.4, 15.0, 13.7
Casting 2	375	246	24.3	14.0, 13.6, 12.4

In case 3, first step inoculation is 0.4 – 0.5% Ca/Ba containing ladle inoculation, second step 0.2% Zr containing inoculation during pouring. Microstructures from 70 mm cast on sample from one casting produced by the revised treatment method is shown in Figure 10 and mechanical properties are given in Table 4. The tensile strength requirement is 370 N/mm^2, however 360 N/mm^2 is accepted.

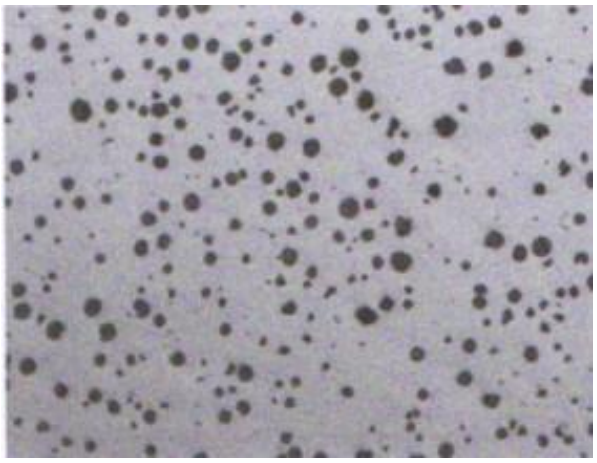

Figure 10. Case 3, microstructure, 70 mm cast on sample X100

Table 4. Mechanical properties, case 3. Results after changing the process

	Tensile strength R_m N/mm^2	**0,2 % proof stress** $R_{p0,2}$ N/mm^2	**Elongation** A *%*	**Impact resistance** *J*
Required	370*	220	12	10
70 mm cast on sample	364	224	25.5	16, 15, 16

*Customer accept min. 360 N/mm^2

CONCLUSIONS

The article gives an overview of the effects of different elements in treatment alloys for cast iron. It also gives examples of improvement in both the structure and mechanical properties by changing the raw material composition and the composition of nodularisers and inoculants.

REFERENCES

[1] EN-ISO 945-1:2008.
[2] T. Skaland, A new approach to ductile iron inoculation, American Foundry Society (AFS), 2001.
[3] I. Riposan, M. Chisamera, S. Stan, D. White, Complex (Mn,X) S compounds – major sites for graphite nucleation in grey cast iron, China Foundry, 6 (2009) 4, pp. 352-357.
[4] T. Skaland, A model for the graphite formation in ductile cast iron, PhD thesis, 1992.
[5] I. Riposan, M. Chisamera, S. Stan, C. Ecob., D. Wilkinson, Role of Al,Ti and Zr in Gray iron Preconditioning/Inoculation, Journal of Materials Engineering and Performance 18 (2009) 1, pp.83-87.
[6] Internal Elkem Report, 2004.
[7] Internal Elkem report, 1999.
[8] Internal Elkem report, 2015.
[9] Internal Elkem report, 2015.
[10] Internal Elkem report, 2015.

15th INTERNATIONAL FOUNDRYMEN CONFERENCE
INNOVATION – The foundation of competitive casting production
Opatija, May 11th-13th, 2016
http://www.simet.hr/~foundry/

HIGH-ZINC ALUMINIUM CAST ALLOYS WITH IMPROVED MECHANICAL PROPERTIES

W. K. Krajewski[1], J. Buraś[1], P. Lisowski[1], G. Piwowarski[1] and A.L. Greer[2]

[1]AGH University of Science and Technology Faculty of Foundry Engineering, Krakow, Poland
[2]University of Cambridge Department of Materials Science & Metallurgy, Cambridge, United Kingdom

Plenary lecture
Original scientific paper

Abstract

The paper reports investigations of the grain refinement of high-zinc Al alloys having a tendency to develop coarse primary Al(Zn) dendrites when cast in sand moulds. This microstructure reduces the plasticity; therefore the grain refinement is aimed at breaking up the primary dendrites of the Al(Zn) solid solution of zinc in aluminium. In these investigations binary Al-20 wt.% Zn and ternary Al-20wt.%Zn-3wt%Cu alloys were inoculated with different additions of Al-Ti- or Zn-Ti-based master alloys. The sand-cast samples were subjected to mechanical-properties measurements (tensile strength and elongation), image analysis aimed at determination of grain size, measurements of the attenuation of 1 MHz ultrasound, and pin-on-disc measurements of tribological properties. It is found that the observed significant grain refinement increases elongation by about 40% with tensile strength and friction coefficient practically preserved. The attenuation coefficient decreases by about 25%, but still remains at the high level of 100 – 150 dB/m.

Keywords: *Al-Zn-based foundry alloys, structure modification, grain refinement, damping properties, tribological properties*

*Corresponding author (e-mail address): *krajwit@agh.edu.pl*

INTRODUCTION

The high-zinc aluminium alloys containing 15–40 wt.% Zn with the addition of third alloying elements have a high resistance to elongation (about 200–250 MPa) and have also good damping properties, which places them in the group of the so-called high-damping alloys, within the field of high-technology alloys [1–3]. Published research indicates that the high-zinc aluminium alloys also have good tribological characteristics, formed in the soft matrix by the presence of secondary phases, formed as a result of the addition of third alloying ele-

ments, e.g. Cu [4–7]. However, these alloys have relatively low plasticity due to high tendency to form coarse grain structures, especially after being cast in a sand mould [8,9], Figure 1. It is therefore vital to perform structural modifications (refinement).

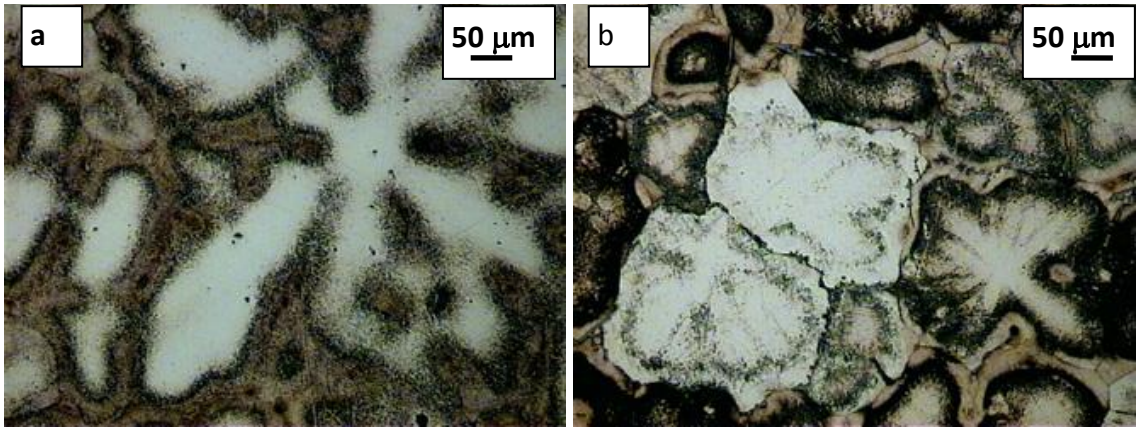

Figure 1. Micrographs of the sand-cast Al-20Zn alloy: (a) non-refined, mean grain size ~1800 μm; (b) Inoculated with 400 ppm Ti in Al-3Ti-0.15C, mean grain size ~ 250 μm

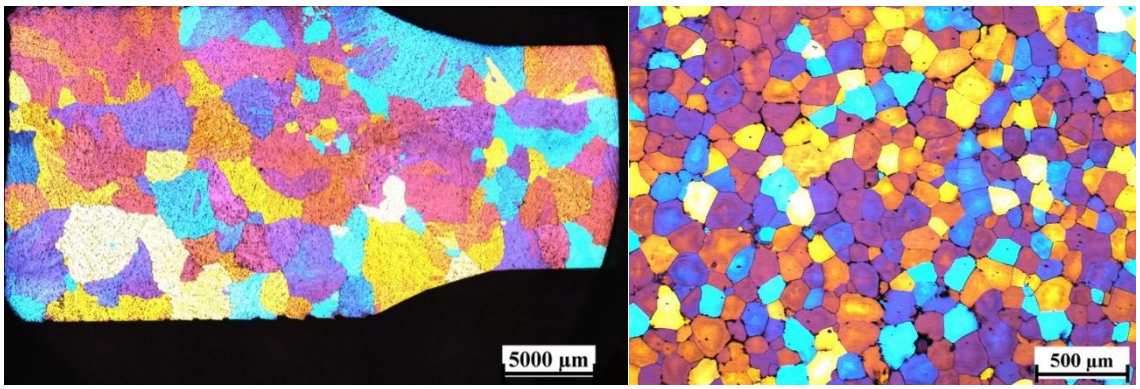

Figure 2. Macrostructures of the alloys shown in Figure 1 [9]

Significant structure refinement of this alloy indeed allows us to improve its plasticity, yet, at the same TIME, it may negatively affect its damping properties, Figure 2. In particular, a finer grain structure usually reduces the damping, which should be taken into consideration when this property is of interest [10–12]. The present paper summarizes work on the grain refinement, damping and tribological property measurements of the selected binary and ternary high-Zn aluminium cast alloys on the basis of joint investigations performed over the last four years at AGH University of Science and Technology, Krakow, Poland – Faculty of Foundry Engineering and at University of Cambridge, UK – Department of Materials Science & Metallurgy.

MATERIALS AND METHODS

The alloys Al–20%Zn and Al-20%Zn-3%Cu were melted from commercial-purity elements of minimum purity 99.8 % (all compositions in wt. %). Melting was performed in an electrical

furnace, in a clay-graphite crucible of 0.5 litre capacity (the details of melting and casting are given in Refs. [8–11]). During these experiments the melt was not flushed or fluxed. The melted charge of the examined alloys was superheated to about 720–740 °C and an amount of Al-3%Ti-0.15%C master alloy (TiCAl) was added to the melt to introduce about 25, 50, 100, 200 and 400 ppm of Ti. The inoculated melt was held for 2–3 minutes to ensure complete dissolution of the added master alloy. Next, the melt was stirred for about 2 minutes with a silica-glass tube, and finally the alloy was cast into dried sand moulds to obtain 30x100 mm castings for structural and damping tests. Structural observations were performed. Light-microscopy (LM) microsections were ground on abrasive paper (grit200–1000) and then polished using sub-µm aluminium oxide in a water-alcohol suspension. The samples used in macrostructure examinations were etched chemically with Keller's or electrochemically with Barker's reagent. Wear-resistance investigations were performed using the pin-on-disc method (T-01M device, made in Poland) and using samples 3.5 mm in diameter and 35 mm in length cut from the ∅30 x 100 mm castings – Figure 3.The dry sliding wear test was performed against a rotating steel disc of 110 mm in diameter and 10 mm in height, and hardness of 50 HRC. The test was carried out under a load giving 0.65 MPa pressure and at a sliding speed of about 1.57 m/s, for a total sliding distance of 2 km. The ambient temperature during the test was about 23 ^{o}C, at air humidity of 45 %. The coefficient of friction was directly measured during these tests [10,12].The attenuation coefficient of the ultrasound longitudinal wave, as a measure of damping properties, was evaluated by the echo method, using a Krautkramer USLT2000 instrument with a frequency of 1 MHz – Figure 3, using samples ∅30 x 100 mm cut from the ∅30 x 100 mm castings. The examinations were carried out using white paraffin oil as lubricant.

Figure 3. The damping Krautkramer USLT 2000 (left) and wear T-01 M (right) instruments used during the experiments

RESULTS AND DISCUSSION

The attenuation coefficient changes, as a function of the addition level of Ti, are collected in Figure4, where the series from the initial alloy through inoculation with 25, 50, 100, 200 and 400 ppm Ti are shown. In the figure, *Am*(total) is the arithmetic mean of the total measurements in a series, *Am*(+) is arithmetic mean of the results above *Am*(total), and *Am*(–) is the arithmetic mean of the results below *Am*(total). From Figure 2, it can be seen that the addition of TiCAl master alloy, in the amount of about 25–100 ppm slightly decreases the attenu-

ation coefficient in comparison with the initial, non-inoculated alloy. This can be attributed to the significant structure refinement, as can be clearly seen in Figures 1 and 2. From the data collected in Figure 4, it appears that series of 200 and 400 ppm Ti addition show very large discrepancies as compared with those of 25–100 ppm Ti addition. On the other hand, it is well known that the common Ti addition to the aluminium alloys in foundry practice is about 50–100 ppm Ti in relation to the mass of the melted alloys. It should be noted that a wide range of individual values is observed within each series, which is seen in Figure 5.

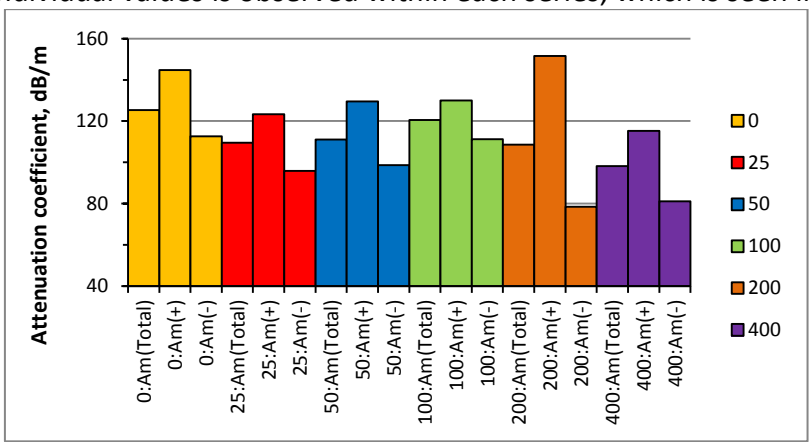

Figure 4. Summary of the effect of the addition of Ti in the Al-3Ti-0.15C (TiCAl) master alloy on the mean values of the Al-20Zn-3Cu attenuation coefficient

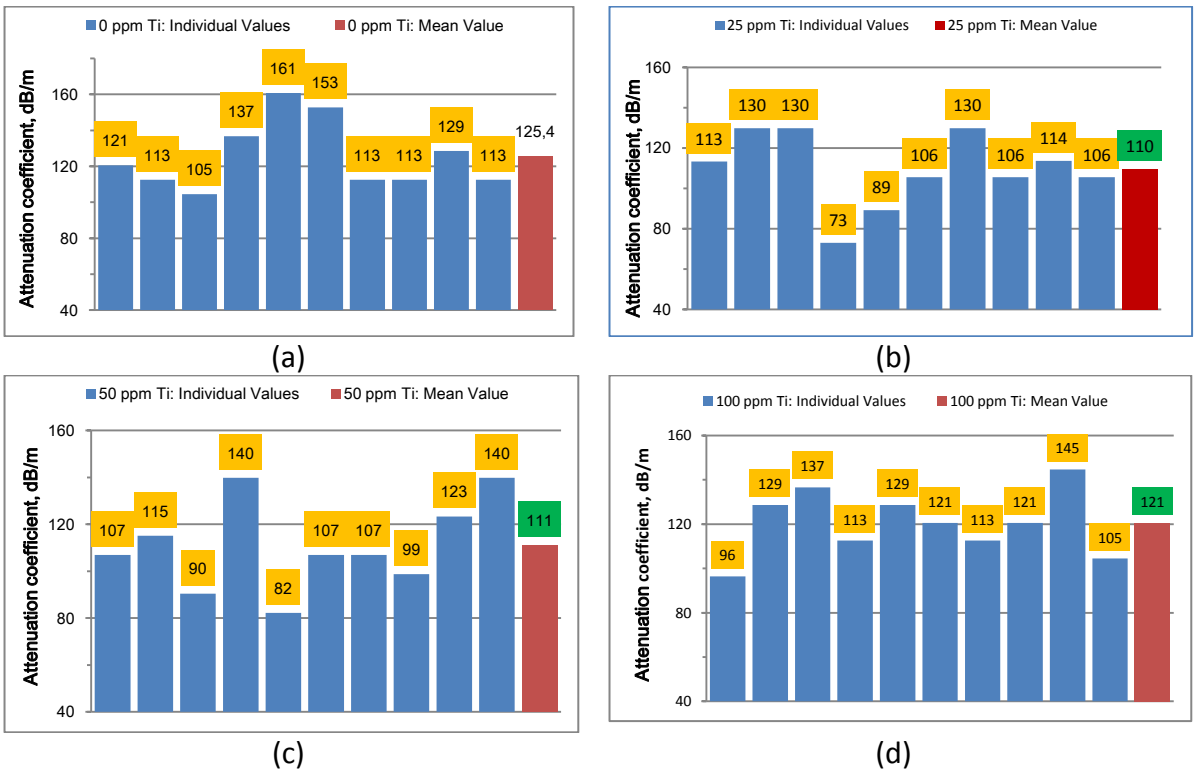

Figure 5. Individual values from 10 samples and their arithmetic means obtained for: (a) initial non-nucleated alloy and (b) for the same alloy inoculated with 25, 50 and 100 ppm Ti

The mean values shown in Figure 5 are collected in Figure 6. It should also be noted that the observed attenuation coefficient decreases only by 10–15 %, so the examined alloys are still high-damping, with attenuation coefficient above 100 dB/m.

In Figure 7(a) there are collected the individual series shown in Figure 5, however with only values from the range ±15% around their mean values shown in Figure 7(b). Comparing results from Figs 6(a) and 7(b), one can see that the courses of the changes are nearly the same for series with 25, 50 and 100 ppm addition. One observed difference is the lower value of mean attenuation coefficient obtained for the initial alloy without Ti addition.

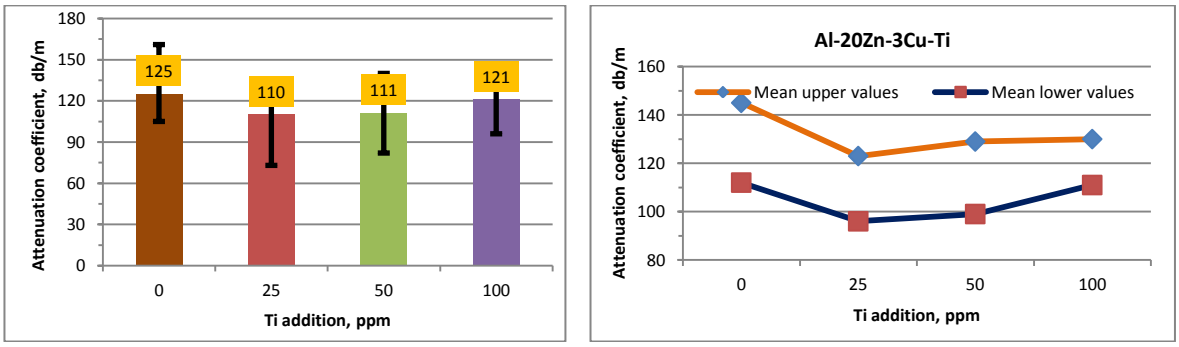

(a) (b)

Figure 6. Mean values of series collected in Figure 5 (a) and the range between their mean maximum and minimum values (b)

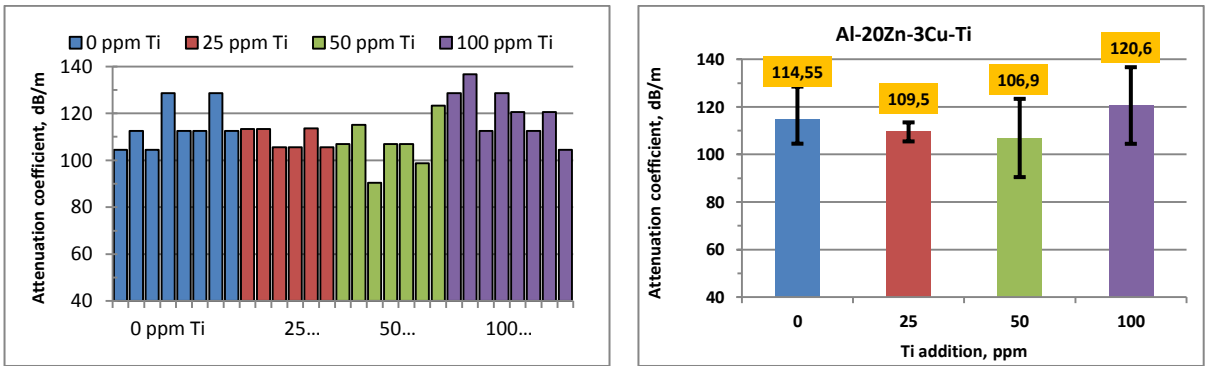

(a) (b)

Figure 7. Series of individual results from the range ±15% around the mean values in a series (a) and their mean arithmetic values (b)

The results obtained during the sliding test of the examined alloys on the T-01 M device are collected in Table 1. The Ti-based particles introduced with the Al-3Ti-0.15C refiner increase the coefficient of friction compared to the initial alloyAl-20Zn-3Cu. The coefficient of friction increases for 50-200 ppm Ti addition. Surprisingly, the value for the alloy with 400 ppm Ti decreases — elucidation of this should be a subject of further detailed examination.

Table 1. Results of pin-on-disc wear tests: load – 10 N, track diameter – 30 mm, rotational speed – 100 rpm

Alloy	Volume loss of sample, mm^3	Coefficient of friction (COF)	Delta COF, %
Al-20Zn-3Cu	1.9455	0.370	0
Al-20Zn-3Cu-25 ppmTi	1.9455	0.370	0
Al-20Zn-3Cu-50 ppmTi	2.1077	0.380	2.7
Al-20Zn-3Cu-100 ppm Ti	2.1401	0.430	16.2
Al-20Zn-3Cu-200 ppm Ti	2.4968	0.450	21.6
Al-20Zn-3Cu-400 ppm Ti	2.2050	0.390	5.4

CONCLUSIONS

Based on the obtained results, the following conclusions can be drawn:

1. Doping the Al-20Zn-3Cu alloy with small Ti additions refines the microstructure, which is beneficial for increasing its ductility [10–11].

2. The attenuation coefficient of Al-20Zn-3Cu alloy with refined microstructure decreases by about 10 % in comparison with the initial alloy without Ti addition. However, the attenuation remains at a high level (above100 dB/m) typical for high-damping alloys.

3. The coefficient of friction is practically unchanged for the alloy doped with 25 and 50 ppm Ti. For an addition of 100 ppm Ti, it increases by about 15% in relation to the non-inoculated alloy. This suggests that addition of 50–100 ppm Ti with the Al-3Ti-0.15C grain refiner should be used to ensure that good mechanical properties can be obtained in the examined alloy.

REFERENCES

[1] I.G. Ritchie, Z-L. Pan, High damping metals and alloys, Metallurgical Transactions A, 22A (1991) pp.607–616.
[2] W.K. Krajewski, The Alloys of Zinc with Aluminium: Types, Properties, Usage. AKAPIT, Krakow, 2013 (in Polish).
[3] W.R. Osorio, J.E. Spinelli, N. Cheung, A. Garcia, Secondary dendrite arm spacing and solute redistribution effects on the corrosion resistance of Al–10 wt% Sn and Al–20 wt% Zn alloys, Materials Science and Engineering, A ,420 (2006) pp.179–185.
[4] Sang-Soo Shin, Kyoung-Mook Lim, Ik-Min Park, Characteristics and microstructure of newly designed AlZn-based alloys for the die-casting process, Journal of Alloys and Compounds, 671 (2016) pp.517–526.
[5] Y. Alemdag, T. Savaskan, Mechanical and tribological properties of Al–40Zn–Cu alloys, Tribology International, 42(2009) pp.176–182.
[6] A.F. Abd El-Rehim, M.S. Sakr, M.M. El-Sayed, M. Abd El-Hafez, Effect of Cu addition on the microstructure and mechanical properties of Al‑30 wt% Zn alloy, Journal of Alloys and Compounds, 607 (2014) pp.157–162.

[7] G. Purcek, O. Saray, I. Karaman, M. Haouaoui, Microstructural evolution and mechanical response of equal-channel angular extrusion-processed Al-40Zn-2Cu alloy, Metallurgical and Materials Transactions A, 40A (2009) pp.2772–2783.
[8] W.K. Krajewski, J. Buraś, M. Żurakowski, A.L. Greer, Structure and properties of grain-refined Al-20wt% Zn sand cast alloy, Archives of Metallurgy and Materials, 54 (2009) pp.329–334.
[9] K. Haberl, W.K. Krajewski, P. Schumacher,Microstructural features of the grain-refined sand cast alloy AlZn20,Archives of Metallurgy and Materials, 55 (2010) pp.837–841.
[10] W.K. Krajewski, A.L. Greer,P.K. Krajewski, Trends in developments of high-aluminium zinc alloys of stable structure and properties, Archives of Metallurgy and Materials, 58 (2013) pp.859–861.
[11] W.K. Krajewski, J. Buras,P.K. Krajewski, A.L. Greer, K. Faerber, P. Schumacher,New developments of Al-Zn cast alloys, Materials Today: Proceedings, 2 (2015) Part A, pp.4978–4983.
[12] P. Lisowski, Effect of grain refinement on damping and tribological properties of high-zinc aluminium alloys, B.Sc. Thesis, AGH University of Science and Technology – Faculty of Foundry Engineering, Krakow, 2016 (in Polish).

Acknowledgements

The authors are grateful to the NCN Polish Science NationalCentre for financial support under grant No. UMO-2012/05/B/ST8/01564. The AGH University of Science and Technology, Krakow, Poland – Faculty of Foundry Engineering and The University of Cambridge, UK – Department of Materials Science and Metallurgy are warmly acknowledged for provision of laboratory facilities.

15th INTERNATIONAL FOUNDRYMEN CONFERENCE
INNOVATION – The foundation of competitive casting production
Opatija, May 11th-13th, 2016
http://www.simet.hr/~foundry/

SULPHUR – KEY ROLE IN GRAPHITE FORMATION IN CAST IRONS - a review

I. Riposan, M. Chisamera, S. Stan, I.C. Stefan, M.C. Firican and V. Uta

Politehnica University of Bucharest, Bucharest, Romania

Plenary lecture
Conference paper

Abstract

Sulphur is a key element in graphite nucleation in all of cast irons, so optimum sulphur content in the base iron is a prerequisite for each iron type. The effect of sulphur in cast irons varies greatly depending on the presence of Group IIA, IIIB, IVB and III A elements in the periodic table. This research summarizes much of the original data obtained by the present authors on the effects of sulphur in cast irons as well as new, experimental work on the inter-relationships between sulphur with other graphitizing elements.
In grey cast irons, excessive sulphur levels can lead to slag inclusions, graphite flake degeneration and affect chill tendency. Sulphur levels less than 0.04% may solidify with high eutectic undercooling, promoting undercooled graphite and/or carbides. In ductile irons, low sulphur levels generally favor reduced nodulizer additions, reduced inclusion formation and result in higher magnesium recovery. However, excessively low sulphur levels may retard or minimize nodular graphite formation. In compacted graphite iron, controlling sulphur and magnesium to tighter ranges involves the aid of sophisticated thermal monitoring software. However, because of concerns regarding future availability of rare earth elements [REE], other production alternatives may be needed. An alternative involves making small and controlled S-addition after Mg-treatment [solo or in combinations with other elements] to promote less eutectic undercooling.
Controlled re-sulphurization with briquetted FeS instead of pyrite powders is the most reliable method for precise sulphur control. Inoculation enhancing through additions of S, O and oxy-sulphides forming elements to commonly used conventional inoculants in a 1:3 ratio, had beneficial effects on solidification of all of standard irons [grey, ductile and compacted graphite irons]. Inoculant consumption was reduced by 50% or more. Using this approach may eliminate the need for rare earth bearing treatment alloys in both nodularizers or/and inoculants.

Keywords: *casting, rare earth, sulphur, grey iron, ductile iron*

*Corresponding author (e-mail address): *iulian.riposan@upb.ro*

SULPHUR – KEY ROLE IN GRAPHITE FORMATION IN CAST IRONS

[a review]

I. Riposan, M. Chisamera, S. Stan, V. Uta, I.C. Stefan, M.C. Firican

POLITEHNICA University of Bucharest, Bucharest, ROMANIA

[15th International Foundrymen Conference, May 11 – 13, 2016, Opatija, CROATIA]

SULPHUR – KEY ROLE IN CAST IRONS

[I. RIPOSAN, M. CHISAMERA, S. STAN et al]

Three stage model for graphite nucleation in grey cast iron – Sulphur contribution

*Undercooling - Chill Size - Structure Relationship in the Ca/Sr Inoculated Grey Cast Iron

64th WFC, Sept. 2000, Paris, FRANCE, Paper No. 62

*Analyses of Possible Nucleation Sites in Ca/Sr Overinoculated Grey Cast Iron

AFS Transactions, 2001, Vol. 109, pp. 1151-1162

*Graphite Nucleants Characterization in Ca/Sr Inoculated Grey Cast Iron

SPCI-7, Barcelona, SPAIN, 2002 / Int. J. Cast Met. Res., 2003, 16 (1-3), 105-111

*A New Approach on the Graphite Nucleation Mechanism in Grey Cast Iron

AFS Cast Iron Inoculation Conference, Sept. 2005, Schaumburg, IL, USA, pp.31- 41

*Graphite Nucleation Control in Grey Cast Iron

10th Asian Foundry Congress (AFC10), JAPAN, 2008 / Int. J. Cast Met. Res., 2008, 21 (1-4), 39

*Three-Stage Model for the Nucleation of Graphite in Grey Cast Iron

"Carl Loper" Cast Iron Symp., 2009, USA / Panel 115th AFS Congr. 2011 / Mater. Sci. Tech. 2010 , p.1439

*Enhanced quality in electric melt grey cast irons / *70th WFC, MEXICO / ISIJ Int., 2013, 53 (10), p.1683*

*New Developments in High Quality Grey Cast Irons / *CHINA FOUNDRY, 10th Anniversary, 2014, p.351*

*Modification and Inoculation of Cast Iron. *Chapter, ASM Handbook, Volume 1A: Cast Irons, 2017*

Complex graphite nucleation sites in ductile iron

– Sulphur contribution

*S - Inoculation of Mg-treated Iron - An efficient way the control graphite morphology and nucleation

SPCI-7, Nancy, France, 1994 / Advanced Mater. Research, 1997, 4-5, pp. 293-300

*High Active Inoculant Ferroalloy to control Graphite Morph. and Nucleation Ability in Cast Iron

7th International Ferroalloy Congress (INFACON 7), 1995, Trondheim, NORWAY, vol. 1, pp. 320-324

*The Importance of Sulfur to Control Graphite Nucleation in Cast Irons

AFS Inoculation Conference, April 1998, Rosemont, IL, USA, Paper no. 3

*Contributions to the Development of the Nodular and Vermicular Cast Irons Technologies

63rd WFC-World Foundry Congress, 1998 (WORLD FOUNDRY CONGRESS – THE BEST PAPER AWARD)

*Role of Residual Aluminium in Ductile Iron Solidification

AFS Transactions 2007, Vol. 115, pp. 423-433 / Modern Casting, May 2008 [on line publication]

*Al Benefits in Ductile Iron Production

"Keith Millis" Symp. on the Ductile Iron, Las Vegas, USA, 2008, 206-214 / JMEP, 2011, 20 (1), 57- 64

Intermediate graphite morphologies in Compacted [V] graphite cast irons – *S contribution*

*Control of the degree of Graphite Compactness in Vermicular & Coral Graphite Cast Irons

FOCOMP'86 International Conference, Krakow, POLAND, June 1986, pp. 269-278

*S - Inoculation of Mg-treated Cast Iron - An efficient way the control graphite morphology and nucleation ability

SPCI - 7, Nancy, FRANCE, 1994 / Advanced Materials Research, 1997, 4-5, pp. 293-300

*Study on the Graphite Compactness Degree in Modified Cast Irons

EUROMET 1995, Progress in Metallography, pp. 163-166 , GERMANY

*New Aspects Regarding Contact Parameters between Graphite Shape & Metallic Base in Modified Iron

EUROMAT 97: 5th European Conf. on Adv. Mater. & Proc. & Applic., Vol. 1, pp. 729-734, 1997.

*Experience Producing Compacted Graphite Cast Irons by Sulfur Addition after Magnesium Treatment

AFS Transactions, 2002, Vol.110, pp. 851-860

*Mg – S Relationship in Ductile and Compacted Graphite Irons as Influenced by Late Sulfur Additions

AFS Transactions, 2003, Vol.111, 869-883 [AFS Congress - The BEST OPERATING PAPER AWARD]

Demystifying the Effects of S in Irons / 120th AFS Congress, April 2016, Minneapolis, MN, USA, 16-080

Sulphur contribution in inoculation enhancing of cast irons

*Importance of REE contribution and Their Subsequent Effect on the Inoculation of Ductile Iron
"Keith Millis" Symposium, Oct. 2013, *Nashville, USA, 256-275* / Int. J. Metalcasting, 2014, 8 (2), 65-80

*The Effect of Minimizing REE during Nodulizing &Inoculation of DI / *AFS Trans. 2014, Vol. 122, 219-236*

*Inoculant enhancer plus Ca-FeSi alloy in DI, low RE / *SPCI-10, Nov. 2014, Mar del Plata, ARGENTINA*

*Increasing the Inoculant Potency of Commercial Inoculating Alloys in Induction Melting Grey Cast Iron
AFS Transactions, 2015, Vol. 123, pp. 227 - 242

*S in cast irons – friend or enemy? *AFS Int. Ferrous Melting Conf., October 2015, Nashville, TN, USA, 03*

*Cast Iron Inoculation Enhancing by S, O and Oxy-Sulphides Forming Elements Contribution.
The 7th European Cast Iron Conference, March 2015, Zwijnaarde, BELGIUM

*Cast Iron Inoculation Enhancing – Solution for Critical Production Conditions
55th Int. Foundry Conference, Sept. 2015, Portoroz, SLOVENIA, Paper 06-Plenary Lecture

*Demystifying the Effects of S in Cast Irons /*120th AFS Congr., April 2016, Minneapolis, MN, USA, 16-080*

INTERNATIONAL RECOGNITION

***63rd World Foundry Congress [WFC] – THE BEST PAPER AWARD– 1998**

Contributions to the Development of the Nodular and Vermicular Cast Irons Technologies

***107th AFS Congress, 2003 [USA]-The BEST OPERATING PAPER AWARD**

Mg – S Relationship in Ductile & Compacted Graphite Irons as Influenced by Late S Additions

***American Foundry Society [AFS] – AWARD OF SCIENTIFIC MERIT–2012**

"for advancing the knowledge of the cast iron industry through extensive research and for generously sharing his knowledge and expertise with the industry".

"This is the highest recognition the American Foundry Society and your peers can give to the individuals who have served the industry honorably and well. In presenting this award, we are confident it will bring you the recognition you so well deserve. The spirit in which you have fulfilled AFS' mission of sharing knowledge has been one of the main considerations in making this award".

OUTLINE

- **INTRODUCTION**
  - *Cast iron in world metalcasting industry
  - *Important changes in cast irons production
- **BACKGROUND**
  - *Graphite formation in commercial cast irons [GI, DI, CGI]
- **EFFECTS OF SULPHUR IN CAST IRONS**
  - *Specific effects in GI, DI, CGI
  - *Inter - relationships between Sulphur and active elements
- **GENERAL CONCLUSIONS**
  - *Sulphur - Friendly element in cast irons

WORLD CASTING PRODUCTION [Mil. Tons]
[1998-2014]

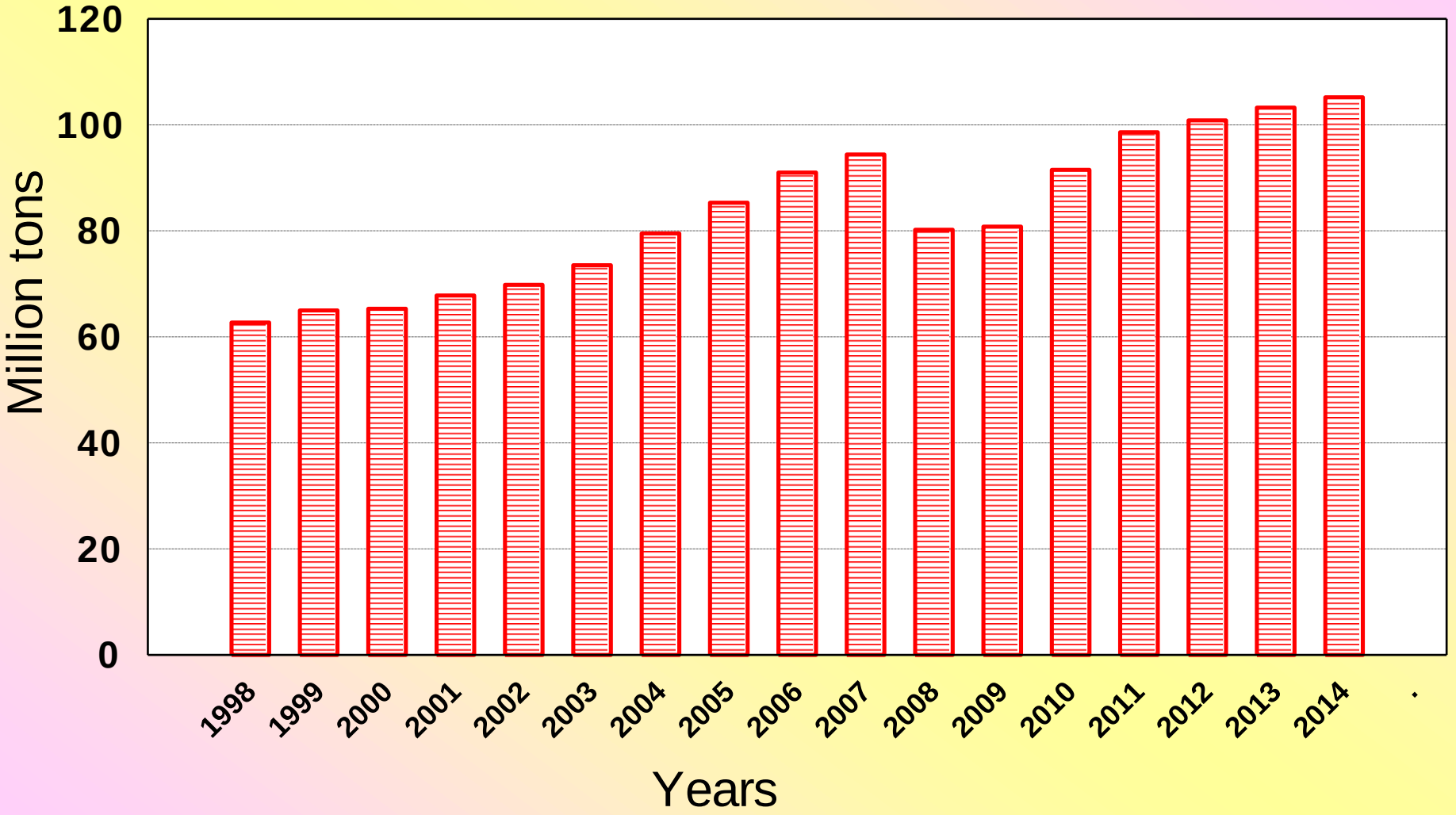

WORLD METALCASTING PRODUCTION EVOLUTION 2004 - 2014

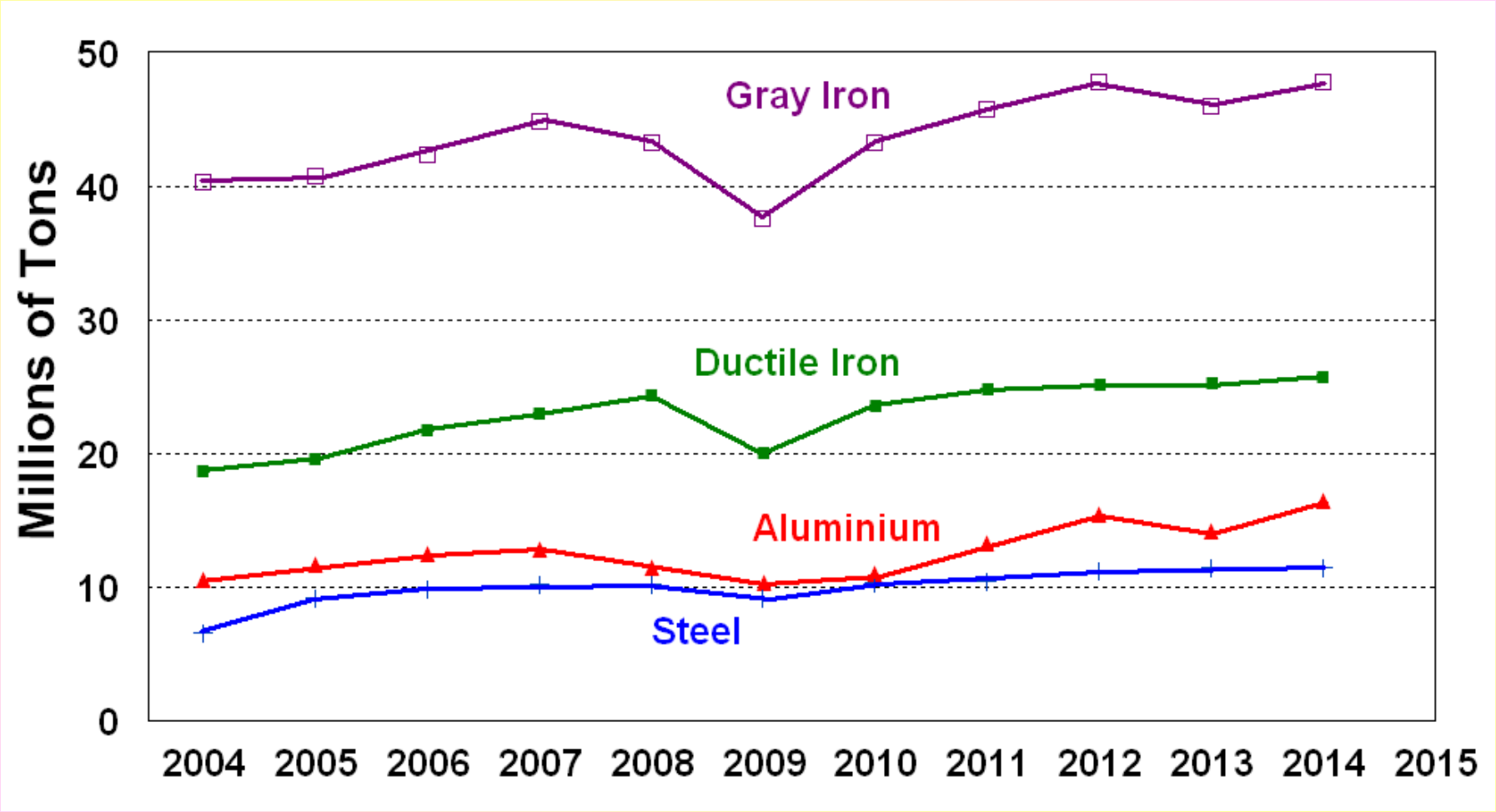

2014 WORLD METALCASTING PRODUCTION
[103.64 Million Metric Tons]

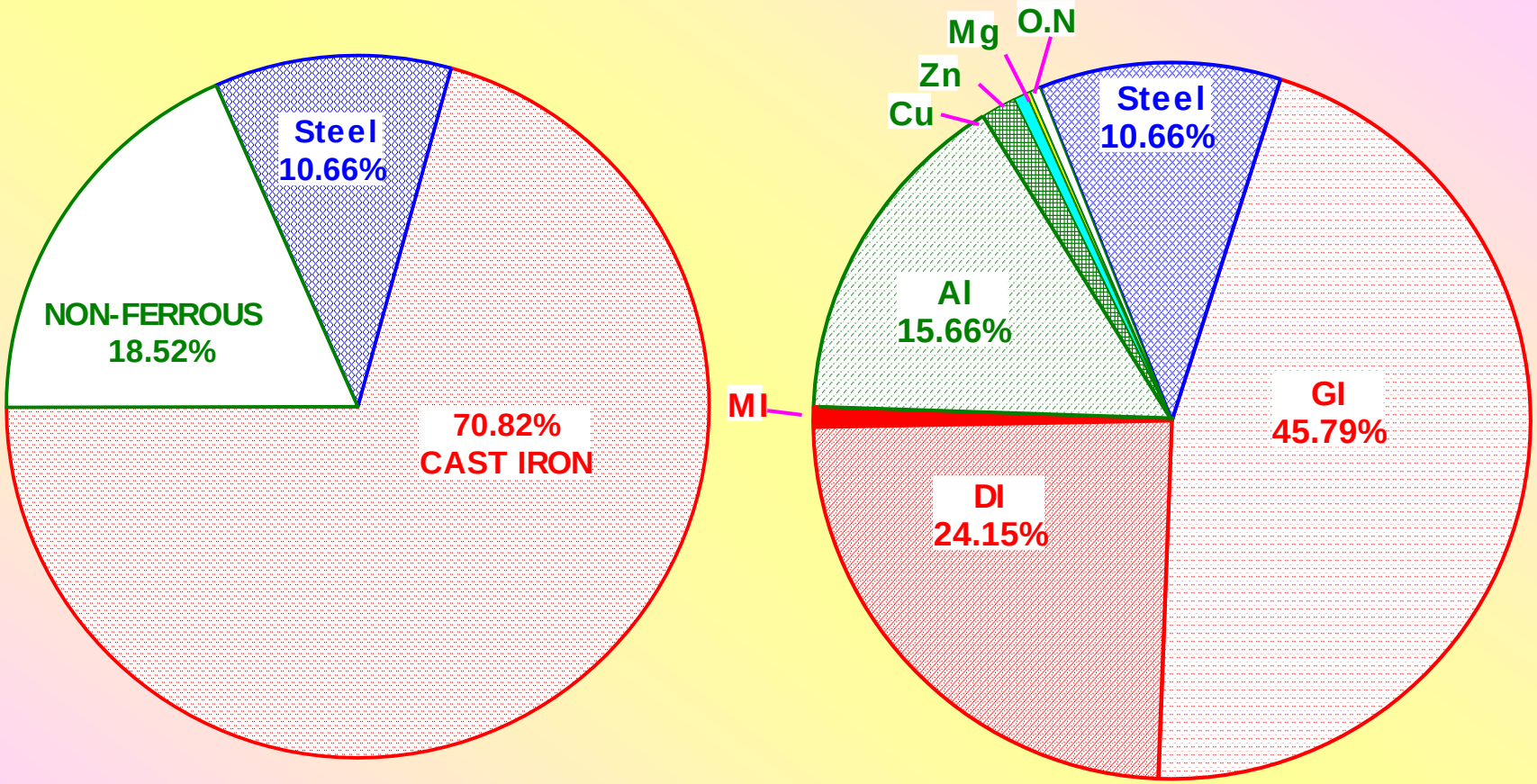

[Modern Casting, December 2015, pp. 26 - 31]

[15th International Foundrymen Conference, May 11 – 13, 2016, Opatija, CROATIA]

IMPORTANT CHANGES IN CAST IRONS PRODUCTION
[Critical Production Conditions]

I. Thin Wall Castings [< 5mm wall thickness]

+ reduced final product weight / reduced energy consumption

- High cooling rate / carbides / excessive hardness / reduced machinability

- undercooled graphite in GI / excessive graphite nodularity in CGI

Metallurgical solutions

- **complex liquid state treatments:** base metal control – preconditioning - inoculation
- **strong inoculation** [graphite nucleation promoting]
- **special formulated inoculants / rare earth elements-REE / inoculation enhancing**

(a) Un – Inoculated (b – 0.15%, c – 0.25% alloy) Inoculated Irons

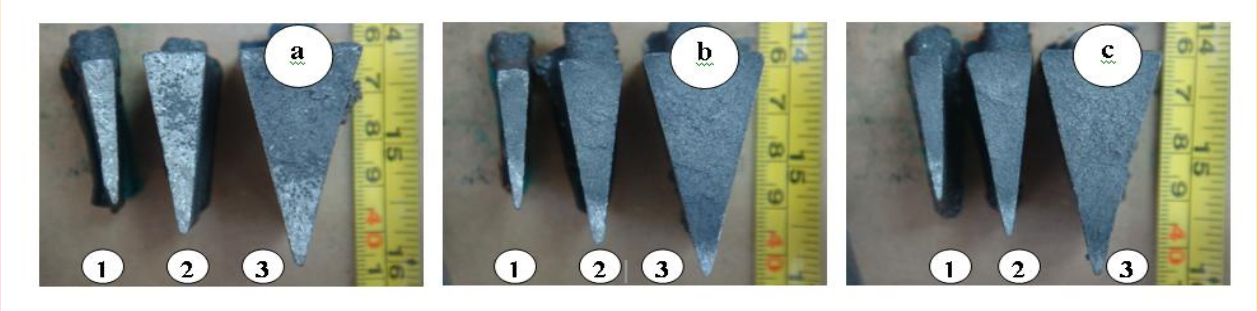

[S. Stan, M. Chisamera, I. Riposan, E. Stefan, M. Barstow. AFS Trans., 2010, Vol. 118, pp 295-309]

II. Important Melting Procedure Changes

***Historically:** Cupola Melted Irons

***Small or / and inefficient Cupolas** – replaced by a new generation of Coreless Induction Furnaces [200 – 1000 Hz, > 250 kW/t, acidic refractory lined]
- high melting rate, no heel, steel charge, stirring, > 1500°C / 2732F

***GI, DI & CGI** Production in the same Foundry: a single Low S Base Iron

TENDENCY IN CAST IRON MELTING

- electrically melting, induction coreless furnaces, high superheating
  - ferrous scrap charge, mainly steel scrap, limited foundry [graphitized] pig iron
  - low and very low Sulphur content base iron [<0.05%S / <0.03%S / <0.02%S]
- low amount of residual graphite and high its dissolution [S<<, T>>]
  - heterogeneous graphite nucleation, sulphides and oxides / silicates:
    - melting practice, iron chemistry, molten iron treatments, solidification
    - thermodynamic conditions of compounds formation, *and*
    - lattice parameters difference compound - graphite **[δ, %]**

DIFFICULTY IN INOCULATING

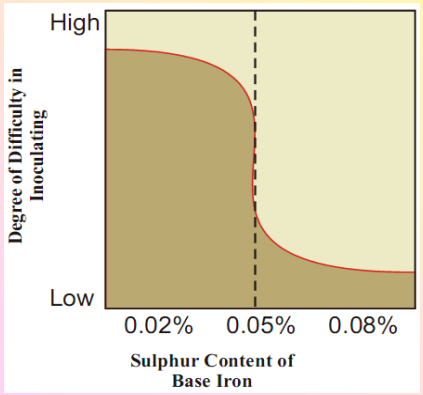

[www.elkem.no]

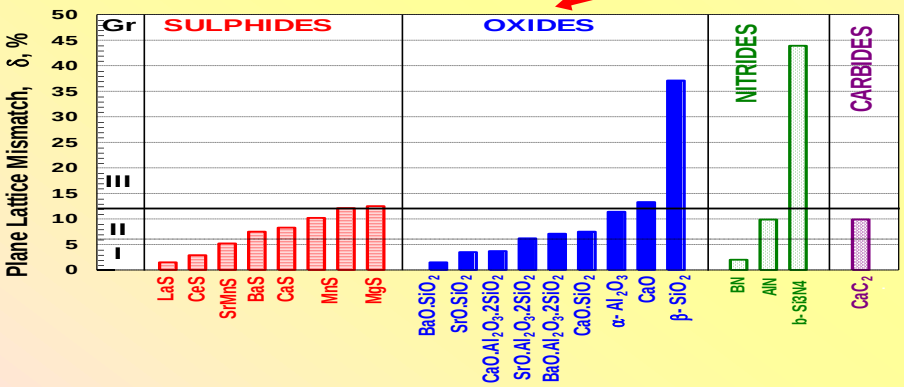

III. RARE EARTH ELEMENTS [REE] IN CAST IRON

Importance *and* Problems

IMPORTANCE

- strong inoculation capacity in low S, electric melting **Grey Cast Iron [REE + Ca, Ba, Sr]**
- capacity to counteract antinodularising elements effect in **Ductile Iron [Mg + REE]**
- improving graphite nodularity and nodule compactness in **Ductile Iron [Mg + REE]**
- improving inoculation capacity in **Ductile Iron [Ca, Ba, Sr....+ REE]**
- the main treatment agent to produce **Compacted Graphite Iron [REE + Mg]**
- improving inoculation capacity in **Compacted Graphite Iron [Ca, Ba, Sr....+ REE]**

PROBLEMS

***GENERAL FORECAST - NOT FAVOURABLE FOR APPLICATION IN FOUNDRIES**

- World REE crisis will continue at least in the short and medium term.
- REEs: important / critical to hundreds of high-tech applications

***Light REE [La, Ce, Pr, Nd]: generally used in metallurgy**

- more attractive for other high - tech applications / less available for cast iron use

***RE extraction / production: pollution industries**

- toxic acids / toxic radioactive [Th, U] byproducts / hard working conditions
- new environmental rules are expected to raise global REE prices

□ BACKGROUND

***Graphite formation in commercial cast irons**

- **Grey Iron**
- **Nodular Graphite Iron**
- **Compacted Graphite Iron**

I. A Three – stage Model for the Nucleation of Graphite in Grey Iron

[1 - 3 %Si, 0.5 – 1.5%Mn, 0.02 – 0.2%S, 0.002 – 0.05%Al, 0.002 – 0.02%Ti, 0.0002 – 0.0005%Zr]

1. Small oxides [XO< 3μm] **2.**(Mn,X)S Compounds [1-10μm] **3.** Graphite

Si – Mn – O [< 0.003%Al_{res}]

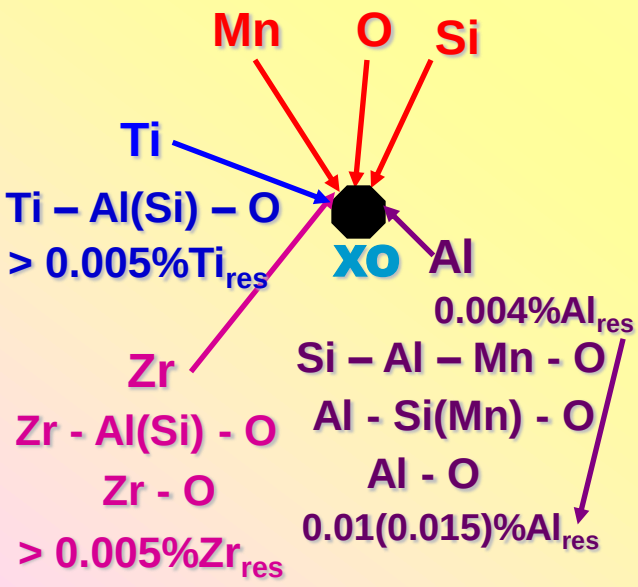

[Mn < Si < (Ti) < Al ≤ Zr]

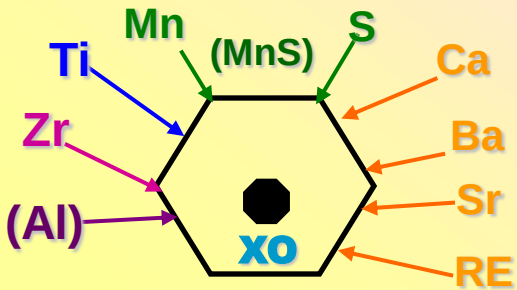

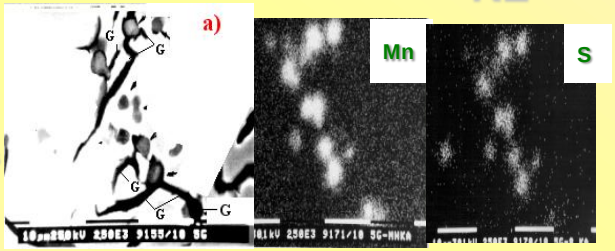

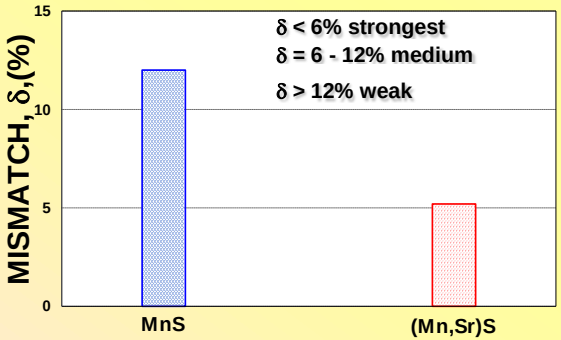

Mismatch δ(%) between a special lattice face of MnS and the (0001) face of graphite

[Jiyang, Rong De, Ueda, Chunqi]

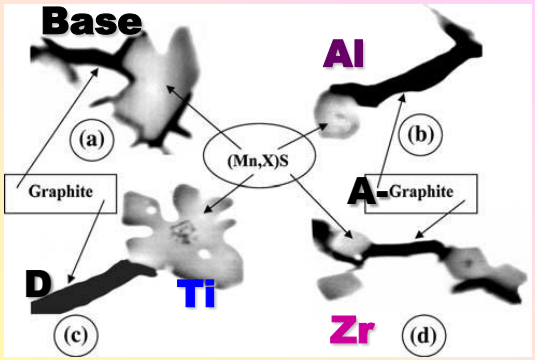

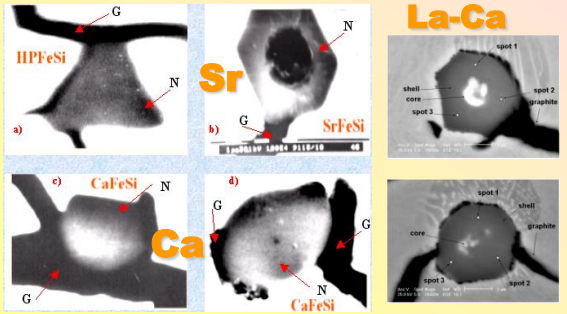

[X = Mn, Si, Al, Zr, Ti, Ca, RE, Sr...]

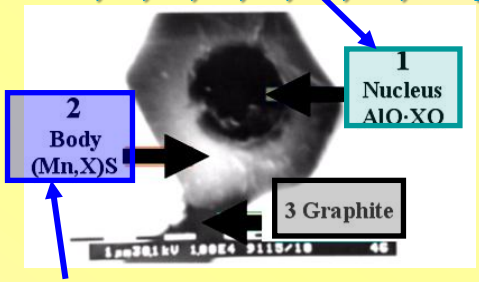

[X = Zr, Ti, (Al), Ca, Sr, Ba, RE...]

[I. Riposan, M. Chisamera, S. Stan, T. Skaland. 64th W F C, 2000, France; AFS Trans., 2001 / SPCI7, 2002 / Int. J. Cast Met. Res. 2003 / AFS Inoc. Conf. 2005 / C. Loper Symp., 2009 / Mat. Sci. & Technol., 2010]

Three groups of elements are important to sustain graphite nucleation in grey irons

1) strong deoxidizing elements, such as Al / Zr,

to promote formation of very small micro - inclusions

[0.005 – 0.010% (0.015%) Al beneficial; *I. Riposan et al*]

[Mn < Si < Al ≤ Zr] [Ti could be harmful: D-type graphite promoter]

2) Mn *and* S to sustain MnS sulphide formation

[(%Mn) x (%S) = 0.03 – 0.06; *R. Gundlach*]

[generally, in a 0.4 – 1.2%Mn / 0.04 – 0.12%S range]

3) inoculating elements (Ca, Sr, Ba, Ce, La etc)

which act in the first stage *and / or* in the second stage of graphite formation,

to improve the capability of (Mn,X)S compounds to nucleate graphite.

REMARK: importance of control / addition of active elements, such as O, S, Oxy - Sulphides forming elements [Mn, Al, Zr, Ca, La, Ce....]

II. DUCTILE IRON - Graphite nodules nucleate heterogeneously on particles formed in the melt, with a duplex structure (sulphide / oxide)

[M.H. Jacobs et al, Metals Technology, [UK] Nov. 1974, 490-500; March 1976, 98-108]

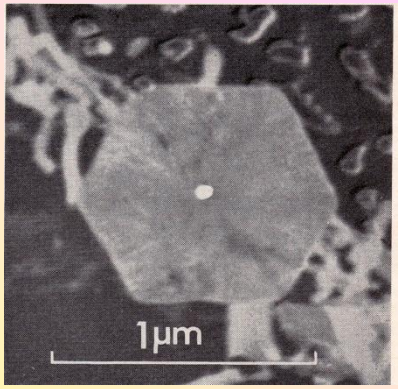

The nucleating particles have a duplex structure *consisting of*

*** Central seed,** ***surrounded by an*** **Outer shell**

of different crystal structure and chemical composition

- **Ca-FeSi / Sr-FeSi** inoculated, FeSiMg treated iron:
  - *** Central seed: (Ca,Mg)S** *vs* **(Sr,Ca,Mg)S compounds**
  - *** Outer Shell: (Mg,Al,Si,Ti) Oxyde with the spinel structure**
- **Two roles of Mg, Ca, Sr in Ductile Iron:**
  - *** To combine with and remove the free S from the melt**
  - *** Formation of sulphide particles, as necessary step in graphite nucleation**

NODULAR GRAPHITE *vs* LAMELLAR GRAPHITE NUCLEATION

NODULAR GRAPHITE
[M. Jacobs + T. Skaland]

FeSiMg - treatment

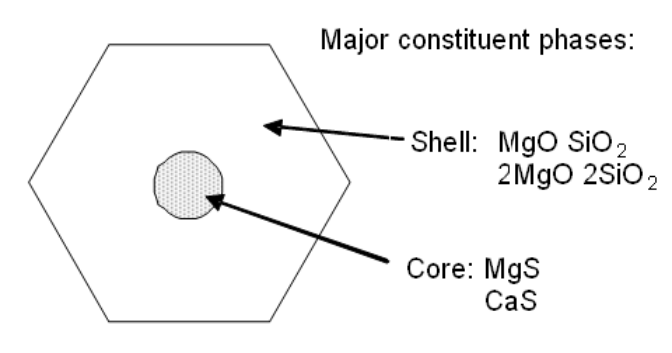

Ca/Sr/Ba-FeSi - inoculation

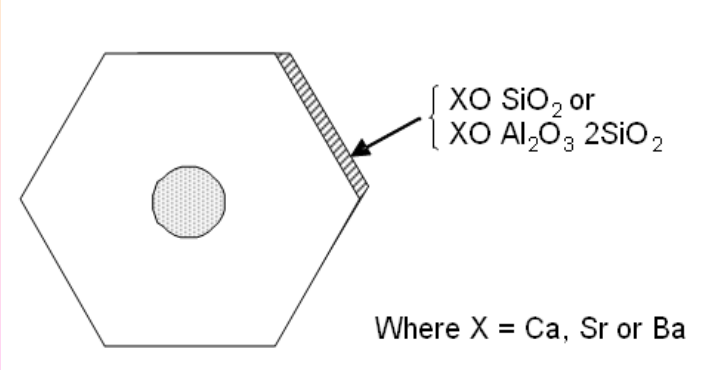

[S, O, Al, Si, Ca, Mg, Ce, La, Ba, Sr..]

LAMELLAR GRAPHITE
[I. Riposan, M. Chisamera, S. Stan]

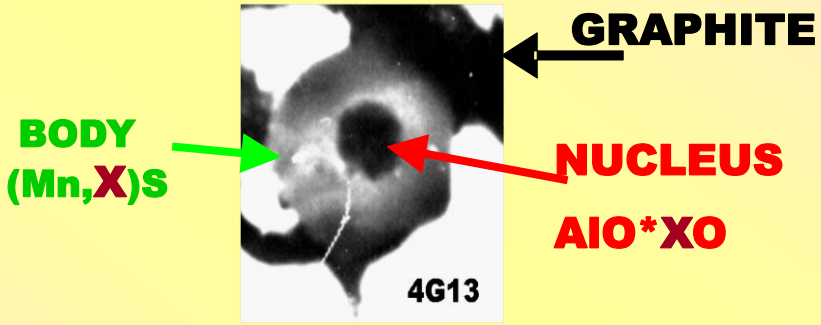

[O, S, Mn, Si, Al, Zr, Ti, Ca, Sr, Ba, Ce, La..]

COMPLEX NODULAR GRAPHITE MICRO-INCLUSIONS AS NUCLEANTS

MATRIX

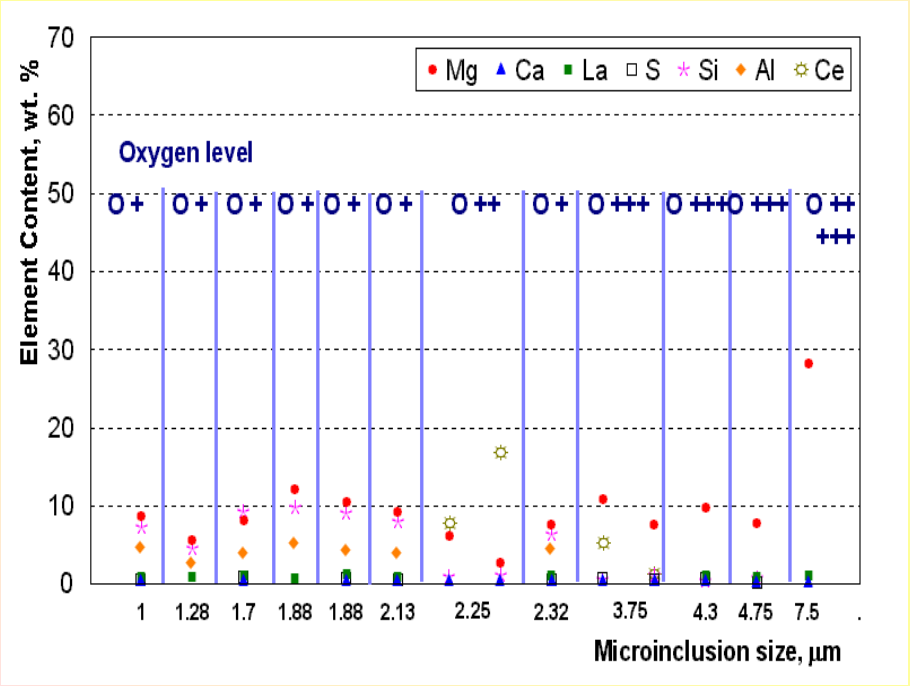

GRAPHITE

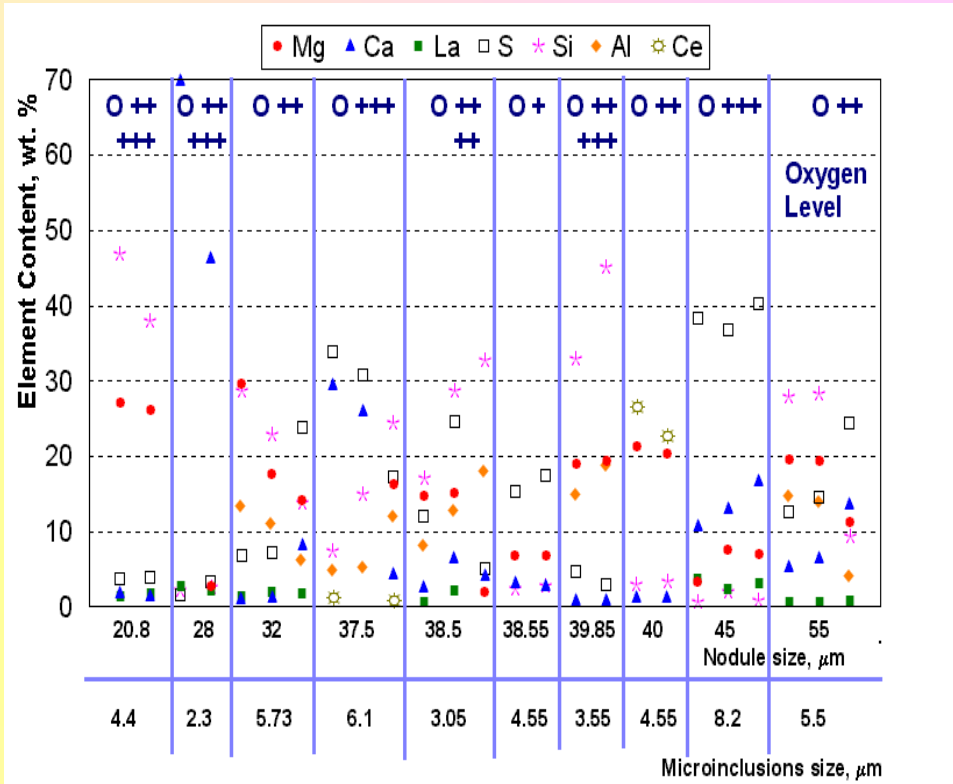

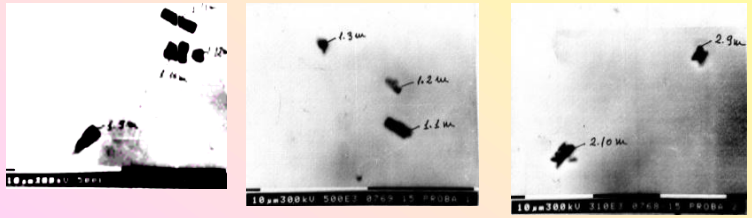

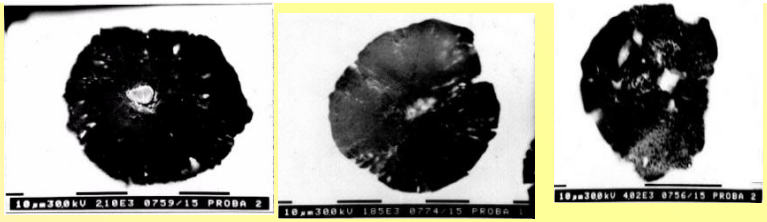

[I. Riposan, M. Chisamera, S. Stan, P.Toboc, D. White, C. Ecob, C. Hartung. 4th Keith Millis Duct. Iron Symp. 2008, Las Vegas, NV, US / J. Mater. Eng. Perform., 20 (1), 2011, 57- 64]

Aluminium decreases Eutectic undercooling (ΔTm) relative to stable (graphitic) eutectic temperature (Tst) in Ductile Iron

[TEU = TElow]

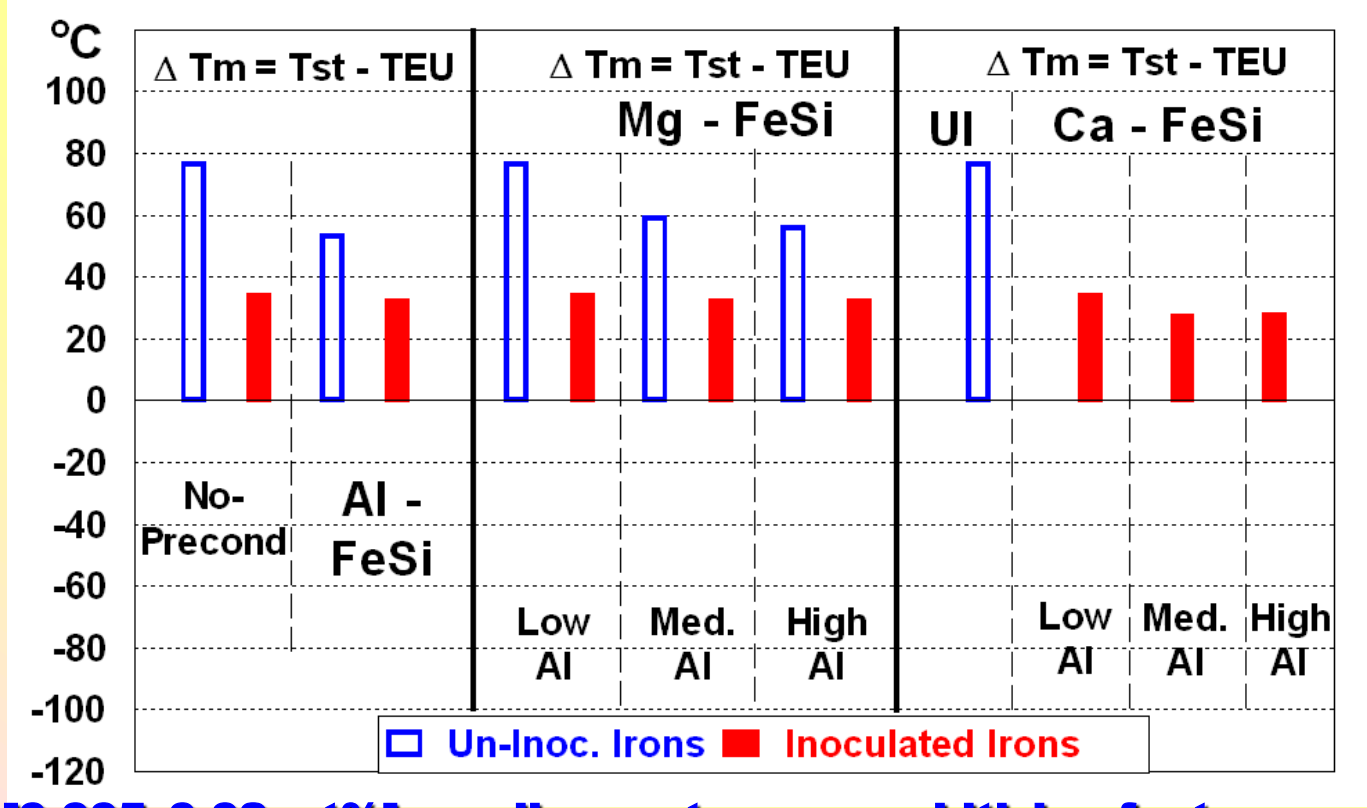

Al-residual [0.005–0.02 wt%]: medium potency graphitizing factor

- in both un-inoculated and inoculated irons; the most representative parameters of thermal analysis were improved; carbides amount decreased / nodule count increased

[I. Riposan, M. Chisamera, S. Stan, P. Toboc, G. Grasmo, D. White, C. Ecob, C. Hartung, AFS Trans., 2007, 115, 423-433 / Proc. Keith Millis Symp. Ductile Iron, Las Vegas, NV, SUA, 2008, 206–214 / JMEPEG, 2011, 20 (1), 57- 64]]

III. COMPACTED GRAPHITE IRON – Graphite Characterization

ISO/FDIS 16112 : 2005 (E)

Roundness Shape Factors

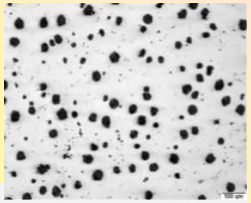

NG

K

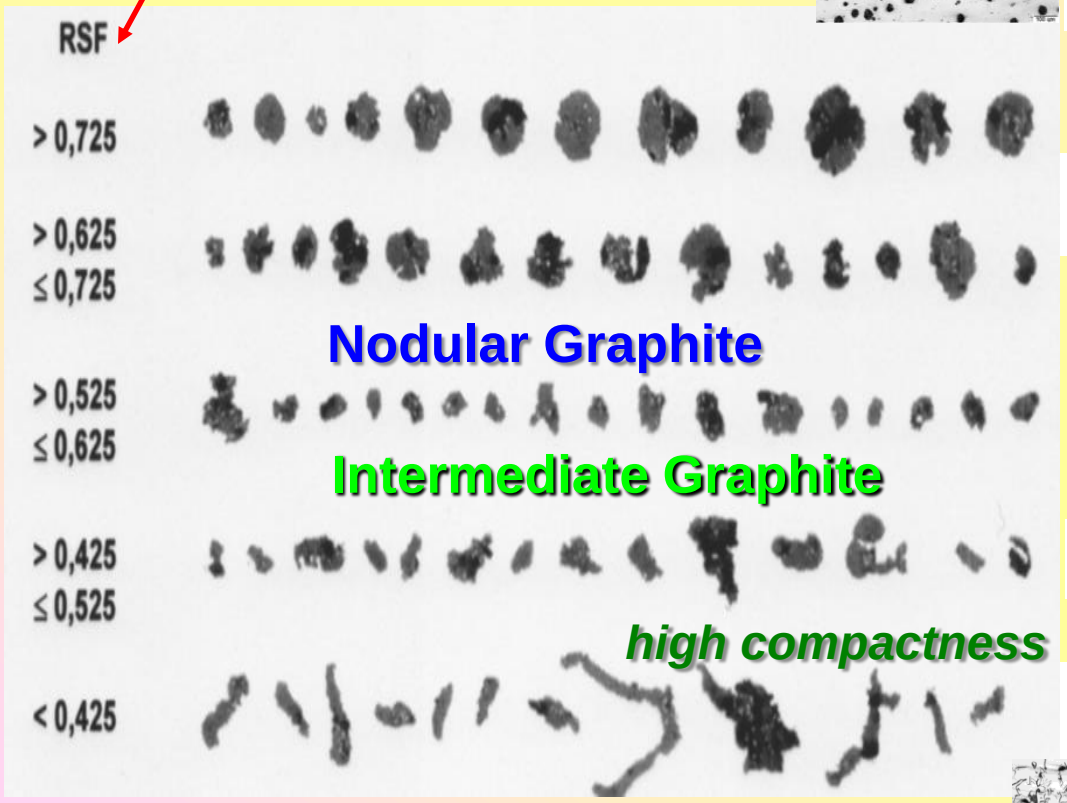

L

M

P

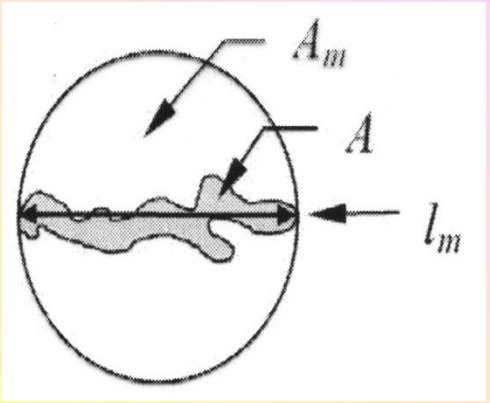

$$Roundness = \frac{A}{A_m} = \frac{4 \times A}{\pi \times l_m^2}$$

$$Percent\ Nodularity = \frac{\sum A_{nodules} + 0.5 \times \sum A_{intermediates}}{\sum A_{all\ particles}} \times 100$$

[in Compacted Graphite Iron]

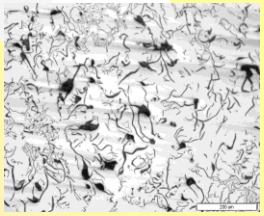

LG

VERMICULAR / COMPACTED GRAPHITE PARTICLES SHAPE FACTORS

[Type I Type II] [Type III Type IV]

NG ← *GRAPHITE COMPACTNESS DEGREE* → **LG**

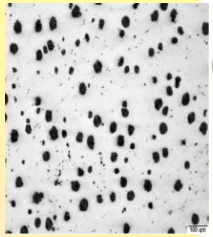

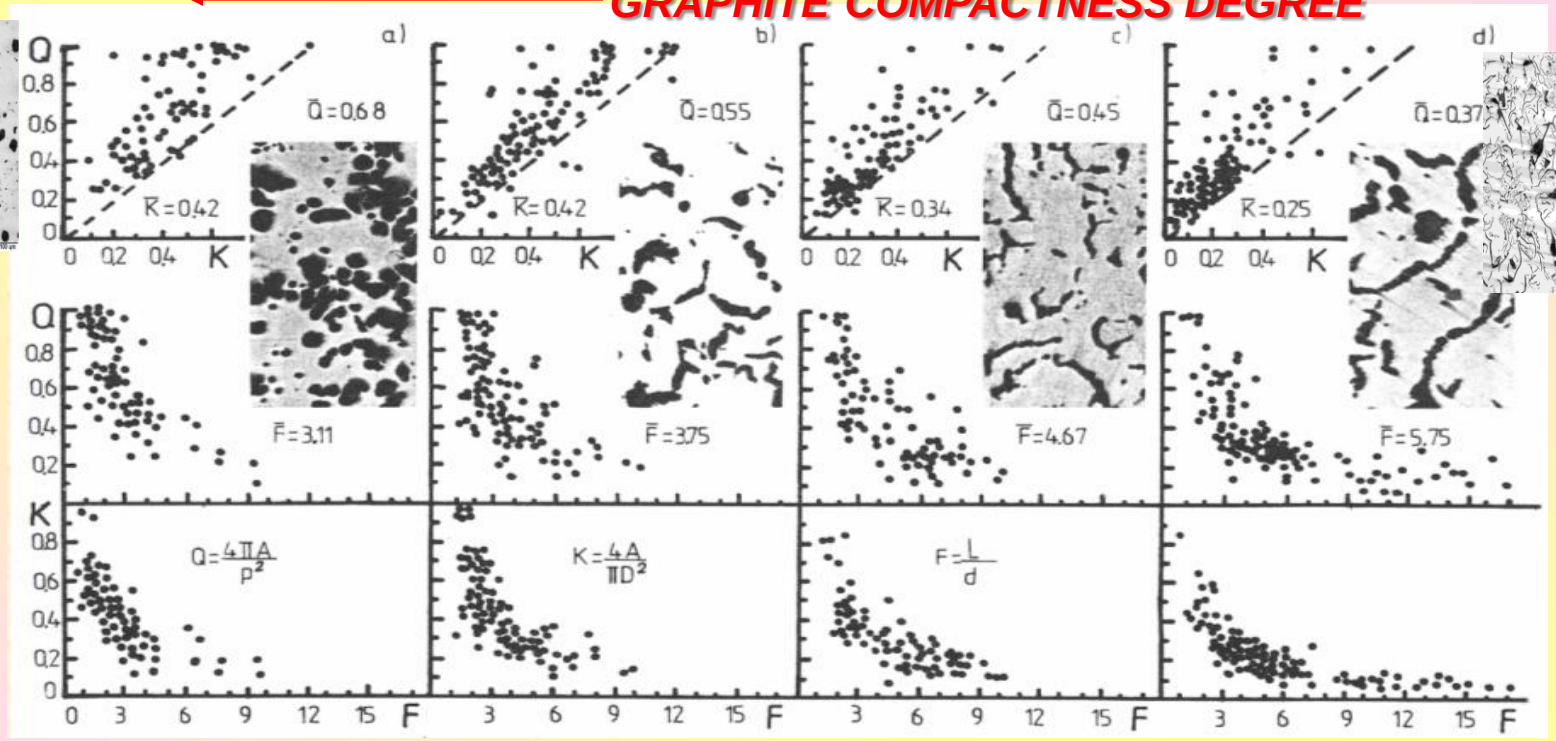

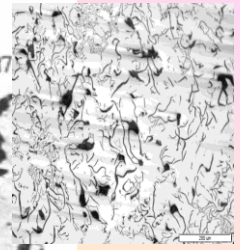

[M. Chisamera, I. Riposan, M. Datcu, M. Liliac, FOCOMP'86, 1986, Krakow, Poland, 269-278 / Progress in Metallography, EUROMET 1995, Germany, 163-166]

EXPECTED APPLICATIONS OF DIFFERENT COMPACTNESS VERMICULAR / COMPACTED GRAPHITE

*** High compactness graphite particles [I + II - Authors]**

M-type; RSF > 0.425 [ISO Standard CGI]

$F = L_G / d_G$ < 6.0, K (RSF) > 0.4

Application: **High mechanical properties necessity,**

- Ferritic or Pearlitic Matrix,

- Rm > 350 MPa, $Rp_{0.2}$ > 250 MPa, A > 3.0%

*** Low compactness graphite particles [III + IV -Authors]**

P-type; RSF < 0.425 [ISO Standard CGI]

$F = L_G / d_G$ > 6.0 (to 10-15), K (RSF) < 0.4

Application: **Thermal Cond.** *or / and* **Vibration Damping Capacity**

Improved Machinability, especially as Pearlitic Matrix

Example: engine block and engine head, heavy cars

☐ EFFECTS OF SULPHUR IN CAST IRONS

***Specific effects:**

- **Grey Iron**
- **Nodular Graphite Iron**
- **Compacted Graphite Iron**

***Inter - relationships between Sulphur and active elements**

I. EFFECTS OF SULPHUR IN HIGH PERFORMANCE GREY CAST IRONS

Graphite nucleation incite by inoculation enhancing in critical solidification conditions:

- **low S, Al, Zr residuals content [<0.03%S, <0.003%Al, <0.0003%Zr]**
- **in high superheated, electric melted base iron [>1500^{0}C / 2732F]**
- **No Rare Earth Elements [REE] contribution**
- **thin wall castings [< 10mm, also < 5mm or < 3mm wall thickness]**

OBJECTIVES: Carbides *and* Undercooled Graphite Avoidance

❑ Solutions for low S, electrically melting grey cast irons, thin wall castings:

*** Resulphurization to 0.05 – 0.10%S [(%Mn) x (%S) = 0.03-0.06]**

- briquetted FeS makes adding controlled amounts of S easy and accurate, especially as proprietary formulas

*** More Potent Inoculant, usually at higher cost**

- Ca,Ba,Al-FeSi [formulated Ca/Ba/Al ratio], Ca,Zr,Al-FeSi, Ca,RE,Al-FeSi…

*** Preconditioning + Conventional Inoculation treatment**

- Al,Zr,Ca-FeSi Preconditioner – action on the first stage in nucleation

*** Inoculation + Inoculant Enhancer treatment**

- **S,O,Al,Ca-FeSi Enhancer** - improves the inoculating ability of current inoculants, lowering consumption up to 50% or more

REMARK: focus on S - addition, in low – S content base iron, before / during inoculation, solo / with active elements

SULPHUR IN BASE IRON - KEY PROBLEM IN GREY IRON

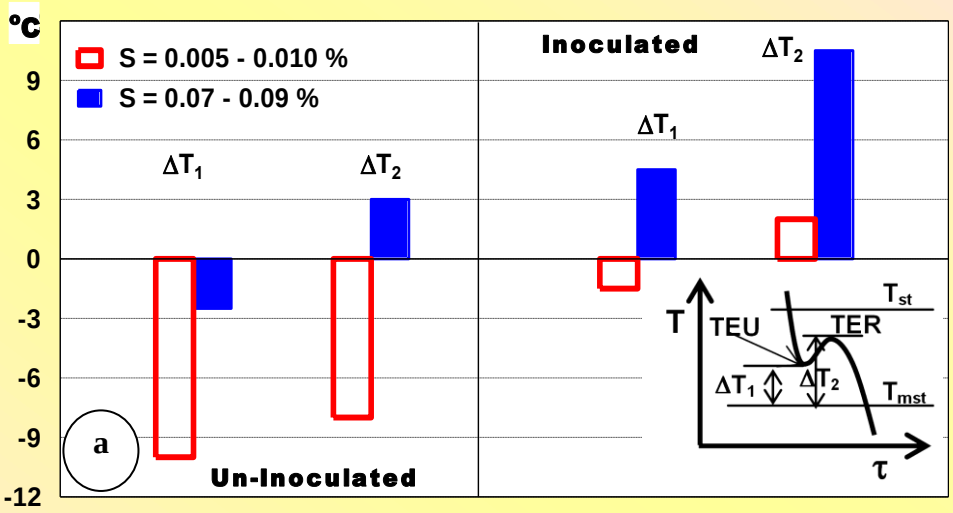

Base Iron:
As-Melted *vs* Resulphurized Irons
(%Mn) x (%S):
0.018 *vs* 0.055

[M.Chisamera, I.Riposan, S.Stan, D.White, G.Grasmo – Asian Foundry Congress, 2008, Japan; Int. J. Cast Met. Res., 2008, 21(1- 4), 39 - 44]

Base Iron:
Ductile Iron *vs* Grey Iron

$\Delta T_1 = TEU\ [TE_{low}] - T_{mst}$

$\Delta T_2 = TER\ [TE_{high}] - T_{mst}$

[M. Chisamera, I. Riposan, S. Stan, T. Skaland. 64th World Foundry Congress, 2000,Paris, France]

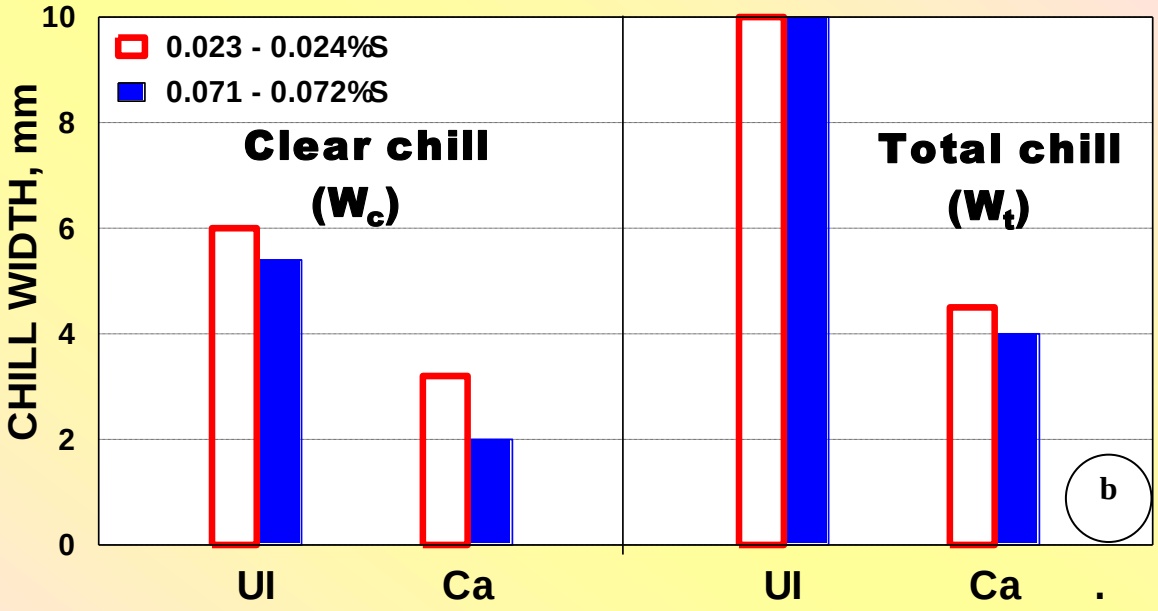

Simultaneous addition of S with potent Oxy - sulphides forming elements [S + Ce] – the beginning

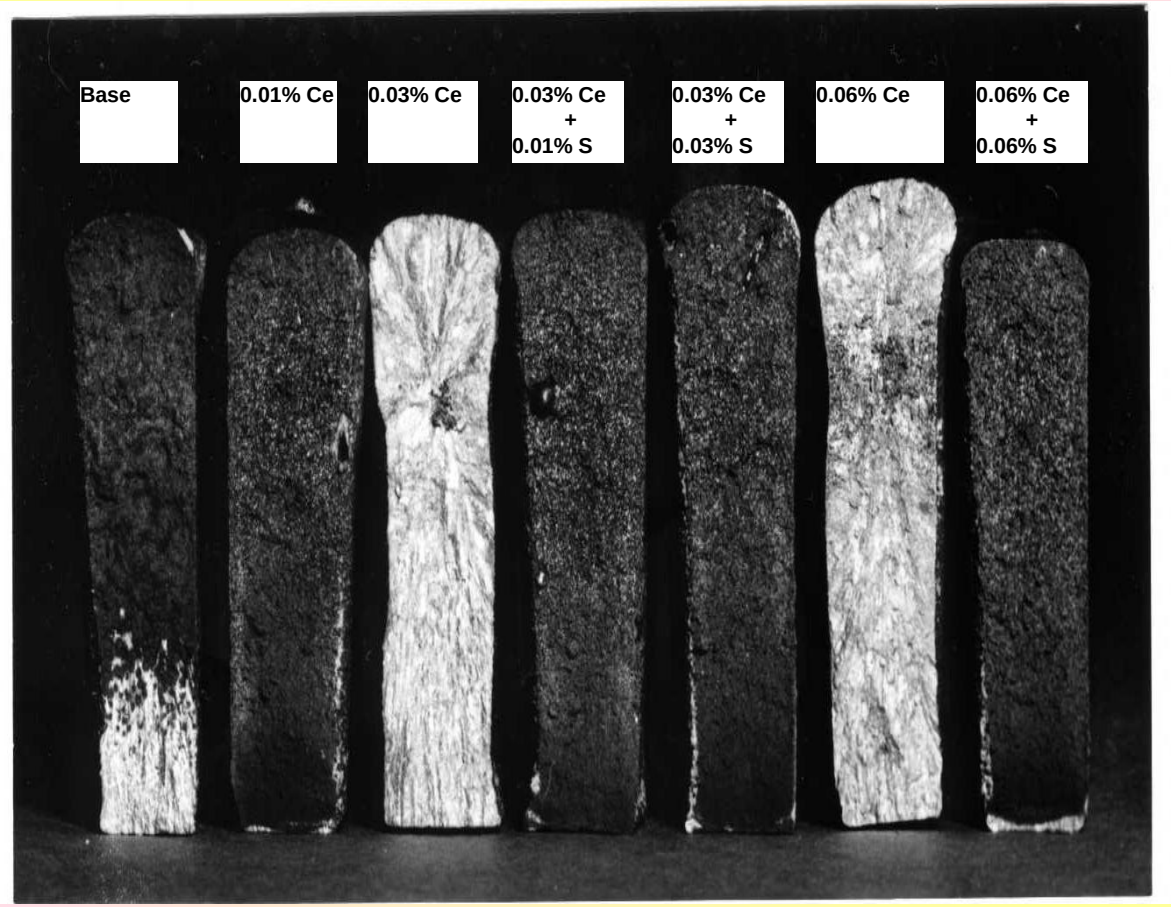

[R.L. Naro and J.F. Wallace: AFS Transactions, 1969, 77, 311; 1970, 78, 229]

Addition of an Inoculant Enhancer to the Conventional Ca-FeSi foundry alloys

- **Grey Cast Iron, Induction Furnace Melting: critical conditions**
  - **CE = 3.7 – 3.9%, 0.035 – 0.045%S, 0.45%Mn, (%Mn) x (%S) = 0.013 – 0.016**
  - **0.0019-0.0024%Al, 0.0005-0.0006%Zr, 0.0045-0.007%N, 0.008-0.0095%Ti**

- **Conventional Ca-FeSi inoculants: Ca-FeSi, Ca,Ba-FeSi, Ca,RE-FeSi**
  - similar **Si** (72.6-73.8wt.%), **Ca (0.87-1.02wt.%) and Al (0.77-0.96wt.%)**
  - 1.68wt.%**Ba** *or* 1.86wt.**%TRE** (Total Rare Earth)
  - **0.077 – 0.085wt**.% inoculant consumption, In-mold inoculation

- **Inoculant Enhancer [En]: S,O,Al,Ca - FeSi [RES-IEP alloy]**
  - (wt.%): 12.24Si, 5.24Ca, 17.48Al, 21.17S, 7.49O, bal Fe
  - separate addition to the conventional inoculants in the reaction chamber,
  - **0.045wt.%** [0.033wt.% Inoc. + 0.012wt.% Enhancer] In-mold inoculation

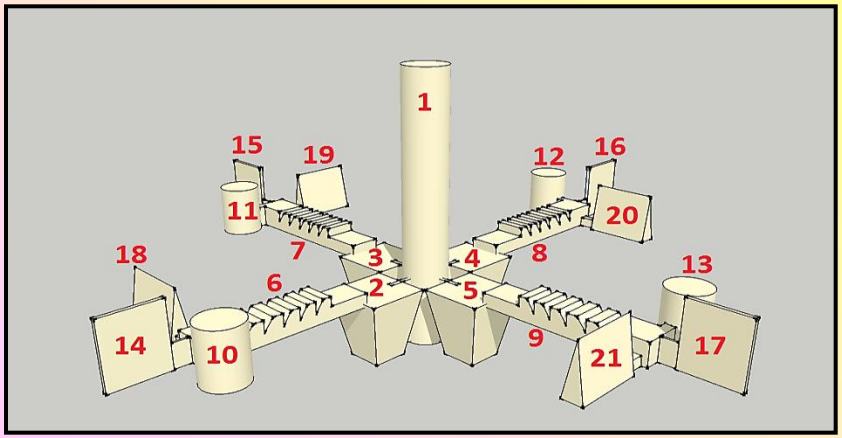

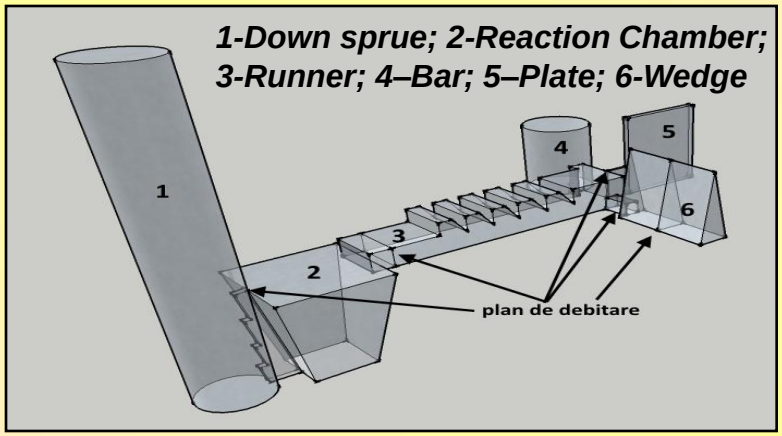

A New Proposed Method to Measure Inoculation Effectiveness

ISF – Inoculation Specific Factor [X]

ISF = |Inoculation Effect| / |Inoculant Consumption|

ISF = ΔX / [% Inoculant] = | $X_{[I]}$ – $X_{[UI]}$ | / [% Inoculant]

$X_{[UI]}$ is the un-inoculated iron *and* $X_{[I]}$ of the nominal inoculated iron considered characteristic.

ΔX, improvement by inoculation, divided by the actual inoculant consumption, which led to that beneficial effect = ISF

X: - thermal analysis parameters: TAL, TEU [TE_{low}], TER [TE_{high}], TES, ΔTr [R, TER-TEU], ΔTm [Tst-TEU], ΔT_1 [TEU-Tmst], ΔT_3 [TES-Tmst]…

- structure characteristics: % carbides, % undercooled graphite, nodule count, eutectic cells count……

- mechanical properties: tensile strength, elongation, hardness…

ISF – Inoculation Specific Factor [%K]

ISF = ΔK / [% Inoculant] = [$\%K_{[UI]}$ – $\%K_{[I]}$] / [wt.% Inoculant]

$K_{[UI]}$ - carbides of Un-inoculat. Iron [%]; $K_{[I]}$ – carbides, Inoc. Iron [%]

[En]: S,O,Al,Ca-FeSi [RES-IEP alloy]; W_3 – ASTM A367 wedge test]

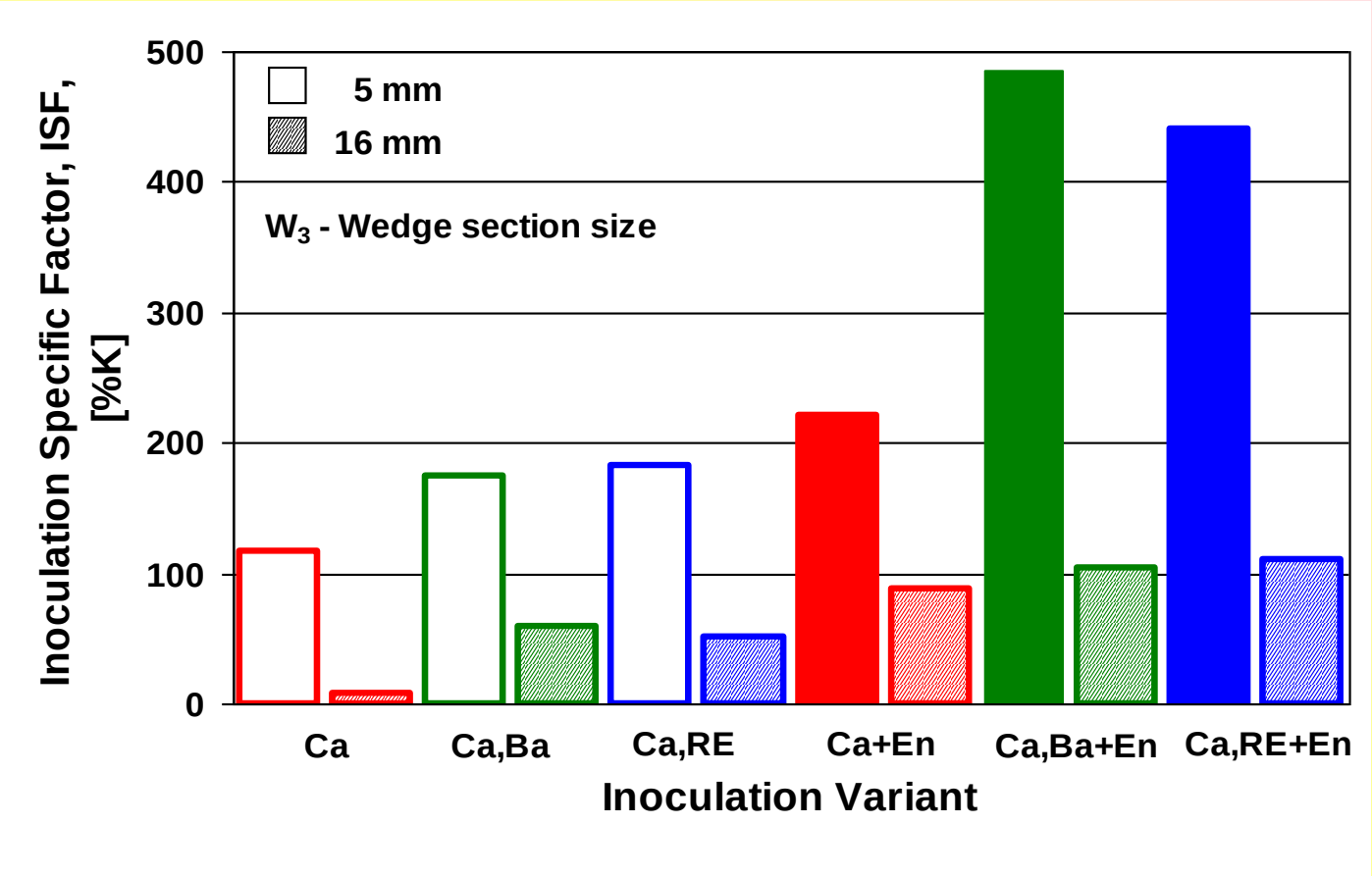

II. DUCTILE CAST IRON–SULPHUR IMPORTANCE

- **Low S Base Iron efficiency**
  - Mg-treatment alloy consumption reduction
  - Limitation of dross defects
  - Process control improving
  - Low Mg-content in treatment alloy [3-6%Mg]
- **Low Mg-residual favorable effects**
  - Low tendency to carbide formation
  - Low eutectic undercooling degree
  - Preservation of graphite nucleants
  - Avoidance of degenerate graphite
  - Low inoculant consumption
- **0.005 – 0.015%S [base iron]**
  - acceptable for most treatment processes
  - tendency to use excessive low sulphur content before nodularization
    - difficult graphite formation, excessive carbides

OBJECTIVES: *low treatment cost, limited / no REE use, carbides avoidance, high nodule count,* **increased inoculation efficiency**

- especially for very low S / high cooling rate

LATE SULPHUR ADDITION EFFICIENCY IN DUCTILE IRON

CHILL TENDENCY

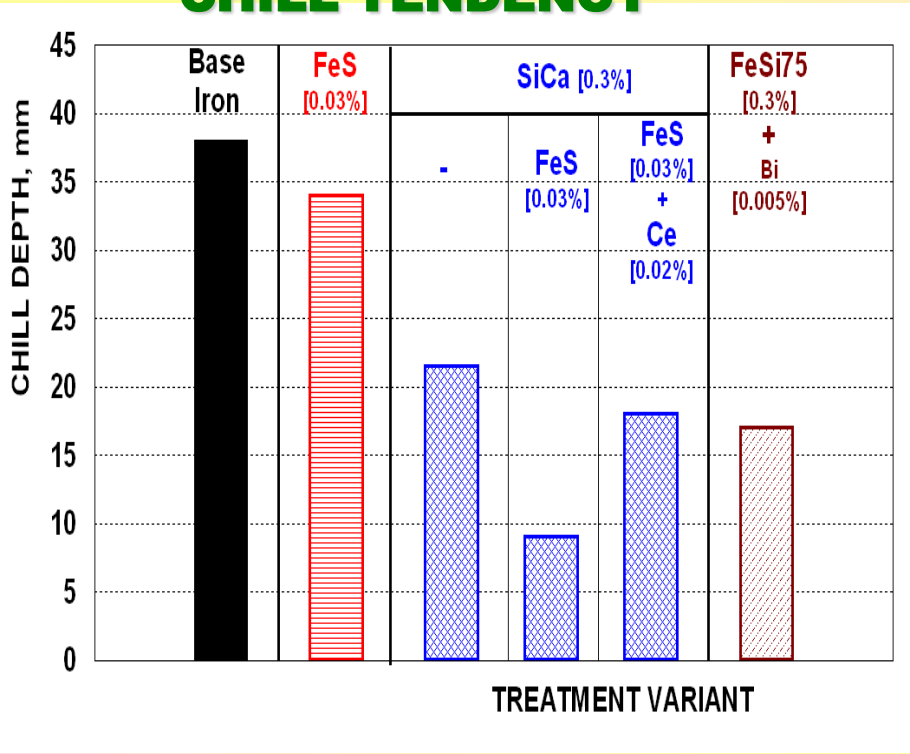

NODULE COUNT

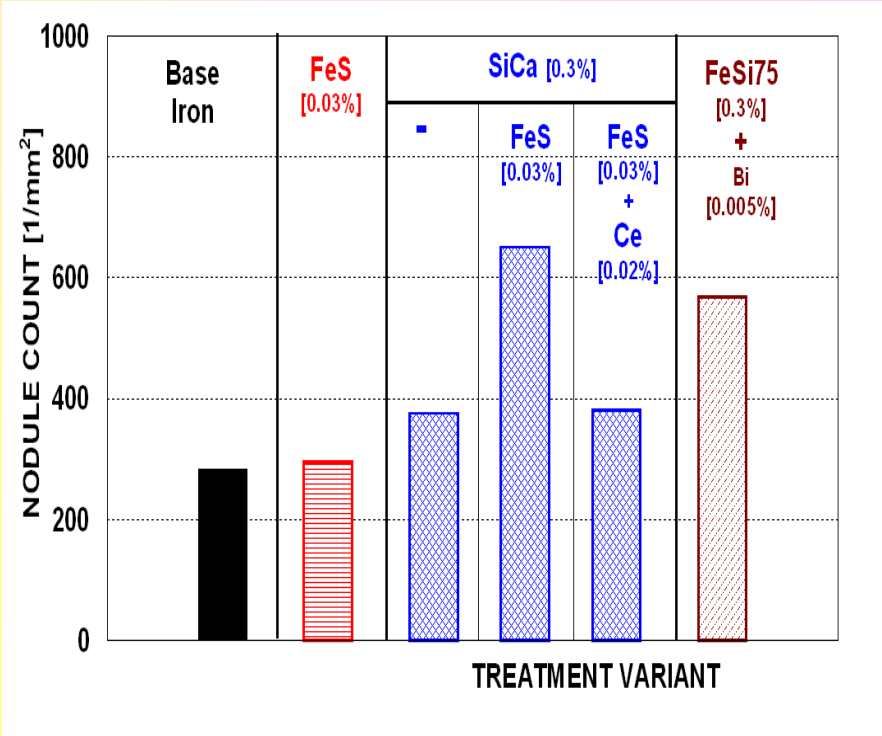

***FeS simple addition: limited benefits**
***SiCa + FeS: the best results [the lowest chill / the highest nodule count]**
***SiCa + FeS better than FeSi75 + Bi**

[M. Chisamera, I. Riposan, M. Liliac-SPCI-5, 1994, Nancy, France / Adv. Mater. Res., 4-5, 1997, 293-300; 7th Int. Ferroalloy Congress, 1995, Trondheim, Norway, 1, 320-324; AFS Trans., 1996, 104, 581-588]

DI - INOCULATION ENHANCING: S,O,Al,Mg–CaSi Enhancer [En]

[W_3 Wedge ASTM A367, In Mould Inoculation]

CARBIDES AMOUNT [3mm section size]

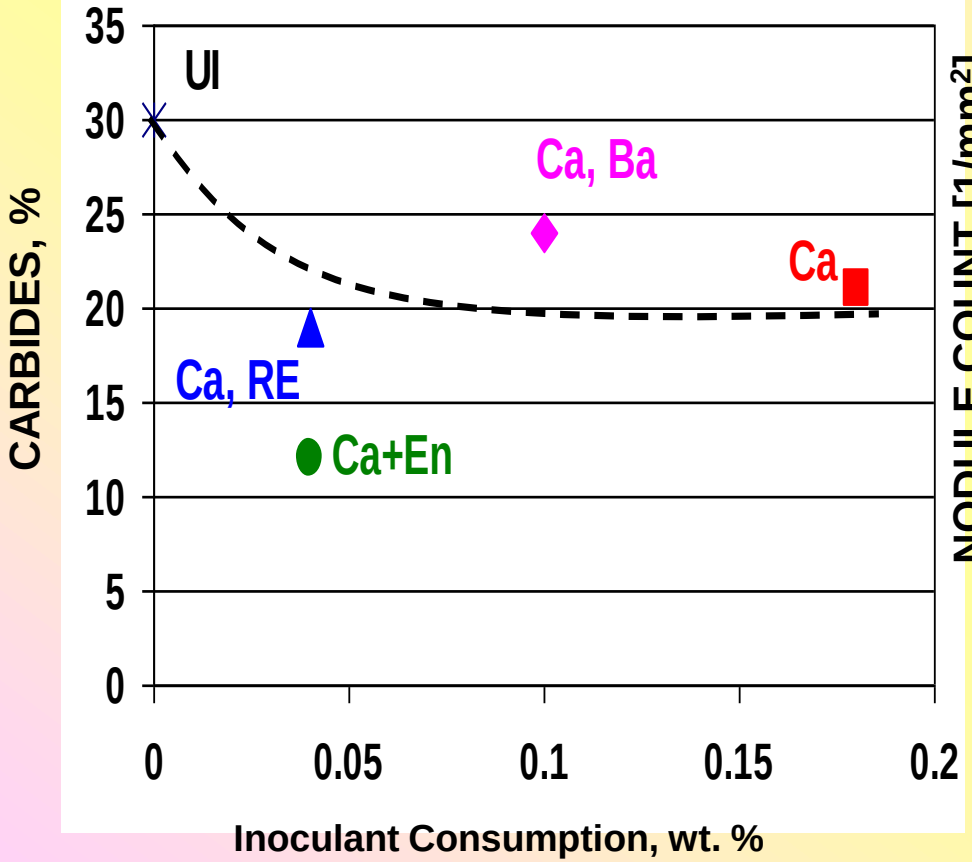

NODULE COUNT [5mm section size]

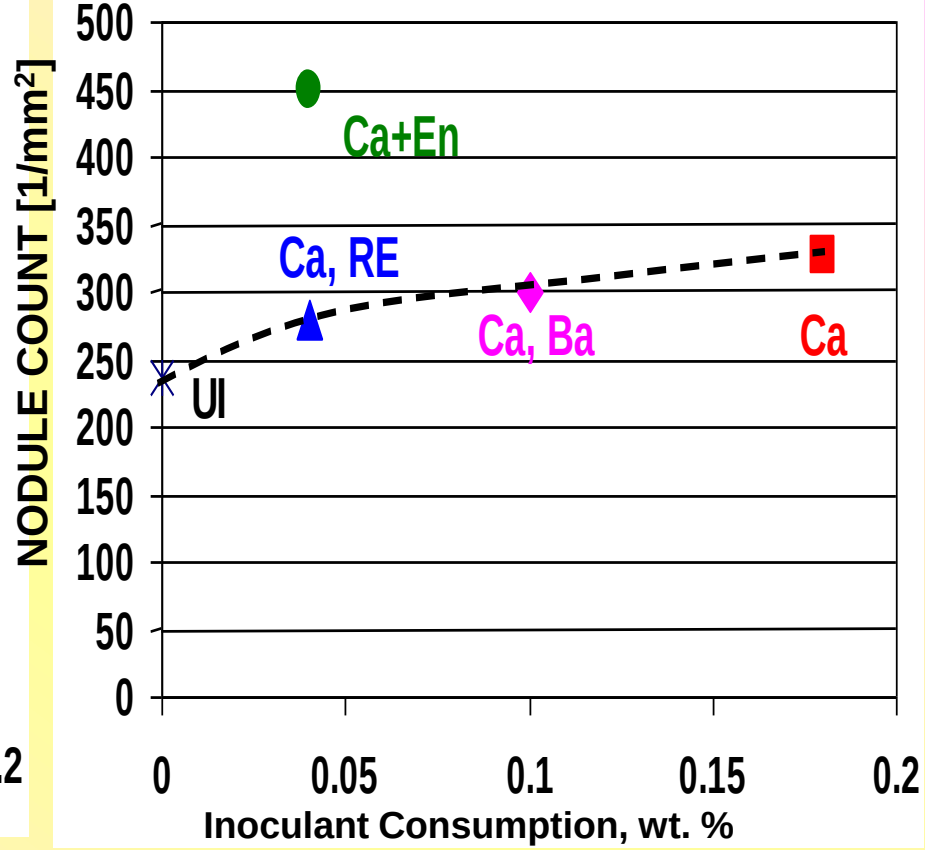

DI - INOCULATION ENHANCING: S,O,Al,Mg–CaSi Enhancer [En]

[W_3 Wedge ASTM A367, In Mould Inoculation]

ISF, [%K] [3mm section size]

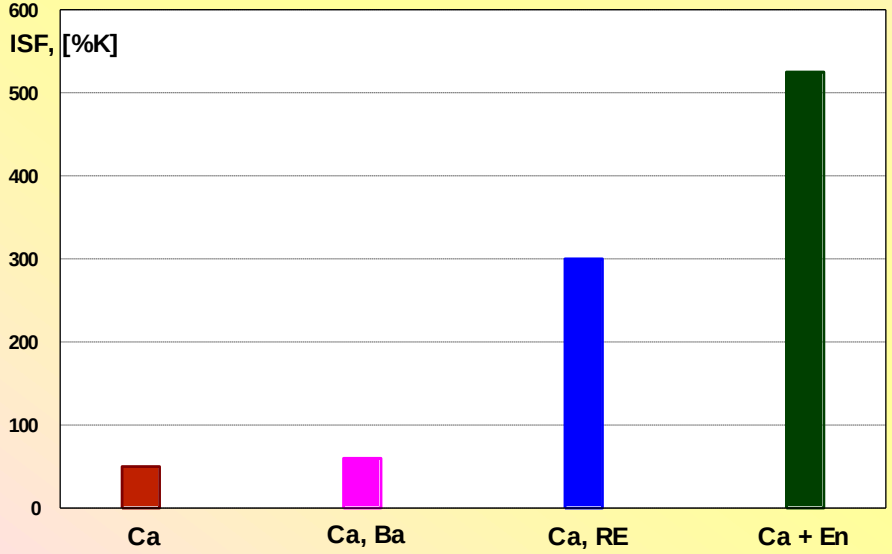

ISF = ΔK / [% Inoculant] =
[$\%K_{[UI]}$ – $\%K_{[I]}$] / [wt.% Inoculant]

ISF = ΔNC / [% Inoculant] =
[$NC_{[I]}$ – $NC_{[UI]}$] / [wt.% Inoculant]

ISF [Nodule Count, NC] [5mm sect. size]

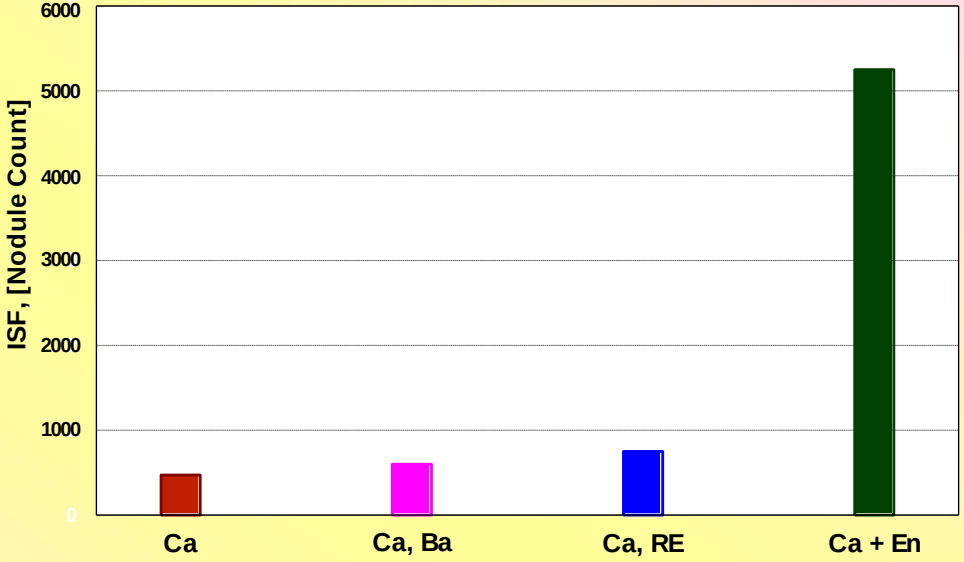

III. CONVENTIONAL WAYS TO PRODUCE CG IRON

- ✓ **The Use of Anti-Spheroidizing Elements (Ti, Al...)**
- ✓ **Higher level Rare Earth (RE) in FeSiMg Alloys**
  - ***Typical Ratio: 3 – 6 %Mg / 5 – 7 %RE**
- ✓ **Process Variation Avoid - High Volume Production**
  - ***The qualification of molten base iron by thermal analysis**
  - ***Corrective addition of Mg *and* Inoculant, prior to casting**

NON - CONVENTIONAL WAY TO PRODUCE CGI

- S - addition after Mg - treatment,

- to convert nodular graphite to compacted graphite

S - ADDITION AFTER Mg - TREATMENT

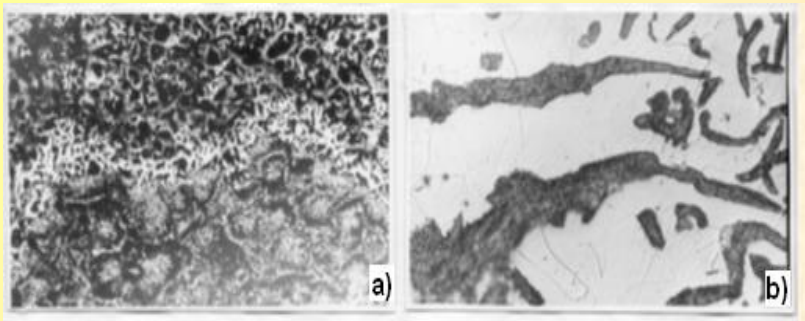

'Hybrid' Graphite:
S - addition
in Mg - treated Iron

Mg – treated Irons

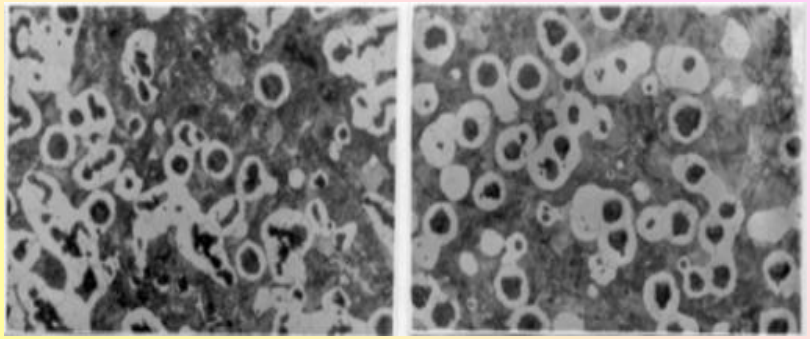

Mg_r = 0.030% Mg_r = 0.045%

+ 0.004%S + 0.012%S

S - addition in Mg – treated Irons

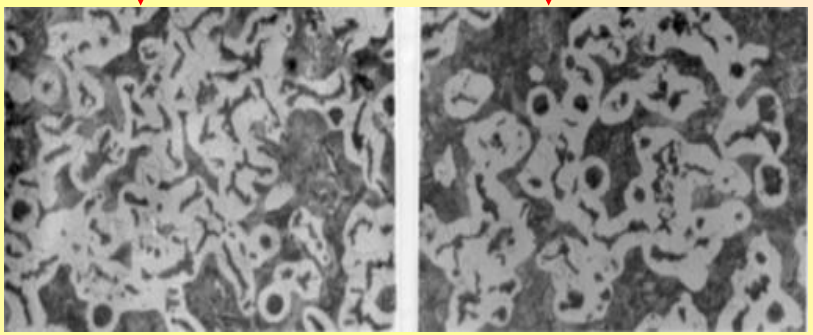

S_{ad} = 0.004% S_{ad} = 0.012%

[M. Chisamera, I. Riposan. SPCI-5, Nancy, France, 1994 / Adv. Mater. Research, 1997, 4-5, 293-300]

US Production Foundry Tests [castings]

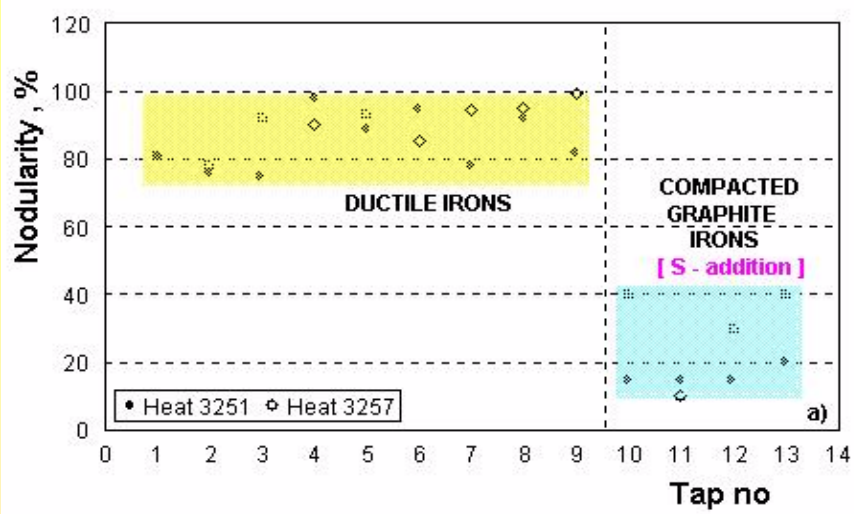

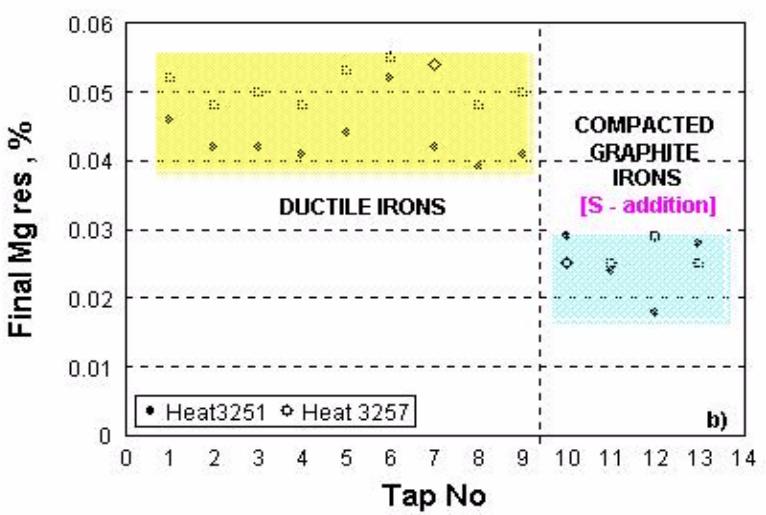

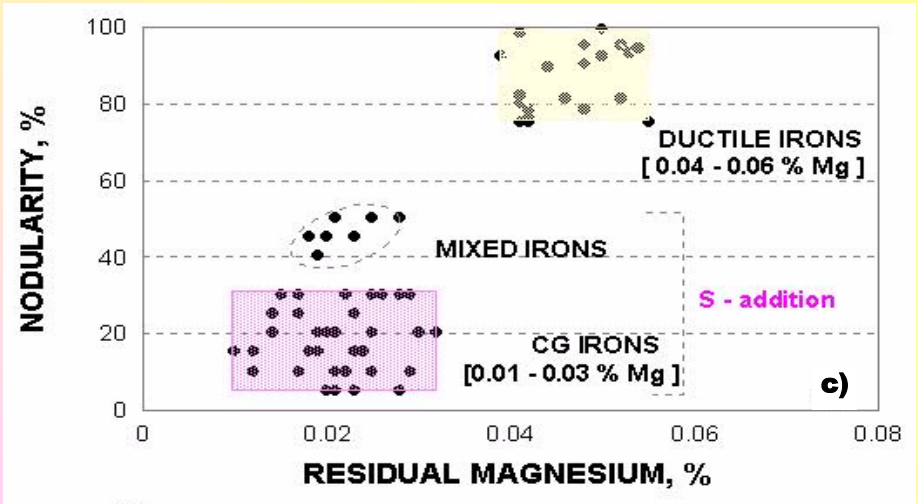

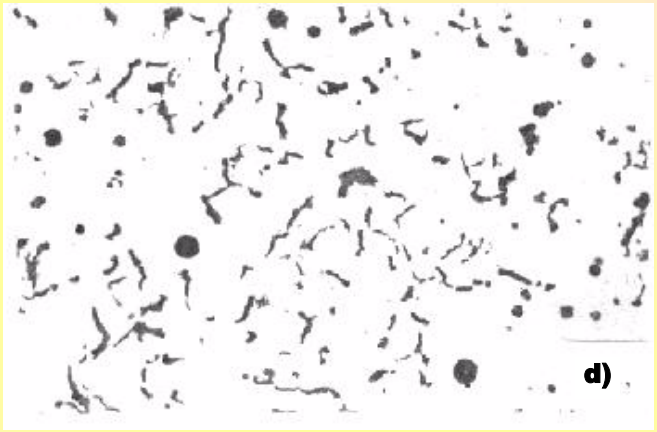

[M. Chisamera, I. Riposan, S. Stan, M. Barstow, D. Kelly, R.Naro, AFS Trans., 2002, 110, 851-860; AFS Trans. 2003, 111, 869-883 [AFS, The BEST OPERATING PAPER AWARD].

Flow chart for DI inoculation improving and CGI production by late S - addition, after Mg - treatment

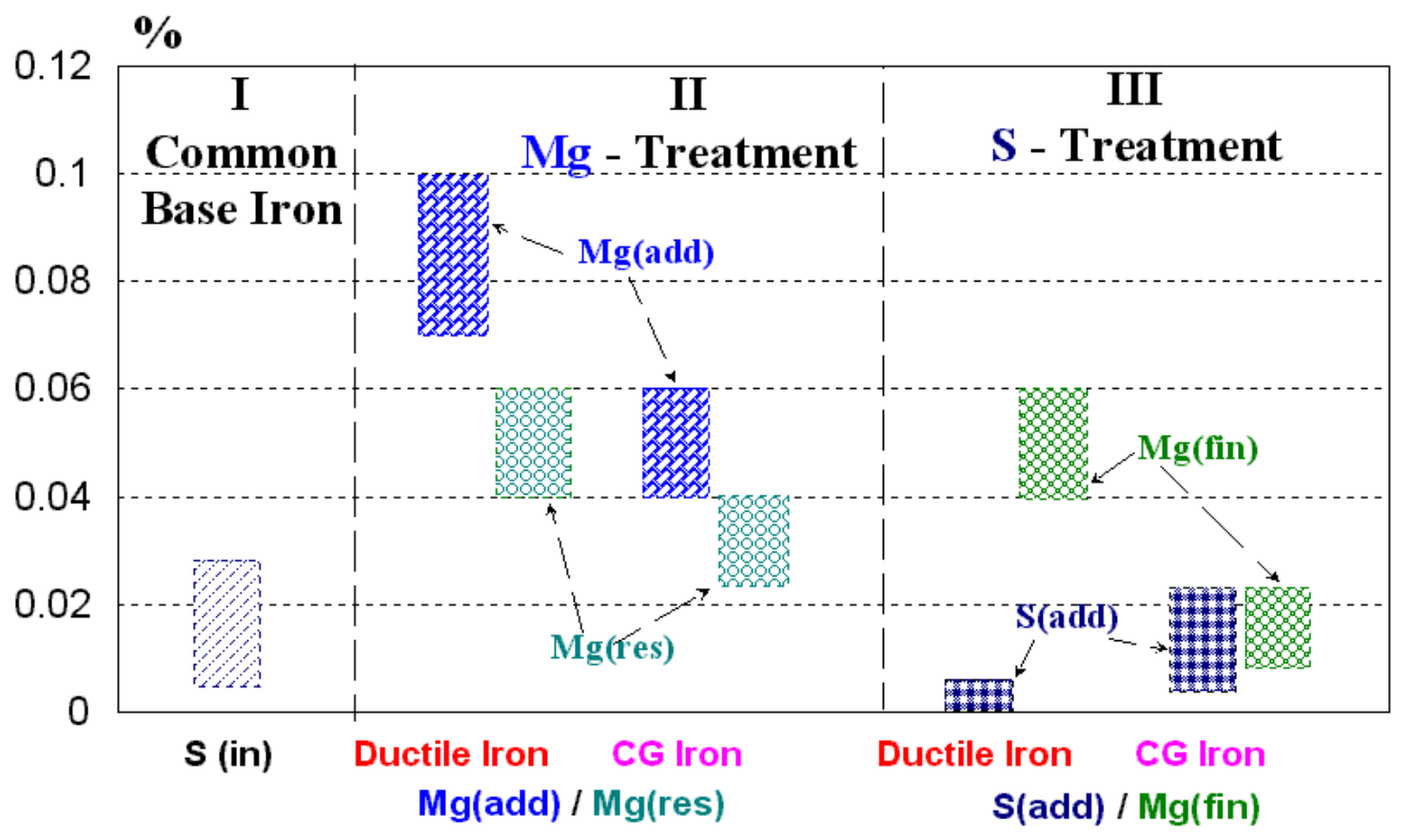

COMPACTED GRAPHITE CAST IRON [CGI] – In – Cup [Mould] Inoculation

INOCULATION ENHANCING: S,O,Al,Mg–CaSi Enhancer

COOLING CURVES ANALYSIS: TE_{low} [TEU]

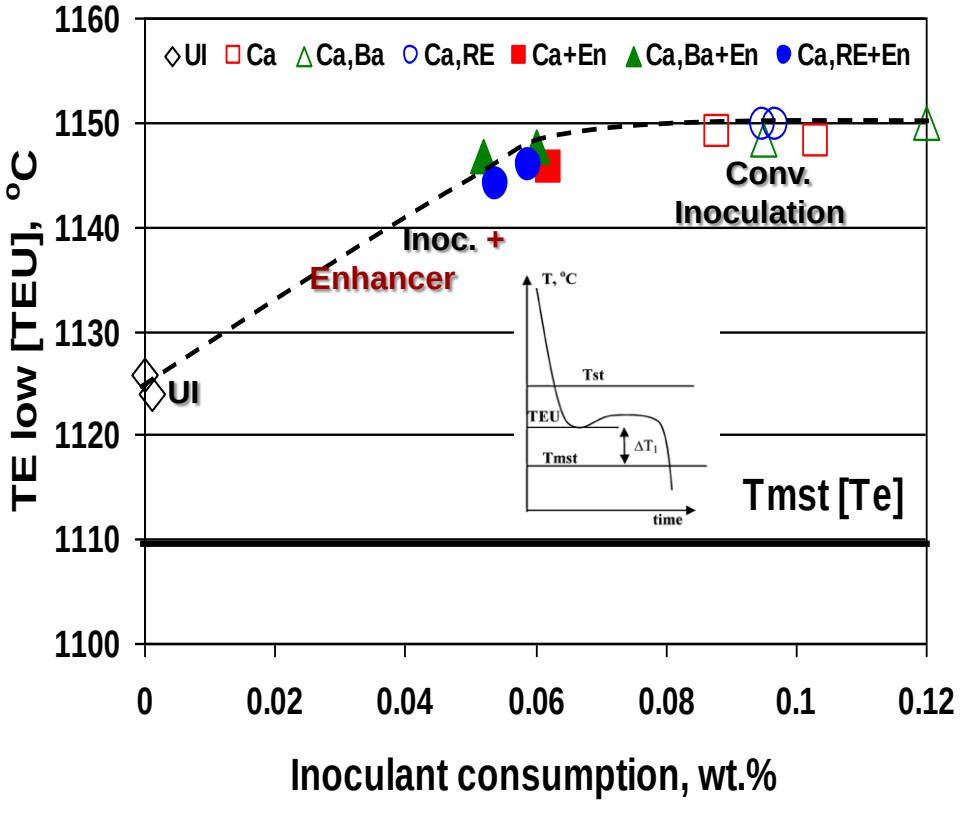

INOCULATION SPECIFIC FACTOR, ISF

ISF = ΔTEU / [wt.% Inoculant] = [$TEU_{[I]}$ – $TEU_{[UI]}$] / [wt.% Inoc.]

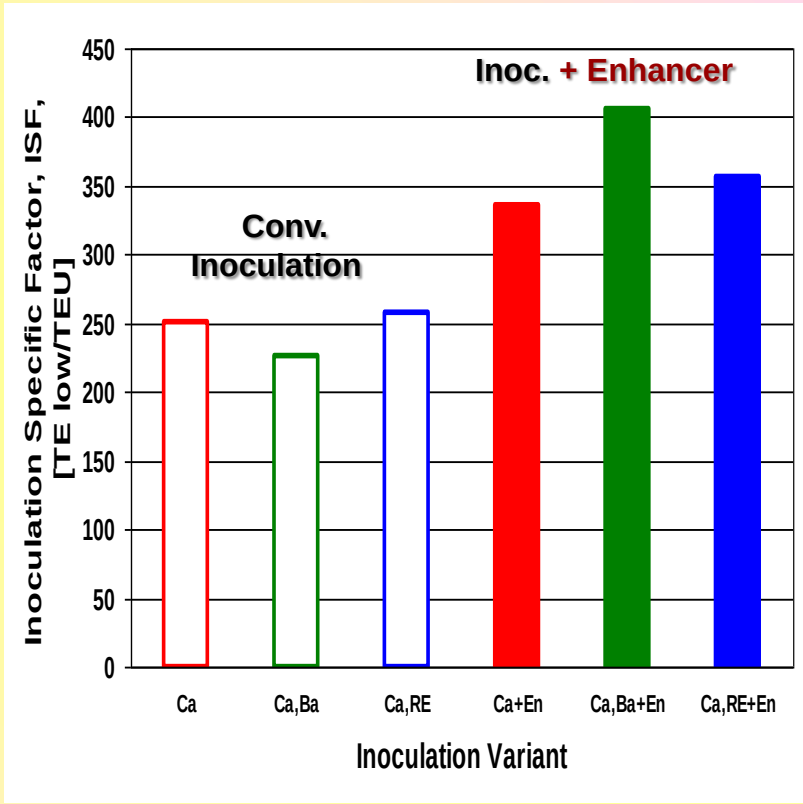

Microstructures of Un-inoculated [UI], Ca – FeSi *and* Ca - FeSi + Enhancer, In-Mould Inoculated CGI

[5mm from the surface, 25mm diameter samples; Nital etched]

[0.019–0.023%Mg_{res}, 4.3– 4.4%CE, 3.5-3.7%C, 2.4-2.5%Si, 0.4-0.5%Mn, 0.010-0.015%Al, 0.009-0.012%Ti, K = 0.50 - 0.65, P_x= 4.0 - 5.0]

UI **0.1wt.% Ca-FeSi** **0.04wt.%Ca-FeSi + 0.015%wt.% [S,O, Al,Mg - CaSi]**

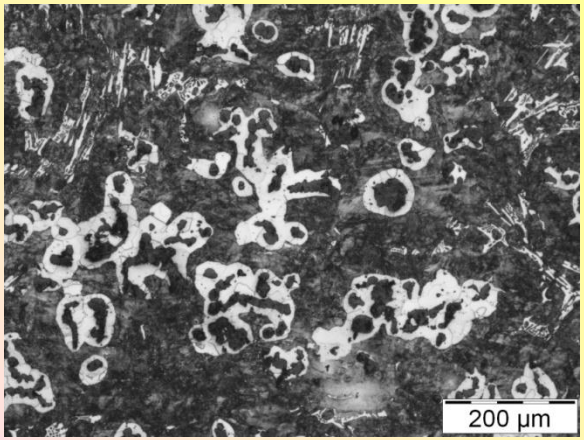

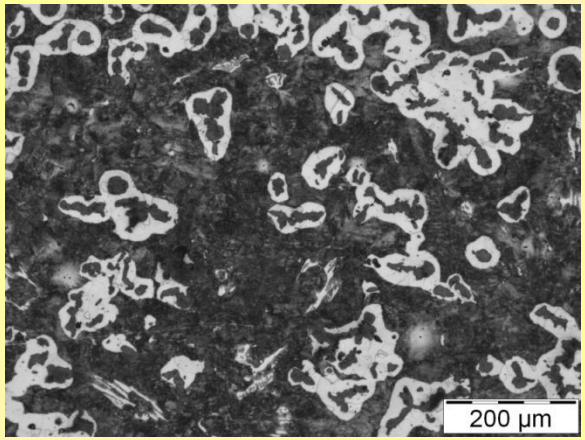

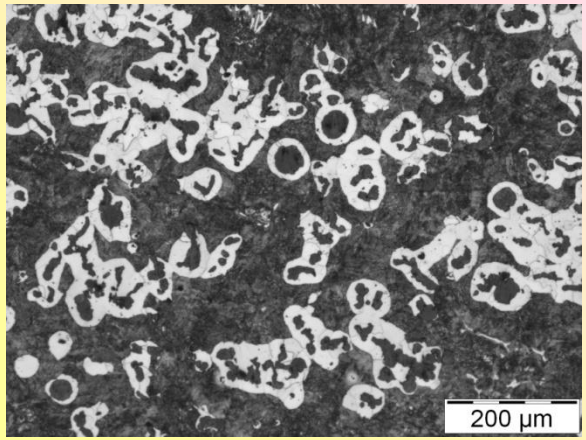

GENERAL CONCLUSIONS

SULPHUR - Friendly element in cast irons

- no excessive High / Low S – content in Base Iron

- **Optimum Sulphur range in the Base Iron:**
  - **0.05 – 0.1wt.% S in Grey Iron**
  - **0.005 – 0.015wt.% S DI / CGI**

- **Key element in graphite nucleation mechanism in Grey *and* Ductile Irons / CGI**
  - Second Step in Grey Iron [oxide/silicates – first one]
  - First Step in Ductile Iron [oxide/silicates–second one]
  - Compacted Graphite Cast Iron [NG to CG transition]

❑ Re - sulphurization before Inoculation

Briquetted FeS: adding controlled amounts of S easy and accurate:

- without the odors normally associated with fine mesh sized iron pyrites
- eliminates the inconsistent recoveries with the use of iron pyrites

*Just one 20g FeS briquette provides approximately 6g of S

- and will increase the S level of 1,000 lbs of molten iron by exactly 0.001%.

*Good results in all of cast irons [Grey / Ductile / Compacted Graphite Irons]

❑ Sulphurization, with O and active elements [Al, Ca, Mg, Ce...] contribution, during Inoculation

➢ **Typical examples:**

Ca,Ce,S,O – FeSi alloy: U.S. Patent 6,102,983

S,O,Al,Ca – FeSi alloy: U.S. Patent 6,866,696B1

S,O,Al (Mg) – CaSi alloy: U.S. Patent 6,293,988B1

Three inoculation variants could be considered, for critical solidification conditions of iron castings

(a) conventional Ca-FeSi inoculant, at a high level of consumption

(b) improved conventional Ca-FeSi alloy, by including active inoculating elements, such as Ba or REE [Ce, La, Y..], for a medium consumption level

(c) association of commercial inoculant, such as Ca-FeSi alloy, with an oxy-sulphide inoculant enhancer alloy [based on a proprietary blend of FeSi or CaSi, Al and oxy-sulphide elements], for the lowest consumption level

❑ Inoculation enhancing by S, O *and* Oxy-sulphides forming elements–bearing alloy addition to Conventional Inoculants

- **Graphite nucleation at lower eutectic undercooling degree**
  - Grey Iron / Ductile Iron / Compacted Graphite Iron
- **A - type graphite in Grey Iron,**
  High Nodule Count / High Compactness degree in Ductile Iron,
  Possible Graphite Nodularity influence in C/V Graphite Iron
- **Low incidence of free carbides**
- **Low inoculant consumption**

Make Good Iron Castings !!!

Inoculation enhancing by S, O *and* oxy – sulphides forming elements

15th INTERNATIONAL FOUNDRYMEN CONFERENCE
INNOVATION – The foundation of competitive casting production
Opatija, May 11th-13th, 2016
http://www.simet.hr/~foundry/

THE INFLUENCE OF CLASSICAL QUENCHING AND TEMPERING AND AUSTEMPERING ON TRIBOLOGICAL PROPERTIES OF DUCTILE IRON

UTJECAJ KLASIČNOG I IZOTERMIČKOG POBOLJŠAVANJA NA TRIBOLOŠKA SVOJSTVA NODULARNOG LIJEVA

I. Kladarić[1], S. Kladarić[2] and A. Milinović[1]

[1]J.J. Strossmayer University of Osijek Mechanical Engineering Faculty, Slavonski Brod, Croatia
[2]College of Slavonski Brod, Slavonski Brod, Croatia

Invited lecture
Preliminary note

Abstract

The paper presents the results of the research on influence of classical quenching and tempering treatment as well as austempering treatment on tribological properties of EN-GJS-400-18 and EN-GJS-600-3 ductile irons. Untreated ductile iron EN-GJS-600-3 has higher abrasive wear resistance when compared to untreated EN GJS 400-18 ductile iron. Results of tribological testing show that quenched and tempered ductile iron has a higher resistance to abrasive wear compared to the untreated ductile iron. After classical quenching and tempering, EN-GJS-400-18 and EN-GJS-600-3 ductile irons have approximately equal resistance to abrasive wear. Based on results of tribological examinations it was determined that the best resistance to abrasive wear is obtained by classical quenching and tempering.

***Keywords**: ductile iron, classical quenching and tempering, austempering, abrasive wear resistance*

*Corresponding author (e-mail address): *ikladar@sfsb.hr*

Sažetak

U radu su prikazani rezultati istraživanja utjecaja klasičnog i izotermičkog poboljšavanja na tribološka svojstva nodularnih ljevova EN-GJS-400-18 i EN-GJS-600-3. Toplinski neobrađeni nodularni lijev EN-GJS-600-3 ima veću otpornost na abrazijsko trošenje od toplinski neobrađenog nodularnog lijeva EN-GJS-400-18. Rezultati triboloških ispitivanja pokazuju da poboljšani nodularni lijev ima veću otpornost na abrazijsko trošenje od toplinski neobrađenog nodularnog lijeva. Nakon klasičnog poboljšavanja nodularni ljevovi EN-GJS-400-18 i EN-GJS-600-3 imaju približno jednaku otpornost na abrazijsko trošenje. Na temelju dobivenih rezultata triboloških ispitivanja utvrđeno je da se najbolja otpornost na abrazijsko trošenje postiže klasičnim poboljšavanjem.

***Ključne riječi:** nodularni lijev, klasično poboljšavanje, izotermičko poboljšavanje, otpornost na abrazijsko trošenje.*

UVOD

Najčešća definicija nodularnog lijeva je:

"*Nodularni lijev je ljevačka pseudo binarna legura željeza i ugljika, koji se pretežnim dijelom izlučio u obliku kuglastog grafita*" [1].

Kuglasti grafit se postiže legiranjem, odnosno cijepljenjem taljevine neposredno prije ulijevanja u kalup, globuratorima magnezijem i cerijem. Podeutektički nodularni lijev dobiva se cijepljenjem s oko 0,5 %Mg, a nadeutektički s oko 0,5 % Ce [1, 2, 3].

Grafit kuglastog oblika, pri konstantnom volumenu, ima najmanju ploštinu. Zbog toga je smanjenje nosivosti presjeka uzrokovano grafitom kod nodularnog lijeva manje nego kod sivog lijeva, a nema ni zareznog djelovanja kao kod listića grafita.

Po mehaničkim svojstvima nodularni lijev nalazi se između sivog i čeličnog lijeva, s tim da se nodularni lijev djelomično može toplo ili hladno oblikovati (valjati, kovati itd.). Nodularni lijev ima veću čvrstoću i žilavost u odnosu na sivi lijev, ali sivi lijev ima bolju sposobnost prigušenja vibracija i bolju obradivost. Nodularni lijev ima bolju obradivost i bolju livljivost u odnosu na čelični lijev, ali čelični lijev ima veću čvrstoću i žilavost [1, 2, 3].

Dobra mehanička svojstva nodularnog lijeva postižu se odgovarajućim kemijskim sastavom, ispravnom provedbom proizvodnog postupka te pravilnim odabirom i provedbom naknadne toplinske obrade.

Posljednjih godina u strojarstvu je prisutan trend razvoja i primjene poboljšanog nodularnog lijeva,naročito za dinamički opterećene dijelove. Ovdje se posebno ističe primjena izotermički poboljšanog nodularnog lijeva ausferitne strukture [4, 5].

Izotermičko poboljšavanje se sastoji od ugrijavanja na temperaturu austenitizacije, držanja pri toj temperaturi, brzog hlađenja do temperature izotermičke transformacije (obično 200 ^{o}C do 500 ^{o}Cu solnoj kupki), držanja pri toj temperaturi dok se potpuno ne završi transformacija u ausferit i ohlađivanja na zraku [4, 5, 6].

Izotermički poboljšani nodularni lijevima dvostruko veću čvrstoću u odnosu na toplinski neobrađeni nodularni lijev, a istovremeno zadržava iste vrijednosti duktilnosti [1, 5]. Na slici 1. prikazana je usporedba mehaničkih svojstava toplinski neobrađenog nodularnog lijeva te klasično i izotermički poboljšanog nodularnog lijeva.

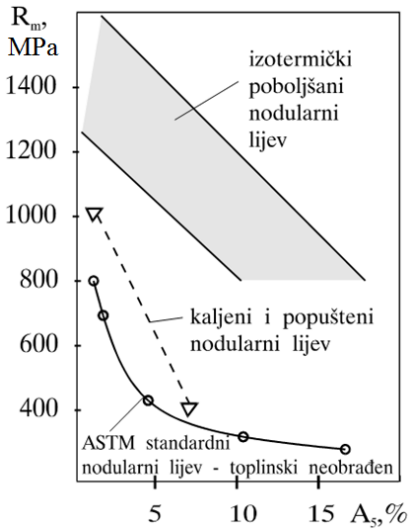

Slika 1. Usporedba mehaničkih svojstava toplinski neobrađenog nodularnog lijeva i poboljšanog (klasično i izotermički) nodularnog lijeva [1]

Utjecaj poboljšavanja na tribološka svojstva nodularnog lijeva nije u potpunosti istražen. U ovom radu prikazani su rezultati istraživanja utjecaja klasičnog i izotermičkog poboljšavanja na tribološka svojstva nodularnih ljevova EN-GJS-400-18 i EN-GJS-600-3.

EKSPERIMENTALNI DIO

U eksperimentalnom dijelu rada provedena je toplinska obrada klasičnog i izotermičkog poboljšavanja nodularnih ljevova EN-GJS-400-18 i EN-GJS-600-3. Prije i nakon toplinske obrade izmjerene su površinske tvrdoće Vickersovom metodom HV5 i provedena su tribološka ispitivanja otpornosti na abrazijsko trošenje.

Toplinska obrada, ispitivanja tvrdoće i tribološka ispitivanja provedena su na ispitnim uzorcima promjera 6 mm i duljine 18 mm.

Toplinska obrada nodularnog lijeva

U tablici 1. navedeni su parametri toplinske obrade klasičnog i izotermičkog poboljšavanja nodularnih ljevova EN-GJS-400-18 i EN-GJS-600-3.

Tablica 1. Parametri toplinske obrade

Materijal	Klasično poboljšavanje	Izotermičko poboljšavanje
EN-GJS-400-18	ϑ_a =900°C/t_a=90′ /ulje ϑ_p =520°C/t_p=60′ /zrak	ϑ_a =900°C/t_a=90′ / solna kupka ϑ_i =390°C/t_i=60′ / zrak
EN-GJS-600-3	ϑ_a =900°C/t_a=90′ /ulje ϑ_p =520°C/t_p=60′ /zrak	ϑ_a =900°C/t_a=90′ / solna kupka ϑ_i =390°C/t_i=60′ / zrak

Na slici 2. prikazan je dijagram postupka klasičnog poboljšavanja nodularnih ljevova EN-GJS-400-18 i EN-GJS-600-3.

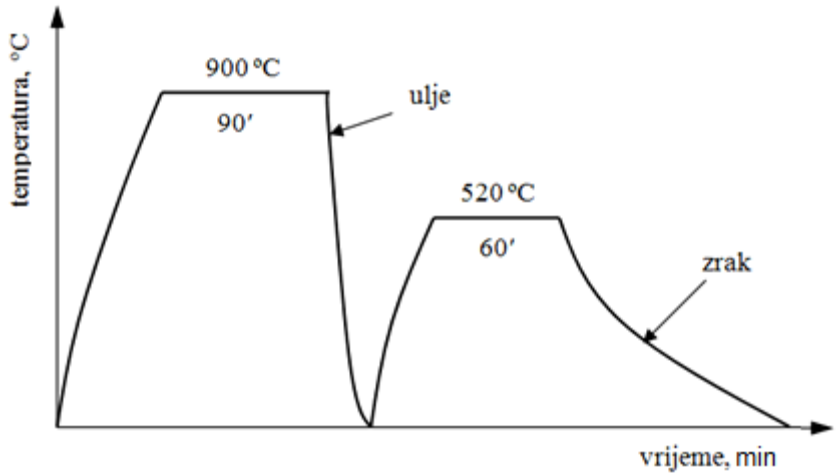

Slika 2. Dijagram postupka klasičnog poboljšavanja nodularnih ljevova EN-GJS-400-18 i EN-GJS-600-3

Pri klasičnom poboljšavanju austenitizacija je izvedena u komornoj peći sa zaštitnom atmosferom metanola (CH_3OH), a gašenje u ulju (Kalenol S22). Popuštanje je izvedeno u komornoj peći.

Na slici 3. prikazan je dijagram postupka izotermičkog poboljšavanja nodularnih ljevova EN-GJS-400-18 i EN-GJS-600-3.

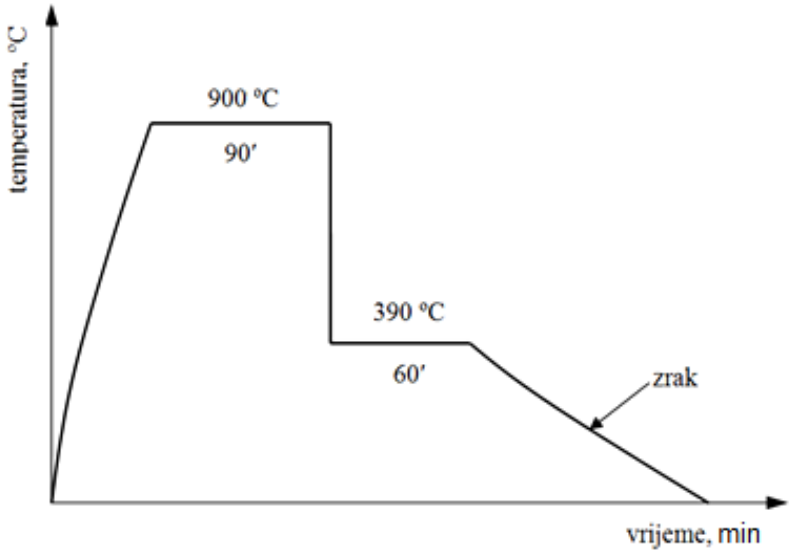

Slika 3. Dijagram postupka izotermičkog poboljšavanja nodularnih ljevova EN-GJS-400-18 i EN-GJS-600-3

Pri izotermičkom poboljšavanju austenitizacija je izvedena u komornoj peći sa zaštitnom atmosferom metanola (CH_3OH), a izotermička transformacija u solnoj kupki (sol AS 140) s maksimalnom brzinom strujanja soli 0,6 m/s.

Ispitivanje tvrdoće

Prije i nakon poboljšavanja nodularnih ljevova EN-GJS-400-18 i EN-GJS-600-3 izmjerena je tvrdoća Vickersovom metodom HV5. Provedena su po tri mjerenja tvrdoće svakog ispitnog uzorka. U tablici 2. navedene su vrijednosti izmjerenih tvrdoća i izračunatih srednjih vrijednosti tvrdoća nodularnih ljevova EN-GJS-400-18 i EN-GJS-600-3.

Tablica 2. Izmjerene tvrdoće, HV5

Redni broj mjerenja	Bez toplinske obrade		Klasično poboljšano		Izotermički poboljšano	
	EN-GJS-400-18	EN-GJS-600-3	EN-GJS-400-18	EN-GJS-600-3	EN-GJS-400-18	EN-GJS-600-3
1.	164	265	332	306	332	306
2.	175	274	336	305	321	299
3.	177	262	313	310	328	313
Srednja vrijednost	172	267	327	307	327	306

Na slici 4. dan je histogramski prikaz srednjih vrijednosti izmjerenih tvrdoća prije i nakon toplinske obrade nodularnih ljevova EN-GJS-400-18 i EN-GJS-600-3.

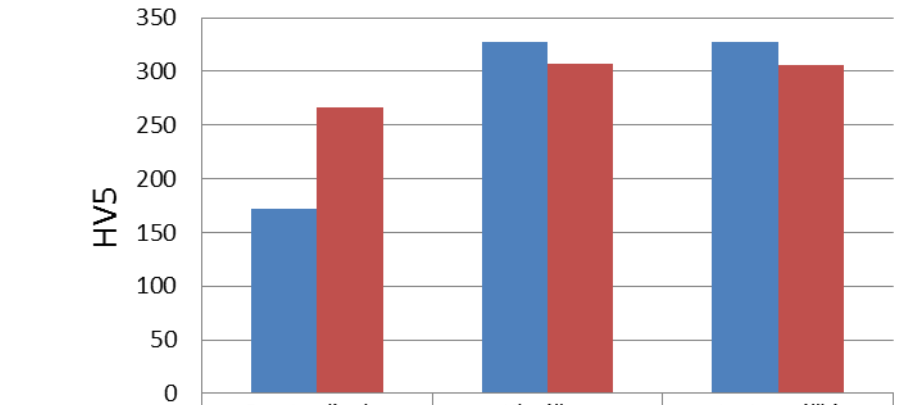

Slika 4. Histogramski prikaz srednjih vrijednosti izmjerenih tvrdoća

Analizom vrijednosti izmjerenih tvrdoća navedenih u tablici 2. i prikazanih na slici 4. utvrđeno je sljedeće:

- Poboljšani nodularni lijev ima veću tvrdoću od toplinski neobrađenog nodularnog lijeva. Kod nodularnog lijeva EN-GJS-400-18 tvrdoća je porasla sa 172 HV5 na 327 HV5, a kod nodularnog lijeva EN-GJS-600-3 tvrdoća je porasla s 267 HV5 na 307 HV5.
- Klasičnim i izotermičkim poboljšavanjem nodularnog lijeva prema parametrima navedenima u tablici 1. postignute su približno jednake vrijednosti tvrdoća; 327 HV5kod nodularnog lijeva EN-GJS-400-18 i 307 HV5kod nodularnog lijeva EN-GJS-600-3.
- Poboljšavani nodularni lijev EN-GJS-400-18 ima više vrijednosti tvrdoće (327 HV5) u odnosu na poboljšani nodularni lijev EN-GJS-600-3 (307 HV5).

Tribološka ispitivanja otpornosti na abrazijsko trošenje

Tribološka ispitivanja otpornosti na abrazijsko trošenje provedena su na ispitnim uzorcima prije i nakon klasičnog i izotermičkog poboljšavanja. Ispitivanje je provedeno na uređaju Taber Abrazer model 503.

Na rotirajuću ploču uređaja postavljena je brusna ploča površinske hrapavosti N6 (R_a=0,8 μm, R_z=3,2 μm, R_{max}=5,12 μm). U držače opterećene silom vrijednosti 10 N postavljeni su ispitni uzorci od nodularnog lijeva EN-GJS-400-18 (lijevo) i EN-GJS-600-3 (desno). Postupak ispitivanja trajao je do 5000 okretaja po ispitnom uzorku. Rezultati ispitivanja izraženi su preko vrijednosti indeksa trošenja prema metodi mjerenja gubitka mase. Niže vrijednosti indeksa trošenja imaju materijali bolje otpornosti na abrazijsko trošenje. Indeks trošenja kod metode mjerenja gubitka mase izračunava se prema izrazu (1).

$$i_t = \frac{\Delta m \cdot 1000}{n} \qquad (1)$$

gdje je: i_t – indeks trošenja; Δm – gubitak mase, mg; n– broj okretaja.

U tablici 3. navedene su vrijednosti izmjerenih gubitaka mase i izračunatih indeksa trošenja ispitnih uzoraka nodularnih ljevova EN-GJS-400-18 i EN-GJS-600-3 prije i nakon toplinske obrade.

Tablica 3. Vrijednosti izmjerenih gubitaka mase i izračunatih indeksa trošenja

Gubitak mase i indeks trošenja	Bez toplinske obrade		Klasično poboljšano		Izotermički poboljšano	
	EN-GJS-400-18	EN-GJS-600-3	EN-GJS-400-18	EN-GJS-600-3	EN-GJS-400-18	EN-GJS-600-3
Δm, mg	20	6,8	4,8	4,7	6,7	5,3
i_t	4	1,36	0,96	0,94	1,34	1,06

Na slici 5. dan je histogramski prikaz indeksa trošenja nodularnih ljevova EN-GJS-400-18 i EN-GJS-600-3 prije i nakon toplinske obrade.

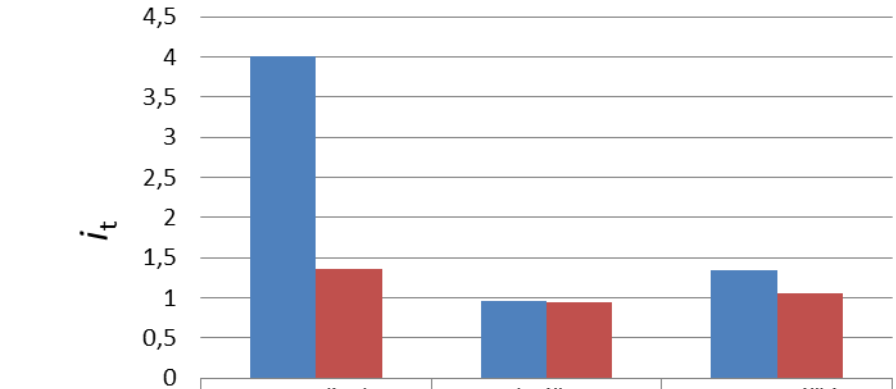

	Bez toplinske obrade	Klasično poboljšano	Izotermički poboljšano
EN-GJS-400-18	4	0,96	1,34
EN-GJS-600-3	1,36	0,94	1,06

Slika 5. Histogramski prikaz indeksa trošenja

Na osnovi rezultata triboloških ispitivanja otpornosti na abrazijsko trošenje nodularnih ljevova EN-GJS-400-18 i EN-GJS-600-3 navedenih u tablici 3.i prikazanih na slici 5.utvrđeno je sljedeće:

- Toplinski neobrađeni nodularni lijev EN-GJS-600-3 ima veću otpornost na abrazijsko trošenje (i_t = 1,36) od toplinski neobrađenog nodularnog lijeva EN-GJS-400-18 (i_t = 4).
- Klasičnim poboljšavanjem nodularnog lijeva EN-GJS-400-18 indeks trošenja smanjen je s i_t = 4 na i_t=0,96, a izotermičkim poboljšavanjem s i_t= 4 na i_t= 1,34.
- Klasičnim poboljšavanjem nodularnog lijeva EN-GJS-600-3 indeks trošenja smanjen je s i_t = 1,36 na i_t = 0,94, a izotermičkim poboljšavanjem s i_t= 1,36 na i_t = 1,06.

ZAKLJUČAK

Na osnovi analize rezultata eksperimentalnog istraživanja utjecaja klasičnog i izotermičkog poboljšavanja na tvrdoću i tribološka svojstva nodularnih ljevova EN-GJS-400-18 i EN-GJS-600-3 može se zaključiti sljedeće:

- Poboljšavanjem nodularnog lijeva postiže se značajno povećanje tvrdoće u odnosu na toplinski neobrađeno stanje.
- Klasičnim i izotermičkim poboljšavanjem povećava se otpornost na abrazijsko trošenje nodularnih ljevova EN-GJS-400-18 i EN-GJS-600-3.

Primarno svojstvo koje utječe na povećanje otpornosti na abrazijsko trošenje je tvrdoća. Klasičnim poboljšavanjem nastaje martenzit, a izotermičkim poboljšavanjem ausferit, što ima za posljedicu povišenje tvrdoće nodularnog lijeva.

- Otpornost na abrazijsko trošenje je bolja nakon klasičnog poboljšavanja u odnosu na izotermičko poboljšavanje, iako su vrijednosti tvrdoća približno istih razina.

Osim tvrdoće kao primarnog svojstva, sekundarni utjecaj na otpornost na abrazijsko trošenje imaju svojstva duktilnosti matrice. Matrice nižih duktilnosti imaju veći otpor abrazijskom

trošenju od matrica viših duktilnosti. Klasično poboljšani nodularni lijev s martenzitnom matricom ima nižu duktilnosti, dok izotermički poboljšani nodularni lijeva s ausferitnom matricom ima višu duktilnost.

LITERATURA

[1] M. Novosel, D. Krumes, Željezni materijali (metalografske osnove i tehnička primjena željeznih ljevova), Strojarski fakultet u Slavonskom Brodu, Slavonski Brod, 1997.
[2] M. Novosel i dr. Inženjerski priručnik 4, Proizvodno strojarstvo, prvi svezak, Materijali, Školska knjiga, Zagreb, 1998.
[3] T. Filetin, F. Kovačiček, J. Indof, Svojstva i primjena materijala, Fakultet strojarstva i brodogradnje, Zagreb, 2002.
[4] M. Pawar, M. Harne, S. Patil, Effect of Microstructure on Wear Behavior of Carbidic Austempered Ductile Iron (CADI), International Journal of Advance Research in Science and Engineering, 4 (2015) 1, pp.266 – 274
[5] ADI Treatments, Accessible on Internet: http://www.aditreatments.com/, 21. 4. 2016.
[6] D. Krumes, Toplinska obradba, Strojarski fakultet u Slavonskom Brodu, Slavonski Brod, 2000.

15th INTERNATIONAL FOUNDRYMEN CONFERENCE
INNOVATION – The foundation of competitive casting production
Opatija, May 11th-13th, 2016
http://www.simet.hr/~foundry/

INFLUENCE OF MODIFICATION OF Al-Mn-BASED ALLOY ON ABILITY TO FORM QUASICRYSTALS

B. Leskovar[1], I. Naglič[1], Z. Samardžija[2] and B. Markoli[1]

[1]University of Ljubljana Faculty of Natural Sciences and Engineering,
Department of Materials and Metallurgy, Ljubljana, Slovenia
[2]Jožef Stefan Institute, Department for Nanostructured Materials, Ljubljana, Slovenia

Invited lecture
Original scientific paper

Abstract

This work deals with the influence of small additions of assorted chemical elements on the formation and morphology of primary metastable quasicrystals. It also investigates the impact of modification of Al-Mn-based alloy by the immersion of stable quasicrystal and crystal phases into the melt. These injected particles should promote the formation of primary metastable quasicrystalline phase. Al-Mn-based alloys were prepared by electric-heated furnace and cast into a copper mold. Castings with 5 mm in diameter were characterized by means of light microscopy, scanning electron microscopy (SEM), energy dispersive x-ray spectroscopy (EDS) and electron backscattered diffraction (EBSD). It was found that the presence of certain chemical elements can ease the formation of dendritic structure of primary metastable quasicrystalline phase. By a method of deep etching the morphology of pentagonal dodecahedron with dendritic branches growing in the direction of the 3-fold symmetry axis, was revealed. Based on EBSD analysis, while introducing stable quasicrystal into Al-Mn-based alloy melt, it was found that the primary metastable quasicrystalline phase, which grew from the surface of stable quasicrystal phase, had the same orientation as the stable quasicrystalline phase. That can lead to the conclusion that the epitaxy between the phases mentioned, does exist. While introducing crystal phases into Al-Mn-based alloy, metastable quasicrystal phase formed around the crystal particles, which led us to the conclusion, that crystal phase served as a substrate for the nucleation of quasicrystalline phase.

Keywords: *Quasicrystals, aluminium alloys, morphology, microstructure*

*Corresponding author (e-mail address): *leskovarblaz@gmail.com*

INTRODUCTION

Long range order with aperiodicity and 5-fold symmetry axes was first revealed by Shechtman in 1984 [1]. Since then, many metastable and stable icosahedral quasicrystalline (iQc) phases were discovered. For metastable quasicrystals it was long considered that they

form only at high cooling rates (10^6 °C/s). Contrary, novel researches show that presence of beryllium and silicon in Al-Mn alloys significantly reduce those high cooling rate, which now value around few 100 °C/s [2-7].

Even small amount of silicon in Al-Mn alloy can significantly change the morphology of primary metastable iQc phase. In such an alloy one can easily obtain dendrite branches with the 5-fold symmetry. When cooling rates are lower than critical, which is the minimum cooling rate needed for the formation of metastable quasicystals, cubic phase α-AlMnSi is formed. This crystalline phase also formed, when samples are annealed at temperatures higher than 500 °C when transformation of metastable quasicrystals occurred [3, 5]. Short after the discovery of quasicrystals the specific orientation relationships between crystalline-quasicrystalline phases were found. Symmetry between specific crystalline-quasicrystalline planes enables transformation and growth of the crystalline or quasicrystalline phases within specific crystallographic directions [8].

Quasicrystals became interesting for researchers mainly because of their unique properties, such as: high absorption of infra-red light, reduced adhesion and friction, heat insulation and as reinforcement component in composites for mechanical devices. To obtain good mechanical properties the homogeneous dispersion of iQc phases with equiaxed shape is preferred. With an increase in the volume fraction of the iQc phase the yield strength of alloy also increased [9-16].

In this paper we report on enhanced growth of the primary iQc phase, while introducing certain amounts of chemical elements. iQc phase is faceted with morphology of pentagonal dodecahedron and its dendritic branches are growing in the direction of the 3-fold symmetry axes. In the case of promoting the formation of primary metastable quasicrystalline phase by immersion of stable quasicrystaline particles the same crystallographic orientation was obtain. These particles or inoculants served as a substrate for the nucleation of quasicrystalline phase, as metastable quasicrystal phase formed around these crystalline particles.

MATERIALS AND METHODS

Alloys were prepared in a chamber furnace using pure aluminum (99.8 mas. %), manganese (99.9 mas. %), zinc (99.99 mas. %), silicon (99.99 mas. %), and master alloys AlSr10 KBM and AlCa6 KBM that are usually made of technical aluminum (99.8 mas. %) and additional elements with purity of 99.9 mas. % or more. Alloys were prepared at temperature 880 °C and cast into a copper mould. Copper mould was made of copper block with dimensions 100x100x120 mm with round casting cavity starting with 15 mm in diameter and further continuing with 5 mm in diameter. Only castings with 5 mm in diameter were analyzed in this work as the cooling rate for this diameter was fixed at approx. 500 °C/s. Castings were then cut, mount and prepared by grinding and final polishing with 3 μm grade diamond paste. Samples for light microscopy were etched by NaOH after polishing, while samples for

electron microscopy and microanalysis were additionally polished with 0.05 μm grade colloidal silica.

Optical microscope Axio Imager A1m from company ZEISS with digital camera AxioCam ICc 3 (3.3 million pixels) and software AxioVision was used to analyze microstructure in bright field.

A field-emission gun scanning electron microscope JEOL JSM-7600F equipped with energy dispersive x-ray spectroscopy (EDS) and electron backscatter diffraction (EBSD) was used for microstructural characterization. The analyses were performed using Oxford Instruments INCA Microanalysis Suite, with X-Max 20 SDD-EDS detector and CHANNEL5 EBSD software with Nordlys detector. Elemental compositions of microscopic iQc phases were measured using optimized low-voltage quantitative EDS approach at a 5 kV SEM accelerating voltage. The crystallinity of the samples was studied by EBSD analysis at a 20 kV voltage.
Quasicrystalline and intermetallic phases were extracted from matrix using etchant (6.9578 g Iodine, 14.0204 g tartaric acid ($C_4H_6O_6$), 100 mL methanol) and ultrasonic vibration for a further morphology observation.

RESULTS AND DISCUSSION

Microstructure of Al-Mn- based alloys

For comparison of primary phase distribution and morphology two alloys with different composition were made. Figure 1 shows microstructures in the central part of castings of Al-Mn-Si alloy (Fig. 1a) and Al-Mn-Si alloy with addition of calcium, strontium and zinc (Fig. 1b).

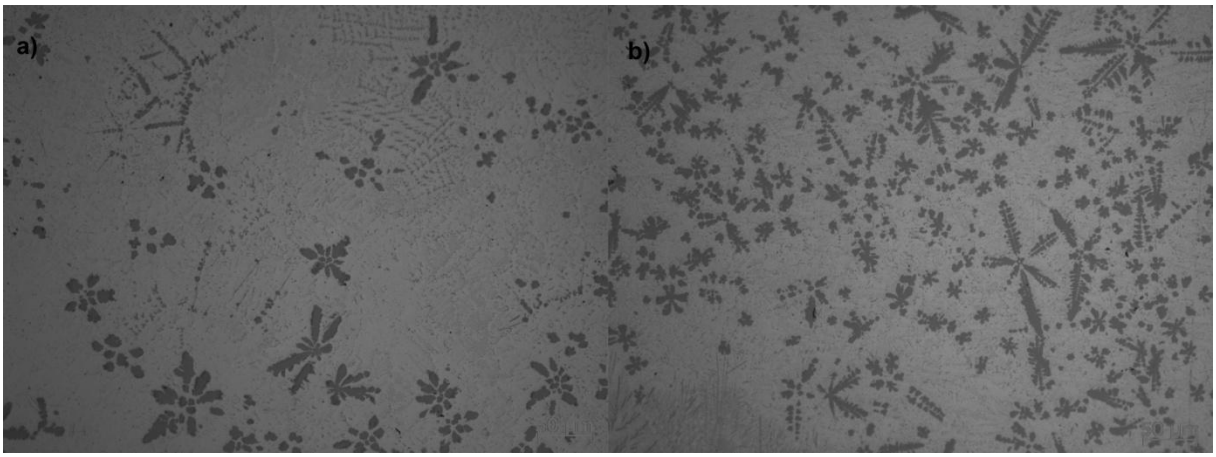

Figure 1. Microstructures of a) Al-Mn-Si and b) Al-Mn-Si-Ca-Sr-Zn alloy

In both alloys morphology of primary dendritic phase indicates that there is a presence of 5-fold symmetry. Many literature sources confirmed that the presence of silicon in Al-Mn alloy facilitates the formation of iQc phase [3, 6, 17-19]. On the other hand, the influence of additional elements to Al-Mn-Si alloy is still not well investigated. Dendritic primary phase in

the central part of the sample Al-Mn-Si-Ca-Sr-Zn alloy (Fig. 1b) has larger and longer dendritic branches. As well, the 5-fold symmetry is obtained easier, because of sharper faceted and dendritic growth. It is clear that additional elements facilitated growth of the primary phase.

Figure 2 represent an electronic image of the microstructure with marked spots of EDS analyses performed to investigate the chemical composition of iQc particles. The intent was to reveal whether the added elements, i.e. calcium, strontium and zinc, get incorporated into the structure of primary iQc particles.

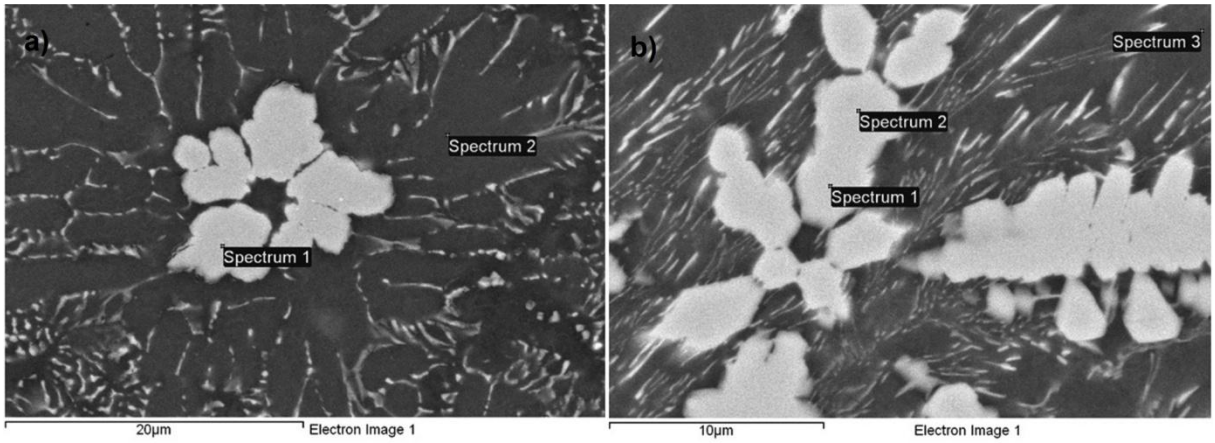

Figure 2. Backscattered electron image of the primary iQc phase in a) Al-Mn-Si and b) Al-Mn-Si-Ca-Sr-Zn alloy with marked spots of EDS analyses

Table 1. Results of EDS measurements in at. %

Location	Al	Mn	Zn	Si
Spectrum 1(Fig. a)	79.2	17.0	0.0	3.8
Spectrum 2(Fig. a)	97.5	2.5	0.0	0.0
Spectrum 1(Fig. b)	80.5	16.7	0.2	2.6
Spectrum 2(Fig. b)	80.8	16.3	0.0	2.9
Spectrum 3(Fig. b)	97.1	2.2	0.7	0.0

The main difference between analyzed primary iQc phases shows that small amount of zinc is present in the iQc phase. Calcium and strontium were not found in the iQc phase of Al-Mn-Si-Ca-Sr-Zn alloy. There is also a little more manganese and silicon in the iQc phase in Al-Mn-Si than in Al-Mn-Si-Ca-Sr-Zn. The reason for the difference could be the presence of zinc in the iQc phase which in turn changes the solubility of other elements during the solidification of the melt.

In order to confirm that primary particles with dendritic morphology do have the structure of the icosahedral quasicrystals EBSD method was used. Electron backscattered diffraction (EBSD) pattern from the iQc phase in the Al-Mn-Si-Ca-Sr-Zn alloy is shown in Figure 3.

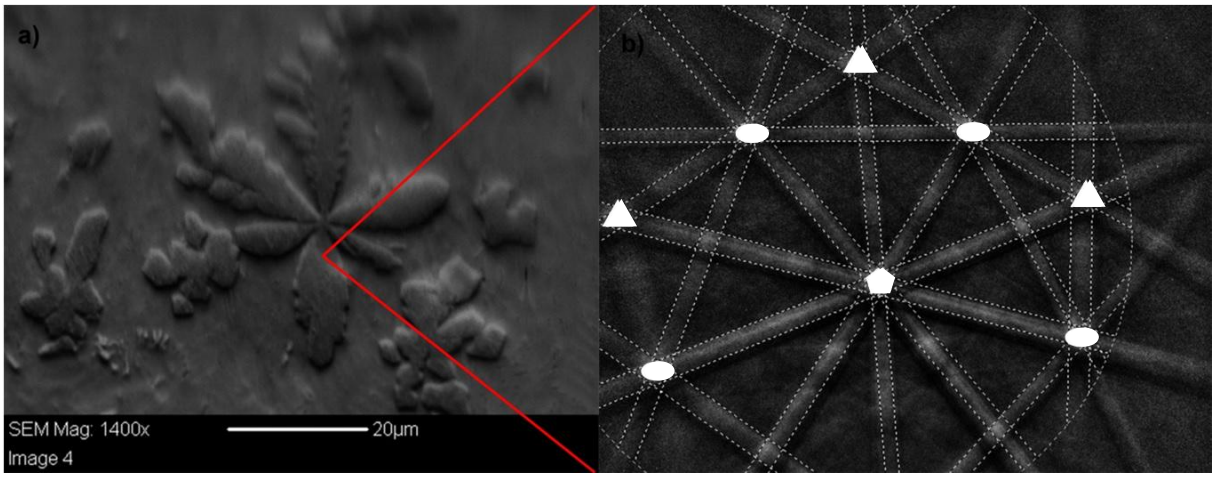

Figure 3. The electronic image of primary dendritic phases (SEI), a), and the corresponding EBSD pattern with marked 5- (white pentagon), 3- (white triangle) and 2-fold (white ellipse) symmetry axes, b)

From the EBSD pattern one can easily recognize the 5-, 3- and 2-fold symmetry axes which are characteristic for the iQc symmetry. Axes are arranged in a way that 5-fold axis is surrounded by five 3-fold axes and five 2-fold axes. It is important to note that the angles between the 5-, 3- and 2-fold axes correspond to those in the reference for the iQc structure. Obtained EBSD pattern from quasicrystalline particle corresponds well to the patterns published in other literature sources and thus confirms the presence of icosahedral symmetry [1, 20].

EBSD analysis confirmed that our particles have the structure related to the icosahedral quasicrystalline phases. Yet, using the deep etching method, by which Al-based matrix had been removed, the 3D structure of iQc particles was revealed. Figure 4 shows the electronic image of morphology of primary iQc phase. The phase was extracted by deep etching process.[21] There is little doubt that the etched particles have the structure of icosahedral quasicrystals as they readily exhibit the morphological features unique to icosahedral quasicrystals.

Primary branches, Fig. 4a and 4b, of iQc dendrites grow in the direction of 3-fold symmetry axis. Figure 4b shows the tip of the primary dendritic branch, featuring the typical 3-fold symmetry as indicated by the red triangle in the Fig. 4b. Secondary dendritic branches in the Fig. 4c and d apparently also grow in the direction of 3-fold symmetry axes as indicated by three pentagons. This is supported by the characteristic shape of pentagonal dodecahedron of primary and secondary branches thus confirming the presence of icosahedral symmetry. Namely, the pentagonal tips of the primary and secondary branches should be at an angle of 41.8° against the 3-fold symmetry axes, which is what we measured in our Fig. 4.

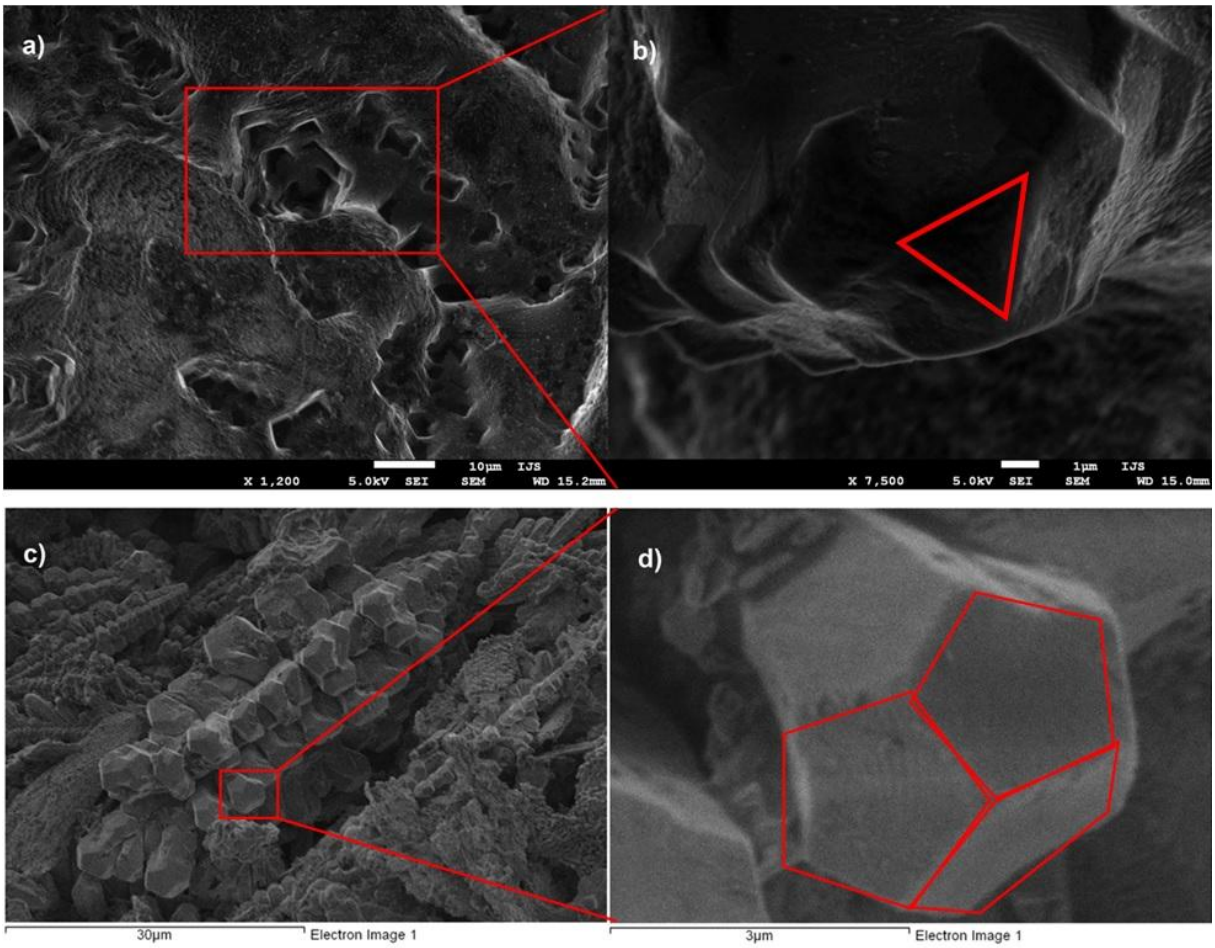

Figure 4. Morphology of extracted icosahedral quasicrystals: a) single primary dendritic branch exhibiting 3-fold symmetry at its tip, b) dendritic branch tip with an triangle denoting the symmetry, c) secondary branches with 3-fold symmetry at an angle of 41,8° and d) secondary branch tip with a pentagons indicating the morphology and symmetry of the tip

Introducing stable quasicrystal into Al-Mn-Si-based alloy

Stable quasicrystal particles were immersed into the Al-Mn-Si alloy in order to minimize interfacial free energy between the stable and metastable quasicrystalline phases. In other words, the stable quasicrystal phase was meant to serve as a substrate for the initial growth of metastable quasicrystalline phase.

While casting the Al-Mn-Si alloy the particles of stable iQc phase from Al-Fe-Cu system were added into the melt flow. The temperature of the melt was around 850 °C. In order to found the particles of stable iQc the solidified sample was cut on more places. Following figure 5 has the electronic image of the microstructure with marked spots of EBSD analysis with their EBSD patterns where can be seen that immersed particle is enveloped with new phases.

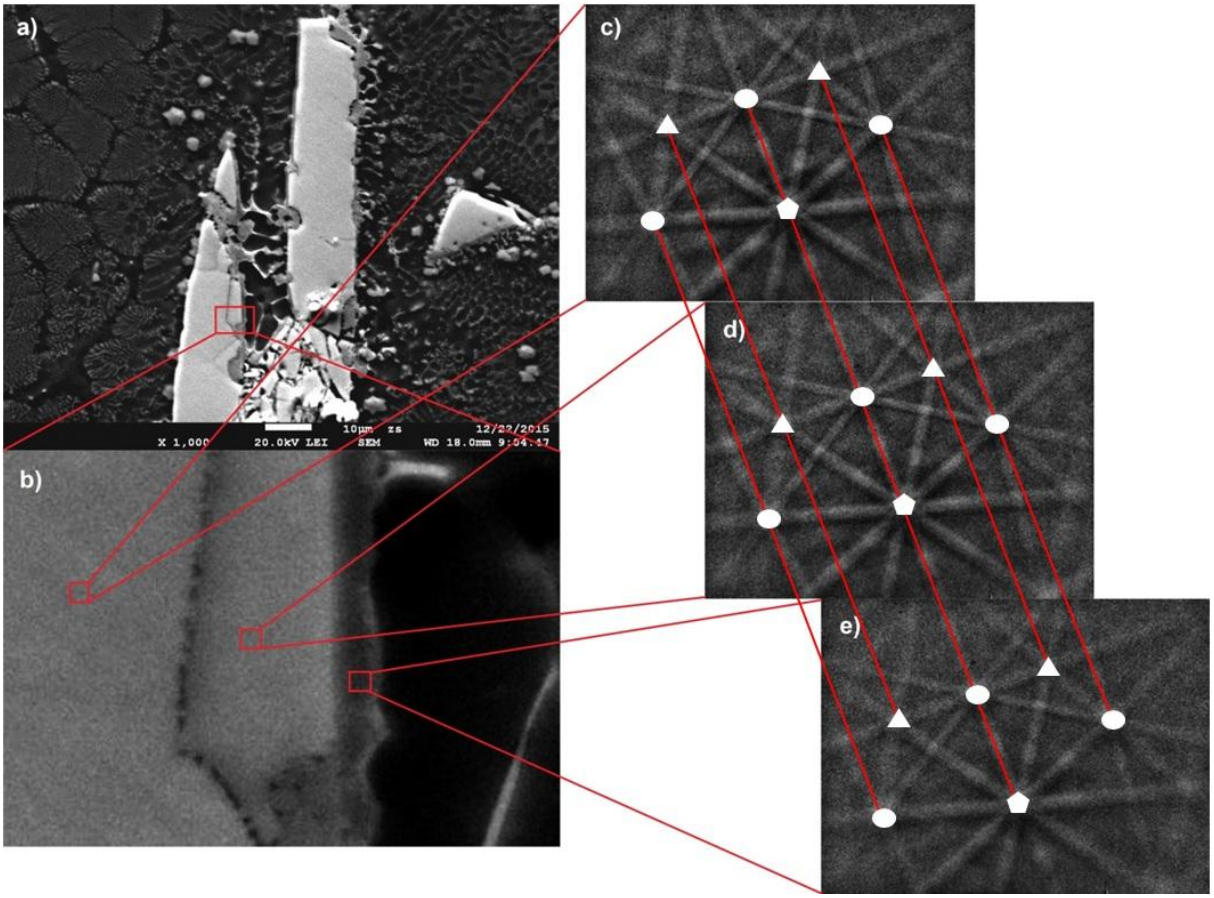

Figure 5. Electronic image of stable iQc phase, a), in microstructure of Al-Mn-Si alloy with marked spots of EBSD analyses, b), with their EBSD patterns from the stable iQc quasicrystal c) and d), and metastable iQc layer, e), with marked 5- (white pentagon), 3- (white triangle) and 2-fold symmetry axes (white ellipse)

LEI image, Fig. 5a, shows particles of stable AlFeCu quasicrystal (the brightest white color) around which the layer has formed, of what is believe to be, a metastable quasicrystal (Fig. 5b). The thickness of layer is around 1 μm. Primary metastable phases have also formed near stable quasicrystal phase. Morphology of primary dendritic phase indicates the presence of 5-fold symmetry. EBSD patterns from stable iQc particle, Fig. 5c and 5d, and metastable iQc layer, Fig. 5e, confirmed the icosahedral symmetry. What's more, the same orientation between these two phases was obtained as the line-up of the Fig. 5c, 5d and 5e clearly indicates. It is obvious that the phase growing on the surface of a stable iQc AlCuFe particle has the exact same orientation proving that immersed particles have served as a substrate for the metastable iQc from the initial Al-Mn-Si melt to grow on them.

Introducing crystal phase into Al-Mn-Si-based alloy

In order to assess the ability to ease the formation of iQc phases the crystalline phases were also immersed into the Al-Mn-Si alloy. Figure 6 shows primary iQc particle in the middle of which plates of crystalline TiB_2 phase can be seen.

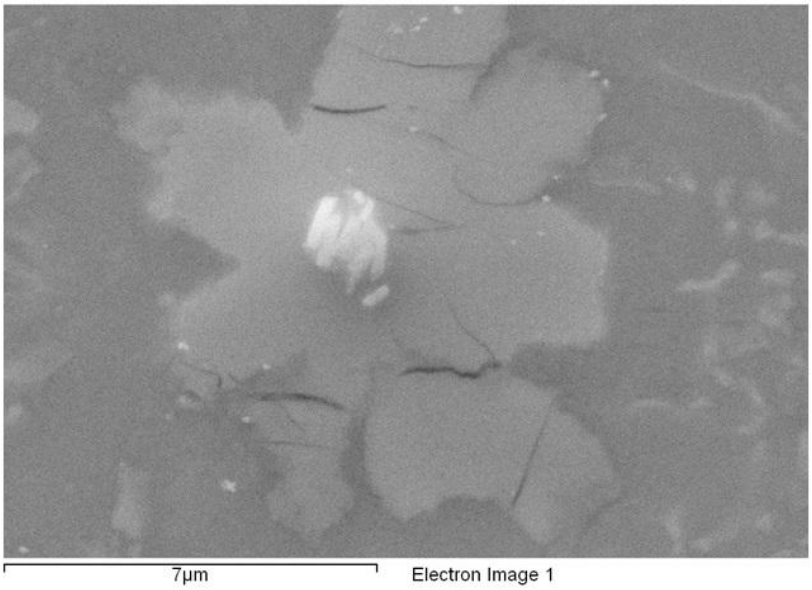

Figure 6. Electronic image of primary particle with the plates of TiB_2

Plates of TiB_2 phase (brighter white color) are located in the middle of primary metastable iQc, what indicates that TiB_2 phase serve as substrate for metastable iQc phase. As metastable iQc phase fully overgrew the TiB_2 particles good wettability between these two phases must have existed. With respect to good wettability and structure similarity in some crystallographic planes that has the lowest interfacial free energy, the growth of metastable iQc with respect to specific crystal-quasicrystal direction must also exist.

CONCLUSIONS

Based on the research results of EDS, EBSD and morphology analysis the following can be concluded:

- Silicon has large positive impact on the formation of iQc phase, but in combination with calcium, strontium and zinc the impact is even higher. Strontium and calcium were not found within the metastable iQc phase. Due to the higher content of iQc phases with more characteristic dendritic shape and larger branches apparently the addition of strontium and calcium have strong influence on the formation and amount of primary iQc phases which is not well understood to date.
- Primary iQc phases were separated from the matrix by dynamical deep etching. The morphology of extracted primary particles was investigated with scanning electron microscopy (SEM). Electronic images showed that these particles are faceted with

morphology of pentagonal dodecahedron and that their dendritic branches grow in the direction of the 3-fold symmetry axis.

- With the EBSD method the presence of the primary dendritic iQc phase and orientation relationship between quasicrystal phases was checked. It was also confirmed that the orientation relationship between stable particle and metastable quasicrystal layer around it, does exist.
- Injected crystal phase serve as a substrate for the nucleation of quasicrystalline phase, as metastable quasicrystal phase formed around the crystal particles.

REFERENCES

[1] D. Shechtman, I. Blech, D. Gratias, J. W. Cahn, Metallic Phase with Long-Range Orientational Order and No Translational Symmetry, Physical Review Letters, 53(1984)20, pp.1951-3.
[2] A. P. Tsai, Discovery of stable icosahedral quasicrystals: Progress in understanding structure and properties, Chemical Society Reviews, 42(2013)12, pp.5352-65.
[3] G. T. De Laissardière, D. Nguyen-Manh, D. Mayou, Electronic structure of complex Hume-Rothery phases and quasicrystals in transition metal aluminides, Progress in materials science, 50(2005)6, pp.679-788.
[4] T. Bončina, B. Markoli, F. Zupanič, Characterization of cast Al86Mn3Be11 alloy, Journal of microscopy, 233(2009)3, pp.364-71.
[5] H. J. Chang, E. Fleury, G. Song, M. Lee, W.-T. Kim, D. Kim, Microstructure modification and quasicrystalline phase formation in Al–Mn–Si–Be cast alloys, Materials Science and Engineering: A, 375(2004) pp.992-7.
[6] N. Rozman, T. Bončina, I. Anžel, F. Zupanič, The influence of cooling rate on the microstructure of an Al-Mn-Be alloy, Materiali in tehnologije, 42(2008)2, p.65.
[7] H. Kang, X. Li, Y. Su, D. Liu, J. Guo, H. Fu, 3-D morphology and growth mechanism of primary Al 6 Mn intermetallic compound in directionally solidified Al-3at.% Mn alloy, Intermetallics, 23(2012) pp.32-8.
[8] E. Widjaja, L. Marks, Models for quasicrystal–crystal epitaxy, Journal of Physics: Condensed Matter, 20(2008)31, 314003
[9] J. M. Dubois, Properties- and applications of quasicrystals and complex metallic alloys, Chemical Society Reviews, 41(2012)20, pp.6760-77.
[10] H. Kang, S. Wu, X. Li, J. Guo, Y. Wang, Improvement of microstructure and mechanical properties of Mg–8Gd–3Y by adding Mg 3 Zn 6 Y icosahedral phase alloy, Materials Science and Engineering: A, 528(2011)16, pp.5585-91.
[11] F. Schurack, J. Eckert, L. Schultz, Synthesis and mechanical properties of cast quasicrystal-reinforced Al-alloys, Acta materialia, 49(2001)8, pp.1351-61.
[12] G. Yuan, K. Amiya, H. Kato, A. Inoue, Structure and mechanical properties of cast quasicrystal-reinforced Mg–Zn–Al–Y base alloys, Journal of materials research, 19(2004)05, pp.1531-8.
[13] A. Inoue, H. Kimura, High-strength aluminum alloys containing nanoquasicrystalline particles, Materials Science and Engineering: A, 286(2000)1, pp.1-10.

[14] A. Inoue, H. Kimura, K. Sasamori, T. Masumoto, Ultrahigh Strength of Rapidly Solidified Al 96− x Cr 3 Ce 1 Co x (x= 1, 1.5 and 2%) Alloys Containing an Icosahedral Phase as a Main Component, Materials Transactions, JIM, 35(1994)2, pp.85-94.
[15] D. Bae, S. Kim, D. Kim, W. Kim, Deformation behavior of Mg–Zn–Y alloys reinforced by icosahedral quasicrystalline particles, Acta Materialia, 50(2002)9, pp.2343-56.
[16] D. Bae, M. Lee, K. Kim, W. Kim, D. Kim, Application of quasicrystalline particles as a strengthening phase in Mg–Zn–Y alloys, Journal of Alloys and Compounds, 342(2002)1, pp.445-50.
[17] K. Kita, K. Saito, High-strength aluminum-based alloy, Google Patents, 2000
[18] V. Elser, C. L. Henley, Crystal and quasicrystal structures in Al-Mn-Si alloys, Physical review letters, 55(1985)26, p.2883.
[19] H. Chen, D. Koskenmaki, C. Chen, Formation and structure of icosahedral and glassy phases in melt-spun Al-Si-Mn, Physical Review B, 35(1987)8, p.3715.
[20] D. Naumović, P. Aebi, L. Schlapbach, C. Beeli, K. Kunze, T. A. Lograsso, et al., Formation of a stable decagonal quasicrystalline Al-Pd-Mn surface layer, Physical review letters, 87(2001)19, p.195506.
[21] T. Boncina, F. Zupanic, B. Markoli, Procedure of dynamic deep etching and particle extraction from aluminium alloys, Google Patents, 2012.

15th INTERNATIONAL FOUNDRYMEN CONFERENCE
INNOVATION – The foundation of competitive casting production
Opatija, May 11th-13th, 2016
http://www.simet.hr/~foundry/

DEVELOPMENT OF INNOVATIVE ALUMINIUM ALLOYS

J. Medved, P. Mrvar and M. Vončina

University of Ljubljana Faculty of Natural Sciences and Engineering,
Department for Materials and Metallurgy, Ljubljana, Slovenia

Invited lecture
Conference paper

Abstract

In modern casting practice standard materials do not satisfy the rigorous requirements for applications. Paper represents thermodynamic modeling of innovative aluminum alloys with better mechanical properties for high temperature applications. The thermodynamic predictions are needed for the study of the effect of additions to the thermodynamic stability, crystallization and precipitation kinetics of lightweight alloys. Thermodynamic characterization of castable Al-alloys with the predicted and experimental determined data will increase the basic understanding of Al-alloys that can be used as lightweight castings alternatives for real industrial applications. Nevertheless, the experimenting is still needed to confirm or to optimize the thermodynamic predictions. Using the different combinations of elements in specific temperature regions the information of which specific phase (solid solution, intermetallic compound) is formed is important. Determination of composition and types of phases, amount of phase and study of equilibrium and non-equilibrium processes, the characteristic temperatures of diferent aluminium based systems for lightweight usage was done. Alloys from Al-X-Zr system were investigated using thermodynamic equilibrium calculations (ThermoCalc), thermal analysis, and optical and scanning electron microscopy, in order to identify the corresponding properties.

Keywords: *aluminium alloys, thermodynamic, solidification*

*Corresponding author (e-mail address): *jozef.medved@omm.ntf.uni-lj.si*

15th INTERNATIONAL FOUNDRYMEN CONFERENCE
INNOVATION – The foundation of competitive casting production
Opatija, May 11th-13th, 2016
http://www.simet.hr/~foundry/

ANALYSIS OF WAX MODELS DEFECTS

ANALIZA GREŠAKA NA VOŠTANIM MODELIMA

D. Novoselović[1], I. Budić[2] and I. Mijić[1]

[1]J.J. Strossmayer University of Osijek Mechanical Engineering Faculty, Slavonski Brod, Croatia
[2]Osječka 66, Slavonski Brod, Croatia

Invited lecture
Professional paper

Abstract

The introductory part of paper describes the investment casting (lost-wax casting), the process of making wax models and the most common defects in the wax models are also listed.
In the experimental section the influence of wax temperature and injection pressure on the occurrence of defects in the ring wax models is examinated. Tests were carried out according to 3^2plan of experiment were two technological parameters changed on three levels. After the tests and analysis of results, optimal technological parameters are selected.

***Keywords**: investment casting wax models, defect*

*Corresponding author (e-mail address): *daniel.novoselovic@sfsb.hr*

Sažetak

U uvodnom dijelu rada opisana je tehnologija točnog lijeva, postupak izrade voštanih modela te su navedene najučestalije greške na voštanim modelima.
U eksperimentalnom dijelu ispitan je utjecaj temperature voska i tlaka ubrizgavanja na pojavu grešaka na voštanim modelima prstena. Ispitivanja su provedena prema planu pokusa 3^2 gdje su promatrani tehnološki parametri mijenjani na tri razine. Nakon provedenih ispitivanja i analize rezultata određeni su optimalni tehnološki parametri za odabrani model.

***Ključne riječi**: točni lijev, voštani model, greške*

UVOD

Osnovni principi točnog ili preciznog lijeva bili su poznati još u antičko doba. Dinastija Čang u Kini koristila je postupak ''izgubljenog modela'' za izradu bakrenih filigranskih predmeta, te novčića (1776. do 1222. god. pr. Kr.). Na drugoj strani svijeta, u Kolumbiji i Meksiku, u doba

Azteka izrađeni su mnogi predmeti od zlata, čija tehnologija izrade upućuje na korištenje osnovnih principa ''izgubljenog modela''. U Europi prvi pisani tragovi o ovom postupku potječu iz autobiografije talijanskog renesansnog kipara B. Cellinija. Prva šira objašnjenja korištenja voštanih modela pri oblikovanju kipova od bronce dao je 1897. godine V. Biringuccio. Postupak točnog lijeva prvi put je u SAD primijenjen 1897. god., gdje su ovim postupkom lijevana zubala i nakit [1].

U industrijski razvijenom svijetu postupak točnog lijeva nije bio značajan za industriju sve do Drugog svjetskog rata. Tada je došlo do masovnih zahtjeva vojne industrije za izradom složenih dijelova vojne opreme (industrija oružja, dijelovi u zrakoplovstvu, lopatice turbina mlaznih motora, šivaći strojevi), koji su spremni za ugradnju bez velike naknadne obrade. Ovi zahtjevi bili su ispunjeni korištenjem tehnologije točnog lijeva, kojim se mogu lijevati složeni odljevci nepravilnih oblika, glatkih površina i točnih dimenzija. Unapređenjem tehnologije posebno automatizacije, do veće primjene točnog lijeva došlo je nakon drugog svjetskog rata u raznim granama industrije kao npr. vojnoj, automobilskoj, tekstilnoj, optičkoj, elektrotehničkoj, u industriji alata i drugdje [1]. Primjeri odljevaka točnog lijeva prikazani su na slici 1. i 2.

Slika 1. Dijelovi za industriju naoružanja [1]

Slika 2. Nakit [1]

TEHNOLOGIJA TOČNOG LIJEVA

Točni lijev se često puta naziva i precizni lijev, a dobiva se ulijevanjem litine u kalupe izrađene jednokratnim (npr. voštanim) modelima. U postupku točnog lijeva i modeli i kalupi su jednokratno upotrebljivi. Postupkom točnog lijeva izrađuju se dijelovi kompliciranog oblika, čija bi izrada drugim postupcima bila otežana i neekonomična. Odljevci imaju kvalitetnu površinu i točne dimenzije, pa su pri završnoj obradi odljevaka potrebni mali zahvati radi postizanja konačnih dimenzija (npr. samo brušenje ušća uljevnog sustava). To je naročito važno kod složenih i razvedenih odljevaka, gdje bi eventualna dodatna obrada bila gotovo nemoguća.Postupkom točnog lijeva proizvode se odljevci manjih dimenzija. Masa željeznih odljevaka proizvedenih postupkom točnog lijeva kreće se od nekoliko grama do 20 kg, aluminijskih odljevaka od nekoliko grama do 10 kg. U ovom postupku dimenzije i masa odljevka ograničene su mogućnošću izrade alata za modele i školjke za ulijevanje metala. Zato se odljevci većih dimenzija proizvode unikatno ili u pojedinačnoj proizvodnji. Postupak točnog lijeva smatra se ekonomičnim ako se lijeva najmanje 50 istovrsnih odljevaka. Shema proizvodnje točnog lijeva prikazana je na slici 3 [1].

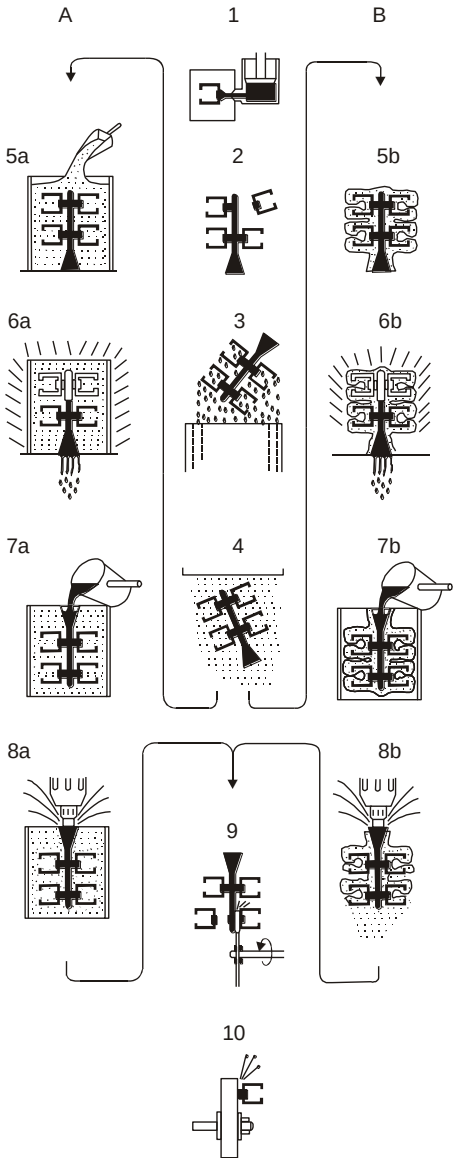

Opis oznaka prema:

A	točni lijev proizvodi se u kalupu
B	točni lijev proizvodi se u školjci
1	ubrizgavanje voštanog modela u metalni alat
2	izrada voštanog grozda (ugrozdavanje); ugrozdavanje je spajanje voštanih modela pomoću električnog lemila na prethodno izrađen voštani uljevni sustav
3	uranjanje voštanog grozda u keramičku suspenziju, te njeno ocjeđivanje s voštanog grozda
4	posipavanje voštanog grozda pijeskom
5.a	ulaganje voštanog grozda u kalup i zasipavanje pijeskom
6.a	zagrijavanje kalupa radi odstranjivanja voska
7.a	ulijevanje metala
8.a	razbijanje (istresanje) kalupa
5.b	izrada keramičke školjke nanošenjem većeg broja slojeva veziva i pijeska
6.b	zagrijavanje školjke radi odstranjivanja voska i daljnje zagrijavanje kada školjka keramizira na visokoj temperaturi (≈ 800 ^{0}C), te postaje spremna za ulijevanje metala
7.b	ulijevanje metala
8.b	razbijanje (istresanje školjke)
9	odrezivanje odljevaka od uljevnih sustava
10	brušenje ostatka uljevnog sustava

Slika 3. Shema proizvodnje točnog lijeva [1]

Prednosti točnog lijeva su [1]:

- mogućnost izrade velikih serija odljevaka vrlo složenog oblika koje je teško ili nemoguće proizvesti klasičnim načinima lijevanja ili strojnom obradom
- kalupni materijal i sama tehnologija omogućuju dobivanje finih detalja, proizvodnju odljevaka velike dimenzijske točnosti i kvalitete površine (glatka površina odljevaka), koji se ne mogu proizvesti klasičnim načinima lijevanja
- odljevci zahtijevaju malu ili nikakvu strojnu obradu, što omogućuje izbor lakših, a time i jeftinijih strojeva za strojnu obradu
- kako ovaj način lijevanja ne zahtijeva veće naknadne obrade tako se može lijevati puno više vrsta metala, kao što su npr. kvalitetni čelici koji se teško obrađuju skidanjem strugotine
- postupak je primjenjiv gotovo za sve materijale koji se mogu taliti i lijevati
- moguće je lijevati i odljevke koji se sastoje od više dijelova (npr. rotori nekih motora)
- moguća je precizna kontrola metalurških svojstava, kao što je veličina zrna, orijentacija i usmjereno skrućivanje, a to rezultira preciznom kontrolom mehaničkih karakteristika odljevaka
- proces se može primijeniti za taljenje i lijevanje legura koje zahtijevaju lijevanje u vakuumu ili inertnoj atmosferi
- kod točnog lijeva ne javljaju se neke klasične greške (npr. pojava srha) zbog sklapanja kalupa, jer je kalup monolitan (iz jednog komada).

Nedostaci točnog lijeva su [1]:

- veličina i masa odljevaka su ograničene
- za veće dimenzije odljevaka troškovi opreme su vrlo visoki.

IZRADA VOŠTANIH MODELA

Vosak je najstariji termoplastični materijal i njime se izrađuje većina modela za točni lijev. Rijetko se koristi samo jedna vrsta voska, već se koriste mješavine sa raznim dodatcima. Vosak je smjesa velikog broja komponenata raznih duljina molekula i to daje ovom materijalufizikalna svojstva drugačija od drugih materijala. Vosak se ne tali kao homogene kemijske supstance već prolazi kroz nekoliko faza taljenja. Postepenim zagrijavanjem, vosak postaje sve mekši, ulazi u plastičnu fazu, pa u polu plastičnu fazu. Dodatnim zagrijavanjem postaje viskozna tekućina (polu tekućina), a dolaskom u područje potpunog taljenja ponaša se kao Newtonovski fluid.

Voštani modeli mogu se izrađivati obrađivanjem voštanog sirovca ručnim alatom poput pilica, turpija, brusilica, alata za rezbarenje i grijanim alatom. Vosak se može rezati, taliti i zavarivati, te se na taj način mogu izraditi razni oblici modela. Takav način obrade je spor, zahtjeva vještinu kod radnika i nije moguća izrada preciznih dijelova konstantnih dimenzija. Iz tih razloga ovakav postupak izrade nije značajan za industrijsku proizvodnju, već je bitan u umjetnosti, kod izrade jedinstvenog nakita i matičnih modela te u zubotehničkim laboratorijima.
U industrijskoj proizvodnji za izradu modela izrađuju se kalupi u koje se strojno ubrizgava vosak. Time se omogućava velika proizvodnost, konstantne dimenzije i uske tolerancije dimenzija i oblika. Osim toga, modeli se mogu izrađivati i obradom voštanih pripremaka na

strojevima za obradu metala i drva ili korištenjem aditivnih tehnologija. Vrijeme izrade modela ovim tehnologijama mjeri se u satima za razliku od ciklusa ubrizgavanja modela koji traje nekoliko minuta. Iz tog razloga strojna izrada ograničena je na pojedinačnu izradu ili izradu malih serija modela.

GREŠKE NA VOŠTANIM MODELIMA

Kao i kod svakog proizvodnog procesa, kod izrade voštanih modela javljaju se greške. Svaki korak procesa izrade voštanih modela utječe na pojavu grešaka.

Greške mogu biti uzrokovane:

- lošom konstrukcijom kalupa i modela
- pogrešnim postavljanjem parametara procesa izrade modela (taljenje voska, temperiranje, ubrizgavanje)
- nestručnim osobljem
- neispravnim rukovanjem i skladištenjem gotovih modela.

Najučestalije greške pri izradi voštanih modela su [2]:

- mjehurići – uključine zraka
- nepotpuno ispunjen kalup
- prekomjerno punjenje kalupa
- lako savitljiv voštani model
- prekomjerno skupljanje
- usahline.
- teško lomljivi voštani modeli
- izvitoperenje.

Zbog složenosti procesa izrade modela jedan tip greške može imati više uzroka, a jedan uzrok može uzrokovati više tipova grešaka. Radi tako složene veze potrebno je obratiti pažnju tijekom svakog koraka procesa izrade te strogo kontrolirati kako bi se broj grešaka sveo na prihvatljivu razinu.

Najutjecajniji tehnološki parametri koji utječu na kvalitetu voštanih modela su:

- tlak ubrizgavanja
- tlak stezanja kalupa
- temperatura voska
- temperatura mlaznice
- temperatura kalupa
- vrijeme ubrizgavanja voska.

PROVOĐENJE ISPITIVANJA

Ispitivanja su provedena na Strojarskom fakultetu u Slavonskom Brodu. Cilj ispitivanja bio je ispitati utjecaj promjene tlaka ubrizgavanja voska i temperature voska na pojavu grešaka na voštanim modelima prstena.
Ispitivanja su provedena prema planu pokusa 3^2 (tablica 1.) gdje su dva parametra (temperatura voska θ, °C i tlak ubrizgavanja p, bar) mijenjani na 3 razine.

Tablica 1. Plan pokusa

	Temperatura voska θ, °C	Tlak ubrizgavanja p, bar
1.	70	0,8
2.	70	1
3.	70	1,2
4.	75	0,8
5.	75	1
6.	75	1,2
7.	80	0,8
8.	80	1
9.	80	1,2

Za izradu voštanih modela odabran je strojno izrađeni gumeni kalup prema slici 4.

Slika 4. Otvoreni gumeni kalup za izradu modela

Za izradu voštanih modela korišten je vosak u listićima proizvođača Freeman Flakes. Voštani modeli izrađeni su na ubrizgavalici „Waxy kompresor“ tip B.009316. (slika 5). Na ubrizgavalici je moguće podesiti tlak ubrizgavanja i temperaturu voska.

Slika 5. Ubrizgavalica Waxy kompresor tip B.009316

Da bi se spriječilo otvaranje gumenog kalupa prilikom ubrizgavanja voska kalup je stegnut sa stegom (slika 6). Na taj način je spriječeno isticanje voska prilikom ubrizgavanja. Vrijeme punjenja kalupa bilo je 3 sekunde. Vrijeme hlađenja voska u kalupu bilo je 15 s. Slika 7. prikazuje izrađeni voštani model.

Slika 6. Zatvoreni gumeni kalup stegnut sa stegom

Slika 7. Voštani model

ANALIZA REZULTATA

Prema planu pokusa 3^2 (tablica 1.) za svako stanje odlivena su po 3 uzorka. U tablici 2. prikazani su voštani modeli izrađeni prema planu pokusa te je na njima analizirana pojava grešaka.

Tablica 2. Prikaz voštanih modela odlivenih prema planu pokusa [4]

	Voštani modeli	Vrste greške
1. θ = 70°C, p= 0,8 bar		- nepotpuno ispunjen kalup - lako savitljiv voštani model - usahline
2. θ = 70°C, p= 1,0 bar		- usahline - nepotpuno ispunjen kalup - mjehuravost
3. θ = 70°C, p= 1,2 bar		- nema grešaka na modelima
4. θ = 75°C, p= 0,8 bar		- izvitoperenje - nepotpuno ispunjen kalup
5. θ = 75°C, p= 1,0 bar		- mjehuravost - nepotpuno ispunjen kalup - izvitoperenje
6. θ = 75°C, p= 1,2 bar		- mjehuravost -nepotpuno ispunjen kalup
7. θ = 80°C, p= 0,8 bar		- mjehuravost - nepotpuno ispunjen kalup - prekomjerno punjenje kalupa - prekomjerno skupljanje

8. θ = 80°C, p= 1,0 bar		- nepotpuno ispunjen kalup - prekomjerno punjenje kalupa - prekomjerno skupljanje
9. θ = 80°C, p= 1,2 bar		- prekomjerno punjenje kalupa - izvitoperenje - usahline

Nakon provedenih ispitivanja može se uočiti da su modeli pod brojem 3 jedini bez grešaka. Modeli su izrađeni s temperaturom voska od 70°C i tlakom ubrizgavanja od 1,2 bar.

Ovo možemo objasniti da s povećanjem temperature vosak postaje rjeđi te dolazi do prekomjernog punjenja kalupa, prekomjernog skupljanja te pojave usahlina. S druge strane premali tlak ubrizgavanja uzrokuje nepotpuno ispunjen kalup, savitljive modele te usahline i mjehuravost.

Zbog toga je važno da se za svaki voštani model prije izrade odrede njegovi optimalni tehnološki parametri.

ZAKLJUČAK

Izrada voštanih modela jedan je od zahtjevnijih koraka kod točnog lijeva jer je vosak osjetljiv materijal koji zahtjeva pažljivo rukovanje. Nedostaci na voštanim modelima mogu biti mnogobrojni, a uzroci nastanka su vrlo različiti. Stoga je utjecaj tehnologije na kvalitetu izrade vrlo bitan.

Vosak koji se ubrizgava u kalupe mora imati odgovarajući sastav. Temperatura i vrijeme držanja voska u kalupu moraju biti pouzdano kontrolirani. Odstupanja propisanih parametara u fazi ubrizgavanja mogu dovesti do promjene skupljanja voštanih modela. Temperatura na kojoj se obavlja priprema voska i ubrizgavanje mora odgovarati propisanoj granici $\pm$ 2 °C.

Pri samom ubrizgavanju voska, tlak stezanja kalupa mora biti veći od tlaka pod kojim se ubrizgava voštana masa, kako ne bi došlo do otvaranja kalupa. Također je potrebno izabrati pogodna mjesta uljevnog sustava, da bi se izbjegle turbulencija i stvaranje zračnih mjehurića. Poželjno je iz upotrebe izbaciti loš ili istrošen kalup, kako ne bi došlo do pojave viška neželjenog materijala (voska) na voštanom modelu.

Nepridržavanje temperaturnih režima pri ulijevanju voska i metala, nepažnja u radu, loše sastavljanje dijelova modela, upućuje na povećanje broja potencijalnih grešaka.

LITERATURA

[1] I. Budić, Z. Bonačić-Mandinić, Osnove tehnologija kalupljneja: Jednokratni kalupi II. dio, Strojarski fakultet u Slavonskom Brodu, Slavonski Brod, 2004.

[2] V. Faccenda, Handbook on investment casting, The lost wax casting process for carat gold jewellery manufacture, World Gold Council, London, 2003.

[3] D. Ott, Handbook on casting and other defects, In Gold Jewellery Manufacture, World Gold Council, London, 2001.

[4] I. Mijić, Analiza grešaka na voštanim modelima, Diplomski rad, Slavonski Brod: Strojarski fakultet u Slavonskom Brodu, 2015, str.48.

15th INTERNATIONAL FOUNDRYMEN CONFERENCE
INNOVATION – The foundation of competitive casting production
Opatija, May 11th-13th, 2016
http://www.simet.hr/~foundry/

COMPUTER SIMULATION OF MICROSTRUCTURE AND MECHANICAL PROPERTIES OF CAST STEEL

B. Smoljan, D. Iljkić and L. Štic

University of Rijeka Faculty of Engineering, Department of Materials Science and Engineering, Rijeka, Croatia

Invited lecture
Original scientific paper

Abstract

The research purpose is to upgrade the mathematical modelling and computer simulation of casting of steel.
Based on theoretical analyses of physical processes which exist in casting systems the proper mathematical model is established and computer software is developed.
On the basis of control volume method, the algorithm for prediction of mechanical properties and microstructure distribution in steel casting has been developed. The computer simulation of casting of steel is consisted of two parts: numerical calculation of transient temperature field in process of solidification and cooling of casting to the final temperature, and of numerical calculation of mechanical properties. The hardness and microstructures of casting has been predicted based on CCT diagrams.
Physical properties that were included in the model, such as heat conductivity coefficient, heat capacity and surface heat transfer coefficient were obtained by the inversion method.
The algorithm is completed to solve 3-D situation problems such as the casting of complex cylinders, cones, spheres, etc. The established model of steel casting can be successfully applied in the practice of casting.

***Keywords**: steel casting, hardness, microstructure, computer simulation*

*Corresponding author (e-mail address): *dario.iljkic@riteh.hr*

INTRODUCTION

The numerical simulation of mechanical properties distribution in castings and ingots has one of the highest priorities in simulation of phenomena of casting. Initially, the attention of numerical computation has been focused on solidification mechanisms and the development of algorithms for microstructure prediction, with tendency to model the rising and growth of

numerous types of defects. During the casting, many different physical processes, such as, solidification, solid state phase transformation, evolution of microstructure, diffusion, heat conduction, and mechanical stressing and distortion are at once taking place inside metal [1, 2, 3, 4, 5]. Computer programs for simulation of the casting can be developed by considering the issues such as achievement of tolerable casting defects, desired mechanical property distribution, microstructure distribution and required workpiece shape.

Process simulation capabilities have been extended beyond thermal and flow modelling for casting. Despite very useful software for the calculation of grain structure, porosity, hot tearing, and solid-state transformation, such are coupled modules MAGMASOFT, ProCAST, NovaCast, MAVIS2000, FLOW-3D, CAPCAST, PAM-CASTSIMULOR, SOLIDCast, ConiferCAST, PowerCAST, CalcoSOFT, SUTCAST, dieCAS, ADSTEFAN, MICRESS, etc., that can be used for computer simulation of casting, there are still questions on which answers should be given to satisfy all industry needs in mathematical modelling and simulation of casting [3, 6, 7].

The input of the simulation is composed of the following categories: geometry of casting and moulds, physical characteristics of the alloy and the moulds, kinematic boundary conditions and thermal boundary conditions. Simulation of heat transfer is thermodynamical problem. It is necessary to establish the appropriate algorithm which describes cooling process and to involve appropriate input data in the model. The accuracy of numerical simulation of thermal process directly depends on the applied input data. Inverse heat transfer problems should be solved to determine thermal properties for casting based on experimentally evaluated cooling curve results [8].

Usually simulations of microstructural transformations are based on the both, CCT diagrams using linear alignment with the actual chemical composition, or on the thermo-kinetic expressions. The first approach is more consistent, but the second approach gives good results for the chemical composition of the steel for which expressions have been established.

Proposed numerical model is based on finite volume method (FVM). The finite volume method (FVM) has been established as a very efficient way of solving fluid flow and heat transfer problems. Recently, FVM is used as a simple and effective tool for the solution of a large range of problems in the thermoplastic analysis [9, 10]. The key feature of the FVM approach is that the FVM is based on flux integration over the control volume surfaces. The method is implemented in a manner that ensures local flux conservation, regardless of the grid structure [9].

COMPUTER MODELLING OF HEAT TRANSFER AND SOLIDIFICATION

Numerical simulation of solidification gives consideration to both the motions of molten metal during the mould cavity filing process and convective motions after pouring. Hot liquid is poured into colder mould and specific heat and heat of fusion of the solidifying metal pass through a series of thermal resistances to the cold mould until solidification is complete. Figure 1 schematically shows this process for solidification of cast metal.

Complete process of solidification and cooling of casting is based on the following system of differential equations [2, 3, 11]:

- *the Navier-Stokes equations*

$$\begin{aligned}\mu\left(\frac{\partial^2 v_r}{\partial r^2}+\frac{1}{r}\frac{\partial v_r}{\partial r}+\frac{\partial^2 v_r}{\partial z^2}-\frac{v_r}{r^2}\right)-\frac{\partial p}{\partial r}+\rho g_r\beta\left(T-T_\infty\right)&=\rho\frac{\mathrm{d}v_r}{\mathrm{d}t}\\ \mu\left(\frac{\partial^2 v_z}{\partial r^2}+\frac{1}{r}\frac{\partial v_z}{\partial r}+\frac{\partial^2 v_z}{\partial z^2}\right)-\frac{\partial p}{\partial z}+\rho g_z\beta\left(T-T_\infty\right)&=\rho\frac{\mathrm{d}v_z}{\mathrm{d}t}\end{aligned} \tag{1}$$

- *the continuity equation*

$$\frac{\partial v_r}{\partial r}+\frac{v_r}{r}+\frac{\partial v_z}{\partial z}=0 \tag{2}$$

- *the Fourier's heat conduction equation including the convection term*

$$\frac{\lambda}{r}\frac{\partial T}{\partial r}+\frac{\partial}{\partial r}\left(\lambda\frac{\partial T}{\partial r}\right)+\frac{\partial}{\partial z}\left(\lambda\frac{\partial T}{\partial z}\right)=\rho c_{\mathrm{ef}}\left(\frac{\partial T}{\partial t}+v_r\frac{\partial T}{\partial r}+v_z\frac{\partial T}{\partial r}\right) \tag{3}$$

Characteristic boundary condition is:

$$-\lambda\left.\frac{\delta T}{\delta n}\right|_{\mathrm{s}}=\alpha\left(T_{\mathrm{s}}-T_{\mathrm{a}}\right) \tag{4}$$

where T/K is the temperature, t/s is the time, $\rho = \rho$(T)/kgm^{-3} is the density, λ/Wm^{-1}K^{-1} is the thermal conductivity coefficient, T_{s}/K is surface temperature, T_{a}/K is air temperature, α/Wm^{-2}K^{-1} is heat transfer coefficient, v_{r}, v_{z}/ms^{-1} are the r- and z-component of velocity, respectively, $\mu(T)$/Nsm^{-2} is dynamical viscosity coefficient, $c_{\mathrm{ef}} = c + L/(T_\beta - T_\alpha)$/Jkg^{-1}K^{-1} is the effective specific heat of a mushy zone, L/Jkg^{-1} is the latent heat of solidification, c/Jkg^{-1}K^{-1} is the specific heat, p/Nm^{-2} is the pressure, g_{r}, g_{z}/ms^{-2} are the r and z-component of gravitational acceleration, respectively, β/K^{-1} is the volume coefficient of thermal expansion, r, z/m are the coordinates of the vector of the considered node's position, T_∞/K is the reference temperature $T_\infty = T_{\mathrm{in}}$, r/m is the radius.

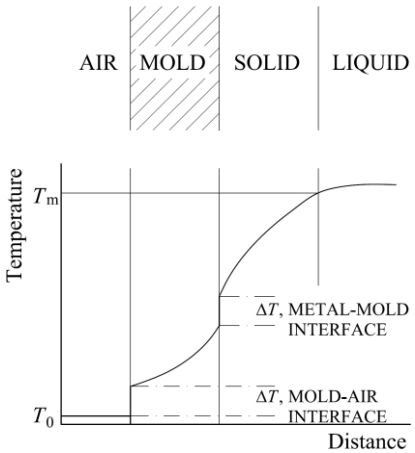

Figure 1. Temperature profile in solidification of a pure metal

Equations (1) to (3) can be found out using the finite volume method, but physical properties included in equations (1) to (4) should be defined [9, 10].

In this model was presumed that convection term has no relevant role and that liquid metal flow could be neglected after pouring [12]. Quantity of growth of solidified part of casting was predicted by calculation of solidification rate in control volume (Figure 2).

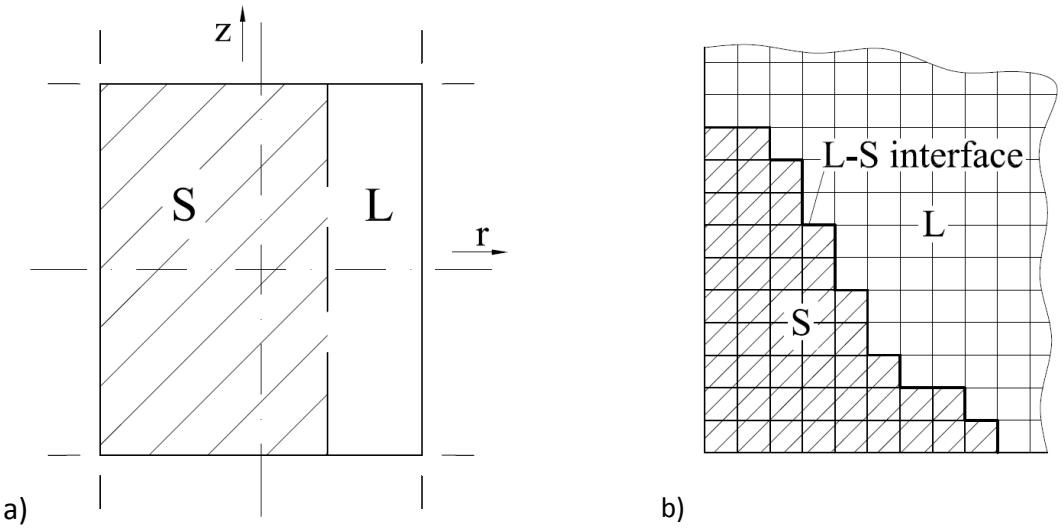

Figure 2. Liquid-solid interface, a) control volume, b) casting

Increment of solidified part in control volume can be calculated by:

$$f_{\mathrm{i}} = \frac{m_{\mathrm{i}}}{m_{\mathrm{vol}}} = \frac{c_{\mathrm{m}}\left(T_1 - T_2\right)}{L} \tag{5}$$

where m_i/kg is mass quantity increase of solidified part in control volume, m_{vol}/kg is mass quantity of control volume, c_m/Jkg^{-1}K^{-1} is heat capacity of liquid and solid mixture, T_1/K is the temperature at the beginning and T_2/K is the temperature at the end of time step Δt.
When $\Sigma f_i = 1$, the mass of solidified part of casting will grow up for mass of control volume.

Accuracy of the heat transfer prediction directly influences to the accuracy of both, calculations of phase transformation kinetics and calculations of mechanical properties of steel. Variable ρ for steel is equal ~7800 kgm^{-3}. Accepted values of specific heat capacity, c are shown in Table 1 [13].

Table 1. Specific heat capacity of different microstructural compositions of steel

	Temperature, T/°C	Ferrite + Pearlite (Bainite)	Martensite	Austenite
Specific heat capacity, c/Jkg^{-1}K^{-1}	0	378	376	415
	300	446	445	440
	600	509	507	467
	800	570	-	490
	950	596	-	520

If the variables ρ and c were accepted, variable λ and specially variable α must be estimated, i.e., calibrated according to variables ρ and c (Table 2) [8].

Table 2. Heat conductivity coefficients

	Temperature, T/°C	Ferrite + Pearlite (Bainite)	Martensite	Austenite
Heat conductivity coefficients, λ/Wm^{-1}K^{-1}	0	49	43	15
	300	42	37	18
	600	34	30	22
	800	27	-	25
	950	21	-	28

Total heat conductivity coefficients of steel at some temperature, T can be estimated by:

$$\lambda_T = \left(x_{\mathrm{F}}\lambda_{(\mathrm{F+P})T} + x_{\mathrm{P}}\lambda_{(\mathrm{F+P})T} + x_{\mathrm{B}}\lambda_{\mathrm{B}T} + x_{\mathrm{M}}\lambda_{\mathrm{M}T} + x_{\mathrm{A}}\lambda_{\mathrm{A}T}\right)/100 \quad (6)$$

where x_{F}, x_{P}, x_{B}, x_{M}, x_{A} are contents ferrite + pearlite, bainite, martensite and austenite at temperature, T, respectively. Heat transfer coefficients of air are given in Table 3.

Table 3. Calibrated values of heat transfer coefficient of air

Temperature, T/°C	20	100	200	400	600	800	1000
Heat transfer coefficient, α/Wm^{-2}K^{-1}	12	15	21	33	50	84	113

COMPUTER MODELLING OF HARDNESS AND MICROSTRUCTURE COMPOSITION

In the developed computer simulation of casting, the hardness at different workpiece points is estimated by the conversion of the calculated cooling time $t_{8/5}$ to the hardness and microstructure composition by using CCT diagram [14]. Other mechanical properties of steel can be estimated based on hardness of steel. Contents of ferrite, pearlite, bainite, martensite and austenite at some temperature can be estimated using the diagram in the Figure 3.

Characteristic cooling times in Figure 3 are equal to:

$$t_1 = t_{\mathrm{M95}} \quad (7a)$$

$$t_2 = \exp\left(\log t_{\mathrm{M95}} + 0.25\left(\log t_{\mathrm{M50}} - \log t_{\mathrm{M95}}\right)\right) \quad (7b)$$

$$t_3 = \exp\left(\log t_{\mathrm{M95}} + 0.75\left(\log t_{\mathrm{M50}} - \log t_{\mathrm{M95}}\right)\right) \quad (7c)$$

$$t_4 = \exp\left(\log t_{\mathrm{M50}} + 0.25\left(\log t_{\mathrm{P100}} - \log t_{\mathrm{M50}}\right)\right) \quad (7d)$$

$$t_5 = \exp\left(\log t_{\mathrm{M50}} + 0.75\left(\log t_{\mathrm{P100}} - \log t_{\mathrm{M50}}\right)\right) \quad (7e)$$

$$t_6 = \exp\left(\log t_{\mathrm{P100}} + 0.25\left(\log t_{\mathrm{P50}} - \log t_{\mathrm{P100}}\right)\right) \quad (7f)$$

$$t_7 = \exp\left(\log t_{\mathrm{P100}} + 0.75\left(\log t_{\mathrm{P50}} - \log t_{\mathrm{P100}}\right)\right) \quad (7g)$$

where t_{M95}, t_{M50}, t_{P100}, t_{P50} are cooling time from 800 to 500 °C for characteristic points in Jominy specimen with 95 % of martensite, 50 % of martensite, 100 % of pearlite and 50 % of pearlite in microstructure, respectively.

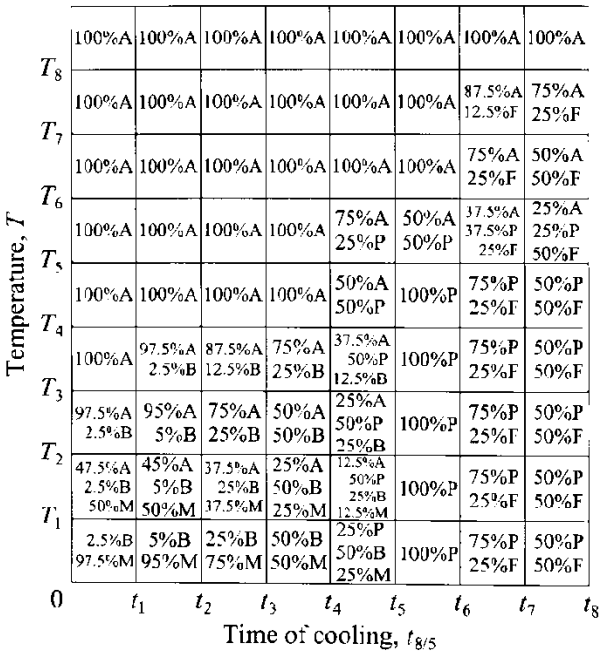

Figure 3. Contents of ferrite, pearlite, bainite, martensite and austenite at some temperature

Characteristic temperatures in diagram shown in Figure 3 are equal to:

$$T_1 = M_s - 0.75(M_s - M_f) \tag{8a}$$

$$T_2 = M_s - 0.25(M_s - M_f) \tag{8b}$$

$$T_3 = B_s - 0.75(B_s - M_s) \tag{8c}$$

$$T_4 = B_s - 0.25(B_s - M_s) \tag{8d}$$

$$T_5 = A_1 - 0.75(A_1 - B_s) \tag{8e}$$

$$T_6 = A_1 - 0.25(A_1 - B_s) \tag{8f}$$

$$T_7 = A_3 - 0.75(A_3 - A_1) \tag{8g}$$

$$T_8 = A_3 - 0.25(A_3 - A_1) \tag{8h}$$

where M_s is temperature of start of martensitic transformation, M_f is temperature of finish of martensitic transformation, B_s is temperature of start of bainitic transformation, A_1 is equilibrium temperature of eutectoid transformation, A_3 is equilibrium temperature at which transformation of austenite to ferrite begins. Between critical temperatures A_3, B_s, M_s and M_f of austenite decomposition and maximum hardness, regression relations are established:

$$A_3 = 862 - 0.04(\mathrm{HRC}_{\max.} - 20)^2 - \frac{2.5t_{8/5}}{\mathrm{HRC}_{\max} - 20} \tag{9a}$$

$$B_s = 586 - 0.02(\mathrm{HRC}_{\max} - 20)^2 - \frac{12t_{8/5}}{\mathrm{HRC}_{\max} - 20} \tag{9b}$$

$$M_s = 502 - 0.09(\mathrm{HRC}_{\max} - 20)^2 - \frac{3.5t_{8/5}}{\mathrm{HRC}_{\max} - 20} \tag{9c}$$

$$M_f = 502 - 0.2(\mathrm{HRC}_{\max} - 20)^2 - \frac{3.5t_{8/5}}{\mathrm{HRC}_{\max} - 20} \tag{9d}$$

It was accepted that equilibrium temperature of eutectoid transformation A_1 is equal to 721 °C.

APPLICATION

The developed method for prediction of mechanical properties and microstructure distributions were applied in design of casting. Computer simulation of mechanical properties and microstructure distribution of steel casting was done using the computer software BS-CASTING.

The casting was made of steel EN 42CrMo4. Pouring temperature during the casting was 1514 °C and the temperature of the mould was 105 °C. The steel casting is poured from the open top of the mould. The chemical composition of casting was: 0.44 %C, 0.14 %Si, 0.62 %Mn, 0.011 %P, 0.025 %S, 1.19 %Cr, 0.23 %Mo, 0.16 %V. The geometry of the mould and casting is shown in Figure 4.

The hardness distribution of the casting is shown in Figure 5. The distributions of ferrite, pearlite, bainite and martensite of steel casting are shown in Figure 6.

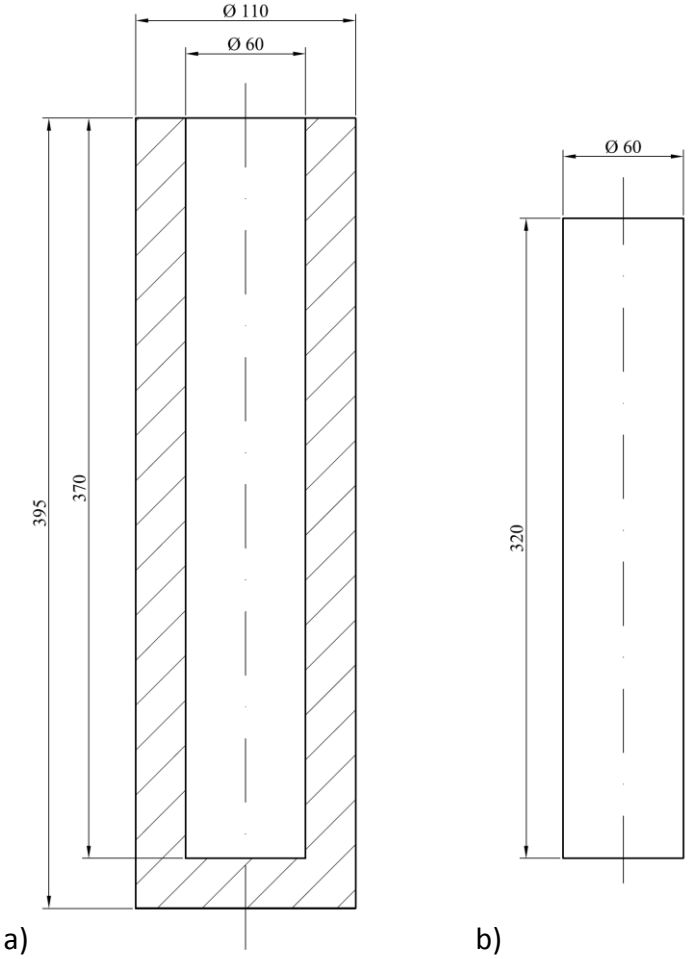

Figure 4. Geometry, a) mould, b) steel casting

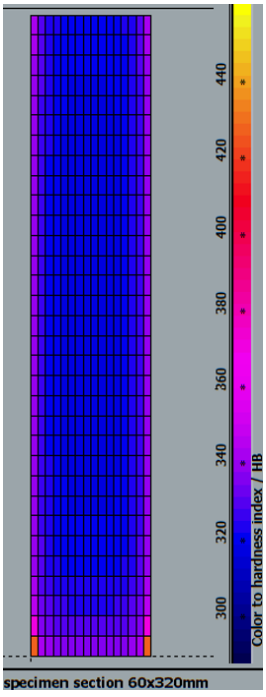

Figure 5. Distribution of hardness of steel casting

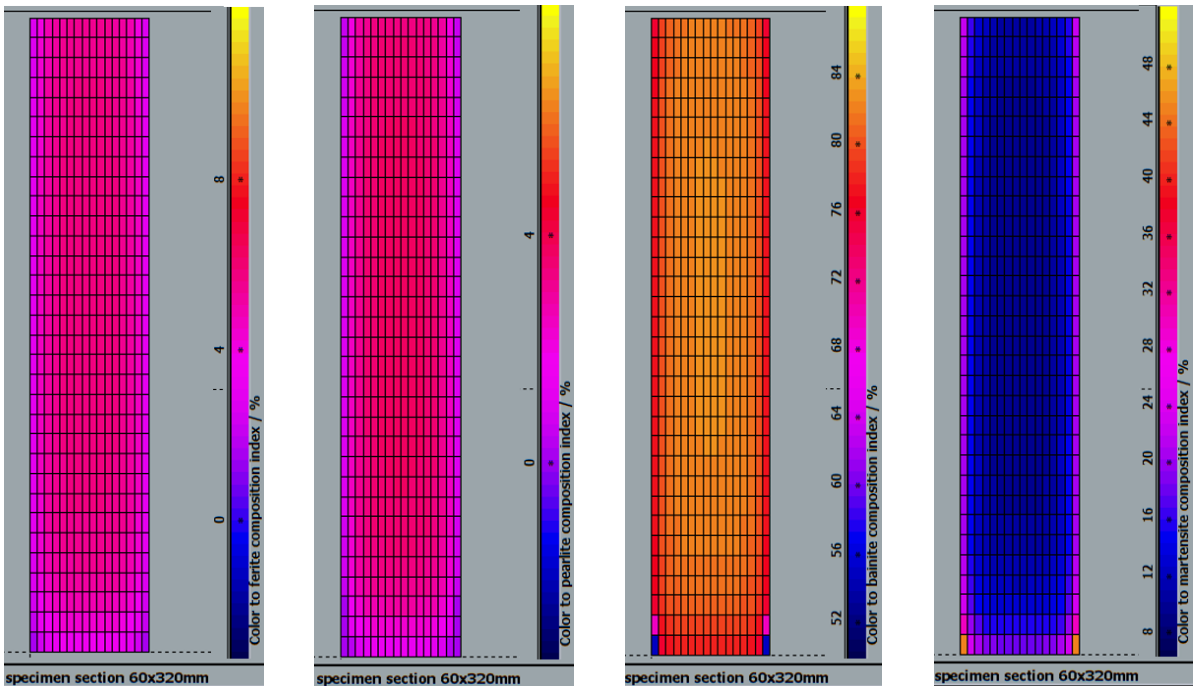

a) b) c) d)

Figure 6. Distributions of, a) ferrite, b) pearlite, c) bainite, d) martensite of steel casting

CONCLUSIONS

The mathematical model of steel casting has been developed to predict the mechanical properties and microstructure distribution in a specimen with complex geometry. The model is based on the finite volume method.

The numerical simulation of casting is consisted of numerical simulation of solidification, transient temperature field of cooling process, numerical simulation of mechanical properties and microstructure transformation in solid state.

Input material data involved in mathematical model of casting, i.e., density and specific heat capacity of steel have been accepted from literature. Specific heat capacity, heat transfer coefficient and heat conductivity coefficient were accepted from literature. Moreover, heat transfer and heat conductivity coefficients are additionally calibrated.

Hardness and microstructure composition in specimen points was calculated by the conversion of calculated time of cooling from 800 to 500 °C to hardness and microstructure composition using the CCT diagram.

A developed mathematical model has been applied in computer simulation of casting of steel bar. It can be concluded, that hardness and microstructure composition in casted steel can by successfully calculated by proposed method.

REFERENCES

[1] N. M. Vanaparthy, M. N. Srinivasan, Modelling of solidification structure of continuous cast steel, Modell. Simul. Mater. Sci. Eng., 6(1998), pp. 237–249.

[2] T. C. Tszeng, S. Kobayashi, Stress analysis in solidification process: Application to continuous casting, Int. J. Mach. Tools Manuf., 29(1989), pp. 121-140.

[3] M. Rosso, Modelling of Casting, in Handbook of Thermal Process Modelling Steels, eds. C.H. Gur, J. Pan, CRC Press, 2008.

[4] A. Grill, J. K. Brimacombe, F. Weinberg, Mathematical analysis of stresses in continuous casting of steel, Ironmak. Steelmak., 3(1976)1, pp. 38-47.

[5] J. R. Williams, R. W. Lewis, K. Morgan, An elasto-viscoplastic thermal stress model with applications to the continuous casting of metals, Int. J. Numer. Meth. Eng., 14(1979), pp. 1-9.

[6] M. Schneider, C. Beckermann, Formation of Macrosegregation by Multicomponent Thermosolutal Convection during the Solidification of Steel, Metallurgical and Materials Transactions A, 26(1995)9, pp. 2373-2388.

[7] A. Sommerfeld, B. Böttger, B. Tonn, Graphite nucleation in cast iron melts based on solidification experiments and microstructure simulation, J. Mater. Sci. Technol., 24(2008), pp. 321-324.

[8] C. H. Gur, J. Pan, Handbook of Thermal Process Modelling Steels, CRC Press, 2008

[9] S. Patankar: Numerical Heat Transfer and Fluid Flow, McGraw Hill Book Company, New York, 1980.

[10] B. Smoljan, D. Iljkić, H. Novak, Estimation of coefficient of heat conductivity and heat transfer coefficient in the numerical model of the steel quenching, *Proceedings of the 2nd Mediterranean Conference on Heat Treatment and Surface Engineering,* 11-14 June 2013, Dubrovnik - Cavtat, Croatia.

[11] L. Sowa, Mathematical Model of Solidification of the Axisymmetric Casting While Taking Into Account its Shrinkage, Journal of Applied Mathematics and Computational Mechanics, 13(2014)4, pp. 123-130.

[12] M. Flemings, Solidification Processing, McGraw-Hill Book Company, 1984.

[13] H. Bhadeshia, Material Factors, in Handbook of Residual Stress and Deformation of Steel, eds. G. Totten, M. Howes, T. Inoue, ASM International, 2002.

[14] B. Smoljan, D. Iljkić, L. Štic, Mathematical modelling and computer simulation of non-monotonic quenching, *Proceedings of the 23rd IFHTSE Congress,* 18-21 April 2016, Savannah, Georgia, USA.

Acknowledgements

This work has been supported in part by Croatian Science Foundation under the project 5371.

This work has been supported in part by University of Rijeka, Support No 13.09.1.1.02.

15th INTERNATIONAL FOUNDRYMEN CONFERENCE
INNOVATION – The foundation of competitive casting production
Opatija, May 12th-13th, 2016
http://www.simet.hr/~foundry/

DEVELOPMENT OF SLOVAK FOUNDRY INDUSTRY IN 21. CENTURY

I. Vasková[1], J. Cibuľa[2] and M. Conev[1]

[1]Technical University of Košice Faculty of Metallurgy, Institute of Metallurgy, Košice, Slovakia
[2]Cibula Consultant, Žiar nad Hronom, Slovakia

Invited lecture
Subject review

Abstract

Production of castings on Slovak ground has a longtime tradition and went through a different phases of development. Slovakia was a heart of industry in Hungarian part of Austria-Hungary until 1918 and in the beginning of 20th century it was studded by iron mills, which among the pig iron spread also the casting production. Creation of Czechoslovakia had a negative influence on castings production. Competition of more developed foundry industry of Czech lands led to reduction of industry in Slovakia. It has changed in 30ties when the military production was replaced away from the western borders of Czechoslovakia from a strategic reason. At the time of WW2 an industry boom had shown, naturally with a dominance of military industry and castings production began to increase. After the year 1948 many of plants were built in Slovakia, but most of them for production of raw materials and semi-finished product, which were then finished in Czech. It took almost 20 years after the Federation creation since the foundry production was on expansion in Slovakia again. Significantly helpful was the moving of production of die pressure machines to Snina, also a start of aluminium castings production with export to Czech, but mainly the military industry. Although a decreased production at the beginning of nineties they were able to stabilize the production by the end of the century. The beginning of 21th century was for Slovak foundries guided by a surprisingly high increase of production. Development of automotive production in Slovakia became such a strong customer, that in recent years, more foreign producers are incoming to Slovakia.

Keywords: *Slovak foundry industry, Development in 21. Century, Military industry, Automotive industry*

*Corresponding author (e-mail address): *Iveta.vaskova@tuke.sk*

INTRODUCTION

Castings production on Slovak land has a longtime tradition and went through a many phases. If we are not thinking about bronze castings from a renaissance time, then the first industrially produced castings at the beginning of 19th century were mainly art-decorated castings from cast iron made in Prakovce, or later industrial castings in Krompachy or Cinobaňa. Slovakia was a heart of industry in Hungarian part of Austria-Hungary until 1918 and in the beginning of 20th century it was studded by iron mills, which among the pig iron spread the casting production too, foundries in Trnava and Fiľakovo. Creation of Czechoslovakia had a negative influence on castings production, compared to Czech lands, which were the industrial base of the Austrian part of monarchy. Slovakia (although in Hungarian greatly advanced) was much more behind. Competition of more developed foundry industry of Czech lands led to reduction of industry in Slovakia. It changed in 30ties when the military production was replaced away from the western borders of Czechoslovakia (Škoda Plzeň to Dubnica nad Váhom, Zbrojovka Brno to Považská Bystrica) from a strategic reason. At the time of WW2 an industry boom has shown, naturally with a dominance of military industry and castings production began to increase. After the year 1948 many of plants were built in Slovakia, but most of them for production of raw materials and semi-finished products, which were then finished in Czech. If there was a higher demand for castings, it was not covered by expanding of existing foundries, but by import - e.g. from Český Liberec to Brezno, even when in near Hronec was a foundry. It took almost 20 years after the Federation creation since the foundry production was on expansion in Slovakia again. The moving of production of die pressure machines to Snina, also a start of greater production of aluminium castings with export to Czech (for Avia, Tatra or Zetor), but mainly military industry (in Prakovce there were a special moulding lines for a tank treads segments) significantly helped.

Development until year 2000

In the 80ties, in the former Czechoslovakia 800 000 tons of castings was poured, more than 70% was made of grey cast iron. Crushing majority of production was for a military industry, in 1989 we were even one of the world greatest producers of weapons. For ilustration in 1989 Závody ťažkého strojárstva (ZTS) made a products for cost of 8,4 billion euro and were employing a little over 87 thousand people. If we were producing these volumes of weapons today, Slovakia could theoretically compete even with Russia, which in 2014 officially exported weapons in cost of 13 billion euro to the world.

Figure 1. Military industry took a significant place in Slovak foundry development

Almost 4 thousand tanks T-55 (Figure 1.) were exported to countries like Hungary, Romania, India, Morocco, Syria, Egypt and today not anymore existing German democratic republic and Yugoslavia (therefore into lands of today´s Croatia). In times when Slovakia was falling apart with Czech (in 1993) from the military industry only torso was left and most of Slovak foundries had to find a different customer. It also came to a significant restriction of export to civil sector of Czech Republic and a loss of these two large sales outlets had reflected very negatively. It came to a sudden decrease of production, stop of investing into foundry industry and almost third of foundries were even closed. A significant moment in 90ties was privatizing of most plants producing castings, mostly by their own management. Despite of initial decrease of production, until the end of last century a production of castings was stabilized and even progressively increased through the export into the West European countries. Gray cast iron and ductile iron castings were exported mainly into the Italy and Germany, aluminium castings were exported to the markets in Germany, France, Denmark etc. Slovak owners were successfully developing foundries by themself and through the increasing production volumes were investing into the modern and efficient equipment, which further granted them a good competitive pros needed for export. Despite all of this the production at the end of century started to stagnate (see Table 1. and Figure 2.), because competition from Germany and other West European countries started to produce a part of castings in countries of Eastern Europe and simple product from grey cast iron were imported from China. Until 2000 these negative aspects caused a decrease of castings production in all technologies the aluminium castings including.

Table 1. Production of castings in ton/year between years 1993 and 2000 [1]

	1993	1994	1995	1996	1997	1998	1999	2000
Grey cast iron castings	34 765	37 938	42 224	44 678	38 683	37 260	39 000	39 447
Ductile cast iron castings	1 834	1 437	3 034	3 926	3 836	3 594	2 375	2 147
Steel castings	7 546	7 146	9 588	9 700	8 241	7 140	5 125	2 024
Investment casting							95	98
Non-ferrous castings	22 776	21 243	21 363	21 350	15 269	13 398	14 517	13 925
Casting in all	**66 921**	**67 764**	**76 209**	**79 654**	**66 029**	**61 392**	**61 112**	**57 641**

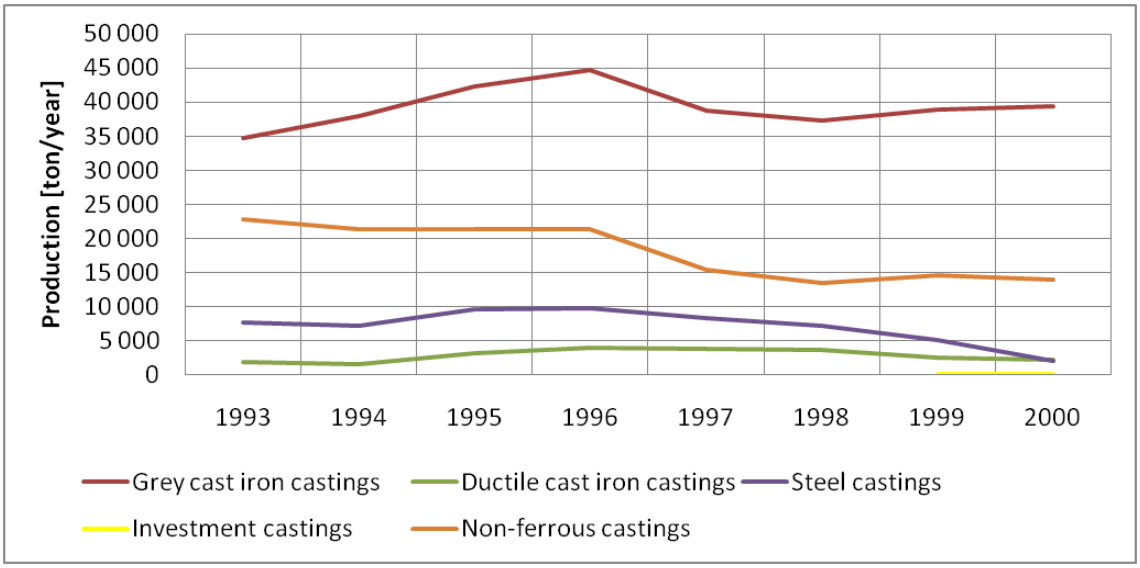

Figure 2. Graph of production development in 1993 – 2000

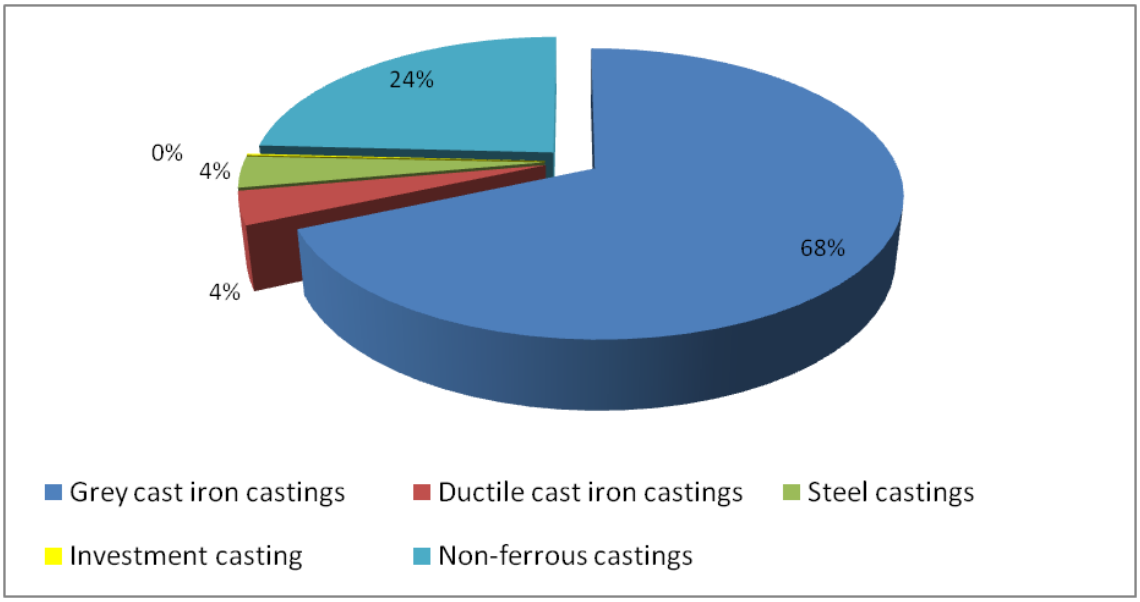

Figure 3. Graph of production in year 2000

Situation in 21st century

The beginning of 21st century was for Slovak foundries guided by a surprisingly high increase of production. After year 2000 an expanding industry of European countries became an acquisitive customer of Slovak castings. In first five years of this century practically 70-90% of produced castings were exported from Slovak foundries. Development of automotive production in Slovakia became such a strong customer, that in recent years, more foreign producers are incoming to Slovakia. Conditions of trade co-operation in the export were improved by Slovakia entering the EU and later Eurozone! It wasn´t a technology of grey cast iron though, but the Slovak foundries succeeded to get a ductile iron cast markets. In first five years of new century the increase of this commodity was over 600%! (Table 2. and Figure 4).

Table 2. Production of castings in ton/year after 2000 [1]

	2000	2004	2008	2009	2010	2012	2014	2015
Grey cast iron castings	39 447	40 850	34 852	22 450	24 500	25 310	25 200	24 950
Ductile cast iron castings	2 147	14 010	16 230	10 480	13 120	14 800	15 400	17 520
Steel castings	2 024	5 820	6 450	3 200	3 510	3 840	3 920	4 050
Investment casting	98	102	98	100	110	118	115	124
Non-ferrous castings	13 925	34 260	36 500	38 250	43 580	43 880	44 850	48 560
Casting in all	**57 641**	**95 042**	**94 130**	**74 480**	**84 820**	**87 948**	**89 485**	**95 204**

It managed to obtain also foreign markets for steel castings and double their production. Excellent outcome had managed also in production of aluminium alloy castings, where almost tripled production compared to the end of 20th century was achieved. However, this production segment was not about new foreign markets, but about the coming of multinational corporations producing castings to the Slovak foundries. Their ownership of Slovak foundries was initiated mainly by development of automotive industry in Slovak ground. Besides the Volkswagen assembly plant, other car factories were opened - Peugeot and later KIA. Practically the whole volume of growing production of castings from aluminium alloys, made by both pressure die casting and mould casting, is already not exported, but stays in Slovakia and is supplying directly Slovak automobile plant branches. Automotive production development (last year more than million cars was made in Slovakia) in Slovakia became such a strong customer, that in recent years, other foreign producers are coming and building new and modern plants (latest Spain company Funderia Condals). Recently the British car factory Jaguar Land Rover has started building a new car assembling plant in Slovakia.

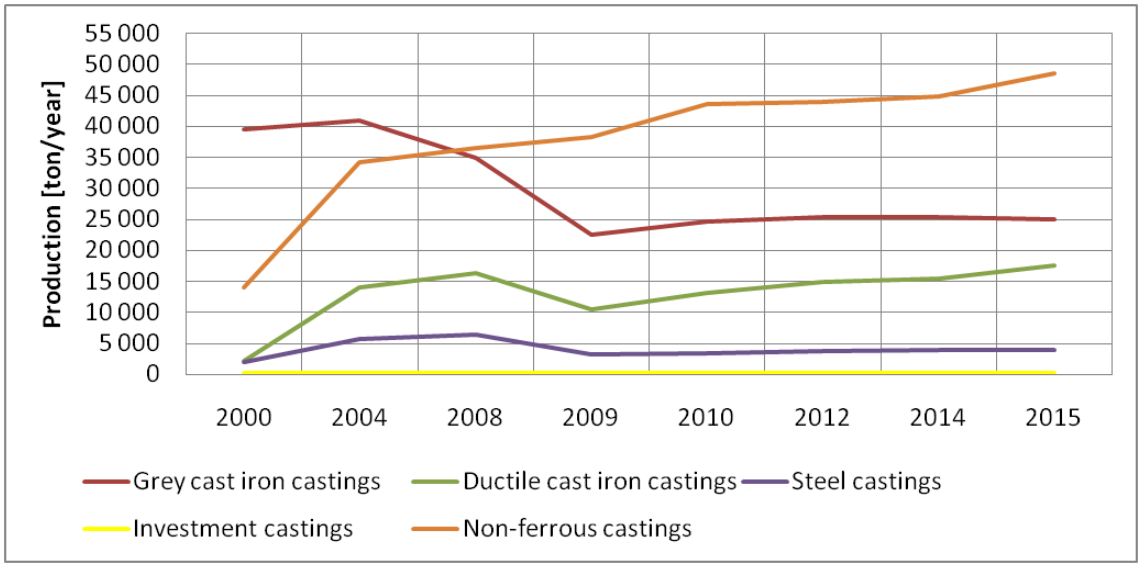

Figure 4. Graph of production development since 2000

Promising start of castings production increase was disrupted by year of crisis 2009 in Slovakia too, which had a significant impact on production. Mainly the production of iron alloys castings was decreased. Production of castings from aluminium was kept in mild increase, considering minimal impact of crisis on automotive industry.

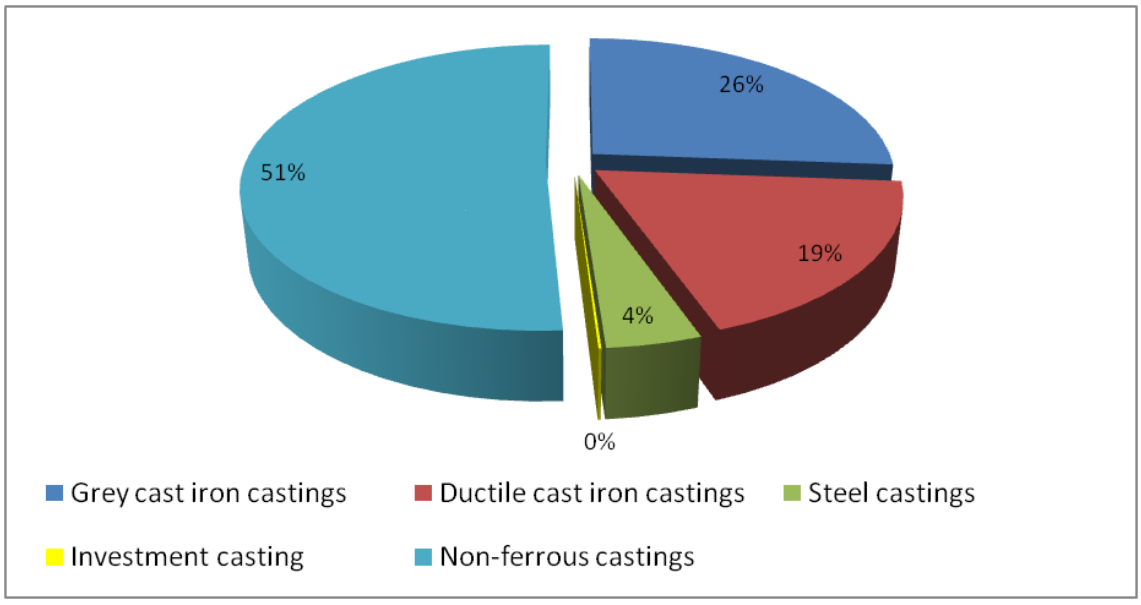

Figure 5. Graph of production in year 2015

CONCLUSIONS

Nowadays, there are 16 foundries producing castings from iron alloys, 27 foundries producing castings from aluminium alloys and 7 foundries producing castings from other non-ferrous metals. In the range of product composition the importance of gray cast iron

had decreased and more than 50% of castings are made from aluminium alloys. Foundries in Slovakia are on a different level, regarding a technology of production and also a volume of production. They are able to manufacture castings from small-scaled castings from zinc or brass (100 grams) to castings over 500 kg from gray cast iron. In total, foundries were mostly greatly upgraded or more precisely automated and they are able to achieve high productivity with a small amount of employees. On average foundries are employing 126 of employees, but it depends on the volume of production from 10 to more than 300 people. Salaries in the sector are significantly varying and depend on a size of foundry, a nature of work and the differences can be in hundreds of euro. The average salary is around 880 €. Production of castings in Slovakia, if there will be no decrease in automotive industry or another crisis, is growing and perspective. Also foundries started developing of machining castings to a final shape and dimensions and are delivering them straight to assembling in machinery.

REFERENCES

[1] Association of Foundries and Forges of Slovakia

15th INTERNATIONAL FOUNDRYMEN CONFERENCE
INNOVATION – The foundation of competitive casting production
Opatija, May 11th-13th, 2016
http://www.simet.hr/~foundry/

INFLUENCE OF MEDIUM AND MICROSTRUCTURE ON CORROSION RATE OF FRICTION WELDED COPPER AND ALUMINIUM ALLOY

UTJECAJ MEDIJA I MIKROSTRUKTURE NA BRZINU KOROZIJE BAKRENE I ALUMINIJSKE LEGURE ZAVARENE TRENJEM

A. Begić Hadžipašić, Z. Zovko Brodarac and D. Mašinović

University of Zagreb Faculty od Metallurgy, Sisak, Croatia

Oral presentation
Original scientific paper

Abstract

In this work, the influence of the media and microstructure on the corrosion rate of copper and aluminium alloy joined by friction welding process are shown. Metallographic investigations indicate a significant effect of parent materials purity. Impurities with the significant impact at particular alloy as an integral connection part, can deteriorate the electrical properties, as well as stimulate electrochemical corrosion. Electrochemical measurements have shown that corrosion rate of aluminium and copper was lower in the medium of artificial rain, rather than in the medium of 3.5% NaCl. Also, the order of the material tested according to the resistance to atmospheric corrosion varies depending on the test medium. Thus, Al-alloy showed the minimum corrosion rate in the medium of 3.5% NaCl, and Cu-alloy showed the minimum corrosion rate in the medium of artificial rain. In both media, the maximum corrosion rate showed a Cu-Al connection, i.e., the area of the friction weld.

***Keywords**: corrosion resistance, copper, aluminium, friction welding, microstructure*

*Corresponding author (e-mail address): *begic@simet.hr*

Sažetak

U ovom radu ispitan je utjecaj medija i mikrostukture na brzinu korozije bakrene i aluminijske legure zavarene trenjem. Metalografska ispitivanja ukazuju na značajan utjecaj čistoće osnovnih materijala. Primjese sa značajnim utjecajem na pojedinu leguru – kao sastavni dio spoja mogu pogoršati električna svojstva, ali i uzrokovati elektrokemijsku koroziju. Elektrokemijskim mjerenjima je ustanovljeno da je brzina korozije aluminija i bakra manja u mediju umjetne kiše, nego u mediju 3,5 % NaCl. Također, poredak materijala prema otpornosti na ispitanu atmosfersku koroziju se razlikuje ovisno o ispitnom mediju. Tako je najmanju brzinu korozije u mediju 3,5 % NaCl pokazala Al-legura, dok je u mediju umjetne kiše najmanju brzinu korozije pokazala Cu-legura. U oba medija, najveću brzinu korozije je pokazao Al-Cu spoj, tj. područje zavara trenjem.

***Ključne riječi:** korozijska otpornost, bakar, aluminij, zavarivanje trenjem, mikrostruktura*

UVOD

Za izradu elektrotehničkih proizvoda na raspolaganju su brojni materijali koji se razlikuju po sastavu i podrijetlu: osnovni kemijski elementi, kemijski spojevi, legure te umjetni spojevi i složeni materijali. Vodljivi materijali se mogu podijeliti prema više kriterija: veličini električne provodnosti, sastavu (čiste metale i legure), položaju u periodnom sustavu elemenata (alkalni i zemnoalkalni), strukturi elektronskog omotača, boji (crni i obojani), temperaturi taljenja (teško i lako taljivi), primjeni (vodiči, električni kontakti, elektrode) [1]. Prema vrsti nositelja naboja vodljivi materijali se dijele na:

- vodiče prvog reda (metali i legure)
- vodiče drugog reda (elektroliti).

Kod vodiča prvog reda slobodni elektroni su nositelji naboja. Kod elektrolita ioni su nositelji naboja. Vodiči prvog reda se uglavnom koriste u polikristalnom stanju. Mehanička svojstva ovih materijala su bitno određena mehaničkom i toplinskom obradom. Vodiči prvog reda dijele se na metale velike električne provodljivosti, metale male električne provodljivosti, specijalne vodljive materijale i otporne legure [1].

Metali velike električne provodljivosti (bakar, aluminij) imaju najmanju električnu otpornost ($\rho \sim 10^{-8} \Omega m$) i zato se koriste za izradu vodiča.

U elektrotehničkim spojevima najčešće se upotrebljavaju meke bakrene i gnječive aluminijske legure visoke čistoće. Usporedna svojstva bakra i aluminija prikazana su tablicom 1.

Tablica 1. Karakteristična svojstva bakra i aluminija [2, 3]

Svojstvo / Materijal	Cu	Al
Specifična masa, kg/dm^3	8,9	2,7
Atomska težina, g/cm^3	63,57	26,98
Redni broj	29	13
Električna provodljivost, Sm/mm^2	56-59	34,8-38
Temperaturni koeficijent istezanja, K^{-1}	17x10^{-6}	24x10^{-6}
Talište, °C	1083	657
Vrelište, °C	2300	2270
Toplinska vodljivost, W/Km	401	209,3
Latentna toplina taljenja, kWs/kg	211,5	396
Temperaturni koeficijent otpora, K^{-1}	43x10^{-3}	4,2x10^{-3}

Usporedni prikaz ovisnosti električne otpornosti i koeficijenta linearnog širenja bakra i aluminija od temperature prikazana je slikom 1 [4].

Materijal	Cu	Al
a)	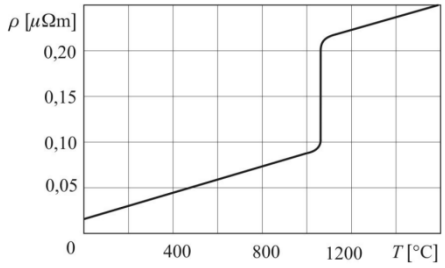	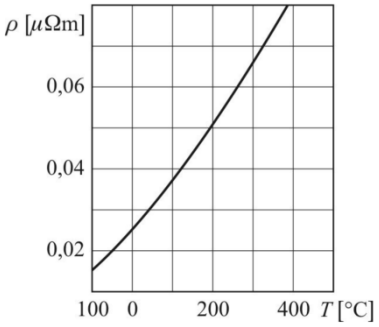
b)	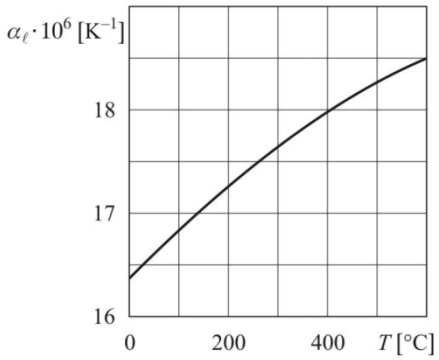	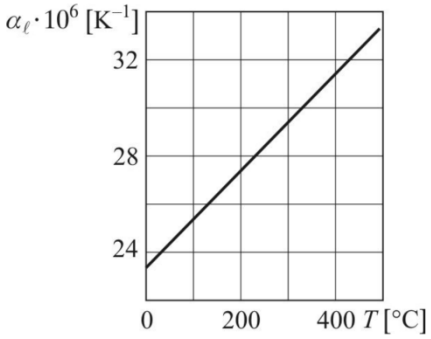

Slika 1. Utjecaj temperature na svojstva bakra i aluminija [4]:
a) električna otpornost
b) koeficijent linearnog širenja

Bakar je najbolji vodič električne struje i topline. Električna provodnost ovisi o postotku primjesa i nečistoća te o stupnju plastične deformacije i rekristalizicije tijekom proizvodnje [5-7].

Kisik vezan u okside Cu_2O (0,02-0,04 %) povoljno utječe na vodljivost bakra jer na sebe veže druge primjese. Međutim, veće količine kisika su štetne, stoga se meka legura bakra proizvodi taljenjem u CO_2 atmosferi. Elektrolitski bakar je najčišći bakar, normom je definirana vodljivost od 58 Sm/mm^2 kao 100% vodljivost. Bakar na zraku oksidira i prekriva se patinom koja ga štiti od daljnje oksidacije, što čini osnovu njegove otpornosti na koroziju. Oksidacija se ubrzava pri višim temperaturama (iznad 400 °C). Specifičnost lijevane teksture je grubo i neorijentirano zrno s oksidima izlučenim po granicama zrna (Cu_2O). Lijevana mikrostruktura se hladnim valjanjem prevodi u sitnozrnatu, usmjerenu mikrostrukturu s povećanom čvrstoćom i tvrdoćom, ali smanjenom vodljivosti. Toplim valjanjem dolazi do rekristalizacije (200-500 °C) kojom se anulira usmjerenost zrna uz još uvijek prisutne okside. Takva mikrostruktura omogućava najbolji odnos vodljivosti i istezljivosti, a čvrstoća i tvrdoća se smanjuju [7]. Elementi poput Cd, Zn i Ag imaju mali utjecaj, Ni, Sn i Al srednji, dok Be, Cr, As, Si i Co, Fe, P imaju veliki utjecaj na električnu otpornost bakra [4].

Dobra svojstva aluminija i njegovih legura kao vodljivog materijala su: visoka električna i toplinska vodljivost, mala specifična masa, dobra tehnološka i mehanička svojstva, kemijska

postojanost i otpornost na električni luk. Vodljivost aluminija najviše ovisi o njegovoj čistoći. U elektrotehnici je standardiziran aluminij čistoće 99,5 % dok je ostatak ispunjen primjesama [8]. Primjese elemenata poput Ni, Si, Fe i Zn imaju mali utjecaj na električnu vodljivost, Cu, Ag i Mg imaju srednji utjecaj, dok Ti, V, Mn i Cr imaju veliki utjecaj na električnu vodljivost, stoga se ograničavaju na ukupan sadržaj od 0,03 % [2].

Najveća čistoća aluminija koja se postiže u praksi je 99,99 % (rafinal) koja se koristi za obloge kondenzatora [8]. Aluminij je otporan prema koroziji jer se prekriva tankom opnom oksida na početku oksidacije (Al_2O_3). Ovaj sloj predstavlja zaštitni sloj koji može stvarati poteškoće pri spajanju vodova u elektrotehnici. Otporan je na kiseline, ali ne i na morsku vodu. Elektrotehnički poluproizvodi od aluminija su žice, profili, cijevi, trake, limovi i folija. Ovi poluproizvodi se proizvode valjanjem ili prešanjem, odnosno dubokim izvlačenjem. Primjena aluminija u elektrotehnici je velika. Aluminij i njegove legure primjenjuju se na onim mjestima gdje je kritični zahtjev na masu vodiča (npr. instalacije u zrakoplovima). Aluminij zauzima prvo mjesto u primjeni za zračne vodove.

Osnovni kriteriji pri izboru materijala za ugradnju u elektrotehnički proizvod su funkcionalni (električki, magnetski, izolacijski) zahtjevi, mogućnosti obrade te ponašanje materijala u zadanim tehnoklimatskim uvjetima. Izraziti utjecaj na svojstva materijala u zadanim uvjetima ima kemijski sastav, odnosno čistoća materijala. Usporedan utjecaj primjesa na električna svojstva bakra i aluminija prikazan je slikom 2.

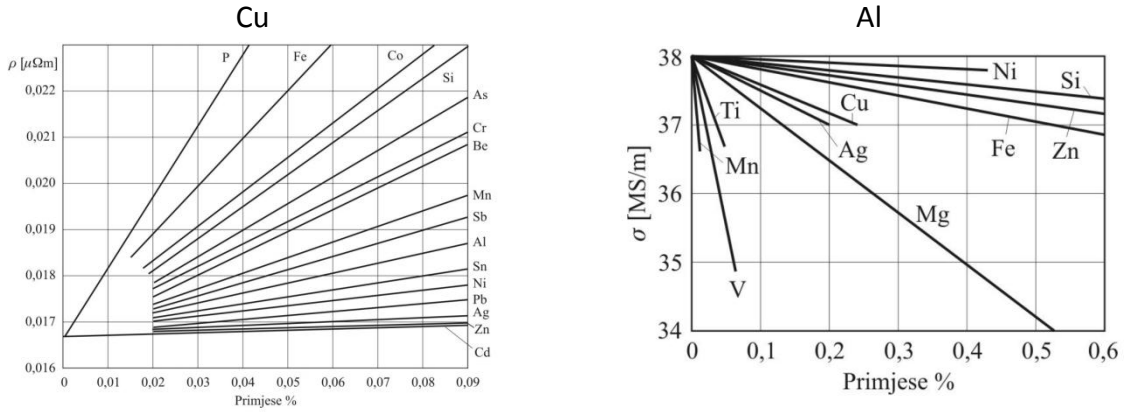

Slika 2. Utjecaj primjesa na:
a) električnu otpornost bakra [4]
b) električnu vodljivost aluminija [2]

Spajanje aluminija i bakra uobičajenim metodama zavarivanja nije dopušteno jer se u prisustvu vlage stvara galvanski članak koji uzrokuje elektrokemijsku koroziju, pri kojoj aluminij kao anoda nestaje.

U ovom je radu ispitana Cu/Al spojnica za primjenu u dalekovodima. Proizvod čini spoj legure mekog bakra Cu-ETP (CW004A) i gnječive aluminijske legure EN AW-1050A. Specifičnost

spojeva visokovodljivih legura je potencijalna opasnost od nastajanja galvanskih članaka. Slijedom navedenog je za spajanje primijenjena metoda zavarivanja trenjem (*engl. Friction welding, FRW*). Proces FRW je tehnika zavarivanja u čvrstom stanju u kojemu zavar nastaje pod utjecajem tlačne sile na kontaktu između radnih komada, koji se rotiraju ili gibaju relativno u odnosu jedan prema drugome i tako stvaraju potrebnu toplinu za nastajanje zavarenog spoja. Također, tlačnom silom i rotacijom, odnosno, relativnim gibanjem radnih komada miješa se materijal radnih komada na dodirnim površinama.

Cilj ovog istraživanja bio je utvrditi mikrostrukturna svojstva materijala bakrene i aluminijske legure te njihova spoja i korelirati ih s utjecajem simuliranih tehnoklimatskih uvjeta u mediju umjetne kiše i 3,5% otopine NaCl.

MATERIJALI I METODE

Materijali

U ovom je radu ispitana Cu/Al spojnica za primjenu u dalekovodima. Proizvod čini spoj legure mekog bakra Cu-ETP (CW004A) i gnječive aluminijske legure EN AW-1050A, pri čemu je za spajanje primijenjena metoda zavarivanja trenjem (*engl. Friction welding, FRW*).
Ispitani su kemijski sastavi meke bakrene legure Cu-ETP (CW004A) sukladno normi EN 13601 i gnječive aluminijske legure EN AW-1050A sukladno normi EN 573-3 te prikazani tablicom 2.

Tablica 2. Kemijski sastav ispitanih legura

Kemijski element/%	Cu-legura	Al-legura
Si	-	0,11
Fe	-	0,28
Cu	99,900	0,030
Mn	-	0,022
Mg	-	0,003
Zn	-	0,003
Ti	-	0,021
Pb	-	0,001
Cd	-	0,0002
Hg	-	0,0003
Pb+Cd+Hg+Cr6+	-	0,0018
P	0,001	-
Al	-	99,51

Mehanička svojstva bakrene i aluminijske legure navedena su u tablici 3.

Tablica 3. Mehanička svojstva ispitanih legura

Materijal	Cu-legura	Al-legura
Granica razvlačenja $R_{p\,0,2}$ /Nmm^{-2}	58,8	107,0
Vlačna čvrstoća R_m / Nmm^{-2}	235,5	100,5
Istezljivost A / %	50,0	23,9
Tvrdoća HB / Min:30	51,0	36,6

Metode

Metalografska ispitivanja

Metalografska ispitivanja provedena su na uzorcima prije simulacije specifičnih tehnoklimatskih uvjeta. Uzorci su pripremljeni na standardni način brušenjem, poliranjem i nagrizanjem. Metalografska analiza provedena je na svjetlosnom mikroskopu Olympus GX51 opremljenom digitalnom kamerom Olympus DP70 i programskom podrškom za analizu slike Analysis® Materials ResearchLab. Mikrostrukturna ispitivanja provedena su na pretražnom elektronskom mikroskopu TescanVega TS 5136 MM. Pretražni elektronski mikroskop opremljen je Bruker energijskim disperzivnim spektrometrom koji omogućava uvid u distribuciju kemijskih elemenata na određenoj površini te analizu kemijskog sastava u određenoj točki.

Elektrokemijska ispitivanja

Elektrokemijska priroda procesa korozije omogućuje primjenu različitih elektrokemijskih mjernih tehnika za određivanje intenziteta korozije. Razlikuju se tehnike s istosmjernom strujom (DC tehnike) i tehnike s izmjeničnom strujom (AC tehnike) [9,10]. Pri elektrokemijskim ispitivanjima procesa korozije upotrebljavaju se polarizacijske metode mjerenja, potenciostatička i galvanostatička polarizacija. Cilj mjerenja je snimanje krivulja polarizacije struja-napon te na temelju anodnih i katodnih krivulja dobivanje slike o korozijskom ponašanju određenog materijala u određenom mediju. Na potenciostatičkoj polarizaciji zasniva se više metoda za određivanje brzine korozije, kao što su Tafelova ekstrapolacija i određivanje polarizacijskog otpora. U ovom radu izvedena je potenciodinamička polarizacija u području potencijala od -250 mV do +250 mV vsE_{corr}, uz brzinu promjene potencijala od 1mV/s, a korozijski parametri su određeni pomoću softvera PowerCorr^{TM}primjenom Tafelove metode ekstrapolacije i Faradayevih zakona [11]. Prije svakog mjerenja potenciodinamičke polarizacije pokrenuta je stabilizacija potencijala kod otvorenog strujnog kruga E_{ocp}, pomoću računalom upravljanog potenciostata/galvanostata („Parstat 2273“) u trajanju od 30 minuta. Elektrokemijska ispitivanja izvedena su pomoću uzoraka očišćenih brusnim papirima gradacije No. 100, 220, 320, 400, 500 i 600, ispranih u destiliranoj vodi i odmašćenih u etanolu. Uzorak se kao radna elektroda postavljao u ispitivani medij u troelektrodnoj staklenoj ćeliji u kojoj su se nalazile zasićena kalomel elektroda (eng. *SaturatedCalomelElectrode,* SCE), kao referentna elektroda i Pt-elektroda kao protuelektroda, slika 3 [11, 12]. Uzorci bakra, aluminija i Cu/Al spoja ispitani su pri sobnoj temperaturi u mediju 3,5 % NaCl i u mediju umjetne kiše (0,2 g L^{-1} Na_2SO_4 + 0,2 g L^{-1} $NaHCO_3$),

kako bi se dobili podaci o korozijskoj otpornosti ispitanih materijala u slučaju primjene u primorskom i kontinentalnom području.

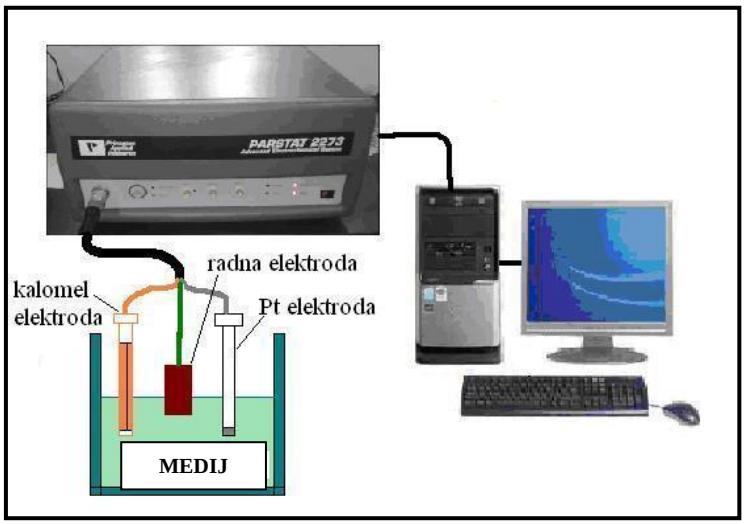

Slika 3. Shema aparature za elektrokemijska mjerenja

REZULTATI I RASPRAVA

Metalografska analiza ukazuje na ispravno vođenu metodu zavarivanja trenjem legura bakra i aluminija. Ispitivanjem svjetlosnom mikroskopijom nije uočeno miješanje spoja već jasno izražena granica Cu/Al spoja kako je prikazano slikom 5.
Mikrostrukture pojedinačnih legura i Al/Cu spoja prikazane su usporedno pri povećanjima od 500X i 1000X na slici 4.

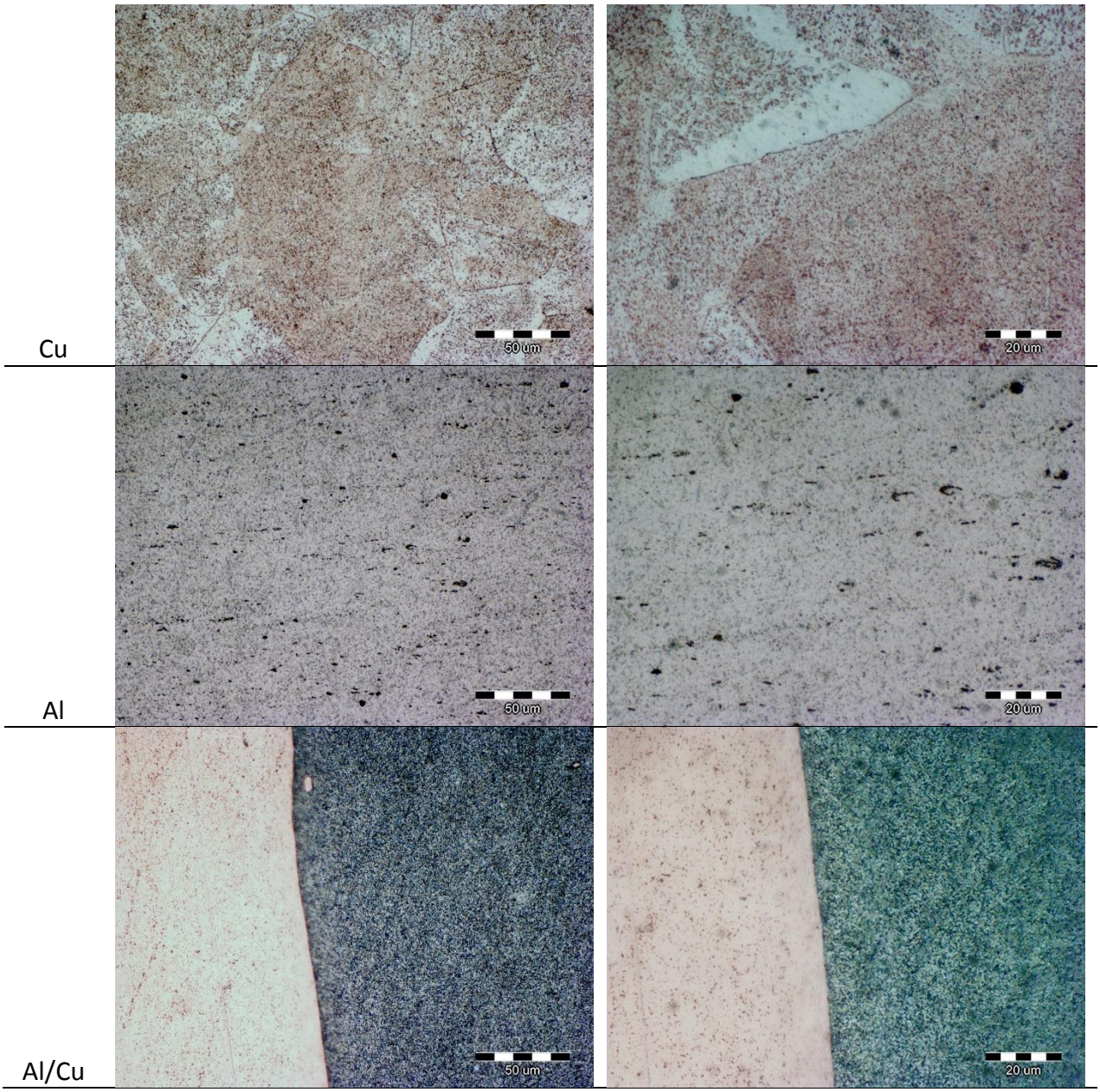

Slika 4. Mikrostruktura sastavnih komponenti i Al/Cu spoja

Uvid u mikrostrukture ukazuje na leguru bakra visoke čistoće s grubozrnatom neusmjerenim zrnima s ravnomjerno raspoređenim precipitatima unutar i po granicama zrna. Legura aluminija visoke je čistoće mikrostrukture s usmjerenim precipitatima. Spoj Al i Cu legure ne otkriva promjene u materijalu u rubnoj zoni. Granica materijala je precizna i bez precipitata. Pretražna elektronska mikroskopija spoja Cu/Al prikazana je slikom 5.

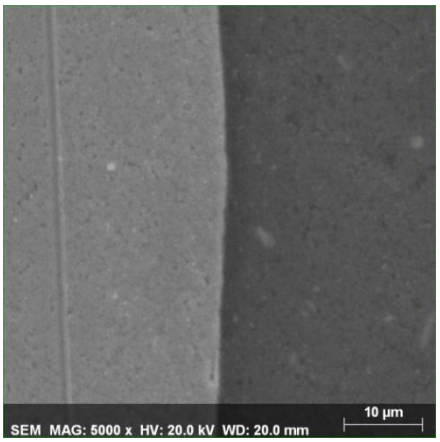
SEM MAG: 5000 x HV: 20.0 kV WD: 20.0 mm
10 µm

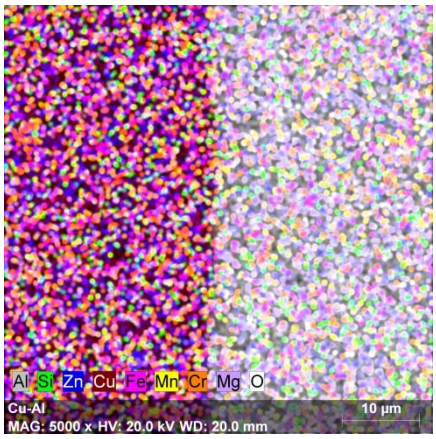
Al Si Zn Cu Fe Mn Cr Mg O
Cu-Al
MAG: 5000 x HV: 20.0 kV WD: 20.0 mm
10 µm

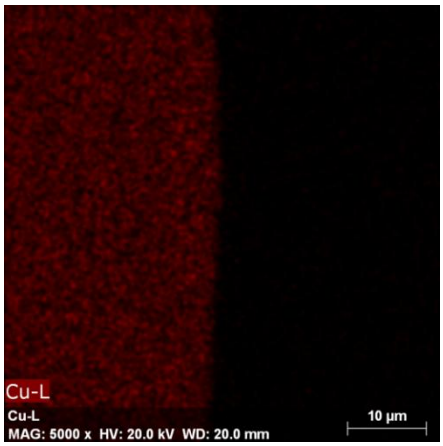
Cu-L
Cu-L
MAG: 5000 x HV: 20.0 kV WD: 20.0 mm
10 µm

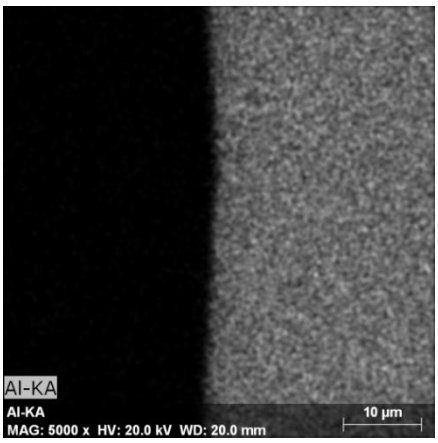
Al-KA
Al-KA
MAG: 5000 x HV: 20.0 kV WD: 20.0 mm
10 µm

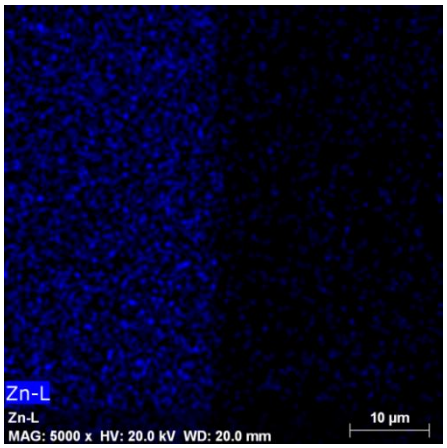
Zn-L
Zn-L
MAG: 5000 x HV: 20.0 kV WD: 20.0 mm
10 µm

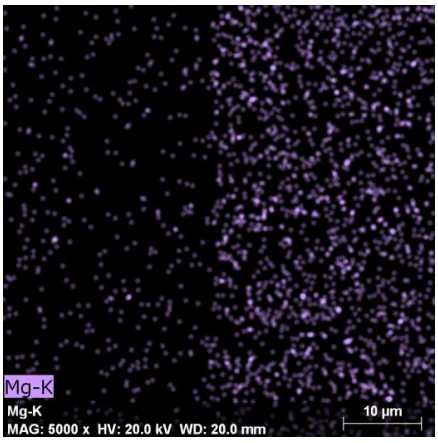
Mg-K
Mg-K
MAG: 5000 x HV: 20.0 kV WD: 20.0 mm
10 µm

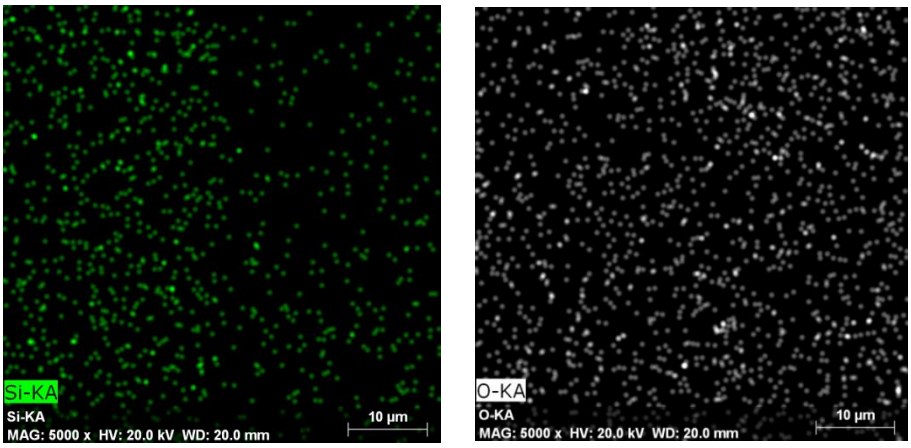

Slika 5. Maping analiza spoja legure Cu/Al

Maping analiza spoja ukazuje na visoki udio ravnomjerno raspoređenog Zn i nešto veći udio Si u bakrenoj leguri. Aluminijska legura sadrži veći udio ravnomjerno raspoređenog Mg. Kisik je podjednako zastupljen u obje legure. Granica spoja je oštra i ravnomjerna što upućuje na ispravno vođen postupak zavarivanja trenjem kojim nije došlo do miješanja materijala.
Linijska analiza spoja Cu/Al legure prikazana je slikom 6.

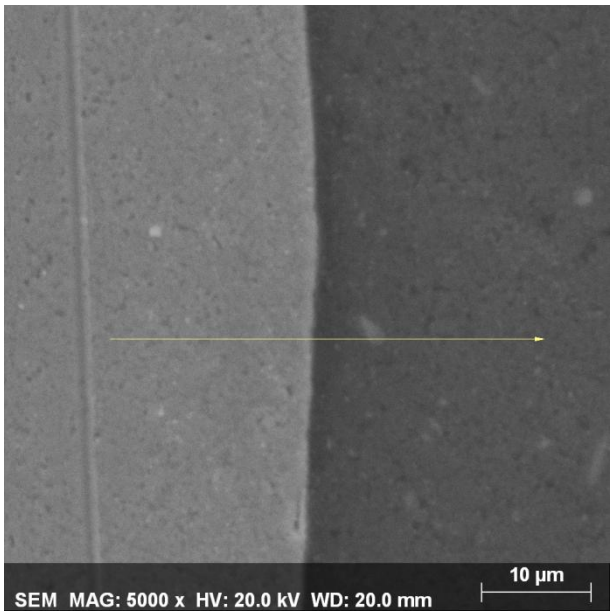

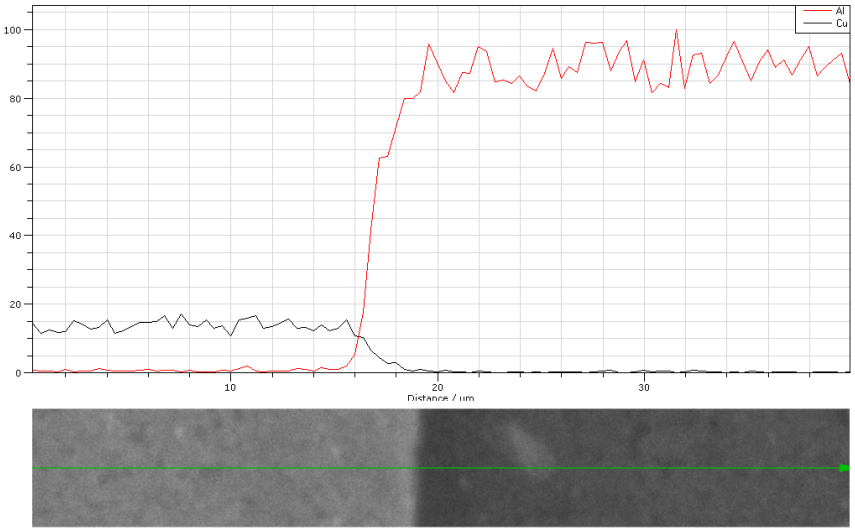

Slika 6. Linijska analiza spoja Cu/Al

Linijska analiza ukazuje na jasnu granicu spoja i nemiješanje materijala u zoni zavara.
Točkasta analiza provedena je na oba materijala radi utvrđivanja prisustva primjesa u osnovnom materijalu, kako je prikazano slikom 7.

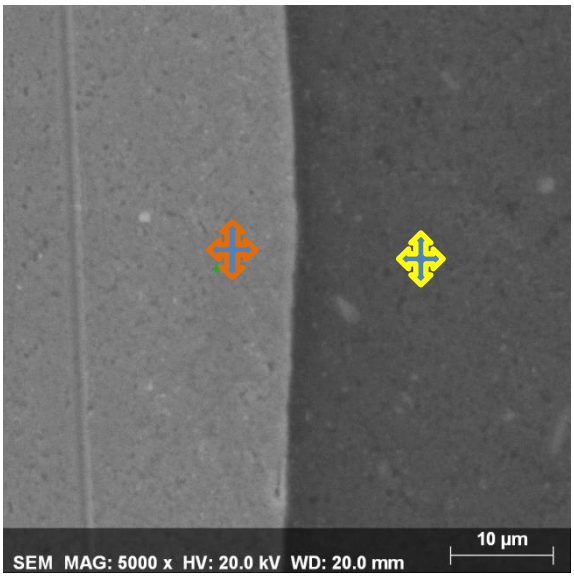

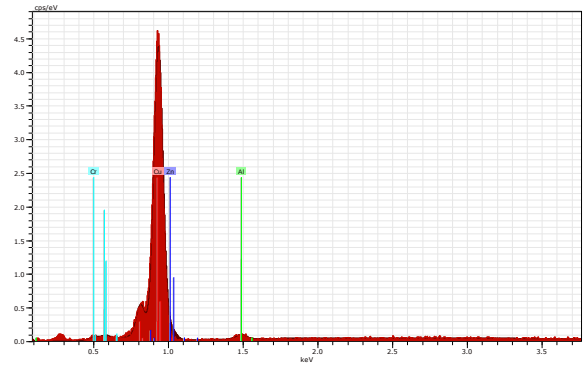

Element	C norm. [wt.%]	C Atom [at.%]
Cu	95,04	93,28
Al	1,29	2,99
Zn	2,71	2,58
Cr	0,96	1,15

a)

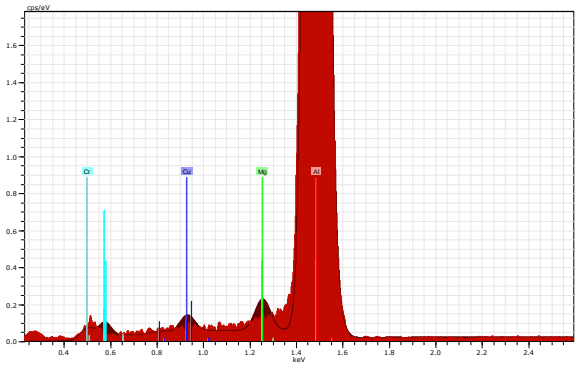

Element	C norm. [wt.%]	C Atom [at.%]
Al	96,50	97,63
Mg	1,15	1,29
Cu	1,65	0,71
Cr	0,69	0,36

b)

Slika 7. Točkasta analiza legura bakra (a) i aluminija (b)

Legure su visoke čistoće. Legura bakra sadrži 95,04 mas.%Cu, dok legura aluminija sadrži 97,63 mas.% Al. Točkasta analiza materijala spoja ukazuje na značajni udio primjesa cinka, aluminija i kroma u leguri bakra. Krom spada u skupinu najutjecajnijih elemenata na povećanje električne otpornost bakra, dok aluminij ima nešto manji utjecaj. Legura aluminija otkriva značajan udio magnezija, bakra i kroma. Magnezij i bakar imaju srednji utjecaj, dok krom značajno pogoršava električnu vodljivost aluminija.

Nakon mjerenja potencijala otvorenog strujnog kruga E_{ocp}, a u svrhu određivanja sljedećih korozijskih parametara: korozijskog potencijala E_{corr}, gustoće struje korozije I_{corr}, anodnog nagiba b_a, katodnog nagiba b_c i brzine korozije v_{corr} izvedena je potenciodinamička polarizacija u području potencijala od −250 mV do +250 mV vs E_{corr}u mediju 3,5 % NaCl i mediju umjetne kiše. Ovisnosti potencijala kod otvorenog strujnog kruga o vremenu za ispitane materijale prikazane su na slikama 8-10. Polarizacijske krivulje ispitanih legura pri različitim temperaturama prikazane su na slikama 11-13, a korozijski parametri određeni iz polarizacijskih krivulja navedeni su u tablicama 4 i 5.

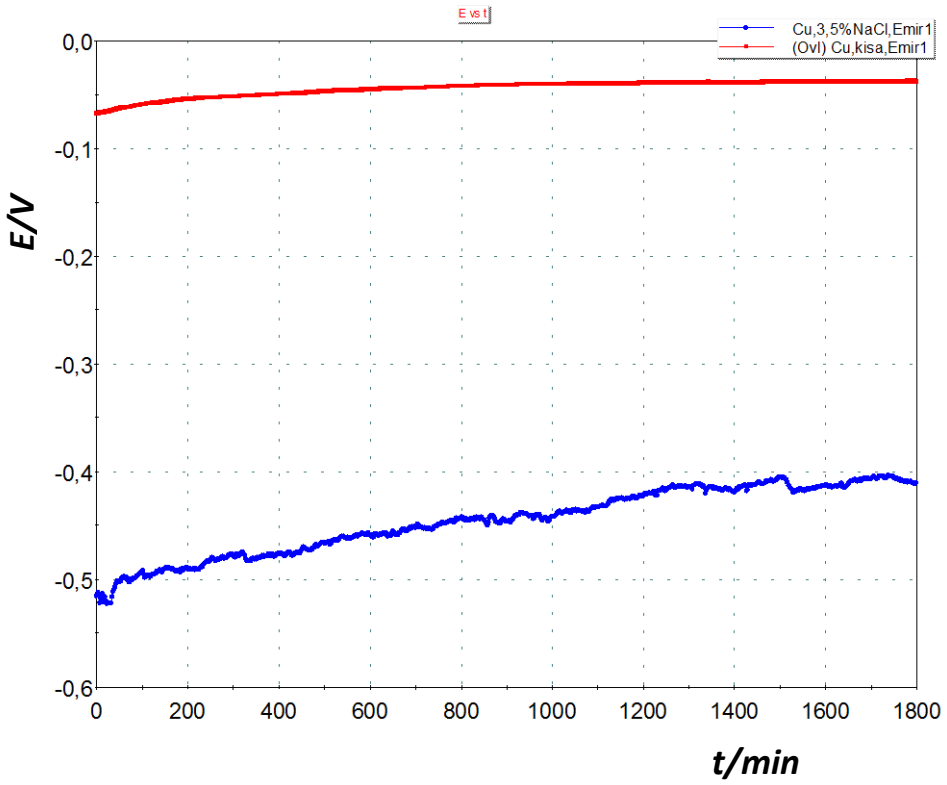

Slika 8. Ovisnost mirujućeg potencijala bakrene legure o vremenu u ispitanim medijima

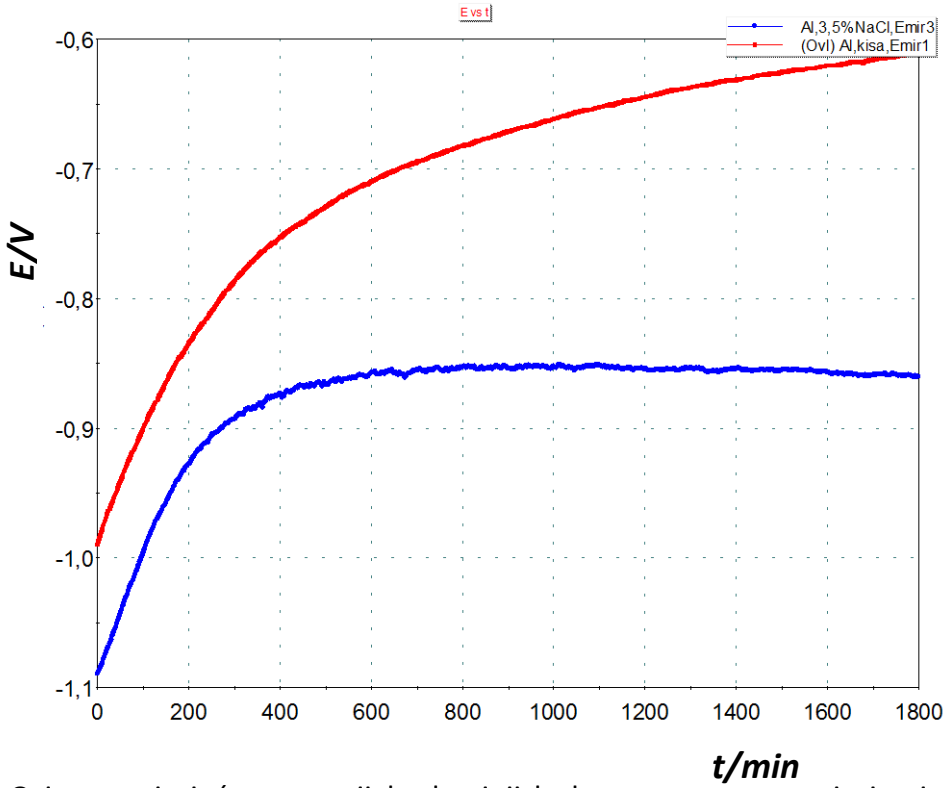

Slika 9. Ovisnost mirujućeg potencijala aluminijske legure o vremenu u ispitanim medijima

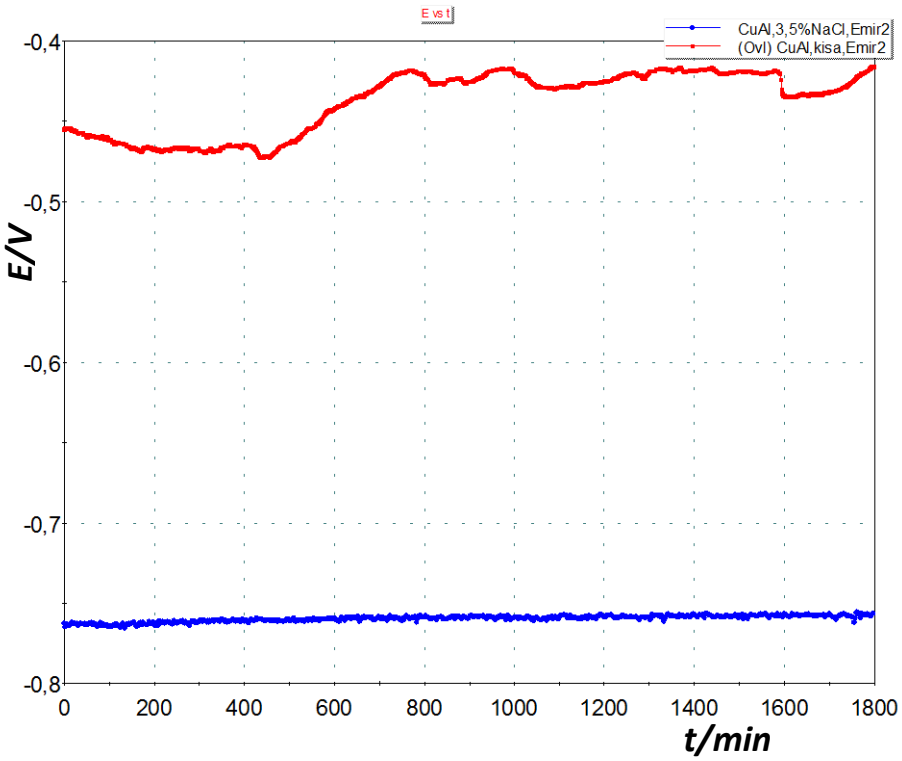

Slika 10. Ovisnost mirujućeg potencijala Al-Cu spoja o vremenu u ispitanim medijima

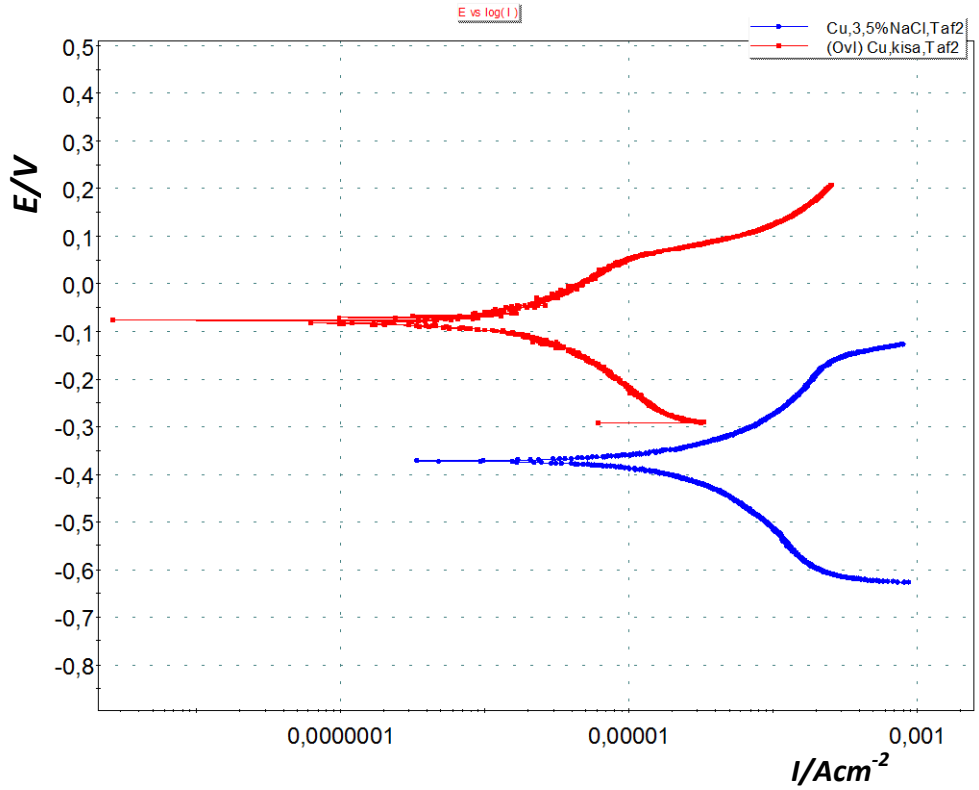

Slika 11. Polarizacijska krivulja bakrene legure u ispitanim medijima

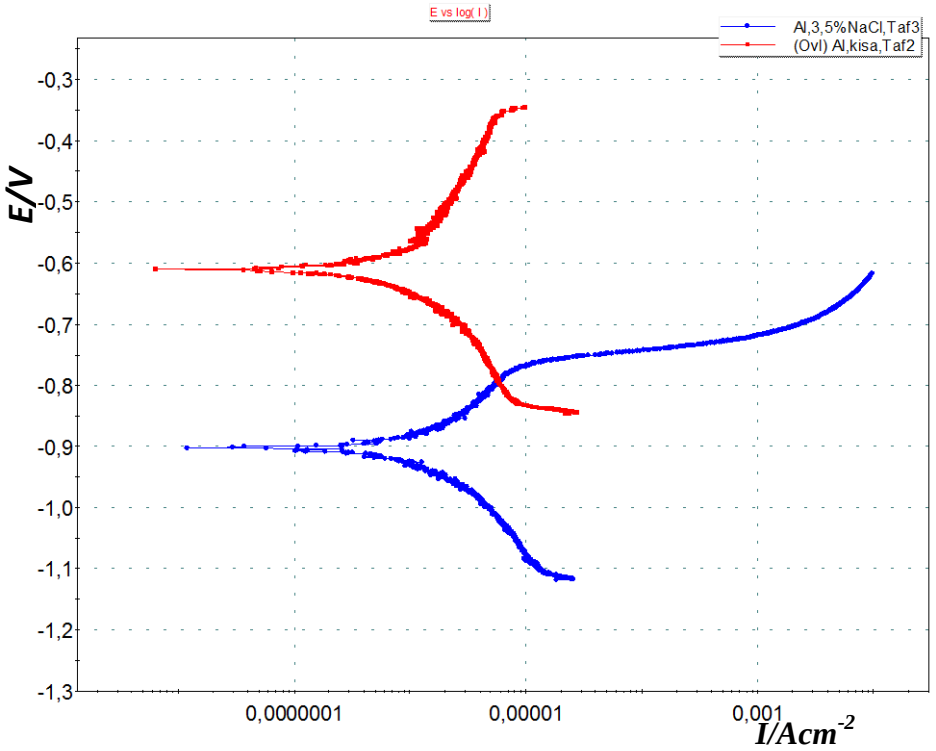

Slika 12. Polarizacijska krivulja aluminijske legure u ispitanim medijima

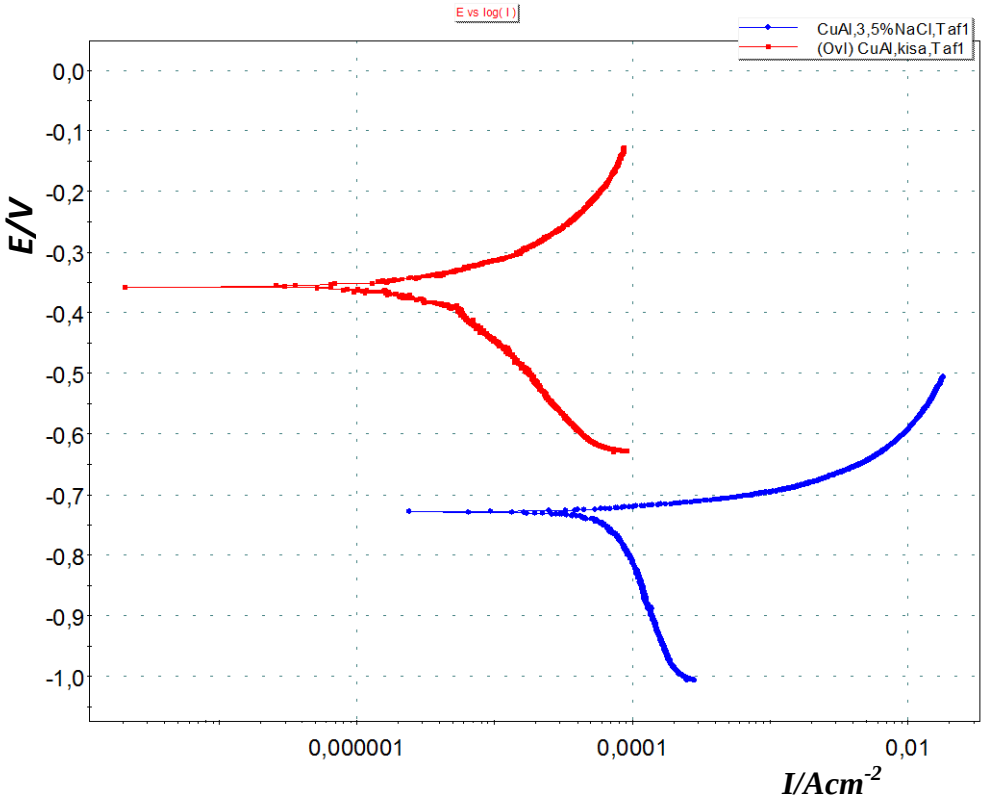

Slika 13. Polarizacijska krivulja Cu/Al spoja u ispitanim medijima

Tablica 4. Korozijski parametri ispitanih materijala u mediju 3,5 % NaCl

Materijal	***P***	***E_{corr}* vs. SCE**	***b_a***	***b_c***	***I_{corr}***	***v_{corr}***
	cm^2	mV	mV/dec	mV/dec	Acm^{-2}	mm god^{-1}
Cu-legura	1,43	-372,55	254,98	356,86	$3,29\times10^{-5}$	0,77
Al-legura	0,52	-799,70	90,58	221,31	$3,07\times10^{-6}$	0,10
Cu/Al spoj	1,92	-728,52	124,17	852,66	$5,67\times10^{-5}$	1,46

Tablica 5. Korozijski parametri ispitanih materijala u mediju umjetne kiše

Materijal	***P***	***E_{corr}* vs. SCE**	***b_a***	***b_c***	***I_{corr}***	***v_{corr}***
	cm^2	mV	mV/dec	mV/dec	Acm^{-2}	mm god^{-1}
Cu-legura	1,43	-78,45	117,74	152,54	$0,81\times10^{-6}$	0,019
Al-legura	0,52	-609,35	246,71	178,02	$1,41\times10^{-6}$	0,046
Cu/Al spoj	1,92	-357,61	200,20	393,76	$4,70\times10^{-6}$	0,121

Promatrajući slike 8-10 može se uočiti da ispitani materijali brzo postižu svoj mirujući potencijal u oba ispitana medija, tj. potencijal otvorenog strujnog kruga. Međutim, važno je za primijetiti da se potencijal kod otvorenog strujnog kruga u mediju umjetne kiše pomiče ka pozitivnijim vrijednostima, što upućuje na činjenicu da u tom mediju dolazi do stvaranja pasivnog zaštitnog sloja, koji dalje štiti materijal od korozije. Iz tog razloga, dobivene su i manje brzine korozije u mediju umjetne kiše.

Iz dobivenih rezultata prikazanih na slikama 11-13 i u tablicama 4 i 5 može se uočiti da su svi ispitani materijali pokazali najmanju korozijsku otpornost u mediju 3,5 % NaCl, o čemu svjedoče veći iznosi za brzinu korozije i gustoću brzine korozije. Također, iz rezultata je vidljivo da je u mediju 3,5 % NaCl najmanju brzinu korozije pokazala Al-legura, nju slijedi Cu-legura pa onda Cu/Al spoj. U mediju umjetne kiše situacija je malo drugačija, jer je najveću korozijsku otpornost pokazala Cu-legura pa tek onda Al-legura i Cu/Al spoj. Dobiveni rezultati su u skladu s već provedenim znanstvenim istraživanjima i ako promotrimo podatke u tablici 6, ispitani materijali su pokazali dobru otpornost na atmosfersku koroziju i stoga, mogu se primjenjivati u primorskom i kontinentalnom području [13].

Tablica 6. Prosječna brzina prodiranja korozije za razne metale i otopine [14]

Metal ili legura	**Prosječna brzina prodiranja korozije (mm/god)**				
	Gradska atmosfera	Morska voda	H_2SO_4 (5 mas.%)	HNO_3 (5 mas.%)	NaOH (5 mas.%)
Ugljični čelik	1,182-7,88	0,1182-11,82	15,76-394	VRLO VELIKA	< 0,197
Aluminij	< 0,512	1,182-51,22	7,88	15,76-78,8	VRLO VELIKA
Bakar	< 1,97	1,97-19,7	3,15-39,4	VRLO VELIKA	1,97-19,7
Olovo	< 0,197	0,197-15,76	<1,97	98,5-591	5,91-591

Također, vidljivo je da su sva tri ispitana materijala pokazala manje anodne i katodne nagibe u mediju umjetne kiše, što upućuje na činjenicu da su u tom mediju manje izražene reakcije na anodi i katodi. Drugim riječima, u mediju 3,5 % NaCl više su izražene katodna reakcija i reakcija anodnog otapanja ispitanih materijala.

ZAKLJUČAK

Metalografskim ispitivanjima ispitana je kvaliteta dvaju materijala spoja Cu/Al te njihova granica. Elektrokemijskim ispitivanjima proučavana je korozijska otpornost bakrene i aluminijske legure te njihova spoja zavarena trenjem u mediju 3,5 % NaCl i mediju umjetne kiše.

1. Metalografskom analizom utvrđeno je da se radi o legurama bakra i aluminija visoke čistoće. Legura bakra sadrži potencijalno visok sadržaj kroma koji može narušiti njezinu vodljivost te visok sadržaj aluminija koji u dodiru s kisikom i vlagom može uzrokovati elektrokemijsku koroziju. Aluminijska legura ima nešto viši sadržaj kroma, koji potencijalno narušava električnu vodljivost legure. Precizna granica spoja, koja ne pokazuje miješanje dvaju materijala, ukazuje na ispravno vođen postupak zavarivanja trenjem.
2. Metodom potenciodinamičke polarizacije je ustanovljeno da je brzina korozije aluminija i bakra manja u mediju umjetne kiše, nego u mediju 3,5 % NaCl. Pritom je Al-legura pokazala najmanju brzinu korozije u mediju 3,5 % NaCl, dok je u mediju umjetne kiše najmanju brzinu korozije pokazala Cu-legura. U oba medija, najveću brzinu korozije je pokazao Cu/Al spoj, tj. područje zavara izvedenog trenjem.
3. S obzirom na male iznose brzine korozije ispitanih materijala u oba medija može se zaključiti da je Cu/Al spojnica od legura visoke čistoće, spojena primjenom metode zavarivanja trenjem, otporna na atmosfersku koroziju i stoga primjenjiva u primorskom i kontinentalnom predjelu.

LITERATURA

[1] V. Šunde, Z. Benčić, T. Filetin, Materijali u elektrotehničkim proizvodima, Graphis Zagreb, https://www.fer.unizg.hr/_download/repository/Skripta_Materijali_u_elektrotehnickim_proizvodima.pdf, 15.4.2016.
[2] Ž. A. Spasojević , Z. V. Popović, Elektrotehnički i elektronski materijali, Naučna knjiga , Beograd, 1979.
[3] V. Bek, Tehnologija elektromaterijala, Sveučilište u Zagrebu Elektrotehnički fakultet, Zagreb, 1972.
[4] J. I. Frenkelj, Uvod u teoriju metala, Moderna fizika, Školska knjiga, Zagreb, 1996.
[5] S. O Kasap, Principles of Electrical Engineering Materials and devices, McGraw-Hill, Boston, 2000.
[6] W. D. Callister, Fundamentals of Materials Science and Engineering / An interactive e-text, John Wiley&Sons, Inc., New York, 2001.

[7] T. Filetin, F. Kovačiček. J. Indof, Svojstva i primjena materijala, Sveučilište u Zagrebu Fakultet strojarstva i brodogradnje, Zagreb, 2009.
[8] V. Knapp, P. Colić, Uvod u električna i magnetna svojstva materijala, Školska knjiga, Zagreb, 1997.
[9] E. Stupnišek-Lisac, Korozija i zaštita konstrukcijskih materijala, Fakultet kemijskog inženjerstva i tehnologije, Zagreb, 2007.
[10] L. Pomenić, Zaštita materijala, skripta, Tehnički fakultet Rijeka, 2011.
[11] A. Begić Hadžipašić, H. Hadžipašić, S. Vrbanjac, The Influence of Medium and Microstructure on Corrosion Rate of Dual Phase High-Strength Structural Steels, The Holistic Approach to Environment 2 (2012) 2, 73-84.
[12] V. Novak, Primjena metalnih prevlaka u zaštiti metala od korozije, Završni rad, Metalurški fakultet, Sisak, 2012.
[13] B. S. Pijanowski, I. Mahmud, A Study of the Effects of Temperature and Oxygen Content on the Corrosion of Several Metals, Report 69-2, Cooperative Program in Ocean Engineering, Institute of Ocean Science and Engineering, The Catholic University of America, Washington, D. C., June 1969.
[14] S. Martinez, I. Štern, Korozija i zaštita-Eksperimentalne metode, HINUS, Zagreb, 1999.

Zahvala

Ovaj je rad izrađen u okviru Financijske potpore istraživanjima Sveučilišta u Zagrebu TP167 „Dizajn i karakterizacija inovativnih inženjerskih legura“.

15th INTERNATIONAL FOUNDRYMEN CONFERENCE

INNOVATION – The foundation of competitive casting production

Opatija, May 12th-13th, 2016

http://www.simet.hr/~foundry/

HOW HARD CAN BE TO PRODUCE „GJL PIPE“ FOR DRAINAGE SYSTEM?

KOLIKO TEŠKO MOŽE BITI PROIZVESTI „GJL CIJEV“ ZA ODVODNJU?

B. Branković[1], D. Petrović[1], G. Gojsević Marić[2] and B. Čeh[3]

[1]Ferro-Preis d.o.o., Čakovec, Croatia
[2]Elkem AS, Sisak, Croatia
[3]Feal-Inženiring, Ptuj, Slovenia

Oral presentation
Professional paper

Abstract

After the start of pipe production in 2016 a new fault, “color in color” breakthrough (micro porosity), that has not been observed in previous production have appeared. During 2015 the transition from work with cupola furnaces to work with MF furnaces was achieved, so ultimately the emergence of fault was connected with the change of way of melting and preparing melt, which was confirmed with cooling curves done by ATAS MetStar®NovaCast. Improvement of metallurgical quality of melt from MF furnaces was achieved by addition of preconditioner Preseed®Elkem, as ATAS curves confirmed. By comparing the chemistry of melts for the production of pipes is observed that the higher content of phosphor (P) in melt results in better surface quality of the pipe, and also that with higher content of sulfur (S) effect of inoculant INOCULIN®Foseco is more noticeable which is reflected through higher metallurgical quality. Addition of preconditioner Preseed®Elkem and control of chemical composition (P and S) results in removing of “color in color” breakthrough fault, the occurrence of porous places on tubes.

Keywords: *centrifugal casting, cooling curves, gray cast iron, preconditioner*

*Corresponding author (e-mail address): *branislav.brankovic@ferro-preis.com*

Sažetak

Nakon početka proizvodnje cijevi 2016. godine pojavljuje se greška prodora „boje u boju“ (poroznost definirana na jednostavan i nepogrješiv način) koja do tada nije bila primijećena. Tijekom 2015. godine je ostvaren prelazak rada s kupolnim pećima na rad s indukcijskim pećima pa se u konačnici pojava greške povezala s promjenom načina taljenja i pripreme taline. Krivulje hlađenja dobivene pomoću uređaja ATAS MetStar®NovaCast, to su i potvrdile. Poboljšanje metalurške kvalitete taline indukcijskih peći postignuto je dodatkom sredstva za pripremu taline Preseed®Elkem, a isto je potvrđeno ATAS krivuljama. Usporedbom kemijskih sastava talina za proizvodnju cijevi uočeno je da se višim udjelom fosfora ostvaruje bolja kvaliteta površine cijevi, te isto tako da je kod viših udjela sumpora izraženiji efekt cjepiva INOCULIN®Foseco što se očituje kroz višu metaluršku kvalitetu. Upotrebom Preseed®Elkem te kontrolom kemijskog sastava (P i S) postignuto je uklanjanje greške proboja boje u boju, odnosno pojava poroznosti cijevi.

Ključne riječi: *sivi lijev, centrifugalno lijevanje, krivulja hlađenja*

UVOD

Godine 2009. ideja o proizvodnji cijevi u Ferro-Preisu implementirana je, na način da je veliki dio potrebne linije napravljen na osnovu zamisli i izuzetno malo dostupnih podataka izvan Ferro-Preisa, što je razumljivo s obzirom na specifičnost same proizvodnje.
Kako je svaki početak težak, važno je spomenuti i koji je bio redoslijed rješavanja navedene problematike da bi dobili korektan proizvod:

1. Hladni test cijele linije
2. Test lijevanja i proizvodnje cijevi
3. Uvođenje neutralne atmosfere unutar peći kapaciteta 28 tona bruto
4. Promjene načina i postupka lijevanja
5. Prerada same peći za kapacitet 15 tona bruto taline
6. Implementacija boja, unutarnje i vanjske
7. Testiranja kvaliteta boja prema svim zahtjevima normi i dobivanja certifikata za svaku boju neovisnih instituta
8. Razvoj kokila za proizvodnju cijevi
9. Eliminacija područja cementita ispod dozvoljenog područja prema zahtjevima norme, odnosno njegova potpuna eliminacija
10. Poboljšavanje kvalitete lijevane površine s obzirom na greške
11. Poboljšavanje kvalitete gruboće lijevane površine
12. Sve navedeno sukladno **normama EN 877 i Quality Assurance RAL-GZ 698** ili i izvan njih (npr. estetika) na zahtjev kupaca
13. Razlikovanje i razumijevanje razlika taline kupolne peći i elektro peći unutar proizvodnje i samo postupanje
14. Kontinuirana optimizacija svih procesa

U ovom radu ćemo se uglavnom posvetiti točci 13, a to je: razlikovanje i razumijevanje razlika taline kupolne peći i elektro peći unutar proizvodnje i samo postupanje.

Tijekom investicije u periodu 01.08.2014. – 20.12.2014. pored samog značajnog proširenja zgrade kaluparne, preseljenja dviju linija ručnog kalupovanja, instalacija novih filtra kao i same nove pripreme pijeska za kemijski vezan proces, Ferro-Preis je uložio i u novu elektro topionicu. Sam postupak edukacije i primjene istoga je vođen pažljivo i paralelno s kupolnim pećima do potpunog zaustavljanja istih tijekom četvrtog mjeseca 2015. godine. Tada je u prvom dijelu godine 2015. radila i proizvodnja cijevi sukladno tržišnim potrebama. Ponovno proizvodnja cijevi počinje s radom u prvom mjesecu 2016. godine.

Obzirom da nema ničeg jednostavnog unutar navedene proizvodnje, i sama uspostava iste traje nekoliko dana. Iskustvo svih ovih godina govori nam da se nije pojavio niti jedan problem, a na koji utjecaj nije imalo minimalno 5 različitih faktora u istom vremenskom okviru. To dovoljno govori o samoj osjetljivosti proizvodnje lijevanja cijevi.

Jedan iz niza elemenata provjere unutar same linije proizvodnje cijevi u Ferro-Preis-u je i kontrola pritiska cijevi zrakom, a o čemu ovisi da li cijev ide dalje u proces prema bojanju ili ne. Uočena su povremena odstupanja, te smo odlučili kontrolirano pustiti te cijevi na bojanje i promatrati rezultate. Dobili smo vizualnu potvrdu samog testa, odnosno dobili smo cijevi s greškom. Vizualizacija greške dolazi kao prijelaz ili prodor jedne boje u drugu kroz stjenku cijevi iako u nekim situacijama nema nigdje vidljive rupice, poroznosti (slika 1).

Slika 1. Prikaz prodora "boje u boju" na prijelomu cijevi

Statistika tijekom tih dana je bila za nas poražavajuća, što je vidljivo iz slijedećeg grafičkog prikaza grešaka u razdoblju od 25.01. do 18.02.2016 (slika 2).

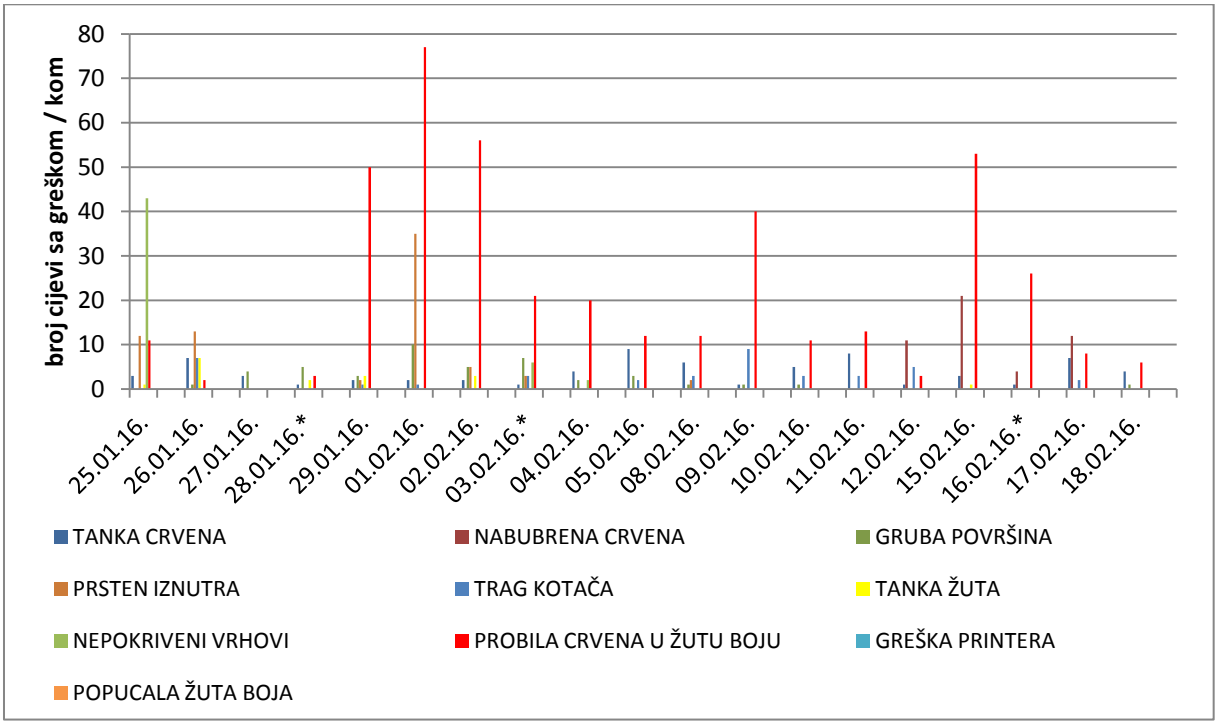

Slika 2. Grafički prikaz pojave grešaka u proizvodnji cijevi za razdoblje od 25.01. do 18.02.2016.

Zbog svega navedenog uslijedio je *„brainstorming"* zajedno s kolegom iz firme Feal-Inženiring. Obzirom da se greška nije pojavljivala u periodu rada s kupolnim pećima, odlučili smo se fokusirati na razliku metalurške kvalitete taline kupolne i indukcijske peći, te postići

što bolju metaluršku kvalitetu kako bi pokušali ukloniti pojavu ovakvih grešaka u proizvodnji cijevi.

Prednost rada s kupolnim pećima; talina proizvedena u kupolnoj peći posjeduje izvrsnu metaluršku kvalitetu zbog prirodnijeg procesa taljenja. Uložni materijal kupolne peći ima veći oksidni faktor te se neki nepoželjni elementi u ulošku oksidiraju i uklanjaju troskom (Al, Cd, Zn…), a preostali kisik pomaže pri cijepljenju taline te time smanjuje pojavu karbida. Nedostatak rada s kupolnim pećima je visok sadržaj sumpora iz koksa u talini i nemogućnost trenutne promjene kemijskog sastava taline, u slučaju nepostojanja predpećice.

Prednosti indukcijskih peći u odnosu na kupolne; brže zagrijavanje i taljenje uloška, mali odgor elemenata i ukupnog materijala, jeftiniji uložni materijal, proizvodnja taline s nižim sadržajem sumpora, lakša kontrola procesa, legiranje, mogućnost postizanja viših temperatura, mogućnost korekcije kemijskog sastava taline. Ukratko brži i efikasniji način proizvodnje taline s mogućnosti korekcije u svakom trenutku.

Unatoč navedenim prednostima glavni nedostatak indukcijskih peći u odnosu na kupolne je lošija metalurška kvaliteta taline, niska reaktivnost troske i manje naugljičenje taline. Obzirom na sastav uložnog materijala i tijek taljenja u elektro peći činjenica je da talina proizvedena u elektro peći ima niži sadržaj O_2 (30-80 ppm) od taline proizvedene u kupolnoj peći (70-150 ppm) [1]. Zbog sastava uložnog materijala, načina taljenja i brzine taljenja u elektro peći uklanja se mogućnost oksidacije štetnih elemenata troskom kao i prirodan proces naugljičenja koksom što talini daje niži oksidni potencijal te time povećava mogućnost nastajanja karbida. No, predkondicioniranjem i naugljičavanjem taline te boljim i učinkovitijim cijepljenjem taj nedostatak elektro peći možemo nadoknaditi.

Zbog lošije metalurške kvalitete taline kod rada s indukcijskim pećima potreban je drugačiji tretman taline kako bi se povećao nukleacijski potencijal. Kod zadržavanja taline u receptoru PRESSPOUR-u na visokim temperaturama s vremenom opada nukleacijski potencijal koji potječe od uloška (sivo sirovo željezo, hrđa sa čelika, SiC, način taljenja). Kako bi se korigirao, odnosno održavao nukleacijski potencijal prilikom taljenja u uložak mogu se (moraju se) dodavati razni materijali za poboljšavanje (pripremu) same taline. Korištenjem takvih sredstava (“predkondicioneri”) u talini nastaju i zadržavaju se postojeće stabilne klice koje osiguravanju metaluršku kvalitetu taline. U ovom području smo aktivno surađivali sa firmama Feal Inženiring i Elkem, odnosno s njihovim proizvodima uz obaveznu tehničku podršku.

METODOLOGIJA ISPITIVANJA

Kako se greška prodora “boje u boju” nije pojavljivala prije, nakon provjere dijelova procesa lijevanja, posumnjalo se na kvalitetu taline. Metaluršku kvalitetu taline najbolje opisuju krivulje hlađenja koje smo dobili pomoću *ATAS MetStar®Nova Cast* uređaja. Za primjer su uzete krivulje iz razdoblja pojave greške, te nakon eliminiranja iste. Isto tako su prikazane

krivulje uzete za vrijeme rada sa kupolnim pećima da se prikaže razlika taline iz različitih talioničkih agregata.

Usporedbom krivulja taline kupolne i indukcijske peći je ustanovljeno da iz taline kupolne peći posjeduje veću metaluršku kvalitetu taline što pogoduje boljoj strukturi materijala. Uvjet za povećanje metalurške kvalitete je povećanje nukleacijskog potencijala, odnosno potrebno je povećati broj nukleacijskih mjesta za nastanak grafita. U tu svrhu je korišten *Preseed*®Elkem, odnosno povremeno i *INOCULIN 390*® Foseco.

Preseed®Elkem je ferolegura sa 75 % Si koja sadrži umjerene količine aktivnih elemenata cirkonija, aluminija i kalcija (tablica 1). Prijašnja istraživanja su pokazala da su navedeni elementi potrebni za formiranje i zadržavanje postojećih stabilnih klica u talini. Dodatak od 0.1 % (do 0.2 %) kod taljenja zajedno sa FeSi i naugljičivačem pokazuje pozitivne efekte, uz neophodno vrijeme za reakciju od minimum 5 minuta prije samog čišćenja troske. Stvaranjem stabilnih klica rano u procesu i stabiliziranjem klica nastalih iz uložnih materijala smanjuje se gubitak nukleacijskog potencijala. Uobičajeno bi klice nestale zbog oksidacije, zadržavanja taline na višim temperaturama gdje iste prelaze u trosku, ali sa dodatkom *Preseed*®Elkem nastale klice se i zadržavaju u talini, te sudjeluju u izlučivanju grafita u željeni oblik.

Tablica 1. Kemijski sastav sredstva za pripremu taline Preseed®Elkem [2]

Silicij	62 - 69 %
Cirkonij	3 - 5 %
Aluminij	3 – 5 %
Kalcij	0,6 – 1,9 %
Željezo	ostatak

Kao cjepivo za cijevi koristi se *INOCULIN 33*®Foseco, dodaje se u mlaz taline koja se izljeva u lonac za cijevi. To je cjepivo na bazi ferosilicija koja sadrži niske udjele aluminija i kalcija, te kontrolirani udio stroncija (tablica 2). Aluminij i kalcij osiguravaju minimalan nastanak troske. Zbog dodatka stroncija smanjuje se pothlađenje, čime se smanjuje mogućnost nastanka mikroporoznosti. Učinak je najbolje zapažen kod talina s višim sadržajem sumpora (>0,05% za sivi lijev).

Tablica 2. Sastav cjepiva Inoculin®Foseco [3]

Silicij	73 – 78 %
Kalcij	0.1 % max
Aluminij	0.5 % max
Stroncij	0,6 – 1,1 %
Željezo	ostatak

REZULTATI I DISKUSIJA

Pošto se kroz rad spominje razlika u metalurškoj kvaliteti taline iz kupolne i elektro peći (srednje frekventne) ona je ovdje prikazana preko krivulja hlađenja koje su snimljene s ATAS MetStar®NovaCast uređajem. U radu su prikazane krivulje za 3 različite kvalitete taline. Za svaku kvalitetu su prikazane 2 krivulje, prva prikazuje metaluršku kvalitetu taline u agregatu za lijevanje PRESSPOUR, dok druga prikazuje kvalitetu taline iz lonca za lijevanje cijevi koja je cjepljena dodatkom INOCULIN®Foseco. Količina dodavanja samog cjepiva INOCULIN®Foseco je kontrolirana preko ATAS MetStar®NovaCast uređaja i ona se mijenja sukladno potrebi.

Primjeri ATAS krivulja talina iz kupolnih peći, dobivenih “na sivo”, čašicama bez Te, 2015.

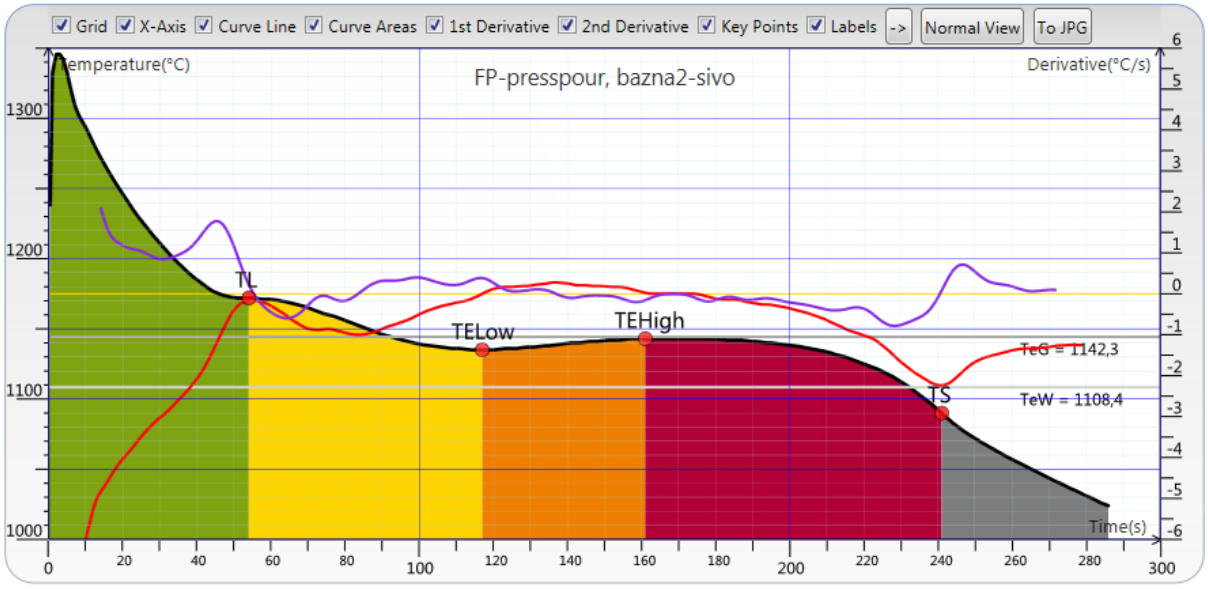

Slika 3. ATAS krivulje taline iz PRESSPOURA

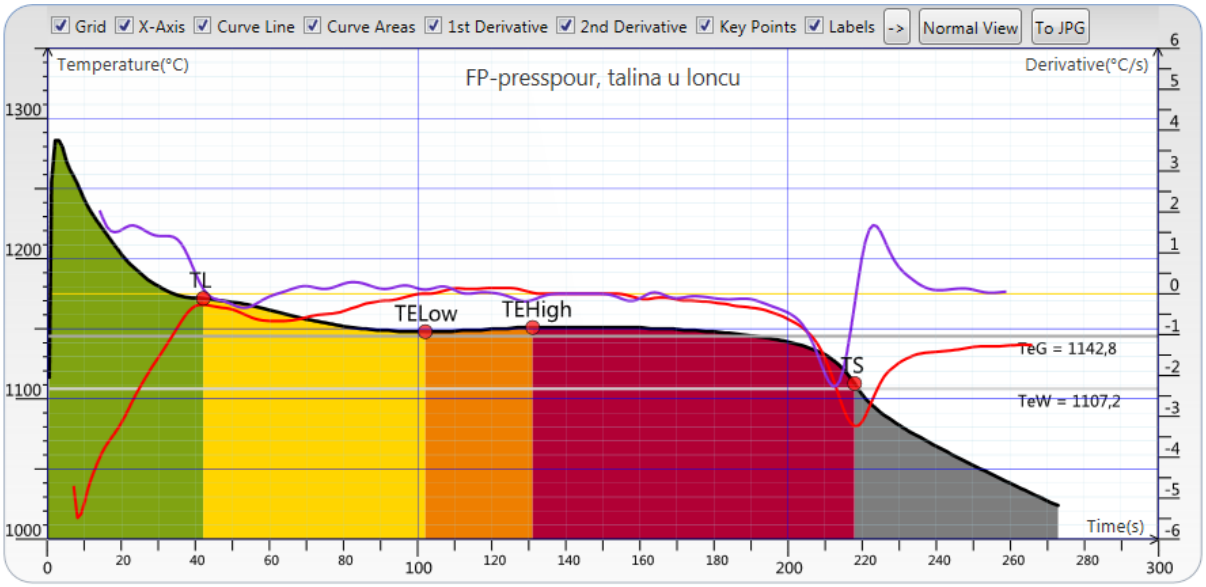

Slika 4. ATAS krivulja talina iz lonca za lijevanje cijevi cjepljene s INOCULIN®Foseco

Tablica 3. Parametri ATAS krivulja sa slika 3 i 4

PARAMETAR	PRESSPOUR	Lonac za cijevi
TL	1172	1171,7
TElow	1135	1148
R	8	3
GRF1	60	85
GRF2	79	32
TS	1090,8	1109,6
dT/dt TS	-2,24	-3,24

Primjer ATAS krivulja taline iz elektro peći u periodu pojave greške prodora “boje u boju”, dobivenih “na sivo”, čašicama bez Te, 2016.

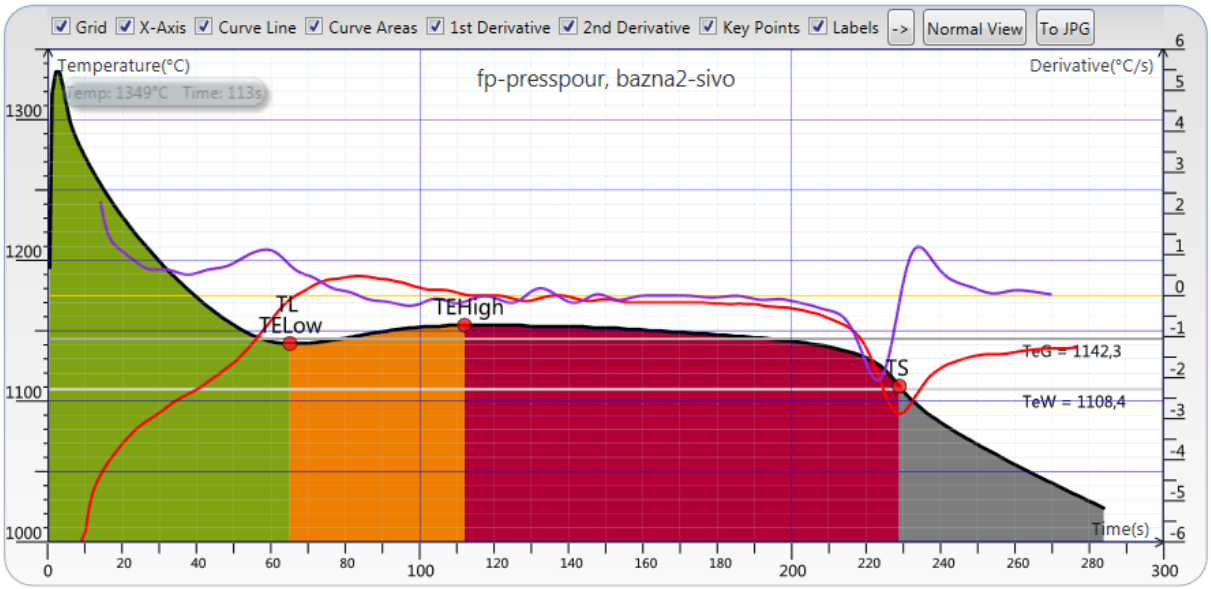

Slika 5. Primjer ATAS krivulje iz PRESSPOURA

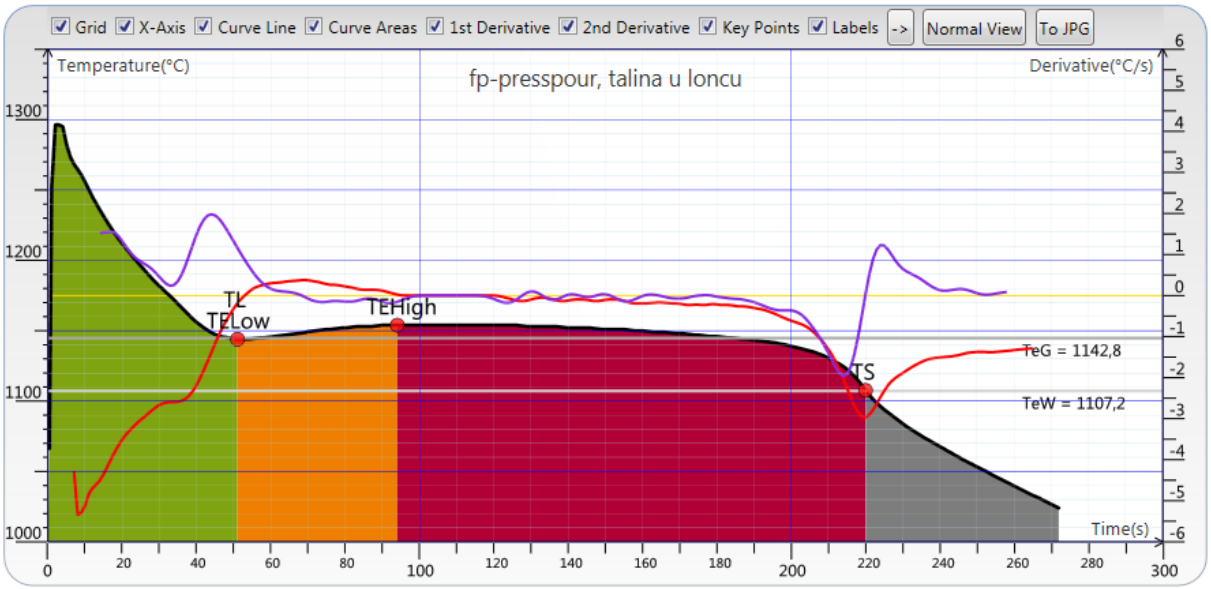

Slika 6. ATAS krivulja talina iz lonca za lijevanje cijevi cjepljene s INOCULIN®Foseco

Tablica 4. Parametri ATAS krivulja sa slika 5 i 6

PARAMETAR	PRESSPOUR	Lonac za cijevi
TL	1141	1144
TElow	1141	1144
R	13	10
GRF1	78	82
GRF2	40	41
TS	1110,1	1108,3
dT/dt TS	-2,21	-2,72

Primjeri ATAS krivulja talina iz elektro peći s dodatkom Preseed®Elkem i FeP, dobivenih "na sivo", čašicama bez Te, 2016.

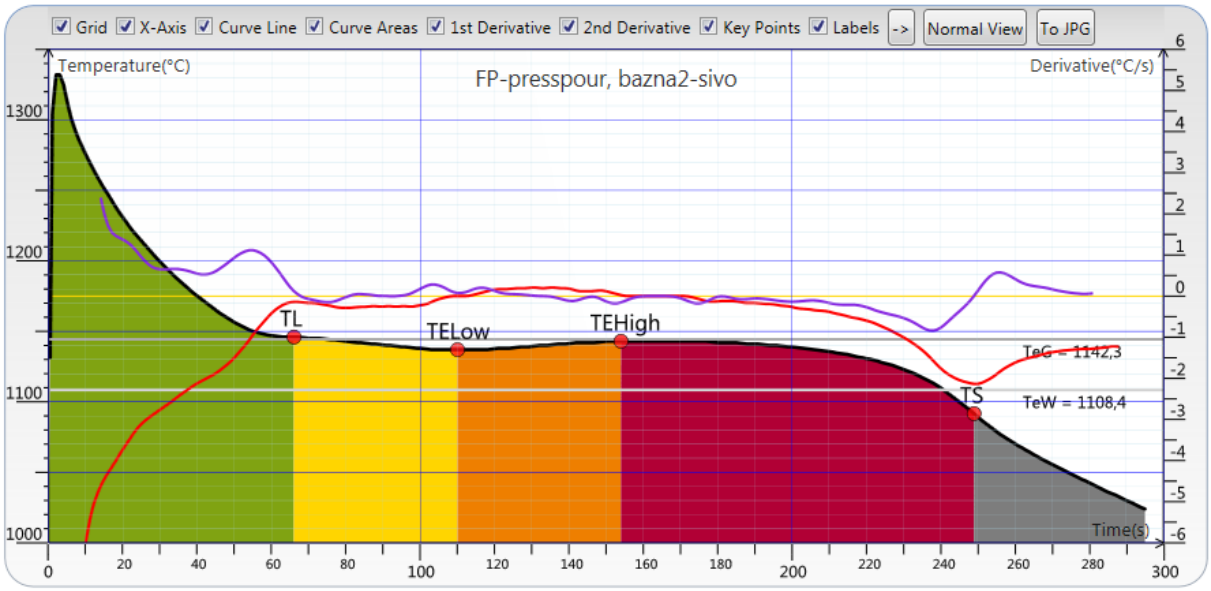

Slika 7. Primjer ATAS krivulje iz PRESSPOURA

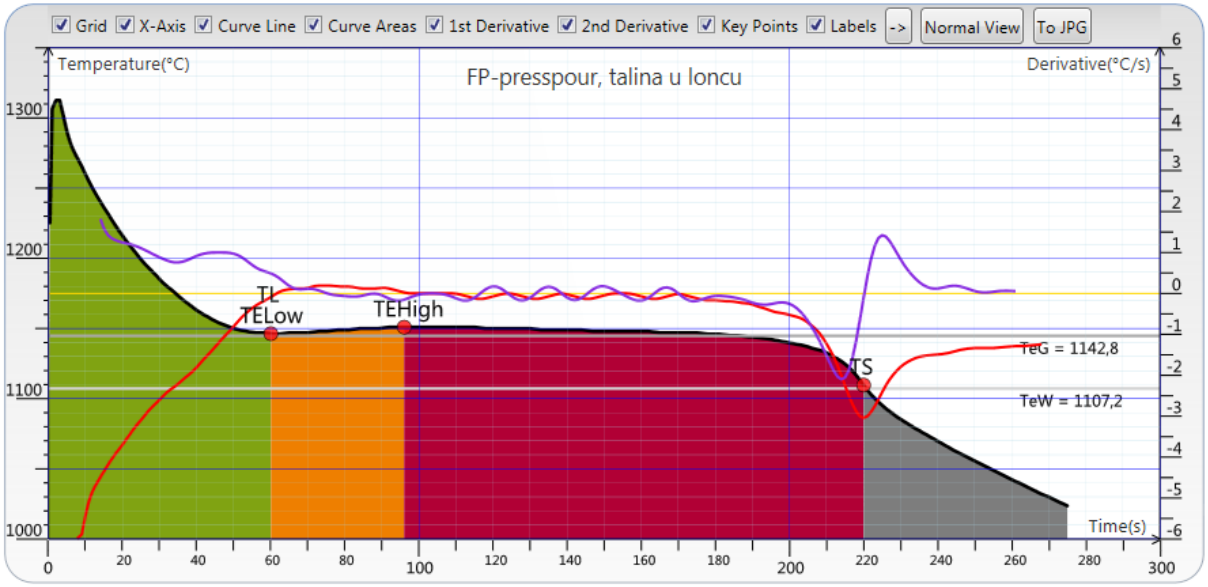

Slika 8. ATAS krivulja talina iz lonca za lijevanje cijevi cjepljene s INOCULIN®Foseco

Tablica 5. Parametri ATAS krivulja sa slika 7 i 8

PARAMETAR	PRESSPOUR	Lonac za cijevi
TL	1146	1146,3
TElow	1137	1146,3
R	6	4,7
GRF1	66	90
GRF2	87	36
TS	1091,4	1109,4
dT/dt TS	-2,13	-3,04

Parametri iz tablice 3 pokazuju da talina dobivena iz kupolne peći, a uzorkovana iz receptora PRESSPOUR, ima visoku metaluršku kvalitetu. Iz njih se vidi pozitivan učinak cjepiva koji se karakterizira kroz povišenje solidus temperature TS, pad likvidus temperature TL i oporavka R. Solidus temperatura nakon cjepljenja se nalazi iznad temperature metastabilnog skrućivanja što smanjuje mogućnost nastanka karbida. Niska vrijednost grafitnog faktora GRF2 ukazuje na visoku toplinsku vodljivost što je znak velike količine izlučenog grafita. Pokazatelj visoke toplinske vodljivosti je i niska vrijednost prve derivacije krivulje hlađenja na solidusu dT/dt TS također ukazuje na visoku toplinsku vodljivost te je povezana s visokom količinom eutektičkog grafita na kraju skrućivanja. Sagledavši sve parametre talina ima visoku metaluršku kvalitetu, zbog čega je umanjena mogućnost nastanka grešaka tijekom skrućivanja.

Parametri iz tablice 4 ukazuju na lošiju metaluršku kvalitetu taline iz elektro peći od one iz kupolne peći, na istom mjestu uzorkovanja. Visoka vrijednost oporavka ukazuje na veliku količinu grafita koji se izlučio na početku eutektičke reakcije u kratkom vremenu što ukazuje na slaba nukleacijska svojstva taline. Pad solidus temperature nakon cjepljenja ukazuje na veću mogućnost pojave karbida u mikrostrukturi. Grafitni faktor GRF2 te prva derivacija krivulje hlađenja na solidusu dT/dt TS ukazuju na nižu toplinsku vodljivost , odnosno manju količinu izlučenog grafita i veću mogućnost nastanka B, C ili D tipa grafita. Parametri iz tablice 4 ukazuju na veliku mogućnost nastanka grešaka prilikom skrućivanja taline.

Parametri iz tablice 5 pokazuju utjecaj dodatka Preseed®Elkem i FeP u talinu iz elektro peći. Vidljiva je razlika u odnosu na prethodne krivulje taline elektro peći. Temperatura solidusa je porasla nakon dodatka cjepiva te se nalazi iznad temperature metastabilnog skrućivanja što ukazuje na manju mogućnost nastanka karbida. Također nakon cjepljenja GRF2 poprima nisku vrijednost kao I dT/dt TS što ukazuje na visoku toplinsku vodljivost i nastanak grafita A i B tipa. Iz parametara je vidljivo da je dodatak Preseed®Elkem imao pozitivan utjecaj na metaluršku kvalitetu taline, što znači manju mogućnost pojave grešaka prilikom skrućivanja taline.

U tablici 6 su prikazani tipični kemijski sastavi taline za proizvodnju cijevi iz kupolne peći, elektro peći te iz indukcijske peći sa povećanim udjelom FeP i FeS u šarži.

Tablica 6. Usporedba kemijskih sastava talina za proizvodnju cijevi

AGREGAT	CE	C	Si	Al	Mn	Ti	P	S
Kupolna peć	4.27	3.54	2.51	0.01	0.52	0.02	0.19	0.09
Elektro peć	4.22	3.45	2.78	0.004	0.52	0.02	0.09	0.07
Elektro peć + Preseed®Elkem + dodatak FeP i FeS	4.31	3.52	2.76	0.01	0.55	0.02	0.17	0.10

Korištenjem elektro peći za taljenje dobiva se puno bolja mogućnost kontrole fosfora i sumpora u talini. Udjeli prikazani u tablici su postignuti odgovarajućim dodatkom ferolegura FeP i FeS. Kod svakodnevog rada te vrijednosti iznose kao u drugom redu u tablici (red "elektro peć"). Testiranjima je uočeno da viši udio fosfora u talini kod proizvodnje cijevi pogoduje boljoj kvaliteti površine, a viši udio sumpora pogoduje boljoj metalurškoj kvaliteti (+ INOCULIN®Foseco), pa se tako prilikom izrade taline za cijevi u uložak dodaju potrebne količine FeP i FeS.

Nakon primjene svega navedenoga, greška proboja "boje u boju" je eliminirana kao što se može vidjeti iz grafa na slici 9.

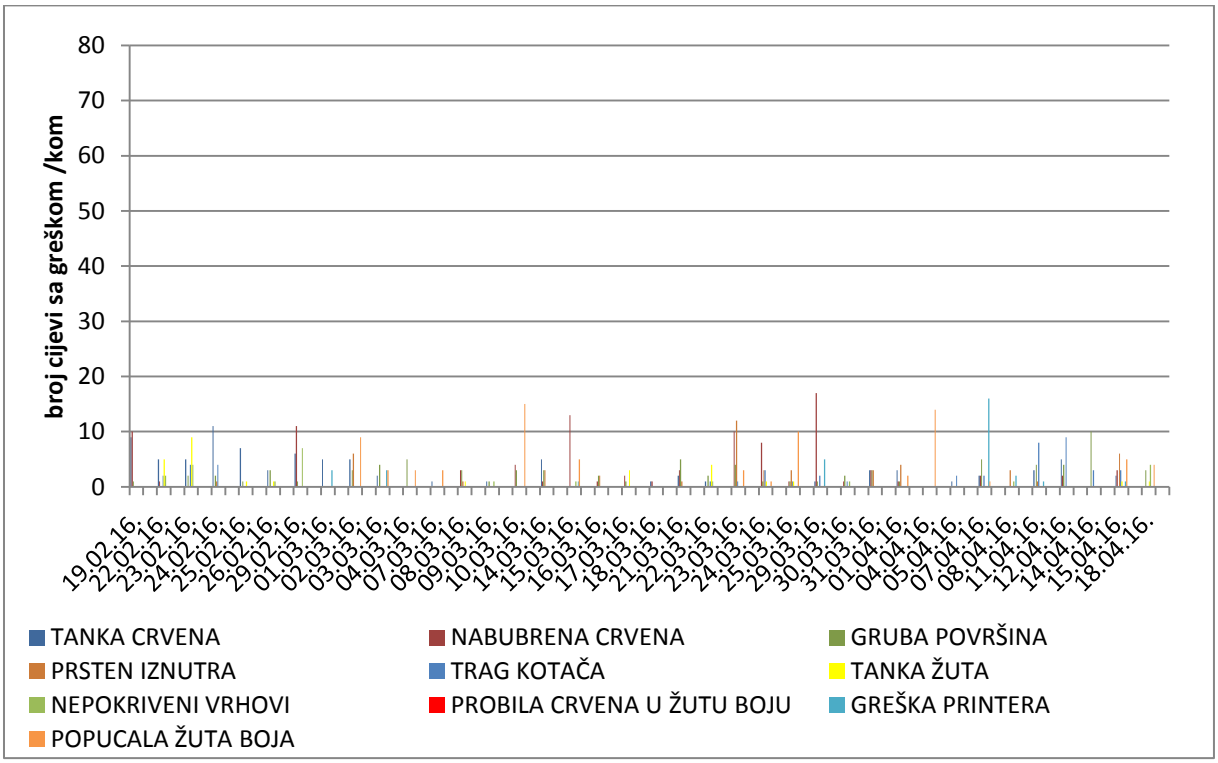

Slika 9. Grafički prikaz pojave grešaka u proizvodnji cijevi za razdoblje od 19.02. do 18.04.2016.

ZAKLJUČAK

1. ATAS krivulje taline kupolne peći pokazuju da takva talina ima dobru metaluršku kvalitetu s stajališta sivog lijeva, to možemo pripisati samom talioničkom agregatu. Talina iz elektro peći ne pokazuje tako dobre rezultate, pa je potrebno, ovisno o proizvodu i njegovim zahtjevima, koristiti sredstva kao što je Preseed®Elkem kako bi se ostvario veći nukleacijski potencijal.
2. Povećanje sadržaja fosfora i sumpora u talini je pridonijelo poboljšanju kvalitete površine gotovog proizvoda kao i poboljšanju metalurške kvalitete taline.
3. Upotrebom navedenih koraka postignuto je uklanjanje greške proboja "boje u boju" u kratkom vremenskom roku te je postignuta potrebna visoka kvaliteta proizvedenih cijevi.

LITERATURA

[1] Official Journal of WORLD FOUNDRYMEN ORGANIZATION (WFO), GIESSEREIFORSCHUNG International Foundry Research, 1/2008, GIESSEREIFORSCHUNG 60 (2008) No. 1 Pp. 2–66; 1 Quarter; ISSN 0046-5933.
[2] Product datasheet Preseed ™ preconditioner, Revised February 2006 © Copyright Elkem AS Hoffsveien 65B, P.O.Box 5211 Majorstua, NO-0303 OSLO.
[3] Leaflet – Ferreus Metal Treatment INOCULIN* 33 (also called INOCULIN*SR75) Edition 12/03, Foseco GmbH, 46322 Borken, Germany.

15th INTERNATIONAL FOUNDRYMEN CONFERENCE
INNOVATION – The foundation of competitive casting production
Opatija, May 12th-13th, 2016
http://www.simet.hr/~foundry/

ECOLOGICAL AND ECONOMIC EFFECTS OF APPLYING A NEW GENERATION BURNER TO DRYING AND SOAKING OF CASTING LADLES

S. Gil, W. Bialik, B. Machulec, J. Ochman and A. Fornalczyk

Silesian University of Technology Faculty of Materials Engineering and Metallurgy,
Katowice, Poland

Oral presentation
Original scientific paper

Abstract

The paper presents the analysis of a potential for reducing gaseous fuel consumption in the process of drying and soaking of casting ladles. The new solution is proposed for ladles used in the ferroalloy industry for casting liquid metals. The observed destruction of the refractory lining during intensive operation requires continuous reconditioning associated with replacement or partial recovery. This problem can grow as a result of the impact of external and internal factors interfering with the normal rhythm of liquid metal tapping. The drying, heating and sustaining of ladle lining at a suitable temperature are carried out by means of a gas burner. In the present paper, the use of a new generation self-recuperative burner, instead of a conventional design, has been proposed. The burner is characterized by better energy efficiency and lower pollutant concentrations in exhaust gas. A decrease in fuel consumption could reach, under favourable conditions, up to 20% compared with traditional solutions. The proposed design of the burner can be used in other areas of casting technologies.

Keywords: *casting ladles, burner, economic effects*

*Corresponding author (e-mail address): *stanislaw.gil@polsl.pl*

INTRODUCTION

Global economy requires continuous improvement of a product and reduced costs of its production. Similar issues are valid for the smelting and metal processing industry. This industry is more challenging for the product advancement but it is usually possible to reduce production costs. An important component of production costs, particularly in metallurgical and metal processing plants, is expenditure related to energy carrier purchase. Even slight improvements may result in markedly lowered energy consumption in applied technological or auxiliary processes. Reduction in energy carrier consumption means economic profits for a company but also its limited effects on the natural environment due to reduced emissions

of harmful or adverse substances. One of the most attractive methods of lowering fuel consumption in processes is utilization of energy from e.g. exhaust gas for preheating combustion substrates in recuperative or regenerative systems. The methods are relatively simple and the combination with the same energy process ensures its concurrent generation and consumption. Currently, all modern gas-fired industrial furnaces, used in production lines, are fitted with exhaust energy recovery systems. This guarantees considerable fuel savings and increased energy efficiency [1, 2]. There are attempts to implement similar solutions in auxiliary devices that are not directly related to production technology and are mostly intended for temporary use. In such cases, however, effective implementation of energy recovery systems is more difficult in view of technological and economic issues. The use of sophisticated technical solutions generally results in additional complications during operating procedures and requires adequately trained employees as well as higher technological awareness. Usually small thermal power of auxiliary devices is a reason of a minor economic profit related to new, more cost-effective solutions due to the absence of so-called economies of scale. Nonetheless, during reconditioning work or purchasing new devices, those which feature lower levels of energy consumption and more advanced technological solutions should be preferred.

APPLICATION OF THE NEW BURNER

In the paper, the analysis of potential application of a new, self-recuperative burner at the casting ladle drying and soaking unit has been presented. The ladles are used for collecting liquid metal from two submerged arc furnaces intended for ferroalloys production. The daily capacity of each furnace is approx. 48 ÷ 50 Mg of liquid metal which is collected during 12 tapping operations. The average liquid metal weight for each operation is 4 Mg and the metal temperature amounts to 1650 °C [3]. Steel walls of the ladle shell are fitted with refractory material; its thickness and production technology are developed experimentally based on the analysis of its functionality. For ferrosilicon alloys, refractory mass, composed of 2 ÷ 20 mm quartzite grains and quartzite sand, is preferred as the external tamped layer. Water glass (4 % of the whole mixture volume) is used as binding material. Additionally, the lining that is formed during operation from remaining solidified metal serves as protective material for the refractory layer. Liquid FeSi alloy is transferred from the ladle into moulding pots or boxes. It cools there, forming thin layers that are easier to crush into grains of required sizes. In Figure 1, a ladle placed under the furnace tapping hole is presented.

Figure 1. Ladle placed under the furnace tapping hole

Figure 2. Ladle and its lid with a thermal insulation layer

Liquid metal tapping, its pouring into moulding boxes and empty ladle weighing last approx. 30 minutes. Following these procedures, the ladle is put aside and prepared for liquid metal tapping from the neighbouring furnace. Between the tapping operations, the ladle is covered using a lid with a thermal insulation layer to limit the temperature drop, which is illustrated in Figure 2. Figure 3 presents a thermogram of the temperature distribution.

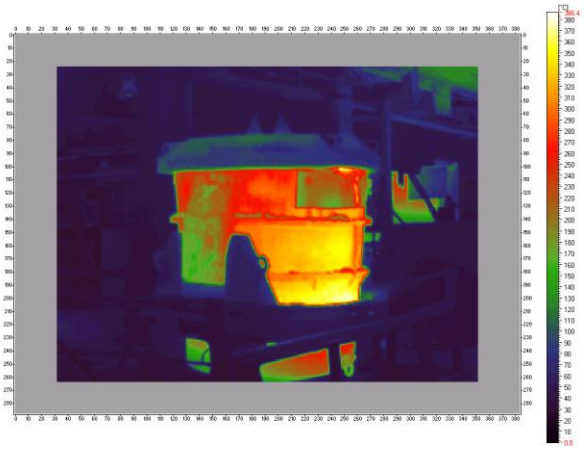

Figure 3. Thermogram of the ladle shell temperature distribution

Figure 4. Unit intended for drying and soaking of casting ladles

If damaged refractory lining is reported, the ladle is repaired or reconditioned depending on the level and size of defects. A complete assessment of necessary work is performed after ladle cooling which lasts approx. 8 hours. Reconditioning works are carried out in a designated area within the production floor where materials for repair and reconditioning of ladles are stored and a drying unit is located. Following reconditioning of ladle shell refractory layers, the ladle is dried and soaked according to appropriate procedures. The instructions for casting ladle reconditioning include guidelines on recommended temperatures and drying times for ladles of various volumes. A ladle during the initial drying phase is shown in Figure 4. The drying times following complete refractory layer

replacement depend on the ladle sizes and amount to approx. 10 hours for a 3 m^3 ladle and approx. 8 hours for a 2 m^3 ladle. Over the course of the drying process, a gap between the lid with a gas burner and the ladle edge is reduced to decrease the radiation heat flux transfer to the surrounding environment and to raise the temperature. The thermal power of the burner in the movable lid is 150 kW and the temperature of exhaust gas leaving the ladle space during the final drying stage amounts to about 900 °C. Its approximate value is measured by means of a thermocouple placed in the lid (Fig. 4). In the case of exhaust gas temperature measurements, some interference is observed due to radiation interactions between the ladle inner space, the lid and the surrounding environment. The calculated average drying and soaking efficiency, determined based on the energy balance, amounts to approx. 20 ÷ 25 % and depends on the stage of the process and conformity to the technical guidelines. Low energy efficiency results from high-temperature exhaust gas leaving the heated area and the radiation energy flux transferred to the surrounding environment from the soaked refractory layer through the gap between the lid and the edge of the ladle. Losses by conduction through the lining refractory layer and the furnace shell were determined based on the temperature distribution in the thermograms but they are small and amount to 6 ÷ 9 %. A potential for improvement in the ladle drying and soaking efficiency is seen in application of one of the series of modern self-recuperative burners. Its schematic design is presented in Figure 5. The series of burners has been developed at the Department of Process Energy, Silesian University of Technology [4].

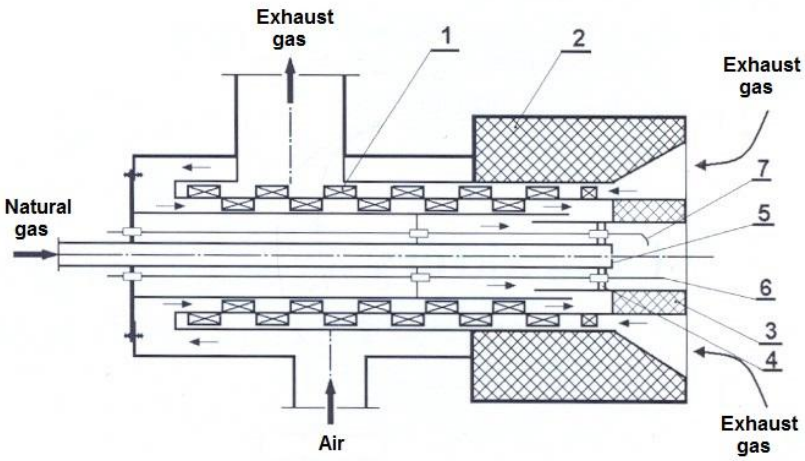

Figure 5. Diagram of a low-emission, automatic self-recuperative diffusion burner:
1 - recuperator; 2 - burner stone; 3 - flame stabilizer; 4 - air nozzle; 5 - gas nozzle;
6 - animating electrode; 7 - starting electrode [5]

The burner installed in the modernized unit will markedly reduce two major factors that cause low efficiency of the present solution. High-temperature exhaust gas that freely flows out to the surrounding environment will be drawn into the burner recuperator where it will preheat the combustion air, leading to reduced gas fuel consumption. The temperature of combustion air preheating can be determined based on the profile presented in Figure 6. It has been assumed that the temperature of exhaust gas, drawn axially within the ladle space,

will amount to approx. 950 ÷ 970 °C. The analysis of the profile in Figure 5 shows that the combustion air preheating temperature will be approx. T_a = 280 °C. In practice, a slightly higher temperature should be expected due to extra enthalpy flux of steam floating in the exhaust gas and a higher rate of exhaust gas flow in the recuperator. While the profiles of self-recuperative burner series were being determined at the Department of Process Energy, Silesian University of Technology, the steam content in the exhaust gas only related to the process of natural gas combustion [6,7]. To achieve effective suction of exhaust gas into the recuperator, its uncontrolled outflow through the gap between the lid and the edge of the ladle (see Figure 4) should be eliminated. A lower lid position and gap elimination will result in the absence of the other important component of energy losses to the surrounding environment i.e. radiation heat transfer from hot inner walls of the ladle to the environment. The exhaust gas is extracted from the self-recuperative burner to the environment by means of an extra fan intended to operate with hot gases. To protect the fan from destruction by too hot exhaust gas, a three-way mixing system is fixed on the exhaust pipeline to lower the temperature using the ambient air.

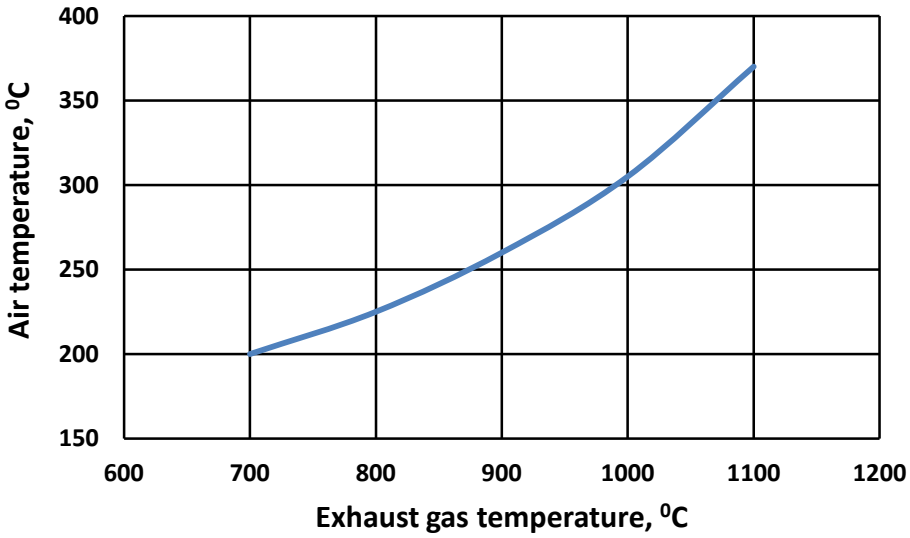

Figure 6. Self-recuperative burner: a profile of combustion air preheating [5]

To develop a proper design of the burner unit flow system, flow profiles of its components are necessary. In Figure 7, pressure losses during exhaust gas flow through the burner versus the burner power are shown. Based on the presented profile and pressure losses in the other components, the type of exhaust gas fan can be selected. The burner automatic control system ensures a safe start-up and smooth transition of the burner power from 50 ÷ 150 kW.

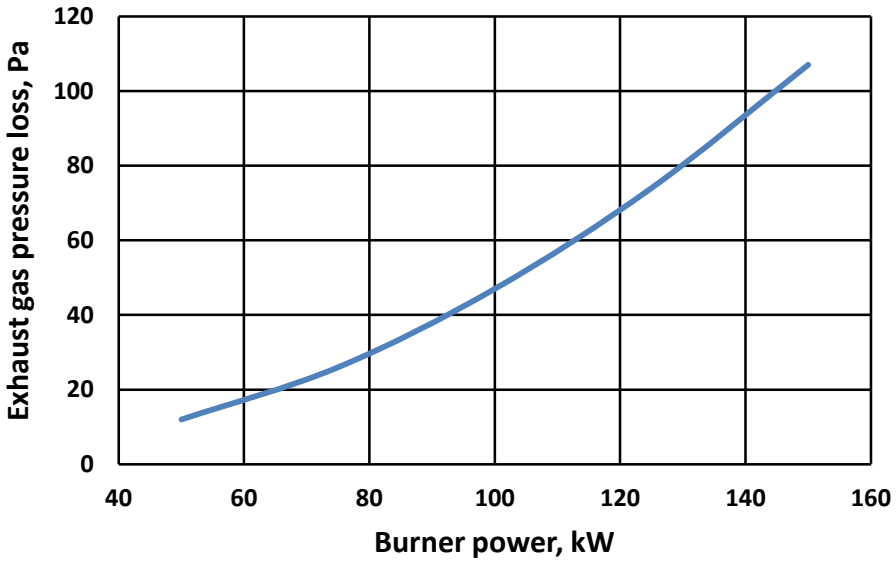

Figure 7. Exhaust gas pressure loss in the burner versus the burner power

CONCLUSIONS

- ✓ The combustion air preheating temperature will amount to approx. T_a = 280 °C. In practice, a slightly higher temperature should be expected due to extra enthalpy flux of steam floating in the exhaust gas and a higher rate of exhaust gas flow in the recuperator.
- ✓ To achieve effective suction of exhaust gas into the recuperator, its uncontrolled outflow through the gap between the lid and the edge of the ladle should be eliminated.
- ✓ The burner automatic control system ensures a safe start-up and smooth transition of the burner power from 50 ÷ 150 kW.
- ✓ Due to application of the new self-recuperative burner, the radiation energy flux loss through the gap between the lid and the edge of the ladle will be minimized.
- ✓ Balancing calculations show that average fuel savings will amount to approx. 4,5 m^3/h of natural gas. However, it should be noted that the new solution involves an additional component, the exhaust gas extraction fan, that is electrically driven.
- ✓ The power of engine in the laboratory research unit was 1,5 kW but its efficiency was not optimized for the 150 kW burner and it was not fitted with a rotary speed control system.

REFERENCES

[1] J. Szargut, Energetyka cieplna w hutnictwie, Wydawnictw Śląsk, Katowice, 1983.

[2] W. Bialik, B. Machulec, Analysis of the possibilities using of the post-reaction gases enthalpy from the ferrosilicon smelting process, Solid State Phenomena, 226 (2015), pp. 215-218.
[3] M. Gasik (Editor), Handbook of Ferroalloys. Theory and Technology, Elsevier, Oxford, 2013.
[4] Opis Patentowy PL 182846. Urządzenie do suszenia i grzania kadzi odlewniczej.
[5] M. Rozpondek, J. Góral, Charakterystyki dyfuzyjnych palników gazowych dla hutniczych urządzeń cieplnych, Hutnik 75 (2008) 5, pp. 257-261.
[6] J. Tomeczek, M. Rozpondek, Racjonalne nagrzewanie kadzi metalurgicznych, Hutnik 68 (2001) 4, pp. 144-147.
[7] J. Tomeczek, M. Rozpondek, B. Gradoń, J. Góral, J. Ochman, Konsekwencje technologiczne i ekologiczne wyrównywania pola temperatury w wysokotemperaturowych piecach przemysłowych, Hutnik 69 (2002) 3, pp. 92-95.

15th INTERNATIONAL FOUNDRYMEN CONFERENCE
INNOVATION – The foundation of competitive casting production
Opatija, May 11th-13th, 2016
http://www.simet.hr/~foundry/

APPLICATION OF THERMOGRAPHY IN THE PRODUCTION AND PROCESSING OF METALLIC MATERIALS

I. Jandrlić, T. Brlić and S. Rešković

University of Zagreb Faculty of Metallurgy, Sisak, Croatia

Oral presentation
Subject review

Abstract

By development of the detectors for measuring the infrared radiation, thermography becomes more and more accessible, and in the same time suitable, for various measurements of temperature. Today thermography is widely used method in various fields of medicine, production and processing industry, energetics, etc. In the last 20 years thermography finds it's more and more frequent application in control of processes during the production and processing of metallic materials, in which is necessary to measure temperature changes and distributions. Recent studies describe the possibilities of thermographic method and ways how to measure temperature changes at different points of metal production processes, where it begins to be widely used. The most common examples of use of thermography in the control of the various processes in the production, processing and control of metallic materials are presented. An overview of some advantages and disadvantages of thermographic method compared to the conventional contact temperature measurement methods is given. As the thermographic method is very sensitive to certain parameters, some of the conditions that are required in order to achieve accurate measurement are highlighted. From the aforesaid, it follows that this method will have the increasing importance in research of metal properties, as well as the technologies in their production.

***Keywords**: thermography, infrared camera, process, non destructive testing, emissivity factor*

*Corresponding author (e-mail address): *ijandrli@simet.hr*

INTRODUCTION

Thermography in metallurgy has more and more frequent applications and presents a relatively new method for testing the various processes in the production and processing of metals and metal alloys. Often used terms for this method are thermographic recording, infrared thermography, or thermal video. It is well known fact that all bodies with a temperature above absolute zero emit heat to the environment in the form of infrared electromagnetic waves [1-3]. Thermography is based on detecting this infrared radiation in

invisible spectrum (900 to 14.000 nanometers wavelength). Depending on the temperature of the body, larger or smaller portion of the emitted energy is in the infrared spectrum. At temperatures below 500 °C, all of objects heat energy is emitted completely within the infrared spectrum. Infrared cameras, as according to the second law of thermodynamics which says that warmer bodies radiate their energy in the environment, detect that radiation. Basic device for thermographic testing is so-called infrared camera which measures the temperature of the observed object. Thermal imaging cameras are similar in appearance to conventional video cameras, and have a radiation detector embedded in them. Today, commercially available cameras have resolutions of 320 x 240 to 640 x 512 pixels.

Infrared cameras contain logic circuits by which detected radiations are visualized on their screens as the distribution of the surface temperature of observed body. Depending on type of camera, there are various commercial software packages for analyzing thermographic images. Using the associated software packages, results of thermographic analysis can be processed in the form of quantitative values and/or qualitative values, with the results shown as thermal images and/or thermal video. Depending on the type of thermographic camera, it is possible to measure the temperature in the range approximately from -50 to 2000 °C.

THEORETICAL BACKGROUND

In thermographic research it should take into account that the infrared cameras detect the total energy coming to its detector [1,2]. This energy consists of emitted energy from the body that radiates energy, transmitted energy that passes through the observed object from a radiation source behind the body, and reflected energy which object reflects from surrounding on the radiation detector (Figure 1).

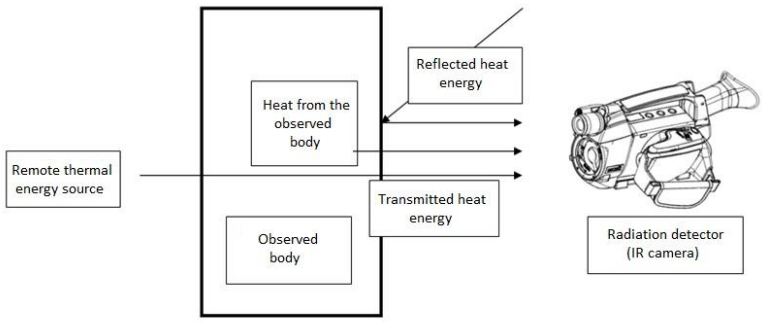

Figure 1. Total energy detected by the infrared camera from the surface of the observed object

Relevant information on the observed body is only in the emitted radiation energy. For this reason, in order to conduct quality thermographic material testing, before testing there is a need for solid preparation of experiments to avoid detection of the reflected and

transmitted energy. Most of the materials that occur in metallurgical plants do not have the possibility of transmission of infrared radiation. Only a few materials possess this property and do not appear in the metallurgical practice unless it is specifically required in certain parts of the plants. In that way we can ignore transmitted energy right from the start of testing. On the other hand, in metallurgical plants, there is a large variety of environmental sources of heat. For this reason, a very common problem for accurate thermographic testing represents the reflected energy from the observed object. The influence of reflected energy from the environment can be eliminated or reduced by applying special curtains to prevent aeration of energy from the environment or by removing all of possible environmental sources of thermal energy.

When using infrared cameras for measurements of temperature distribution or changes in industrial conditions, it is necessary to consider the possibility of reflected energy which represents the area of higher temperature levels during the test. It is also necessary to take into account various other external influences, such as air flow, different relative humidity of environment, as well as differences in the emissivity factor of the observed objects. Infrared cameras measure the surface temperature of observed object (T_{obj}) from the measured changes of voltage, which detector gives from detected infrared radiation [1,2]:

$$T_{obj} = \sqrt[n]{\frac{U - C \cdot T_{at}^n + C \cdot \epsilon \cdot T_{at}^n + C \cdot T_{ct}^n}{C \cdot \epsilon}} \quad (1)$$

Where is: C – constant specific for camera
T_{at} – ambient temperature
T_{ct} – temperature of camera
ϵ – emissivity factor
U – voltage of the electric signal
n – factor which depends on the wavelength measured by the detector

Equation 1 takes into account the ambient temperature, temperature of the radiation detector, the emissivity factor, and in which wave spectrum measurements were taken. The equation is based on the basic equation, which is known in the literature as Stephan-Boltzmann law of radiation of ideal thermal black body:

$$W = \sigma_B \cdot T^4 \quad (2)$$

Where is: σ_B – Stephan-Boltzmann constant for ideal thermal black body

Equation 2 for real bodies (thermal grey) is modified with so-called emissivity factor, since only an ideal thermal black body has an emissivity factor equal to 1, other bodies have a smaller amount. So equation for the real body is:

$$W = A \cdot \epsilon \cdot \sigma_B \cdot T^4 \quad (3)$$

Where is je : A – body surface,

It can be seen that emissivity factor of the body is one of the most influential factors on the temperature measurement accuracy. Emissivity factor of materials describes the ability of materials to emit or release absorbed thermal energy. The emissivity of the object depends on the type of material, surface state or quality of object, and the temperature of the object. It can said that this is the ratio of total radiation energy of the real body in order to the total radiation energy of an ideal thermal black body at the same temperature [4,5]:

$$\epsilon = \frac{W_0}{W_{ct}} \quad (4)$$

Where is: W_o – the total energy of real body radiation
W_{ct} – total energy radiation of ideal thermal black body

Emissivity factor values for practical all common materials are known and available in the literature. In certain cases it is necessary to determine the emissivity factor. For that it is necessary to measure the exact temperature of the body with one of the contact methods, and then accordingly set the parameters in infrared camera. Often on the surface of objects is applied a coating with well known emissivity to achieve uniform emissivity factor [6-9]. This is not applicable in larger metal processing industry, due to significantly large areas that are observed. In those cases is mainly a temperature distribution measured, and there is no need to determine the exact value of temperature, and emissivity factor can be ignored. This is more often case in foundries and metallurgical plants because the different elements have different values of emissivity factors.

THERMOGRAPHY IN THE METALLURGICAL PRACTICE

In the production and processing of metals by casting, the use of thermography has a wide application, from observation of the production conditions and thermal loads alone of plants, to the analysis and detection of defects during casting and cooling of castings. Any errors on the installations of metal production plant can result from large financial losses, to even work injuries and casualties. In metallurgical practice, this primarily refers to the condition of the insulation, state of lining, and condition of openings for loading and ejecting metal on metallurgical furnaces. The smallest openings in the joints of the doors can lead to significant financial costs due to lose of heat energy. Wear of the refractory lining on the ladles and furnaces for melting metal is a serious problem and possible danger in the metal production. Thermography in this area has some advantages over other temperature distribution measuring methods: it gives the possibility of determining the exact place of heat losses due to the wear of lining (Figure 3 a)), or not fully closed doors (Figure 3b)).

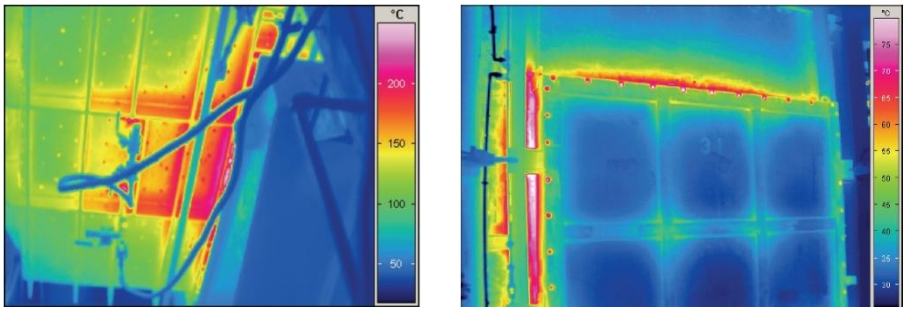

a) b)

Figure 3. Thermographic testing of melting furnace [10]
a) point of the leak of heat due to poor insulation,
b) inadequate closing of door

Example given in Figure 3 a) shows how the thermographic analysis can predict the place where it is possible to be a significant failure of melting furnace. In doing so, one can stop the production on time in order to prevent greater damage and do the necessary repairs of the lining. By using the contact methods it would be required a larger number of measurements on the surface of the furnace to obtain only a general overview of the same temperature distribution as is given in Figure 3. In production of steel there are used a different types of ladles and during production they wear out. From time to time it is necessary to carry out their repair. In the metallurgical practice this is usually done after a certain number of melting cycles and from visual inspection of the ladles. But sometimes it is possible that due to various factors the lining wears out much earlier on some parts. This sometimes is not visible to the naked eye, and it poses a danger to workers. Figure 4 shows the view of the steel casting ladle: a) visible spectrum, and b) thermal imaging camera recorded temperature distribution on the full ladle.

a) b)

Figure 4. Steel casting ladle [11]
a) in visible spectrum
b) in infrared spectrum

It is clear that using thermography it is possible to predict the eventual flaws in lining, which in addition to material savings, give additional safety for employees [11]. The steel plant Hüttenwerke Krupp Mannesmann GmbH (HKM), located in Duissburg, Germany, noted thermography as a very useful method, and they use it in inspection of various production

processes in order to increase productivity, reduce costs, and to increase the employee's safety. They emphasize that they daily find various new applications of thermography in the production of steel. In addition to the overall observation of plants, thermography finds application in foundries for observation of process during melting and solidification of metal when casting into moulds [12, 13]. It has proven to be a very efficient method for determining cooling curves of metal during casting [12]. Using infrared cameras as detector of changes in emissivity factor, one can accelerate the process of casting and reduce the amount of impurities (such as slag) in the castings [13].

Furthermore, thermographic cameras are becoming standard equipment for inspecting and control the temperature of permanent casting tools in foundries of aluminium alloys using gravity die casting (GDC) and high pressure die casting (HPDC) technologies [14,15]. It is shown that usage of thermographic cameras has its advantages in temperature monitoring of casting tools. As the right temperature of preheating is of great importance for the longer lasting time of permanent casting tools, there have been developed a computer software's which uses thermographic cameras to monitor tool temperatures for each cycle of casting.

As thermography is contactless non-destructive temperature measuring method, specific systems are developed for error detection in metal workpieces [16-18]. Thus, in [16] describe the use of thermography as a method for testing of steel blocks before rolling process. As defects change metals thermal conductivity in their area, a new method for detecting defects in metal is developed, just by measuring the distribution of temperature on the surface of metals. In presence of defect temperature distribution on surface is changed. A similar principle is used to detect errors in the testing of railway tracks [18], which greatly accelerated the testing of train tracks.

Thermography has proven to be a very suitable method for the observation and analysis of the changes in deformation zone during plastic deformation [8, 9, 19, 20]. By using thermographic method in the studies of the deformation zone and the material plastic flow, it can be observed elastic and plastic material behaviour. In the elastic area during stretching of metal materials thermography showed the temperature drop at some tested materials [9, 21, 22]. This is related to the thermo-elastic effect. Figure 5 shows the measured changes in temperature of the samples during the static tensile testing using thermography.

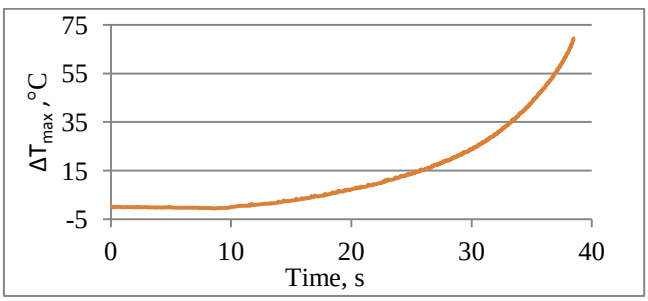

a)

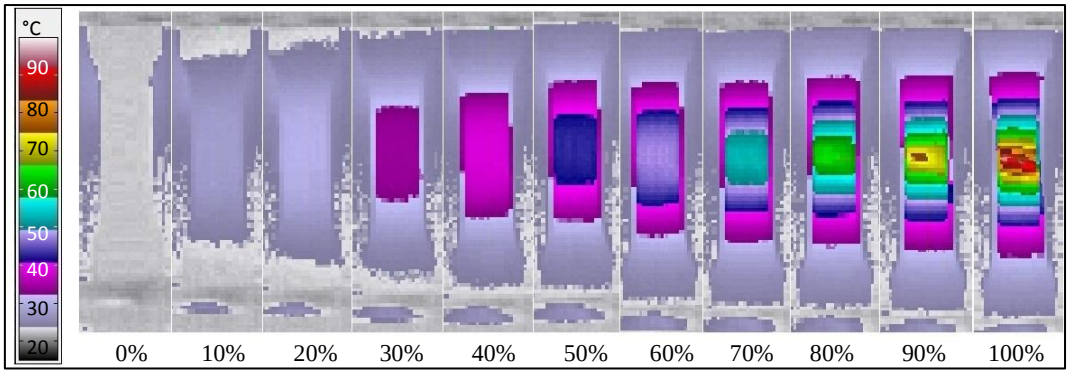

b)

Figure 5. Elastic and plastic deformations measuring using thermography [9]
a) quantitative measurements of temperature changes
b) temperature distribution during plastic deformation

In the first part of temperature analysis (Figure 5 a)), it can be seen the mentioned temperature drop due to thermo-elastic effect. The start of plastic flow is characterized by first increasing in temperature, which allows the determination of the start of plastic deformation using the thermographic method [9, 23-24]. Thermography can even detect a very small changes in temperature due to localized deformations such as Lűders bands [9, 23, 24]. Figure 5 b) shows the temperature distribution within the deformation zone, which is related to distribution of plastic deformation in test material [9]. From the obtained thermographs it is possible to obtain quantitative and qualitative information about deformation zone, as well as to spot any cracks due to inadequate selection of plastic deformation parameters.

ADVANTAGES AND DISADVANTAGES OF THE METHOD

The main advantage of this method is that provides immediate results in real time, enabling early detection of certain temperature changes due to faults or plastic deformation. Thermography is a non-contact method and allows investigations in areas that are hard to reach, and even dangerous for people to be in. Using thermography those areas can be inspected from greater distance, and without significant impact on the measurement accuracy. It allows the automation of the production process by shorter time for spotting errors, for example during casting from ladles, which increases the safety of the workers reducing manufacturing costs and increases product quality. The method itself is simple to use, and can be implemented at various locations in the production process.

As main disadvantage of this method it can be highlighted the strong sensitivity on the surrounding sources of heat radiation. It is necessary to know the emissivity factor, or to determine it before testing. Another disadvantage is that one can measure the temperature of the body that is directly in front of the camera lens, without the possibility of measurement through some barriers, for example behind the wall of furnace or behind glass openings. In special cases it can be used a special filter that has a possibility of transmission

of infra-red radiation, which serve as a screen between the measured object and the camera. If such material is mounted on the opening of the furnace, then the thermographic camera can measure the processes inside through the "screen". The disadvantage is relative high prizes of cameras, although today there are available relatively cheap models.

CONCLUSIONS

It can be concluded that thermography is a very effective method, which can be implemented in different areas of metallurgy.

It represents perspective method of finding errors and defects in the production and processing in metal production. It becomes an indispensable tool for the maintenance of production facilities for in real time indication of defects, and thus one can react on time and remove any deficiencies in short period. Its application in the studies on deformation of metals and alloys gives a clearer picture on the processes that take place during plastic deformation.

Measurements of temperature changes during deformation, with knowledge of the amount of deformation, enable the implementation of this method in the processes of plastic processing of metals, during monitoring of changes in the deformation zone.

REFERENCES

[1] J. Nowacki, A. Wypych, Application of thermovision method to welding thermal cycle analysis, Journal of Achievements in Materials and Manufacturing Engineering, 40 (2010) 2, pp.131-137.
[2] M. Hrvoje, Đ. Damir, Primjena infracrvene termografije u održavanju stambenih objekata, Accessible on Internet http://www.huict.hr/images/pictures/impl_doc_1_20.pdf, (20.03.2012) 76.
[3] http://www.lenalighting.pl/en/knowledge/spectrum-of-visible-radiation/, (13.02.2015.)
[4] Basic Principles Of Non-Contact Temperature Measurement, Accessible on Internet http://www.optris.com/applications?file=tl_files/pdf/Downloads/Zubehoer/IR-Basics.pdf, (25.01.2015.)
[5] Principle of thermal imaging, Accessible on Internet https://www.google.hr/url?sa=t&rct=j&q=&esrc=s&source=web&cd=1&cad=rja&uact=8&ved=0CBwQFjAA&url=http%3A%2F%2Fwww.inmes.hr%2Fpdf%2Fthermography.pdf&ei=Xm5AVYrzBcGMaLfogegM&usg=AFQjCNHcPBSX_0BSY-joA1UZ2g5kTbrRAg, (20.04.2015.)
[6] I. Jandrlić, S. Rešković, L. Lazić; Značaj faktora emisivnosti kod termografskih ispitivanja plastičnosti čelika, Proceedings of 12th International Foundrymen Conference, Sustainable Development in Foundry Materials and Technologies, ur. N. Dolić, Z. Glavaš, Z. Zovko Brodarac, Metalurški fakultet, Opatija, 24. – 25. svibanj 2012., pp.169-175.

[7] I. Jandrlić, S. Rešković, Application of thermographic method in determining the onset of plastic deformation, Proceedings of 13th International Foundrymen Conference, Innovative Foundry Processes and Materials, ur. Z. Glavaš, Z. Zovko Brodarac, N. Dolić, Metalurški fakultet, Opatija, 16. – 17. svibanj 2013., pp.163-170.
[8] I. Jandrlić, S. Rešković, Choosing the optimal Coating for thermographic inspection, The Holistic Approach to Environment, 5(2015)3, pp.127-134
[9] I. Jandrlić, Raspodjela naprezanja u zoni deformacije niobijem mikrolegiranog čelika, Faculty of metallurgy, University of Zagreb, 2015.
[10] Thermography for Insulation Checks VarioCAM® high resolution – precise, efficient and reliable, Accessible on Internet http://www.infratec-infrared.com/fileadmin/downloads/pdf/furnace_lining_thermal_ceramics.pdf, 17.3.2016.
[11] HKM's steelworks use FLIR P-Series infrared cameras to inspect, maintain and optimize production processes, Accessible on Internet, http://www.flir.com/uploadedFiles/Thermography/MMC/Brochures/T559271/T559271_EN.pdf , 17.3.2016.
[12] R. Władysiak, A. Kozuń, An Application for Infrared Camera in Analyzing of the Solidification Process of Al-Si Alloy, Archives of foundrye ngineering, 15 (2015) 3, 81-84
[13] Detection of Slag Impurities in Molten Metals for Improved Yield and Quality, Accessible on Internet, http://www.sensorsinc.com/applications/thermography/detecting-metal-impurities, 17.03.2016.
[14] B. Kosec, Failures of dies for die-casting of aluminium alloys, Metalurgija 47 (2008) 1, pp.51-55
[15] B. Kosec, G. Kosec, M. Soković, Temperature field and failure analysis of die-casting die, Archives of Materials Science and Engineering, 28 (2007) 3, pp.182-187
[16] S. Štarman, V. Matz, Automated system for crack detection using infrared thermographic testing, Proceeding book of 17th World Conference on Non-Destructive Testing 2008 (WCNDT 2008) 25-28 October 2008., Shanghai, China, Vol. 1, pp.1238-1243.
[17] X.G. Wang, V. Crupi, X.L. Guo, Y.G. Zhao, Quantitative Thermographic Methodology for fatigue assessment and stress measurement, International Journal of Fatigue 32 (2010), pp. 1970–1976.
[18] J. Wilson, G. Tian, I. Mukriz, D. Almond, PEC thermography for imaging multiple cracks from rolling contact fatigue, NDT&E International 44 (2011), pp.505–512.
[19] W. Oliferuk, M. Maj, R.Litwinko, L. Urbanski, Thermomechanical coupling in the elastic regime and elasto-plastic transition during tension of austenitic steel, titanium and aluminium alloy at strain rates from 10^{-4} to 10^{-1} s^{-1}, European Journal of Mechanics A/Solids, 35 (2012), pp.111-118.
[20] A. Rusinek, J.R. Klepaczko, Experiments on heat generated during plastic deformation and stored energy for TRIP steels, Materials and Design, 30 (2009), pp.35–48.

[21] I. Jandrlić, S. Rešković, M. Lovrenić-Jugović; On the thermoelastic behaviour of low carbon steel, Summaries of absracts of 11th International Symposium of Croatian Metallurgical Society "Materials and Metallurgy", Metalurgija 53(2014)3, p. 421.
[22] G. Risitano, A. Risitano, C. Clienti, Determination of the fatigue limit by semistatic tests, In: Proceedings of Convegno Nazionale IGF XXI, Cassino (FR), Italia, 2011, 322-330.
[23] S. Rešković, I. Jandrlić, F. Vodopivec, Influence of testing rate on Lüders band propagation in niobium microalloyed steel, Metalurgija, 55 (2016) 2, pp.157-160.
[24] S. Rešković, I. Jandrlić, Influence of niobium on the beginning of the plastic flow of material during cold deformation, The Scientific World Journal, 2013 (2013), pp.1-5.

15th INTERNATIONAL FOUNDRYMEN CONFERENCE
INNOVATION – The foundation of competitive casting production
Opatija, May 11th-13th, 2016
http://www.simet.hr/~foundry/

MANAGEMENT OF SCIENTIFIC INNOVATION IN METALLURGICAL INDUSTRY

Ž. Kamberović[1], D. Rajić[2], J. Uljarević[2] and K. Delijić[3]

[1]University of Belgrade Faculty of Technology and Metallurgy, Belgrade, Serbia
[2]Innovation Center of Faculty of Technology and Metallurgy in Belgrade Ltd., Belgrade, Serbia
[3]University of Podgorica Faculty of Metallurgy and Technology, Podgorica, Montenegro

Oral presentation
Subject review

Abstract

Realizing the vision of creating scientific innovation and achieving significant economic impact beneficial to the development of countries in transition generally represents widely accepted requirements. In the situation of brain drain and lack of R&D private sector, the scientific innovation is the main driver which can lead a country to the success, so it is necessary to for organizations to parallel enforce both QMS and integrated innovation standard TS 16555. Innovation management standard is consisted of following parts: innovation management system, strategic intelligence management, innovation thinking, intellectual property management, collaboration management, and creativity management and innovation management assessment. However, the standards themselves are not a guarantee that the innovation productivity will rise in the business entities, thus it is necessary to include creative engineering in daily practice. It is based on TRIZ- methodology of innovative creativity. TRIZ itself comprises tools for efficient solving of technical and technological problems of different complexity levels. Creating infrastructure for knowledge transfer in scientific institutions is of great importance, due to the expanding influence of marketing at universities, and also possibility of increasing market potential of academic knowledge. This paper will present examples of energy and materials efficiency in metallurgical industry, especially molten metal production, casting of mill balls and high tech refractory automotive parts. In this approach environmental issues and cleaner production takes important segment.

***Keywords**: innovation management, TRIZ, metallurgy, foundry, economy*

*Corresponding author (e-mail address): *juljarevic@tmf.bg.ac.rs*

Sažetak

Realizacija vizije stvaranja znanstvenih inovacija i dostizanja ekonomskih beneficija razvoju zemalja u tranziciji općenito predstavlja široko prihvaćen zahtjev. U situaciji odljeva mozgova i nedostatka R&D u privatnom sektoru, znanstvene inovacije su glavni pokretač koji može dovesti zemlju do uspjeha, tako da je za organizacije najpotrebnije da paralelno provode oba sustava upravljanja kvalitetom, integrirani inovacijski standard TS 16555. Inovacijski standard sastoji se od sljedećih dijelova:

inovacijski sustav za upravljanje, strateško inteligentno upravljanje, inovacijsko razmišljanje, upravljanje intelektualnim vlasništvom, upravljanje suradnjom i kreativnošću i ocjenjivanje upravljanja inovacijama. Međutim, sami standardni nisu garancija da će produktivnost inovacija rasti u poslovnim subjektima, tako da je potrebno uključiti kreativni inženjering u svakodnevnoj praksi. On se temelji na TRIZ metodologiji inovacijske kreativnosti. Sam TRIZ sadrži alate za učinkovito rješavanje tehničkih i tehnoloških problema različitih razina složenosti. Stvaranje infrastrukture za prijenos znanja u znanstvenim institucijama od velike je važnosti s obzirom na širi utjecaj marketinga na sveučilištu ali i mogućnost povećanja tržišnog potencijala akademskog znanja. Ovaj rad će predstaviti primjere učinkovitosti energije i materijala u metalurgiji, naročito proizvodnja rastaljenog metala, lijevanje u topionici za loptice i visokotehnološki, vatrostalni automobilski dijelovi. U ovom pristupu pitanja okoliša i čistije proizvodnje su važan segment.

Ključne riječi: *inovacijski menadžment, TRIZ, metalurgija, ljevaonica, ekonomija*

UVOD

Koncept stvaranja znanstvenih inovacija, kao poslovna strategija za nadilaženje ekonomskih teškoća u zemljama u tranziciji, s velikim uspjehom, a u različito vrijeme, primjenjivan je u nizu zemalja (npr. Južna Koreja, Singapur, Irska, Japan, Finska, Kina, Njemačka, Izrael...) na osnovu modela koje su primijenile SAD za svoj ekonomski oporavak i izlazak iz stanja velike recesije 1929. godine [1]. Danas se ovaj koncept koristi i na mikro planu, za nadilaženje krize u poslovanju poduzeća. Inoviranje postojećih proizvoda, u kratkom vremenu i s malo utrošenih resursa, uvjet je opstanka poduzeća na tržištu.

U uvjetima kada većina privrednih subjekata posjeduje integrirani sistem kvalitete (IQMS), jasno je da samo poslovanje bazirano na sistemu kvalitete nije garancija opstanka na tržištu. Kada dva privredna subjekta posjeduju IQMS, ono što ih međusobno izdvaja prema kriteriju uspješnosti je spremnost na značajan inovativni angažman i ulaganje u ovo područje, jer će rezultat te investicije biti u ostvarenoj komparativnoj prednosti na tržištu.

Cilj ovog rada je da ukaže na relevantnost implementacije novog integriranog sistema menadžmenta kvalitetom (QMS), koji bi obuhvatio i primjenu inovacijskih standarda TS16555 [2-7] u funkciji opstanka i razvoja privrednih subjekata. Inovacijski standardi imaju potencijalnu primjenu kod inovacije proizvoda, usluga, marketinga, same organizacije itd. Međutim, samo njihovo uvođenje u privredne subjekte nije garancija uspješnosti u inovacijskom stvaralaštvu. Za to je neophodna primjena uspješne inovacijske metodologije poput TRIZ-a i njegovih inovacijskih standarda [1] ali i drugih TRIZ alata koji povezuju QMS i TRIZ [8]. Također je neophodna edukacija stručnjaka iz tehničkih područja(onih od kojih se očekuje stvaranje inovacija), ali i menadžmenta poduzeća (onih od kojih se očekuje da stvore uvjete za uspješan inovacijski rad).

ZNANSTVENE INOVACIJE KAO PRAVAC RAZVOJA

Glavne karakteristike suvremenog tehničkog napretka sastoje se u spajanju znanosti i tehnike, tj. u zatvaranju lanca od fundamentalnih znanstvenih istraživanja, preko usmjerenih, primijenjenih i razvojnih, do same proizvodnje. Inovatorstvo u razvijenim zemljama zasniva se na timskom radu obrazovanih specijalista tehničke struke, koji planskim istraživanjem, uz izdašnu financijsku potporu svojih investitora, programirano „ciljaju“ na određena nova tehnička rješenja. U tom smislu, ključni resursi inovatorstva su: obrazovanje, organizacija, infrastruktura i kapital.

Postoji bitna razlika između shvaćanja inovacije u visoko razvijenim zapadnim državama u odnosu na dalekoistočne zemlje, pri čemu treba naglasiti da obe grupacije imaju najrazvijenije ekonomije u svijetu bazirane na znanju. U prvom slučaju, pažnja je usmjerena ka stvaranju radikalne inovacije, koja predstavlja tehnološki prodor i koja prouzrokuje značajne promjene na tržištu. U drugom slučaju se na inovaciju gleda kao na novi tehnološki progres do koga se dolazi kroz niz malih, sukcesivnih poboljšanja postojećeg proizvoda, tehnologije ili usluge.

U zakonskoj regulativi i u stručnoj literaturi spominju se terminološki slični, a ipak različiti pojmovi invencije i inovacije. Invencija je koncept, ideja i metoda za dobivanje novog proizvoda ili procesa, uključujući otkriće nove tehnologije (proizvoda ili procesa) za iskorištavanje prirodnih resursa. Inovacija je uspješna tržišna primjena invencije, odnosno primjena novog ili značajno poboljšanog proizvoda, procesa ili usluge [1].

Svjetski ekonomski forum definira konkurentnost kao skup institucija, propisa i drugih čimbenika koji određuju nivo produktivnosti zemalja. Pokazatelj nivoa konkurentnosti naziva se Globalni indeks konkurentnosti (Global competitiveness index - GCI) i bavi se mjerenjem prosjeka više mikroekonomskih i makroekonomskih komponenata, koji se pojedinačno vrednuju na skali od 1 do 7. Svi mjereni pokazatelji su grupirani u dvanaest stupova i odražavaju različite aspekte složene ekonomske stvarnosti. Dvanaesti stup odnosi se na inovacije. Poduzeća u razvijenim zemljama moraju sama da osmišljavaju i razvijaju nove proizvode i procese, kako bi održavale konkurentsku prednost. To zahtjeva okruženje koje podržava razvoj inovativnosti, odnosno ulaganja u istraživanje i razvoj, ostvarivanje suradnje između sveučilišta i privrede, zaštitu intelektualne svojine itd. [9].

IZAZOVI PRED KOJIMA SU SE NAŠLE INOVATIVNE ORGANIZACIJE

Znanost, kao područje koje stvara novo znanje, dobiva sve više na značaju prilikom kreiranja strategija razvoja europskog društva. Istraživanje i inovacije u Srbiji su sastavni element većine strateških dokumenata koji su usvojeni u prethodnih nekoliko godina i samim time su vezani za djelatnost većeg broja ministarstava. Mada suštinsku odgovornost za razvoj znanosti i inovacija imaju u svojoj domeni sva ministarstva, osnovni poslovi u ovoj djelatnosti su povjereni Ministarstvu prosvete, znanosti tehnološkog razvoja (MPNTR). Usprkos brojnim teškoćama s kojima su se društvo i zemlja suočavali u proteklom periodu, znanost u Srbiji

sačuvala je svoju kritičnu masu, a u pojedinim segmentima se osnažila i zabilježila rast i uspjehe na međunarodnom nivou.

U nacrtu nove Strategije znanstvenog i tehnološkog razvoja Republike Srbije za period od 2016.-2020. godine pod nazivom „Istraživanje za inovacije“, ključne izazove predstavljaju:

1. Upravljanje znanstvenim i inovacijskim sistemom koje nije dovoljno efikasno i ne postoji koordinacija između relevantnih institucija,
2. Izvrsnost znanstvenih istraživanja i njihova relevantnost za ekonomski razvoj zemlje i društva u cjelini nisu dovoljno podržani trenutnim sistemom financiranja,
3. Ne postoje adekvatni financijski instrumenti i institucionalni okvir za povezivanje znanstvenosti i privrede,
4. Postoji nedostatak ljudskih resursa u znanstvenoistraživačkim organizacijama i u privatnom sektoru i ne postoje dugoročne mjere za rješavanje ovog problema,
5. Znanost u Srbiji nije u potpunosti integrirana na u Europski istraživački prostor i nedovoljan broj znanstvenika sudjeluje u međunarodnim projektima [10].

Misija MPNTR je da pripremi i provede paket reformskih mjera koje će stvoriti uvjete za ostvarivanje vizije i strategije. EU također prepoznaje značaj utjecaja razvoja i primjene znanstvenih i tehnoloških dostignuća na razvoj ekonomije i cjelokupnog društva. Europska komisija formirala je novi tim znanstvenih savjetnika. Sedam znanstvenika, koji potječu iz sedam zemalja i sedam znanstvenih disciplina usredotočiti će se prvenstveno na hitna i dugoročna pitanja. Europska komisija promovira međusobnu suradnju privrednog i znanstveno-istraživačkog sektora i potiče znanstveno-istraživačku djelatnost i tehnološko-razvojne projekte, kako razvojnih centara poduzeća, tako i sveučilišta i istraživačkih instituta u cilju efikasnijeg korištenja i postizanja sinergijskog efekta [11].

INOVACIJSKE METODOLOGIJE I INOVACIJSKI STANDARDI

Samo sistemski pristup u rješenju problema pruža najveće šanse za njegovo efikasno rješenje. Sistemsko mišljenje podrazumijeva interdisciplinarno, istovremeno promatranje istog predmeta sa stanovišta raznih znanstvenih disciplina. Zato je, pored korištenja metodologije kreativnog inženjeringa, za proces stvaranja inovacija poželjan timski, a ne individualni rad.

Inovatori uglavnom koriste metodologije koje su im poznate iz drugih disciplina, a koje su savladali u okviru svog redovnog školovanja. Ipak, najčešća metodologija koju koriste je metoda pokušaja i pogreške, koja je najmanje efikasna i zahtjeva najveći utrošak resursa. Od svih kreatoloških metoda koje se danas primjenjuju, teorija rješavanja inventivnih zadataka (TRIZ) je među najefikasnijom u oblasti inovacijskog stvaralaštva, jer se jedina bazira na heuristici, a ne psihologiji [12].

Kreatološke metode (brainstorming, lateralno mišljenje, SCAMPER metoda, mapiranje misli) bazirane su na emocionalnoj osnovi, zbog čega postoji teškoća da se savlada psihološka inercija u procesu ljudskog razmišljanja. Psihološka inercija ili inercija mišljenja navodi pojedinca da razmišlja na standardni način, onako kako su ga učili kroz proces obrazovanja i odgoja. Jedna od najpogodnijih metodologija za nadilaženje problema psihološke inercije je TRIZ [13-22]. TRIZ se jedini od poznatih kreatoloških metodologija bazira na empirijskoj osnovi, a ne psihološkoj. Autor TRIZ-a je G. Altuler koji je bio zaposlen u Patentnom uredu sovjetske mornarice na radnom mjestu - ispitivač patenata. On je proučavanjem pronalazaka identificirao 39 standardnih parametara i 40 zajedničkih inventivnih principa za rješavanje proturječnosti u pronalascima, na osnovu kojih je razvio svoju TRIZ teoriju. Od 90-ih godina prošlog stoljeća, nakon raspada bivšeg Sovjetskog Saveza, TRIZ je postao dostupan i zapadnim zemljama, pri čemu je doživio daljnji procvat i primjenu u skoro svim područjima ljudskog stvaralaštva.

TRIZ se kao metoda stvaralaštva izučava na više od 40 najprestižnijih sveučilišta u svijetu i praktično primjenjuje u više od 500 najmoćnijih svjetskih kompanija. TRIZ rješenja se direktno manifestiraju u poboljšanju proizvoda i smanjenju cijene proizvodnje. Danas postoji TRIZ softverska baza podataka koja obuhvaća preko 3 miliona najjačih svjetskih patenata.

Općenito govoreći, TRIZ koristi sljedeće korake pri rješavanju tehničkih problema (sl. 1):

1. Sistemska analiza uzročno-posljedičnih veza koja inovatora treba da dovede do mjesta primarnog uzroka, do tzv. operativne zone problema;
2. Formuliranje idealnog konačnog rezultata (IKR);
3. Izdvajanje proturječnosti koje ometaju IKR i
4. Razrješenje proturječnosti uključivanjem zakona razvoja tehničkih sistema i instrumenata TRIZ-a namijenjenih za rješavanje zadataka.

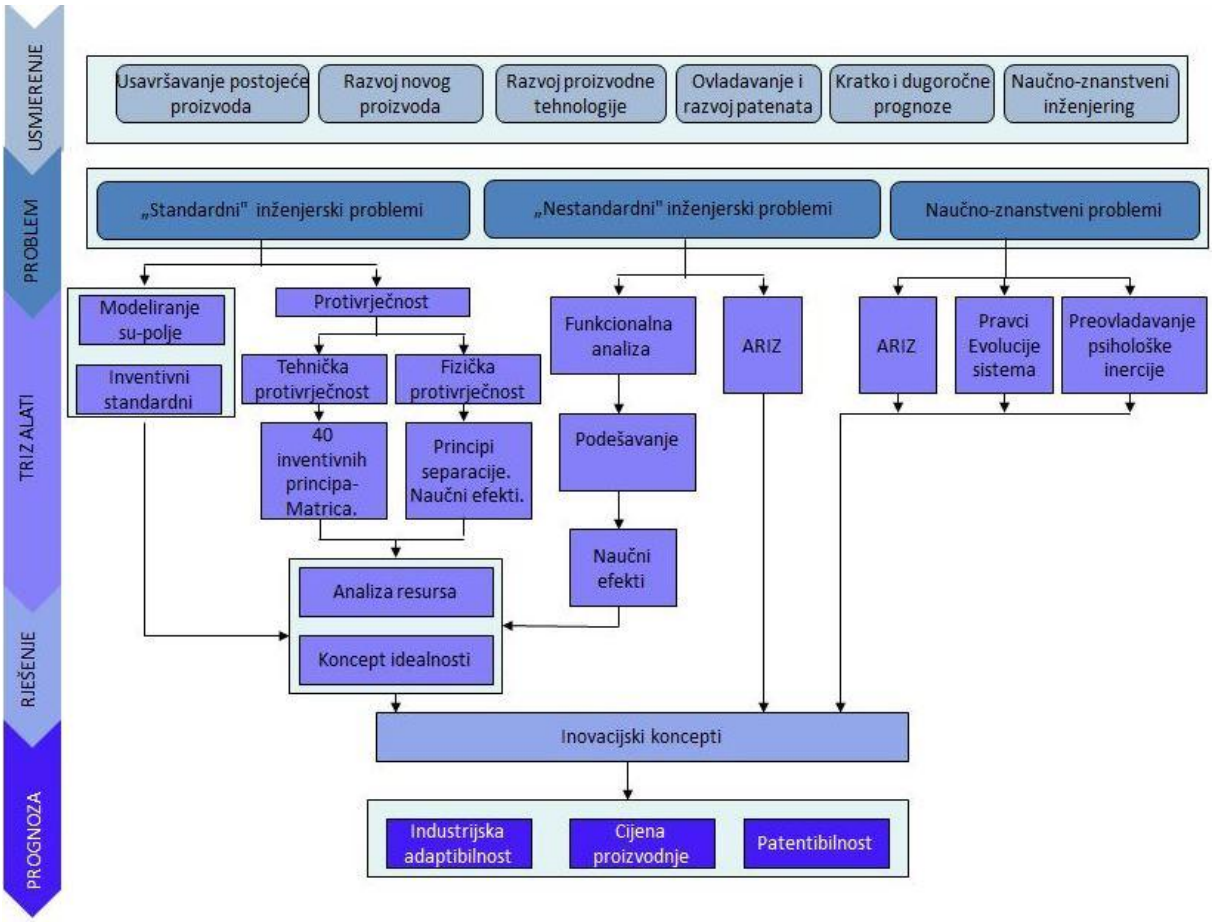

Slika 1. Procesi rješavanja problema pomoću TRIZ metodologije

Dakle, u privrednim subjektima, neophodna je primjena TRIZ metodologije kao jedine znanstvene metodologije inovacijskog stvaralaštva kako bi se na efikasan način riješili brojni tehničko-tehnološki problemi koji se javljaju u privrednim subjektima.

Kako su inovacije glavni pokretači koji organizaciju mogu dovesti do uspjeha, potrebno je primjenjivati, paralelno sa sistemom kvalitete i inovacijski sustav kvalitete TS 16555. On obuhvaća: sistem menadžmenta inovacijama, menadžment strateškim informacijama, inovativno razmišljanje, intelektualnim vlasništvom, suradnjom i kreativnošću kao i ocjenjivanje menadžmenta inovacijama. Implementacija ovog sistema organizacijama može donijeti razne benefite, koji se pored rasta prihoda i povećanja profita, odnose i na uvođenje novog načina razmišljanja i stvaranje novih vrijednosti, omogućuje bolje razumijevanje potreba i tržišnih mogućnosti, pomaže sagledavanju rizika poslovanja i daje prijedloge za njihovo nadilaženje, doprinosi sveukupnom kreativnom razmišljanju organizacije i potiče uključivanje svih zaposlenih kroz timski rad [2-7].

U literaturi [26] dan je prikaz mogućnosti primjene metodologije kreativnog inženjeringa u oblasti ljevarstva. Primjenom Altshulerove matrice definiran je problem izdvajanjem proturječnosti koje utječu na efikasnost procesa lijevanja flotacijskih kugli. Kao karakteristika

sistema koji treba korigirati izdvaja se smanjenje trošenja alata za lijevanje kugli. Uvođenjem funkcije zaštite alata, koja se provodi na načine dobivene korištenjem Altshulerove matrice, značajno se doprinosi povećanju radnog vijeka kokile primjenom TRIZ metode u procesu lijevanja flotacijskih kugli.

Također, uspješan primjer realizacije inovacija u procesu taljenja nestandardnih šarži željezonosnih materijala prikazan je u literaturi [27].

PRIJEDLOG OPERATIVNIH SMJERNICA RADI OSIGURANJA PREDUVJETA ZA UPRAVLJANJE INOVACIJAMA

Inovativne organizacije u Srbiji našle su se pred nizom poteškoća u realizaciji svoje misije, kako na strateškom, tako i na operativnom nivou. Kroz nacrt srpske strategije iskazana je potreba za strateškim upravljanjem inovacijama. Međutim, potrebno je u akcijskom planu dati konkretne prijedloge kako potaći suradnju znanosti i privrede, točno definirati tko osigurava novčana sredstva za financiranje znanosti i istraživanja koja bi rješavala konkretne probleme privrede i poticala njenu konkurentnost kroz inovacije. Novčana sredstva trebao bi osigurati Inovacijski fond, koji je osnovan Zakonom o inovacijskoj djelatnosti radi poticanja inovativnosti i osiguravanja sredstava za financiranje inovacijske djelatnosti, prvenstveno kroz suradnju s međunarodnim financijskim institucijama, organizacijama, donatorima i privatnim sektorom. Cilj Fonda je poticanje i financiranje inovativnosti u prioritetnim područjima znanosti i tehnologije, odnosno da se pruži podrška da nove tehnologije stignu iz akademskih okvira do privrede, kao i da se pomogne malim i srednjim poduzećima koja razvijaju inovacijske tehnologije [23]. Jednu od uspješnih mjera planira da provodi Ministarstvo privrede kroz dodjelu inovacijskih vaučera, davanje bespovratnih sredstava poduzetnicima, koji imaju za cilj poticanje suradnje sektora malih i srednjih poduzeća sa znanosti. Također, inovacijskim organizacijama treba da bude dozvoljeno da direktno provode transfer tehnologije iz znanosti u privredu. Na slici 2. predstavljen je alternativni model transfera znanja na sveučilištima.

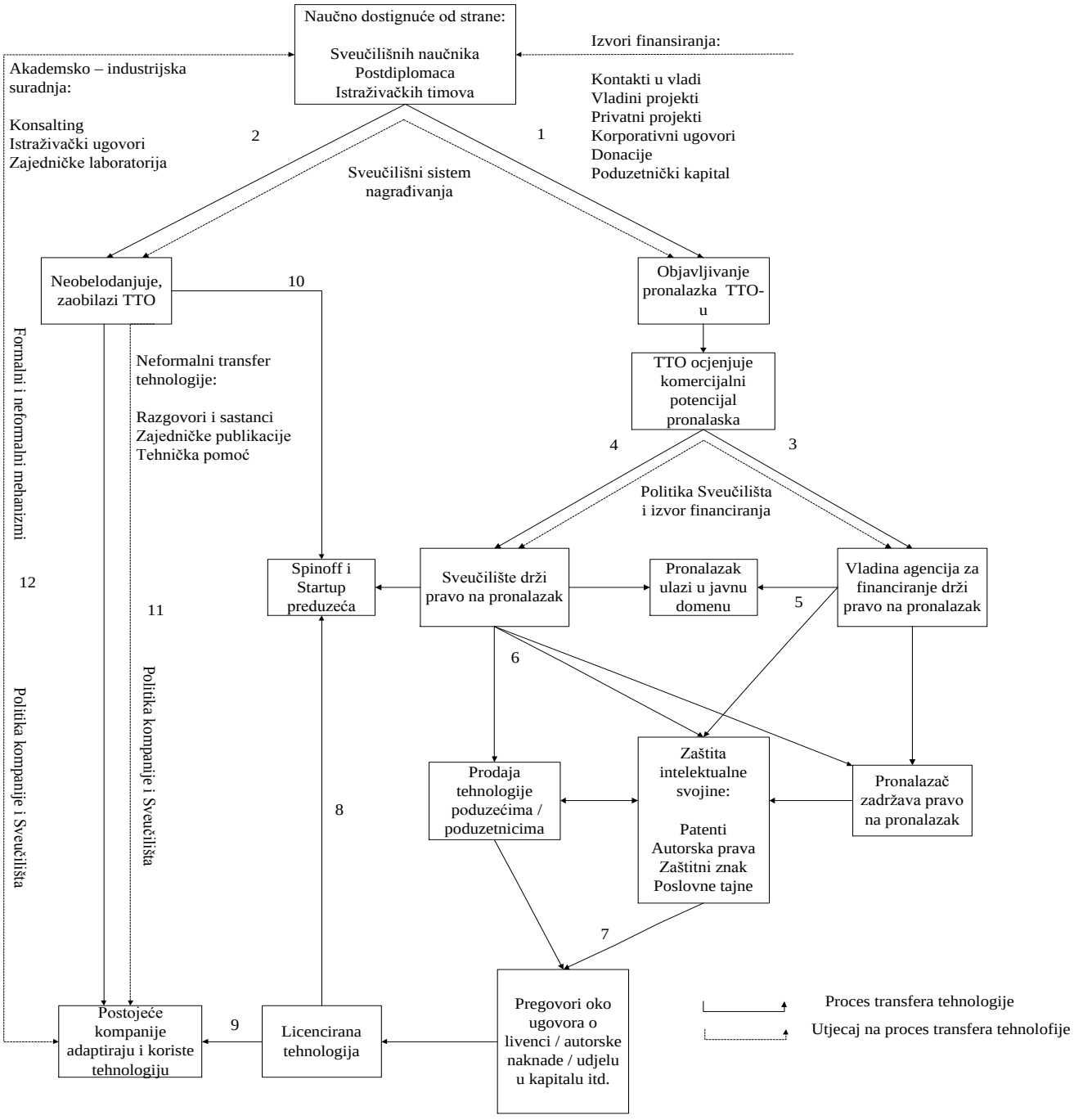

Slika 2. Alternativni model transfera znanja na sveučilištima

Kako bi sve inovacijske organizacije doprinosile definiranoj misiji, potrebno je da kroz sistem kvaliteta, u kojem je integriran i inovacijski standard, prate i ključne indikatore uspjeha koji treba da se oslanjaju na prijedloge iz strategije, prikazane na slici 3.

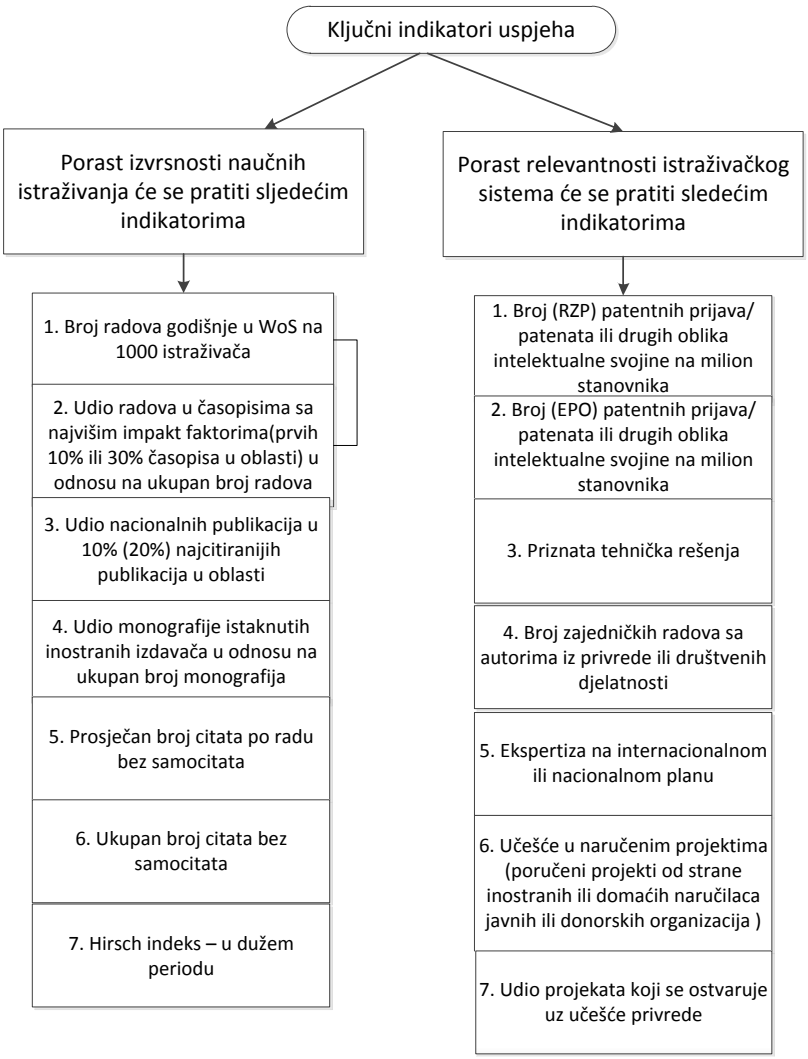

Slika 3. Ključni indikatori uspjeha [10]

Potrebno je osigurati i infrastrukturu neophodnu za razvoj tehnoloških inovacija kao i okruženje za ekološki rizične tehnologije. Nakon licenciranja veliki broj inovacija nastalih na sveučilištu su na nivou potvrde koncepta u laboratorijskim uvjetima i još uvijek su u fazi razvoja, tako da su neophodni dodatni napori istraživača kako bi se stekli realni uvjeti za komercijalni uspeh, što je i osnovni cilj formiranja T_HUB-OFF-a [24]. Projekt „Tehnološki hub i inovacijski spin-off centar“ spada u infrastrukturna ulaganja u oblasti komercijalizacije akademskog znanja. T_HUB-OFF je specijalistički organiziran istraživački prostor namijenjen za transfer inovacija iz uvećanih laboratorijskih u poluindustrijske i tržišne uvjete [24].
Stvaranje infrastrukture za transfer znanja u znanstvenim institucijama je od velikog značaja, ne samo zbog proširivanje utjecaja marketinga na univerzitete, već i zbog mogućnosti uvećavanja tržišnog potencijala akademskog znanja [25].

ZAKLJUČAK

U eri sve bržeg tehnološkog napretka, gdje znanstveno-tehnološka dostignuća prožimaju sve aspekte ljudskog života, znanost, tehnološki razvoj i inovacije imaju značajnu ulogu u poticanju ekonomskog razvoja. Inovacijske djelatnosti smatraju se glavnim faktorima za stabilnu ekonomiju usmjerenu ka znanju, koja je postala osnova konkurentnosti i dinamičnog razvoja.

Primjenom TRIZ-ovih standarda rješavaju se na efikasan način brojni tehničko-tehnološki problemi koji se javljaju u privrednim subjektima. Za uspješno inovacijsko stvaralaštvo neophodna je i kontinuirana edukacija lica od kojih se očekuje da stvaraju inovacije, kako bi se stvorili preduvjeti za generiranje inovacija koje se baziraju na znanstvenoj metodologiji, a ne individualnoj intuiciji i nadahnuću.

U radu je ukazano na značaj i potrebu uvođenja inovacijskih standarda TS16555 za uspješnije poslovanje privrednih subjekata. Predlaže se uključivanje ovih standarda u integrirani sistem menadžmenta kvalitetom (IQMS). Primjenom inovacijskih standarda unapređuje se rad uspješnih privrednih subjekata, a onima koji su neuspješni pruža se mogućnost izbjegavanja najgoreg – stečaja, promjenom vlastite pozicije na tržištu.

Ovaj rad je doprinos uspostavljanju operativnog sistema suvremene inovacijske djelatnosti zasnovane na principima moderne znanosti i pozitivnim praktičnim iskustvima iz tog područja, na primjeru iz metalurške industrije. Ukazano je na glavne operativne smjernice koje je neophodno primijeniti na svim nivoima upravljanja, s akcentom na inovacijske organizacije, kako bi se ostvario potreban nivo kooperativnosti i kohezije između različitih aktera i tako došlo do progresa u okviru poduzeća i ostvarivanja vizije stvaranja znanstvenih inovacija, koje bi imale značajan utjecaj na privredni razvoj zemalja u tranziciji.

LITERATURA

[1] D. Rajić, Ž. Kamberović, B. Žakula, Kreativni inženjering, Inovacioni centar TMF, Beograd, 2015, ISBN 978-86-919829-0-4.
[2] CEN/TS16555 Innovation Management – Part 1: Innovation Management System, 2013.
[3] CEN/TS16555 Innovation Management – Part 2: Strategic intelligence management, 2014.
[4] CEN/TS16555 (2014) Innovation Management – Part 3: Innovation thinking,2014.
[5]CEN/TS16555 (2014) Innovation Management – Part 4: Intellectual property management, 2014.
[6] CEN/TS16555 Innovation Management – Part 5: Collaboration management, 2014
[7] CEN/TS16555 Innovation Management – Part 6: Creativity management, 2014.
[8] TRIZ software, Dostupno na internetu https://play.google.com/store/apps/details?id=com.mj.triz&hl=en, datum 05.04.2016.

[9] S. Klaus, S. Xavier, Global Competitiveness report 2010- 2011, World Economic Forum, 2011.
[10] Strategija znanstvenog i tehnološkog razvoja Republike Srbije za period od 2016.-2020. godine -,,Istraživanje za inovacije" 2015, Beograd, Mistarstvo prosvete, znanosti i tehnološkog razvoja, Republika Srbija.
[11] European Commission, Research and Innovation, Dostupno na internetu https://ec.europa.eu/research/index.cfm?pg=newsalert&year=2015&na=na-101115, datum 25.03.2016.
[12] D. Rajić, B. Žakula, V. Jovanović, (2006), Uvod u TRIZ ili kako postati kreativan u tehnici, Beograd, SIG, http://www.sigonline.rs/files/File/knjige/uvodutriz.pdf, 9. 5.2015.
[13] Altshuler algoritm, Dostupno na internetu http://www.altshuller.ru/triz/ariz85v.asp, 9. 5. 2015.
[14] Г. Альтшуллер, СТворчество как точная наука. М., "Советское радио", 2-е изд., дополненное. - Петрозаводск: Скандинавия,.- с., 2004.
[15] Г. Альтов, И ТУТ ПОЯВИЛСЯ ИЗОБРЕТАТЕЛЬ. М., "Детская литература", 3-е изд.,перераб. и доп., 1989.
[16] Г.С. Альтшуллер, НАЙТИ ИДЕЮ (1991) Новосибирск,"Наука", 2-е издание.
[17] Г.С. Альтшуллер, И.М. Верткин, (1994) КАК СТАТЬ ГЕНИЕМ: Жизненная стратегия творческой личности, Минск, "Беларусь".
[18] Н. Ф. Овчинников, Новый взгляд на мышление, Ростов на Дону, 2008.
[19] S. Savransky, Engineering of Creativity, London, CRC Press, 2000.
[20] K. Rantanen, E. Domb, Simplified TRIZ, Boca Raton, St. Lucie Press, 2002.
[21] D. Silverstein, N. DeCarlo, M. Slocum, Insourcing Innovation, NW, Aurbach Publications. 2008.
[22] Orloff, M., (Inventive Thinking Through TRIZ – A Practical Guide, Second Edition, Berlin Heidelberg, Springer - Verlag., 2006.
[23] Inovacioni fond, www.inovacionifond.rs, datum 04.04.2016.
[24] Elaborat o izvodljivosti projekta ,,Tehnološki hub i Inovacioni spin-off centar", Beograd, Inovacioni centar TMF-a, 2015.
[25] H. Etzkowitz, (2003) Research groups as 'quasi-firms': the invention of the entrepreneurial university,' Research Policy, 32(1), 109-121.
[26] V. Miltrenović, N. Dučić, R. Slavković, S. Radonjić, N. Bošković, Increase of the Operating Life of a Mould During the Casting Process of Flotation Balls With the Aid of Triz Method, Facta Universitatis, Series: Mechanical Engineering, 10 (2012) 1, pp. 31 – 40.
[27] H. Issa, M. Korać, Ž. Kamberović, M. Gavrilovski, T. Kovačević, A two-stage metal valorisation process from electric arc furnace dust (EAFD), Metallurgy, 55 (2016) 2, 2016.

15th INTERNATIONAL FOUNDRYMEN CONFERENCE
INNOVATION – The foundation of competitive casting production
Opatija, May 11th-13th, 2016
http://www.simet.hr/~foundry/

DETERMINISTIC AND STOCHASTIC COMPUTING OF SCRAP-INTENSIVE WROUGHT ALUMINIUM ALLOYS COMPOSITIONS

V. Kevorkijan[1], B. Hmelak[2], T. Šuštar[3] and P. Cvahte[1]

[1]Impol Aluminium Industry, Slovenska Bistrica, Slovenia
[2]The Alcad Company, Slovenska Bistrica, Slovenia
[3]C3M – Centre for Computational Continuum Mechanics, Ljubljana, Slovenia

Oral presentation
Original scientific paper

Abstract

The current standard wrought aluminium alloys (WAAs) are with the limited recyclability. The main obstacle for that is in the narrow compositional tolerance limits. Because of this, the grades of scrap suitable for WAAs production are usually the most expensive ones, with well-defined chemical compositions, such as new industrial scrap or well-sorted fractions of old scrap with very limited potential for performance-to-cost improvements.
One way of overcoming these limitations is to encourage the formulation of new WAAs, focusing on the desired performances and not on the exact chemical composition. However, before completing the development of new alloys it will be necessary to attain a fundamental understanding of the complex influence of the chemical composition on the properties of the WAAs of the standard composition. The effective way to do that is the data mining, using existing data from the production.
The purpose of this work is to present the deterministic and the stochastic algorithms developed for calculating the optimum combination of scrap grades, each with a proper and well-controlled chemical composition, for providing the standard composition of the pre-melting mixture, the required mechanical properties of the alloy and the minimum cost of production within the entire processing chain. Algorithms do not favour in advance the formulation of alloys with an increased amount of scrap, but select a solution with the desired combination of properties based on the optimum cost of production. In addition, they are also useful for tailoring recycling-friendly compositions of wrought aluminium alloys and for optimizing the production technology.
The preliminary results of the investigation are demonstrated using some alternative compositions of the alloy AA 6082 and the experimentally determined correlation between the alternative chemical compositions and the corresponding mechanical properties of the as-cast samples, measured with a room-temperature tensile test.

***Keywords**: recycling, wrought aluminium alloys, modelling, concentrations, alloying elements*

*Corresponding author (e-mail address): *varuzan.kevorkijan@impol.si*

INTRODUCTION

The improved global market position of competitive advanced materials, especially the ultra-high-strength steels (recently promoted as functionally lighter and cheaper than wrought aluminium alloys) will influence the future costs of wrought aluminium alloys significantly.

To remain competitive with advanced high-strength steels and other engineering materials, wrought aluminium alloys should offer the customer a favourable cost-performance ratio, or, in other words, enhanced mechanical properties ensured by cost-effective production. To achieve this goal, it is necessary to enhance the alloy's properties (especially the tensile strength), while at the same time minimizing the costs. The properties of wrought aluminium alloys are the result of a complex interaction between the chemical composition and the microstructural features obtained during the solidification, thermal treatments and deformation processing [1]. Thus, under constant processing parameters, the properties are a consequence of the chemical composition of the alloy, and, vice-versa, the tolerance limits for the concentration intervals of the alloying elements depend on the required properties. On the other hand, cost reduction mostly depends on the technological possibilities of replacing as many of the expensive raw materials (the primary aluminium and the alloying elements) as possible with scrap. The extent of such a replacement depends on the ability of the production technology to preserve the standard composition and quality of the alloy or, to put it another way, to meet customer requirements by offering scrap-intensive alloys. In other words, the difficulty in recycling wrought aluminium alloys is the problem of achieving the standard tolerances, or more generally, the ability of an alloy to absorb elements not normally present in its composition [2]. This is the starting point for designing the so-called "recycling-friendly wrought aluminium alloys".
To ensure more recycling of wrought aluminium alloys, it is necessary to organize the scrap yard [3, 4] so that it consists of different material streams, each with a proper and well-controlled chemical composition. In addition, it is necessary to develop the software for calculating the proper combination of material streams that is essential for achieving the required alloy composition – standard alloys or the alternative, so-called "recycling friendly alloys" [5].

In this work an algorithm for calculating the optimal combination of material streams for providing the standard composition of the pre-melting mixture, the required mechanical properties of the alloy and the minimum cost of production within the entire processing chain will be presented.

THE DESCRIPTION OF THE MODEL

The model provides a procedure for: (i) selecting the proper material streams from those available in the scrap yard and (ii) calculating their shares in order to achieve the prescribed composition of the pre-melting mixture for the production of wrought aluminium alloys with a standard composition.

The individual material streams represent the fractions of aluminium scrap sorted from the incoming material to an exactly defined chemical composition, Fig. 1. In addition, as well as fractions of aluminium scrap, the model also involves material streams of alloying elements as well as the primary aluminium and the impurities. The compositions of the individual material streams are represented in the model by vectors, the components of which are concentrations (i.e., shares) of particular elements involved in the material streams. In this way, a vector with n components describes the composition of a material stream that consists of n different elements – among which are all the alloying elements, impurities and aluminium.

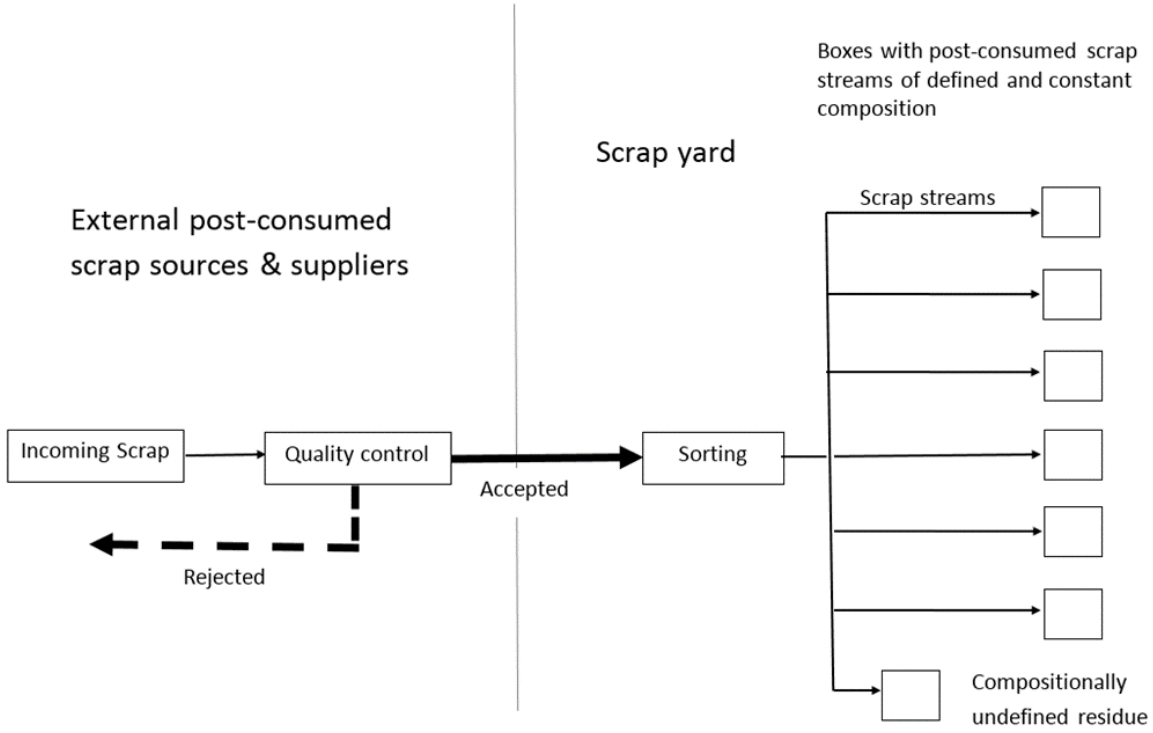

Figure 1. Organization of the scrap yard for the recycling of wrought aluminium alloys from post-consumed scrap in accordance with the model

According to the model, the scrap yard consists of *m* different material streams. The compositions of all the material streams are written using a matrix of the material streams or, in the more developed form, using a matrix of the composition of the material streams. The shares of the individual elements are presented as intervals using technologically prescribed widths.

The unknowns calculated are the shares of the particular material streams that are necessary to achieve the proper composition of the pre-melting mixture of scrap and raw materials. The composition of the pre-melting mixture defined the vector with *n*

components corresponding to the shares of the individual elements appearing in the stream. In addition, also in this case, the shares as the components of the vector are intervals, using the interval widths prescribed by the standard.

In addition to all the possible solutions (the shares of the various material streams), the algorithm searches for that particular solution which provides the minimum cost of the pre-melting mixture. To do this, it is necessary to introduce a matrix of the cost of the material streams and define the matrix of the cost of formation of the pre-melting mixture, in which the individual articles appear as the costs of each of the material streams. The unknown shares of the material streams calculated under the condition that the sum of the articles of the matrix of the cost of formation of pre-melting mixture is a minimum.

DEFINITIONS OF THE BASIC VARIABLES APPLIED IN THE MODEL

Matrix of material streams

The material streams existing in the scrap yard are described using the following matrix of the material streams:

$$\boldsymbol{R}_m = \begin{pmatrix} r_1 \\ \vdots \\ r_m \end{pmatrix} \tag{1}$$

The compositions of the individual material streams are described using a vector, the components of which represent the shares of particular elements appearing in the stream:

$$r_i = (x_{i1}, x_{i2}, x_{i3}, \ldots\ldots\ldots x_{in}) \tag{2}$$

The index *i* corresponds to the *i* materials stream, while x_{ij} denotes the share of the element *j* (j = 1,2,3,…n) in the stream *i* (i = 1,2,3,… m).

Based on the above, the matrix of the material streams $\boldsymbol{R}_m$ can be transformed into the matrix of the composition of material streams $\boldsymbol{X}_{mn}$ in which the components of the matrix correspond to the shares of the chemical elements in the material streams:

$$R_m = X_{mn} = \begin{pmatrix} x_{11} & \cdots & x_{1n} \\ \vdots & \ddots & \vdots \\ x_{m1} & \cdots & x_{mn} \end{pmatrix} \tag{3}$$

Moreover, it is important to note that the sum of the shares inside an individual material stream *i* is always equal to 1:

$$\sum_{j=1}^{n} x_{ij} = 1 \tag{4}$$

Vector of the shares of the material streams

The components of this vector are the shares of the individual material streams, which are the main outputs calculated by the model:

$$A_m = (a_1, a_2, a, \ldots\ldots a_n) \tag{5}$$

Vector of the chemical composition of the pre-melting mixture

This vector defines the chemical composition of the pre-melting mixture:

$$V_n = (v_1, v_2, v_3, \ldots\ldots v_n) = \sum_{i=1}^{m}\sum_{j=1}^{n} a_i \cdot r_{ij} \tag{6}$$

Here, the symbols $v_1, v_2, v_3, \ldots\ldots v_n$ represent the shares of the individual chemical elements appearing in the pre-melting mixture.
Again, for the sums of the shares of the material streams and the chemical elements it is the case that:

$$\sum_{i=1}^{m} a_i = 1 \tag{7}$$

$$\sum_{i=1}^{n} v_i = 1 \tag{8}$$

Vector of the cost of the material streams

The components of this vector represent the costs of the individual material streams:

$$\boldsymbol{C}_m = (c_1, c_2, c_3, \ldots\ldots c_n) \tag{9}$$

Finally, combining all the above-defined matrices, one can formulate the matrix of the cost of the production of the pre-melting mixture, $\boldsymbol{V}_m$:

$$\boldsymbol{V}_m = \boldsymbol{A}_m \cdot \boldsymbol{C}_m \cdot \boldsymbol{R}_{mn} = \begin{pmatrix} c_1 a_1 r_1 \\ \vdots \\ c_m a_m r_m \end{pmatrix} \tag{10}$$

It is important to note that the components of this matrix define the cost of the individual streams applied for the formation of the pre-melting mixture.

DEFINITIONS OF THE BASIC VARIABLES APPLIED IN THE MODEL

The mechanical properties of the wrought aluminium alloys processed in this model are the yield strength $\boldsymbol{YS}$, the tensile strength, $\boldsymbol{TS}$, the elongation $\boldsymbol{A}$ and the hardness $\boldsymbol{H}$.
In all cases considered in this study, the general assumption is made that under the constant conditions of the thermal treatments and the deformation processing, the mechanical properties of the alloy are functions of the chemical composition:

$$\boldsymbol{YS} = \boldsymbol{f_1}(\boldsymbol{v_1}, \boldsymbol{v_2}, \boldsymbol{v_3}, \dots\dots\dots, \boldsymbol{v_n}) \tag{11}$$

$$\boldsymbol{TS} = \boldsymbol{f_2}(\boldsymbol{v_1}, \boldsymbol{v_2}, \boldsymbol{v_3}, \dots\dots\dots, \boldsymbol{v_n}) \tag{12}$$

$$\boldsymbol{A} = \boldsymbol{f_3}(\boldsymbol{v_1}, \boldsymbol{v_2}, \boldsymbol{v_3}, \dots\dots\dots, \boldsymbol{v_n}) \tag{13}$$

$$\boldsymbol{H} = \boldsymbol{f_4}(\boldsymbol{v_1}, \boldsymbol{v_2}, \boldsymbol{v_3}, \dots\dots\dots, \boldsymbol{v_n}) \tag{14}$$

In practice, the functions $\boldsymbol{f_1}, \boldsymbol{f_2}, \boldsymbol{f_3}$ $\boldsymbol{inf_4}$ are usually polynomial, with the unknowns being the shares of the alloying elements in the alloy $v_1, v_2, v_3, \dots\dots\dots, v_m$.
The shares of the alloying elements $v_1, v_2, v_3, \dots\dots\dots, v_m$ are presented as the intervals of the concentration:

$$v_i = \overline{v_i} \pm \Delta v_i \tag{15}$$

where $\overline{v_i}$ is the average value of the interval, and $2\Delta v_i$ is its width.

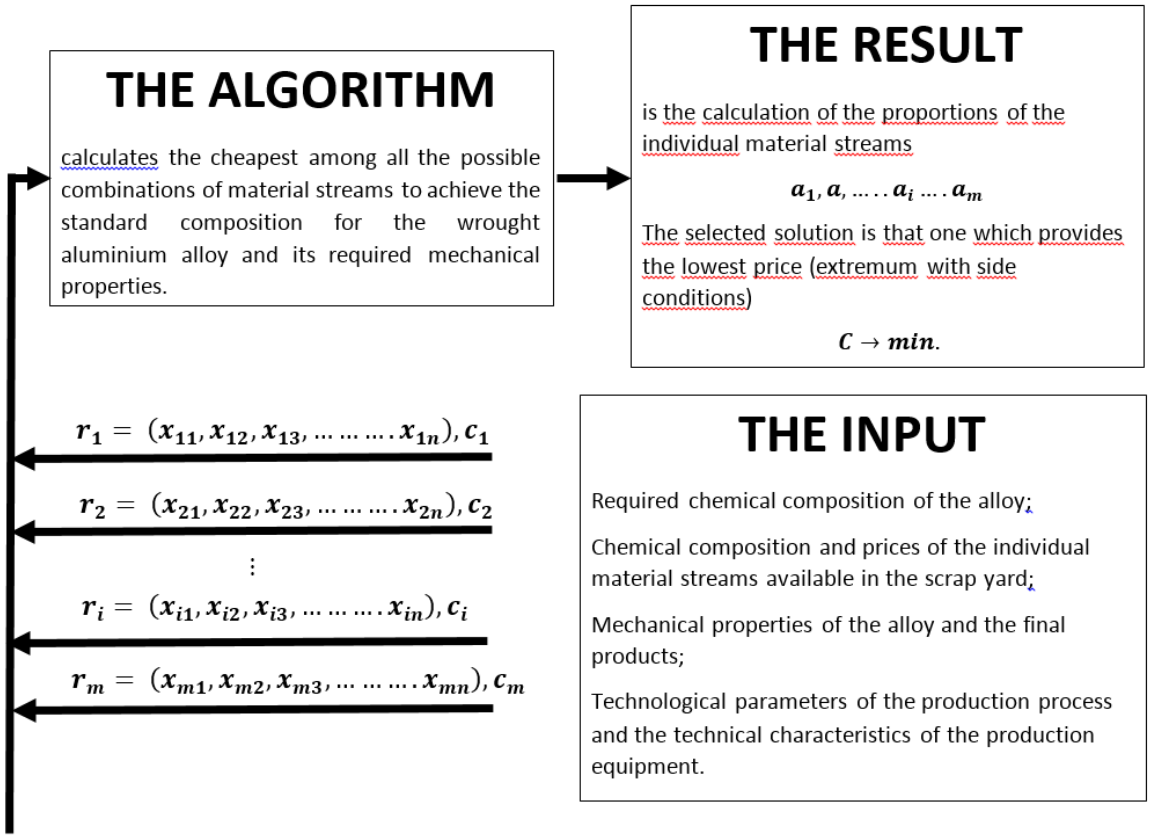

Figure 2. Flowchart of the developed algorithm

CALCULATION OF THE SHARES OF THE MATERIAL STREAMS

The algorithm is looking for the cheapest combination of material streams to achieve the standard composition of the pre-melting mixture and the required mechanical properties in the alloy. The following data is used in the algorithm:
- The alloy chemical composition, prescribed by the vector of the pre-melting mixture, $V_n = (v_1, v_2, v_3, \ldots \ldots . v_n)$,
- The mechanical properties (yield strength $\boldsymbol{YS}$, tensile strength, $\boldsymbol{TS}$, elongation $\boldsymbol{A}$ and hardness $\boldsymbol{H}$),
- The number and the chemical compositions of the material streams, defined by the vectors of the individual material streams, $r_i = (x_{i1}, x_{i2}, x_{i3}, \ldots \ldots \ldots . x_{in})$,
- The parameters of the technological process (thermal treatments, deformation processing),
- The technical characteristics of the production equipment (useful for the proper estimation of the total cost of the losses within the production chain).

The algorithm calculates the shares of the material streams, which are defined by the matrix of the shares of the material streams, $A_m = (a_1, a_2, a, \ldots\ldots a_n)$ and among all possible solutions. In this way it is possible to achieve the proper composition and mechanical properties of the alloy, while selecting the solution with the lowest cost. With respect to all the costs applied in the algorithm, in addition to the costs of the materials, also the costs of the production and all the losses caused by using scrap are included. Fig. 2 presents the complete procedure for the calculation.

The difficulty is in the fact that theoretically there are an unlimited number of possible solutions or linear combinations by which it is possible to achieve the desired composition of the pre-melting mixture. Because of this, it is necessary to introduce the cost criterion, according to which there is only one cheapest combination, ensuring in that way the explicitness of the solution to the problem.

The base for the development of the algorithm is the previously formulated assumption that the properties of the wrought aluminium alloys are created by a complex interaction of the chemical composition and the microstructural features obtained during the solidification, the thermal treatments and the deformation processing. Consequently, from the mathematical point of view, the mechanical properties and the chemical composition of the wrought aluminium alloy cannot be independent variables. The mechanical properties are a consequence of the chemical composition of the alloy and vice-versa, while the tolerance limits of the intervals of the concentrations of alloying elements depend on the required mechanical properties. The problem is in the fact that these correlations between the chemical composition and the mechanical properties are not necessarily functional or bijective (based on a one-to-one correspondence, where every element of one set is paired with exactly one element of the other set), and not linear, which additionally aggravates the programing of the algorithm.

The vector of the pre-melting mixture, V_n, which defines with its components (shares of elements) the desired composition of the pre-melting mixture, can be written as a linear combination of the material streams, r_{ij}, where the coeficients of the linear combination appear as the shares of the individual material streams (unknowns determined by the model).

In industry, the number of material streams and their shares in the pre-melting mixture, *m*, which are unknowns, is usually higher than the number of alloying elements, *n*. Hence, in practice it is often the case that m>>n. Consequently, the number of unknowns in the system is higher than the number of equations and, therefore, the system has several possible solutions. In other words, the algorithm will recognize several possible ways of combining different streams (different solutions) in order to achieve the proper composition of the pre-melting mixture and the required mechanical properties of the alloy. Because of that, it is necessary to introduce the cost criterion, according to which there is only one cheapest combination, ensuring in this way the explicitness of the solution to the problem.

The optimum composition of the pre-melting mixture is defined by the shares $(a_1, a_2, \ldots . a_m)$ calculated under the condition that the cost of the pre-melting mixture, $C(a_1, a_2, a_3, \ldots . . a_m)$, or in another words the sum of elements of the matrix $\boldsymbol{V}_m$, should be a minimum:

$$C(a_1, a_2, a_3, \ldots . . a_m) = \sum_{i=1}^{m} c_i a_i \rightarrow min. \tag{16}$$

The algorithm is looking for the minimum of the function $C(a_1, a_2, a_3, \ldots . . a_m)$ for more variables:

$$dC(a_1, a_2, a_3, \ldots . . a_m) = \sum_{i=1}^{m} \frac{\partial C}{\partial a_i} da_i = 0 \tag{17}$$

A CASE STUDY

In this study, the results of standard room-temperature tensile tests and the corresponding concentrations of the alloying elements for the AA 6082 alloy were numerically processed and written as a polynomial alloy property-composition functional dependence. The details of the modelling methodology can be found in Ref. [6]. The obtained numerical correlations are determined based on the results of the experimental testing of as-cast samples from regular production. The investigation was performed on 120 samples (discs cut from billets) of the AA6082 alloy in the as-cast state. The as-cast state was selected in order to exclude the influence of subsequent processing steps (homogenisation, heat treatment and forming) on the correlation between the concentration of alloying elements and the selected mechanical properties.

The measurements of the tensile strength, the yield strength and the elongation involved standard room-temperature tensile tests. The bars with a standard geometry for the tensile tests were machined perpendicular to the direction of the individual billet casting.
The chemical compositions of the samples were analysed using optical emission spectroscopy (OES) with an average accuracy of ±10 ppm.

The several numerically predicted compositions to provide the desired combination of properties are reported in Table 1, while all 120 experimentally determined compositions, as well as the 8 computed compositions, are plotted in Fig. 3.

The accumulated results clearly confirm that even slight differences in the initial chemical compositions of the individual alloys cause, in the as-cast state, significant changes in the individual and the combined mechanical properties.

It is important to note that under the constant parameters of melting and casting, the initial, as-cast processing state of the alloy is a function of the concentrations for the seven alloying elements (i.e., variables) considered in this study, Table 1. However, for samples taken from any subsequent stages of processing, the number of variables increases rapidly, involving not only the concentrations but also the various processing parameters.

The experimentally determined dependence of the mechanical properties of the AA6082 alloy on the changes in the alloy compositions, as illustrated in Fig. 3, clearly confirms that, in principle, the same combination of mechanical properties could be ensured by applying various alloy compositions. This experimental finding is particularly important and represents part of the still-missing information that is necessary for the successful development of the next generation of so-called "recycling friendly wrought aluminium alloys".

Table 1. The numerically predicted compositions of the AA6082 alloy in the as-cast state to provide the desired combination of mechanical properties

Point	YS (MPa)	TS (MPa)	A (%)	Si (%)	Fe (%)	Cu (%)	Mn (%)	Mg (%)	Cr (%)	Ti (%)
A1	85	178	17	0.861	0.216	0.042	0.551	0.641	0.103	0.037
A2	85	224	17	0.975	0.220	0.056	0.544	0.705	0.129	0.034
A3	117	224	17	1.093	0.220	0.056	0.551	0.763	0.139	0.030
A4	117	178	17	0.979	0.216	0.043	0.558	0.699	0.113	0.033
B1	85	178	9	0.963	0.217	0.044	0.564	0.673	0.121	0.034
B2	85	224	9	1.077	0.221	0.058	0.558	0.737	0.148	0.030
B3	117	224	9	1.195	0.221	0.058	0.565	0.794	0.158	0.026
B4	117	178	9	1.081	0.217	0.045	0.571	0.731	0.131	0.030

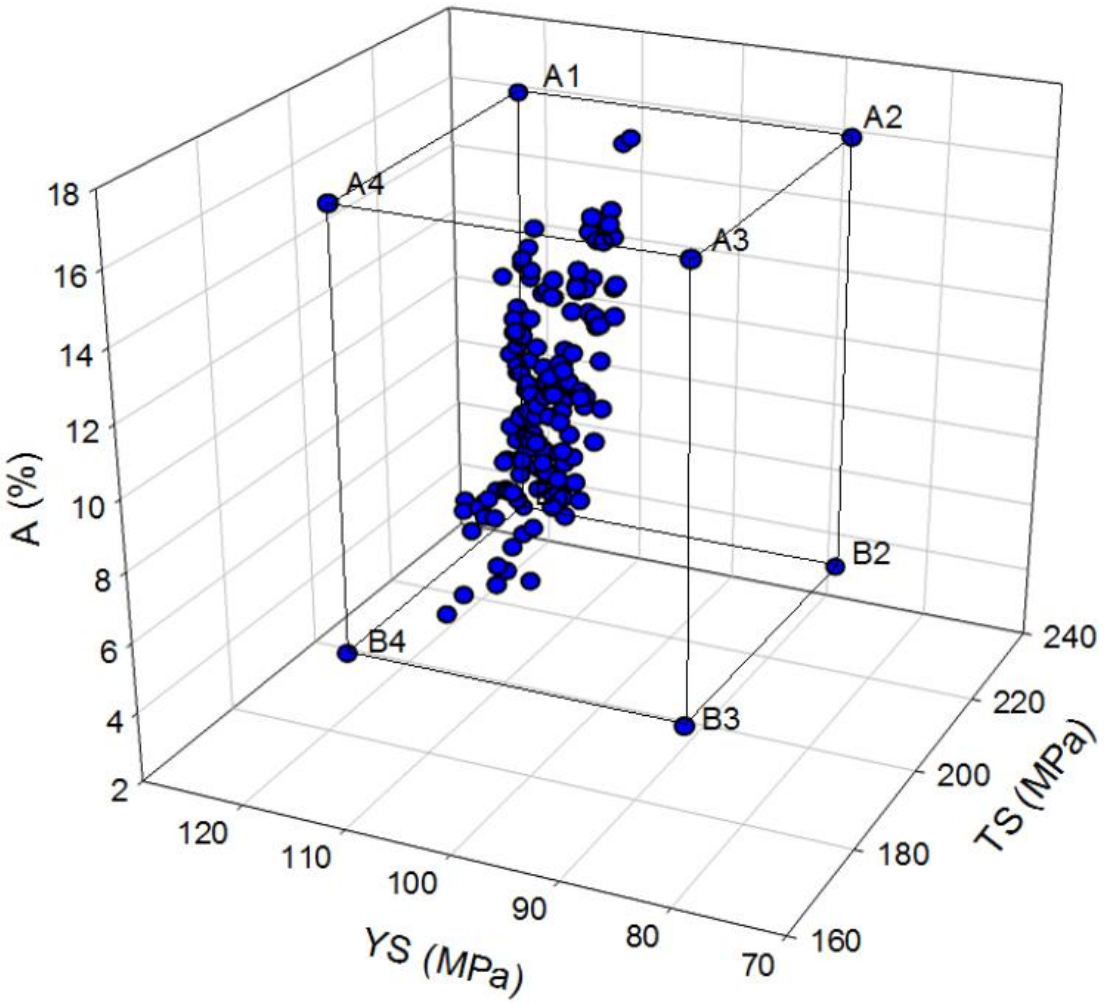

Figure 3. The experimentally tested compositions of the AA6082 alloy in the as-cast state, with the corresponding mechanical properties. The boundary compositions (from A1 to B4) are reported in Table 1.

CONCLUSIONS

The algorithm developed in this work offers several advantages in tailoring a pre-melting mixture for the production of wrought aluminium alloys by combining the material streams of different sources of aluminium and alloying elements (old or new aluminium scrap, returning material, primary aluminium, pure alloying elements).

One of the important advantages is that the algorithm does not favour, in advance, the obtaining of alloys with an increased amount of scrap, but enables a decision-making procedure to achieve the best choice of constituents based on the resulting cost of the mixture. In other words, the algorithm will follow the requirements relating to the chemical composition and the mechanical properties and, based on that, defines the shares of the

material streams from the digitalized stock of raw materials (primary aluminium and alloying elements) and different kinds of aluminium scrap, but in a way that will provide the minimum cost of production (within the entire production chain). In this way, the cost of production involves not only the cost of the raw materials and scrap, but also the cost of all the processing losses caused by an increased amount of scrap.

The algorithm also offers an option by which, based on the prescribed mechanical properties, it determines the proper chemical composition (the standard one, but, if necessary, a composition with narrower compositional tolerances) and after that computes the shares of the material streams from digitalized stock, again under the condition of the minimum cost of production.

The algorithm could also be applied in the opposite direction; therefore, in such a way as to correlate the changes in the concentrations of the alloying elements into the changes of the mechanical properties, enabling in this way the tailoring of the standard, but more recycling-friendly, compositions of the wrought aluminium alloys.

Finally, the algorithm, which correlates the incoming chemical composition and the processing parameters with the properties of the final products, could also be applied for the optimization of the production technology, especially the thermal treatments and the deformation processing as a way of achieving the desired alloy properties.

REFERENCES

[1] M. Tiryakioğlu and J. T. Staley, Handbook of Aluminum, Vol. 1, CRC Press, Taylor & Francis Group, Boca Raton, FL, 2003.
[2] M. E. Schlesinger, Aluminum Recycling, CRC Press, Taylor & Francis Group, Boca Raton, FL, 2014.
[3] D. B. Spencer, The high-speed identification and sorting of nonferrous scrap, JOM, 57 (2005) 4, pp.46.
[4] A. Gesing, L. Berry, R. Salton and R. Wolansky, Aluminum 2002, TMS, Warrendale, PA, 2002.
[5] S. K. Das, , Light Metals 2006, TMS, Warrendale, PA, 2006.
[6] V. Kevorkijan, Modeling of Alternative Compositions of Recycled Wrought Aluminum Alloys, JOM, 65 (2013) 8, 2013.

15th INTERNATIONAL FOUNDRYMEN CONFERENCE
INNOVATION – The foundation of competitive casting production
Opatija, May 11th-13th, 2016
http://www.simet.hr/~foundry/

ANALYSIS OF THE STRESS, STRAIN AND MOLD LIFETIME IN CASTING PRODUCTION APLICATIONS

V. Kolda
Mecas ESI, Brno, Czech Republic

Oral presentation
Subject review

Abstract

Today, in all industries numerical simulation is considered as one of the tools used in product design, process development and solving problems in the production phase. Big challenge for die casting technology is solving problems with tearing and cracking due to the stress and deformation of the casting, heat fatigue, together with the prediction of actual deformations. Powerful, multi-physics simulation tools are now available to solve such problems. The new die can be designed on a computer, eliminating inefficient way by trial and error. This new approach brings drastic cost savings associated with the phases of development of new dies and leads to improved production and optimization of existing dies.
This paper will address some of the factors that influence the accuracy of filling, solidification and stress analysis of the casting. After reviewing different models implemented in ProCAST different applications will be illustrate as the possibilities of how numerical simulations can be used to assess the causes of cracks and tears, die fatigue and dimensional tolerances.

Keywords: *Stress, deformation, cracks, hot tears, fatigue, FEM*

*Corresponding author (e-mail address): *Vlastimil.Kolda@esi-group.com*

INTRODUCTION

Besides the defects related to filling and solidification, there are a number of stress related issues which can affect the final integrity of the die-cast component, as well as result in die failures. Factors which influence the stress behavior and fatigue life of the die include geometry, thermal history, thermo-mechanical properties of the die and casting, thermal/mechanical contact algorithm, and external forces and pressures.

In order to accurately simulate the stress behavior, one should consider the full coupling between the thermal, fluid and mechanical stress analysis of all the relevant materials, including casting, cores and dies. The gap formation caused as a result of shrinkage during

solidification and inversely contact pressure, will affect the heat transfer between the casting and the dies and needs to be taken into account.

Furthermore, dies may experience some local plastic deformation and thus one needs to consider both the elastic and plastic behavior of the die. Any local plastic deformation in the die would severely limit its life time and should therefore be avoided. Even when dies operate within the elastic region, their life time is influenced by the cyclic stresses which occur during processing.

A realistic assessment of these issues requires a fully coupled thermal-fluid-stress simulation. The finite element method has been found to be superior for this type of simulation. Some of the considerations involved in the implementation of such a program include; 1) use of an appropriate material model, 2) unstructured mesh 3) thermal/mechanical contact algorithm, 4) fatigue life prediction, 5) hot tearing prediction, 6) cracking prediction, and 7) inverse displacements.

MATERIAL MODELS

In order to simulate a variety of materials, several mechanical material models have been adopted in ProCAST. For cast parts and molds, the models include a thermo-elasto-viscoplastic model of the Perzyna type [1], a thermo-elastoplastic counterpart and an elastic model. The elastoplastic model and elasto-viscoplastic model, in which all the parameters and functions are temperature dependent, are described in [2]. The first example demonstrates the importance of using proper material models in the stress analysis. The problem considered is an aluminum casting in a sand mold. The mold material model is chosen as elastoplastic with linear strain hardening. The casting material model is treated with two alternatives, elastic and elasto-viscoplastic. An isotropic linear hardening law is assumed for the elasto-viscoplastic model. The initial temperature of the casting is taken as 650°C and the mold temperature as 25°C. All material data are temperature dependent. The results in Figure 1 show the accumulated plastic strain for both material models (casting and mold). Naturally, with an elastic model for the casting, on the left, the only plastic strain occurs in the mold. Figure 2 depicts the corresponding final effective or von Mises stress. The elastic model results in a maximum stress in the casting more than twice that in the other model. The viscoplastic model can relieve stress through plastic deformation. Thus, if the absolute value of the stress in a casting is desired, it is necessary to utilize one of the nonlinear material models.

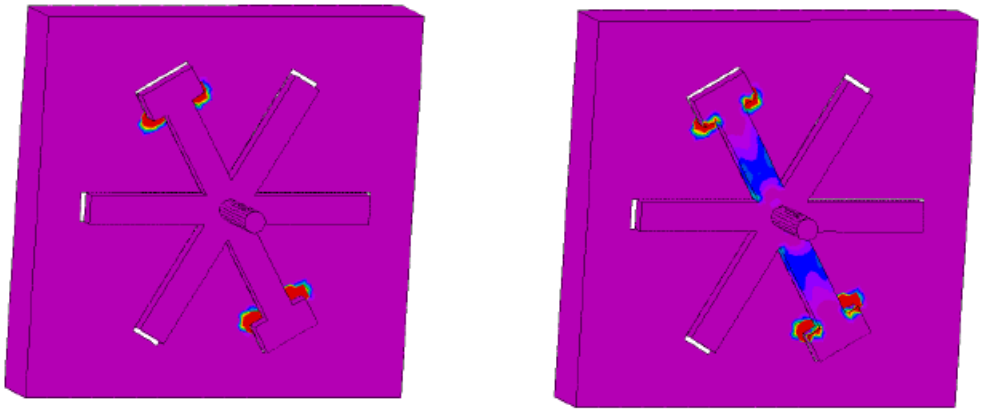

Figure 1. Accumulated Plastic Strain, Elastic Model (left) and Viscoplastic (right) (ProCAST)

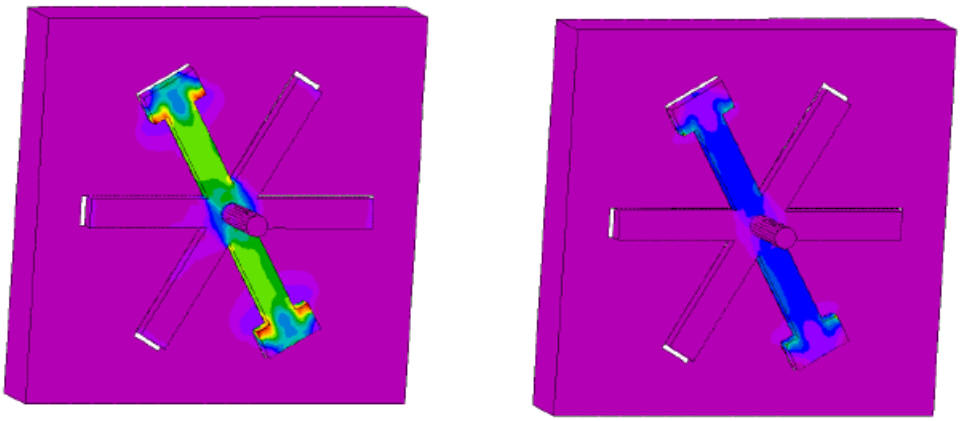

Figure 2. Effective Stress, Elastic Model (left) and Viscoplastic (right) (ProCAST)

UNSTRUCTURED MESH

The Finite Element Method, based on unstructured meshes, has its roots in mechanical engineering and all major software for the simulation of stress and deformation are using this method today. Since structured meshes (used in Finite Difference Method, FDM) are constrained to follow the coordinate axes, deformation calculations with such meshes are limited to small deformations, often in the elastic regime (see figure 3 (right) illustrating the problem of stair-like interfaces). As is well known, deformation of metals during cooling occurs to a large extent in the viscoplastic regime and this component must be absolutely considered if realistic simulations are to be obtained. This is necessary in particular to handle the loss of contact of two parts of a casting (e.g. the metal and the mold) when an air gap forms or the friction between them when they are in contact, thus influencing heat transfer (see figure 5). With unstructured meshes, the new position of the mesh points can be calculated at each time step. Thus, the mesh can be deformed and the contact/loss of contact events can be detected.

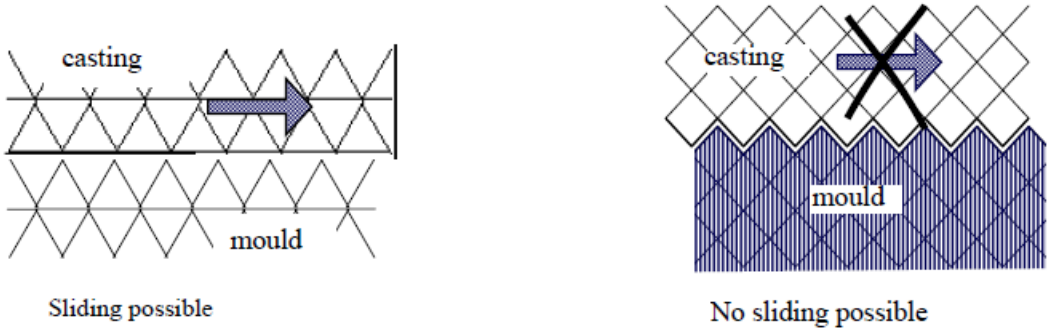

Figure 3. Comparison between unstructured mesh used in FEM (left) and structured mesh use in FDM (right) in regards to stress calculations issues.

THERMAL AND MECHANICAL CONTACT OF CASTING AND MOLD

For demonstration purposes, a simple T shaped casting of A356 in a H13 mold is simulated, as shown in Figure 4. The effective interface heat transfer coefficient at two different points on the casting is plotted in Figure 5. The top curve is from a point experiencing increasing contact pressure as the casting contracts. The middle curve is from a point where a gap is opening up between casting and mold, assuming the presence of air. The bottom curve is from that same point, but assuming a vacuum. The large variation in the coefficient illustrates the importance of accounting for local conditions. In addition, this example illustrates the value of the reverse coupling of the mechanical deformations with the energy solution. This effect can be seen in Figure 4 on the right where the heat flux contours are plotted. The heat flux is greatest where the contact pressure is highest.

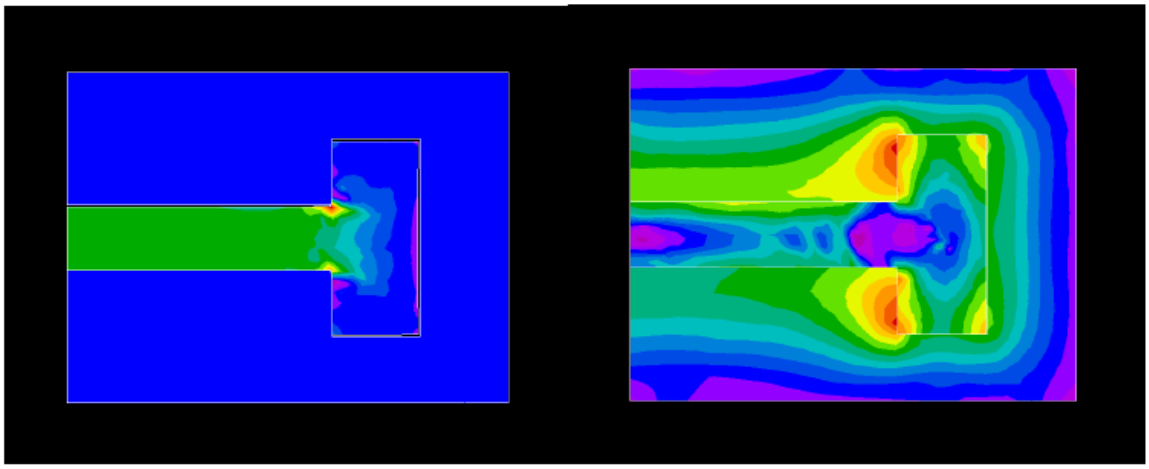

Figure 4. Principal Stress 1 and Heat Flux Contours (ProCAST)

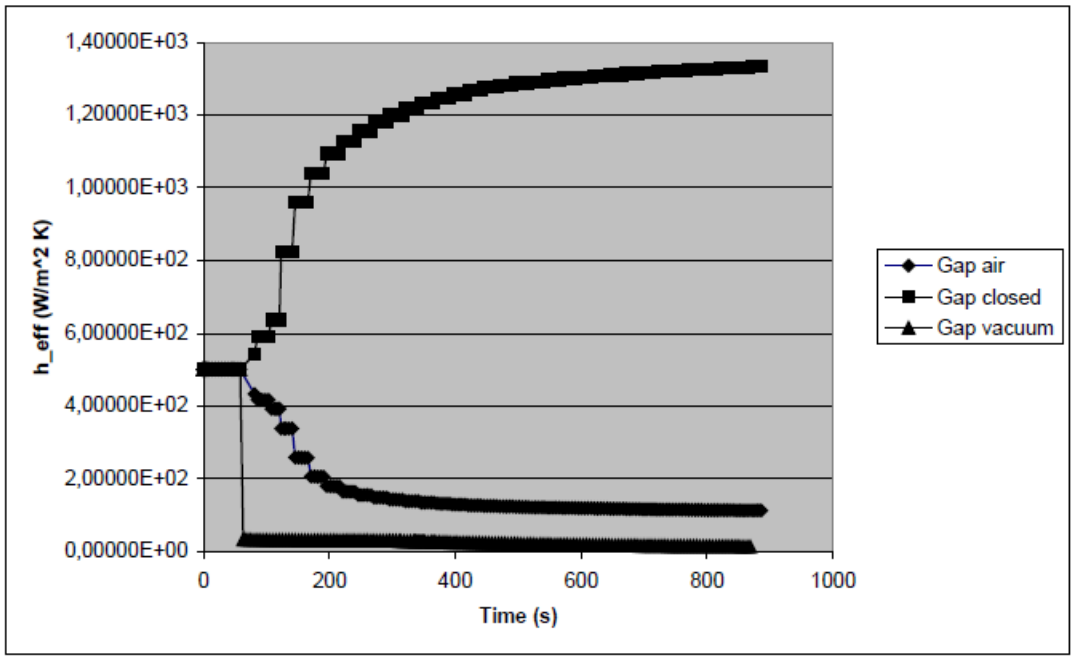

Figure 5. Interface heat transfer coefficients adjusted for mechanical contact

FATIGUE LIFE PREDICTION

The fatigue life model is applied to a simple example of a high pressure die cast aluminum alloy component (see Figure 6), cast at 720°C, with one die half having a cooling channel positioned at the end of the casting. The full cycle includes filling, solidification, ejection and spraying. In a first scenario, we consider the cooling channel at 20°C and in a second scenario we remove the cooling channel. The effect of the cooling channel on the effective stress, as well as on the die fatigue, is clearly evidenced on Figure 7. The increased temperature gradient between the casting/die interface and the cooling channel increases cyclic stresses in the die. In the second scenario, as shown in Figure 8, the high stress regions have disappeared with the cooling channel and an improvement in fatigue life prediction is obtained.

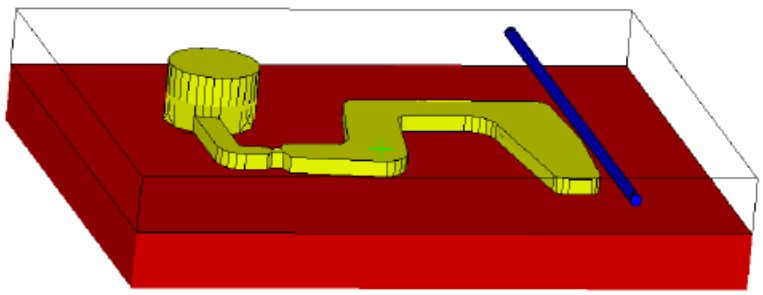

Figure 6. Geometry showing casting (yellow), cooling channel (blue) and dies (red)

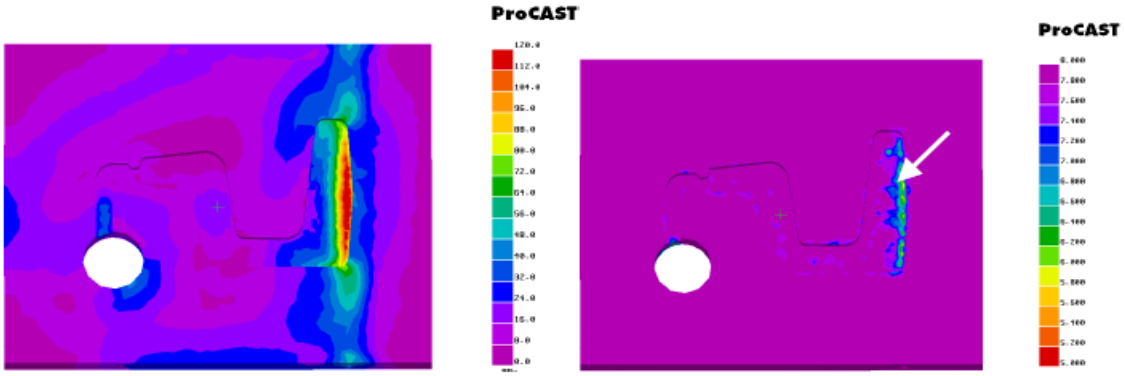

Figure 7. Effective stress in bottom die (left) showing high stress and fatigue life prediction (right) showing regions with limited fatigue life (with cooling channel)

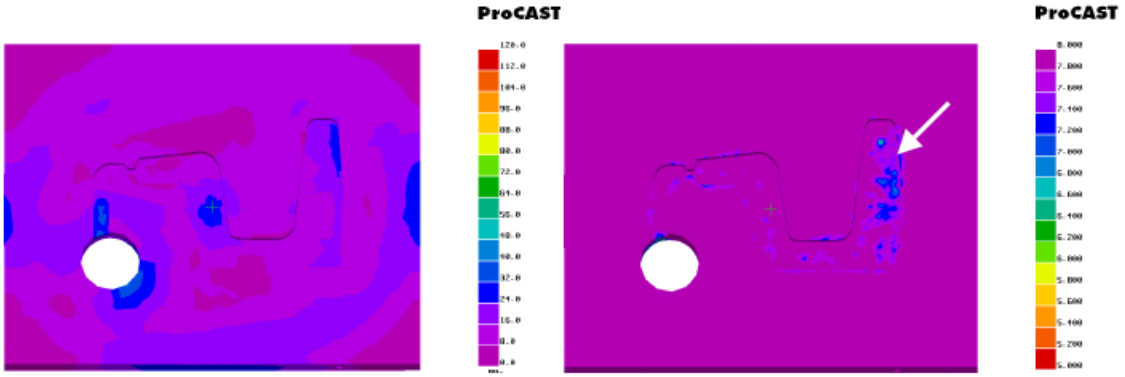

Figure 8. Effective stress in bottom die (left) showing limited stress and fatigue life prediction (right) showing regions with limited fatigue life (w/o cooling channel)

HOT TEARING PREDICTION

Hot tearing occurs when the strains that appear while the metal is still partially solidified cannot be compensated by liquid feed metal due to the low permeability of the mushy zone [3]. Longer freezing range alloys, where a liquid film persists between grain boundaries for a greater time, are more prone to hot tearing. Whether or not it occurs depends on the mechanical loads that develop due to thermal contraction and the contact constraints of the die wall. We have found that the total strain, plastic plus elastic, that accumulates between a critical value of fraction solid and fully solid metal, is a useful indicator of hot tearing. Relatively high values of this quantity correlate well with the probability of hot tearing (see Figure 9).

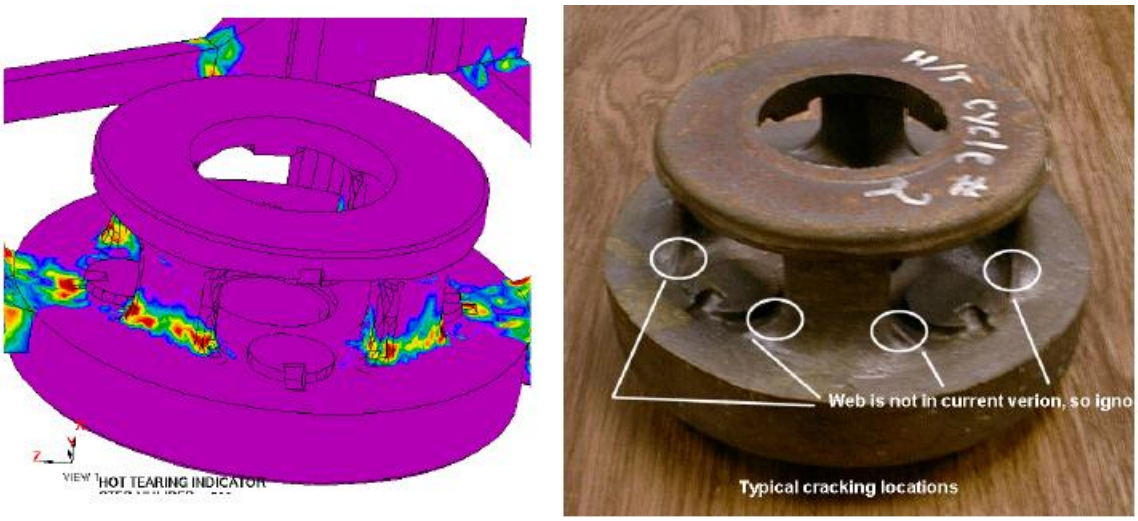

Figure 9. Industrial validation of a hot tearing prediction within ProCAST

CRACKING PREDICTION

The cracking indicator model of ProCAST corresponds to cracks occurring after completion of solidification. The model is based upon the modified Gurson model. It corresponds to a plastic strain driven model, where accumulated plastic strains allow cracks to nucleate and grow. All the plastic strain is considered, including plastic strains formed in the mushy zone. The model couples the stress calculation with the porosity calculation. The presence of porosity, corresponding to a void fraction indicator, will increase the risk of cracking.

INVERSE DISPLACEMENTS

One of the more challenging tasks of designing a die casting is figuring out the shrinkage allowance to add to the casting geometry. With a complex 3D geometry, shrinkage will be non-uniform. The presence of cores, inserts, or re-entrant corners of the dies further complicates the task.

A very powerful technique for coming up with an initial die geometry is afforded by the coupled casting simulation, starting with a CAD model of the desired net shape of the casting. It is meshed and simulated in a direct way, starting from filling, through ejection, and then cooling down to room temperature. This results in displacement values at every node in the mesh due to contraction and distortion. The software then inverts those displacements, applying them to the original mesh to produce an expanded initial geometry. This new initial geometry produces a casting that shrinks quite accurately to the desired net shape.

In Figure 10, a simple example of an aluminum male cross sign is used to demonstrate the method for correcting the distortions of the part. On the left, a part is shown distorted after casting due to constraints from the die. These distortions were automatically inverted in

order to determine the correct die shape. On the right, the final corrected shape of the part is shown after casting.

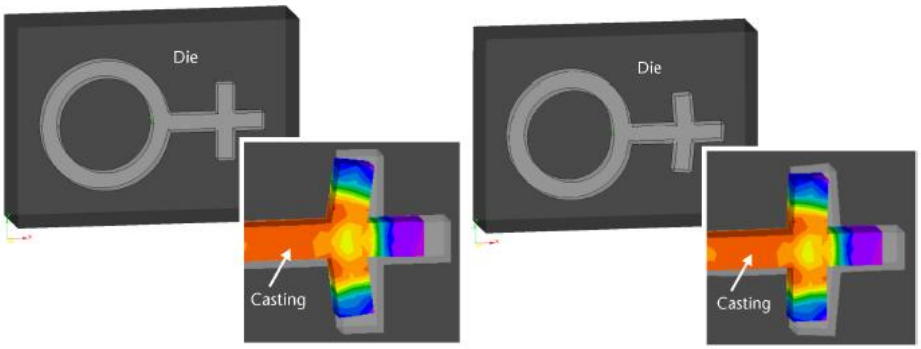

Figure 10. Effective stresses in the part after casting (left) and effective stresses in the part after modifying the die cavity in order to produce the required part shape (right). (ProCAST)

CONCLUSION

Casting process simulation has now reached a state where a relevant input for the design of a die can be given to the process engineers. Gating systems, overflows and venting channels can be optimized using numerical simulation. Solidification related defects can also be predicted taking into account cooling channels and die cycling so as to accurately reproduce production conditions.

ProCAST readily addresses all these issues but also includes advanced features to better assess the casting quality. These advanced features include fully coupled thermo-mechanical analysis with hot tearing, cracking and fatigue life predictions. The generalization of CAD modeling and the increase in performance of computers now allows for these technologies to be applied by the casting industry to full industrial applications.

REFERENCES

[1] P. Perzyna, 1966, Fundamental Problems in Viscoplasticity, Advance in Applied Mechanics, Vol.9, pp. 243-377.
[2] M. Samonds, J.Z. Zhu, A. Sholurwalla, Integration of Thermal Stresses Simulation with Process Development in the Modern Foundry, Nadca 2002.
[3] J. Campbell, 1993, Castings, Butterworth-Heinemann Ltd.

15th INTERNATIONAL FOUNDRYMEN CONFERENCE
INNOVATION – The foundation of competitive casting production
Opatija, May 11th-13th, 2016
http://www.simet.hr/~foundry/

MICROSTRUCTURE OF Cu-Al-Mn SHAPE MEMORY RIBBONS CASTED BY MELT SPINNER

S. Kožuh[1], I. Ivanić[1], M. Bizjak[2], B. Kosec[2], T. Holjevac Grgurić[1], I. Bogeljić and M. Gojić[1]

[1]University of Zagreb Faculty of Metallurgy, Sisak, Croatia
[2]University of Ljubljana Faculty of Natural Sciences and Engineering, Ljubljana, Slovenia

Oral presentations
Original scientific paper

Abstract

Cu-Al-Mn shape memory alloy could have a wide application due to their ductility. In this work the microstructure analysis of Cu-Al-Mn alloy after smelting (ingot) and casting (rapidly solidified ribbons) are shown. Alloy of composition Cu - 8.96%Al – 7.08 %Mn (wt.%) was prepared from pure metals and casted using melt spinning technique in Ar atmosphere. Before casting CuAlMn in the form of ingot (ϕ45x55 mm, weight 684 g) is produced, this is used as input for melt spinner. Microstructure was analyzed by optical microscopy (OM) and scanning electron microscopy (SEM) equipped by device for energy dispersive spectroscopy (EDS). Microstructure analysis of rapidly solidified ribbons was performed before and after annealing at 900 °C (60 and 30 min) and quenching in water. Also, sequence of the microstructural changes in the rapidly solidified ribbons were determined by the in-situ measurement of the electrical resistance. Preliminary metallographic analysis of ingot confirmed that microstructure consisted from two-phases (α+β), while in rapidly solidified ribbons presence of martensite was observed. Measurements of electrical resistance shows that phase transformations can be associated with precipitation of equilibrium α phase and with the order-disorder transition of austenite.

Keywords: *Cu-Al-Mn, shape memory alloys, microstructure, martensite, electrical resistance*

*Corresponding author (e-mail address): *kozuh@simet.hr*

INTRODUCTION

Shape memory effect (SME) is a remarkable characteristic that some alloy exhibit and this special property which allows them to regain and remember their original shape. Also, such materials have super-elasticity properties. Alloys that exhibit mentioned properties are called shape memory alloys (SMAs). SMAs have two stable phases: austenite which is stable

at high temperature, and martensite at low temperature. Additionaly, the martensite can be in one of two forms: twinned or de-twinned. Phase transformations can be illustrated with four characteristic temperatures, which are defined as: M_s – martensite start, M_f – martensite finish, A_s – austenite start, A_f – austenite finish.

Cu-based SMAs are the most promising in practical use and they have been extensively investigated because of their good shape memory properties, high electrical and thermal conductivity and low cost. But, most popular Cu-based SMAs, like Cu-Al-Ni and Cu-Zn-Al, are too brittle to be sufficiently cold worked. This had lead to development of ductile Cu-Al-Mn shape memory alloy. By adding Mn into Cu-Al alloys, it has been gained on the magnetic properties, the excellent ductility, large super elasticity and damping capacity [1-4]. In literature [5] is mentioned that the Cu-Al-Mn SMAs with an Al content below 18 at.%, which have a low degree of order in the β phase, shows excellent cold-workability over 60% in cold rolling reduction and also exhibit SME and pseudoelasticity based on cubic $\beta_1(L2_1)$ to monoclinic β_1`(18R) transformation. Excellent cold-workability was observed even if the β phase grain size of those alloys is extremely large (~ 1 mm) [3].

Also, rapidly casted copper based shape memory ribbons are intensively studied [6, 7]. In the present study, the microstructure of Cu-Al-Mn rapidly solidified ribbons was investigated.

MATERIALS AND METHODS

The shape memory alloy used for this investigation belongs to the family of Cu-Al-Mn alloys. Alloy with nominal composition of Cu- 8.96%Al – 7.08 %Mn (wt.%) was remelted by induction melting of pure copper (99.9%), aluminium (99.5%) and manganese (99.8%) in a graphite crucible. The aforementioned induction melting produces ingot, which was used as the input material for the melt. Dimensions of solidified ingot were ϕ45x55mm and 684 g in weight. This ingot was smelted and injected through a nozzle (rectangular) onto a cold surface of the melt spinner (Fig. 1). The melting temperature of ingot was around 1450 °C. Under the argon overpressure in the graphite crucible the molten alloy was sprayed through the nozzle on the rotating disc made from the copper alloy. Because of very fast heat transfer, test ribbons with the width 1.5-2.5 mm and thickness 170-206 μm are produced (Fig. 2). By means of this technique a fine jet of melt solidifies on a solid substrate. After casting the ribbons are heated at 900 ^{o}C in the furnace for 60 and 30 min and then quenched in room temperature water. Microstructural characterization of samples was carried out by optical microscopy (OM) and scanning electron microscopy (SEM) equipped by device for energy dispersive spectroscopy (EDS). The samples for microstructural analysis were prepared by mechanical grinding and polishing and then were etched using 2.5 g $FeCl_3$, 48 ml methanol and 10 ml HCl solution.

For the measurement of the electrical resistance the D.C. method was used and it was applied on a ribbon which was coiled up on the 50 mm long ceramic tube. During the heating of the samples the electrical resistance was measured in the tube furnace and a

temperature change is observed by the thermocouple of Pt - Pt 10 % Rh, which was attached to the sample, respectively. The temperature heating program of the furnace was controlled by the Eurotherm control system. The electrical resistance was simultaneously calculated at known electric current through the sample and a measured voltage drop.

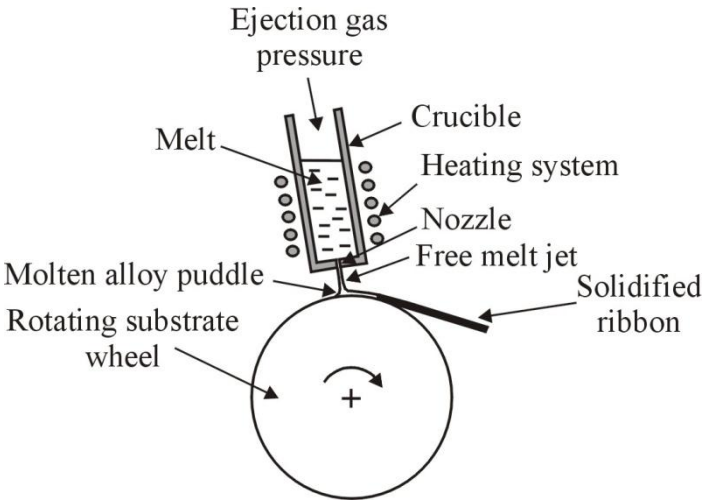

Figure 1. Schematic illustration a free jet melt spinner device

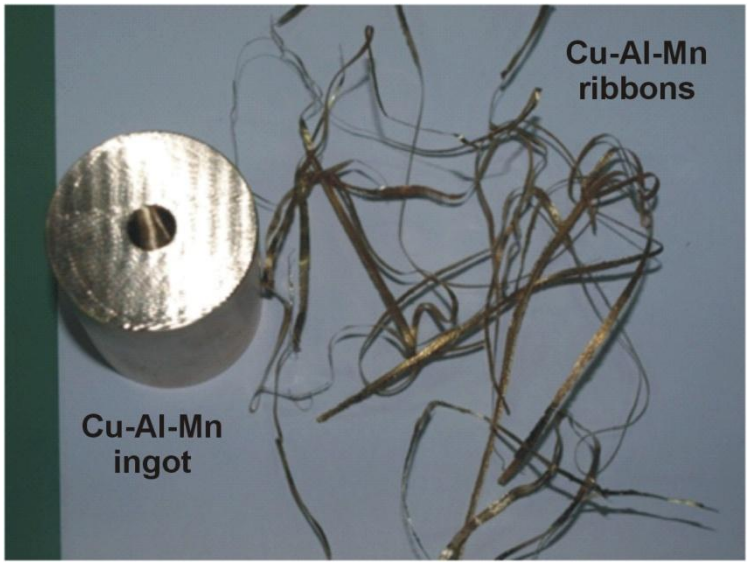

Figure 2. Photography of Cu-Al-Mn ingot and rapidly solidified ribbons

RESULTS AND DISCUSSION

Addition of some alloying elements in Cu-Al system can significantly improve its properties. For example, the addition of Mn to binary Cu-Al alloy stabilizes the bcc phase, widens the single phase region to lower temperature and lower Al content and improves ductility in low

Al alloys by decreasing the degree of order. Thus, 2% of Mn substituting Al may suppress the eutectoid reaction $\beta_1 \rightarrow \alpha+\gamma_2$ while maintaining necessary transition temperature. Content of Mn strongly influences on both, ordering and stabilization kinetics [4].

Figs. 3 and 4 show results of metallographic analysis by OM method of ingot and ribbons in as-cast state. As can be seen, the Cu-Al-Mn ingot has two-phase ($\alpha+\beta$) microstructure. It is known that Cu-Al-Mn alloys undergo a martensitic transformation from β phase. This β phase is stable only at high temperatures. Thereby, three types of martensite may arise: α`(3R), $\beta_1$`(18R) and γ_1`(2H), and this depends on amount of Al and Mn. The $\beta_1$` martensite is predominant at lower Al content, whereas γ_1` martensite is associated with higher content of Al [8]. From literature [9] is known that in vertical section of phase diagram of Cu-Al-10 at.%Mn the single phase region is broadened by addition of Mn and $\alpha+\beta$ microstructure exists. As opposed to that can be seen that the ribbons produced by melt spinner exhibits presence of martensite phase (Fig. 4). The grains into microstructure of the ribbons contain martensite lamellaes.

The typical SEM micrograph with EDS spectrum of the ribbons under study was shown in Fig. 5. Also, the morphology of the SEM micrograph on the Fig. 5 suggests the presence of martensite (Positions 3 and 5) and particles of non transformed α phase (Positions 1, 2 and 6). The EDS results of Cu-Al-Mn ribbons in as-cast state are listed in Table 1. The analysis performed using the energy dispersive spectroscopy system indicated a relative similar composition between different positions marked on Fig. 5. For example, from analysis of EDS results can be seen that martensite plate contains about 85.85 % Cu, 6.90 %Al and 7.26 %Mn. Jiao et al. [10] were investigated Cu-7.66%Al-9.52%Mn alloy and concluded that blocky α phase particles and martensite after solution treatment at 750 °C were present. Increasing solution temperature to 800 °C, caused the α phase disappeared, hence Cu-rich α phase dissolved into β phase and spear-like martensite was introduced. Higher solution temperature leads to thicker martensite plates. It is known that after β(A2) $\rightarrow$ β(B2) $\rightarrow$ β_1($L2_1$) follows the martensitic transformation β_1($L2_1$) $\rightarrow$ β_1`(18R) [10]. Probably, for this investigation of Cu-Al-Mn alloy, next principle can be applied: the disordered bcc high temperature $\beta$ phase undergoes $DO_3$ ordening to $\beta_1$ during quenching and then transforms to 18R $\beta_1$` martensite at lower temperatures. In contrast, Sutou et al. [2] mentioned that two-phase microstructure (martensite + α) obtained by heat treatment at 850 °C in Cu-Al-Mn-Ni-Si alloy. Also, we after quenching of Cu-Al-Mn ribbons at 900 °C martensitic microstructure with sporadically presence of α phase were observed (Figs. 6 and 7). The EDS results of Cu-Al-Mn ribbons after quenching at 900 °C are listed in Table 2, and they are very similar to results obtained in as-cast state alloy. The microstructure of ribbons after quenching mainly is composed of the β phase matrix and a thin plate of martensite phase which crossed austenite grains. Also, sporadically presence of α phase was observed.

(a) (b)

Figure 3. Optical micrographs of Cu-Al-Mn ingot at different magnifiations

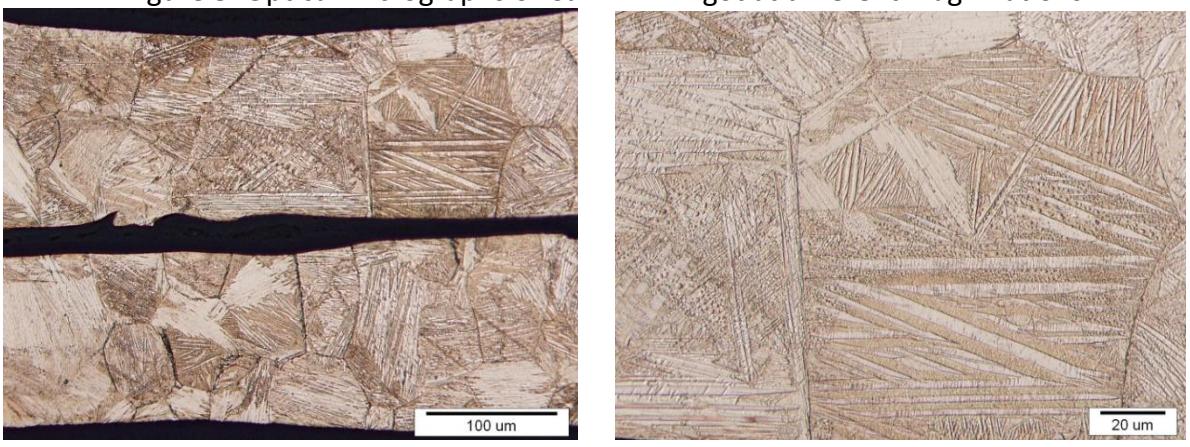

(a) (b)

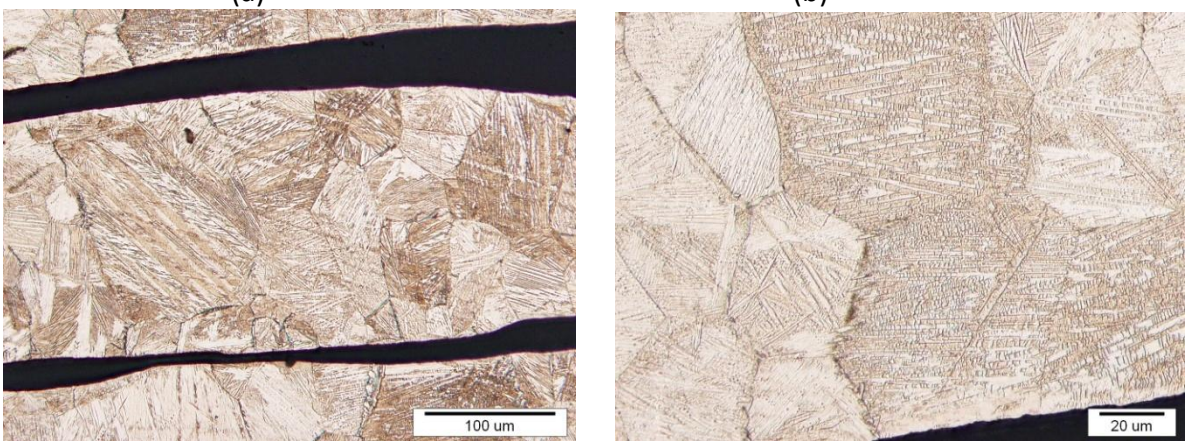

(c) (d)

Figure 4. Optical micrographs of Cu-Al-Mn rapidly solidified ribbons at different magnifiations
(a, b – Position 1; c,d – Position 2)

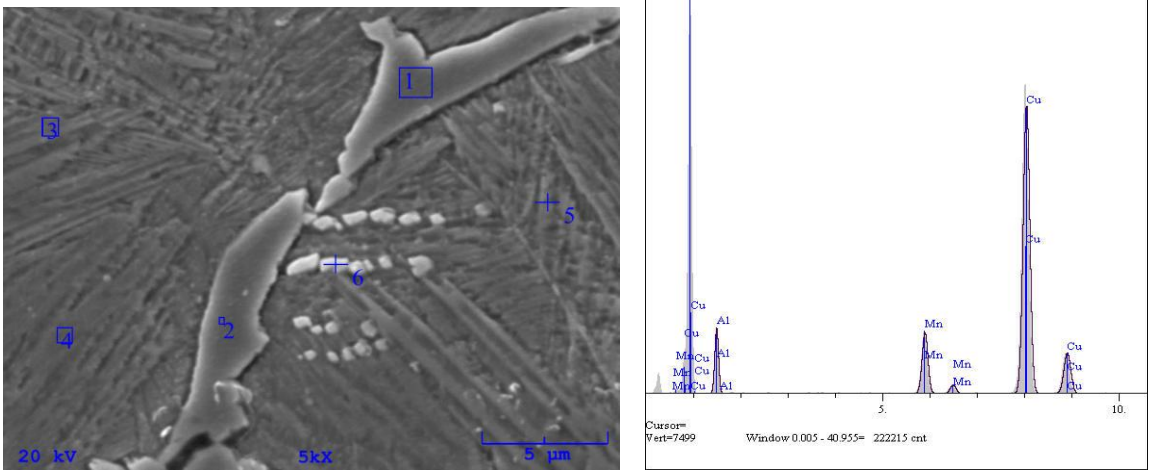

(a) (b)

Figure 5. SEM micrograph (a) and energy dispersive spectrum – Position 1 (b) of Cu-Al-Mn rapidly solidified ribbons after casting by melt spinner

Table 1. Chemical composition of the Cu-Al-Mn rapidly solidified ribbons after casting, the positions marked on Fig. 5.

Position marked on Fig. 5	Chemical composition, wt.%		
	Cu	Al	Mn
1	87.572	5.908	6.520
2	86.899	6.092	7.008
3	85.503	7.541	6.956
4	85.643	7.204	7.153
5	85.846	6.898	7.257
6	87.302	5.581	7.217

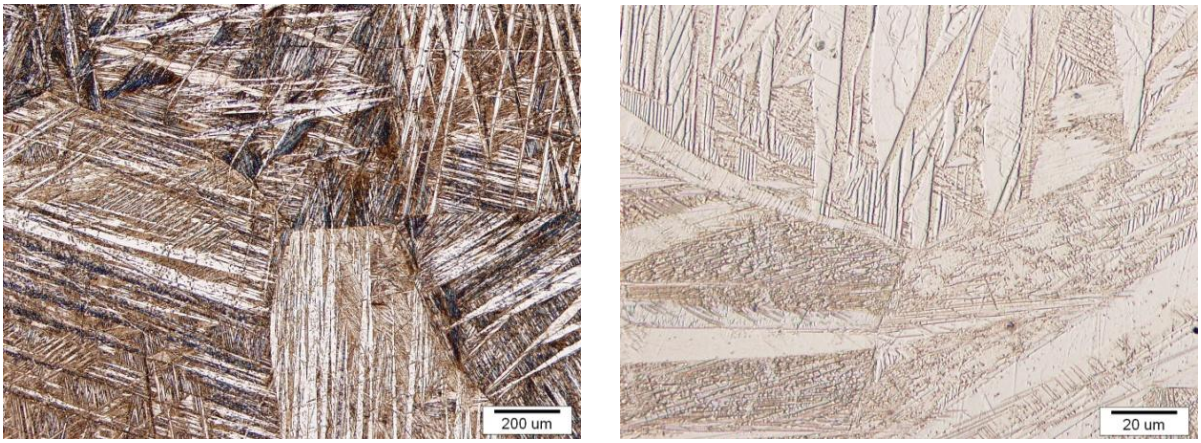

(a) (b)

Figure 6. Optical micrographs of Cu-Al-Mn rapidly solidified ribbons after heat treatment at 900 °C/60 min/water; at different magnifications

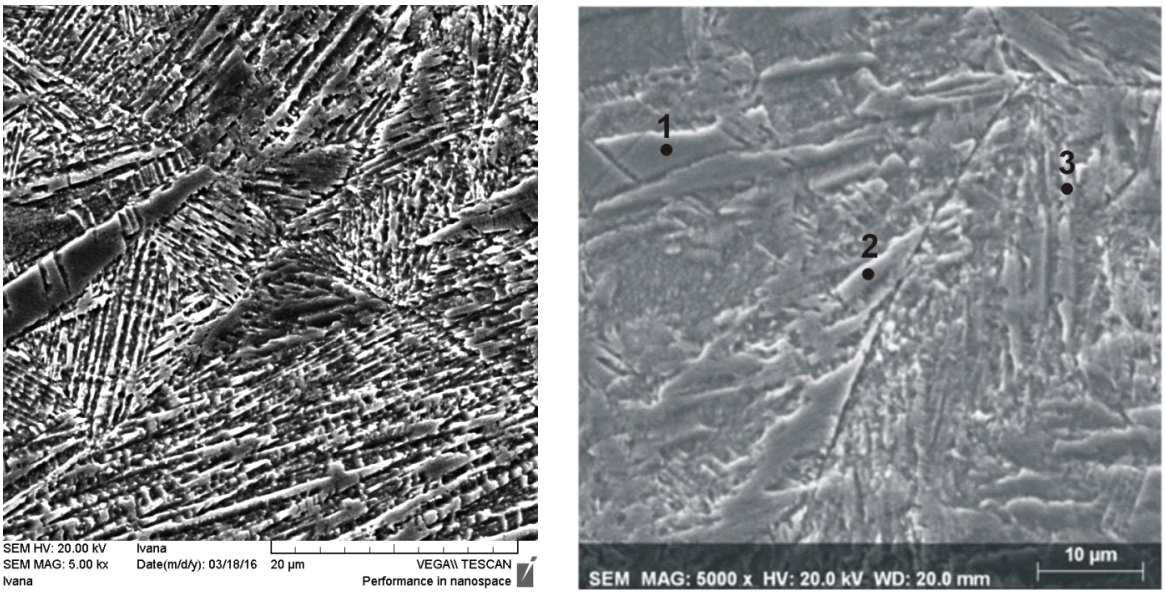

(a) (b)

Figure 7. SEM micrographs of Cu-Al-Mn rapidly solidified ribbons after heat treatment at 900 °C/30 min/water; (a) Position 1, (b) Position 2

Table 2. Chemical composition of Cu-Al-Mn rapidly solidified ribbons after heat treatment at 900 °C/30 min/water, the positions marked on Fig. 7b.

Position marked on Fig. 7b	Chemical composition, wt.%		
	Cu	Al	Mn
1	85.35	7.51	7.13
2	85.02	7.84	7.15
3	84.35	8.87	6.78

The electrical resistance measurement method was used in attempt to determine the eventual existence of phase transformation i.e. microstructure development. Fig. 8 show result of electrical resistance measurements on Cu-Al-Mn ribbons in form of electrical resistance vs. temperature curves. These curves (heating and cooling) were observed after second cycle of measurements. As can be seen the obtained curve have uncharacteristic shape. It can be assumed that present peaks on curves probably represent precipitation of α phase and order-disorder transition of austenite. This can be in accordance with investigations of Stanciu et al. [11]. They are mentioned that two phase transformations are noticeable during heating, which could be associated with precipitation (at 327 °C) of equilibrium α phase and with the order-disorder transition (at 483 °C) of austenite. Also, during cooling, a two step disorder-order transition can become noticeable. Considering that cooling was interrupted at room temperature, they assumed that direct martensitic transformation did not occur, since critical temperature M_s would be located below room temperature.

Also, Sutou et al. [12] mentioned that the group of Cu-Al-Mn alloys with a higher Mn content (> 8 at.%) and a lower Al content (< 18 at.%) with decreased degrees of order in the parent $L2_1$ phase exhibit excellent cold-workability. The transition temperatures associated with two types of order-disorder transitions, $\beta(A2) \rightarrow \beta(B2)$ and $\beta \rightarrow \beta_1(L2_1)$ decrease with decreasing of Al content. Also, below about 14 at.% Al the ordering transition from A2 to $L2_1$ structure is suppressed by quenching from 900 °C and the martensite phase has the 2M or 6M crystal structure. On the other hand, Kainuma et al. [13] were investigated Cu-Al-Mn system and concluded that at 700 °C exists A2-B2 ordering reaction while at 600 °C B2-$L2_1$ ordering reaction.

Since the research of electrical resistance in this work was stopped at 30 and 100 °C, can be assumed that M_s temperature in this case likewise is not covered. This is in accordance with our previously investigation on Cu-16Al-(6-10)Mn (at.%) cylindrical rod (ϕ8x130 mm), where we found that the martensite transformation temperatures are below room temperature (M_s= -19 °C and M_f =-22 °C) [14]. For that reason, further research of phase transformations temperatures should be carried out at lower temperatures range, at cryogenic condition (for example by DSC) to identify M_s and M_f temperatures.

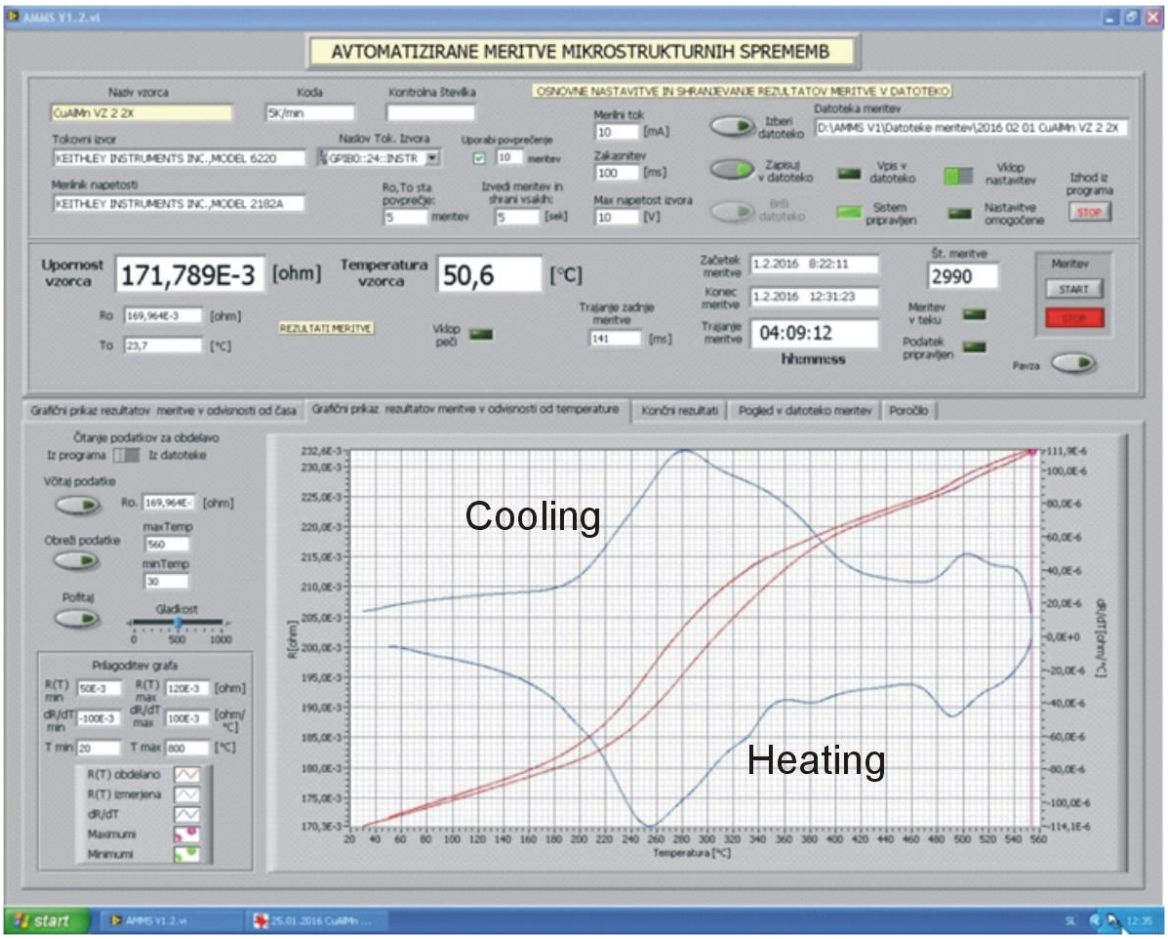

Figure 8. Thermographs electrical resistance vs. temperature of rapidly solidified Cu-Al-Mn ribbon

CONCLUSIONS

After casting of Cu - 8.96%Al – 7.08 %Mn (wt.%) ingot a two-phase (α+β) microstructure is obtained. From this ingot, the ribbons by melt spinning technique were produced. Results of microstructure analysis of ribbons in as-cast state show a formation of martensite structure and presence of α phase in Cu-Al-Mn alloy. Also, after quenching of the ribbons, martensitic microstructure with sporadically presence of α phase was observed. The EDS results of ribbons before and after quenching at 900 °C showed very similar results. The peaks observed on electrical resistance vs. temperature curves represent precipitation of α phase and order-disorder transition of austenite. In general, next principle of transformations can be applied: the disordered bcc high temperature β phase undergoes DO_3 ordering to β_1 during quenching and then transforms to 18R β_1` martensite at lower temperatures.

REFERENCES

[1] Y. Sutou, T. Omori, J.J. Wang, R. Kainuma, K. Ishida, Characteristics of Cu-Al-Mn-based shape memory alloys and their applications, Materials Science and Engineering A 378 (2004), pp.278-282.
[2] Y. Sutou, T. Omori, N. Koeda, R. Kainuma, K. Ishida, Effects of grain size and texture on damping properties of Cu-Al-Mn based shape memory alloys, Materials Science and Engineering A 438-440 (2006), pp.743-746.
[3] Y. Sutou, T. Omori, R. Kainuma, K. Ishida, Grain size dependence of pseudoelasticity in polycrystalline Cu-Al-Mn-based shape memory sheets, Acta Materialia 61 (2013), pp.3842-3850.
[4] Y. Sutou, T. Omori, R. Kainuma, K. Ishida, Ductile Cu-Al-Mn based shape memory alloys: General properties and applications, Materials Science and Technology 24 (2008) 8, pp.896-901.
[5] Y. Sutou, T. Omori, K. Yamauchi, N. Ono, R. Kainuma, K. Ishida, Effect of grain size and texture on pseudoelasticity in Cu-Al-Mn-based shape memory wire, Acta Materialia 53 (2005), pp.4121-4133.
[6] J. Dutkiewicz, T. Czeppe, J. Morgiel, Effect of titanium on structure and martensic transformation in rapidly solidified Cu-Al-Ni-Mn-Ti alloys, Materials Science and Engineering A 237-275 (1999), pp.703-707.
[7] J. Dutkiewicz, J. Morgiel, T. Czeppe, E. Cesari, Martensitic Transformation in CuAlMn and CuAlNi Melt Spun Ribbons, Journal of Physics IV France 7 (1997) C5-167-C5-172.
[8] U.S.Mallik, V. Sampath, Effect of composition and ageing on damping characteristics of Cu-Al-Mn shape memory alloys, Materials Science Engineering A 478 (2008), pp.48-55.
[9] Y. Sutou, T. Omori, R. Kainuma, N. Ono, K. Ihida, Enhancement of Superelasticity in Cu-Al-Mn-Ni Shape-Memory Alloys by Texture Control, Metallurgical and Materials Transactions A 33A (2002), pp.2817-2824.
[10] Y.Q. Jiao, Y.H. Wen, N. Li, J.Q. He, J. Teng, Effect of solution treatment on damping capacity and shape memory effect of a CuAlMn alloy, Journal of Alloys and Compounds 491 (2010), pp.627-630.
[11] S. Stanciu, L.G. Bujoreanu, R.I. Comanenci, N. Cimpoesu, I. Ionita, V.V. Moldoveanu, Particularities of phase transitions in thermomechanically processed Cu-Al-Mn shape memory alloys, Proceedings of 8th European Symposium on Martensitic Transformations ESOMAT, 07-11. September, Prague, 2009, 1-6 (DOI:10.1051/esomat/200905004)
[12] Y. Sutou, R. Kainuma, K. Ishida, Effect of alloying elements on the shape memory properties of ductile Cu-Al-Mn alloys, Materials Science Engineering A237-275 (1999), pp.375-379.
[13] R. Kainuma, N. Satoh, X.J. Liu, I. Ohnuma, K. Ishida, Phase equilibria and Heusler phase stability in the Cu-rich portion of the Cu-Al-Mn system, Journal of Alloys and Compounds 266 (1998), pp.191-200.
[14] T. Holjevac Grgurić, M. Gojić, D. Živković, A. Kostov, S. Kožuh, Z. Zovko-Brodarac, D. Ćubela, Characterization of Cu-Al-Mn shape memory alloy, Proceedings the 45th

International Conference on Mining and Metallurgy, Bor-Serbia, 16-19. October 2013., pp.844-847.

Acknowledgements
This work has been fully supported by Croatian Science Foundation under the project IP-2014-09-3405.

15th INTERNATIONAL FOUNDRYMEN CONFERENCE
INNOVATION – The foundation of competitive casting production
Opatija, May 11th-13th, 2016
http://www.simet.hr/~foundry/

APPLICATION OF HIGH EMISSIVITY COATING IN FOUNDRY ALUMINIUM MELTING FURNACES

L. Lazić, M. Lovrenić-Jugović and Ž. Grubišić

University of Zagreb Faculty of Metallurgy, Sisak, Croatia

Oral presentation
Original scientific paper

Abstract

Energy efficiency of foundry furnaces for aluminium melting is much lower than in most other furnace aggregates, especially because of low emissivity of conventional refractory at operating furnace temperatures as well as low aluminium emissivity and low heat conductivity of molten aluminium. In this paper the application of high emissivity coating in foundry aluminium melting furnaces in order to intensify the heat transfer by radiation and increase the furnace energy efficiency was analyzed. The objective is to find out effectiveness of the emissivity coatings on the fuel consumption.

Keywords: *foundry, furnace, aluminium, energy efficiency, coating emissivity*

*Corresponding author (e-mail address): *lazic@simet.hr*

INTRODUCTION

The main problems in the process of aluminium melting in foundry practice are as follows:

- Inherently low efficiency of aluminium and conventional refractory at operating furnace temperatures;
- Recuperation is difficult due to dirty gases;
- Contamination of melted aluminium with oxide.

Heat is transferred to the bath from above by radiation and convection. In high temperature furnaces the radiative heat transfer often dominates so that the convective heat transfer is small (5 - 10%) because of low gas velocities.

Radiation interchange in a furnace depends upon:

- Flame temperature;
- Load temperature;

- Flame emissivity;
- Load emissivity;
- Lining temperature & emissivity.

Most aluminum melting and molten aluminum holding (alloying) furnaces are refractory-lined 'reverberatory' or 'reverb' furnaces composed of a rectangular refractory-lined box and burners are located in one wall or in the roof (Fig. 1). The exhaust may be in the roof or in one of the walls, often in between the burners. The burners are used primarily to heat the refractory walls which then re-radiate or reverberate the heat energy to the load. The surface emissivity of molten aluminum ranges from 0.004 to 0.55 and a slag layer formed on the surface of molten aluminum, consisting of aluminum oxide, has an emissivity of 0.11 to 0.19 [1]. This result in poor heat transfer by radiation to the surface. Therefore, compared to some other furnace designs, the furnace is designed to compensate for this by having a high bath surface area-to-melt ratio to ensure that the bath surface accepts the needed heat transfer rate.

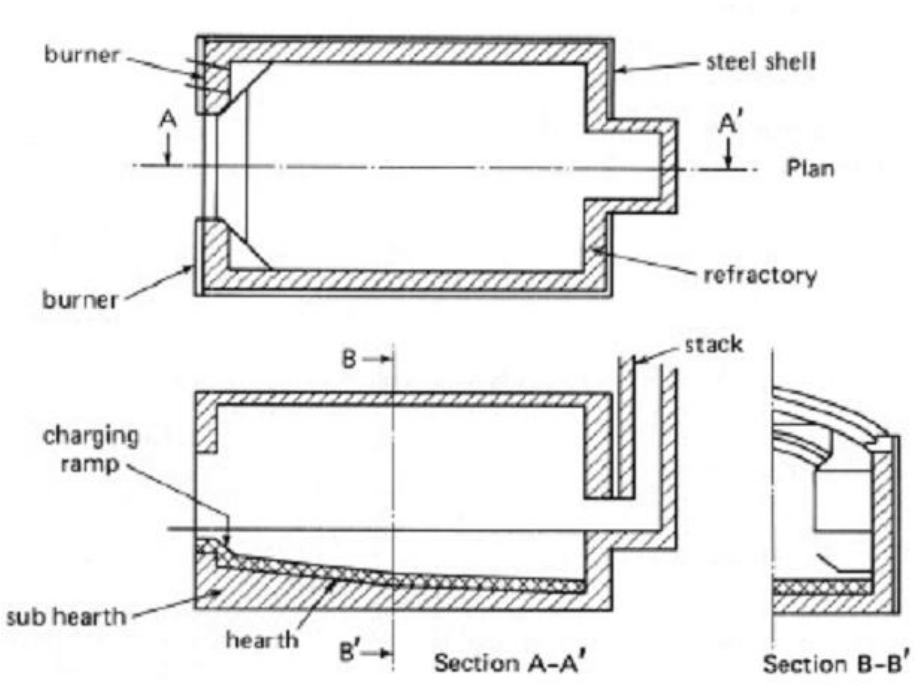

Figure 1. Aluminium melting and holding furnace [1]

One of the essential ways to reduce these problems is to increase the refractory wall emissivity. The objective of this paper is to find out effectiveness of the emissivity coatings on the fuel consumption.

REFRACTORY WALL EMISSIVITY

The emissivity here is characterized to describe the surface radiative property which involves the transfer of heat by electromagnetic radiation arising due to the temperature of a body.

The emissivity is defined as the ratio of energy radiated by the material to energy radiated by a black body (*A* body that emits the maximum amount of heat for its absolute temperature is called a black body), meaning that a black body completely absorbs all radiation incident upon it, and at the same time it emits all the energy that it absorbs with the same absorbing spectrum.
The efficiency by which materials radiate is defined as emissivity ($\boldsymbol{\varepsilon}$). Its value depends on the surface temperature and material properties of the radiating object's surface, and on the radiation wavelength ($\boldsymbol{\varepsilon_n, \Delta\lambda}$).

Furnace refractories are often assumed to have an emissivity of about 0.9. However, in the case of most refractory materials the emissivity significantly decreases with temperature increase. Conventional refractories have low wall emissivity at high temperatures, so e.g. ε can be <0.5 at 1000°C (Fig. 2). For instance, if the emissivity of a given type of a chamotte refractory brick is 0.9 at a temperature of 130 °C, at 1000°C the emissivity might be 0.5 only (Fig.2). Ceramic fibre insulating materials (such as Al_2O_3) have poor heat radiation properties (Fig. 2.) but their insulating property is good at operating temperatures up to 1200-1400 °C [2]. Ceramic fibre linings may also have an emissivity as low as 0.5-0.6 at high temperatures (Fig. 3). An end-on or "stock-bonded" fibre orientation (the fibres are aligned normal to the hot face) has a slightly higher emissivity than when the fibres are aligned parallel to the hot face (Fig.3) [3].

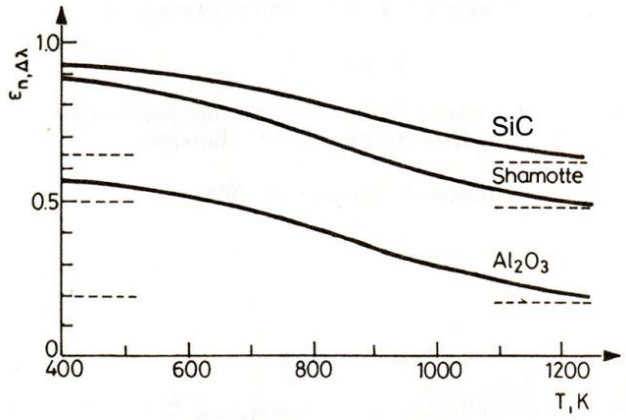

Figure 2. Normal spectral emissivity of SiC, shamotte and ceramic fibre (Al_2O_3) against material surface temperature [2]

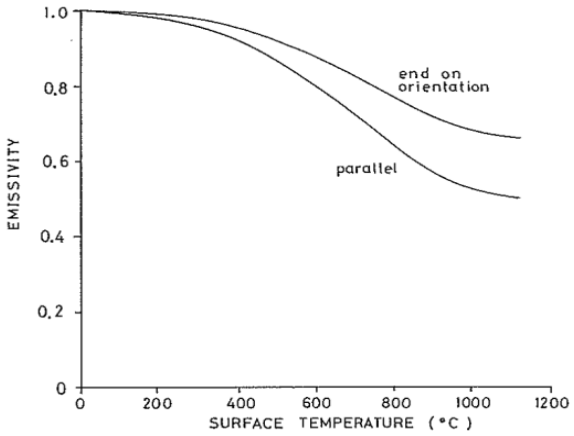

Figure 3. Emissivity of ceramic fibre as a function of surface and fibre orientation [3]

However, ceramic fibre has much lower mechanical strength than traditional fireclay based materials. A recently opened way of dealing with these drawbacks is the application of suitable coating materials. Their purpose is on one hand to improve the strength and surface properties of the ceramic fibre, and on the other hand to increase the infrared emissivity of the surface.

In the past forty years great attention has been paid to studying the emissivity of furnace linings [4] as well as to energy conservation through utilization of high emissivity coatings [5], the latter well complementing the use of low density insulating materials, such as ceramic fibres and refractory bricks [6]. Recent research has been focused on high emissivity coating of ceramic fibres, which increase the fibres' mechanical strength and the emitted energy. Experiments revealed that by employing a silicon carbide (SiC) based coating the emissivity of a ceramic fibre can be increased to 0.63 from 0.2 at 730°C temperature (Fig. 2) [2].

When high emissivity coating is applied in a high temperature furnace, radiant energy from the burners and convective energy from furnace atmosphere is absorbed by the surface face of the coating and re radiated to cooler furnace load, where the temperature of wall furnace is higher than furnace load. Namely, in gas or oil fired furnace, the gases are fired and after combustion in presence of air they absorbed and emit radiation at specific wave length corresponding to the spectra of CO_2 and H_2O. Radiant energy from hot gases reflected back from the furnace wall does not change its wavelength and hence can be significantly absorbed by gas before reaching to the load surface. Radiation that is absorbed by the wall on account of its emissivity is reemitted. If the wall is black or a high emissive then more radiation will reach the load surface without reabsorption by the gas. Thus net redistribution of energy occurs across the spectrum resulting in an increase in heat transfer to the load.

High emissivity coatings are widely used in many high temperature applications to effectively transfer the heat by radiation [7-9]. The application of high-emissivity coatings in furnace chambers promotes rapid and efficient transfer of heat, uniform heating, and extended life of refractories and metallic components such as radiant tubes and heating elements. For intermittent furnaces or where rapid heating is required, use of such coatings was found to reduce fuel or power to tune of 25-45%. Other benefits are temperature uniformity and increased refractory life. Furnaces, which operate at high temperature, have emissivities of 0.3. By using high emissivity coatings this can go up to 0.9 thus effectively increasing the radiative heat transfer [10].

Emissivity, the measure of a material's ability to both absorb and radiate heat, has been considered by engineers as being an inherent physical property which like density, specific heat and thermal conductivity, is not readily amenable to change. However, the development of high emissivity coatings now allows the surface emissivity of materials to be increased, with resultant benefits in heat transfer efficiency and in the service life of heat transfer components. High emissivity coatings are applied in the interior surface of furnaces. The Figure 4 shows emissivity of various insulating materials including high emissivity coatings. High emissivity coating shows a constant value over varying process temperatures.

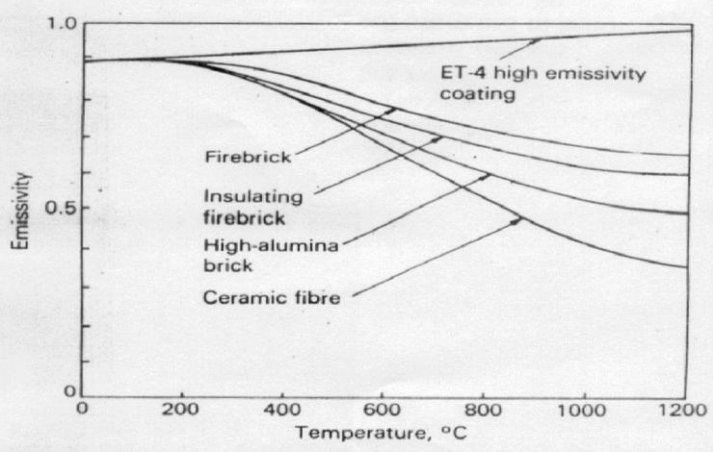

Figure 4. Emissivity of refractory materials at different temperatures [10]

The high emissivity coating is applied on refractory or metal substrate to expose at high temperature. It should be remembered that high emissivity coating are not insulator or reflector. They are not barrier to conductivity of thermal energy through a furnace wall. Insulating refractories are generally place behind dense refractories at the cold phase of refractory design [11].

Emissivity is often considered as inherent physical property that does not normally change. A surface with high emissivity has the ability to absorb radiant and convective energy at high temperature and re radiate up to 95% of that energy. In turn these get absorbed by the surface of gas which is cooler than coating. When hot face emissivity of a substrate is increased by applying coating, radiant energy from burner or electric arcs and convective heat from contract with furnace gases are absorbed and re radiated [12]. In general, the emissivity of furnace that operate at high temperature is found to be 0.3. But with the help of emissivity coating, this can go to up to 0.85-0.95. This significantly results in increase of heat transfer through radiation. Emissivity is a property of the coating, which is in this case, remains between 0.85 and 0.95 up to temperatures in excess of 1650°C [13].

Emissivity coating is prepared by two major components: a high emissivity agent and a binder. A mix of various constituents is weighed in a weighing scale and added water to maintain a coating consistency after milling for certain duration. Ceramic coating thus prepared with desired rheological characteristics have been applied onto the surface of ceramic substrates by spraying /brushing. The settling of the slip is made to a minimum level with a higher solid content. The slip is coated on suitable ceramic substrate such as refractory insulation bricks, ceramic insulation fiber for attaining desired thickness. The details of the formulation of the coating materials are described in Ref. [12]. All the ceramic substrates can be spray and brush coated. The sprayed coated material looked to be more uniform as compared to that of brushing.

MATHEMATICAL MODEL

The single gas zone model was used to analyze the impact of the emissivity of refractory lining on the heat transfer, and hence, on the energy efficiency as well as on the fuel consumption of the furnace.

The most significant development of a simple furnace model, so-called simple well-stirred furnace model, was made by Hottel [14] and is based on the presumption that many industrial furnaces operate with sufficient momentum in the air and/or fuel streams to create a reasonably well-stirred furnace chamber. This assumption allows most of the complex geometric problems associated with radiative heat transfer calculations to be reduced to a numerically simple solution.

Otherwise, zone models provide accurate calculations of thermal radiation and have very short computing times so that they can yield transient predictions and can be used to quickly analyse the relative effect of design options such as fuel type and refractory selection, and operating parameters such as air preheating, oxygen enrichment and excess air.

For this type of model, the following simplifying assumptions are made:

1. Combustion gas mass and flame are assigned a single temperature T_g
2. The combustion gases leave the radiant section of the furnace at a temperature below T_g
3. Spectral effects of combustion gases were included in the single well-stirred zone mode
4. Surface of load, area A_m, is grey, with an emissivity ε_m, and can be assigned a single temperatureT_1
5. External heat losses and convective heat transfer to the walls (internal and external) are calculated
6. The load and refractory wall surfaces are intimately mixed, such that the view factors to load surface are the same from all points (speckled wall assumption)
7. Convection from the gases to the load is taken into account through the calculation of the coefficient of convection heat transfer.

This type of model belongs to the category of the steady-state models, which is based on the following balances:

- The mass balance: Mass Flow In = Mass Flow Out
- The energy balance: Energy Inputs = Energy Outputs

In the present case, the basic structure of the model is described by the following equation:
Rate of enthalpy derived from fuel + Rate of enthalpy with preheated combustion air - Rate of enthalpy (energy loss) with flue gases = Radiative and convective heat transfer (heat flow) to the load + Heat losses (heat flow) through the walls.

RESULTS

In this article, energy efficiency and fuel consumption of the furnace were compared for two cases:

- using the convectional refractory,
- using the convectional refractory with high emissivity coating,

observed at the beginning and at the end of the melting process.

The convectional refractory lining consists of hi-alumina brick in the metal contact area and high strength brick (40% alumina firebrick, density 2000 kg/m^3, maximum service temperature 1500°C, thickness 300 mm, thermal conductivity 1.0 W/mK, emissivity 0.3) in the upper portion of the furnace, which is sprayed with high emissivity coating with emissivity of 0.9.

The furnace is fired with natural gas of the low heating value 48.5 MJ/kg. The internal dimensions of the furnace filled with combustion gases are: L x B x H = 4.0m x 2,5m x 1,80m. The input data are as follows: T_g, T_m , ε_w, ε_m, $h_{g\text{-}m}$, U.

In Table 1 are presented input and calculated values for the convectional refractory lining, and in Table 2 for coated lining.

Table 1. Input and calculated values for the convectional refractory lining

T_g °C	T_w °C	T_m °C	ε_w	ε_m	$h_{g\text{-}m}$ W/m^{2}K	U W/m^{2}K	Φ_m kW	η
Beginning of melting								
1200	1096	30	0.3	0.15	4	1.56	361.5	38.79
End of melting								
1200	1087	700	0.3	0.25	8	1.56	426.6	39.4

Table 2. Input and calculated values for the coated lining

T_g °C	T_w °C	T_m °C	ε_w	ε_m	$h_{g\text{-}m}$ W/m^{2}K	U W/m^{2}K	Φ_m kW	η
Beginning of melting								
1200	1144	30	0.9	0.15	4	1.56	404.7	39.04
End of melting								
1200	1132	700	0.9	0.25	8	1.56	496.7	39.76

Nomenclature:

T_g- temperature of combustion gases, °C
T_m- load temperature, °C
T_w- refractory hot face temperature, °C
ε_m- emissivity of load
ε_w- emissivity of walls

$h_{g\text{-}m}$- convective heat transfer coefficient between combustion gases and load, W/m^{2}K
η- thermal efficiency of the furnace
U- overall heat transfer coefficient through the walls, W/m^{2}K
Φ_m- heat flow to the load, kW

CONCLUSIONS

From Table 2 it is evident that the heat flow from the combustion gases and walls to the load, in the period from the beginning to the end of the melting process, at the coated lining in relation to the convectional refractory lining is increased in the range from 10.7% to 14.1%. This means that the time of the melting is shortened by approximately 12%. It is expected that the same amount of fuel consumption would be reduced because the energy efficiency is increased in the interval from 0.6% to 0.9%.

The replacement of the existing conventional convectional refractory lining or the choice of a high emissivity coating for furnaces in foundries is one of the key factors in minimization of energy consumption per unit of product. It should be the objective to choose the optimal refractory lining under which the furnace should be operated in order to maximize the energy efficiency and minimize the fuel consumption, taking into account the profitability of the investment i.e. the payback period.

It is noteworthy that the factors affecting the infrared radiation of furnace surfaces and high temperature industrial equipment have not yet been studied widely enough.

REFERENCES

[1] W. Trinks et al., Industrial furnaces, Sixth edition, John Wiley & Sons Inc., New Jersey, 2004, pp. 111,112,182.
[2] I. Benko, Improvement of IR-emissivity of ceramic fibre by silicon carbide coating in furnaces, Proceedings of 9th International Conference on Quantitative InfraRed Thermography, July 2-5, 2008, Krakow – Poland
[3] http://texasthermalanalysis.com/Appendix%20A%20Properties%20of%20Ceramic%20Fibres.PDF, 15.03.2016.
[4] A. Goldsmith, T.E. Waterman and H.J. Hirschhorn: Handbook of thermophysical properties of solid materials, Pergamon Press, Oxford (1961,1963).
[5] Inst. of Energy, London: Ceramics in energy applications, Adam Hilger, Bristol and New York, 1990.
[6] I. Benko, High infrared emissivity coating for energy conservation and protection of inner surfaces in furnaces, Int. J. Global Energy Issues, 17 (2002) 1/2, pp.60-67.
[7] B.V. Cockeram, D.P. Measures, A.J. Mueller, The Development and Testing of Emissivity Enhancement Coating for Thermophotovoltic (TPV) Radiator Applications, Thin Solid Films, 355–356 (1999), pp. 17-25.

[8] T. Sumita, M. Imaizumi, S. Kawakita, S. Matsuda, S. Kuwajima, T. Ohshima, T. Kamiya, Terrestrial Solar Cells in Space, Proceedings of 2004 IEEE Radiation Effects Data Workshop Record, J. Black (Ed.), Atlanta, U.S.A., July 19–23, 2004, pp. 130-136.
[9] X. He, Y. Li, L. Wang, Y. Sun and S. Zhang, High emissivity coatings for high temperature application: Progress and prospect, Thin Solid Films, 517 (2009), pp. 5120–5129.
[10] https://beeindia.gov.in/sites/default/files/2Ch5.pdf, 15.03.2016.
[11] http://www.naref.com/products/Publications/Electric_Furnaces.pdf, 15.03.2016.
[12] D.V. Chauhan, S.N. Misra, R.N. Shukla, Synthesis of high emissivity coating for ceramic substrate towards energy conservation, International Journal of Scientific Engineering and Technology, www.ijset.com, 1 (2012)3, pp. 36-40.
[13] P.C. Sheil and T.R. Kleeb, High emissivity Coating for Improved Performance of Electric Arc Furnaces, Iron Steel Technol., 3(2006), 2, pp. 49-53.
[14] H.C. Hottel, First estimates of industrial furnace performance – the one-gas-zone model re-examined, in *Heat Transfer in Flames*, Chapter 1, edited by Afgan and Beer, Wiley, New York, 1974, pp. 5-28.

15th INTERNATIONAL FOUNDRYMEN CONFERENCE
INNOVATION – The foundation of competitive casting production
Opatija, May 12th-13th, 2016
http://www.simet.hr/~foundry/

NUMERICAL SIMULATIONS AS A SUCCESSFUL TOOL FOR SOLVING CASTING PROBLEMS

NUMERIČKE SIMULACIJE KAO USPJEŠAN ALAT KOD RJEŠAVANJA LJEVAČKIH PROBLEMA

A. Mahmutović[1], S. Kastelic[1,2], M. Petrič[2] and P. Mrvar[2]

[1]TC Livarstvo, Ljubljana, Slovenia
[2]University of Ljubljana Faculty of Natural Science and Engineering, Ljubljana, Slovenia

Oral presentation
Conference paper

Abstract

Paper presents the ProCAST computer program for numerical simulations as a tool for simulation of all foundry technologies. In past years the need for implementation of numerical simulations in solving most foundry problems has increased. With correct and precise input data for simulation program the realistic results in sequences of casting, solidification and cooling of casting can be met. With experimentally obtained data such as thermal expansion coefficient we can predict the contraction of casting during cooling. In this manner we can solve the problem of dimensional stability since the casting does not contract evenly in all directions.
The use of pin squeeze technology in high pressure die-casting, low pressure die-casting and in die-casting technology can be simulated. The results offer optimization of squeeze depth in order to eliminate the shrinkage porosity in the casting. ProCAST simulation program is based on finite element method (FEM) so the results of calculations can be imported to other FEM programs such as Abaqus for further analyses.

Keywords: *ProCAST, numerical simulation, squeeze, FEM method*

*Corresponding author (e-mail address): *almir.mahmutovic@tc-liv.eu*

Sažetak

U radu je predstavljen program za numeričke simulacije ProCAST kao alat sa kojim je moguće simulirati sve tehnologije ulijevanja. U zadnjih nekoliko godine je povećana potreba za uvođenjem računalnih simulacija kod rješavanja većine ljevački problema. Sa točnim ulaznim parametrima koje unosimo u program za izračun numeričke simulacije možemo se dosta približiti realnom stanju odljevka u sekvenci punjenja skrućivanja i hlađenja. Eksperimentalno dobiveni rezultati kao što je toplinsko istezanje materijala (koeficijent toplinskog istezanja) nam omogućava da sa numeričkom simulacijom predvidimo skupljanja odljevka. Na takav način možemo riješiti problem sa točnošću dimenzija odljevaka jer odljevci u odvisnosti od kompleksnosti se ne skupljaju isto u svim smjerovima.

Upotreba „squeeza“ u tehnologiji tlačnoga i niskotlačnoga lijeva kao i kokilnoga lijeva s numeričkom simulacijom moguće je optimizirati parametre squeeza i na takav način eliminirati pojavljivanje poroznosti koja nastaje zbog skupljanja materijala. Program ProCAST računa s metodom konačni elemenata tako da izračunane rezultate naprezanja u odljevaku možemo izvoziti u druge programe za FEM analizu kao što je Abaqus.

Ključne riječi: *ProCAST, numerička simulacija, squeez, FEM analiza*

15th INTERNATIONAL FOUNDRYMEN CONFERENCE
INNOVATION – The foundation of competitive casting production
Opatija, May 11th-13th, 2016
http://www.simet.hr/~foundry/

EFFECT OF Bi ADDITION ON MICROSTRUCTURE AND MECHANICAL PROPERTIES IN HEAVY-SECTION SPHEROIDAL GRAPHITE CAST IRON PARTS

UTJECAJ DODATKA BIZMUTA NA MIKROSTRUKTURU I MEHANIČKA SVOJSTVA DEBELOSTIJENIH ODLJEVAKA OD NODULARNOG LIJEVA

I. Mihalic Pokopec[1], M. Petrič[2], P. Mrvar[2] and B. Bauer[1]

[1]University of Zagreb Faculty of Mechanical Engineering and Naval Architecture, Zagreb, Croatia
[2]University of Ljubljana Faculty of Natural Sciences and Engineering, Ljubljana, Slovenia

Oral presentation
Preliminary note

Abstract

In this study, the effect of Bi addition on the microstructure and mechanical properties of heavy-section spheroidal graphite cast iron EN-GJS-400-15 was investigated. The addition of bismuth in proper content can prevent the formation of degenerate graphite and result in increased nodule count and improved graphite nodularity. However, the effect of Bi is highly dependent on presence of Ce; only when the correct balance between the presence of cerium and bismuth is achieved, high-quality castings can be obtained.
Two molds containing cone blocks ϕ 300 mm x 350 mm, with and without bismuth addition were casted. From each block three samples from three different positions in the casting (from the edge to the center), with different cooling rates, were prepared for microstructure observation and three tensile test bar from thermal center of block for tensile test. Bismuth addition was performed with 99,99% pure element to reach level of 0,01 % for one mold, after inoculation sequence, while Ce was added in form of Ce containing commercial inoculant, in the same amount for both molds. Thermal and chemical analyses were used to control the melt.
The graphite degeneration increases with a decrease of cooling rate. Bi addition negatively influenced microstructure, for all cooling rates. The mechanical properties were hardly affected due to Bi addition, except elongation. With Bi addition the elongation values were higher for up to 40 %.

***Keywords**: heavy-section spheroidal graphite cast iron, graphite morphology, bismuth, cooling rate*

*Corresponding author (e-mail address): *branko.bauer@fsb.hr*

Sažetak

U ovom radu ispitivan je utjecaj dodatka bizmuta na mikrostrukturu i mehanička svojstva debelostijenih odljevaka od nodularnog lijeva kvalitete EN-GJS-400-15. Dodavanje bizmuta u

pravilnom udjelu može spriječiti nastanak degeneranih oblika grafita te rezultirati povećanjem broja nodula i poboljšanjem nodularnosti grafita. Djelovanje bizmuta jako ovisi o prisutnom udjelu cerija, tako da samo pravilan omjer između ova dva elementa može rezultirati visokokvalitetnim odljevcima od nodularnog lijeva.
Odlivena su dva ispitna odljevka oblika stošca dimenzija ϕ 300 mm x 350 mm. Iz svakog su stošca uzeta po tri uzorka s tri različita mjesta (od ruba prema centru odljevka), s različitim brzinama hlađenja, radi metalografske analize te tri epruvete iz toplinskog centra odljevka radi određivanja mehaničkih svojstava. Bizmut je dodan u udjelu od 0,01 % kao 99,99 % čisti metal, nakon cijepljenja u mlaz taljevine. Cerij je dodan kao sastavni dio cjepiva. Toplinska analiza i analiza kemijskog sastava provedene su s ciljem kontrole kvalitete taljevine.
Smanjenje brzine hlađenja od rubnih dijelova prema toplinskom centru odljevka potiče degeneraciju grafita. Dodatak bizmuta potiče izdvajanje grafita nepravilnog oblika, neovisno o brzini hlađenja. Na mehanička svojstva dodatak bizmuta nema značajan utjecaj, osim na istezljivost. Dodatak bizmuta uzrokovao je povišenje vrijednosti istezljivosti za 40 %.

Ključne riječi: *debelostijeni odljevci od nodularnog lijeva, morfologija grafita, bizmut, brzina hlađenja*

UVOD

Proizvodnja debelostijenih odljevaka od nodularnog lijeva sve je zastupljenija, a za očekivati je da će se ovaj trend nastaviti barem idućih dvadeset godina. Ovo se prije svega odnosi na proizvodnju odljevaka za vjetroelektrane, industiju teških transportnih vozila te proizvodnju kanistera za trajno skladištenje nuklearnog otpada [1-6]. Buduće primjene debelostijenih odljevaka od nodularnog lijeva zahtijevat će sve veće debljine stijenki. Također će rasti i zahtjevi na mehanička svojstva dovodeći do sve većeg značaja izvrsnost sferoidalne morfologije grafita. Naime, svaka degeneracija grafita, što je kod proizvodnje debelostijenih odljevaka česta i iznad svega nepoželjna pojava, dovodi do pada mehaničkih svojstava i vrlo često rezultira odbacivanjem takvih odljevaka [2]. Do degeneracije dolazi prije svega zbog smanjenja brzine hlađenja, odnosno dugog vremena skrućivanja. Nekoliko je vrsta degeneriranog grafita - vermikularni, šiljasti, koraljni, eksplodirani i chunky grafit. Najštetnija od njih je chunky grafit. Ova se greška najčešće javlja u toplinskom centru debelostijenih odljevaka te uzrokuje pad mehaničkih svojstava, osobito vlačne čvrstoće, istezljivosti i dinamičke izdržljivosti [3-9].

Radi sprječavanja degeneracije grafita te poboljšanja mehaničkih svojstava debelostijenih odljevaka od nodularnog lijeva u taljevinu se često dodaju elementi u tragovima (kao što su Bi, Sb, Sn, Ce). Cerij i ostali elementi rijetkih zemalja dodaju se u obliku MgFeS predlegura za obradu jer povisuju broj nodula, poboljšavaju nodularnost te smanjuju mogućnost pojave karbida. Međutim, ukoliko njihov udio prijeđe kritičnu vrijednost promoviraju nastanak chunky grafita. Da bi se neutraliziralo njihovo štetno djelovanje nodularnom lijevu se dodaju subverzivni elementi, npr. Bi, Sb, Sn [2-4, 10, 11].

U novijim istraživanjima i u ovom radu istražuje se djelovanje dodatka bizmuta na sprječavanje nastanka chunky grafita u debelostijenim odljevcima od nodularnog lijeva kada

su prisutni elementi koji promoviraju nastanak chunky grafita. Dosadašnja istraživanja su pokazala kako povoljni udjeli Bi pozitivno utječu na sferoidalnu morfologiju grafita u nodularnom lijevu tako što se stvaraju brojna heterogena nukleacijska mjesta i smanjuje promjer grafitnih nodula što uzrokuje povećanje broja nodula. Povoljnim dodatkom Bi također se kontrolira rast karbida te se poboljšava čvrstoća i žilavost nodularnog lijeva [1]. Međutim, ako udio Bi prijeđe kritičan udio tada ima negativan utjecaj na sferoidalnu morfologiju grafita. Prema [10] negativno djelovanje viška Ce može se spriječiti dodavanjem do 0,003 % Bi, odnosno prema [12] do 0,006% Bi. Prema [1] udio Bi do 0,011 % pozitivno utječe na morfologiju grafita smanjujući udio chunky grafita i ostalih vrsta degeneriranog grafita kod feritnih debelostijenih odljevaka od nodularnog lijeva.

MATERIJALI I METODE

U eksperimentalnom dijelu ovog rada ispitivan je utjecaj dodatka bizmuta na morfologiju grafita i mehanička svojstva nodularnog lijeva kvalitete EN-GJS-400-15.
Kao ispitni odljevak korišten je stožac dimenzija ϕ 300mm × 350 mm, radi mogućnosti ispitivanja utjecaja različitih brzina hlađenja na morfologiju grafita i mehanička svojstva na istom odjevku. Ulijevanje je izvedeno odozgo, direktnim ulijevanjem kroz KALPUR® uljevni sustav (KALMINEX® pojilo zajedno sa SEDIMEX® filterom). Izrađena su dva kalupa (K1 i K2) CO_2 postupkom kalupljenja, slika 1.

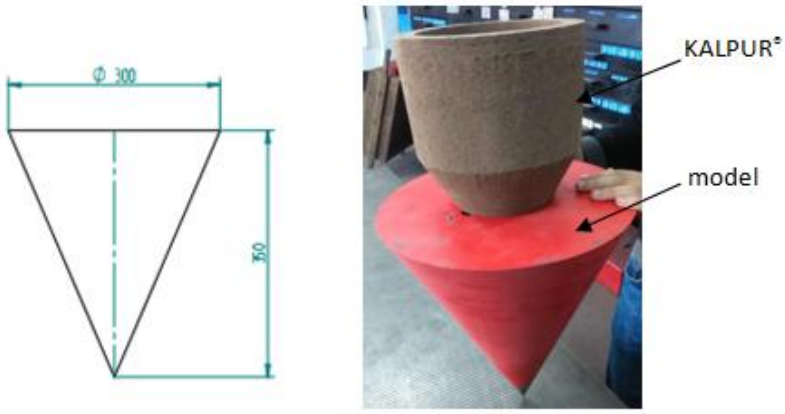

Slika 1. Nacrt i model odljevka sa KALPUR® uljevnim sustavom

Primarna taljevina izrađena je u srednjefrekventnoj indukcijskoj peći kapaciteta 5,6 tona. Metalni zasip sastojao se od sivog sirovog željeza (Sorelmetal®), čelika i povrata, tablica 1.

Tablica 1. Sastav metalnog zasipa

Ukupna masa (kg)	Sivo sirovo željezo (kg)	čelik (kg)	povrat (kg)	FeSi (kg)
5600	3920	504	1176	11,2
	70 mas.%	9 mas.%	21 mas.%	0,2 mas.%

Nakon izrade primarne taljevine ispitan je kemijski sastav; udio ugljika i silicija jednostavnom

toplinskom analizom (ATAS®), a udio ostalih elemenata optičkom emisijskom spektroskopijom.

Obrada nodulacijom primarne taljevine provedena je Sandwich postupkom u loncu kapaciteta 220 kg dodatkom 1,8 % FeSiMg predlegure (44-48 % Si, 3,5-3,8 % Mg, 0,9-1,1 % Ca, 0,5-1,2 Al, 0,6-0,8 RE, Fe ost.) pri 1480 °C. Predlegura je bila postavljena u džep na dnu lonca za obradu i prekrivena s 0,2 % FeSiMg pokrovne legure (46-50 % Si, 1,8-2,2 % Ba, 0,4-0,6 % Ca, 0,6-1,0 % Al, Fe ost.) prije ulijevanja primarne taljevine u lonac. Slijedilo je čišćenje troske s površine i ulijevanje nodulirane taljevine u kalupe. Prilikom ulijevanja u kalup izvedeno je cijepljenje u mlaz dodatkom 0,45 % komercijalnog cjepiva koje sadrži Ce. Kemijski sastav cjepiva dan je u tablici 2. Temperatura lijevanja iznosila je 1400 °C, a vrijeme lijevanja 25 s, kod oba kalupa. Ukupna bruto masa taljevine u kalupu iznosila je 80 kg.

Tablica 2. Kemijski sastav cjepiva

Cjepivo		**Kemijski sastav, mas. %**						
	Si	Mg	Ca	Al	Ce	S	O	Fe
C1	70-76	-	0,75-1,25	0,75-1,25	1,5-2,0	(<1%)	(<1%)	ost.

Radi utvrđivanja djelovanja bizmuta, u drugi je kalup na filter bilo smješteno 0,01 % Bi u obliku 99,99 % čistog metala.
Prije samog ulijevanja u kalupe, odliven je uzorak u bakrenu kokilu za ispitivanje kemijskog sastava optičkom emisijskom spektroskopijom (ARL 3460). Kemijski sastav nodulirane taljevine dan je u tablici 3.

Tablica 3. Kemijski sastav nodulirane taljevine

Kalup br.	**Maseni udio, %**														
	C	**Si**	**Mn**	**S**	**P**	**Mg**	**Co**	**Ni**	**Cr**	**Cu**	**Sn**	**Mo**	**Ti**	**Al**	**ACEL***
K 1	3,66	2,15	0,169	0,010	0,029	0,034	0,016	0,027	0,027	0,020	0,004	0,003	0,007	0,0131	4,12
K 2															

Usporedno sa lijevanjem odljevaka napravljeno je lijevanje u Quik-cup® čašicu radi snimanja krivulja hlađenja jednostavnom toplinskom analizom (ATAS®). Na temelju snimljenih krivulja hlađenja određeni su toplinski parametri eutektičkog skrućivanja.
Nakon lijevanja svaki je stožac u prvom koraku prepiljen na pola uzduž vertikalne ravnine simetrije (slika 2 a). Jedna je polovica podvrgnuta makroanalizi, a druga je polovica poprečno prepiljena na udaljenosti 50 mm od baze stošca, radi uzimanja ploče debljine približno 10 mm za izradu uzoraka za metalografsku analizu (slika 2b). Uzorci su uzimani sa tri različita mjesta na ploči; ruba, između ruba i toplinskog centra i u toplinskom centru – S1, S2 i S3 (slika 2 c). Dimenzije uzoraka iznosile su 25 mm × 25 mm.

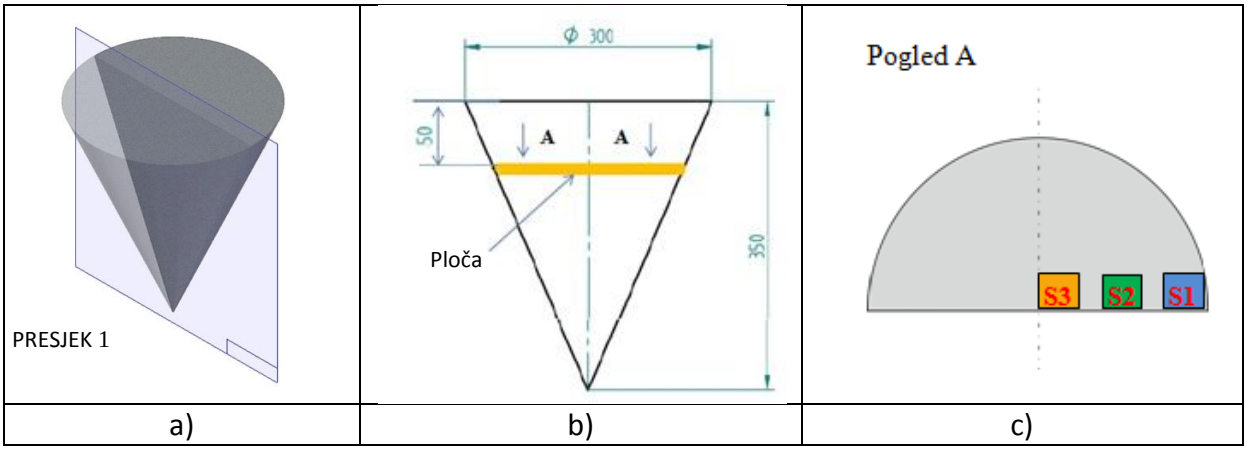

a) b) c)

Slika 2. Shematski prikaz uzimanja uzoraka za metalografsku analizu

Iz stošca 1, uzorci su označeni sa 1-S1, 1-S2 i 1-S3, a iz stošca 2 sa 2-S1, 2-S2 i 2-S3.

Na pripremljenim uzorcima napravljena je metalografska analiza pomoću svjetlosnog mikroskopa. Pri ovoj analizi korišten je mikroskop Olympus BX61, opremljen videokamerom DP70 i programskim paketom za analizu slike AnalySIS® 5.0. Određena su slijedeća mikrostrukturna svojstva: oblik grafita, veličina grafita, nodularnost, površinski udio grafita te distribucija grafita po razredima veličina, sukladno normi EN-ISO-945-1:2012. Analiza oblika, veličine i raspodjele grafita napravljena je nakon brušenja i poliranja, dok je udio ferita i perlita određen nakon nagrizanja uzoraka u 2 %-tnom Nitalu. Svi parametri su mjereni na pet različitih mjesta na uzorku, a kao rezultat je uzeta srednja vrijednost.

Mehanička svojstva odljevaka određena su statičkim vlačnim ispitivanjem. Korištena je univerzalna kidalica EU 40mod proizvođača WMP. Za ovo ispitivanje izrađene su po tri epruvete iz svakog stošca. Epruvute su bile oblika B (d_o = 8 mm, L_o = 40 mm) sukladno normi DIN 50125:2004-01. Određena su sljedeća mehanička svojstva: R_m, $R_{p0,2}$ i A_5.

REZULTATI I DISKUSIJA

Makro- i mikroanaliza

Na presjeku stožaca 1 i 2 nije uočen chunky grafit nakon reza pilom. Iako nije uočen makroanalizom, postojanje chunky grafita utvrđeno je u mikrostrukturi uzorka 2-S3 (toplinski centar stošca 2). Iz literature je poznato da se chunky grafit može uočiti vizualnom metodom pregleda na poprečnom presjeku nakon reza pilom, što u ovom istraživanju nije bio slučaj. Međutim, radi se o vrlo malom udjelu područja zahvaćenog chunky grafitom pa uočavanje golim okom nije bilo moguće.

Mikroanaliza

Slika 3 prikazuje morfologiju grafita u uzorcima iz stošca 1 (bez bizmuta), a slika 4 u uzorcima

iz stošca 2 (dodatak 0,01 % Bi), za tri različite brzine hlađenja. Na temelju rezultata simulacije pomoću programskog paketa ProCAST® određeno je da brzina hlađenja u uzorku 1 iznosi 0,036 K/s, u uzorku 2 0,022 K/s, a u uzorku 3 0,016 K/s.

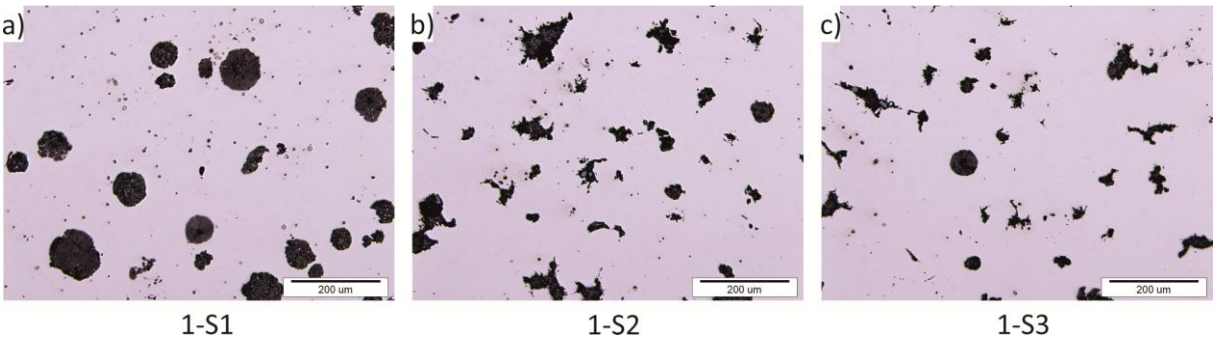

Slika 3. Mikrostruktura uzoraka iz stošca 1 za različite brzine hlađenja: a) 0,036 K/s, b) 0,022 K/s, c) 0,016 K/s

Pregledom slika mikrostrukture stošca 1 može se vidjeti da u uzorku 1-S1 s najvećom brzinom hlađenja prevladavaju nodule grafita sferoidalnog oblika pravilno raspoređene u metalnoj osnovi, uz poneku degeneriranu nodulu manjih dimenzija, slika 3 a). Sa smanjenjem brzine hlađenja dolazi do smanjenja veličine grafitnih čestica i znatnog pogoršanja nodularnosti. Vrlo je malen broj pravilnih nodula i njihove su dimenzije znatno manje u usporedbi s nodulama u uzorku 1-S1, slika 3 b). Daljnjim smanjenjem brzine hlađenja dimenzije nodula se ne smanjuju, ali se dodatno smanjuje broj pravilnih nodula. Prevladavaju degenerirani oblici grafita, a pravilnih nodula gotovo da nema.

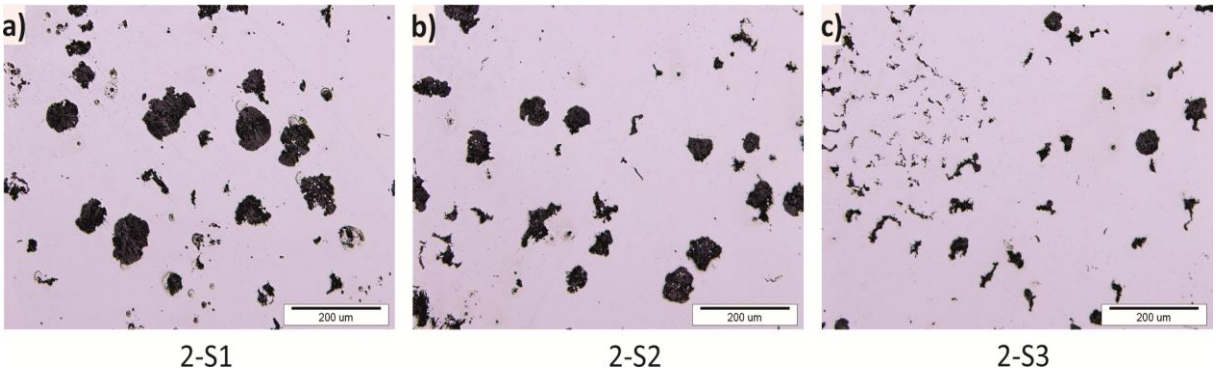

Slika 4. Mikrostruktura uzoraka iz stošca 2 za različite brzine hlađenja: a) 0,036 K/s, b) 0,022 K/s, c) 0,016 K/s

Pregledom slika mikrostrukture stošca 2 kojemu je dodano 0,01 % Bi može se također uočiti negativan utjecaj smanjenja brzine hlađenja na sferoidalnu morfologiju grafita. U mikrostrukturi uzorka 2-S1 s najvećom brzinom hlađenja prisutne su nodule grafita nešto lošije nodularnosti nego kod uzorka 1-S1. Nodule su neravnomjerno raspoređene. Bizmut je

negativno utjecao na sferoidalnu morfologiju grafita. Sa smanjenjem brzine hlađenja broj pravilnih nodula se smanjuje, nodule postaju manje te je sve veći udio degeneriranog grafita. Pojavljuje se kompaktni oblik grafita, vermikularni te u uzorku 2-S3 i chunky grafit, uz poneku nodulu idealno kuglastog oblika. Površinski udio chunky grafita u navedenom uzorku iznosi 10 %. Za razliku od stošca 1, kod ovih je uzoraka negativan utjecaj smanjenja brzine hlađenja na morfologiju grafita slabije izražen, osobito između uzoraka sa srednjom brzinom hlađenja 0,022 K/s.

Na temelju iznešenog, može se zaključiti da je dodatak 0,01 % bizmuta u pravilu negativno utjecao na sferoidalnu morfologiju grafita, a u kombinaciji sa smanjenjem brzine hlađenja od ruba prema sredini stošca uzrokovao je nastanak chunky grafita u toplinskom centru odljevka.

Negativan utjecaj smanjenja brzine hlađenja i dodatka 0,01 % Bi na grafit, prije svega nodularnost, može se vidjeti i u tablici 4 u kojoj su dani rezultati metalografske analize grafita.

Tablica 4. Rezultati metalografske analize grafita

Uzorak	Oblik	Veličina	Nodularnost %	Površinski udio %	Razred veličine, µm							
					1	2	3	4	5	6	7	8
					>	max.1000	max.500	max.250	max.120	max.60	max.30	max.15
1-S1	VI	5	68,8	13,3	0	0	0	5	54	34	44	260
1-S2	IV,II(45%)	5	46,5	7,9	0	0	0	10	29	56	64	202
1-S3	IV,II(30%)	5	42,9	5,2	0	0	0	5	24	74	92	204
2-S1	IV,II(35%)	5	54,6	10,0	0	0	0	4	48	64	111	288
2-S2	IV,II(50%)	5	50,3	7,3	0	0	0	3	44	61	64	212
2-S3	IV,II(35%)	6	44,0	5,7	0	0	0	1	29	124	167	372

Na temelju rezultata metalografske analize grafita može se vidjeti da se u mikrostrukutri ispitanih uzoraka pojavljuju razredi oblika grafita IV i VI, s manjim udjelima oblika razreda II (30 %-50 %). Veličina grafita za sve uzorke ima vrijednost 5.

Nodularnost je u svim uzorcima općenito niska. Vrijednosti se kreću u od približno 43 % do 70 %. To znači da ni jedan uzorak nema zadovoljavajuću vrijednost nodularnosti, koja bi za nodularni lijev prema normi EN 1563:2012-03 trebala biti 80 % ili više kako bi se sa sigurnošću osiguralo, postizanje zahtijevanih mehaničkih svojstava, s pretpostavkom da je metalna matrica feritna ili perlitna te da u strukturi nema karbida i ostalih nepoželjnih uključaka. Najniže vrijednosti nodularnosti određene su u uzorcima u kojima prevladavaju degenerirani oblici grafita uz tek poneku pravilnu nodulu. Najmanja vrijednost nodularnosti (42,9 %) određena je u uzorku 1-S3, a najveća u uzorku 1-S1 (68,8 %). Određene vrijednosti nodularnosti na uzorcima padaju kako se brzina skrućivanja smanjuje. Iz tablice 4 može se vidjeti da se površinski udio grafita kreće u granicama od 5,2 % do 13,3 %. Najniža vrijednost određena je na uzorku 1-S3 (5,2 %), a najviša na uzorku 1-S1 (13,3 %). Pojava chunky grafita

ne utječe na ovaj parametar.

Kod svih uzoraka prevladavaju čestice grafita veličine 8, tj. čestice grafita manje od 0,015 mm. Uz ovu se veličinu, javljaju u nešto manjem udjelu čestice grafita veličina 7, 6 i 5. Čestica grafita veličina 1, 2 i 3 uopće nema, dok se čestice grafita veličine 4 jako rijetko i u jako malom broju pojavljuju u analiziranim uzorcima. Pri analizi su u obzir uzimani svi oblici grafita, i pravilne nodule kao i degenerirani oblici. Uglavnom se manje dimenzije grafitnih čestica odnose na degenerirane oblike grafita, dok su grafitne nodule ipak nešto većih dimenzija. Na temelju rezultata metalografske analize i slika mikrostrukture može se zaključiti da pojava chunky grafita utječe na povećanje broja grafitnih čestica.

Promatrajući rezultate metalografske analize grafita može se vidjeti da gotovo svi uzorci pokazuju trend smanjenja promatranih svojstava sa smanjenjem brzine hlađenja, pogotovo na uzorcima 1-S1 i 1-S2.

Rezultati udjela ferita i perlita u metalnoj matrici prikazani su u tablici 5.

Tablica 5. Udjeli ferita i perlita u metalnoj matrici

Stožac	Uzorak	Ferit %	Perlit %
1	S1	71,3	28,7
	S2	73,8	26,2
	S3	88,0	12,0
2	S1	87,2	12,8
	S2	81,5	18,5
	S3	81,6	18,4

Na temelju rezultata može se zaključiti da je metalna matrica feritno-perlitna s udjelima ferita od približno 71 % do 88 %. Niže vrijednosti udjela ferita uočene su u stošcu 1, izuzev uzorka 1-S3 u kojem je uočen najviši udio ferita. U uzorcima iz stošca 1 sa smanjenjem brzine hlađenja dolazi do povećanja udjela ferita, a u uzorcima iz stošca 2 do smanjenja udjela ferita. Dodatak bizmuta uzrokovao je povećanje udjela ferita u mikrostrukturi.

Mehanička svojstva

U tablici 6 navedena su mehanička svojstva stožaca 1 i 2.

Tablica 6. Rezultati statičkog vlačnog ispitivanja

Oznaka uzorka	R_m N/mm^2	$R_{p0,2}$ N/mm^2	A_5 %	Napomena
1.1	387,21	224,95		lom izvan L_0
1.2	390,07	224,69	11,00	
1.3	387,61	227,22	10,25	
2.1	393,74	208,29	18,70	
2.2	398,78	220,22	21,10	
2.3	399,67	226,97	19,75	

Sve epruvete za statičko vlačno ispitivanje uzete su iz toplinskog centra odljevka (stošca). Na temelju rezultata u tablici 6 može se vidjeti da su vrijednosti vlačne čvrstoće nešto niže od minimalne normom propisane vrijednosti – 400 N/mm^2.

Vrijednosti $R_{p0,2}$ kreću se u granicama od približno 208 N/mm^2 do 227 N/mm^2. Nešto niže vrijednosti zabilježene su kod uzoraka s bizmutom.

Istezljivost nije određena za epruvetu kod koje je došlo do loma izvan L_o područja. Kod stošca 1 nije dobivena zadovoljavajuća istezljivost, vrijednosti su ispod 15 %. Dodatkom bizmuta postignute su značajno veće vrijednosti, oko 20 %, što je približno 40 % više u odnosu na stožac 1.

ZAKLJUČAK

Na temelju provedenog ispitivanja može se zaključiti:

- dodatak 0,01 % bizmuta i smanjenje brzine hlađenja od ruba prema toplinskom centru debelostijenog odljevka od nodularnog lijeva EN-GJS-400-15 negativno su utjecali na sferoidalnu morfologiju grafita
- chunky grafit pojavio se u toplinskom centru odljevka s 0,01 % Bi
- dodatak bizmuta pozitivno je utjecao na istezljivost.

LITERATURA

[1] S. Liang, G. Erjun, T. Changlong: Effect of Bi on graphite morphology and mechanical properties of heavy section ductile cast iron, China Foundry, 2 (2014) 11, pp.125-131.
[2] R. Källbom, K. Hamberg, M. Wessen, L.-E. Björkegren, On the solidification sequence of ductile iron castings containing chunky graphite, Materials Science and Engineering A, 413-414 (2005), pp.346-351.
[3] H. Löblich, Effect of nucleation conditions on the development of chunky graphite in heavy ductile iron castings, Giessereiforschung 58 (2006) 3, pp.28-41.

[4] P. Ferro, A. Fabrizi, R. Cervo, C. Carollo: Effect of inoculant containing rare earth metals and bismuth on microstructure and mechanical properties of heavy-section near-eutectic ductile iron castings, Journal of Materials Processing Technology, 213 (2013), 1601-1608.
[5] R. Källbom, K. Hamberg, L. E. Björkegren: Chunky Graphite - Formation and Influence on Mechanical Properties in Ductile Cast Iron, Proceedings of the Gjutdesign 2005, Espoo, Finska, 2005.
[6] K. Hartung, O. Knustad, K. Wardenaer, Chunky graphite in ductile cast iron castings-Theories and examples, Indian Foundry Journal, 55 (2009), pp.25-29.
[7] J. Lacaze, L. Magnusson, J. Sertucha, Review of microstructural features of chunky graphite in ductile cast irons, 2013 Keith Millis Symp. on Ductile Cast Iron, Nashville, USA, 2013, pp.360-368.
[8] S. Mendez, D. Loper, I. Asenjo, P. Larrañaga, J. Lacaze: Improved analytical method for chemical analysis of cast iron. Application to castings with chunky graphite, ISIJ International, 51 (2011), pp.242-249.
[9] M. Gagné, C. Labrecque: Microstrustural Defects in heavy section ductile iron castings: formation and effect on properties, AFS Transactions, 117 (2009), pp.561-571.
[10] J. Riposan, M. Chisamera, S. Stan, Performance of heavy ductile iron castings for windmills, China Foundry, 5 (2010), pp.163-170.
[11] U. Petzschmann, Vermeidung von Chunky-Graphit in dickwandigen Gussstuecken aus Gusseisen mit Kugelgraphit, AiF-Schlussbericht, IfG, 2013.
[12] M. Koch: Chunky Graphite; effects and theories on formation and prevention, 2013 Keith Millis Symposium on Ductile Cast iron, October 15-17, Nashville, SAD, 2013.

15th INTERNATIONAL FOUNDRYMEN CONFERENCE
INNOVATION – The foundation of competitive casting production
Opatija, May 11th-13th, 2016
http://www.simet.hr/~foundry/

INFLUENCE OF SURFACE FINISH ON THE CORROSION RESISTANCE OF DUPLEX STAINLESS STEEL CASTING

UTJECAJ ZAVRŠNE OBRADE NA KOROZIJSKU OTPORNOST NEHRĐAJUĆEG DUPLEKS ČELIČNOG LIJEVA

V. Rede, Z. Šokčević and A. Budim

University of Zagreb Faculty of Mechanical Engineering and Naval Architecture, Zagreb, Croatia

Oral presentation
Original scientific paper

Abstract

Duplex stainless steel castings have excellent corrosion resistance but in some special conditions corrosion can occur. In this paper the influence of surface finish on the pitting corrosion resistance of duplex stainless steel GX2CrNiMoN 26-7-4 was investigated. Examination was performed according to ASTM G48. Three groups of samples, each one with a different surface finish –-polished, grinded and sandblasted, were used for testing. Obtained results indicated that all tested samples showed excellent corrosion resistance at the temperature of 20 ± 2 ° C. At the temperature of 50 ± 2 ° C, the largest weight loss and corroded surface area (%) were measured on sandblasted sample, while pit density was equal for all tested samples. Obtained results indicated that surface finish has a great impact on corrosion resistance of duplex stainless steel casting.

***Keywords**: duplex stainless steel casting, corrosion resistance, pitting corrosion, surface finish*

*Corresponding author (e-mail address): *vera.rede@fsb.hr*

Sažetak

Nehrđajući dupleks čelični ljevovi imaju izvrsnu korozijsku postojanost ali su u određenim uvjetima ipak podložni nekim oblicima lokalne korozije. U radu je ispitan utjecaj stanja površine na otpornost prema rupičastoj koroziji na uzorcima nehrđajućeg čeličnog dupleks lijeva oznake GX2CrNiMoN 26-7-4. Ispitivanje je provedeno prema normi ASTM G48. Površina ispitnih uzoraka završno je obrađena na tri načina: poliranjem, brušenjem i pjeskarenjem. Svi uzorci su pokazali izvrsnu otpornost pri ispitivanju na temperaturi 20 ± 2°C. Pri temperaturi ispitivanja od 50 ± 2°C najveći gubitak mase i najveći udio površine zahvaćene korozijom izmjeren je kod pjeskarenog uzorka, dok je gustoća rupica podjednaka na svim uzorcima. Dobiveni rezultati pokazuju da stanje površine značajno utječe na korozijsku postojanost nehrđajućeg dupleks čeličnog lijeva.

***Ključne riječi**: dupleks čelični lijev, korozijska postojanost, rupičasta korozija, završna obrada*

UVOD

Dupleks nehrđajući čelici i ljevovi posjeduju izvanrednu kombinaciju mehaničkih i korozijskih svojstava, dobro se zavaruju i lijevaju. Zbog svega navedenog sve više se primjenjuju posebice u prehrambenoj, farmaceutskoj, kemijsko-procesnoj te industriji nafte i plina, u brodogradnji, transportu i sl., gdje uspješno zamjenjuju druge vrste nehrđajućih čelika i ljevova [1].

Struktura dupleks ljevova sastoji se od ferita i austenita u podjednakim volumnim udjelima. Da bi se postigla takva izbalansirana mikrostruktura mora se precizno odrediti kemijski sastav, a osim sastava važnu ulogu u formiranju mikrostrukture ima i režim hlađenja nakon primarne kristalizacije.

Novije vrste dupleks ljevova imaju snižen udio ugljika čime je izlučivanje karbida i pojava interkristalne korozije svedena na najmanju moguću mjeru [2].

Posjeduju puno bolju otpornost na napetosnu koroziju od austenitnih nehrđajućih ljevova. Zbog nižeg masenog udjela nikla i visokog udjela kroma osobito su otporni na napetosnu koroziju u kloridnom okruženju.

Postojanost dupleks ljevova prema rupičastoj koroziji je dobra zbog visokog udjela kroma, volframa, molibdena i dušika. Na otpornost dupleks ljevova prema ovom tipu korozije utječe i mikrostruktura, kao i kvaliteta obrađene površine [3, 4].

U ovom radu ispitano je kako različite završne obrade (poliranje, brušenje i pjeskarenje) utječu na otpornost površine prema rupičastoj koroziji. Ispitivanje je provedeno na nehrđajućem dupleks čeličnom lijevu GX2CrNiMoN 26-7-4 prema normi ASTM G48 [5]. Ovaj lijev se primjenjuje u petrokemijskoj industriji te industriji nafte i plina za izradu dijelova pumpi koje rade u procesima pod visokim tlakom i medijima koji sadrže kloride i spojeve sumpor-vodika.

MATERIJAL I METODE ISPITIVANJA

Utjecaj stanja površine na otpornost prema rupičastoj koroziji ispitana je na nehrđajućem dupleks čeliku oznake GX2CrNiMoN 26-7-4. Uzorci za ispitivanje izrezani su iz odljevka dimenzija 230×60×30 mm. Kemijski sastav lijeva prikazan je u tablici 1.

Tablica 1. Kemijski sastav nehrđajućeg dupleks čeličnog lijeva GX2CrNiMoN 26-7-4 iskazan u masenim udjelima (*w*, %)

Kemijski element	C	S	P	Si	Mn	Cr	Ni	Mo	N	Fe
w, [%]	0,023	0,006	0,028	0,41	0,83	26,19	6,75	3,36	0,44	ostatak

Na slici 1 prikazana je mikrostruktura ispitivanog materijala, snimljena na svjetlosnom mikroskopu *Olympus GX51F-5.* Mikrostruktura se sastoji od ferita i austenita u podjednakim volumnim udjelima. Osim ferita i austenita u mikrostrukturi se mogu vidjeti i sitne tamne nakupine intermetalnih spojeva. Njihov volumni udio je zanemariv.

U okviru kvantitativne analize mikrostrukture izmjerena je i mikrotvrdoća lijeva, a srednja vrijednost od pet mjerenja iznosi 353 HV0,2.

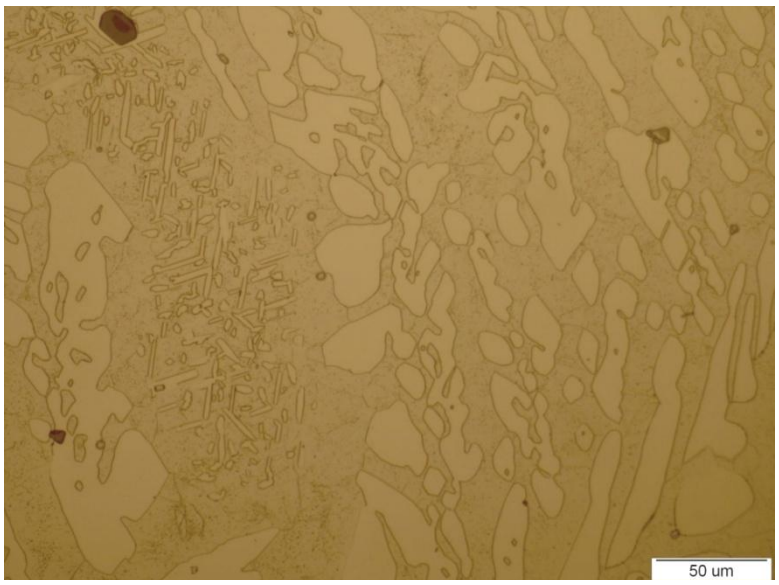

Slika 1. Mikrostruktura dupleks čeličnog lijeva GX2CrNiMoN 26-7-4

Ispitivanje otpornosti na rupičastu koroziju provedeno je prema zahtjevima norme ASTM G 48. Ispitivanje je provedeno u 10 %-tnoj otopini željezno(III) klorida ($FeCl_3$ x $6H_2O$) pri temperaturi od 20 ± 2 i 50 ± 2 °C.

Sklonost materijala prema rupičastoj koroziji određena je mjerenjem gubitka mase po jediničnoj površini, broju rupica po jediničnoj površini i udjelu površine zahvaćene korozijom. Po dva uzorka dimenzija 50×25×3 mm izrezana su i pripremljena za svako od tri stanja: brušeno, polirano i pjeskareno. Kod brušenih uzoraka ispitivana površina završno je obrađena brusnim papirom P1000, a kod poliranih uzoraka završno poliranje provedeno je dijamantnim česticama finoće 1 µm. Treća skupina uzoraka podvrgnuta je pjeskarenju kvarcnim pjeskom granulacije 0,2 do 1 mm, pod tlakom zraka u cijevi od 4 bara.
Uzorci su nakon mehaničke pripreme očišćeni u ultrazvučnoj kupelji, izvagani i nakon toga stavljeni u posudu s otopinom željeznog klorida. Ostavljeni su u otopini 72 sata na temperaturi 20 ± 2 °C.

Nakon 72 sata izlaganja otopini na površini uzoraka nije bilo vidljivih rupica pa je ispitivanje nastavljeno još 24 sata na temperaturi 50 ± 2 °C. Uzorci su nakon toga očišćeni u ultrazvučnoj kupelji, osušeni i ponovo izvagani.

Na slici 2. prikazani su uzorci nakon provedenog ispitivanja.

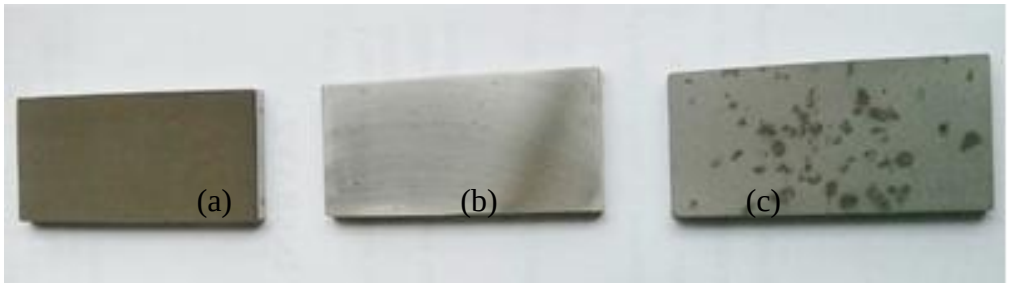

Slika 2. Površine uzoraka nakon ispitivanja otpornosti na rupičastu koroziju: (a) polirana, (b) brušena i (c) pjeskarena

Uz pomoć računalnog paketa *ImageJ* izmjeren je udio korodirane površine i broj rupica na ispitivanoj površini svih uzoraka.

Otvori rupica bili su premali za ulazak šiljastog ticala na uređaju za mjerenje dubine. Stoga nije bilo moguće izračunati maksimalnu neravnomjernost rupičaste korozije, tj. pitting faktor.

REZULTATI I DISKUSIJA

U ovom radu otpornost prema rupičastoj koroziji čeličnog dupleks lijeva oznake GX2CrNiMoN 26-7-4 određena je mjerenjem gubitka mase, prema broju rupica po jediničnoj površini i prema udjelu površine zahvaćene korozijom.

Na temelju izmjerene mase uzoraka prije i nakon ispitivanja otpornosti na rupičastu koroziju izračunat je apsolutni i relativni gubitak mase svih uzoraka.
Rezultati su prikazani na slikama 3 i 4.

Uzorci s pjeskarenom površinom imaju najveći, a uzorci s poliranom površinom najmanji apsolutni i relativni gubitak mase. Relativni gubitak mase kod uzoraka s pjeskarenom površinom je oko 3 puta veći od gubitka mase kod uzoraka s poliranom površinom.

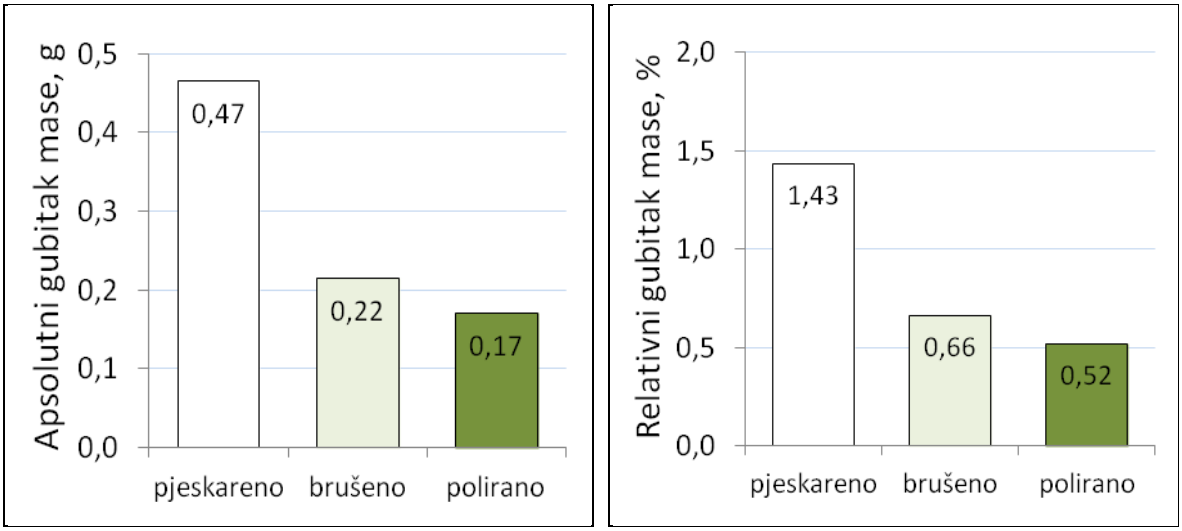

Slika 3. Apsolutni i relativni gubitak mase uzoraka s poliranom, brušenom i pjeskarenom površinom

Na slici 4 predočene su srednje vrijednosti gustoće rupica, a na slici 5 mogu se vidjeti udjeli korodirane površine za sve uzorke.

Broj vidljivih rupica podjednak je za sve uzorke pa je i gustoća rupica ujednačena.
Udio korodirane površine najveći je kod pjeskarenih uzoraka. Dobiveni rezultati pokazuju da je udio površine zahvaćene korozijom kod pjeskarenih uzoraka skoro 7 puta veći od udjela na poliranim uzorcima i 1,5 puta veći od udjela na brušenim uzorcima.

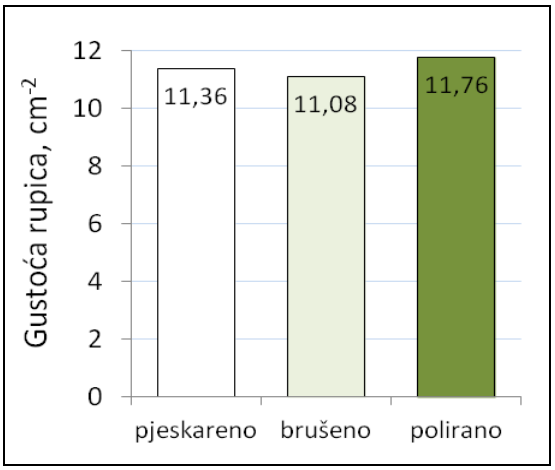

Slika 4. Gustoća rupica za sve uzorke

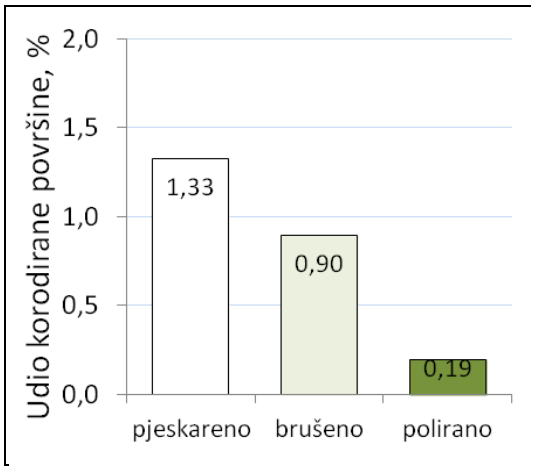

Slika 5. Udjeli korodirane površine

Na slici 6 prikazana je morfologija površine uzoraka snimljena na pretražnom elektronskom mikroskopu *VEGA TESCAN TS5136LS*. Fotografije su snimljene pri istom povećanju i na njima se jasno vidi razlika u veličini rupica i udjelu korodirane površine između uzoraka s poliranom, brušenom i pjeskarenom površinom.

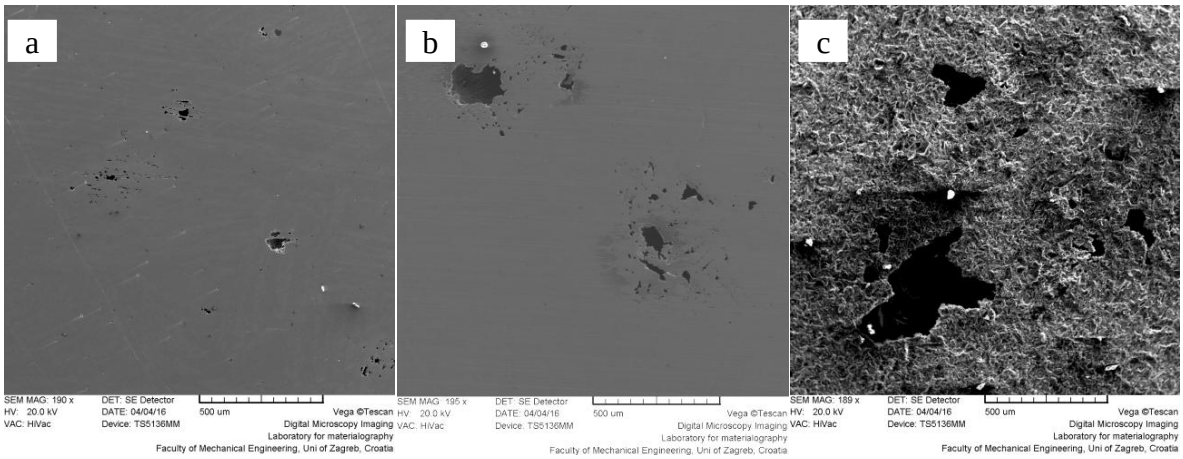

Slika 6. SEM snimke uzoraka (a) polirane, (b) brušene i (c) pjeskarene površine nakon ispitivanja otpornosti na rupičastu koroziju pri temperaturi od 50 $\pm$ 2 °C.

ZAKLJUČCI

Na temelju dobivenih rezultata može se zaključiti sljedeće:

- Kvaliteta površine izrazito jako utječe na otpornost dupleks nehrđajućeg čeličnog lijeva na rupičastu koroziju. Što je kvaliteta površine veća, veća je i otpornost na koroziju.

- Gustoća rupica je podjednaka kod svih uzoraka. Gubitak mase, veličina rupica i udio korodirane površine najveći je kod uzoraka s pjeskarenom površinom.
- Temperatura također značajno utječe na nastanak i tijek rupičaste korozije. Nakon izlaganja svih uzoraka 10 %-tnoj otopini $FeCl_3$ pri temperaturi od 20 ± 2 °C tijekom 72 sata nije bilo vidljivih oštećenja površine, dok je ispitivanje provedeno na 50 ± 2 °C za manje od 24 sata izazvalo znatna oštećenja na površini svih uzoraka.

LITERATURA

[1] A. J. Sedriks, Corrosion of ASTM Steels, SM International, Materials Park, John Wiley & Sons, 1994.

[2] R. Merello, F.J. Botana, J. Botella, M.V. Matres, M. Marcos, Influence of chemical composition on the pitting corrosion resistance of non-standard low-Ni high-Mn–N duplex stainless steels, Corrosion Science, 45 (2003) 5, pp. 909–921.

[3] I. Esih, Z. Dugi, Tehnologija zaštite od korozije II, Školska knjiga, Zagreb, 1992.

[4] N. Ben Salah-Rousset, M. A. Chaouachi, A. Chellouf, Role of surface finishing on pitting corrosion of a duplex stainless steel in seawater, Journal of Materials Engineering and Performance, 5 (1996) 2, pp. 225-231.

[5] ASTM G48-92: "Standard test methods for pitting and crevice corrosion resistance of stainless steels and related alloys by the use of ferric chloride solution".

15th INTERNATIONAL FOUNDRYMEN CONFERENCE
INNOVATION – The foundation of competitive casting production
Opatija, May 11th-13th, 2016
http://www.simet.hr/~foundry/

NANOCOMPOSITES BASED ON AlSi9Cu3(Fe) ALLOY AND CARBON NANOTUBES, PREPARATION AND PROPERTIES

D. Stanić[1], V. Grozdanić[2], I. Brnardić[3], T. Holjevac Grgurić[3], F. Unkić[4] and B. Smoljan[5]

[1]Croatia CIMOS - P.P.C. Buzet d.o.o., Buzet, Croatia
[2]Research Centre for Materials of Region of Istria METRIS, Pula, Croatia
[3]University of Zagreb Faculty of Metallurgy, Sisak, Croatia
[4]Ivane Brlić Mažuranić 16, Sisak, Croatia
[5]University of Rijeka Faculty of Engineering, Rijeka, Croatia

Oral presentation
Original scientific paper

Abstract

Throughout last few decades, the main research area regarding reducing CO_2 footprint is developing new materials, which can be used as lighter parts for transport industry. Majority of work is conducted concerning the potential usage of new nanocomposites based on metal or polymer matrix with improved mechanical properties. This improvement could result in production of smaller and thicker vehicle parts with overall less weight.
In this work, new nanocomposites based on AlSi9Cu3(Fe) alloy and carbon nanotubes were prepared using high pressure die casting machine. Nanotubes, varying in mass ratio, were placed on two different positions inside the machine. Structure and stability of nanotubes in nanocomposite were confirmed using scanning electron microscopy (SEM). Mechanical properties and metallographic investigation of prepared nanocomposites and base alloy were studied using tensile testing machine and optical microscope. According to experiment conditions nanocomposites showed different mechanical properties when compared to base alloy.

Keywords: *AlSi9Cu3(Fe) alloy, carbon nanotubes, high pressure dye casting*

*Corresponding author (e-mail address): *brnardic@simet.hr*

INTRODUCTION

Today's scientific community devotes large number of research to preparation and characterization of nanocomposites based on different nanofillers and matrixes [1-6]. Nanofillers play the major role through their impact on optimization or improvement of numerous properties: chemical, physical and mechanical. Therefore, nanocomposites with improved properties could replace today commonly used materials, and could be used in

wide spectra of different application fields. One of the most commonly used and investigated filler is a carbon nanotube (CNT). That is a consequence or high Young modulus of CNT [7] what results in improvement of nanocomposites mechanical properties compared to pure matrix. Furthermore, researches on nanocomposites based on polymer matrix are dominated, compared to those on metal matrix. The reason could be found in high melting temperature of metals, which destructively effect CNTs through thermal degradation. That represents a challenge for solution of problems like introducing, mixing, overcoming low-wettability and equally dispersing CNTs in metal matrix, which will have crucial influence to end properties of produced nanocomposite. Researchers have tried to solve those problems by using different preparation methods such as cold compaction, sintering, melt stirring with and without inert atmosphere and high pressure die casting [8-13]. Agglomeration causes formation of micro aggregates in nanocomposites, "weak spots" resulting in lousing CNT strengthening potential.

The successfully prepared light metal nanocomposites showed significantly improved mechanical properties already at small CNT contents [9-14]. Such properties could result in dimension (shape) of different parts to be smaller and thicker that can reduce consumption of a metal and energy required for the melting. This new nanocomposite has possibilities to be used in vehicle parts production resulting in lower mass, which directly reduces fuel consumption reducing the CO_2 footprint.

The idea of this work was to prepare nanocomposite samples with commonly used alloy and production method in industry. In this work nanocomposites from AlSi9Cu3(Fe) alloy and multi-walled carbon nanotubes (MWCNT), with varying mass ratio, were prepared using high pressure die casting (HPDC) method. Samples were prepared in two different ways, placing MWCNT in two different positions of HPDC machine. Stability and the influence of MWCNTs (wt% and position) on structure, mechanical properties and microstructure of nanocomposites and base alloy were investigated. This work is a preliminary work with the aim to define further methodology of experiments.

MATERIALS AND METHODS

The MWCNT were obtained from Chengdu Organic Chem. Co. The characteristics of used MWCNT are: diameter from 10 to 30 nm, purity >90% and length from 10 to 30 nm. The base alloy AlSi9Cu3(Fe) for car parts production in Croatia CIMOS - P.P.C. Buzet d.o.o. was used, chemical composition is shown in Table 1.

Table 1 Chemical coposition of AlSi9Cu3(Fe) alloy

Element	Si	Fe	Cu	Mn	Mg	Zn	Ti	Cr	Ni	Pb	Sn	Al
wt %	8.73	0.76	2.88	0.24	0.18	1.02	0.05	0.05	0.05	0.09	0.04	85.91

Nanocomposite samples were prepared by HPDC machine. MWCNTs with different mass ration, 0.05, 0.1 and 0.2 wt%, were prepared by wrapping exact mass in commercially available Aluminium foil. Reference samples from base alloy and nanocomposite samples were prepared in two different ways; firstly by placing wrapped MWCNTs in chamber before piston, and secondly by putting wrapped MWCNTs in the beginning of the tool for exact shape casting formation. The melted alloy was poured in chamber and then pushed into the tool by the piston. When the tool was opened, casted samples were cooled and separated for further testing (Figure 1).

a) b)

Figure 1. Nanocomposite samples a) casted b) separated

Every sample was casted five times by exact procedure and was named as proposed; R (reference sample – base alloy), K1-1 (1 to 5), K1-2, K1-5, K2-1, K2-2 and K2-5. KX-Y-Z, X stand for wt% 5- 0.05%, 1- 0.1% and 2- 0.2%, Y for position of wrapped MWCNTs 1 before piston and 2 at the beginning of the tool, and Z number of casted sample.

Mechanical measurements were performed on a Messphysik BETA 250 testing machine, in uniaxial tension mode at 25 °C. At least three test specimens were tested for sample, according to standards HRN EN ISO 6892-1:2010. Stability and existence of MWCNTs, and structure of samples after mechanical testing were checked with a scanning electron microscopy (SEM) by FEG SEM Quanta 250 FEI microscope. Fracture surface after tensile tests was examined. Metallographic investigation was conducted by optical metallographic microscope BX51 OLYMPUS. All experiments were performed on casted samples with 11 mm in diameter.

RESULTS AND DISCUSSION

Results of mechanical properties of the base alloy and nanocomposites are summarized in Table 2; three from five tested samples were chosen based on deviations.

Table 2. Tensile test values, breaking at elongation and tensile strength

Sample	Breaking elongation / %	Tensile strength / MPa
R	2.1630 ± 0.1310	294.80 ± 3.30
K 5-1	3.0790 ± 0.0970	312.85 ± 1.85
K 1-1	2.5530 ± 0.1860	297.70 ± 5.50
K 2-1	2.5100 ± 0.0830	279.25 ± 4.35
K 5-2	2.6335 ± 0.1995	306.45 ± 4.25
K 1-2	3.0620 ± 0.2010	312,45 ± 5.55
K 2-2	2.9900 ± 0.1650	310.50 ± 3.60

Results for nanocomposites prepared by adding MWCNT on position 2 in HPDC machine (K 5-2, K 1-2 and K2-2) show bigger discrepancy what can be better noticed from figure 2 a) and b).

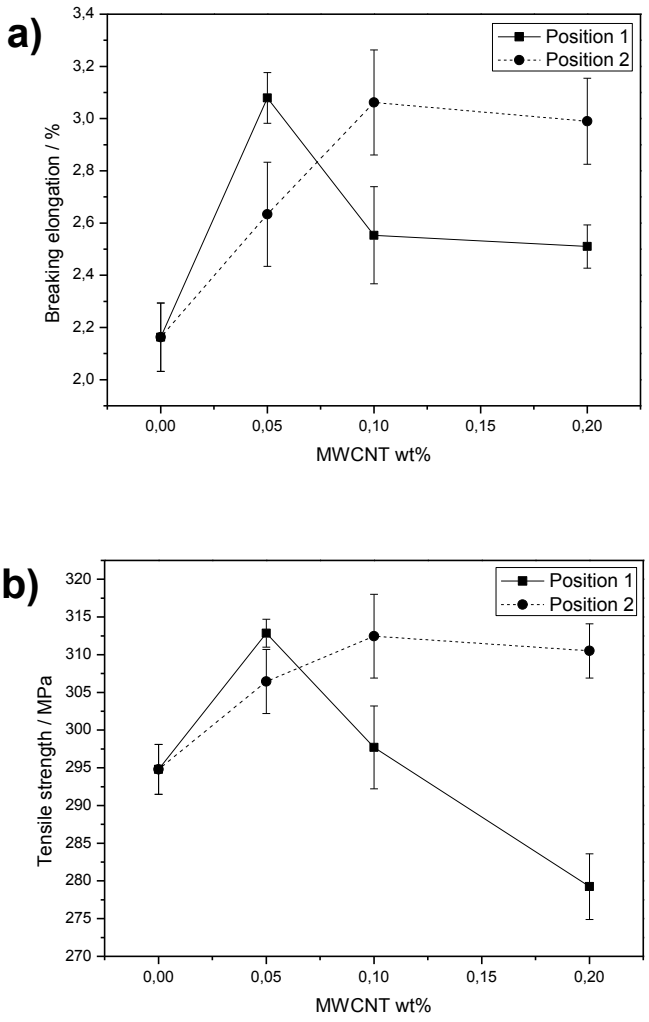

Figure 2. Tensile test values *vs.* MWCNT content,
a) breaking elongation / % and b) tensile strength / MPa

The nanocomposite samples prepared with 0.05 wt% of MWCNTs and by placing them on a position 1 before piston in HPDC machine showed best results regarding improving mechanical properties of base alloy; breaking elongation by ~42% and tensile strength by ~6%. Furthermore, samples prepared at position 2 showed agglomerates of MWCNTs on broken surface that can be correlated to the short period for melting of wrapped foil with hot base alloy resulting in non-homogenous distribution.

Figure 3 shows SEM images with two different magnifications of K 2-1-4 sample.

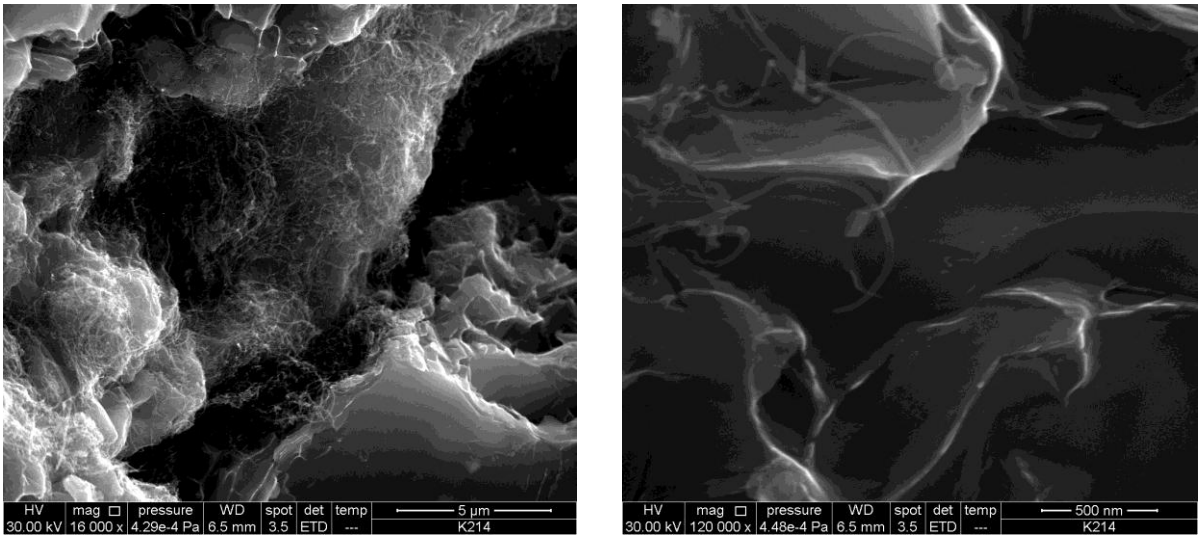

Figure 3. SEM images of MWCNT in K 2-1-4 sample with 16 kX and 120 kX magnification

Microstructural investigations show that thermal degradation of MWCNT did not occur so HPDC method for introducing MWCNT in metal matrix could be used for nanocomposite production. Also, agglomeration is observed resulting in poor distribution of MWCNT and small influence or even negative on mechanical properties of nanocomposites compared to base alloy. The results are in accordance with the mechanical testing.

Influence of MWCNT on microstructure was examined under the optical microscope. In Figure 4 optical microstructure of the a) base alloy and b) nanocomposite sample K 5-1-2 is shown at magnification of 200x and 1000x. Prior to the analysis, samples were metallographically polished. As it can been seen, the microstructure has not been changed under the influence of MWCNTs.

According to literature the reason for obtained results could be found in different procedure of preparation and also in using alloy without magnesium. The cooling rate of casted sample in HPDC method is faster in comparison with methods used in literature, what directly influence on microstructure. Furthermore, Magnesium improves wettability of MWCNT in Al alloys and with incorporation of MWCNT primary Al grains were smaller resulting in better mechanical properties [11, 12, 14, 15].

Regarding all results, we could assume that process of adding of MWCNTs in base alloy needs some improvement. More microstructure experiments need to be done, and in order to overcome agglomeration and non-homogenous distribution future research will focus on finding new ways of introducing MWCNTs in matrix, for example adding of MWCNTs in pre-furnace of HPDC machine with mechanical mixing under inert atmosphere.

a)

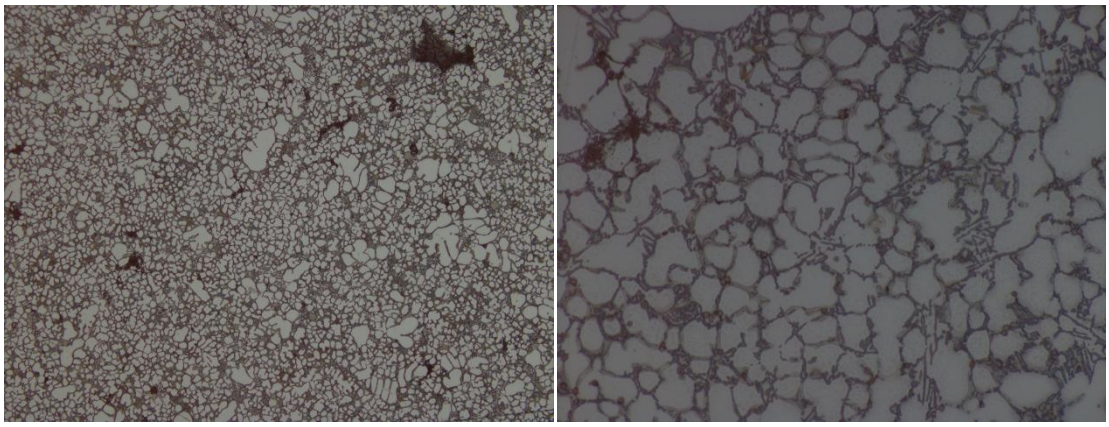

200X 1000X

b)

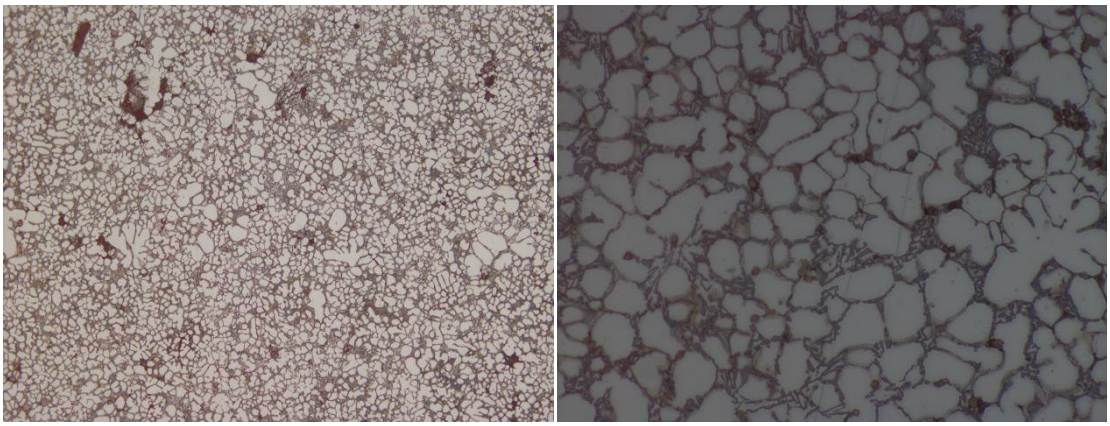

200X 1000X

Figure 4. Micrographs of the a) base alloy, and b) sample K 5-1 2

CONCLUSIONS

MWCNT were used for the preparation of the nanocomposites based on AlSi9Cu3(Fe) alloy. Incorporation of nanotubes without thermal degradation in base alloy through HPDC method was successfully performed and confirmed by SEM.

The best results showed samples with 0.05 wt% of MWCNT wrapped and placed on position 1 before piston in HPDC machine. The changes in mechanical properties were not as good as expected. Also, no impact of MWCNTs on microstructure of base alloy was observed.

Altogether, the main reason for such results could be found in non-homogenous distribution and agglomeration of MWCNTs what results in small surface activity between MWCNTs and base alloy.

The results of this preliminary work will help us in further experiments throughout proposing new methodology for improving homogeneity of nanotubes.

REFERENCES

[1] M.T. Byrne, J.E. McCarthy, M. Ben, R. Blake, Y.K. Gun'ko, E. Horvath, Z. Konya, A. Kukovecz, I. Kiricsi, J.N. Coleman, Chemical functionalization of titanium nanotubes and their utilization for the fabrication of reinforced polystyrene composites, Journal of Materials Chemistry, 17 (2007) pp.2351–2358.
[2] H.-J. Song, Z.-Z. Zhang, X.-H. Men, Tribological behaviour of polyurethane-based composite coating reinforced with TiO_2 nanotubes, European Polymer Journal, 44 (2008) pp.1012–1022.
[3] I. Brnardić, M. Huskić, P. Umek, A. Fina, T. Holjevac Grgurić, Synthesis of silane functionalized sodium titanate nanotubes and their influence on thermal and mechanical properties of epoxy nanocomposite, Physica Status Solidi A, 210 (2013) pp.2284–2291.
[4] L. Valentini, J. Macan, I. Armentano, F. Mengoni, J.M. Kenny, Modification of fluorinated single-walled carbon nanotubes with amino- silane molecules, Carbon, 44 (2006) pp.2196–2201.
[5] J. Zhu, M. Yudasaka, M. Zhang, D. Kasuya, S. Iijima, A surface modification approach to the patterned assembly of single-walled carbon nanomaterials, Nano Letters, 3 (2003) pp.1239–1243.
[6] A. Powell, The Fabrication of Aluminium-Carbon Nanotube Metal Matrix Composites (Master Thesis), University of Birmingham, United Kingdom 2013.
[7] B. Lukić, J.W. Seo, R.R. Basca. S. Delpeux, F. Beguin, G. Bister, A. Fonseca, J.B. Nagy, A. Kis, S. Jeney, A.J. Kulik, L. Forro, Catalytically Grown Carbon Nanotubes of Small Diameter Have a High Young's Modulus, Nano Letters, 2 (2005) pp.2074-2077.
[8] X. Hao, H. Zhang, R. Zheng, Y. Zhang, K. Ameyama, C. Ma, Effect of mechanical alloying time and rotation speed on evolution of CNTs/Al-2024 composite powders, Transactions of Nonferrous Metals Society of China, 24 (2014) pp.2380−2386.
[9] S. Narayanan, M.G. Moorthy, Experimental Investigation of Aluminium alloy with MWCNT Composite to increase the Mechanical Properties by Stir Casting Method, Journal of Mechanical and Civil Engineering, 12 (2015) pp.30-34.
[10] A.K. Srivastava, C.L. Xub, B.Q. Wei, R. Kishorea, K.N. Sood, *Microstructural features and mechanical properties* of carbon nanotubes reinforced aluminium–based metal matrix composites, Indian Journal of Engineering & Materials Sciences, 15 (2008) pp.247-255.
[11] Xi. Zheng, G. Zhoua, Q. Xua, Y. Xiongb, C. Luoa, J. Wua, A new technique for dispersion of carbon nanotube in a metal melt, Materials Science and Engineering A, 527 (2010) pp.5335–5340.

[12] L.H. Manjunatha, P. Dinesh, Fabrication, Microstructure, Hardness and Wear properties of Extruded MWCNT- Reinforced with 6061Al Metal Matrix Composites, International Journal of Scientific & Engineering Research, 4 (2013) pp.974-990
[13] Q. Li, C.A. Rottmair, R.F. Singer, CNT reinforced light metal composites produced by melt stirring and by high pressure die casting, Composites Science and Technology, 70 (2010) pp.2242–2247
[14] R.M. Rashad, O.M. Awadallah, A.S. Wifi, Effect of MWCNTs content on the characteristics of A356 nanocomposite, Journal of Achievements in Materials and Manufacturing Engineering, 58 (2013) pp.74-80.
[15] A.B. Elshalakany, T.A. Osman, A. Khattab, B. Azzam, M. Zaki, Microstructure and Mechanical Properties of MWCNTs Reinforced A356 Aluminum Alloys Cast Nanocomposites Fabricated by Using a Combination of Rheocasting and Squeeze Casting Techniques, Journal of Nanomaterials, (2014) pp.1-14.

15th INTERNATIONAL FOUNDRYMEN CONFERENCE

INNOVATION – The foundation of competitive casting production

Opatija, May 11th-13th, 2016

http://www.simet.hr/~foundry/

INTRODUCTION TO THE MECHANISMS OF FORMATION AND MORPHOLOGY OF MICROPORES IN THE STRUCTURE OF DC CAST AlMgSi ALLOY

UVID U MEHANIZME I MORFOLOGIJU FORMIRANJA MIKROPORA U STRUKTURI DC LIJEVANE AlMgSi LEGURE

I. Buljeta[1], Z. Zovko Brodarac[2], A. Beroš[3] and M. Zeko[4]

[1,3,4]University of Zenica Faculty of Metallurgy and Materials Science, Zenica, Bosnia and Herzegovina
[2]University of Zagreb Faculty of Metallurgy, Sisak, Croatia

Poster presentation
Preliminary note

Abstract

The phenomena defects in the triple junction grain boundaries affect the properties of the microstructure of aluminum alloys. For that purpose the microstructure of the alloy EN AW 6060 on the billet sample cast by DC (Direct Chill) technology was analysed in order to gain insight into the origin and form pores in the final stages of solidification. Mechanisms of solidification shrinkage, thermal contraction and low permeability of interdendritic channels networks were discussed in moment when melt becomes isolated in separate locations forming new structure. Under such conditions, the tensile stress caused by anisotropic thermal contraction of a coherent dendrites network, causing the formation of pores in the corners of the grain boundaries whose morphology is determined by SEM / EDS analysis.

***Keywords**: micro cavity-pores-voids, the triple point of grain boundaries, hot tearing, AlMgSi alloy, Direct Chill Casting*

*Corresponding author (e-mail address): buljeta_ivica@yahoo.com

Sažetak

Pojave grešaka na trojnom spoju (eng. *Triple Junction*) granica zrna utječu na svojstva lijevane mikrostrukture aluminijske legure. S tim je ciljem analizirana mikrostruktura legure EN AW 6060 na uzorku trupca lijevanog DC postupkom (eng. *Direct Chill*) kako bi se dobio uvid u formiranje i oblik mikro pora nastalih u zadnjem stadiju skrućivanja. Razmatrani su mehanizmi stezanja pri skrućivanju, toplinske kontrakcije i niske propusnosti mreže inter-dendritnih kanala kada talina postaje izolirana na odvojenim lokacijama novonastale strukture. Pod takvim uvjetima, vlačna naprezanja uzrokovana neravnomjernom toplinskom kontrakcijom koherentne mreže dendrita, uzrokuju nastanak pora na kutovima granica zrna čija je morfologija utvrđena SEM/EDS analizom.

***Ključne riječi**: mikro šupljine-praznine-pore, trojne točke granica zrna, tople pukotine, AlMgSi legura, Direct Chill lijevanje*

UVOD

Identifikacija izravnim proučavanjem neispravnog odljevka ili opis koji uključuje samo kriterije oblika, izgleda ili dimenzija će pokazati greške kao što su diskontinuiteti, površinske greške, uključci, šupljine, pukotine, itd. Međutim klasifikacija grešaka poput plinske poroznosti, greške nastale uslijed skrućivanja kao i metalurške greške, upućuju na složene mehanizme djelovanja tijekom lijevanja.
Novija razmatranja postojećih kriterija nastanaka pukotina u odljevku koji skrućuje, pretpostavlja uzimanje u obzir različitih mehanizama njihove nukleacije uslijed koncentracijskog gradijenta, te razmatranje napredovanja pukotine na osnovama mehanike loma i razvoja mikrostrukture. Temeljito i sustavno proučavanje lomova u skrućujućem materijalu s ciljem izdavajanja prirode i kritične dimenzije greške ili strukture koje mogu uzrokovati njihovu nukleaciju, još uvijek predstavljaju problem. U uvjetima oblikovanja metala u toplom stanju dominantan mehanizam mikropukotina koje uzrokuju dalji razvoj grešaka ovisit će o mikrostrukturi materijala i brzini deformacije. Nastanak grešaka u metalnim strukturama, uključuje degradaciju materijala uslijed nukleacije i rasta grešaka, kao što su mikropore i mikropukotine te njihovo dalje srastanje u makropukotine [1].

Nukleacija toplih pukotina je gotovo neistraženo fenomen, a izazov danas leži u pronalaženju pravih čimbenika koji uzrokuju stvaranje nukleusa i širenje pukotine. Postojeće teorije djelomično opisuju čimbenike inicijatora pukotina kao što šupljine ispunjene tekućinom [2, 3], oksidi u obliku bi-filma [4] ili mikroporoznost kao rezultat stezanja pri skrućivanju i toplinske kontrakcije na trojnim granicama zrna [5]. Lijevana struktura se formira bez poroznosti ako se stezanje pri skrućivanju i toplinska kontrakcija potpuno kompenziraju protokom taline kroz mrežu dendrita, a kasnije i visoko temperaturnim puzanjem. Suprotno, razvoj pukotine zahtijeva da pora dosegne kritičnu veličinu pod određenim termomehaničkim uvjetima *Griffith*-ovog kriterija krtog loma, tako da je moguće predvidjeti istovremeno pojavu mikroporoznosti i tople pukotine [6]. Osim toga, treba naglasiti da pore kao potencijalni nukleusi vrućih pukotina, mogu potjecati od taloženja plina, skupljanja tijekom skrućivanja ili prekomjernog zasićenja šupljinama (slobodnim mjestima) [6].

Makroskopski nedostaci u odljevku opisuju šupljine kao "udubljenja ili otiske kalupa gdje se odljevak formira", a praznine kao "velike pore ili šupljine uzrokovane zarobljenim plinom". Na mikro skali, šupljine (eng. *Cavities*) karakterizira broj atoma plina u odnosu na broj šupljina (praznih atomskih mjesta u kristalnoj rešetki) potrebnih za proizvodnju određenog volumena šupljine. Kada šupljina sadrži samo šupljine, ali ne i atome plina, tada nosi naziv praznina (eng. *Void*) [7] što praktično podrazumijeva da više praznina ili šupljina mogu formirati pore. Vrlo često se ove razlike ne ističu, pa makro šupljina predstavlja otvorenu, a pora izoliranu zatvorenu prazninu.

Praznina tj. pora se smatra nukleus pukotine, iako se pore nužno ne moraju razviti u pukotinu. Stoga treba uzeti u obzir razliku između stvaranja pore i iniciranja pukotine,

Pukotina može nukleirati ili se razviti iz nekog drugog defekta i nakon toga propagirati kroz lanac pora.

Poroznost uslijed skrućivanja (eng. *Solidification Shrinkage*) u odljevcima ima fundamentalno drugačiji uzrok od plinske poroznosti. Gustoća legure za lijevanje u rastaljenom stanju manja od njegova gustoća u krutom stanju. Stoga, kada se događa fazna promjena legure između ovih stanja, ona se uvijek skuplja po veličini. U središtu debljih dijelova odljevka, ovo smanjenje može rezultirati mnogobrojnim malim šupljinama poznatim kao poroznosti uslijed skupljanja unutar kojih ne postoji zrak ili plin, nego vakum. Veličina ove poroznosti je često funkcija brzine skrućivanja: veliki dendriti nastaju pri nižim brzinama skrućivanja. Tako nastale pore dodatno se mogu povećati zaostalim/zarobljenim plinom. Pore plina su obično prilično kuglastog oblika, a pore koje nastaju skupljanjem uslijed skrućivanja obično imaju više nepravilan i izdužen oblik. Neki odljevci imaju poroznost uslijed skrućivanja i plinsku poroznost, koje je vrlo teško uočiti jedan pored drugog, a u slijedećim fazama obrade ili eksploatacija odljevka mogu se pojaviti kao uzroci nastajanja pukotina materijala. Općenito, formiranje pora uzrokovano toplinskim naprezanjima javlja u dva koraka: nukleacija i rast.

Formiranja mikroporoznosti može često se može uočiti na trojnim točkama granica zrna (engl. *Triple Junctions of Grain Boundaries*). Trostruki spoj je jednodimenzionalni mikro defekt koji se pojavljuje u sustavu spojenih zrna i malo je istraživan u odnosu na granice zrna. Osim toga, u trostrukom spojevima visoka lokalna naprezanja i gustoća grešaka (praznina, sekundarnih faza, uključaka, itd.) mogu predstavljati preferencijalna mjesta nukleacije pora odnosno šupljina. Oni mogu imati suprotan učinak na svojstva materijala: prepreku deformaciji pri niskoj temperaturi, "povlaštenu" putanju za koroziju, vlaženje ili nastanak šupljina kod puzanja [8]. Trostruki spojevi mogu imati dodatnu energiju iznad energije susjednih granica zrna i kod određene deformacije, gustoća dislokacija je znatno veća nego na granicama zrna [9] i zato bitno utječu na razvoj mikrostrukture tijekom rasta zrna [10]. Eksperimentalni rezultati pokazuju da gibanje sustava granica zrna u aluminiju može biti kontrolirano trojnim spojevima [11].

Za mehanizam rasta praznina, postoji mnogo mogućih utjecajnih faktora, a prisutnost toplinskih naprezanja slovi kao dominantan faktor. Rast praznina u aluminiju pretpostavlja difuziju granica zrna pod uvjetima puzanja [12]. Također za strukturu u kojoj postoji znatna razlika u orijentaciji između zrna (> 10°), trostruki spojevi su točke visokog lokalnog naprezanja, i dovode do visokog udjela šupljina [13]. Zato su to mjesta koja preferiraju vjerojatnost nukleacije praznina, a granice visokog kuta pružaju putanje za brzu difuziju praznina po granicama zrna prema trojnim spojevima [14].

Makroskopskom prekidu/diskontinuitetu na obratku u uvjetima toplog oblikovanja metala, odnosno, kada je temperatura deformacije viša od oko polovice temperature taljenja, glavni uzrok razvoja oštećenja se povezuje s intergranularnim oštećenjem koja odgovara nukleaciji pora na granicama zrna za vrlo niske brzine deformacije [15]. Brzina deformacije, temperatura, veličina naprezanja su parametri koji određuju mjesto nastanka, oblik, veličinu

i kinetiku nukleacije te rast mikropora. Makroskopskom prekidu materijala prethode složeni mehanizmi djelovanja kao što su a) mobilne dislokacije, b) nukleacija šupljina, c) kontinuirani rast šupljina, d) superplastični rast praznina, e) duktilni rast praznina, i f) mikro pukotine [15].

Kod vrućeg oblikovanja metala i visoke temperature deformacije, mikro pukotine se pojavljuje na granicama zrna i oko sekundarnih faza, a oblik šupljina na granicama zrna varira s brzinom deformacije. U ovim uvjetima uočene su: (1) sitne/malene praznine na granicama zrna za visoke temperature puzanja ($\varepsilon = 10^{-15}\ s^{-1}$), zatim (2) velike praznine na trojnim spojevima granica zrna kod superplastičnih deformacija ($\varepsilon = 10^{-4}\ s^{-1}$) i (3) klinasta pukotina na trojnom spoju granica zrna ($\varepsilon = 10\ s^{-1}$).

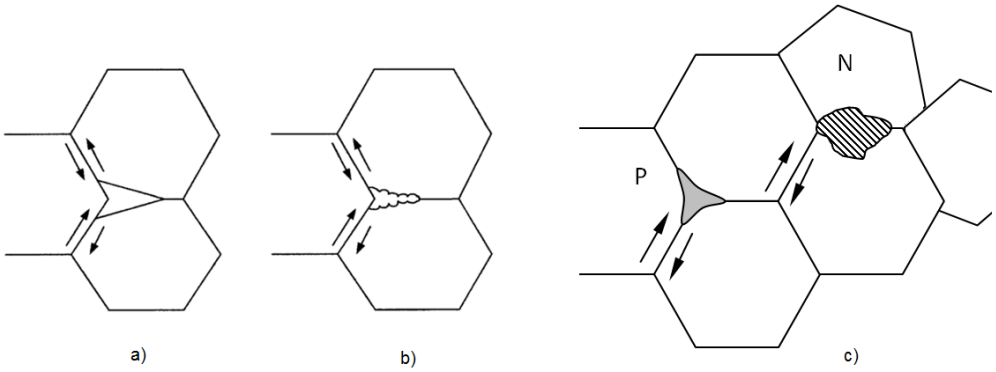

Slika 1. Shema nastanka pukotine a) *w i b) r tipa* [16] i mehanizma superplastičnog nastanka povezanih pora c) na trojnim spojevima [17]

Postoje i mišljenja da pukotina nukleira kao posljedica klizanja granica zrna (kao klinasta *w* - tipa na slici 1.a) ili jednostavno nastaje akumulacijom sferičnih praznina (kao *r* - *tip*, na slici 1.b) [16]. Formiranje praznine na granicama zrna je kinetički fenomen, a način loma pod proizvoljnim stanjem naprezanja ovisi isključivo o brzini nukleacije i brzini rasta pore. Kada su obje brzine velike, postoji jaki potencijal za njihovo međusobno spajanje u šupljinu.

Kod vrućeg oblikovanja metala, brzine deformacije i naprezanja su visoke, mala je difuzija granica zrna, te se smanjuje mogućnost rotacije zrna i klizanja granica zrna, tako da se u ovim uvjetima višestruke pore ne nalaze na granicama zrna, niti se praznine uočavaju na trostrukim točkama zrna. Umjesto toga, samo se mikroklinaste pukotine mogu se pojaviti na granicama zrna kod uvjeta vrućeg oblikovanja. Suprotno tome, u uvjetima superplastičnog oblikovanja/obrade, sa usitnjenom veličinom zrna (<10 μm), pore su uglavnom na trostrukim točkama (slika 1.c), zbog rotacije zrna i klizanja granica zrna pod osrednjim naprezanjima i brzinom deformacija znatno većom od brzine puzanja.

Daljnji mehanizam uključuje formiranje redova pora na smjerovima nagnutim prema vlačnoj osi [17]. Taj postupak je prikazan na slici 1.c te se pretpostavlja da se za vrijeme navale klizanja granica, skupine zrna klize kao cjelina, sve do trenutka kada su blokirane od strane nepovoljno orijentiranih granica zrna. To stvara koncentraciju naprezanja na odgovarajućim trostrukim spojevima zrna, a u nedostatku akomodacije difuzijom, deformacijom i/ili

migracijom granica, lokalna koncentrirana naprezanja se oslobađaju otvaranjem praznine u točki P. Prema rezultatima numeričkih proračuna na granicama klizanja [18], otvaranje takve šupljine rezultira napregnutim površinama N. Kao rezultat toga, daljnja nukleacija praznina ima prednost na tim poprečnim granicama. Ovaj, plastičnošću kontroliran mehanizam oštećenja, je najvažniji u ukupnom rastu pora kod većine superplastičnih materijala. Ipak još uvijek ne postoje fizičke jednadžbe raspoložive za modeliranje nukleacije i rasta praznina na trojnim točkama koje nastaju zbog rotacije zrna i klizanja granica zrna.

Analiza površine tople pukotine nakon njenog nastanka može uputiti na različite mehanizme i prirodu njenog nastanka [18]. Pojedine serije aluminijskih legura za gnječenje kao na primjer 1000, 3000, 5000 i 6000 imaju različite tendencije formiranja pukotina ovisno o rasponu skrućivanja, veličini zrna, količini eutektika, segregacijama metala i sekundarnih faza. Kod tople pukotine legura serije 6000 kao što je EN AW 6111, slobodna površina dendrita može ukazati na činjenicu da je došlo do razdvajanja prije nego je skrućivanja dovršeno tj. prije nego su dendriti potpuno spojeni.

Suprotno, aluminijska legura iz serije 1000 kao što je EN AW 1050, ima uzak raspon skrućivanja (oko 10-20 °C) i pokazuje da su tople napukline ponekad potpuno ili djelomično zarasle zbog upada taline bogate otopljenom tvari u interdendritska područja. Legura iz serije 5000 kao što je EN AW 5182 legura, ima malu tendenciju vrućim napuklinama zbog visoke koncentracije eutektičke faze dok EN AW 3104 legura pokazuje površinu prijeloma žilavog loma na spoju dendritskih vrhova.

MATERIJALI I METODE

Eksperimentalna istraživanja su provedena u pogonu ljevaonice Aluminij d.d. Mostar na aluminijevom trupcu proizvedenom po *Direct Chill* postupkom lijevanja koji je imao termički inducirane tople pukotine. Ispitivan je uzorka legure EN AW 6060 koji je preliminarnim istraživanjima mikrostrukture pokazao prisutnost mikro pora [19,20].

Kod aluminijskih legura serije 6000, ispitivanja toplih pukotina pokazuju površinu prijeloma koja je relativno ravna s vidljivim slobodnim dendritima bez izobličenja, ili jamica te se tople pukotine mogu opisati kao rezultat interdendritskog razdvajanja [18]. Međutim prisutnost stezanja pri skrućivanju, ne može se isključiti. Stoga je u ovom radu bilo potrebno dodatno ispitati ovu mogućnost, jer širok raspon skrućivanja ove legure učinit će posljednja područja koja skrućuju podložnim naprezanjima uslijed kontrakcije tijekom dužeg temperaturnog intervala i tako povećati sklonost nastanku mikroporoznosti.

S tim je ciljem ispitivana legura EN AW 6060 koja ima širok interval skrućivanja (585 – 650°C). U navedenom temperaturnom intervalu kašasta zona egzistira znatno duže te postoji velika tendencija ka formiranju mikro pora tijekom skrućivanja. Osim toga legura EN AW 6060 ima lošu tečljivost zbog malog sadržaja Si i stoga je jako veliku osjetljivost ka nastajanju toplih pukotina.

Ispitivan je primarni (engl. *As-Cast*) trupac legure EN AW 6060 s unutarnjim pukotinama promjera 203 mm i dužine lijevanja 7500 mm gdje se istraživala početna tj. kritična faza lijevanja. Izvršena je SEM/EDS analiza na uzorku stope trupca gdje je formirana struktura pokazala mikropore na trojnom spoju granica zrna.

REZULTATI

Kemijski sastav odlivenog trupca legure EN AW 6060 prikazan je u tablici 1 koji prikazuje niži sadržaj elemenata s visokom temperaturom taljenja: Ti, Mn i Cr. Snižen sadržaj Ti upućuje na mogućnost formiranja krupnijeg zrna, dok su Mn i Cr odgovorni za kinetiku precipitacije sekundarnih AlFeSi faza tokom homogenizacije koja u slučaju škartnog trupca izostaje. Od istog trupca koji je prošao ultrazvučnu kontrolu (slika 2.a) odrezan je cilindrični uzorak stope trupca debljine 60 mm (slika 2.b), a iz samog središta trupca izrezan je cilindrični uzorak promjera 25 -30 mm, koji je brušen i poliran standardnim postupcima za aluminijske legure.

Tablica 1. Kemijski sastav legure EN AW6060

Sastav	Sadržaj elemenata (%)								
	Si	Fe	Cu	Zn	Mg	Mn	Ti	Cr	Na
2	3	4	5	6	7	8	9	10	11
Zahtijevano	0,42 0,48	0,15 0,25	- 0,1	- 0,1	0,42 0,48	- 0,1	- 0,02	- 0,05	0,007
Postignuto	0,4259	0,1751	0,0013	0,0109	0,4302	0,0413	0,0085	0,0014	0,0016

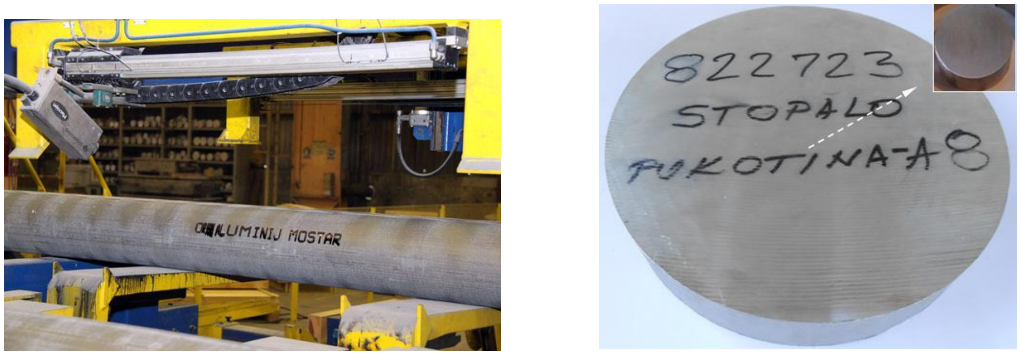

a) b)

Slika 2. a) Kontrola proizvedenog trupca [21] i b)uzorak stope i središnjeg dijela odlivenog trupca legure EN AW 6060

U slijedećoj fazi provedeno je SEM/EDS ispitivanje s ciljem uvida u mehanizam nukleacije pora određivanjem: (1) mjesta nastanka (2) oblika i (3) raspodjele ključnih elemenata u promatranoj pori.

Iako nisu jasno vidljive sve granice zrna, pri povećanju uzorka od 1000x (slika 3.a), jasno je da se pora nalazi na točki granica zrna označenih A, B i C. Na istoj slici 3.a osim otvorene pore,

na granicama zrna vidljive su pločice sekundarne AlFeSi faze duž granica zrna. Velike intermetalne čestice, koje se formiraju u ranoj fazi skrućivanja, mogu premostiti Al - dendritne grane i kao posljedica toga, polu-kruta legura može poboljšati svoju čvrstoću pri nižem udjelu solida kada je osjetljivost na pukotine velika [6].

Na slici 3.b pri uvećanju od 5000 × vidljiv je mogući ostatak polomljene pločice AlFeSi (detalj E) kao i dvije AlFeSi čestice poprečno na granicu zrna (detalj F). Osim što poboljšavaju krutost suprotno, velike intermetalnie AlFeSi čestice mogu učinkovito blokirati napajanje talinom međudendritskih kanala u kašastoj zoni [6], na što upućuju ove poprečno postavljene intermetalne čestice (detalj F, slika 3.b).

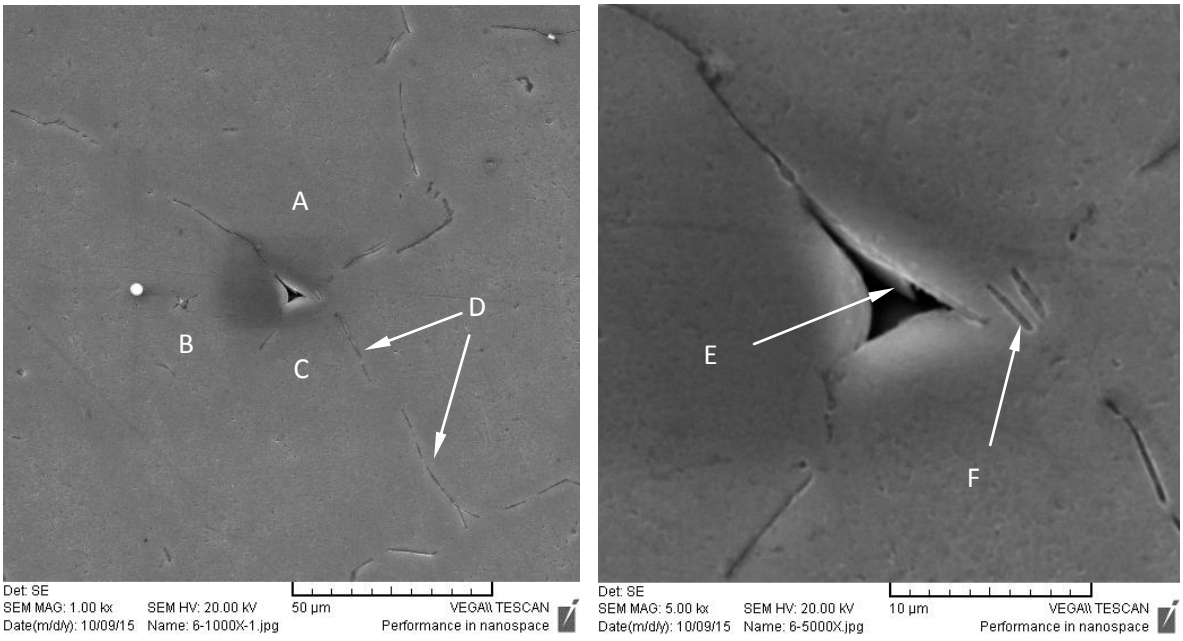

a) b)

Slika 3. a) Pora na trojnoj točki zrna i b) sekundarne AlFeSi čestice legure EN AW 6060

Oblik pore u tri pravca upućuje na to da je nastala u prostorno napregnutom stanju za razliku od praznina *w tipa* koje nastaju kod jednoosnog vlačnog ispitivanja. Gornja slika mikropore u obliku trokuta zaobljenih stranica ~ 5,5 µm i 8 µm, upućuje na njen postanak koji je rezultat: međusobnog djelovanja skupljanja uslijed skrućivanja, toplinske kontrakcije i niske propusnosti taline kroz mrežu dendrita na trojnim točkama granica zrna. Stoga su ova mjesta u uvjetima visokih lokalnih toplinskih naprezanja za vrijeme brzog hlađenja kore trupca, preferencijalna mjesta nukleiranja praznina.

Analiza oblika pore ne ukazuje na kuglaste pore plina nastale kod plinske poroznosti, već na nepravilan i izdužen oblik pore koje nastaju skupljanjem uslijed skrućivanja (engl. *Shrinkage porosity)*. Izgled površine pore može uputiti na koncept vlaženja granica zrna (za slučaj potpunog kvašenja granica zrna, plošni kut 2θ je jednak nuli) [22], ali odsustvo plastične deformacije vjerojatnije upućuje na prisutnost poroziteta uslijed skrućivanja. Uz činjenicu da

je opseg skrućivanja legure EN AW6060 prilično širok, a fluidnost slaba, to će produženo postojanje kašaste zone poduprijeti formiranje mikro pora.

U cilju identifikacije sadržaja ključnih elemenata Al, Si, Fe, Mg koji oslikavaju poru ili neku sekundarnu fazu (Mg_2Si ili AlFeSi) kao i uključke na ovom mjestu, provedena je EDS tehnika mapiranje elemenata (engl. *Elemet Mapping*) istog mjesta čije 2D slike prikazuju prostorni raspored elemenata u uzorku. Slika 4.a pokazuje otopljeni Si, Fe i Mg u aluminijskom matriksu dok je za identifikaciju na gornjem rubu pore teško reći da li pokazuje stvarne elementarne sastave AlFeSi faze (detalj E sa slike 3.b) ili utjecaj sastava iz matriksa koji ga okružuje. Generalno, slika 4.a pokazuje povećanu koncentraciju Si na istom mjestu dok slika 4.b jasno pokazuje odsutnost aluminija na mjestu pore tj. prazan prostor.

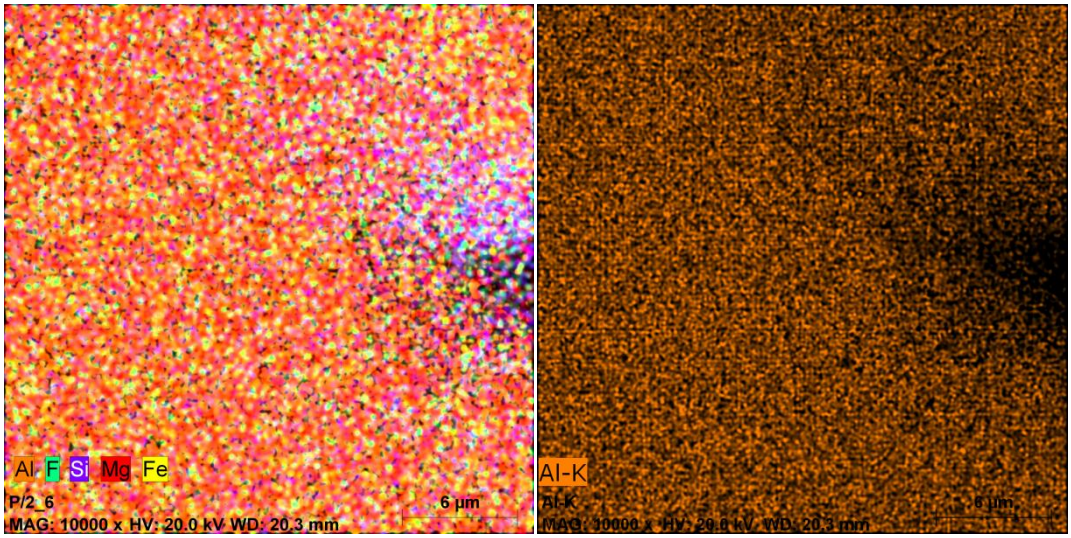

a) b)

Slika 4. a) Maping koncentracije ključnih elemenata i b) samog aluminija na uzorku

Dalje je u cilju preciznijeg potvrđivanja prisutnosti pore, provedena usporedna EDX analiza pore (slika 5) i susjednih zrna (slika 6). Dobivene slike ne pokazuju jasniju predodžbu sadržaja Al, Mg i Si na oba ispitana mjesta. Međutim gotovo identični rezultati unutar pore i u aluminijskoj osnovi, pokazuju da pora niže u dubini nije otvorena, tj. da nije dalje propagirala u pukotinu.

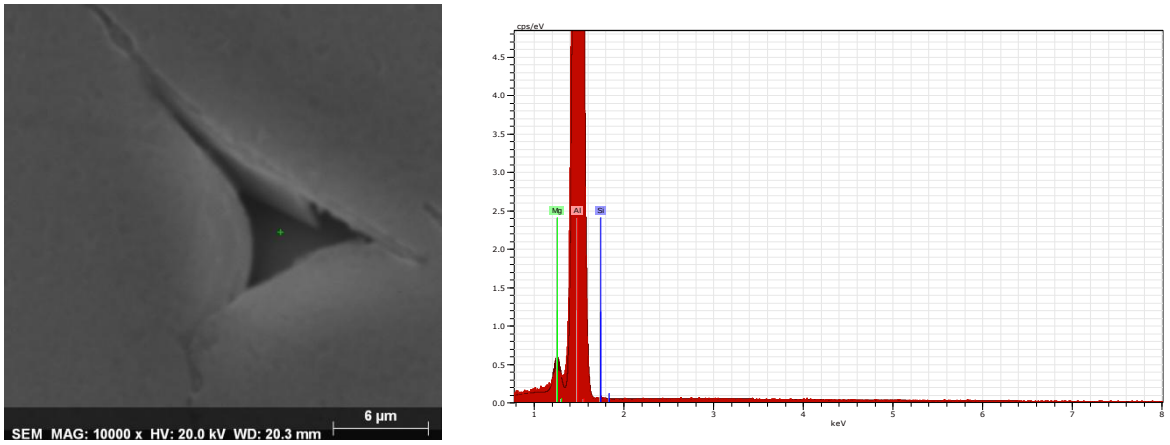

a) b)

Slika 5. a) Mjerno mjesto i b) EDX kvantitativni spektar pore

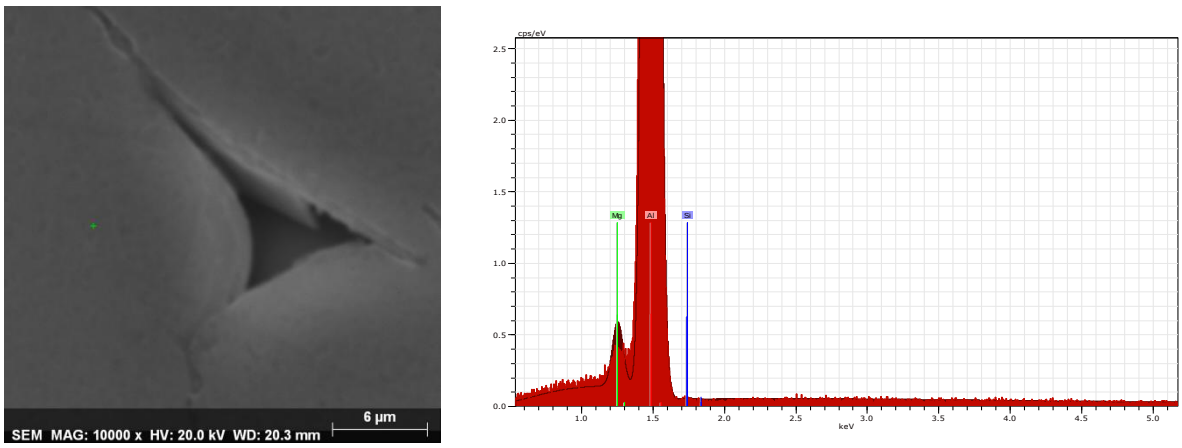

a) b)

Slika 6. a) Mjerno mjesto i b) EDX kvantitativni spektar pore spektar zrna aluminijske osnove

Kako na slikama 5. i 6. očitanja ne pokazuju dovoljno jasnu razliku sadržaja kemijskih elemenata, dodatno je provedena EDS analiza načinjena na presječnoj liniji za isto mjesto što pokazuje slika 7a. EDS dijagram analize uzorka jasno dokazuje pad intenziteta sadržaja aluminija na početku i kraju presječne linije (pore) ukazujući na prazan prostor tj. prostorni defekt na trojnoj točki granica zrna (slika 7.b). Također neznatna promjena intenziteta krivulje za Fe i Si na samom rubu pore nam pokazuje da se zaista radi o ostatku AlFeSi čestice (slika 3.b detalj E) koju se mapiranjem elemenata nije moglo pokazati na slici 4a. Linija presijeca također i poprečnu (slika 3.b, detalj F) AlFeSi česticu na kraju slike 7.a desno, a porast sadržaja Fe i Si registriran na dijagramu potvrđuje da se zaista radi o AlFeSi pločicama koje su mogle sudjelovati u blokiranju protoka tekućine između dendrira.

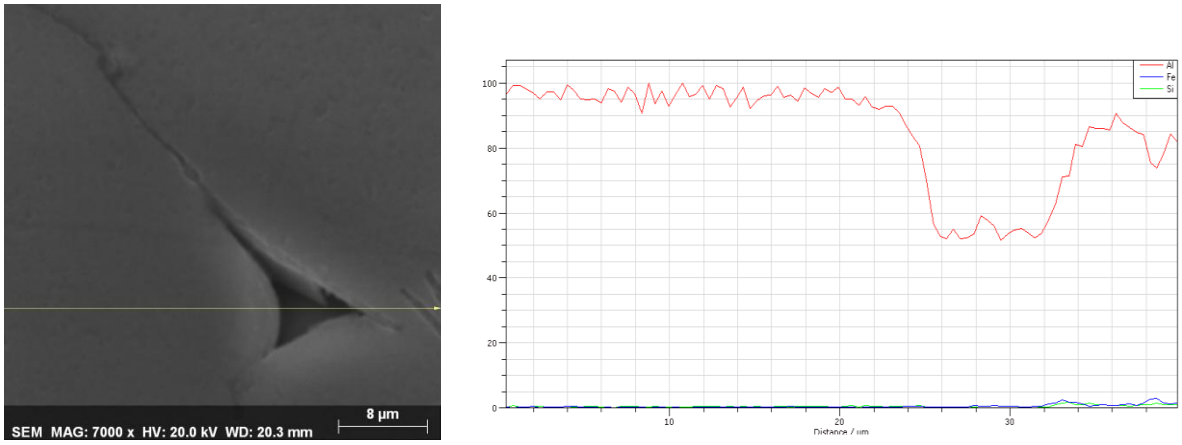

a) b)

Slika 7. a) EDS dijagram intenziteta sadržaja Al,Fe i Si na liniji presjeka zrna i b) pore

DISKUSIJA REZULTATA

Kod legura serije 6××× topla napuklina svojstvena ovoj vrsti legure, sastoji od slobodne dendritne površine što ukazuje na činjenicu da je došlo do njihovog razdvajanja prije nego je došlo do skrućivanja ili može ukazati na mikro pore nastale uslijed skupljanja [18].

Ispitivanja deformacije metala na visokim temperaturama, pokazuje da oblik i veličina pora na granicama zrna varira od brzine deformacije, ali više odgovara smjeru deformacije na trojnim spojevima.

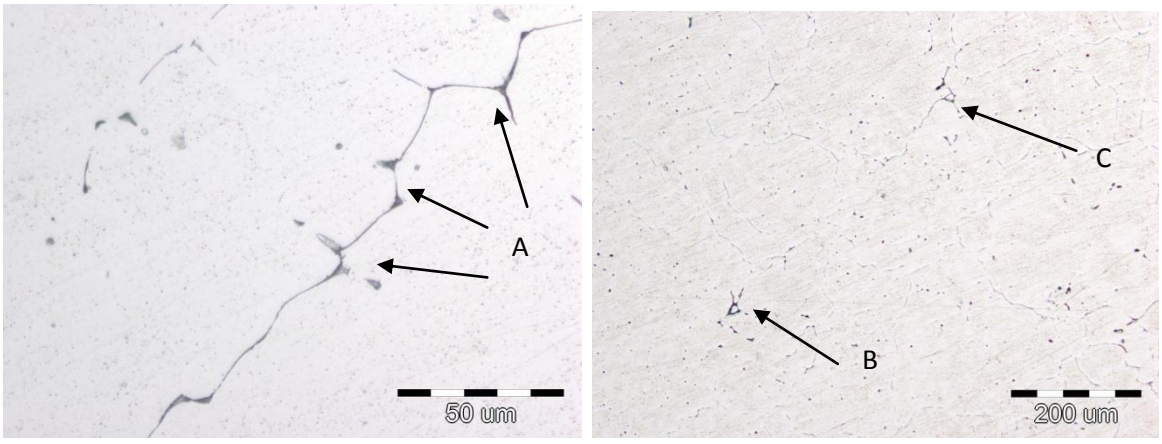

a) b)

Slika 8. a) Mikropukotine uslijed vezanih i b) pojedinačnih pora na istom uzorku centralnog dijela napuknutog trupca legure EN AW 6060 [23]

Teorija superplastičnih materijala kao što je aluminij, za veličine zrna manje od 10 µm, pojašnjava formiranje mikropukotine povezanim porama [17] tokom SPF (engl. *Super plastically forming*) obrade. Međutim, ranija istraživanja napuknutih trupaca u ljevaonici Aluminij d.d. Mostar su pokazala samo djelomično slaganje sa napomenutom teorijom. Kod

aluminijeve legure EN AW 6060 i veličina zrna 80 -120 μm uslijed nametnute brzine deformacije za vrijem brzog hlađenja vodom, uočeno je također formiranje mikropukotine povezanim porama (Detalj A sa slike 8.a), ali mikropukotina čiji je rast zaustavljen (Detalj B i C sa slike 8.a) [23].

U ovom radu je provedeno ispitivanje uzorka stope trupca sa pukotinom kao i rezultati koji (I) opisuju uvjete nukleacije pore na trojnom spoju granica i upućuju na (II) mogući mehanizam rasta mikropukotine u toplom stanju, stoga:

1. Rezultati ispitivanja pukotina u toplom stanju legure EN AW6060 ukazuju da je nukleacija pora na trojnom spoju granica zrna nastala skupljanjem uslijed skrućivanja.
2. EDX analiza dubine pore i susjednih zrna ukazuju da pojedinačne udaljene pore ne mogu biti nukleusi toplih pukotina što potvrđuje detalj B i C sa slike 8.b [23].
3. Oblik mikro pore na SEM slikama ukazuje na nukeaciju koja nije rezultat klizanja granica na susjednim zrnima, što više odgovara stanju ravninskog tj. prostornog naprezanja u trupcu tokom hlađenja.
4. Mehanizam superplastičnosti djelomice nije primjenjiv na legure kod kojih se skupljanjem uslijed skrućivanja na trojnim spojevima formiraju pore, iz razloga što je već otvorena pora mjesto relaksacije nametnutih naprezanja i na taj način kompenzira prijenos deformacija istezanja duž susjedno slično orijentiranih granica zrna.

Vjerojatni mehanizam rasta mikropukotine uzastopnim porama nastaje u slučajevima kada u isušenom interdendritnom kanalu, skupljanje tijekom skrućivanja aluminijske legure serije 6000, osigurava nukleaciju minimalnog (kritičnog) broja pora na trojnim točkama zrna sa sličnim usmjerenjima. Tada uslijed nametnutih termičkih naprezanja, postoje dva moguća mehanizma propagiranja mikropukotina između dvije uzastopne pore na trojnim spojevima: (1) mogućnost razdvajanja granica zrna na krtim AlFeSi česticama ili (2) klizanja granica zrna mehanizmom plastične deformacije. Međutim, ovakvi pretpostavljeni mehanizam daljeg povezivanja uzastopnih susjednih pora na trojnim spojevima zrna i dalji rast mikropukotine, ipak treba dodatno istražiti.

ZAKLJUČAK

Mehanizam rasta mikropukotine nastale u toplom stanju ovisi od vrste aluminijeve legure. Za leguru tipa EN AW 6060 kada legure prelazi iz tekuće u krutu fazu veliki opseg skrućivanja produžuje postojanje kašaste zone, a uvjeti otežanog napajanja i slaba fluidnost interdendritnim kanala omogućuje nukleiranje pora na trojnim spojevima granica zrna. Standardni postupci vlačnih ispitivanja na povišenim temperaturama odgovaraju jednoosnom stanju naprezanja, za razliku od brzog hlađenja trupca kojem odgovaraju prostorna termička naprezanja što mijenja oblik stvarne inicijale pore na trojnim spojevima granica zrna. Mehanizam srastanja ovakvih pora u mikropukotinu još uvijek je nerazjašnjen, a upućuje na pore u neposrednom susjedstvu dvaju ili više slično orijentiranih zrna.

LITERATURA

[1] D. Krajcinovic, Damage Mechanics, Amsterdam, 1996
[2] M. Rappaz, J.-M. Drezet, and M. Gremaud: Metall. Mater. Trans. A, 1999.
[3] Suyitno, W.H. Kool, L. Katgerman: Mater. Sci. Forum, 2002, vols. 396–402, pp. 179.
[4] J. Campbell: Castings, Butterworth-Heinemann, United Kingdom, 2003.
[5] W. Suyitno, H. Kool, L. Katgerman. Mater. Sci. Forum, 2002, vols. 396–402, pp. 179–184.
[6] D. Eskin, Physical Metallurgy of Direct Chill Casting of Aluminum Alloys, New Work, 2008.
[7] Glossary of Terms, http://www.paceind.com/die-casting-101/glossary-of-terms
[8] L. Priester, Grain Boundaries, Springer, 2013.
[9] S. Shekhar, A. H. King, Strain fields and energies of grain boundary triple junctions , Acta Materialia, 56 (2008) 19.
[10] G. Gottstein,a L.S. Shvindlermana,b and B. Zhaoa Thermodynamics and kinetics of grain boundary triple junctions in metals, Recent developments 2010.
[11] S. G. Protasova, Triple junction motion in aluminum tricrystals, Acta mater, 49, 2001.
[12] J. Ho , Thermal stress induced voids in nanoscale cu interconnects by in-situ tem heating, Dissertation, The University of Texas, Austin, 2007.
[13] J. Nucci, et all, Local Crystallographic Texture and Voiding in Passivated Copper Interconnects, Applied Physics Letter**,** 4017-4019, 1996.
[14] R. Keller, J. Nucci, D. Field, Local Textures and Grain Boundaries in Voided Copper Interconnects, Journal of Electronic Materials, 26, 996-1001,1997.
[15] J. Lin, Y. Liu, T. A. Dean, A Review on Damage Mechanisms, Models and Calibration Methods under Various Deformation Conditions International Journal of DAMAGE MECHANICS, Vol. 14—October, 2005.
[16] M. E. Kassner, M.-T. Perez-Prado, Fundamentals of Creep in Metals and Alloys Elsevier, Technology & Engineering, 2004, pp.1-279.
[17] A. Farghalli, A. Mohamed, Micrograin Superplasticity: Characteristics and Utilization, Materials, ISSN 1996-1944, 2011.
[18] S. Lin, A study of hot tearing in wrought aluminum alloys, Dissertation, Université du Québec à Chicoutimi (UQAC), 1999.
[19] A. Beroš, I. Buljeta, The influence of induced thermal stresses on the measured hardness in EN AW 6060 alloy billet produced using direct chill casting procedure, Metallurgical & Materials Engineering Congress of South-East Europe, 2015.
[20] I.Buljeta, A. Beros, Z.Z.Brodarac, The Study Conditions Occurrence of Hot Tearing in the Billets Alloy EN AW6060 Produced with the Process of Direct Chill Casting, Light Metals 2016, Chapt.113, 2016
[21] Proizvodnja, trupci, http://www.aluminij.ba/en/billets
[22] J. Campbell, Castings, ISBN 0750647906 ,Elsevier Science,2003.
[23] I. Buljeta, A. Beroš, Analysis of the Influence of Composition ENAA-6060(AlMgSi0,5) Aluminum Alloy on the Occurrence of Hot Cracks in the Billets, 10st International Foundrymen Conference, Opatija 2010.

15th INTERNATIONAL FOUNDRYMEN CONFERENCE
INNOVATION – The foundation of competitive casting production
Opatija, May 11th-13th, 2016
http://www.simet.hr/~foundry/

GDOES ANALYSIS OF SOL-GEL ZrO_2 THIN FILMS ON AUSTENITIC STAINLESS STEEL

L. Ćurković[1], I. Bačić[2], H. Otmačić-Ćurković[3] and Z. Šokčević[1]

[1]University of Zagreb Faculty of Mechanical Engineering and Naval Architecture, Zagreb, Croatia
[2]Forensic Science Centre Ivan Vučetić, Zagreb, Croatia
[3]University of Zagreb Faculty of Chemical Engineering and Technology, Zagreb, Croatia

Poster presentation
Original scientific paper

Abstract

In this paper, one layer and three layers of yttria stabilized sol-gel ZrO_2 thin films were deposited on the X2CrNiMo17-12-2 (AISI 316L) austenitic stainless steel by dip coating method. For the preparation of sol zirconium (IV) butoxide was used as pre-cursor, *i*-propanol as a solvent with addition of nitric acid as a catalyst, acetylacetone as chelating agent and water for hydrolysis. Deposited films were calcined at the temperature of 400 °C.
Thickness of sol-gel ZrO_2 films deposited on stainless steel was determined by glow-discharge optical emission spectrometry (GD-OES). It was found that thickness of deposited films increases by increasing the number of layers.

Keywords: *GDOES, stainless steel, sol-gel, ZrO_2*

*Corresponding author (e-mail address): *lidija.curkovic@fsb.hr*

INTRODUCTION

Metals and metal alloys are one of the most common materials in engineering applications. Therefore, it is very important to recognize the influence on their service lifetime. One of these influences is corrosion, a destructive process that destroys metallic structure and causes material failures and damage. Special attention thereby is paid to the corrosion behaviour of stainless steels. Although stainless steels have major resistance to the corrosion attributed to the passive oxide film on its surface, there are some environments, like a chloride media, that can permanently harm this protective film, leading to localized corrosion [1-4].

Improvement of stainless steels corrosion resistance can be achieved by chemical modification of metal surface with corrosion inhibitors, as well as protective amorphous or crystalline coatings, such as TiO_2, ZrO_2, SiO_2 thin films-or their mixtures [5-7].

Metal ceramic coatings can be deposited on substrate by number of various techniques that have been developed for this purpose. They include physical vapour deposition (PVD), chemical vapour deposition (CVD), electrochemical deposition, thermal spraying, plasma spraying and sol-gel processes, such as spin, dip and spray coating [8, 9].

Among them, sol-gel techniques are preferred for several reasons: they are simple, low temperature (usually 200-600 °C) techniques, which avoid possible decomposition problems; can provide high purity, high quality and stoichiometric coatings; the adjustment of film thickness can be done easily; dip coating method is suitable for coatings of complex shaped substrate etc.[10-12].

The sol-gel process is a chemical synthesis method and can be used for production of a wide range of materials such as thin films and coatings, monoliths, powder, fibres, composites, porous gels and membranes (Figure 1) [8, 10-12].

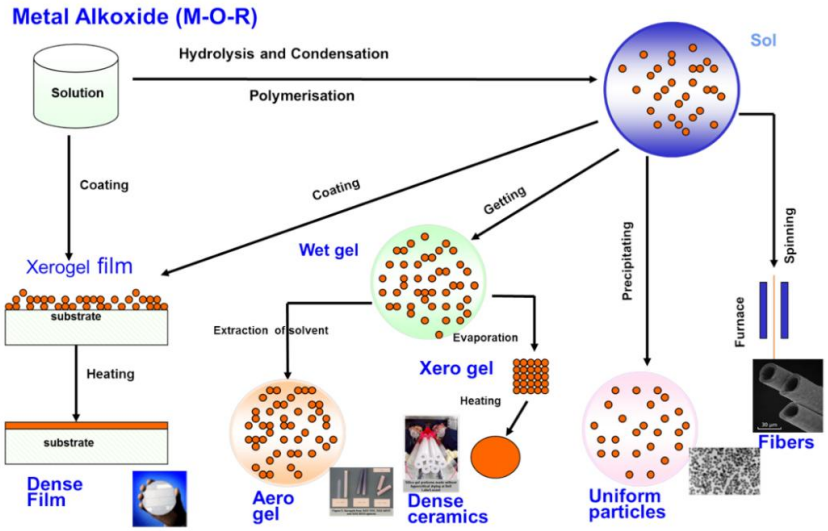

Figure 1. Sol-gel technology and application [8, 10-12]

Examples of possible application of sol-gel films are presented on Figure 2 [8, 10-12].

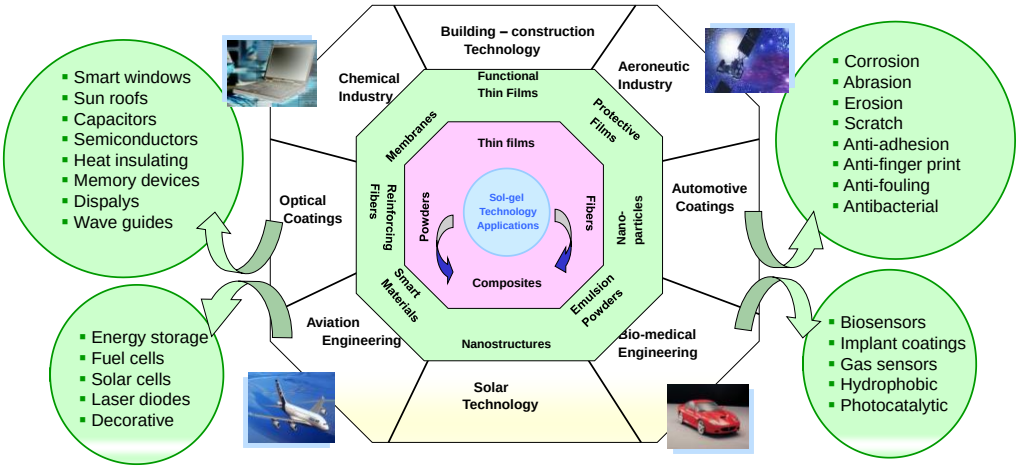

Figure 2. Application of sol-gel film [8, 10-12]

In this paper, nanostructured ZrO_2 films stabilized by 5 mol% Y_2O_3 were deposited on the stainless steel X2CrNiMo17-12-2 (AISI 316L) surface by sol-gel process, dip coating technique. Glow discharge optical emission spectrometry (GDOES) was used for determination thickness and composition of deposited films.

MATERIALS AND METHODS

Deposition of sol-gel ZrO_2 films on stainless steel

Steel disks with diameter 16 mm and height 2 mm were used as substrates. Chemical composition of X2CrNiMo17-12-2 (AISI 316L) stainless steel was determined by glow discharge optical emission spectroscopy (GDS 850A, Leco) and results in *wt*. % are: C-0.026; P-0.0287; S-0.0021; Si-0.37; Mn-1.42; Cu-0.345; Mo-2.17; Cr-16.38; Ni-10.53 and Fe – balance.

For the preparation of sol zirconium(IV) butoxide (ZrB) was used as precursors, *i*-propanol (PrOH) as a solvent, acetylacetone(AcAc) as chelating agent, with addition of nitric acid as a catalyst, and yttrium acetate hydrate (YAc) was used for ZrO_2 stabilization.

The molar ratio of the reagents was: ZrB:PrOH:AcAc:HNO_3=1:18:0.7:0.002:0.028, respectively.

The appropriate quantity for a final composition of 5 mol % Y_2O_3 to ZrO_2 was calculated and used.

After 24 h aging, the stainless steel plates disks were dipped into the sol by an in-house developed, electrically driven pulley system. Steel substrates were dipped into sol at a rate of 30 mm/min, then were held in solution for 3 minutes, in order to allow surface wetting. The withdrawal rate was also 30 mm/min. The steel substrates were then dried at room

temperature for 30 minutes. After drying at room temperature, each steel substrate was dried at 100 °C for an hour. The same procedure followed after each dip, for steel substrates which were dipped multiple times. After dip coating and drying, steel substrates were calcined at 400 °C for 1 hour.

Characterization of sol-gel ZrO_2 films on stainless steel

In this study, glow discharge optical emission spectrometry (GDOES), Leco GDS-850A spectrometer, equipped with a Grimm-type DC lamp for conductive samples was used for analysis of stainless steel substrate as well as for quantitative depth profiling (QDP) and the thickness of films of sol-gel ZrO_2 films deposited on stainless steel. The anode has a diameter of 4 mm, for a sampling area of 12.5 mm^2. The spectrometer is equipped with dual Rowland circles, having curved, holographic diffraction gratings of 1800 lines/mm and 3600 lines/mm, respectively, for a spectral range of 120–800 nm.

RESULTS AND DISCUSSION

Based on the method of Grimm type source, glow discharge optical spectroscopy (GDOES) has been developed as an important analytical tool for direct analyses of solid samples or depth profiling of different deposited coatings. Glow discharge optical emission spectrometry (GDOES) is an important analytical technique for bulk and depth profiling analysis of thin films and coatings with a total analysed depth ranging between a few nanometers and tens of micrometers.

Figures 3 and 4 show the GDOES depth profile of the element composition (at. %) of the selected elements: zirconium, chromium, nickel and iron for the sol-gel ZrO_2 film with 1 layer and 3 layers, respectively.

Results presented in Figures 3 and 4 show that the thickness of the deposited films increases by increasing the number of deposited layers. The thickness of deposited sol-gel ZrO_2 film with 1 layer and 3 layers are approximately 40 nm and 120 nm, respectively. Also, it was found that Cr, Fe and Ni diffusion from substrate through the interface and film.

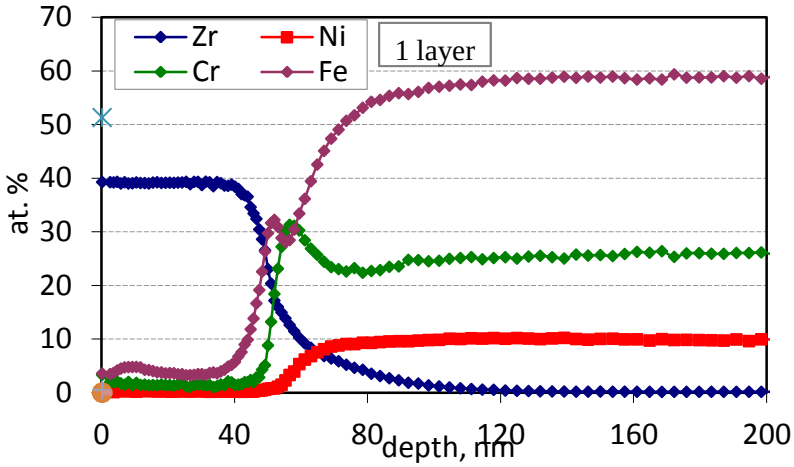

Figure 3. Quantitative depth profile analysis of sol-gel ZrO_2 film with 1 layer on stainless steel obtained by GDOES, heat treated at 400 ˚C for 60 min

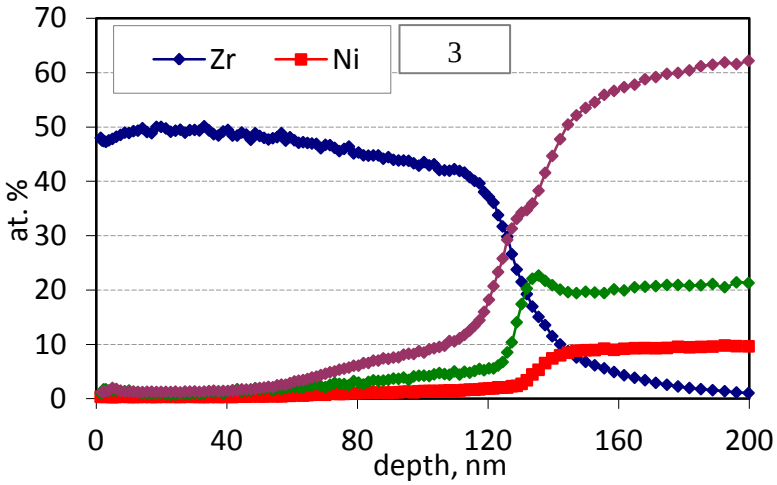

Figure 4. Quantitative depth profile analysis of sol-gel ZrO_2 film with 3 layers on stainless steel obtained by GDOES, heat treated at 400 ˚C for 60 min

CONCLUSIONS

Nanostructured sol-gel ZrO_2 films were deposited on stainless steel X2CrNiMo17-12-2 (AISI 316L) substrate by dip coating method. For preparation of sol zirconium butoxide were used as precursors, *i*- propanol as a solvent, with the addition of nitric acid as a catalyst and acetylacetone for peptization and 5 mol % Y_2O_3.

Deposited sol-gel ZrO_2 films after calcination at 400 °C were characterized by GDOES, from the obtained results the following conclusions can be drawn:

- Glow-discharge optical emission spectrometry (GDOES) as fast, easy-to-use analytical technique has proven to be a powerful tool for the rapid analysis of elements in the

surface of solids as well as for elemental concentrations as a function of depth in nanoscale.

- Thickness of ZrO_2 films with 1 layer and 3 layers were 40 nm and 120 nm, respectively.
- The results of GDOES analysis showed that thickness of the deposited films increases by increasing the number of deposited layers.
- It was found that Cr, Fe and Ni diffusion from substrate through the interface and film.

REFERENCES

[1] Y. Yin, L. Niu, M. Lua, W. Guo, S. Chen, In situ characterization of localized corrosion of stainless steel by scanning electrochemical microscope, Appl. Surf. Sci., 255 (2009) pp.9193–9199.
[2] Y. Wang, W. Wang, Y. Liu, L. Zhong, J. Wang, Study of localized corrosion of 304 stainless steel under chloride solution droplets using the wire beam electrode, Corr. Sci., 53 (2011) pp.2963–2968.
[3] J.J. Kim, Y.M. Young, Study on the Passive Film of Type 316 Stainless Steel, Int. J. Electrochem. Sci., 8 (2013) pp.11847-11859.
[4] H. Yanliang, D. Xiqing , C. Jun, Electrochemical Characteristics of an Austenitic Stainless Steel Under Simulated Solution Film Formed in Marine Atmosphere, Int. J. Electrochem. Sci., 6 (2011) pp.5597-5604.
[5] N. Padhy, U. Kamachi Mudali, V. Chawla, R. Chandra, B. Raj, Corrosion behaviour of single (Ti) and duplex (Ti–TiO_2) coating on 304L stainless steel in nitric acid medium, Mater. Chem. Phy., 130 (2011) pp.962–972.
[6] L. Ćurković, H. Otmačić Ćurković, S. Salopek, M. Majić Renjo, S. Šegota, Enhancement of corrosion protection of AISI 304 stainless steel by nanostructured sol–gel TiO_2 films, Corr. Sci., 77 (2013) pp.176–184.
[7] V. S. Saji, J. Thomas, Nanomaterials for corrosion control, Corr. Sci., 92 (2007) 51–55.
[8] J. D. Wright, N. A. J. Sommerdijk, Sol–Gel Materials Chemistry and Applications, CRC Press, OPA Overseas Publishers Association, 2001.
[9] H. Schmidt, Chemistry of material preparation by the sol-gel process, J. Non-Cryst. Solids, 100 (1988) pp.51-64.
[10] T. L. Metroke, R. L. Parkhill, E. T. Knobbe, Passivation of metal alloys using sol-gel-derived materials- a review, Prog. Org. Coat., 41 (2001) pp.233–238.
[11] R. Gheriani, R. Chtourou, Preparation of Nanocrystalline Titanium Dioxide (TiO_2) Thin Films by the Sol-Gel Dip Coating Method, Journal of Nano Research, 16 (2012) pp.105–111.
[12] D. Wang, G.P. Bierwagen, Sol–Gel Coatings on Metals for Corrosion Protection, Progr. Org. Coat., 64 (2009) pp.327–338.

15th INTERNATIONAL FOUNDRYMEN CONFERENCE
INNOVATION – The foundation of competitive casting production
Opatija, May 11th-13th, 2016
http://www.simet.hr/~foundry/

ALUMINOTHERMIC PROCEDURE AND THERMITE MIXTURE FOR VKD RAILS CROSSOVER WELDING

ALUMINOTERMIJSKI POSTUPAK I TERMITNA SMJESA ZA VKD SPOJEVE TRAMVAJSKIH TRAČNICA

M. Gavrilovski[1], Ž. Kamberović[2], V. Manojlović[3], A. Mihajlović[1], N. Jovanović[1], M. Sokić[3] and B. Marković[3]

[1]Innovation Center of Faculty of Technology and Metallurgy in Belgrade Ltd., Belgrade, Serbia
[2]University of Belgrade Faculty of Technology and Metallurgy, Belgrade Serbia
[3]Institute for Technology of Nuclear and Other Mineral Row Materials, Belgrade, Serbia

Poster presentation
Professional paper

Abstract

The welding of so called “transition joints”, in tram railways, types Ri 60 and VK D 180/150 are typically performed by Electric Arc welding procedure. The huge differences in size of the cross section and geometry, as well as the poor quality of the faces of rails cause the accumulation of internal stresses. Conventional Electric Arc procedure does not provide appropriate mechanical properties and homogeneity of weld, which leads to breakage of rails, seriously harming the security in tram traffic. In this paper, the innovative Aluminothermic welding procedure for this type of rails has been shown. A new technology involves specific conditions of Aluminothermic welding process of transition joints in tram railways, which will provide compact and homogeneous weld. This weld corresponds to the mechanical properties of the base material, and meets all the requirements of international and national standards of welding. The composition of thermite mixture and geometry of inflow system and mould are specially designed for obtaining of optimal structural, mechanical and other properties of welds. Preparation of the thermite mixture, made on the basis of a mathematical model, depends on the characteristics of the starting materials and pre-defined parameters and requires no expensive or complicated equipment. The advantages of this method are demonstrated in real conditions and introduced into regular production.

***Keywords**: aluminothermic process, welding, VKD rails, RV60, Pyrkonit*

*Corresponding author (e-mail address): *m.sokic@itnms.ac.rs*

Sažetak

Zavarivanje tzv. "prijelaznih spojeva", kod tramvajskih tračnica, vrste Ri 60 i VK D 180/150 tipično se izvodi elektrolučnim postupkom zavarivanja. Goleme razlike u veličini presjeka i geometrije, kao i loša kvaliteta lica tračnica uzrokuje stvaranje unutarnjih naprezanja. Konvencionalni elektrolučni postupak

ne daje odgovarajuća mehanička svojstva i homogenost zavara, što dovodi do pucanja tračnica te ozbiljno šteti sigurnosti u tramvajskom prometu. U ovom radu pokazan je inovativni aluminotermijski postupak zavarivanja za ovu vrstu tramvajskih tračnica. Nova tehnologija uključuje specifične uvjete aluminotermijskog procesa zavarivanja prijelaznih spojeva kod tramvajskih tračnica, koji će pružiti kompaktan i homogen zavareni spoj. Zavareni spoj odgovara mehaničkim svojstvima osnovnog materijala, i ispunjava sve zahtjeve međunarodnih i nacionalnih standarda zavarivanja. Sastav termitne smjese i geometrije ulaznih sustava i kalupa su posebno dizajnirani za dobivanje optimalnih strukturnih, mehaničkih i drugih svojstava zavara. Priprema termitne smjese, izrađena je na temelju matematičkog modela, ovisno o karakteristikama polaznih materijala i unaprijed definiranim parametrima i ne zahtijeva skupe i komplicirane opreme. Prednosti ove metode su se pokazali u realnim uvjetima, a uveden je u redovnu proizvodnju.

Ključne riječi: *aluminotermijski postupak, zavarivanje, VKD tračnice, RV60, Pyrkonit*

UVOD

Zavareni spojevi u principu predstavljaju oslabljeno mjesto svake metalne konstrukcije. Ovo se odnosi i na spojeve tramvajskih tračnica koji predstavljaju diskontinuitet u kolosijeku, prouzrokovan njihovim specifičnim mikro i makrostrukturnim karakteristikama i mehaničkim svojstvima. Pored toga, izloženi su eksploatacijskim uvjetima sa visokim naprezanjima prouzrokovanim vertikalnim, horizontalno-poprečnim i horizontalno-uzdužnim silama, naprezanjima i temperaturnim dilatacijama. Najkvalitetniji, najjeftiniji i najbrži postupak zavarivanja spoja tračnica dobiva se primjenom elektrootpornog postupka. Izvodi se robusnom, stabilnom opremom u radioničkim uvjetima. Primjenjuje se kod rekonstrukcija ili izgradnje novih kolosijeka. Dužine tračnica koje se zavaruje su ograničene, zbog čega se intenzivno razvijaju manji uređaji i oprema za elektrootporno zavarivanje tračnica u kolosijeku. Bez obzira na intenzivna istraživanja u ovom području aluminotermijski postupak predstavlja najrasprostranjeniji postupak zavarivanja tračnica. Jednostavnost, ekonomičnost i prenosivost opreme učinili su da se postupak aluminotermijskog zavarivanja široko koristi u industriji zavarivanja tračnica [4]. Primjenjuje se za međusobno povezivanje tračnica u dugom traku, zatim kod završnog zavarivanja, kao i kod tekućeg održavanja kolosijeka za sanaciju pukotina [5]. Također se primjenjuje i za zavarivanje tzv. „prijelaznih spojeva“, između dva različita tračnička profila, ako razlike u njihovim poprečnim presjecima i geometriji nisu velike (prijelaz željezničke tračnice tipa 49E1(62,5cm^2) na tračnicu 60E1(76,8cm^2). Kod velikih razlika ova dva parametra, kao što je to slučaj kod zavarivanja tramvajskih tračnica na ukrštajima kolosijeka, tračnice tipa Ri 60(77,05cm^2) na tračnicu VK D 180/105(134,04cm^2) najčešće se primjenjuje elektrolučni postupak. Međutim i pored rigoroznih procedura izvođenja ovog postupka (prethodno predgrijavanje, pravilan izbor dodatnog materijala, izbor optimalnog postupka elektrolučnog zavarivanja, kontrola brzine hlađenja i dr.), ovaj postupak ne daje dovoljno kvalitetan spoj. Primjena aluminotermijskog postupka zavarivanja sa svojim specifičnostima, u ovom slučaju, pokazala se uspješnijom. Ovaj postupak razvijen je na Tehnološko - metalurškom fakultetu u Beogradu i našao je praktičnu primjenu tijekom rekonstrukcije tramvajskog kolosijeka u Nemanjinoj ulici u Beogradu. Zbog toga i ovaj rad ima za cilj prikaz rezultata ispitivanja radioničkih zavarenih

spojeva, na osnovu kojih je odobren, ovaj potpuno nov i autentičan postupak zavarivanja prijelaznih zavara na tramvajskim ukrštajima u kolosijeke na ovom području. Treba napomenuti da je po ovoj metodologiji napravljeno 112 zavarenih spojeva, još početkom 2005. godine i da su isti, bez obzira što su izloženi teškim eksploatacijskim uvjetima, u funkciji već 9 godina bez pojave, bilo vanjskih, bilo unutarnjih oštećenja i što je najvažnije bez pojave „razbijanja“ na spojevima uslijed udaraca pri prijelazu tramvajskog kotača sa jedne tračnice na drugu, kakav je slučaj kod primjene elektrolučnog postupka.

OPĆENITO O ALUMINOTERMIJSKOM ZAVARIVANJU

Aluminotermijski postupak zavarivanja je najčešće primijenjeni postupak spajanja željezničkih, tramvajskih i kranskih tračnica. Za njegovo izvođenje koristi se aluminotermijska smjesa visoke kalorične vrijednosti, preko 3000 kJ/kg, koja predstavlja mješavinu specijalno pripremljenih željeznih oksida i Al praha, različitih dodataka i mikrododataka [3, 4].

Općenito gledajući, prednosti ovog postupka zavarivanja u odnosu na druge postupke su sljedeće:

- Postupak omogućava usuglašavanje kemijskih, strukturnih i mehaničkih svojstava zavarenog spoja sa svojstvima osnovnog materijala;
- Ovim postupkom ostvaruje se veoma kompaktan i homogen neraskidiv spoj po cijelom poprečnom presjeku krajeva koji se zavaruju;
- Geometrija zavarenog spoja je besprijekorna;
- Oprema za izvođenje ovog postupka je jednostavne konstrukcije, za višekratnu je upotrebu i laka je za rukovanje i manipulaciju.

Za izvođenje zavarenog spoja nije potrebna vanjska energija. Energija koja se oslobađa egzotermnom reakcijom komponenata nakon aktiviranja AT smjese, dovoljna je za zagrijavanje i taljenje dijelova elemenata koji se zavaruju, a visoka čistoća komponenti, dodataka i mikrododataka, njihov međusobni odnos, kao i specijalna tehnologija izrade AT-smjese, garantiraju ostvarivanje zahtijevane kvalitete zavarenog spoja.

IZRADA RADIONIČKIH ZAVARENIH SPOJEVA

Za ispitivanja karakteristika zavarenih spojeva izrađena je serija radioničkih prijelaznih spojeva na radnom stolu za aluminotermijsko zavarivanje tračnica na Tehnološko-metalurškom fakultetu u Beogradu, a u cilju kvalifikacije ovog postupka za primjenu u Nemanjinoj ulici u Beogradu. Zahtjevi za kvalifikaciju postupka usuglašeni su europskim standardima EN 14730-1, EN 14732-2 [6, 7]. Zahtjevi navedeni ovim standardima su u suglasnosti sa preporukama Europske federacije za zavarivanje, spajanje i rezanje (EWF), odnosno tehničkog komiteta (TC) Europskog komiteta za standardizaciju (CEN) 256.

Materijali

Za izradu zavarenih spojeva korištene su tračnice tipa Ri60 i VK D180/105, proizvođača Voestalpine. Materijal za aluminotemijsko zavarivanje (AT porcije, kalupi) proizveden je u firmi Pyrkonit d.o.o tehnologijom čije je autorsko pravo zaštićeno patentima u Zavodu za zaštitu intelektualnog vlasništva. Ispitivanja zavarenih spojeva rađena su na Tehnološko-metalurškom fakultetu i Institutu za materijale u Beogradu.

Na slici 1 prikazani su profili šina Ri 60 i Vk D180/105 koji predstavljaju lijevi i desni poprečni presjek tramvajskog kolosijeka.

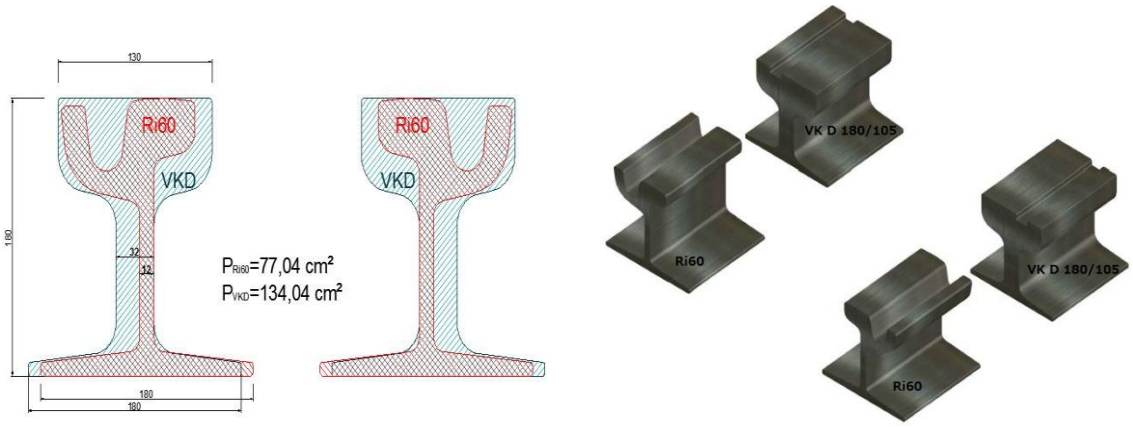

Slika 1. Profili šina Ri 60 i VKD180/105

Geometrija kalupa i uljevni sistem prikazani su na slici 2. Na istoj slici prikazana je i AT smjesa Pyrkonit.

Slika 2. Kalupne polovice i AT smjesa za izradu prijelaznih zavara

Kalupi sa uljevnim sistemom projektirani su tako da osiguravaju ravnomjerno odvođenje topline, kako tijekom izlijevanja čelika u šav, tako i tijekom hlađenja zavarenog spoja.

Za projektiranje sastava AT-smjese, korišten je matematički model. Na osnovu zadanih definiranih ulaznih parametara (tip tračnice i kvaliteta čelika tračnice) dobiveni su veoma brzo i pouzdano izlazni podaci: kvalitativno-kvantitativni odnosi komponenti, dodataka i mikrododataka koji čine AT-smjesu, toplinska bilanca procesa, temperatura reakcije,

temperatura metala pri izlijevanju, optimalna količina metala za ispunu šava i nadvara i dr., za zadane karakteristike zavarenog spoja. Adekvatnost modela potvrđena je tokom njegovog 20 godišnjeg korištenja u masovnoj proizvodnji AT smjese.

Na slici 3 prikazan je tok aluminotermijske reakcije, kao i dio zavarenog spoja, nakon uzimanja uzoraka iz dijela glave, vrata i stope. Aluminotermijska reakcija imala je normalan tok i istjecanje metala u šav bio je blagovremen i ravnomjeran. Nakon obrade zavarenih spojeva brušenjem, vizualnom kontrolom, utvrđena je adekvatna zapunjenost materijala šava, bez uočljivih pukotina ili drugih vanjskih grešaka.

Slika 3. Tok aluminotermijske reakcije i dio zavarenog spoja

REZULTATI ISPITIVANJA PRIJELAZNIH ZAVARENIH SPOJEVA TRAMVAJSKIH TRAČNICA

Ultrazvučna ispitivanja

Na izrađenim zavarenim spojevima, nakon hlađenja koje je trajalo najmanje 24 sata provedena su ispitivanja njihove homogenosti. Ispitivanja su izvršena ultrazvučnom Impuls-Eho metodom koristeći uređaj marke Krautkramer USM-2 sonde 006CM3/KBA 45O, 2.25 MHz. Uzorci su ocijenjeni kao dobri, jer se pri ispitivanju sa vertikalnom sondom pojavio signal koji je pokazao da je ultrazvuk prodro do dna zavarenog spoja, a pri ispitivanju s kutnom sondom nije dobiven povratni signal od refleksne površine koji se nalazi između stope tračnice i površine [8].

Kemijski sastav

Kemijski sastav osnovnog materijala i zavara na svim uzorcima određen je metodom optičke emisijske spektroskopije (OEC) na kvantometru ARL 3640, prema standardu SRPS C.A1.011:2003. Rezultati ispitivanja su prikazani u tablici 1, pri čemu su uzimane srednje vrijednosti.

Tablica 1. Kemijska ispitivanja sastava osnovnog materijala i zavara

Prijelazni zavar Ri60 / VKD180/150	Lokacija uzorka	Udio elemenata, %						ppm
		C	Si	Mn	S	P	Al	H
	Osn.mat.Ri60	0,57	0,26	1,01	0,018	0,021	0,005	1,3
	Term.čelik zavara	0,55	0,33	1,00	0,014	0,018	0,19	1,1
	Osn.mat.VKD180/105	0,56	0,31	0,98	0,029	0,023	0,004-	1,5

Rezultati ispitivanja vlačne čvrstoće

Za ispitivanje vlačne čvrstoće zavara izrađene su epruvete iz uzorka. Tokom izrade epruveta za ispitivanje vlačne čvrstoće nisu utvrđene greške čija bi vrsta i obim onemogućile njihovu izradu, što potvrđuje homogenost zavarenih spojeva. Ispitivanja su provedena prema standardu SRPS EN 10002-1:1996., na kidalici INSTRON 1330, slika 4.

Slika 4. Ispitivanje vlačnih karakteristika i izgled epruvete nakon kidanja

Rezultati ispitivanja vlačnih karakteristika prikazani su u tablici 2, kao na odgovarajućem dijagramu na slici 5.

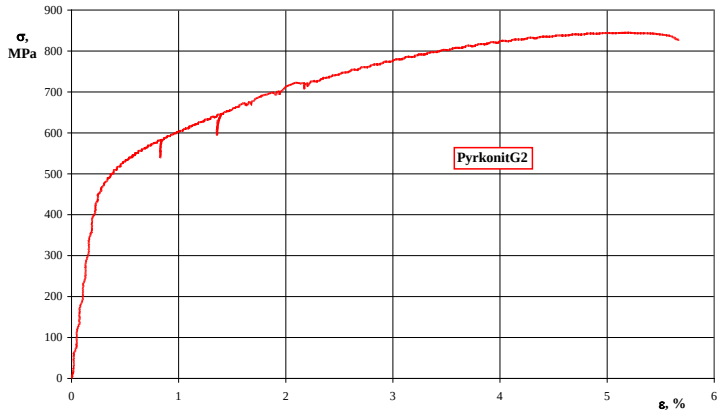

Slika 5. Dijagram naprezanje - istezanje

Tablica 2. Vlačne karakteristike uzoraka

d	A	F	R_{p02}	R_m	A_t	l_0
mm	mm^2	N	MPa	MPa	%	mm
9.99	78.3828	66190	524	844	5.67	50

Ispitivanja tvrdoće

Tvrdoća je ispitivana prema standardu SRPS EN 14730-1:2006. Linijska tvrdoća je određena samo na gazećem sloju tračnice, Vikersovom metodom HV10, sa testom opterećenja od 30 kg, u točkama na udaljenosti od 2 mm.

Tvrdoća termitnog čelika je određena metodom po Brinelu, sa parametrima:
- promjer volframkarbidne kuglice 10 mm,
- test opterećenja 3000 kg,
- vrijeme trajanja opterećenja 15 s.

Rezultati su prikazani i grafički i tabelarno na slici 6.

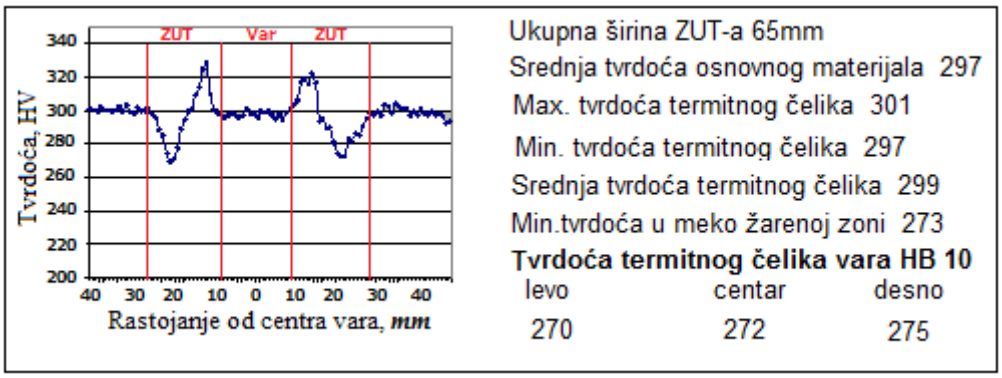

Slika 6. Linijska tvrdoća površine tračnice HV30

Statičko ispitivanje na savijanje

Statičko ispitivanje na savijanje izvedeno je uzorcima zavarenih spojeva, dužine 1,2 m. Ispitivanje je izvedeno na hidrauličnoj preši s razmakom oslonaca od 1,0 m, pri čemu se AT zavar nalazi na sredini razmaka između dva oslonca (slika 7).

Slika 7. Ispitivanje zavarenog spoja na savijanje

Ispitivanje se obavlja postepenim povećanjem pritisaka na glavu tračnice do pojave loma. Istovremeno sa mjerenjem opterećenja mjerio se i ugib. Rezultati ispitivanja prikazani u tablici 4.

Tablica 4. Rezultati ispitivanja sile loma i progiba

Masa zavarenog spoja(kg/m)	Sila loma(KN)	Ugib(mm)
91,1	855	15

Makro i mikrostrukturna ispitivanja

Ispitivanje mikrostrukture izvršeno je na površinama uzetih iz zona osnovnog materijala, ZUT-a i zavara optičkim mikroskopom Carl Zeiss Neophot u odbijenoj svjetlosti.

Mikrostruktura osnovnog materijala (Ri60 i VK D180/105) je sitnozrna perlitno-feritna. Mikrostruktura ZUTa je vrlo bliska strukturi osnovnog materijala, pri čemu se uočava porast zrna u odnosu na osnovni materijal prema liniji spoja. U strukturi linije spoja uočava se nešto grublja feritno-perlitna zrna. Mikrostruktura zavara je perlitno-feritna sa sitnijim zrnima u odnosu na zonu utjecaja topline, ujednačena po presjeku i sa izraženim feritnim zrnima. Na slici 8. prikazane su makro i mikrostrukture uzorka zavarenih spojeva.

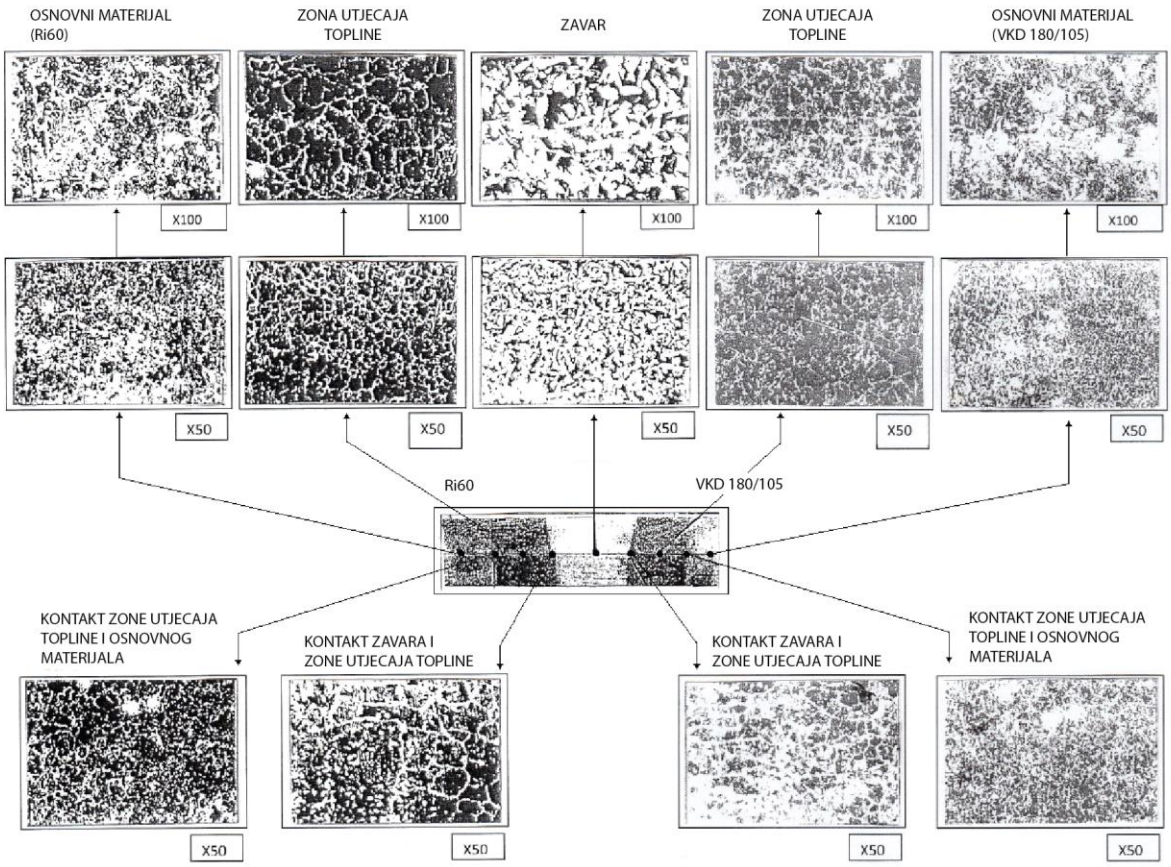

Slika 8. Makro i mikro strukture uzoraka zavarenih spojeva

ANALIZA REZULTATA

Ultrazvučnim ispitivanjima utvrđena je homogenost zavarenog spoja duž cijelog poprečnog presjeka, bez unutrašnjih grešaka.

Na osnovi rezultata ispitivanja kemijskog sastava materijala ispune, konstatira se da su sadržaji elemenata koji u najvećoj meri određuju svojstva zavarenog spoja, u propisanim granicama. Ujednačenost vrijednosti vlačnih čvrstoća ispitivanih uzoraka ukazuju na kemijsku i mikrostrukturnu homogenost zavara, a vrijednosti izduženja su u propisanim granicama, bez većeg rasipanja rezultata.

Prosječna tvrdoća je nešto iznad 275V, pri čemu je profil relativno ujednačen. Linijska tvrdoća je tipična za zavarene spojeve.

Osim sitnih nemetalnih aluminatnih uključaka zavareni spojevi su čisti i sadržaj je manji od 2 po JK-skali, dok sulfidnih i oksidnih uključaka nema. Osnovni materijal je također veoma čist u pogledu sadržaja nemetalnih uključaka (1,5 JK- skali). Struktura zavara je feritno perlitna kao i osnovni materijal sa nešto grubljim zrnima u zoni utjecaja topline (veličina zrna No. 3 ASTM).

ZAKLJUČAK

Na osnovu dobivenih rezultata ispitivanja može se zaključiti sljedeće:

1. Rezultati ispitivanja nedvosmisleno pokazuju da je modificirani aluminotermijski postupak sa predloženim i primijenjenim specifičnostima, adekvatan za dobivanje kvalitetnog prijelaznog zavarenog spoja, shodno zahtjevima srpskih i međunarodnih standarda, koji su karakteristični za ukrštaje tramvajskih kolosijeka.
2. Mehanička svojstva zavarenih spojeva (tvrdoća, vlačne karakteristike) nalaze se u intervalima zahtijevanih vrijednosti za ispitivanu vrstu materijala. Projektirani sastav AT smjese je takav da osigurava dobra plastična svojstva zavarenih spojeva pri visokim vrijednostima vlačne čvrstoće. Postignuta je homogenost mikrostrukture u pogledu sadržaja nemetalnih uključaka, tako da su zavareni spojevi u skladu sa svim zahtjevima za ovu vrstu materijala.
3. U toku zavarivanja nisu uočena odstupanja od uobičajene tehnologije aluminotermijskog zavarivanja i proces se odvijao u kontroliranim uvjetima.
4. Navedena tehnologija je u praksi prvi put primijenjena prije devet godina, tokom rekonstrukcije tramvajskog kolosijeka u Nemanjinoj ulici u Beogradu. Vizualne i ultrazvučne kontrole svih zavarenih prelaznih spojeva dokazuju ispravnost provedene tehnologije.

LITERATURA

[1] N. Ilić, M. Jovanović, M. Todorović, M. Trtanj, Microstructural and Mechanical Characterization of Postweld Heat-Treated Thermite Weld in Rails, Materials Characterizaton, 43 (1999) 4, pp.243-250.
[2] R.N. Hart,Thermite welding process, Lindsay Publications, Inc., Bradely, 1987.
[3] J.E. Brumbaugh, Welders guide, Chapter 10, Howard W. Sams & Co, Inc., Indianapolis, 1975.
[4] J. Myers, G.H. Geiger, D.R. Poirier, Structure and properties of thermite welds in r ails. Welding research supplement, 8 (1982) 258.
[5] B. Pollak, G.A. Bajuć, Posebna oštećenja tračnica na skretnicama, Građevinar 54 (2002) 8, pp.456-471.
[6] EN 14730-1, Railway applications - Track - Aluminothermic welding of rails - Part 1: Approval of welding processes; German version EN 14730-1:2006.
[7] EN 14732-2, Railway applications - Track - Aluminothermic welding of rails - Part 2: Qualification of aluminothermic welders, approval of contractors and acceptance of welds; German version EN 14730-2:2006.
[8] M. Saarna, A. Laansoo, Rail and rail weld testing, Proceedings of 4th International DAAAM Conference“Industrial engineering – innovation as competitive edge for SME”, Eds. J.Papstel/B.Katalinic,29 – 30th April, 2004, Tallinn, Estonia, pp.217-220.

Acknowledgements
This work was supported by the Ministry of Education and Science of the Republic of Serbia through the projects TR34033.

15th INTERNATIONAL FOUNDRYMEN CONFERENCE

INNOVATION – The foundation of competitive casting production

Opatija, May 11th-13th, 2016

http://www.simet.hr/~foundry/

INFLUENCE OF SILICA AND CHROMITE SAND ON THE SOLIDIFICATION SIMULATION OF STEEL CASTINGS

UTJECAJ SILIKATNOG I KROMITNOG PIJESKA NA SIMULACIJU SKRUĆIVANJA ČELIČNIH ODLJEVAKA

V. Grozdanić

University of Zagreb Faculty of Metallurgy, Sisak, Croatia

Poster presentation

Original scientific paper

Abstract

Influence of silica and chromite foundry sand on simulation of solidification of low and middle carbon „L“ shaped steel castings is investigated in the work.

Keywords: *modelling of solidification, steel castings, silica and chromite foundry sand*

*corresponding author: *grozdan@simet.hr*

Sažetak

U radu je istražen utjecaj silikatnog i kromitnog ljevaoničkog pijeska na simulaciju skrućivanja nisko i srednje ugljičnih čeličnih odljevaka u obliku slova „L“.

Ključne riječi: *modeliranje skrućivanja, čelični odljevci, kvarcni i kromitni ljevaonički pijesak*

UVOD

Matematičko modeliranje je znanstvena metoda koja omogućuje rješavanje i najkompleksnijih ljevaoničkih problema, kao što je skrućivanje odljevaka složene geometrije. To je potpomognuto brzim razvojem računala i numeričkih metoda rješavanja parcijalnih diferencijalnih jednadžbi.

Pri postavljanju matematičkih modela skrućivanja polazi se od Fourierove parcijalne diferencijalne jednadžbe provođenja topline. Jednadžba je riješena po domeni odljevka i geometriji kalupa, s time da su inkorporirani početni i rubni uvjeti. Pri operacionalizaciji matematičkog modela korištena je implicitna metoda promjenljivog smjera (eng. Implicit

alternating direction – IAD), iz razloga što je bezuvjetno stabilna i drugog je reda s obzirom na aproksimaciju prostora i vremena. Budući da se temperatura u sustavu odljevak-kalup mijenja za cca $1600\ ^0$C u model su ugrađena temperaturno ovisna toplinska svojstva.
Na temelju matematičkog modela, odnosno provedene numeričke simulacije, moguće je zorno vidjeti skrućivanje nisko i srednje ugljičnog čeličnog odljevka (pomicanje izosolidusa), kao i utjecaj vrste (kvarcnog i kromitnog) ljevaoničkog pijeska.

Matematički model

Simulacija skrućivanja provedena je za nisko i srednje ugljični čelični odljevak u pješčanom kalupu, kao što je prikazano na slici 1.

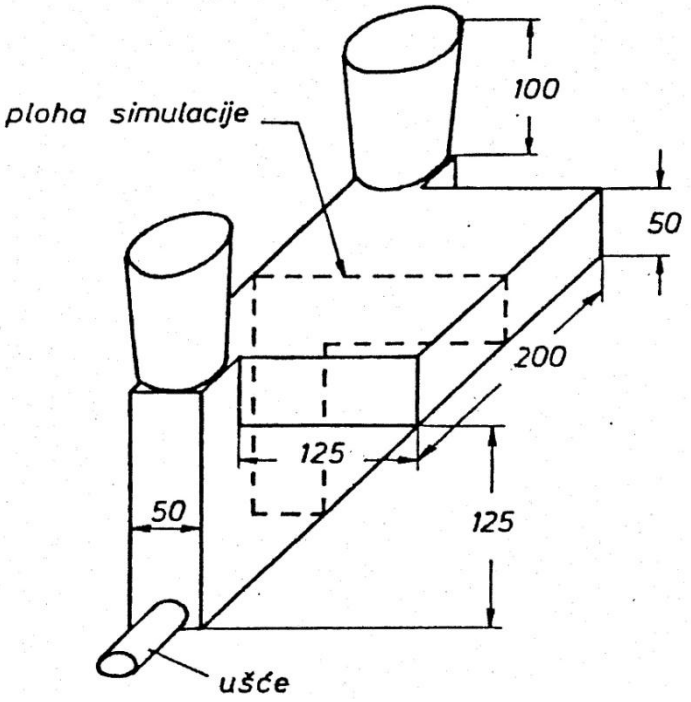

Slika 1. Shematski prikaz odljevka

Pri simulaciji procesa razmatra se presjek kroz kalup i odljevak kao na slici 2.

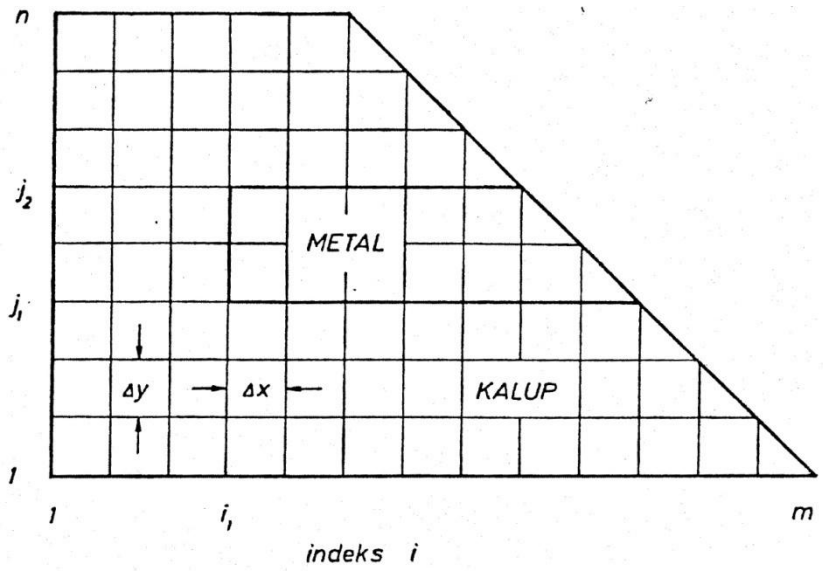

Slika 2. Dio presjeka kroz kalup i odljevak koji se razmatra pri simulaciji procesa

Matematički model skrućivanja odljevka sastoji se od Fourierove parcijalne diferencijalne jednadžbe provođenja topline i odgovarajućih početnih i rubnih uvjeta. Dvodimenzionalna parcijalna diferencijalna jednadžba provođenja topline u pravokutnom koordinatnom sustavu ima oblik [1]:

$$\frac{\partial T}{\partial t} = a\left(\frac{\partial^2 T}{\partial x^2} + \frac{\partial^2 T}{\partial y^2}\right) \quad (1)$$

Početni uvjet dobiven je na temelju toplinske bilance sustava [2]:

t=0 T=T_s

$$T_i = \frac{\rho_m c_{pm} T_L + \rho_k c_{pk} T_s + \rho_m \Delta H_f}{\rho_m c_{pm} + \rho_k c_{pk}} \quad (2)$$

pri čemu je: T_s - površinska temperatura kalupa, K
T_L – temperatura lijevanja, K
T_i - temperatura na graničnoj plohi kalup-metal, K
ρ_m - gustoća metala, kg/m^3
c_{pm} - specifični toplinski kapacitet metala pri konstantnom tlaku, J/kgK
ρ_k - gustoća kalupa, kg/m^3
c_{pk} - specifični toplinski kapacitet kalupa pri konstantnom tlaku, J/kgK
ΔH_f - entalpija taljenja, J/kg

Rubni uvjeti. Vanjska ploha kalupa je pri konstantnoj temperaturi T_s. U blizini plohe koja leži nadi dijagonali pod kutom od 45^0 nema temperaturnih razlika, tako da su toplinski tokovi jednaki. Iz Fourierovog zakona slijedi:

$$\frac{\partial T}{\partial n} = 0 \tag{3}$$

Na dodirnoj plohi kalup-metal kontinuitet je toplinskog toka, tako da vrijedi rubni uvjet četvrte vrste [3]:

$$k_m \frac{\partial T_m}{\partial n} = k_k \frac{\partial T_k}{\partial n} \tag{4}$$

U jednadžbama (3) i (4) n je normala na promatranu plohu.

Toplinska svojstva čeličnog lijeva i kalupnog materijala

Pri skrućivanju i hlađenju čeličnog odljevka u pješčanom kalupu temperatura materijala mijenja se u rasponu od gotovo 1600^0C. Da bi se što bolje opisao realni proces u matematičkom je modelu potrebno uzeti temperaturnu ovisnost toplinskih svojstava materijala. Na slikama 3. do 6. prikazana je temperaturna ovisnost toplinskih svojstava nisko i srednje ugljičnog čeličnog lijeva, na temelju podataka iz literature [4, 5]. Temperature likvidusa i solidusa za nisko ugljični ČL su $1516{,}5^0C$, odnosno $1478{,}4^0C$, a za srednje ugljični ČL su 1482^0C, odnosno 1427^0C. Latentna toplina kristalizacije iznosi 271 kJ/kg, a u slučaju nisko ugljičnog ČL u obzir je uzeta i toplina koja se oslobađa pri peritektičkoj reakciji, koja iznosi 81 kJ/kg.

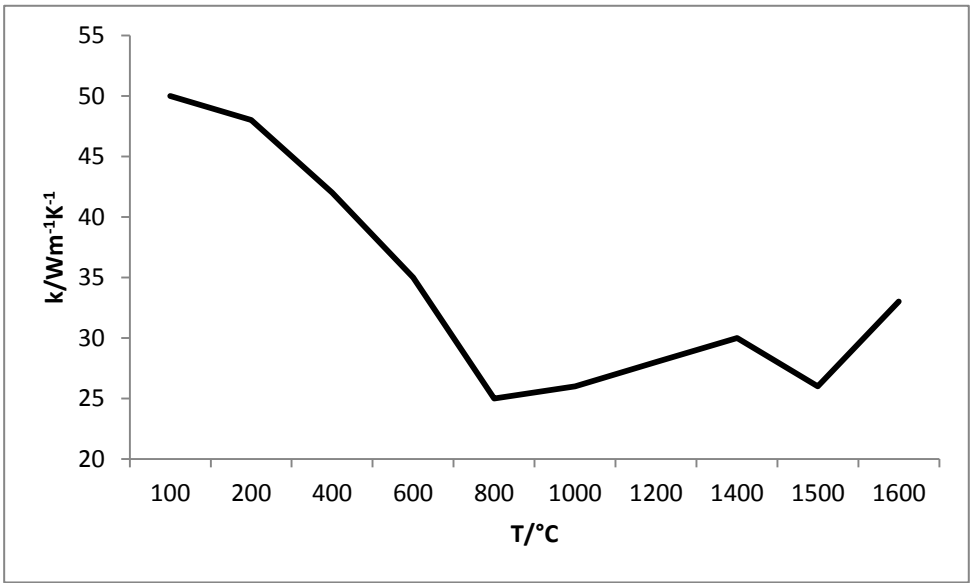

Slika 3. Temperaturna ovisnost toplinske vodljivosti nisko ugljičnog čeličnog lijeva

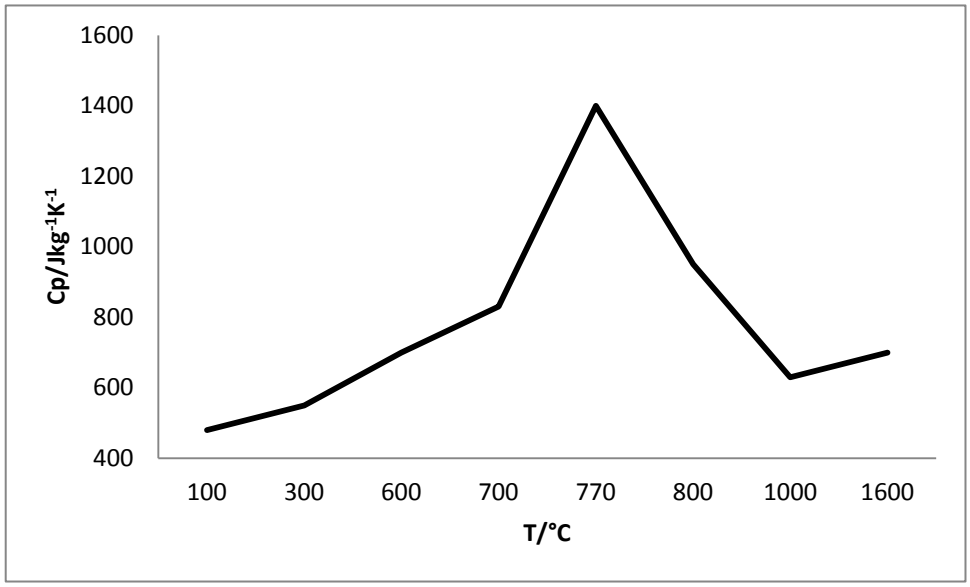

Slika 4. Temperaturna ovisnost specifične topline nisko ugljičnog čeličnog lijeva

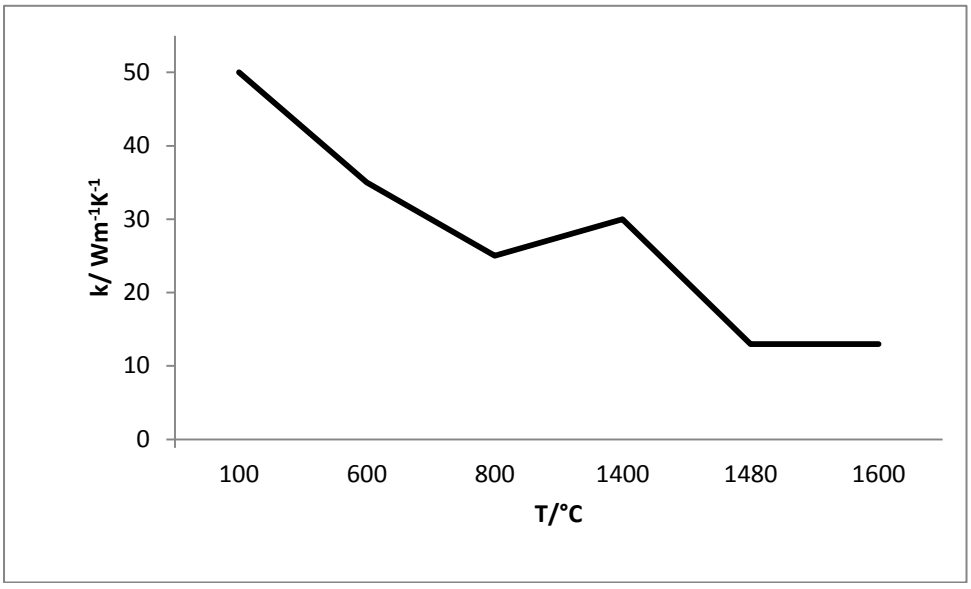

Slika 5. Temperaturna ovisnost toplinske vodljivost srednje ugljičnog čeličnog lijeva

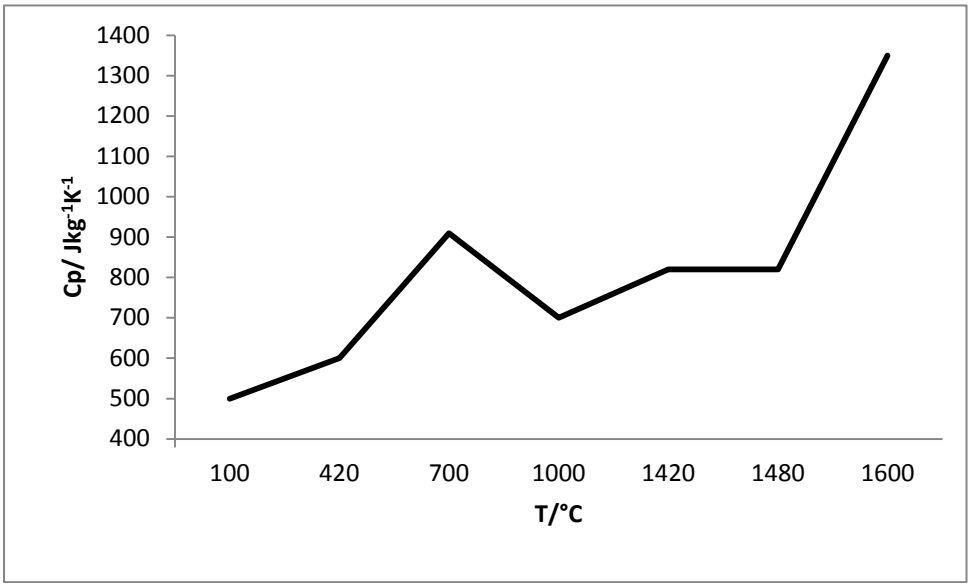

Slika 6. Temperaturna ovisnost specifične topline srednje ugljičnog čeličnog lijeva

Na slikama 7. do 10. prikazana je ovisnost prividne toplinske vodljivost i specifične topline za kvarcni i kromitni pijesak. Gustoća kvarcnog pijeska iznosi 1602 kg/m^3, a kromitnog 4300 kg/m^3.

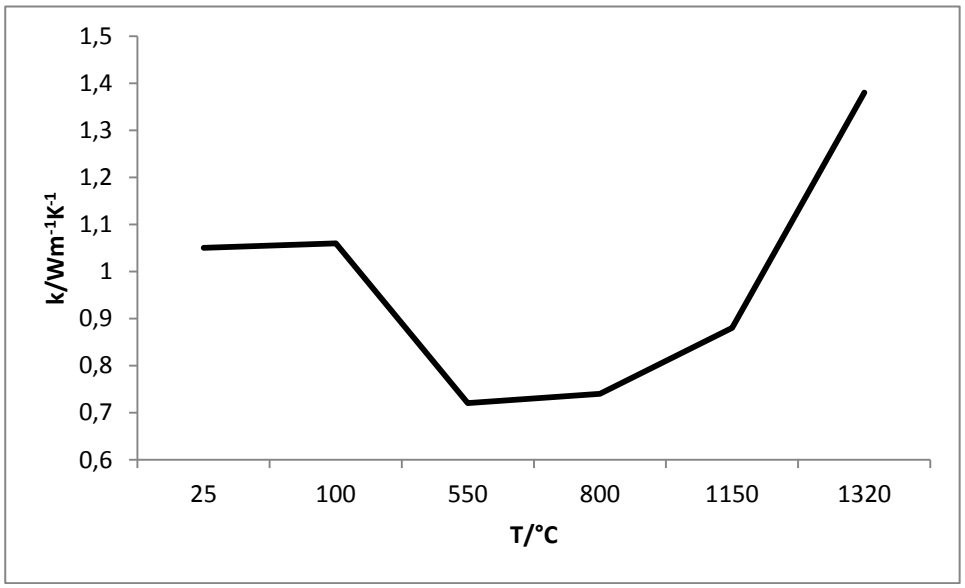

Slika 7. Temperaturna ovisnost toplinske vodljivost kvarcnog pijeska

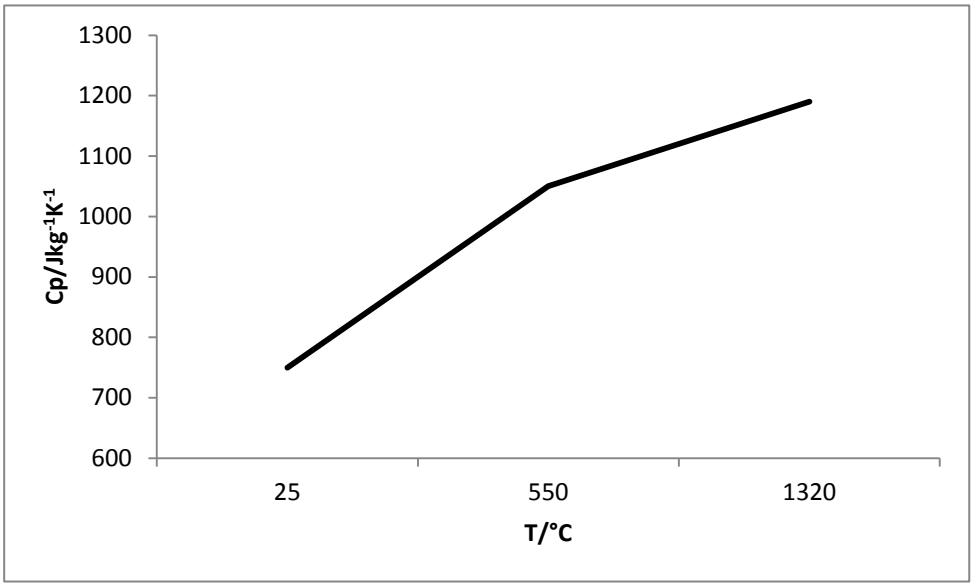

Slika 8. Temperaturna ovisnost specifične topline kvarcnog pijeska

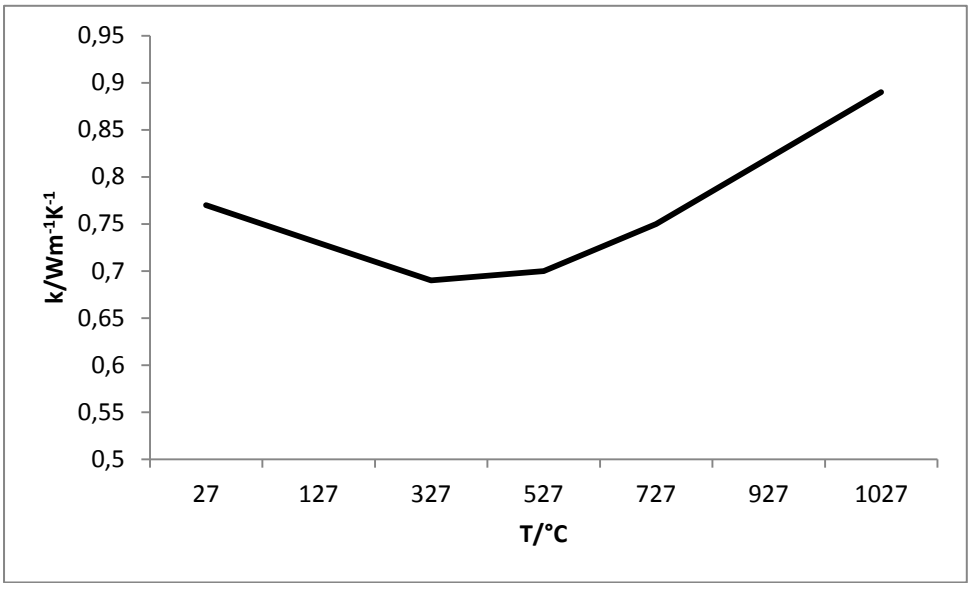

Slika 9. Temperaturna ovisnost toplinske vodljivosti kromitnog pijeska

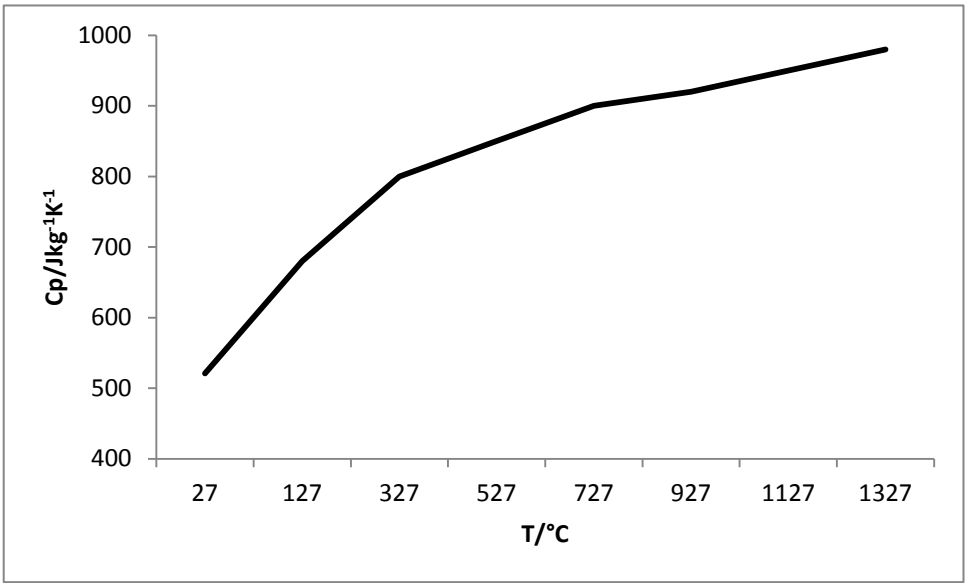

Slika 10. Temperaturna ovisnost specifične topline kromitnog pijeska

IMPLICITNA METODA PROMJENLJIVOG SMJERA (IAD)

Kod IAD metode vremenski interval Δt dijeli se na dva vremenska koraka, od kojih svaki traje $\Delta t/2$. Prostorna derivacija u jednadžbi (1) aproksimira se implicitno u *x* smjeru i eksplicitno u *y* smjeru tokom prvog $\Delta t/2$; postupak je obrnut tokom drugog $\Delta t/2$ - eksplicitno u *x* smjeru i implicitno u *y* smjeru. Neka $T_{i,j}^{*}$ označava temperaturu u točki (i,j) na kraju prve polovine vremenskog koraka, neposredno između t_n i t_{n+1}. Razmotrimo općenitu točku (*i,j*), koja ne leži na granici kao i na međuplohi kalup/metal. Tokom dvaju sukcesivnih vremenskih koraka, od kojih svaki traje $\Delta t/2$, odgovarajuće IAD aproksimacije jednadžbe (1) su:

$$\delta_x^2 T_{i,j}^{*} + \delta_y^2 T_{i,j}^{n} = \frac{1}{a_{i,j,n}} \frac{T_{i,j}^{*} - T_{i,j}^{n}}{\Delta t/2} \tag{5}$$

$$\delta_x^2 T_{i,j}^{*} + \delta_y^2 T_{i,j}^{n+1} = \frac{1}{a_{i,j,n}} \frac{T_{i,j}^{n+1} - T_{i,j}^{*}}{\Delta t/2} \tag{6}$$

Pri čemu $a_{i,j,n}$ označava temperaturnu vodljivost u točki (*i,j*) pri temperaturi $T_{i,j}^{n}$ na početku vremenskog koraka za kalup ili metal. Neka je recipročna vrijednost Fourierove značajke

$$z_{i,j,n} = \frac{(\Delta x)^2}{a_{i,j,n}\Delta t} \tag{7}$$

Odaberemo li pravokutnu mrežu ($\Delta x = \Delta y$), jednadžbe (5) i (6) mogu se pisati kao:

$$-T_{i-1,j}^{*} + 2\left(z_{i,j,n} + 1\right)T_{i,j}^{*} - T_{i+1,j}^{*} = T_{i,j-1}^{n} + 2\left(z_{i,j,n} - 1\right)T_{i,j}^{n} + T_{i,j+1}^{n} \tag{8}$$

$$-T_{i,j-1}^{n+1} + 2(z_{i,j,.n} + 1)T_{i,j}^{n+1} - T_{i,j+1}^{n+1} = T_{i-1,j}^{*} + 2(z_{i,j,n} - 1)T_{i,j}^{*} + T_{i+1,j}^{*} \quad (9)$$

U slučaju vertikalne granične plohe između kalupa i metala dobiju se IAD aproksimacije, i to za prvi $\frac{\Delta t}{2}$:

$$-\frac{2k_k}{k_k+k_m}T_{i-1,j}^{*} + 2(z_{i,j,n} + 1)T_{i,j}^{*} - \frac{2k_m}{k_k+k_m}T_{i+1,j}^{*} = T_{i,j-1}^{n} + 2(z_{i,j,n} - 1)T_{i,j}^{n} + T_{i,j+1}^{n} \quad (10)$$

gdje je

$$z_{i,j,n} = \frac{c_1}{k_k+k_m}\left(\frac{k_k}{a_k} + \frac{k_m}{a_m}\right) \quad (11)$$

i

$$c_1 = \frac{(\Delta x)^2}{\Delta t} \quad (12)$$

Za drugi Δt dobije se:

$$-T_{i,j-1}^{n+1} + 2(z_{i,j,n} + 1)T_{i,j}^{n+1} - T_{i,j+1}^{n+1} = \frac{2k_k}{k_k+k_m}T_{i-1,j}^{*} + 2(z_{i,j,n} - 1)T_{i,j}^{*} + \frac{2k_m}{k_k+k_m}T_{i+1,j}^{*} \quad (13)$$

U slučaju plohe koja leži na dijagonali pod kutom 45^0, odgovarajuće IAD aproksimacije su: prvi $\Delta t/2$:

$$-T_{l-1,j}^{*} + (z_{l,j,n} + 1)T_{l,j}^{*} = T_{l,j-1}^{n} + (z_{l,j,n} - 1)T_{l,j}^{n} \quad (14)$$

drugi $\Delta t/2$:

$$-T_{l,j-1}^{n+1} + (z_{l,j,n} + 1)T_{l,j}^{n+1} = T_{l-1,j}^{*} + (z_{l,j,n} - 1)T_{l.j}^{*} \quad (15)$$

pri čemu je $z_{l,j,n}$ kao u jednadžbi (7).

IAD metoda vodi do sustava simultanih algebarskih jednadžbi koje imaju tridijagonalni oblik, a za koji postoji posebno efikasan algoritam [6]. Prednosti IAD metode su:

a) Vrlo je efikasna zbog algoritma za brzo rješavanje tridijagonalnog sustava jednadžbi;
b) Bezuvjetno je stabilna i konvergira bez obzira na vrijednost Fourierove značajke;
c) Greška diskretizacije je O$[(\Delta x)^2 + (\Delta t)^2]$ te je prema tome drugog reda s obzirom na aproksimaciju prostora i vremena.

Na temelju danog algoritma može se napisati program u FORTRAN-u, a na slici 11. prikazan je dijagram toka.

Osnovna karakteristika programa je da se za pohranjivanje temperature koriste dvije matrice. Matrica T koristi se za pohranjivanje temperatura na početku i kraju cijelog vremenskog koraka, dok se matrica T^* koristi za pohranjivanje temperatura na kraju prvog $\Delta t/2$. Korištenje matrica ponavlja se tokom sukcesivnih vremenskih koraka pa je na taj način

izbjegnuta primjena trostruko indeksiranih matrica. Naravno, temperature treba periodički ispisati inače bi se njihove vrijednosti izgubile.

U glavnom programu prvo se čitaju ulazne varijable, a zatim pridaju početne vrijednosti matricama T i T^*. Ostatak glavnog programa sastoji se u primjeni implicitne metode promjenljivog smjera tokom sukcesivnih vremenskih koraka, prvo na rješavanje tridijagonalnog sustava redak po redak, a zatim stupac po stupac unutar zadane geometrije odljevka i kalupa. Indeks k određuje broj vremenskih koraka. Periodički se nakon svakih K_p koraka ispisuju vrijednosti vremena i temperature za pojedine mrežne točke. U slučaju da vrijeme t premaši propisanu graničnu vrijednost t_{max} računanje se prekida.

Glavni program sastoji se od sljedećih četiri potprograma i dviju funkcija:

1. Potprogram KOEFJ(j),za određivanje različitih tridijagonalnih koeficijenata za bilo koji redak j tokom prve polovine vremenskog koraka,
2. Potprogram KOEFI(i), za određivanje različitih treidijagonalnih koeficijenata za bilo koji stupac i tokom druge polovine vremenskog koraka,
3. Potprogram TRID1 i TRID2, za rješavanje tridijagonalnog sustava linearnih simultanih algebarskih jednadžbi, prvi redak po redak a drugi stupac po stupac.
4. Funkcije SVOJ1 i SVOJ2, za određivanje vrijednosti toplinskih svojstava u ovisnosti o temperaturi za pojedine mrežne točke.

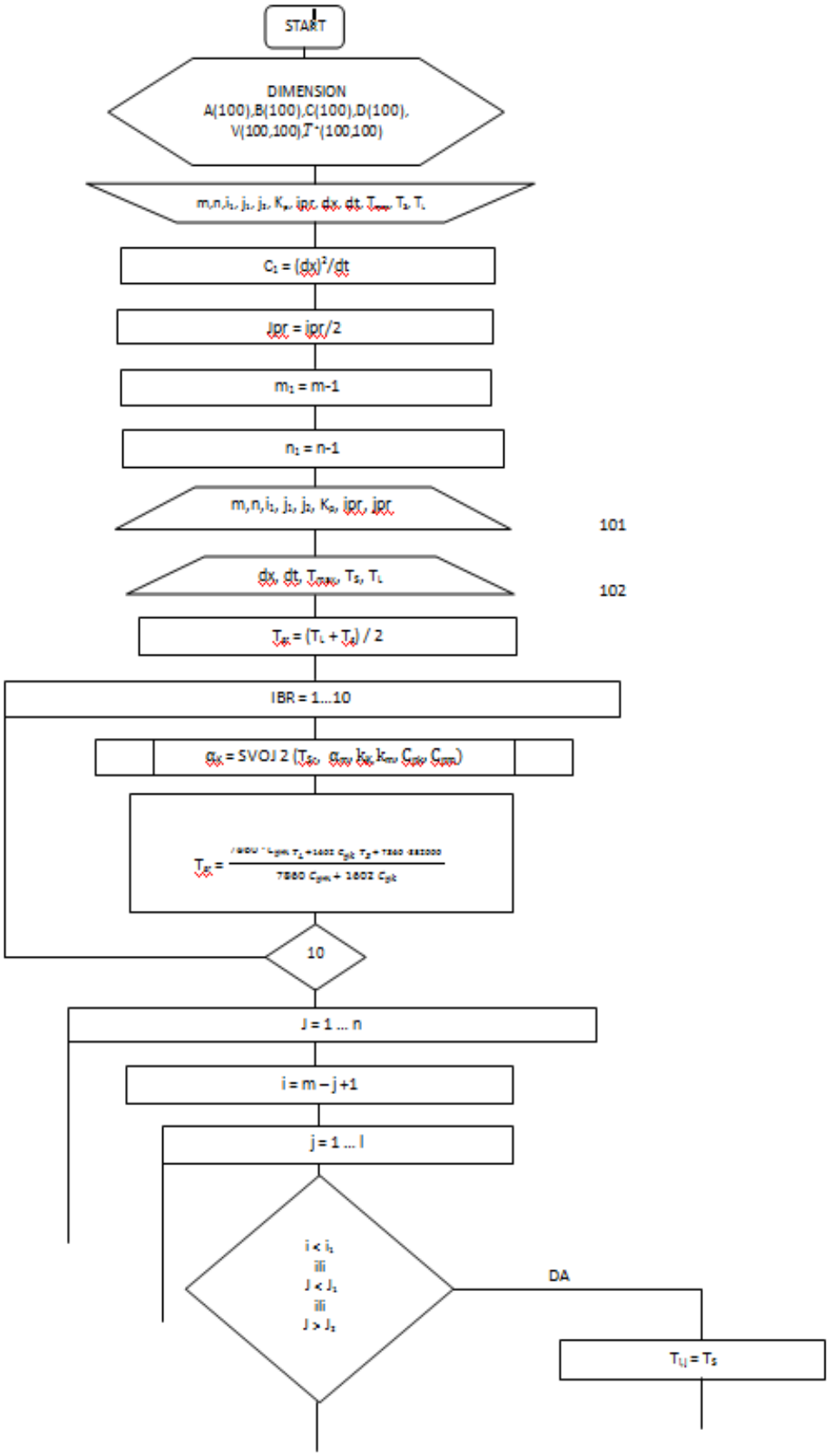
START
DIMENSION A(100),B(100),C(100),D(100), V(100,100),T*(100,100)
m,n,i1, j1, j2, Ks, ipr, dx, dt, Tpov, Ts, TL
C1 = (dx)²/dt
jpr = ipr/2
m1 = m-1
n1 = n-1
m,n,i1, j1, j2, Ks, ipr, jpr
101
dx, dt, Tpov, Ts, TL
102
Tpk = (TL + Ts) / 2
IBR = 1...10
αK = SVOJ 2 (Tpk, αpv, kk, km, Cpk, Cpm)
10
J = 1 ... n
i = m – j +1
j = 1 ... I
i < i1 ili J < J1 ili J > J1
DA
Tij = Ts

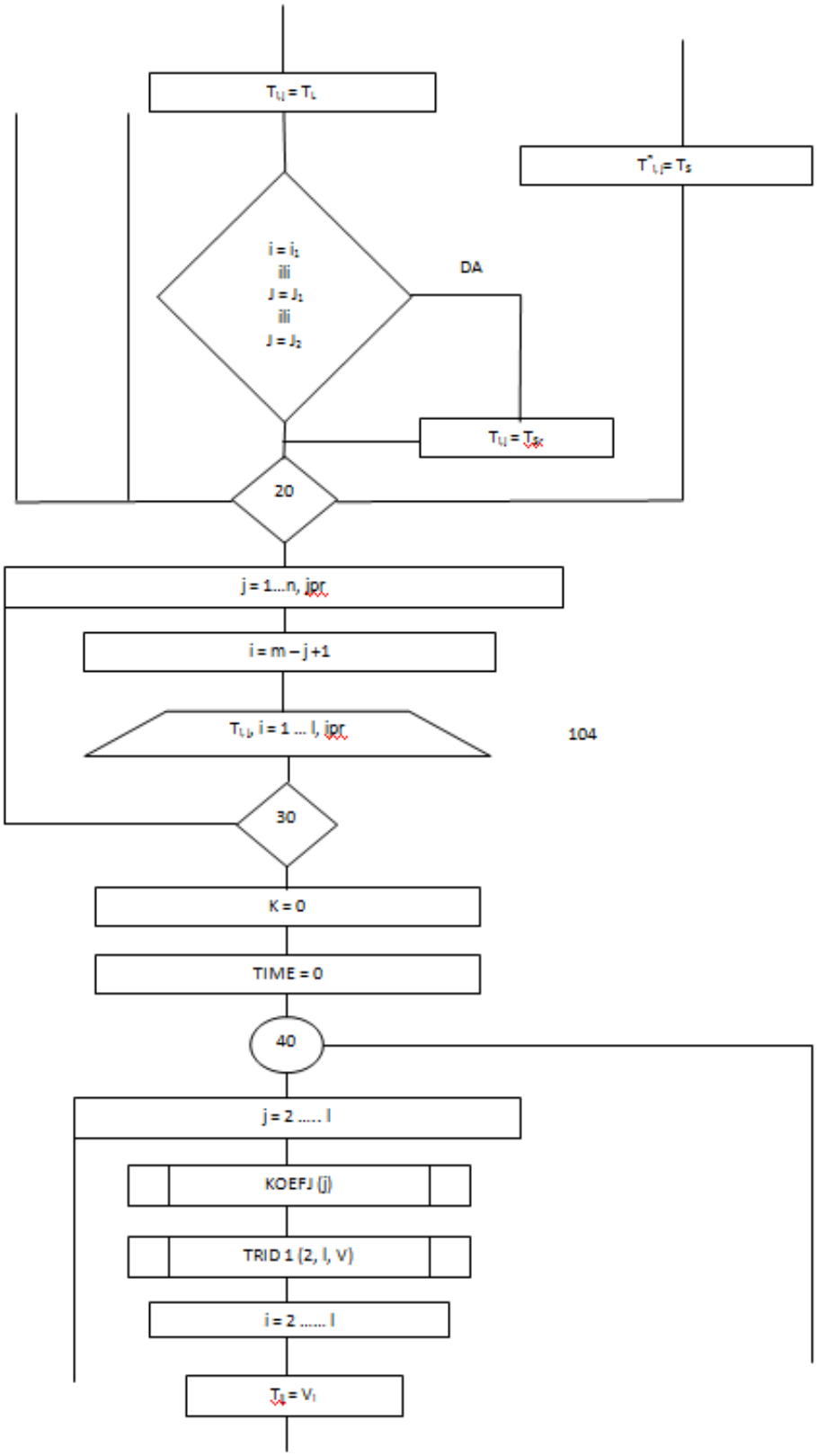
T(i,j) = T(i)
T*(i,j) = T(s)
i = i1
ili
J = J1
ili
J = J2
DA
T(i,j) = T(sk)
20
j = 1...n, jpr
i = m – j +1
T(i,j), i = 1 ... l, jpr
104
30
K = 0
TIME = 0
40
j = 2 l
KOEFJ (j)
TRID 1 (2, l, V)
i = 2 l
T(i) = V(i)

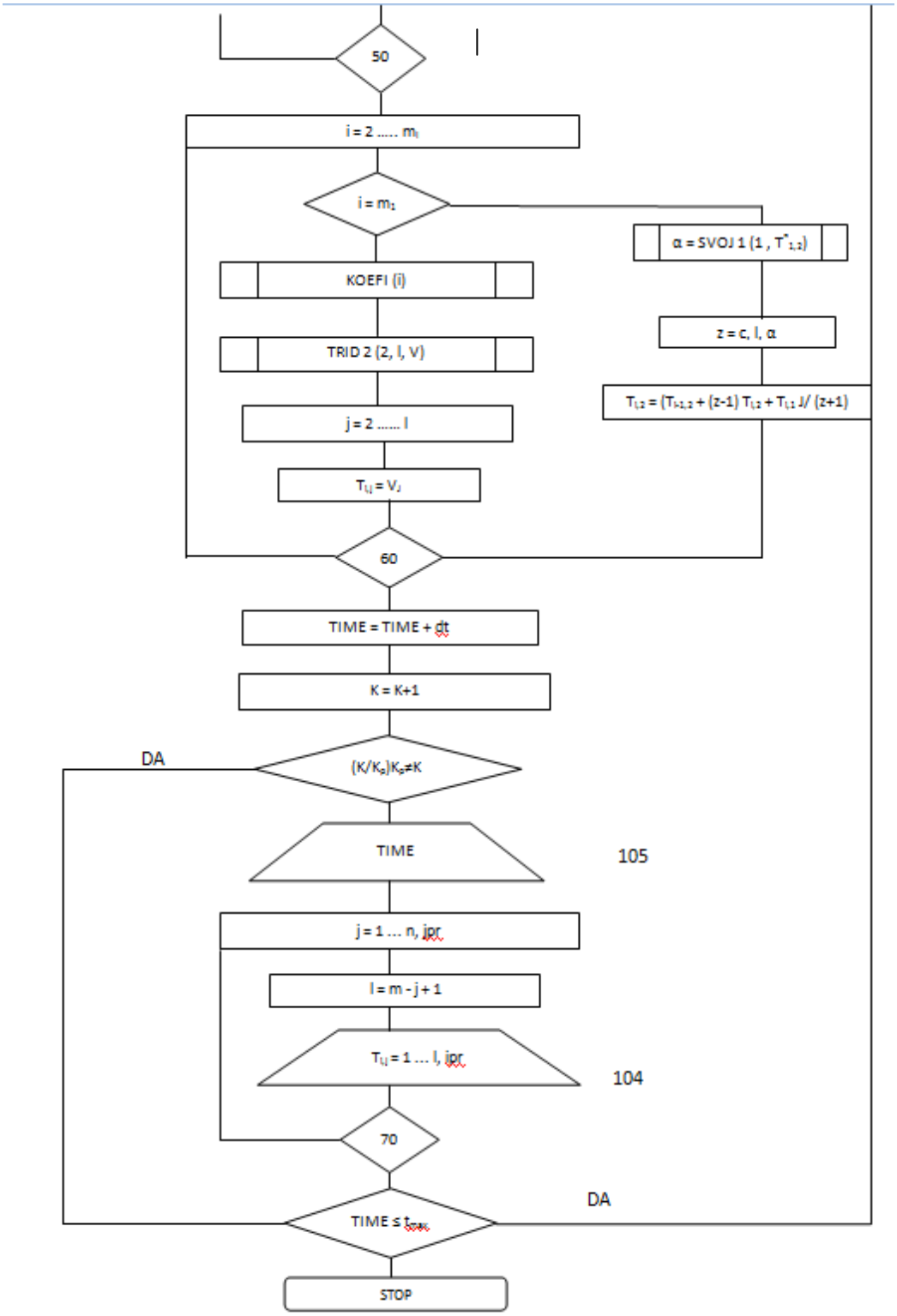

Slika 11. Dijagram toka

REZULTATI SIMULACIJE

U vremenu t=0 kalup i metal su pri početnoj temperaturi 25 °C odnosno 1580 °C. Odgovarajuće temperature na graničnoj plohi kalup-metal su 1538^0C za nisko ugljični čelik i 1565 °C za srednje ugljični čelik lijevan u kvarcni pijesak, odnosno 1500 °C za obadva čelika lijevana u kromitni pijesak. Toplina tokom vremena postupno prelazi iz odljevka u kalup. Odljevci progresivno skrućuju u intervalu temperatura od 1516,5 °C do 1478 °C za nisko ugljični čelični lijev i 1482 °C do 1427 °C za srednje ugljični čelični lijev.

Točnost simulacije uz pomoć računala ograničena je u nekim aspektima zbog potrebe uvođenja pretpostavki pri opisu procesa lijevanja i skrućivanja odljevaka. Međutim, ta ograničenja nisu tako izražena kao npr. ograničeno poznavanje toplinskih svojstava materijala, osobito kalupne mješavine te utjecaj granične plohe na mehanizam prijelaza topline.

Ograničavajući je faktor simulacije uz pomoć računala točnost podataka za toplinska svojstva čeličnog lijeva, a posebno kalupnog materijala. Toplinska svojstva pijeska funkcija su sastava, sadržaja vlage, metode kalupljenja, tvrdoće i njezine jednolikosti, kao i temperature. Iz tog razloga podaci za temperaturnu ovisnost toplinskih svojstava pijeska, naročito toplinske vodljivosti, pokazuju širok raspon rasipanja.

Sljedeći ograničavajući faktor je promjenljivost toplinskog toka tokom skrućivanja na granicama odljevka uslijed stezanja metala i pomicanja stjenke kalupa. Nastajanje zračnog raspora kao i odgovarajuće smanjenje prijelaza topline čak i kod pješčanih kalupa ograničuje točnost simulacije procesa skrućivanja i hlađenja odljevka.
Na slikama 12. do 15. prikazano je progresivno skrućivanje promatranih odljevaka u dvije vrste kalupnog materijala.

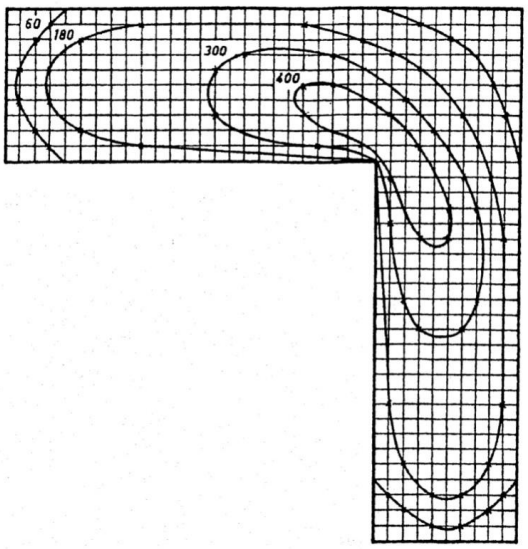

Slika 12. Napredovanje izosolidusa za odljevak od nisko ugljičnog čelika lijevanog u kvarcni pijesak za vremena 60, 180, 300 i 400 s

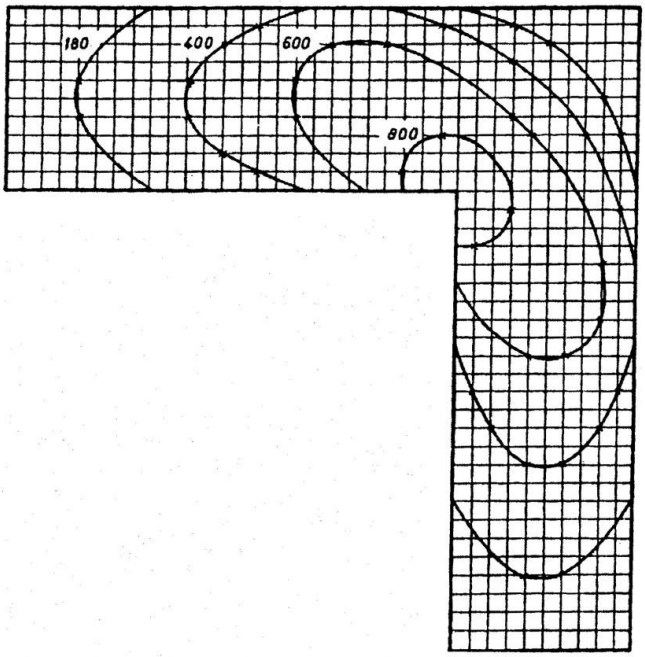

Slika 13. Napredovanje izosolidusa za odljevak od srednje ugljičnog čelika lijevanog u kvarcni pijesak za vremena 180, 400, 600 i 800 s

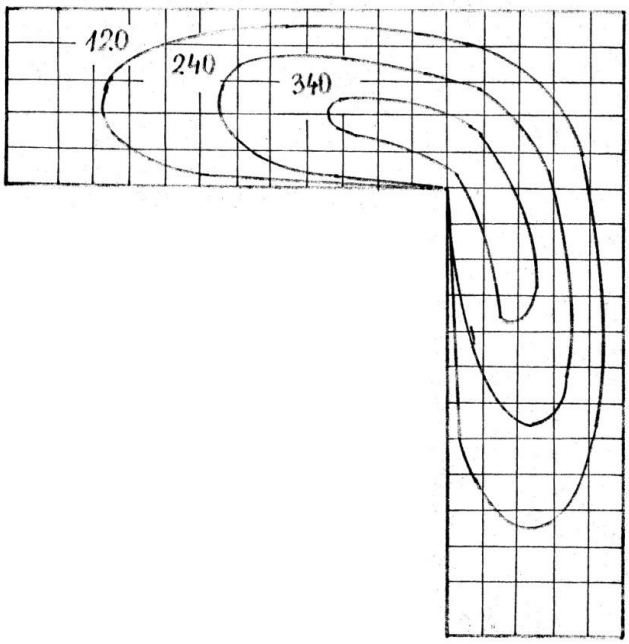

Slika 14. Napredovanje izosolidusa za odljevak od nisko ugljičnog čelika lijevanog u kromitni pijesak za vremena 120, 240 i 340 s

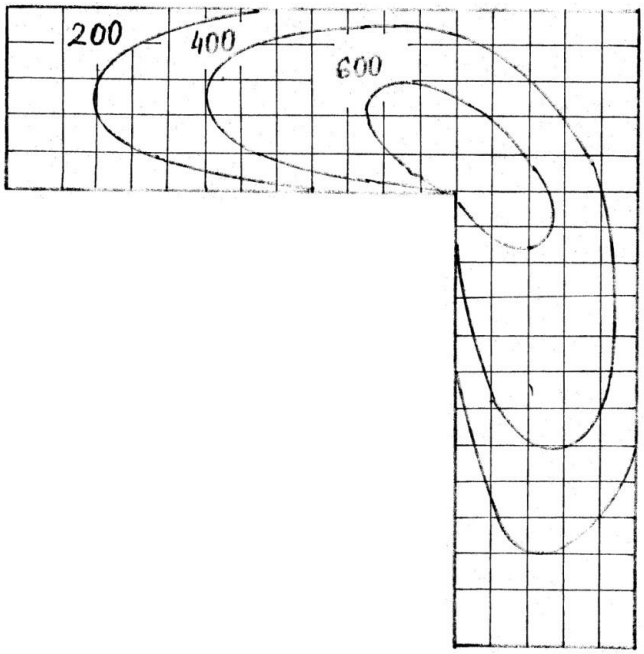

Slika 15. Napredovanje izosolidusa za odljevak od srednje ugljičnog čelika lijevanog u kromitni pijesak za vremena 200, 400 i 600 s

Iz slika se uočava da se vanjski ugao i ekstremiteti odljevka skrućuju prvi, a toplina se relativno sporo uklanja iz unutarnjeg ugla. Skrućivanje završava blizu unutarnjeg ugla, što predstavlja mjesto moguće pojave defekta u odljevku (usahline).

Na temelju predloženog matematičkog modela za vrijeme skrućivanja odljevka od nisko ugljičnog čeličnog lijeva dobije se 470 s, a za odljevak od srednje ugljičnog čelika 840 s, lijevanih u kvarcni pijesak. U slučaju lijevanja u kromitni pijesak vrijeme skrućivanja nisko ugljičnog čeličnog lijeva 360 s, a srednje ugljičnog 750 s. Prema tome, čelični odljevci lijevani u kromitni pijesak brže skrućuju nego oni lijevani u kvarcni pijesak.

ZAKLJUČAK

U radu je formuliran i istražen matematički model skrućivanja i hlađenja čeličnih odljevaka u pješčanim kalupima koji se temelji na prijelazu topline provođenjem. U model su inkorporirani početni i rubni uvjeti, kao i temperaturno ovisna toplinska svojstva materijala (toplinska vodljivost i specifični toplinski kapacitet), a u intervalu skrućivanja, tj. između likvidusa i solidusa, ugrađena je entalpija skrućivanja. Numerička analiza provedena je korištenjem implicitne metode promjenljivog smjera (IAD), koja je odabrana zbog velike preciznosti pri aproksimaciji prostora i vremena. Simulacija je provedena za nisko i srednje ugljični čelik lijevan u kvarcni i kromitni pijesak. Na temelju pomicanja izosolidusa moguće je vidjeti točke u kojima se javlja defekt (točke koje zadnje skrućuju), u blizini unutarnjeg ugla odljevka. Također je definirano trajanje skrućivanja od 470 s za nisko ugljični i 840 s za srednje ugljični čelični odljevak lijevan u kvarcni pijesak, odnosno 360 s i 750 s za čelik lijevan u kromitni pijesak. Dobiveni rezultati omogućuju da se na moderan i znanstveni način vidi

kako odabir pojedine vrste kalupnog materijala utječe na tijek skrućivanja i hlađenja odljevaka.

LITERATURA

[1] E.R.G. Eckert, R.M. Drake, Analysis of Heat and Mass Transfer, McGraw-Hill Kogakusha, Tokyo, 1972.
[2] V. Grozdanić, V. Novosel-Radović, R. Dmitrović, AFS Transactions 100(1992) pp.265-271.
[3] V. Grozdanić, J. Črnko, Železarski zbornik 25(1991)4, pp.149-158.
[4] R.D. Pehlke, A. Jeyarajan, H. Wada, Summary of Thermal Properties for Casting Alloys and Mold Materials, University of Michigan, Ann Arbor, 1982.
[5] P.R. Sahm, P.N. Hansen, Numerical simulation and modelling of casting and solidification processes for foundry and cast-house, CIATF, Zurich, 1984.
[6] B. Carnahan, H.A. Luther, J.O. Wilkes, Applied Numerical Methods, John Wiley, New York, 1969.

15th INTERNATIONAL FOUNDRYMEN CONFERENCE
INNOVATION – The foundation of competitive casting production
Opatija, May 11th-13th, 2016
http://www.simet.hr/~foundry/

EFFECT OF MELT SUPERHEAT ON THE MICROSTRUCTURAL DEVELOPMENT OF CENTRIFUGALLY CAST HIGH CARBON HIGH SPEED STEEL ALLOY

U. Klančnik[1], M. Drobne[1], B. Kosec[1], P. Mrvar[2] and J. Medved[2]

[1]Valji d.o.o., Štore, Slovenia
[2]University of Ljubljana Faculty of Natural Sciences and Engineering, Ljubljana, Slovenia

Poster presentation
Original scientific paper

Abstract

Melt superheat has a profound effect on the development of as-cast microstructure in steels. With decreasing superheat, the density of stable nuclei generally increases thus favoring equiaxed growth to columnar growth. In the case of centrifugal casting, three solidification zones typically occur in the radial cross section of the casting wall: the chilled zone near the mould-metal interface followed by the columnar zone and the equiaxed zone in the final solidification interval. The goal of this research was to study the effect of melt superheat on the columnar to equiaxed zone transitionin centrifugal castings.
The investigation was carried out on a high carbon high speed steel alloy used for working layers in rolls, generally used in the first finishing stands in hot strip mills. The alloy was centrifugally cast in a laboratory-scale centrifugal casting device. Three separate castings were made, each with a different melt superheat upon casting: 40, 80 and 120 °C. Other parameters such as melt preparation, mould pre-heat temperature, mould rotation speed and casting dimensions remained unchanged for all investigated castings. The results showed a considerable difference in the as-cast microstructure between the three sample castings. With decreasing the melt superheat, the thickness of the dendritic zone also decreased. The equiaxed zone in turn increased in accordance with the increased nuclei density theory. The overall microstructure at lower superheats was found to be finer, with evenly distributed eutectic carbides. The results of this study can serve as a basis for as-cast microstructure improvement in centrifugal casting.

***Keywords**: centrifugal casting, melt superheat, microstructure, high speed steel*

*Corresponding author (e-mail address): *urska.klancnik@valji.si*

INTRODUCTION

In examining as-cast macrostructures of ingot casting cross sections, three zones are expected: the outer chilled zone, which appears near the mould-melt interface, the

intermediate columnar zone, appearing adjacent to the chilled zone and finally, the innermost equiaxed zone with a fine grain-like structure. The same is expected in the case of centrifugal casting throughout the radial cross section of the casting [1-4]. Wu *et. al.*[1] have established, that an equiaxed microstructure is beneficial in improving mechanical properties of centrifugal cast ingots, such as wear resistance and tensile strength. High speed steels, especially with a high carbon level, generally exhibit a hypo-eutectic microstructure with a relatively high ratio of MC, M_2C or M_6C type eutectic carbides [5, 6]. Studies have shown that increasing the cooling rate of the solidifying material restrains the precipitation of eutectic carbides, as well as promotes the development of well-oriented columnar grains [1]. Indeed, several studies have been focused on the impact of various physical parameters on the development of microstructure (mould surface texture, gas atmosphere, mould pre-heat temperature, etc.) [4, 7]. Few parameters have been proven to have such a profound impact on solidification as melt superheat.

In this work we shall refer to superheat (ΔT_{SH}) as the increase of temperature in regards to the liquidus temperature (T_L) of the material upon pouring (i.e. pouring temperature, T_P), Eq. 1:

$$\Delta T_{SH} = T_P - T_L \tag{1}$$

The work of Strezov*et. al.* [5] has shown a strong dependence of nucleation density (nuclei per mm^2) on the degree of superheat. In the case of austenitic stainless steel 304, the dependence appears to have a parabolic trend; the nucleation density lowers parabolicallywith increasing superheat. Experiments performed on 17%Cr ferritic stainless steel in the case of twin-roll strip casting give similar results coupled with structural development in dependence on the degree of superheat [8]. It is seen that with decreasing superheat, the structure of fully oriented columnar grains slowly transitions into a fine equiaxed structure.The transition between both structures is termed columnar to equiaxedtransition (CET). CET is strongly dependent on the temperature gradient in front of the solid-liquid interface, the growth speed of the crystal and on the degree of undercooling [3]. By decreasing superheat, the density of heterogeneous nuclei increases and the temperature gradient decreases, both in favor of the equiaxed grain growth.

Oriented columnar grains exhibit a strong anisotropy. In the case of roll production, an anisotropic outer layer could influence the deterioration of sustainability in terms of wear and fire cracking resistance during rolling operations. In this view a finer equiaxed grain structure would be advantageous in assuring overall isotropic properties of the outer roll layer. In this research we intended to study the effect of melt superheat on the CET for quality improvement and better added value of the finished product starting from the as-cast structure.

MATERIALS AND METHODS

In order to study the influence of melt superheat on the as-cast structure of centrifugally cast ingots, three sample castings were made in a laboratory-scale centrifugal casting device. A high carbon high speed steel melt was prepared from steel and cast iron scrap, pig iron and ferroalloys. The chemical composition of the castings was determined with a spectrometer using a spark ignition. The material was melted in an induction furnace with a bearing of 500 kg and heated to 1600 °C before discharge. A quantity of 200 kg was discharged from the furnace to the intermediate ladle. Approximately 50 kg of melt was then poured into a steel mould rotating at 1150 rpm, to form a 310 mm long hollow cylinder casting with an outer diameter of 270 mm. The temperature of the casting during spinning was monitored using a calibrated optical pyrometer. At around 1000 °C the device was stopped and the casting left to cool inside the mould. The casting and the laboratory centrifugal casting device are shown in Figure 1.

Figure 1. High carbon high speed steel hollow cylinder casting in front of the laboratory centrifugal casting device

The pouring temperature represented the variable of melt superheat. The set parameters of melt superheat according to Eq. 1 are presented in Table 1 including the wall thickness of the finished castings.

Table 1. Superheat (ΔT_{SH}) parameters with wall thickness of three investigated sample castings

Sample casting label	**A**	**B**	**C**
ΔT_{SH}(°C)	120	80	40
Thickness (mm)	33	31	36

Samples (shown in Figure 2) were taken from the middle of the castings for metallographic and structural analysis of the casting wall cross section.

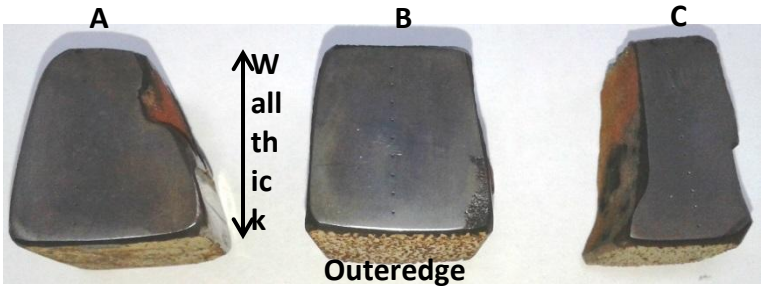

Figure 2. Samples taken from the middle of the centrifugal castings A, B and C for a structural assessment of the casting wall. Outer edge represents the mould interface

The middle of the casting was chosen, since the temperature gradient during solidification there is perpendicular to the mould-melt interface and the solidification front advances unidirectionally. The samples were prepared with a standard metallographic procedure of grinding, polishing and etching in Villela's reagent to reveal the microstructure. Optical microscopy was conducted using an Olympus BX51M optical microscope equipped with Olympus DP-12 camera. Evaluation of the carbide ratio was performed with JMicroVisionv.1.2.7 software. Hardness of the samples was measured using an Emco test Rockwell hardness tester.

RESULTS AND DISCUSSION

The results of the measured chemical composition of all three investigated castings are presented in Table 2.

Table 2. Chemical composition of all three investigated castings (in mass %)

	C	Mn	Cr+Mo+W	V+Nb	Fe
A	1.90	0.76	9.34	5.58	79.55
B	1.91	0.79	9.69	5.14	80.42
C	1.90	0.89	9.83	5.37	79.97

Upon metallographic examination of the samples, two distinct structures were visible: an apparent dendritic and an even equiaxed grain structure. A clear columnar grained zone was not confirmed in the examined samples, most likely due to the complex eutectic carbide composition of the microstructure. It is safe to assume, that potential columnar grains would appear similar to dendrites lacking a familiar unidirectionality. Optical microphotographs of the investigated samples are shown in Figure 3.

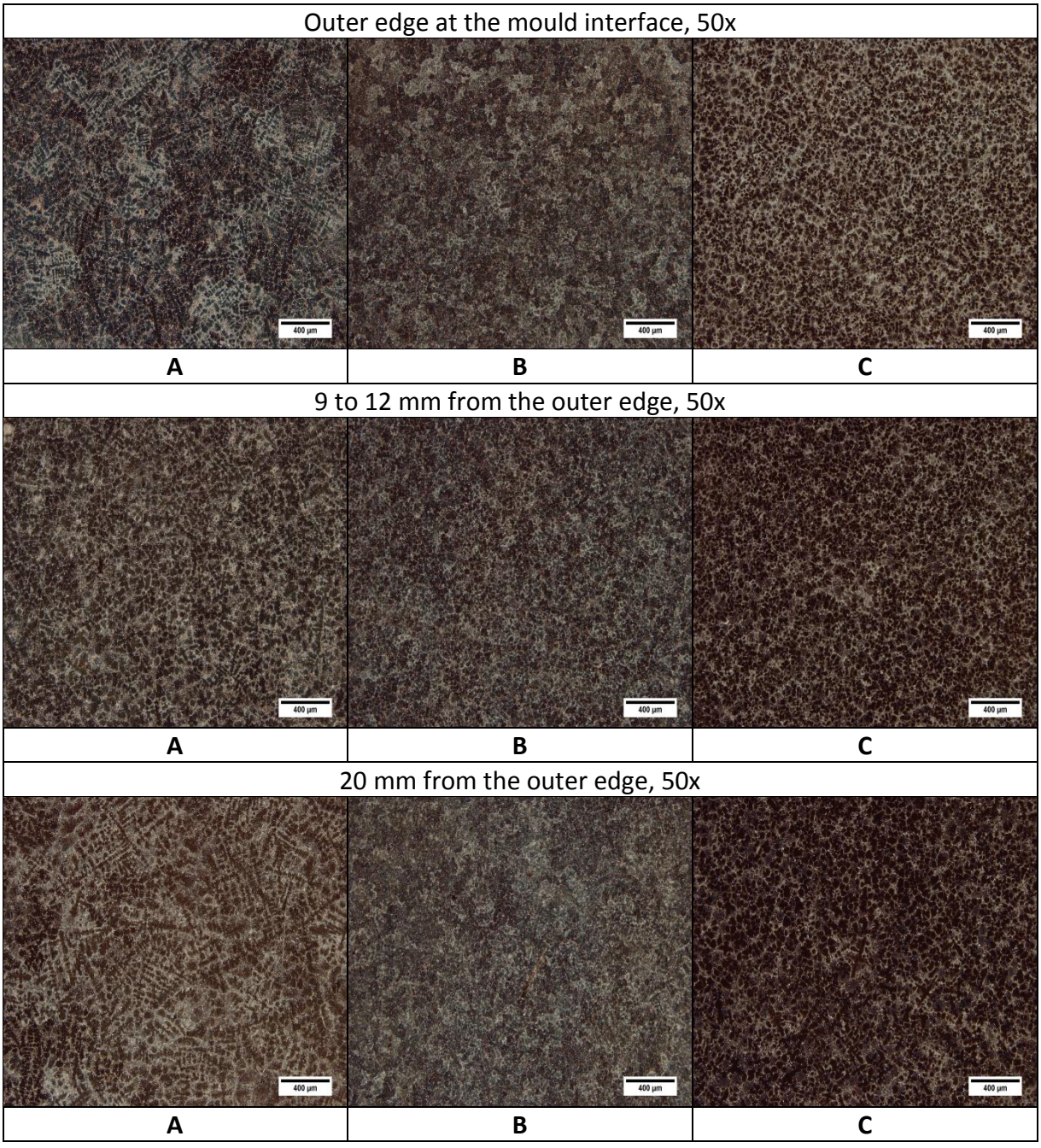

Figure 3. Optical microphotographs of examined samples through the casting wall cross section. Two distinct structures are visible: dendritic and equiaxed grain structure

As is shown in optical microphotographs in Figure 3, both samples A and B reveal a dendritic structure at the outer edge near themould interface. While the dendrites are clearly distinguishable in sample A, the structure in sample B appears to be already somewhat refined as a result of lower melt superheat. A difference in etching coloration reveals a different crystal orientation of dendrite colonies in samples A and B.The outer edge

structure of sample C reveals a structure that appears to consist completely of fine equiaxed grains with evenly distributed eutectic carbides on grain boundaries.

After the initial dendritic structure at the outer edge, both samples A and B exhibit a dendritic to equiaxed grain transition (DET) towards the middle of the casting wall. In sample A, the DET occurs at 9 mm from the outer edge. The equiaxed grain zone in sample Areaches to about 12 mm, where the reverse equiaxed grained to dendritic transition occurs (EDT). This is a direct result of the casting geometry. As a hollow cylinder, the casting wall undergoes two solidification fronts, both advancing inwards the casting wall; one from the outer edge at the mould interface and the other from the inner edge where heat dissipates through contact with air. This gives the wall's cross section a semi-symmetrical structure. In the case of sample B, the DET occurs at 6 mm and the EDT at 18 mm. Sample C does not exhibit a DET as the structure at the outer edge is already equiaxed. However, an EDT is visible in sample C occurring just under 20 mm. A schematic drawing of the sample's cross section is shown in Figure 4.

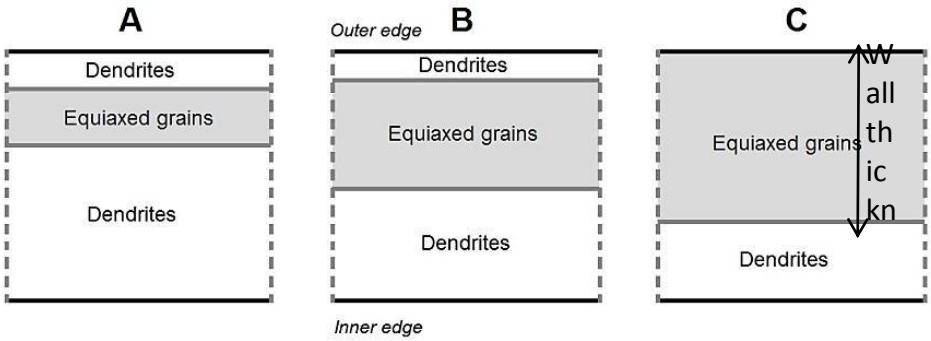

Figure 4. A schematic drawing of the structure through the casting wall cross section for three investigated castings

The drawing in Figure 4 shows the change in structural zones which occurs as a result of melt superheat reduction. At a relatively high melt superheat (sample A) the equiaxed grain zone is quite narrow and appears near the outer edge of the casting wall. As the melt superheat is reduced, the equiaxed zone expands which is in good agreement with the results published in literature [1-3,8]. Another observation shows that the equiaxed zone appears to expand at a fixed position relative to the wall's outer edge. This could be explained in view of dendrite arm breakage and consequent heterogeneous nucleation during solidification. The narrow equiaxed zone shown in Figure 4 for sample A shows the location where the intensity of dendrite arm breakage and nuclei count is sufficiently high to develop an even equiaxed grain structure. This location appears to be located in the same spot regardless of the melt superheat upon pouring. We can assume that the intensenucleation spot is set by different parameters (i.e. mould pre-heat temperature, rotation speed, melt modification, etc.).

The decreasing melt superheat however does affect the thickness of the equiaxed grain zone. This dependence is shown in Figure 5.

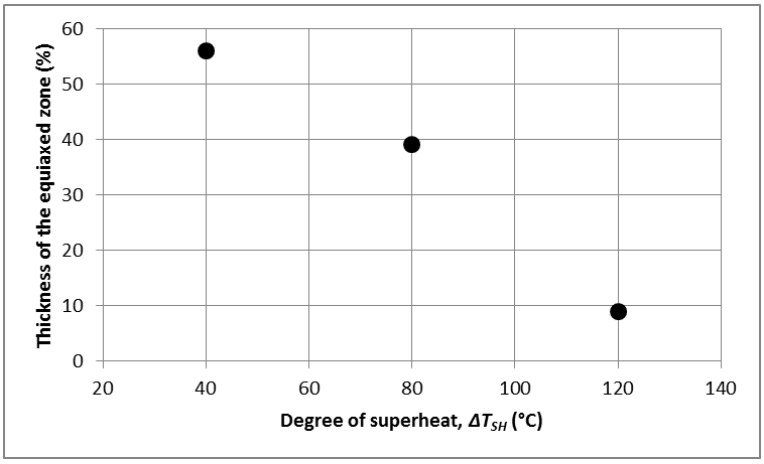

Figure 5. The thickness of the equiaxed zone relative to the casting wall thickness for three investigated samples

Results in Figure 5 show thatthe thickness of the equiaxed zone increases rapidly with decreasing melt superheat. At 40 °C melt superheat, the equiaxed zone encompasses over half of the entire wall thickness compared to less than 10 % at 120 °C melt superheat.

A quantitative analysis of the carbide ratio was performed on the investigated samples in dependence on the wall thickness. Results of the quantitative analysis are shown in Figure 6.

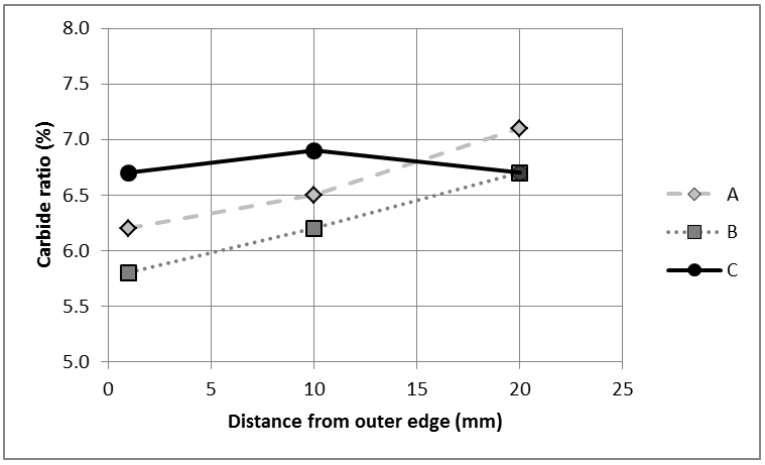

Figure 6. Quantitative analysis of carbide ratio in dependence on casting wall thickness for three investigated samples

The measurement of carbide content shown in Figure 6 reveals an increasing tendency towards the wall's inner edge for samples A and B. A slightly smaller amount of carbide content is detected at the outer edge. This could be explained by the chilled fine dendritic structure as a result of faster solidification. The carbide ratio slowly increases towards the inner edge, where the ratio in sample A is slightly higher than that in sample B. Sample C revealed an almost steady carbide ratio throughout the wall thickness to 20 mm in depth.

This result confirms an even equiaxed grain structure from the outer edge of the sample to the final measured point at 20 mm. The scatter ratio for sample C is thus only 3 %, where for samples A and B it reaches up to 6 %.

Figure 7 shows the results of the hardness measurement in dependence on wall thickness for the investigated samples.

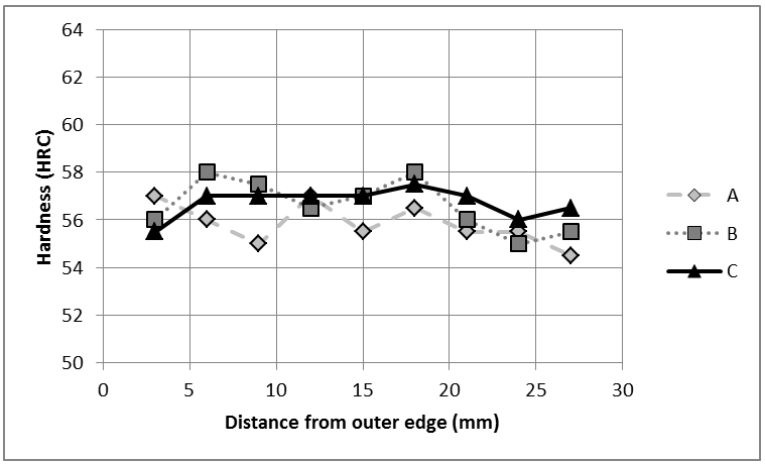

Figure 7. Hardness of the investigated samples in dependence on the wall thickness

The measured hardness shown in Figure 7 shows a rather scattered dependence on wall thickness for samples A and B, while the results for sample C are somewhat more even. While the measured hardness for sample A is strongly scattered throughout the wall thickness, sample B does exhibit an approximate plateau (±0,5 HRC) between 6 and 18 mm which corresponds to the location of the equiaxed zone in sample B. The hardness after 18 mm drops rather suddenly for up to 3 HRC. A similar apparent plateau is visible for sample C ranging from 6 to 21 mm, afterwards it decreases for up to 1 HRC. This also corresponds to the even hardness exhibited at the equiaxed zone with a drop in hardness at the EDT. The average hardness for the three samples is shown in Table 3.

Table 3. Average hardness for three investigated samples

	A	B	C
Average hardness (HRC)	55,8 ± 0,3	56,6 ± 0,4	56,7 ± 0,3

The results shown in Table 3 revealthat for sample A, where the equiaxed zone is the narrowest, the average hardness is the lowest. Both samples B and C show an improvement of about 1 HRC.

CONCLUSIONS

The investigation of structure development in dependence on melt superheat in the case of centrifugal casting gave similar results to those published for twin strip or continuous

casting. Results show that with decreasing melt superheat the equiaxed grain zone increases as a result of a higher nuclei count due to dendrite arm breakage and heterogeneous nucleation. The equiaxed zone appears always in the same location given that the casting parameters remain the same. Carbide ratio measurement showed an even carbide distribution in the equiaxed zone whereas the scatter ratio for samples with a more dendritic structure is higher. Hardness measurement confirmed more constant properties in the equiaxed zone compared to the dendritic region, where hardness dropped to up to 3 HRC. These results give a good basis for material improvement with adjusting melt superheat prior to pouring. With lowering the melt superheat to 40 °C a more even structure can be expected in a larger area thus achieving a more constant carbide distribution and hardness.

REFERENCES

[1]X.Q.Wu, H.M.Jing, Y.G. Zheng, Z.M. Yao, W. Ke, Z.Q. Hu, The eutectic carbides and creep rupture strength of 25Cr20Ni heat-resistant steel tubes centrifugally cast with different solidification conditions, Materials Science and Engineering A, 293 (2000) 1-2, pp. 252-260
[2] K. Ito, R. Sahara, S. Farjami, T. Maruyama, H. Kubo, Evolution of Solidification Structures in Fe-Mn-Si-Cr Shape Memory Alloy in Centrifugal Casting, Materials Transactions, 47 (2006) 6, pp. 1584-1594
[3] L. Zongqiang, Z. Weiwen, X. Baoliang, L. Yuanyuan, Control of equiaxed grains in a complicated Cu-Ni based alloy prepared by centrifugal casting, 69th World Foundry Congress 2010, World Foundry Organization Ltd, November, 2010, Hangzhou, China, pp. 141-144
[4] ASM Metals Handbook Volume 15 – Casting, ASM International, 1998
[5] Z. Tianming, W. Qinjuan, S. Xuding, F. Hanguang, Effectofcastingtechnology on microstructureandphasesofhighcarbonhighspeedsteel, ChinaFoundry, (2011) 2, pp. 197-201
[6] Y. Sano, T. Hattori, M. Haga, CharacteristicsofHigh-carbonHighSpeedSteelRollsforHot Strip Mill, ISIJ International, 32 (1992) 11, pp. 1194-1201
[7] L. Strezov, J. Herbertson, Experimental Studies of Interfacial Heat Transfer and Initial Solidification Pertinent to Strip Casting, ISIJ International, 38 (1998)9, pp. 959-966
[8] H.T. Liu, Z.Y. Liu, Y.Q. Qiu, G.M. Cao, C.G. Li, G.D. Wang, Characterization of the solidification structure and texture development of ferritic stainless steel produced by twin-roll strip casting, Materials characterization, 60 (2009), pp. 79-82

15th INTERNATIONAL FOUNDRYMEN CONFERENCE
INNOVATION – The foundation of competitive casting production
Opatija, May 11th-13th, 2016
http://www.simet.hr/~foundry/

VIRTUAL QUALITY ANALYSIS OF THE CASTS USING CAE TECHNIQUES ON SPECIFIC CASES

S. Manasijević[1], R. Radiša[1], J. Pristavec[2] and V. Komadinić[1]

[1]Lola Institut, Belgrade, Serbia
[2]Exoterm-IT d.o.o., Kranj, Slovenia

Poster presentation
Professional paper

Abstract

The paper shows the application of modern information technology to the virtual analysis of the quality of castings in several samples (Buckets Pelton turbine, LED lamp housing and excavator tooth holder). The MAGMA[5] software package was used to optimize the relevant technological parameters of casting and for analysing the quality of castings. It has been shown from the obtained results that potential problems can be easily identified and eliminated at the design stage of castings, which enables the product and tool designer and engineer to optimize all relevant parameters of the casting process. In addition to shortening the product development time and reducing the costs, this establishes a better process control, increases the quality and reduces the price of new product.

Keywords: *a virtual analysis of the quality, MAGMA[5], CAE, casting process simulation*

*Corresponding author (e-mail address): *srecko.manasijevic@li.rs*

INTRODUCTION

Foundry, as a vital branch of the industry is currently facing many challenges. On one side, founders have to satisfy arising expectations of the buyers in terms of securing quality, shorter time for product realization, smaller-scale series, lower and more competitive prices. On the other hand, the foundries are losing touch in terms of fast technological and managerial changes in manufacturing sectors. This dance of founder's skills and hardly predictable nature of the cast metal is a walk on the fine line separating success from failure, good cast from the one that needs to be returned to the furnace [1].

Today we have primary use of NC processing machines that require dimensionally stable casts with uniform hardness of the surface for preventing damages of cutting tools. Comparing current condition with the one ten years ago it is noticeable that most countries

reduce number of foundries (not only in our country, but in wider region), which is compensated by adequate increase of manufacturing scope.

Increase of competition and survival in the worlds market is visible in speed of technical innovation transfer. This is the reason why is necessary to launch quality new products, produced in the shortest possible period and will smaller costs. Shortening time for replacing new products in the market is followed by increased demands for functionality, design, economy, etc. This means that the following requests are set before the industry: shortening development time, reducing manufacturing expenditures, quality improvement, increasing safety, improving design and functionality and meeting ecological standards. Meet the requests on severe market conditions is only possible by using contemporary software packages, i.e. tools that fasten conquering new products (from idea, construction, selection of materials and procedures, different calculations, simulation, making a prototype, making a cast, to manufacturing a product). This integral approach in conquering new product unquestionably increase competitive power on the market.

By using contemporary techniques (CAD/CAM/CAE) of product design and contemporary techniques for computer simulation of casting process shortens time for cast development and it´s price. Current wide knowledge of the process enables foreseeing impact of relevant technological parameters of the casting and solidification of the casts. This results in modelling solidification process, development of program for computer simulation of the casting simulating events from the very process and graphically displays results. Computer simulation of casting proves is a description of the actual state using a logical mathematical-physical model. All physical laws under which this process unfolds with margin conditions are entered into a mathematical model processed by a computer.

Until recently all this was based on traditional casting technology, on informal skills and intuition of the foundry men, however, it is now a subject of exact calculations with high probability of predicting final results. Nowadays, there are several software packages for simulation of casting and solidification (MAGMA[5], ProCast, Access, etc.). They read graphic formats such as *.stl* and *.step*. Creating 3D geometry model is made by using CAD software packages exporting into these formats [2−4].

Simulation of casting process has been used in foundries for 30 years. In time, software packages were very developed and encompass every segment of a casting. Main goal of using these software packages is optimizing relevant technological casting parameters and increasing process efficiency and cast quality. Practical application of these programs is that they are adjusted for demonstration and optimization in small plants and testing in industrial conditions. It has been showed that in current run of technological development of the foundry where they are not using these software packages lose touch and unfortunately disappear from the market.

Goal of this paper is to use specific cases for showing advantages of using software packages for virtual quality analysis of the casts using CAE techniques.

MATERIALS AND METHODS

MAGMA GmbH is research & development center in Germany that has been known to all foundries in the world for some time now with its software package MAGMASOFT® (now MAGMA^5). This research center has developed an overall program package of the new generation designed for simulating foundry processes. For simulation execution it is necessary to provide: 3D geometric model of a cast and other components (casting tools, firth system, feeder…), technological parameters (cast temperature, casting time, alloy contents, etc.). MAGMA^5 reads graphic formats such as *.stl* and *.step*. This means that previously constructed 3D models can be used (by some CAD software, Figure 1a, 1c and 1d) and entered into graphic station MAGMA^5 as originals (Figures 1b, 1d and 1f). There is an option of constructing simple 3D geometry models in MAGMA^5.

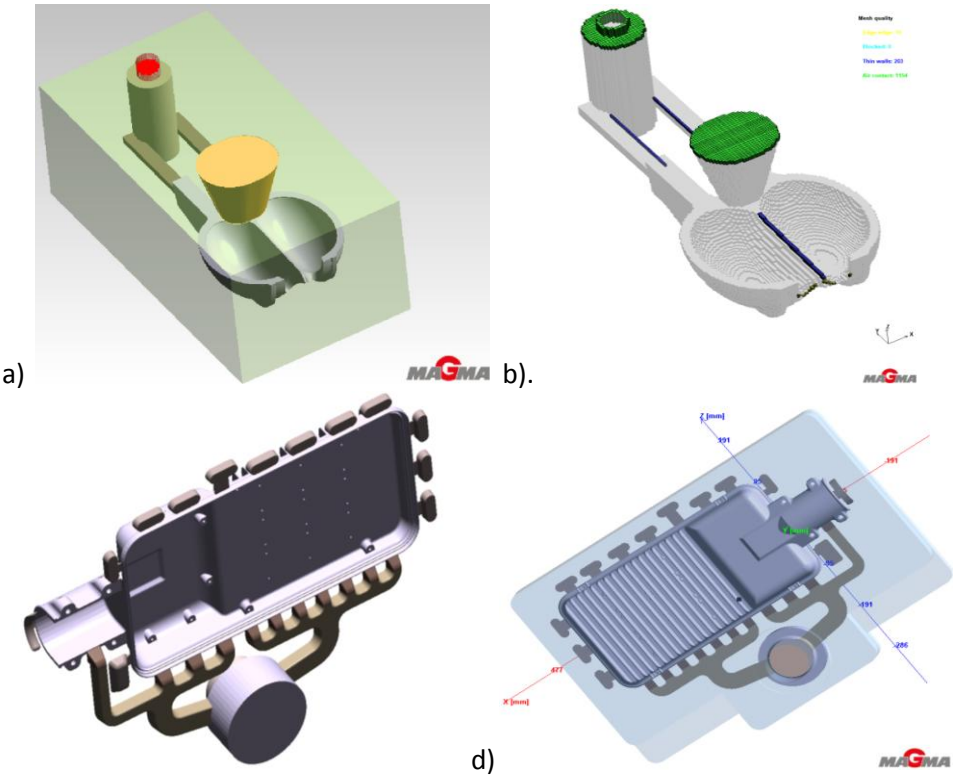

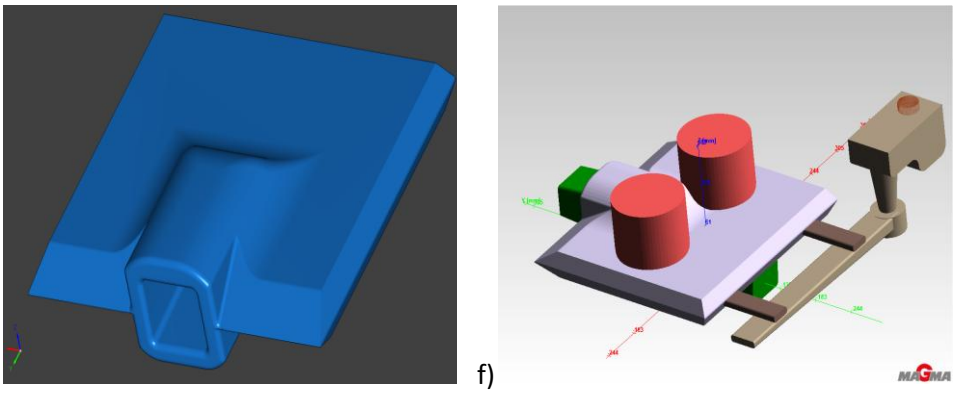

e) f)

Figure 1. a) The Buckets Pelton turbine -3D model, b) Buckets Pelton turbine -MAGMA[5] c) a LED street light housing-3D model, d) a LED street light housing -MAGMA[5], e) an excavator tooth holder -3D model, f) an excavator tooth holder -MAGMA[5] [6–8]

In the next phase, all geometrical assembles are divided into partial elements. Software itself automatically generates the network. Network refinement, i.e. number of network elements can be adjusted by a user in all three directions of coordinate system by defining desired minimal element size. The greater refinement, i.e. the more elements, the more precise calculation of simulation, but with longer simulation time. With more complex and/or thin-walled casts it is necessary to define more refined network.

Prepared network is used for further calculation. For each element, i.e. part of the network, differential equations are used for calculating physical-thermal parameters, and obtained results are margin conditions for calculating parameters in the adjacent element. In this way, a computer makes a calculation between the elements in 3D coordinates and in the end, integrate all partial results in overall geometry.

RESULTS AND DISCUSSION

Results of simulation the Buckets Pelton turbine

Using the Mold Filling Criteria Results after the simulation is terminated, the program automatically calculated several criteria that can be selected at each point. Displaying the criteria results helps find defects in the casting and analyze the filling behavior. In this paper, *Fill_Temp* (Fig. 2a) shows the temperature distribution in the metal during mold filling [°C] (the part filled for 75% of the mold cavity). In addition to the presented *FillTracer* criteria (Fig. 2b).

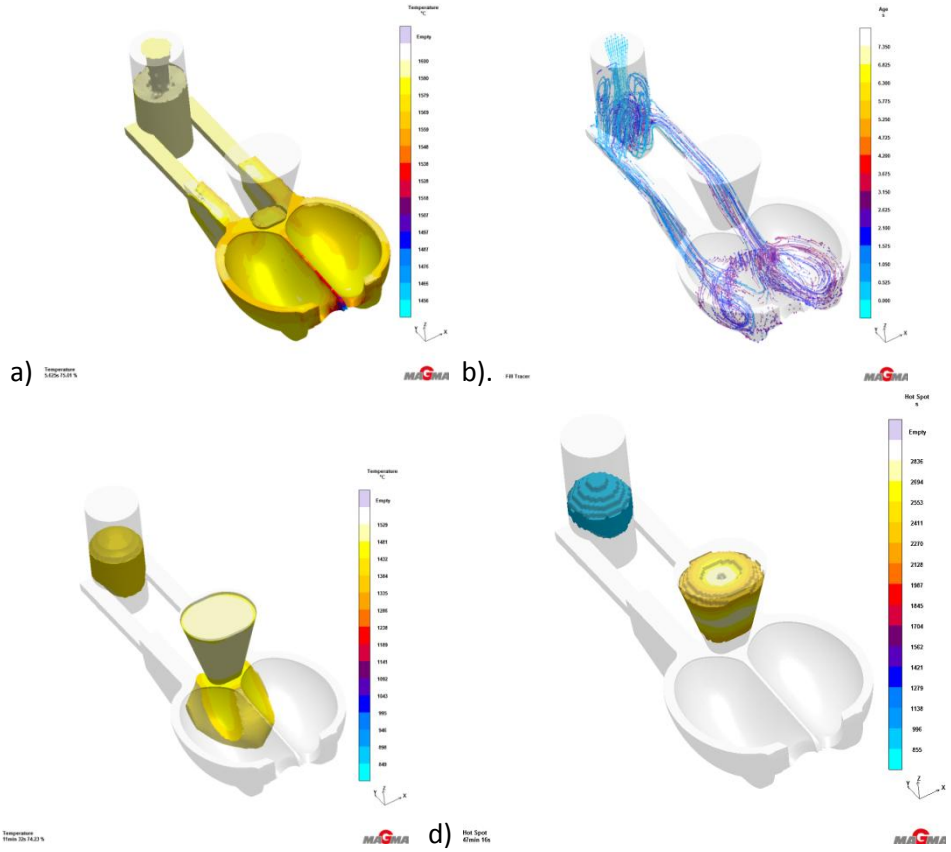

Figure 2. - Results: a) *Fill_Temp* criteria, 75%, b) *FillTracer* criteria, 75%, c) *Fill_Temp* criteria, 75%, and d) *Hotspot* criteria

This function enables observation of the movement of simulated zero-mass particles in the melt. The tracer particles are zero-mass and move just like the metal flow. The particles' positions are saved at each time step during mold filling and solidification simulation. In addition to the functions that are available with all results, special functions for the display of tracer particles are available.

Using the Solidification Criteria Results after the simulation is terminated, the program automatically calculated several criteria that can be selected at each point. Displaying the criteria results helps find defects in the casting and analyze the solidification behavior. The solidification time is 50 min. This paper presents the results of the following criteria: *Fill_Temp* (Fig. 2c), *Hotspot* (Fig. 2d). The results show that the solidification process develops in a directed way and that the last parts that solidify are pour cup and feeder. Using the *Hotspot* criterion, isolated regions of residual melt are determined at any time during solidification. If the feeding calculation option in the simulation setup is checked, this criterion helps to detect porosities in these residual melt regions. The unit is solidification time in seconds (s, color scale). This can determine the time during solidification at which a particular hot spot develops. It can be clearly seen in Figure 2d that the solidification process develops according to expectations and that the last points of solidification are in feeders.

Results of simulation the LED street light housing

Other analyzed case is LED street light housing. For example, *FillTemp* showing the arrangement of metal temperature during mould filling. Using this criterion leads to the first conclusion that the design of gating system is not good.

Due to the long period of piston accelerating to the final speed of filling, the initial part of liquid metal stream is hitting the gate wall (Fig. 3a), starting solidification before it reaches the main mass. This results in a subcooling of the gate (Fig 3b).

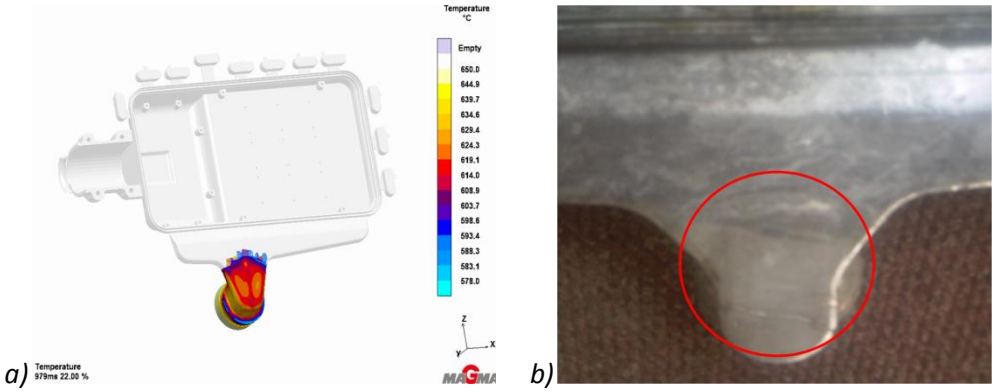

Figure 3. a) The FillTemp criterion and b) a subcooling in the gate [7]

By using the MAGMAhpdc module, the casting process simulation shows turbulent stream motion, resulting in the formation of gaseous inclusions (Fig. 4). The criteria FillTracer (Fig. 4a) and FillVelocity (Fig. 4b) confirms the tendency of making the above errors in a designated area.

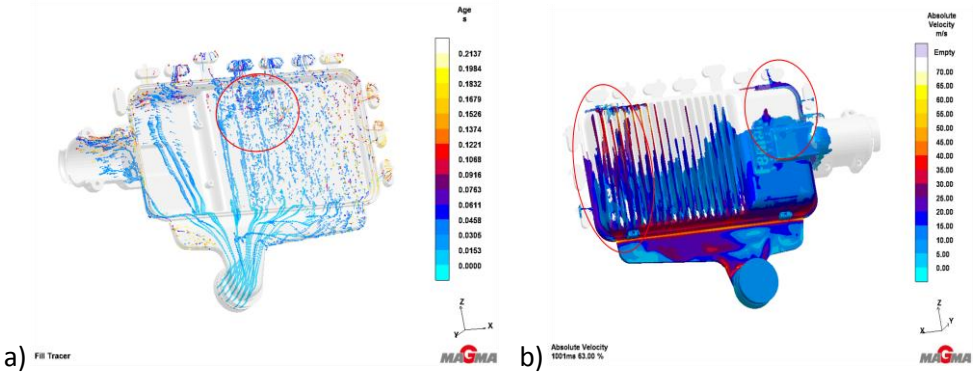

Figure 4. A critical zone analysis for the criteria: a) FillTraces and b) FillVelocity [7]

The examples of simulation results for the criteria *Air Back Pressure* and *Air Entrapment* are presented in Fig. 5. Due to the priority filling on the edges, front filling is encountered in the middle of cast. The positions of trapped gas correspond to the positions of errors in real-cast.

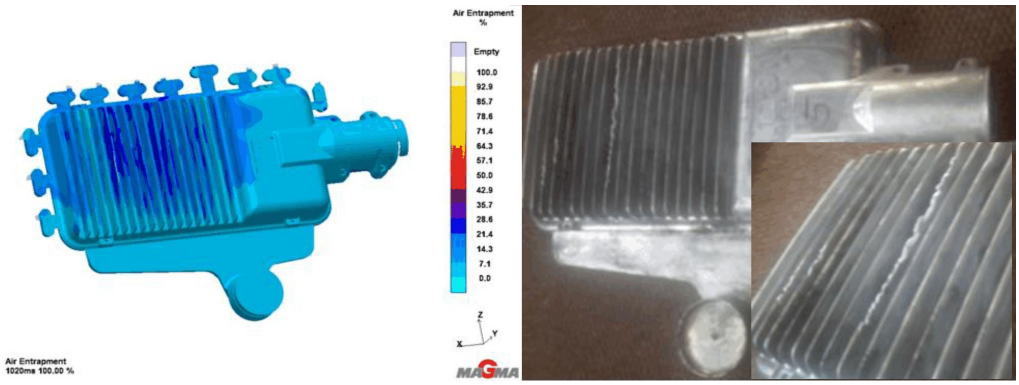

Figure 5. The criterion Air Entrapment and shown errors in cast [7]

The highest suction air is below the beginning of die casting ribs (Fig. 6). Due to the complex-shaped die cast part and the poor design of gating system, the liquid metal at the beginning moves towards the upper edge of the ribs, creating the underpressure and understaffed area of the cast (the highlighted area in Fig. 6a).

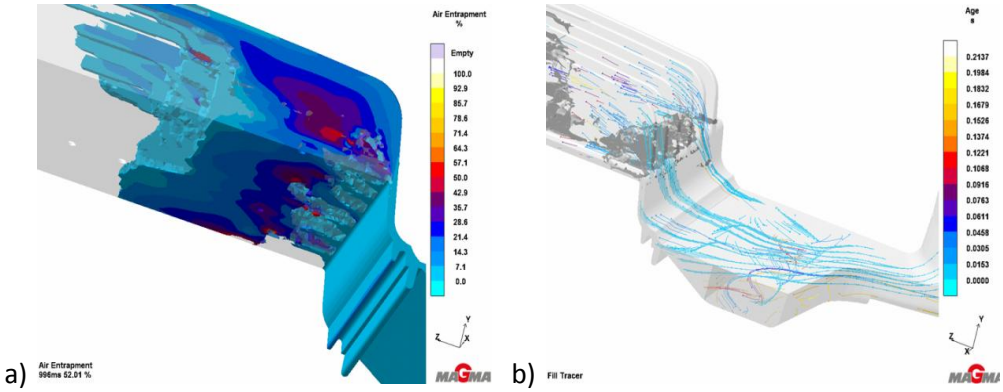

Figure 6. Analysis of the critical areas, of criteria: a) Air Entrapment and b) Age [7]

Using MAGMA[5] software package leads us to the conclusion that the casting machines by which the test casting is carried out, actually is a powerless for this cast shape and design of gating system. If we adopt for the mould closing force of machine a safety factor of 25%, then it can be achieved a maximum pressure of 295 bar for the III phase (Fig. 7b). Therefore, the option of increasing the piston diameter to Ø80 mm was analyzed. Speed of the first phase for both piston diameters was constant: 0.2 m/s (Fig. 7c).

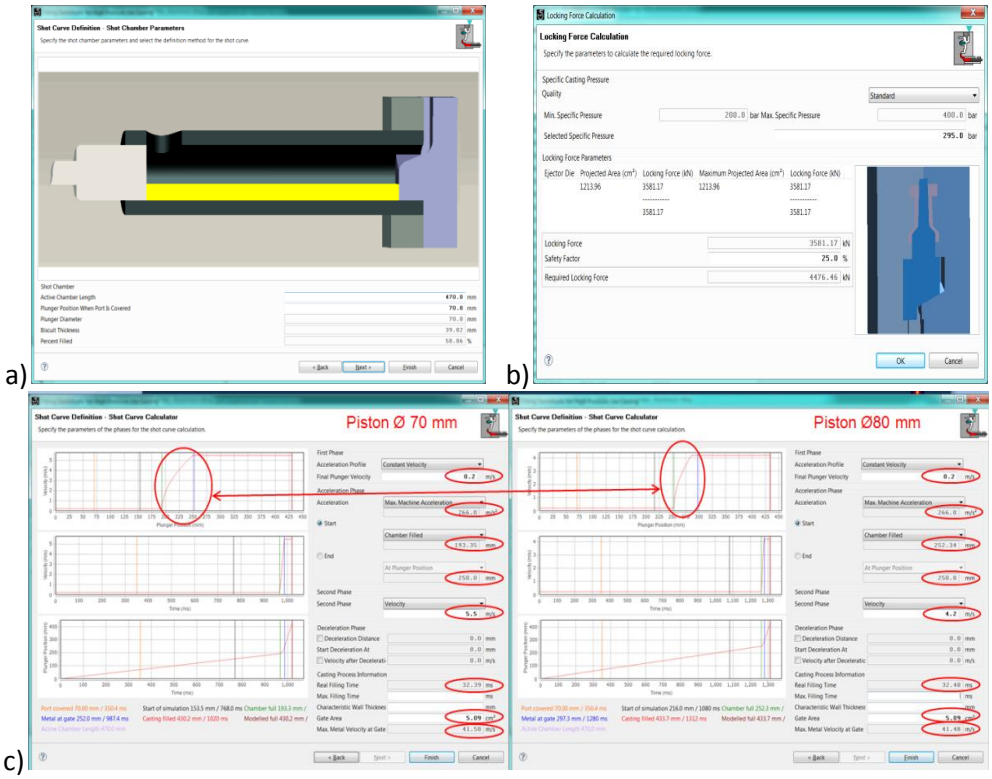

Figure 7. The analysis of casting machine: a) the input data, b) the calculation, and c) the comparative overview of two piston diameters [7]

The piston with diameter Ø70 and a maximal acceleration 266 m/s^2, reaches the speed of the II phase at the position 250 mm. An acceleration starts when the chamber is filled up to the top, which is 193.35 mm. The piston speed in the II phase is 5.5 m/s, while a theoretical speed of molten metal at the ingate is 41.6 m/s.
If we are using piston diameter Ø80 mm, an acceleration starts when the chamber is filled up to the top, which is 252.34 mm. The piston speed in the II phase is 4.2 m/s, and a theoretical speed of molten metal at the ingate then is 41.48 m/s. This leads us to the conclusion that the use of the piston with a diameter Ø80 mm reduces the time for reaching the II phase.

Results of simulation the excavator driver bearer

Third analyzed example is excavator driver bearer. With assistance of *FillTemp* criteria it was immediately agreed that design of firth and feeder is not good (Version_V02, Figure 8a). Adjustment of firth system and feeder led to better allocation of temperature during firth (Version_V07, Figure 8b). Instead of one feeder were put two with insulation shells and dimensions of firth system were changed.

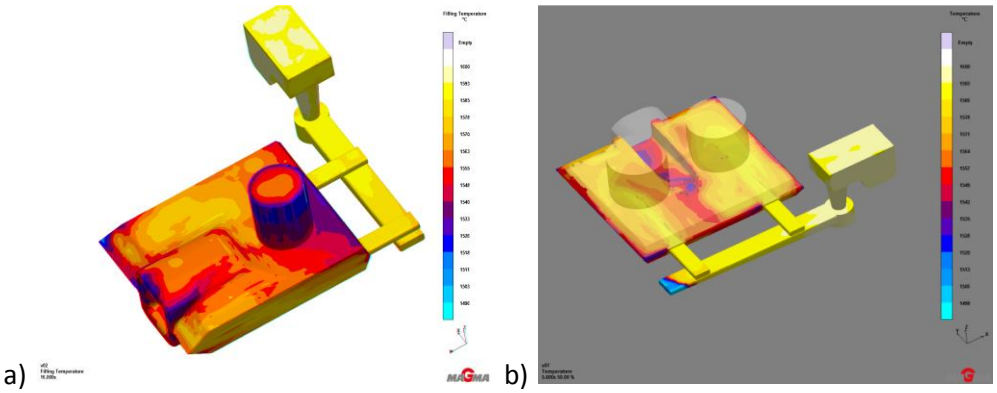

a) b)

Figure 8. The criterion FillTemp: a) V02 and b) V07 [8]

By using *Solidification Criteria Results* after calculation, program automatically calculates several criteria that can be used at any point. Results of these criteria helps analyzing solidification process and find cast deficiencies. Figure 9a shows presence of porosity by using criteria *TotalPorosity* with Version V02, as proved in practice. Figure 9b shows results for criteria *Porosity* for Version V07. With Version V07 is visible no porosity in the cast. This type of firth system in practice proved to yield a "healthy cast".

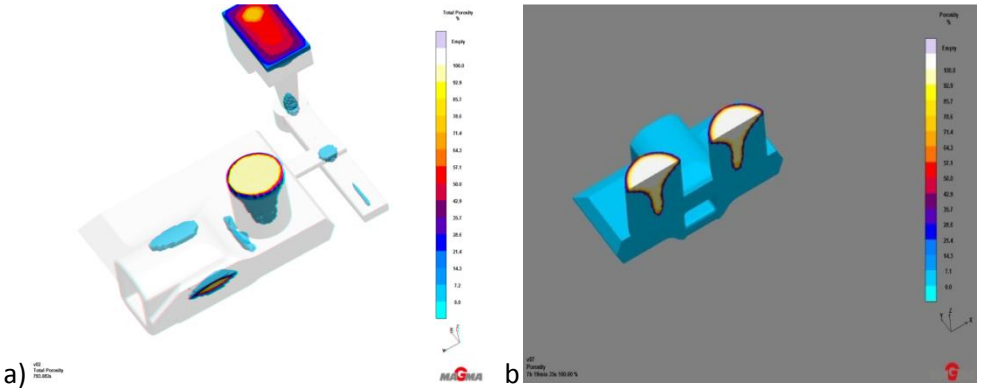

a) b

Figure 9. An analysis of critical areas of the Porosity criterion: a) V02 i b) V07 [8]

CONCLUSIONS

Using informational technologies and virtual casting technology, in this case a software package MAGMA[5] enabled testing different versions for optimizing technological casting parameters. Before experimental casting for each version the testing is done in virtual world of computers. This makes all potential problems visible. Designer can cut a digital cast in any plain and analyze any part for finding discrepancies (presence of porosity, segregation, etc.), also can be analyzed residual strains, metallurgic structure of a cast and many other things. Only after the right solution is found, implementation of results takes place in reality. This method of conquering new products allow avoiding expensive and longtime experimental researches, and the advantage is option of easy implementation in practice for verifying technologies in foundries.

REFERENCES

[1] S. Manasijević, R. Radiša, Skill and intuition of foundrymen or computer assisted casting, Livarstvo, 47 (2008) 1, pp.10−11.
[2] R. Radiša, Z. Gulišija, S. Manasijević, Process optimization of metal casting, MACHINE DESIGN, pp. 111−114, 2009.
[3] S. Manasijević, R. Radiša, Z. Aćimović-Pavlović, K. Raić, S., Marković, Software packages for simulation and visualization of the process of casting pistons, Livarstvo, 48 (2009) 1, pp.14−20.
[4] R. Radiša, S. Manasijević, S. Marković, Optimization of of metal casting technology using software tools, IX international conference on accomplishments in Electrical and Mechanical Engineering and Information –DEMI 2009, Proceedings ISBN 978-9938-39-23-1, Banja Luka, pp.175-180, 2009.
[5] http://www.magmasoft.de/
[6] R. Radiša, S. Manasijević, J. Pristavec, MAGMA^5 use for optimization of technological paarameters of casting a buckets pelton turbine, The 46th International October Conference on Mining and Metallurgy, Proceedings ISBN 978-86-6305-026-6, pp. 441−444, 01−04 October, Bor Lake, Bor Serbia, 2014.
[7] R. Radiša, S. Manasijević, J. Pristavec, V. Mandić, Using MAGMA^5 to optimize relevant technological parameters of the process of casting the housing of LED lamp for street lighting, VI International Congress of Metallurgists of Macedonia, Proceedings ISBN 978-9989-9571-6-1, CM-5, 29 May−01 June, Ohrid, Macedonia, pp. 1−5, 2014.
[8] R. Radiša, S. Manasijević, J. Pristavec, V. Mandić, V. Komadinić, Using MAGMA^5 to optimize the parameters of casting an excavator tooth holder, Metallurgical & Materials Engineering Congress of South-East Europe (MME SEE 2015), Proceedings& Book of Abstracts ISBN 978-86-87183-27-8, 03−05. June, Belgrade, Serbia, pp. 321−326, 2015.

Acknowledgements
This paper is a part of results in experimental researches within the project financed by the Ministry of Education, Science and Technological Development of the Republic of Serbia.

15th INTERNATIONAL FOUNDRYMEN CONFERENCE
INNOVATION – The foundation of competitive casting production
Opatija, May 11th-13th, 2016
http://www.simet.hr/~foundry/

EFFECT OF ANNEALING TIME ON PROPERTIES OF SINTERED Cu-4Au ALLOY DEFORMED WITH 60 % REDUCTION

I. Marković, S. Nestorović†, D. Marković, S. Ivanov and S. Mladenović

University of Belgrade Technical Faculty in Bor, Bor, Serbia
† Deceased 3rd December 2015

Poster presentation
Original scientific paper

Abstract

This investigation was carried out on the copper-gold alloy with 4 at.% of gold obtained by a powder metallurgy (PM) technique. After sintering and thermomechanical treatment which included pre-final cold rolling and annealing followed by quenching, samples were final cold rolled with 60 % reduction. Samples of sintered Cu-4Au alloy deformed with 60 % reduction were isothermal annealed at 250 °C up to the 6,000 minutes. During the isothermal annealing, the values of hardness, microhardness and electrical conductivity were measured. The investigation has shown that low-temperature isothermal annealing at 250 °Cof sintered Cu-4Au alloy deformed with 60 % reduction caused a two-stage increase in all measured properties.

Keywords: *thermomechanical treatment, Cu-Au alloys, hardness, microhardness, electrical conductivity*

*Corresponding author (e-mail address): *imarkovic@tf.bor.ac.rs*

INTRODUCTION

The Cu-Au phase diagram is shown in Fig. 1 [1]. According to the Cu-Au phase diagram, order-disorder transformations occur at some compositions. Long range ordered structures such as Cu_3Au with L12 lattice, AuCu with L10 type lattice, and Au_3Cu with L12 lattice can be formed at the room temperature, depending on gold concentration [2-4]. Above the critical temperature, these alloys are disordered with A1 type structure. During the annealing, disordered alloy hardens on account of order-hardening [5].The chosen alloy for this investigation (Cu-4Au) has no order-disorder phase transformation. It is with a disordered or short range ordered A1 type structure. Despite of no long range ordering in this alloy, some authors have conformed the hardening of previously cold deformed alloy after low temperature annealing [6-10]. This hardening is on account of the anneal hardening effect, which is confirmed only in some binary copper based alloys (with aluminum, gold, gallium,

nickel, palladium, rhodium and zinc) [6]. The described atypical hardening/strengthening of listed diluted solid solutions after cold deformation and annealing up to the recrystallization temperature has been periodically studied since 1970s.

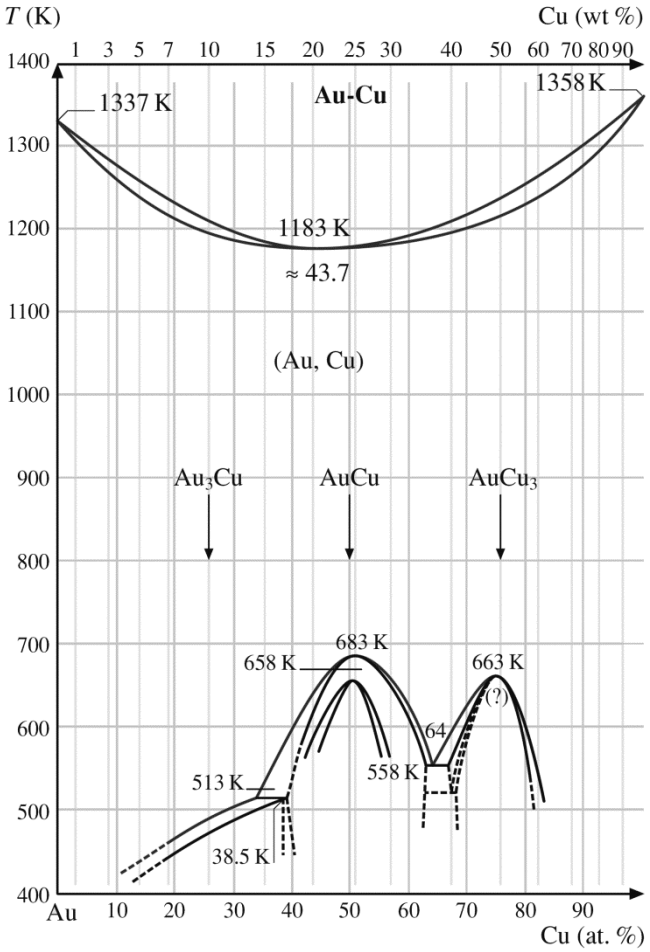

Figure 1. The Cu-Au phase diagram [1]

However, the mechanism of anneal hardening effect has not been fully explained up to today. Two explanations are the most acceptable for describing the origin of this effect – short range ordering and solute segregation to lattice defects. Popplewell and Crane [11] have shown that strengthening in some Cu-Al alloys is related to the occurrence of ordering and strain fields in ordered regions. Nucleuses of ordered domains have preferentially occurred at stacking faults due to the continual tendency for chemical segregation at these faults. Kuwano et al. [12] concluded that annealing of Cu-14.2at.%Al alloy contributed to the annihilation of stacking faults and segregation of the locally ordered regions. According to Miura and Tajima [13], Suzuki locking atmospheres formed near the grain boundaries are the primary responsible for this hardening effect. Varschavsky and Donoso [14] developed the model for the calculation of energy release during the low temperature annealing. They

indicated that a short range ordering occurred parallel with a solute segregation to the partial dislocations.

This paper gives the results of isothermal annealing on the sintered Cu-4Au alloy deformed with 60 % reduction, with the aim of studying the improvement in mechanical and physical properties.

MATERIALS AND METHODS

The samples of Cu-4Au alloy were obtained by a PM technique. The elemental powders of copper and gold were mixed by the triaxial mixer for 2 h. Homogenized mixture of powders is pressed using the uniaxial hydraulic press with 360 MPa. Pressed samples were sintered using the tube furnace with hydrogen atmosphere at 850 °C for 1 h.The chemical composition of the PM obtained samples was (in at.%) 95.95 Cu and 4.05 Au. The PM samples were then pre-finally cold rolled, annealed at 500 °C for 45 minutes, and disordered by quenching from 500 °C. Cold rolled samples in the form of strips were produced from quenched samples by cold rolling with 60 % reduction. Thermo-mechanically treated samples on described route were isothermally annealed at 250 °C from 1 minute to 100 h. The values of hardness, microhardness, and electrical conductivity were measured during the isothermal annealing.

Hardness values were measured using a 10 kg load. Microhardness measurements were made on polished samples using a 100 g load. Hardness and microhardness values were obtained using the ASTM E384 standard. Electrical conductivity measuring was carried out using a conductivity tester. All measured values were obtained as an average of 10 to 15 measurements together with the values of the interval of variation.

RESULTS AND DISCUSSION

Figure2 shows optical microphotograph of the PM Cu-4Au alloy, which is cold rolled with 60 % reduction after quenching. Grain boundaries cannot be seen. It is noted that the spheroidal pores, which are characteristic for sintered materials, are elongated in the direction of deformation.

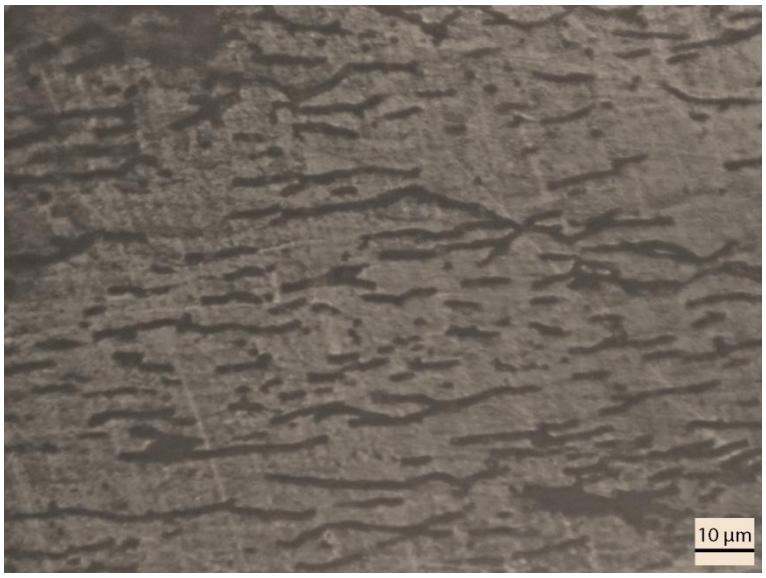

Figure 2. Optical microphotograph of the PM Cu-4Au alloy, which is cold rolled with 60 % reduction after quenching

Figure3 shows the hardness values of PM Cu-4Au alloy (cold rolled with 60 % reduction) during the isothermal annealing at 250 °C.

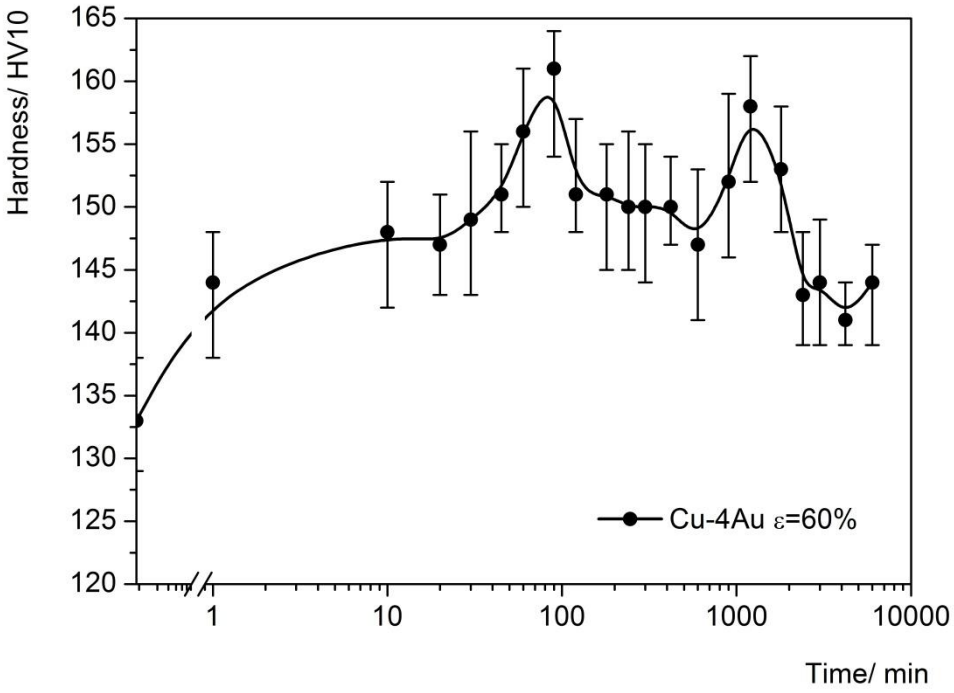

Figure 3. Hardness values of PM Cu-4Au alloy (cold rolled with 60 % reduction) during the isothermal annealing at 250 °C

When cold-rolled PM Cu-Au alloy is annealed at 250 °C from 1 minute to 100 h, it hardens through the two hardness peaks. These two hardness peaks correspond to the primary and secondary hardening. After isothermal annealing at 250 °C for about 90 minutes, the first hardness peak can be seen. Hardness increased for 28 HV10 compared to the cold rolled state. After a slight decrease in hardness, it increased again. The second hardness peak occurred after isothermal annealing at 250 °C for 1200 minutes. In this case, hardness of annealed samples increased for 25 HV10 compared to the cold rolled state. The obtained results showed that the more intensive hardness increase was observed in the first annealing stage than in the second one. Even after isothermal annealing at 250 °C for 100 h, the values of hardness are still higher compared to the hardness of cold rolled state. This indicates that anneal hardening still continues.

Figure4shows the microhardness values of PM Cu-4Au alloy (cold rolled with 60 % reduction) during the isothermal annealing at 250 ^{o}C. The microhardness curve in figure 4 looks similar to the hardness curve shown in figure 3. The first hardening was recognized at an early stage of annealing, followed by some softening and then the second hardening took place. Two microhardness peaks were identified. The first microhardness peak during isothermal annealing at 250 ^{o}C appeared at about 90 minutes. The microhardness increased for 21 HV0.1 in comparison with cold rolled state. A second microhardness peak was evident after annealing for 1200 minutes. This microhardness increase was for 14 HV0.1 in comparison with the microhardness values of cold rolled samples. The intensity of the first hardening is larger than the second one, similar to the results of hardness measurements.

Figure 5 shows the electrical conductivity values of PM Cu-4Au alloy (cold rolled with 60 % reduction) during the isothermal annealing at 250 ^{o}C.

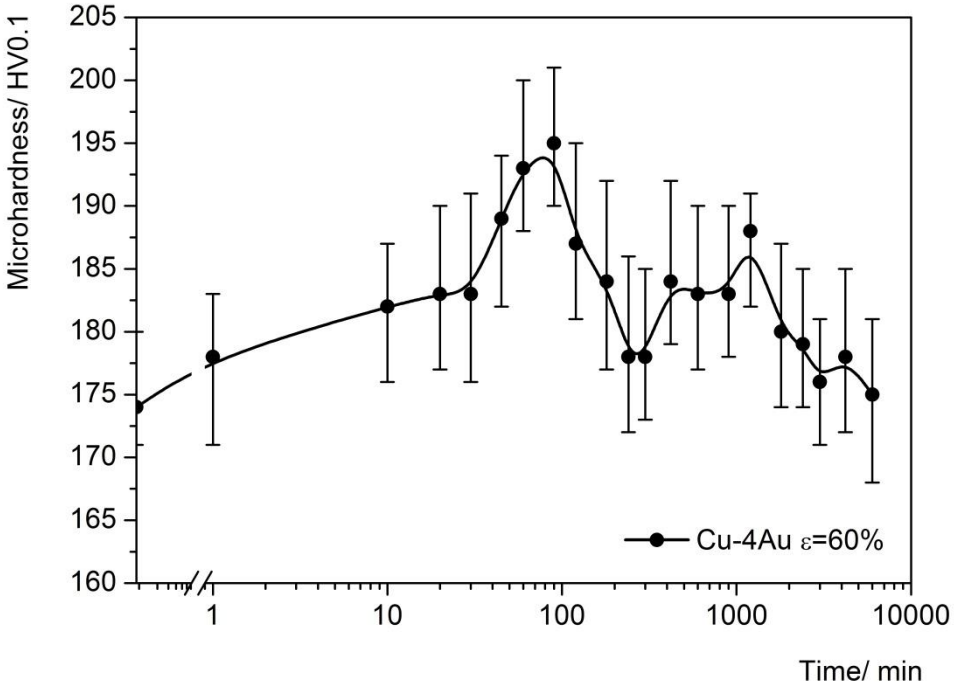

Figure 4. Microhardness values of PM Cu-4Au alloy (cold rolled with 60 % reduction) during the isothermal annealing at 250 °C

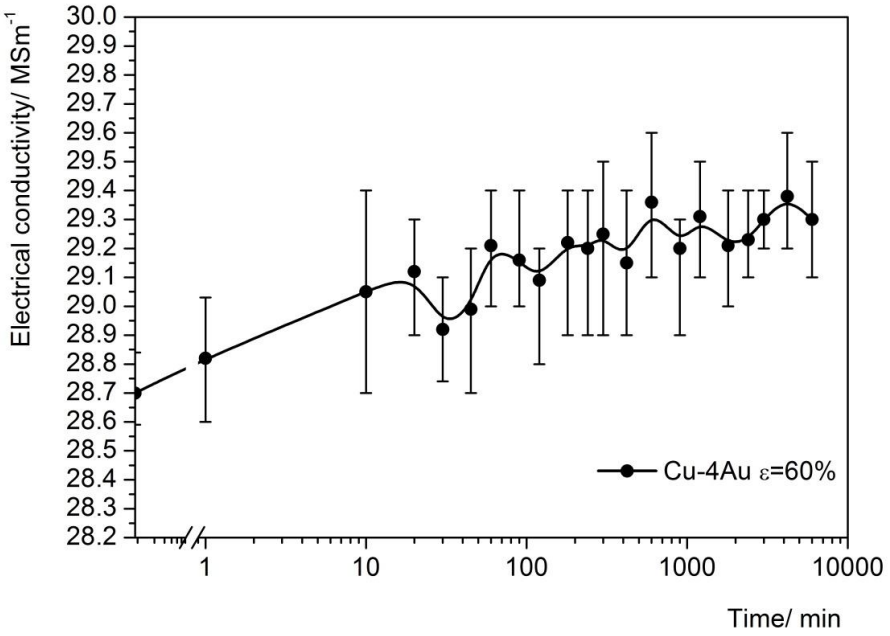

Figure 5. Electrical conductivity values of PM Cu-4Au alloy (cold rolled with 60 % reduction) during the isothermal annealing at 250 °C

Electrical conductivity of PM Cu-4Au alloy (cold rolled with 60 % reduction) slowly increased with time, during the isothermal annealing at 250 °C. The maximum increase in electrical conductivity was achieved during the annealing for 4,200 minute, where electrical conductivity increased from 28.7 MSm^{-1} to 29.38 MSm^{-1}.Bader et al. [15] and Vitek and Warlimont [6] concluded that this increase in electrical conductivity during the annealing at the same temperatures is a result of solute segregation to the lattice defects. The major influence has the segregation of solute atoms to stacking faults, vacancies and dislocations, while the short-range ordering has a significantly lower influence. Segregation effects have influence on the depleting of copper-based matrix on gold atoms, contributing to the decrease in lattice parameter, which is confirmed elsewhere [8].

CONCLUSIONS

The effect of annealing time on properties of sintered Cu-4Au alloy deformed with 60 % reduction was studied, and the following conclusions can be drawn:
– The thermomechanical treatment was effectively established to produce the anneal-hardened alloy.
– Hardness, microhardness and electrical conductivity values were increased during the isothermal annealing at 250 °C. This increase was accomplished through the two hardening stages – the first and the second one hardening.
– The best combination of measured properties was achieved after annealing at 250 °C for 90 minutes, where hardness increased for 25 HV10, microhardness for 14 HV0.1, and electrical conductivity to 29.16 MSm^{-1}.
– Even isothermal annealing at 250 °C for 100 h did not bring a decrease in mechanical properties, which implies that anneal hardening still continues.

REFERENCES

[1] W. Martienssen, H. Warlimont, Springer Handbook of Condensed Matter and Materials Data, Springer, 2005.
[2] A.I. Potekaev, E.A. Dudnik, M.D. Starostenkov, V.V. Kulagina, Thermoactivated Structure Rearrangements in a Binary $CuAu_3$ Alloy Under Deviation from Stoichiometric Composition, Russian Physics Journal, 53 (2010) 5, pp. 465–479.
[3] Ch.E. Lekka, N. Bernstein, M.J. Mehl, D.A. Papaconstantopoulo, Electronic Structure of the Cu_3Au (111) Surface, Applied Surface Science, 219 (2003), pp. 158–166.
[4] Y.S. Puzyrev, G.E. Ice, C.J. Sparks, L. Robertson, Automated Software for the Recovery of the Short Range Order Parameters from Diffuse X-ray Scattering Data, Nuclear Instruments and Methods in Physics Research Section A, 582(2007), pp. 193–195.
[5] V.S. Arunachalam, R.W. Cahn, Order-hardening in CuAu, Journal of Materials Science, 2 (1967) 2, pp. 160-170.
[6] J.M. Vitek, H. Warlimont, The Mechanism of Anneal Hardening in Dilute Copper Alloys, Metallurgical and Materials Transactions A, 10 (1979), pp. 1889–1892.

[7] I. Marković, S. Nestorović, B. Markoli, M. Premović, S. Mladenović, Study of Anneal Hardening in Cold Worked Cu-Au Alloy, Journal of Alloys and Compounds, 658 (2016), pp. 414-421.
[8] I. Marković, S. Nestorović, B. Markoli, M. Premović, S. Šturm, Anneal Hardening in Cold Rolled PM Cu-Au Alloy, Materials Science & Engineering A, 658 (2016), pp. 393–399.
[9] I. Marković, S. Nestorović, D. Marković, Effect of Thermo-mechanical Treatment on Properties Improvement and Microstructure Changes in Copper–gold Alloy, Materials and Design, 53 (2014) pp. 137-144.
[10] I. Marković, S. Nestorović, D. Marković, D. Gusković, Properties Improvement and Microstructure Changes During Thermomechanical Treatment in Sintered Cu-Au Alloy, Transactions of Nonferrous Metals Society of China, 24 (2014) 2, pp. 431−440.
[11] J.M. Popplewell, J. Crane, Order-strengthening in Cu-Al Alloys, Metallurgical Transactions A, 2(1971) 12, pp. 3411–3420.
[12] N. Kuwano, Y. Tomokiyo, C. Kinoshita, T. Eguchi, Study of Annealing Effects on Cold-Worked α Phase of Cu-Al Alloys, Transactions of the Japan Institute of Metals. 15 (1974) 5, pp. 338–344.
[13] S. Miura, T. Tajima, Effect of Grain Boundaries on Anneal Hardening in Cu-Al Alloy, Metal Science, 12 (1978) 4, pp. 183-191.
[14] A. Varschavsky, E. Donoso, Modelling Solute Segregation to Partial Dislocations for DSC Evaluations, Journal of Thermal Analysis, 48 (1997), pp. 1229-1248.
[15] M. Bader, G.T. Eldis, H. Warlimont, The Mechanisms of Anneal Hardening in CuAl alloys, Metallurgical Transactions A, 7 (1976), pp. 249–255.

Acknowledgements

This work was supported by the Ministry of Education, Science and Technological Development of the Republic of Serbia (Grant No. 34003 - Conquering the Production of Cu–Au, Cu–Ag, Cu–Pt, Cu–Pd, Cu–Rh Cast Alloys of Improved Properties by Applying the Anneal Hardening Mechanisms).

15th INTERNATIONAL FOUNDRYMEN CONFERENCE
INNOVATION – The foundation of competitive casting production
Opatija, May 11th-13th, 2016
http://www.simet.hr/~foundry/

INFLUENCE OF CHEMICAL COMPOSITION AND COOLING RATE ON BAINITE MORFOLOGY IN HIGH STRENGTH STEELS

UTJECAJ KEMIJSKOG SASTAVA I BRZINE OHLAĐIVANJA NA MORFOLOGIJU BAINITA VISOKOČVRSTIH ČELIKA

S. Šolić, B. Podgornik and J. Burja

Institute of Metals and Technology, Ljubljana, Slovenia

Poster presentation
Original scientific paper

Abstract

Bainitic steels with a wide range of carbon content (from less than 0.1 % to near 1 %) are being in focus of many research nowadays. Important results and significant developments have been achieved in the area of low carbon bainitic steels (TMCP and HSLA) and detailed research are recently done in the area of medium and high carbon steels with good values of strength but usually accompanied by relatively low values of toughness. To obtain the optimal properties with minimal production costs research has been mainly focused on the optimization of the chemical composition in combination with different continuous cooling rates. It allows various mixed structures of martensite with different types of bainite to be achieved without any additional heat treatment procedures. For that purpose the paper will present the investigation result on the influence of chromium and manganese content in combination with different continuous cooling rate on formation, type and content of the bainite and the resulting mechanical properties. Results show that optimization of continuous cooling rate can significantly affect the increase in toughness while maintaining high strength.

***Keywords**: high strength steel, bainite, microstructure, continuous cooling*

*Corresponding author (e-mail address): *Sanja.Solic@imt.si*

Sažetak

Bainitni čelici sa širokim rasponom ugljika (u području od 0,1 % C do 1 % C) posljednjih su godina u fokusu različitih istraživanja. Značajni rezultati postignuti su u području niskougljičnih bainitnih čelika (TMCP, HSLA), a sve više istraživanja prebacuje se u područje srednje i visoko ugljičnih čelika kod kojih je uz vrlo visoku čvrstoću obično prisutna relativno niska žilavost. Kako bi se postigla optimalna svojstva čelika uz minimalne troškove proizvodnje istraživanja se rade na optimiranju kemijskog sastava u kombinaciji s različitim brzinama kontinuiranog ohlađivanja kako bi se postigle mješovite

strukture martenzita i različitih oblika bainita bez naknadnih toplinskih obrada. S tim ciljem u ovom radu prikazani su rezultati istraživanja utjecaja udjela kroma i mangana u kombinaciji s različitim brzinama kontinuiranog hlađenja na formiranje, vrstu i udio bainita te na mehanička svojstva. Rezultati su pokazali da se optimiranjem brzine ohlađivanja značajno može utjecati na povećanje žilavosti uz zadržavanje visoke čvrstoće.

***Ključne riječi**: visoko čvrsti čelici, bainit, mikrostruktura, kontinuirano hlađenje*

UVOD

Dvadesetih godina prošlog stoljeća pronađena je nova faza u strukturi čelika kao produkt mikrostrukturne transformacije u srednje-temperaturnom rasponu koja je kasnije nazvana bainit. Općenita mikrostrukturna definicija bainita bila je da je to produkt ne-lamelarne, ne-kooperativne eutektoidne pretvorbe početne/roditeljske faze [1]. Iako je opisano šest morfoloških oblika bainita, najčešća podjela bainita je na gornji i donji, u ovisnosti o temperaturi pretvorbe tj. nastanka. Gornji bainit se sastoji od paralelnih kristala ferita, oblika pločica ili letvica, sa nekontinuiranim cementitom između njih. Donji bainit sadrži male čestice cementita unutar feritnih kristala, uobičajeno pod kutom od 55°– 60° u odnosu na granicu zrna. Ostali oblici bainita prema [2] su nodularni bainit, kolumnarni (stupasti) bainit, inverzni bainit te alotriomorfni bainit. Također, postoji još nekoliko podjela bainita predstavljenih od više autora [1-4] obzirom da je pojedine morfološke oblike bainita vrlo teško točno karakterizirati.

Podjela bainita prema Ohmori [3] podrazumijeva da bainit također može biti i bez karbida te ga se svrstava u tri skupine: BI – bainitni ferit bez prisutnih karbida sa zaostalim austenitom između feritnih letvica, BII – karbid prisutan između feritnih letvica i BIII – karbid unutar feritnih letvica. Ta podjela napravljena je za nisko-ugljične čelike gdje se tip bainita BI formira u temperaturnom području između 600° i 500° te se sastoji od feritnih letvica bez karbida između kojih se nalaze slojevi zaostalog austenita i martenzita. Tip BII je klasičan oblik karakteriziran kao gornji bainit koji se formira između 450° i 500°C s karbidima između feritnih zrna. Tip BIII formira se blizu Ms temperature te je više u obliku letvice nego pločice koji se uobičajeno karakterizira kod donjeg bainita (također i kod čelika s većim udjelom ugljika).

Vrlo popularan sustav klasifikacije bainita predstavili su Bramfit i Speer [4]. Prema toj klasifikaciji morfologija bainitnog ferita je acikularna tj. igličasta, nepravilna, te se sve razlike između bainitnih oblika temelje na interakciji drugih faza sa feritom. Problem kod ove klasifikacije je što se terminom acikularni karakteriziraju feriti kod TMCP i HSLA čelika te je acikularni ferit kao karakterizirano različiti oblik ferita od bainitnih oblika karakterističan za zavarivačku literaturu i karakterizaciju zavarenih spojeva.

Sustav klasifikacije bainita prema Zajac et al. [1] najnoviji je te se temelji na morfologiji ferita, koja može biti nekog nepravilnog tipa uz oblik letvice, te nekog drugog

mikrostrukturnog konstituenta. Ovaj sustav opisuje pet morfoloških oblika bainita za srednje i nisko ugljične čelike, a to su granularni bainit (GB), gornji bainit (UB), degenerirani gornji bainit (DUP), donji bainit (LB) i degenerirani donji bainit (DLB). Iako je ova podjela bainita znatno naprednija od prethodno navedenih jer podrazumijeva da morfološki oblici ferita kod bainita mogu biti i nepravilnog oblika, a ne isključivo oblika letvice, nedostatak podjele je što ne prepoznaje feritne oblike koji se formiraju iznad temperaturnog područja formiranja granularnog bainita, kao što su poligonalni i ostali masivni oblici ferita koji se ovdje svrstavaju u granularni.

Iz navedenog je vidljivo da su morfološki oblici bainitne strukture vrlo kompleksni i da svojim svojstvima značajno mogu utjecati na mehanička svojstva čelika. Karakteristike bainita koje utječu na mehanička svojstva čelika su:
- mogućnost formiranja nakupina feritnih zrna oblika letvice gotovo jednake orijentacije
- promjenjiva, ali generalno visoka gustoća dislokacija
- mogućnost mehanizma očvrsnuća legirnim elementima, uglavnom ugljikom i dušikom te supstitucijskim legirnim elementima.
- između feritnih letvica mogu se formirati blokovi martenzita i zaostalog austenita povećanog udjela ugljika
- u strukturi mogu nastati veliki karbidi na feritnim letvicama, nakupinama i granicama prethodnih autenitnih zrna i manji karbidi dispergirani unutar feritnih zrna [5].

Sedamdesetih godina prošlog stoljeća Feng et. al. [6-8] proizveli su bainitne čelike na bazi mangana dobivene kontinuiranim hlađenjem te dokazali da je moguće dobiti bainit kontinuiranim hlađenjem i bez dodavanja skupih elemenata kao što su Mo, W itd. Također, pokazalo se da bainitni čelici na bazi mangana imaju nekoliko prednosti nad onim na bazi molidbena: veću bainitnu prokaljivost pri kontinuiranom hlađenju, nižu temperaturu bainitne pretvorbe, dobru kombinaciju čvrstoće i žilavosti, jednostavan kemijski sastav i nižu cijenu.

Cilj ovog ispitivanja bio je istražiti utjecaj brzine hlađenja te udjela mangana i kroma na oblik i morfologiju bainita, na udio bainita u mikrostrukturi te na čvrstoću i žilavost nisko-ugljičnog čelika.

EKSPERIMENTALNI DIO

Za potrebe ispitivanja napravljene su dvije laboratorijske šarže čelika čiji su kemijski sastavi prikazani u tablici 1.

Tablica 1. Kemijski sastav čelika

oznaka	%C	%Si	%Mn	%S	%Cr	%Ni	%Cu	%Mo	%V	%Nb	%Fe
UA	0,41	1,22	0,82	0,009	1,26	0,20	0,23	0,21	0,29	0,08	ostatak
UB	0,45	1,11	0,58	0,009	1,39	0,21	0,23	0,21	0,28	-	ostatak

Čelik je taljen u laboratorijskoj 50 kW indukcijskoj peći u kojoj je pretaljeno ukupno 18 kg čelika. Čelik je umiren aluminijem te uliven u dva ingota od 9 kg. Ingoti dimenzija 60 mm x 60 mm valjani su u vrućem stanju (u području 1150 °C - 1050 °C) do dimenzija 20 mm x 70 mm. Za svaku šaržu izrezano je šest uzoraka za statičko vlačno ispitivanje te šest uzoraka za ispitivanje udarnog rada loma. Toplinska obrada uzoraka sastojala se od ugrijavanja na temperaturu austenitizacije od 1000 °C brzinom 0,33 °C/s, progrijavanja na toj temperaturi u trajanju od 15 min, te hlađenja na zraku brzinama 1,5 °C/s i 2,5 °C/s. Toplinska obrada pojedinih grupa uzoraka prikazana je u tablici 2. Brzine ugrijavanja i hlađenja praćene su pomoću termo-elementa smještenog u jezgri pomoćnog uzorka oblika CVN.

Tablica 2. Oznake uzoraka u ovisnosti o brzini hlađenja

Oznaka uzorka	v_{hl}, °C/s
UA-1	1,5
UA-2	2,5
UB-1	1,5
UB-2	2,5

Mehanička svojstva ispitana su prema ISO 6892-1 na kidalici Instron 8820. Ispitivanje je provedeno na normalnim kratkim epruvetama, a mjerenje je uključilo ispitivanje konvencionalne granice razvlačenja, $R_{p0.2}$, vlačne čvrstoće, R_m i istezljivosti, A_5. Udarni rad loma proveden je na Charpy-jevom batu s njihalom od 300 J, na uzrocima s V zarezom prema BS EN 10045-1. Ispitivanje je provedeno na temperaturi 21 °C ± 0,5 °C. Za svako stanje ispitane su tri epruvete te iskazani rezultat predstavlja srednju vrijednost tri ispitivanja. Također, analizirane su prijelomne površine uzoraka kako bi se utvrdila i karakterizirala vrsta loma u odnosu na postignutu mikrostrukturu.

Za ispitivanje mikrostrukture uzorci su pripremljeni standardnim metalografskim postupkom pripreme uzorka, te nagriženi u 3 % nitalu. Mikrostruktura i prijelomne površine uzoraka udarnog rada loma ispitani na field-emission skenirajućem elektronskom mikroskopu FE SEM JEOL JSM6500F. Kvantitativna analiza udjela faza napravljena je na temelju analize cijele površine poprečnog presjeka uzorka na FE SEM mikroskopu. Tvrdoća uzoraka izmjerena je Vickers metodom HV 1 na uređaju Instron, Tukon 2100 B. Na svakom uzorku napravljeno je deset mjerenja te rezultat predstavlja srednju vrijednost dobivenih rezultata.

Vrijednosti temperatura početka banitne pretvorbe (B_S) izračunate su pomoću Kunitake i Okada formule [9], a martenzit start temperatura (M_S) pomoću izraza Andrews [10]. Rezultati su prikazani u tablici 3. Vidljivo je da su temperature B_S i M_S gotovo jednake za obje šarže te da ne utječu značajno na mogućnost pojave različitih morfologija bainita.

Tablica 3. Temperature početka bainitne i martenzitne pretvorbe

Šarža	B_S, °C	M_S, °C
UA	523,47	280,55
UB	533,8	280,87

REZULTATI I DISKUSIJA

Na slici 1 prikazana je mikrostruktura uzoraka UA-1 i UA-2. Vidljivo je da je struktura mješovito bainitno martenzitna s različitim bainitnim oblicima na koje je brzina hlađenja imala značajan utjecaj. Kod uzorka hlađenog manjom brzinom vidljivo je da se sastoji uglavnom od gornjeg bainita kod kojeg većinom nije prisutna karbidna faza između feritnih zrna već visokougljični zaostali austenit te su također prisutni martenzitno/austenitni blokovi. Procijenjeni udio faza kod ovog uzorka iznosi 40 % martenzita i 60 % bainita (mješavine gornjeg, degeneriranog bainita i klasičnog gornjeg bainita).

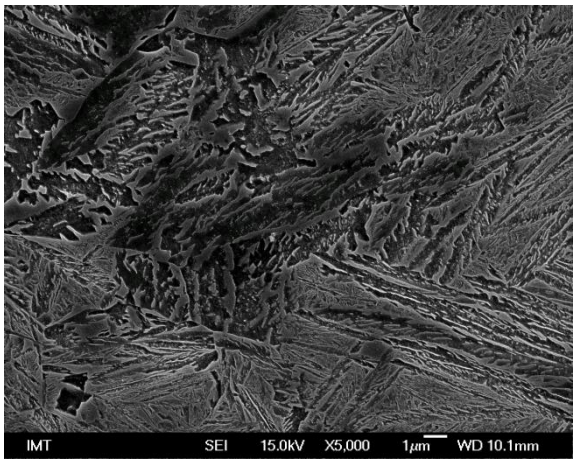

a)

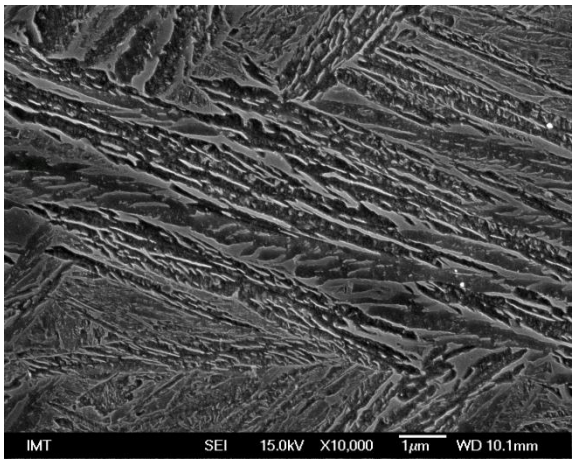

b)

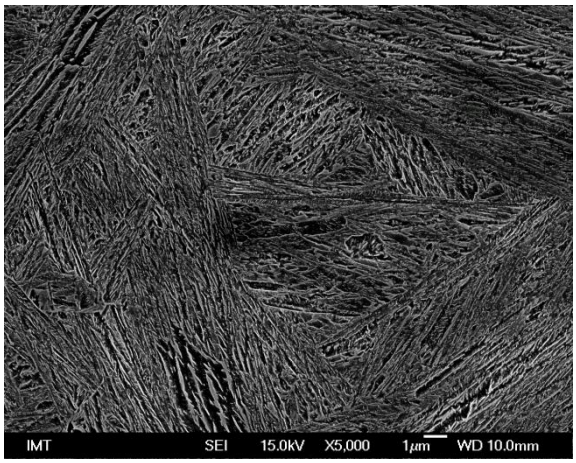

c)

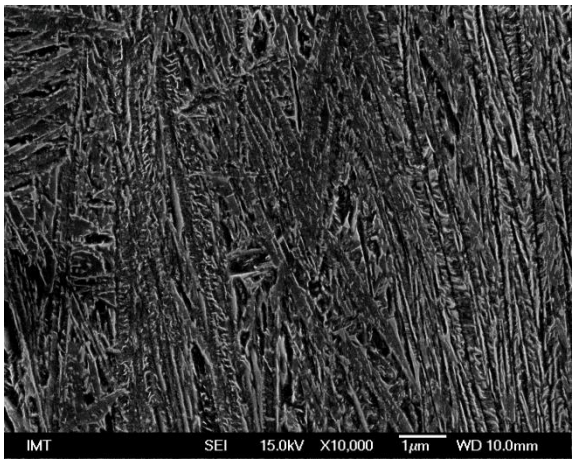

d)

Slika 1. Mikrostruktura uzoraka UA: a) UA-1, v_{hl} = 1,5 °C/s manje povećanje, b) UA-1, v_{hl} = 1,5 °C/s veće povećanje; c) UA-2, v_{hl} = 2,5 °C/s manje povećanje, d) UA-2, v_{hl} = 2,5 °C/s veće povećanje

Uzorak hlađen većom brzinom (slika 1c i d) također ima mješovitu martenzitno bainitnu mikrostrukturu, ali je jasno vidljivo da je udio martenzita veći te da se morfologija bainita značajno razlikuje. Jasno je vidljiva morfologija letvica (engl. lath-like) karakteristična za donji bainit s karbidnim česticama postavljenim pod kutom od 50° do 60° na granicu zrna. Također, vidljiv je i mali udio gornjeg degeneriranog bainita te pločastog donjeg bainita (engl. plate-like), ali i vrlo mali udio zaostalog austenita. Procijenjeni udio faza je 70 % martenzita i 30 % bainita (pretežno letvičastog u manjem udjelu pločastog te do 2 % zaostalog austenita).

Na slici 2 prikazane su mikrostrukture uzoraka UB koji su imali smanjeni udio Mn i Cr u odnosu na uzorak UA.

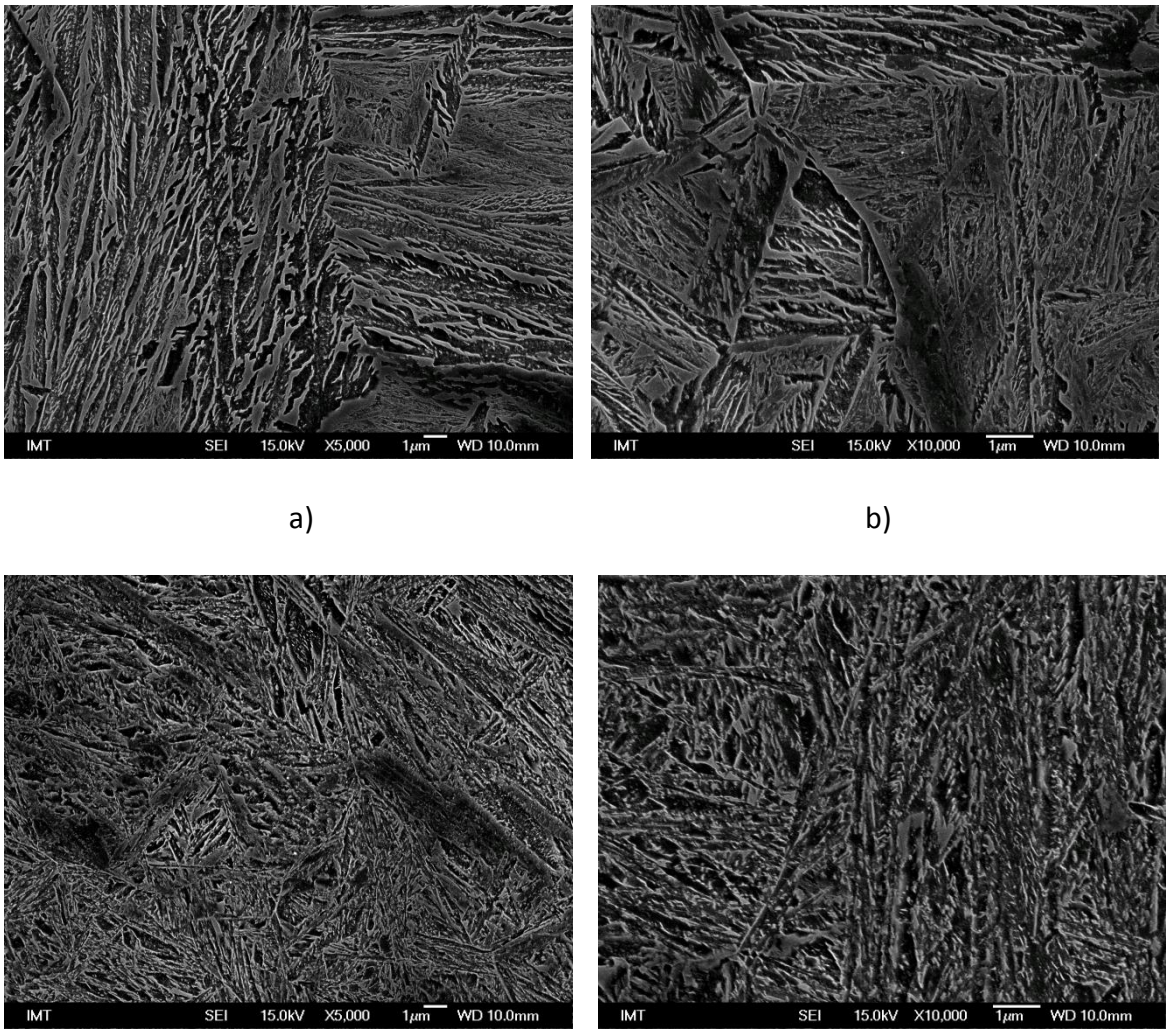

a) b)

c) d)

Slika 2. Mikrostrukture uzoraka UB: a) UB-1, v_{hl} = 1,5 °C/s manje povećanje, b) UB-1, v_{hl} = 1,5 °C/s veće povećanje; c) UB-2, v_{hl} = 2,5 °C/s manje povećanje, d) UB-2, v_{hl} = 2,5 °C/s veće povećanje

Na slikama 2a i b prikazana je mikrostruktura uzorka UB hlađena manjom brzinom. Vidljiva je mješovita bainitno martenzitna struktura uglavnom degeneriranog gornjeg bainita, bainitnog ferita prošaranog cementitom i visokougljičnim zaostalim austenitom te martenzitno/austenitnim blokovima. Udio bainita u ovom uzorku nešto je veći nego kod uzorka UA-1 i iznosi oko 70 %, dok je udio martenzita 30 %. Uzorak UB-2 hlađen većom brzinom ima strukturu donjeg bainita, uglavnom morfologije letvica, ali je vidljivo da je kod ovog uzorka veći udio pločastog donjeg bainita (eng. plate-like).

Iz mikrostrukture je jasno vidljivo da je pri ohlađivanju manjom brzinom došlo do nastanka pretežno gornjeg bainita i martenzita dok je pri ohlađivanju većom brzinom uglavnom nastala mješavina donjeg banita i martenzita. Kod uzorka sa smanjenim udjelom kroma i mangana osim donjeg bainita morfologije letvica došlo je do povećanog udjela pločastog donjeg bainita, slika 3.

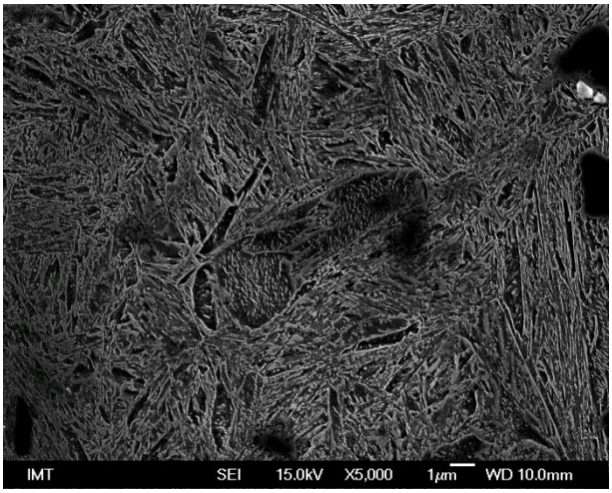

Slika 3. Pločasti (eng. plate-like) donji bainit, uzorak UB-2

Pločasti (eng. plate-like) bainit se naziva još i srasli (eng. coalesced) bainit. Pločasti ili srasli bainit nastaje kada dolazi do srastanja individualno nastalih pločica tj. letvica bainitnog ferita koji imaju identičnu kristalografsku orijentaciju [11]. Predočena su dva uvjeta koja su nužna za nastanak pločastog bainta:

1. kada pojedine pod-jedinice tj. letvice bainitnog ferita imaju jednaku kristalografsku orijentaciju one u principu mogu srasti neprimjetno, ali formiranje tanje pločice/letvice uzrokuje veće naprezanjem uslijed deformacije oblika pri formiranju bainita tako da mora postojati dovoljna pokretačka sila (izmjena slobodne kemijske energije) koja će osigurati formiranje većih ploča bainitnog ferita;
2. mora postojati dovoljno mjesta u primarnom kristalnom zrnu tj. roditeljskoj fazi kako bi se osiguralo nesmetano srastanje i rast pločastog ferita. Ugljik ostaje zarobljen unutar feritnog zrna te kasnije precipitira unutar zrna u karbidne čestice ili djelomično odlazi u zaostali austenit. Prisutnost pločastog bainita u većim udjelima uglavnom se negativno odražava na žilavost čelika [12].

Rezultati ispitivanja mehaničkih svojstava i tvrdoće prikazani su u tablici 4.

Tablica 4. Mehanička svojstva ispitanih šarži

uzorak	$R_{p0,2}$, MPa	*Rm*, MPa	*A*, %	*KV*, J	HV 1	udio faza, %
UA-1	980	1465	4,3	17,5	414	40 %M + 60 %B (UDB)
UA-2	1130	1750	3,0	11, 8	583	70 %M + 30 %B (LLB)
UB-1	910	1375	3,6	24,3	524	30 %M + 70 %B (UDB)
UB-2	1220	1925	5,9	13,5	600	70 %M + 30 %B (LLB)

Rezultati su pokazali da uzorci s većim udjelom bainita u strukturi imaju bolju žilavost, a pretežno martenzitna struktura utjecala je na povećanje konvencionalne granice razvlačenja i vlačne čvrstoće. Niža tvrdoća kod uzorka UA-1 u odnosu na uzorak UB-1 koji ima nešto veći udio martenzita, rezultat je manjeg udjela karbida u degeneriranom gornjem bainitu kod kojeg je karakterizirana morfologija bainitnog ferita bez karbida između feritnih zrna, što odgovara i povećanom udjelu silicija u kemijskom sastavu koji odgađa formiranje karbida u bainitu. Također u kemijski sastav uzoraka oznake UA dodan je i niobij koji pomiče početak bainitne transformacije prema većim brzinama ohlađivanja, ali utječe na smanjenje tvrdoće čelika.

Na slici 4 prikazane su prijelomne površine ispitanih uzoraka. Na slici 4a i 4c prijelomne su površine uzoraka s većim udjelom gornjeg bainita tj hlađenih manjom brzinom. Vidljivo je da su prijelomne površine uglavnom ravne i da je lom propagirao radeći rascjep zrna pod određenim kutom. Takva vrsta prijeloma karakteristična je uglavnom za gornji bainit [13].

Kod uzoraka hlađenih većom brzinom kod kojih je došlo do izlučivanja donjeg bainita (slika 4b i 4d) vidljivo je da na prijelomnom površini prevladava žilavi lom pri čemu su jasno izražene jamice koje su sprečavale propagaciju pukotine. Jamičasta površina karakteristična je za donji bainit, a u dijelovima mikrostrukture u kojima prevladava martenzit pukotina je propagirala rascjepno kroz kristalna zrna pod određenim kutom [13].

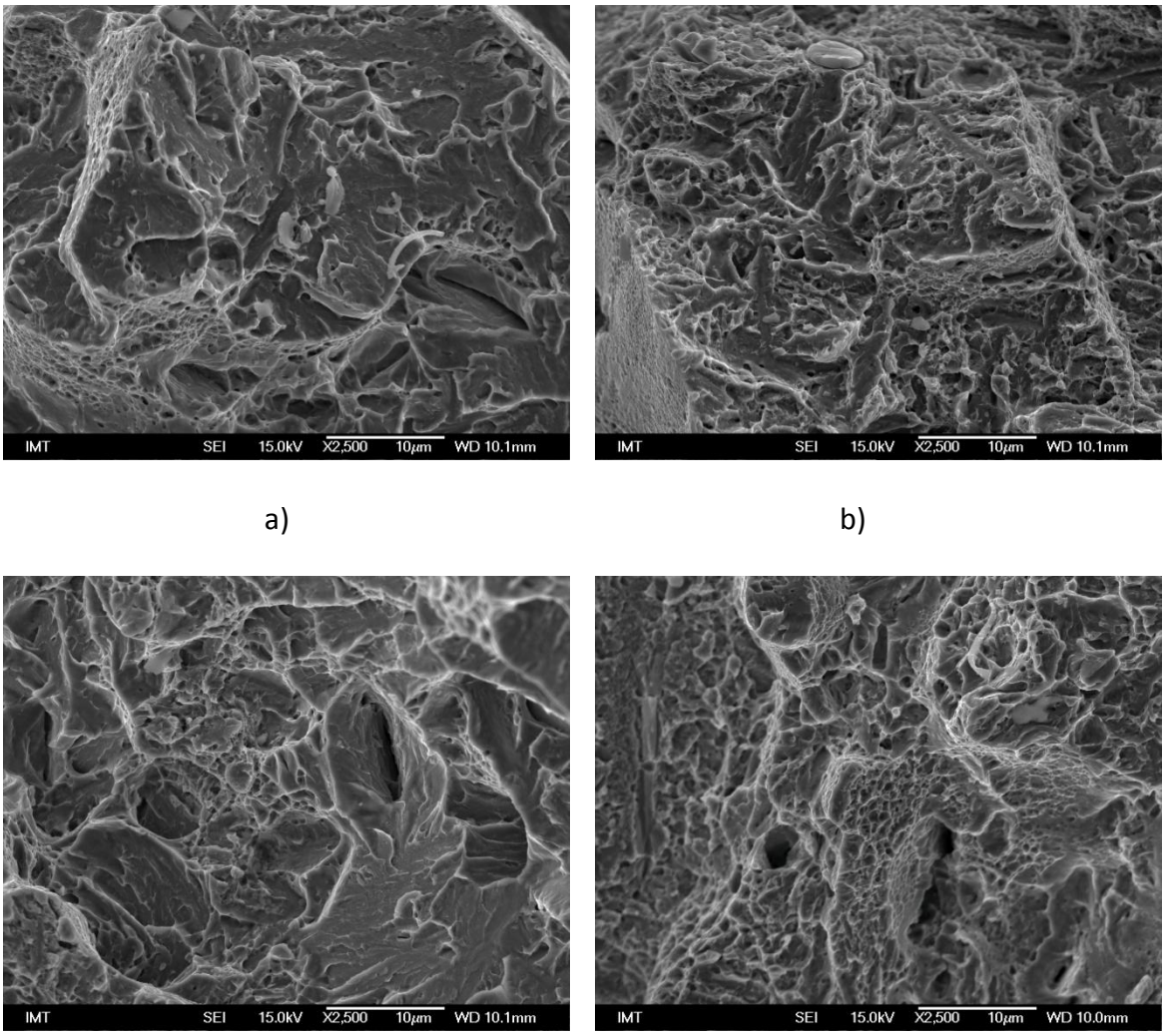

a) b)

c) d)

Slika 4. Prijelomne površine CVN uzoraka a) UA-1, v_{hl} = 1,5 °C/s; b) UA-2, v_{hl} = 2,5 °C/s; c) UB-1, v_{hl} = 1,5 °C/s; d) UB-2, v_{hl} = 2,5 °C/s

ZAKLJUČAK

U radu je istraživan utjecaj brzine hlađenja te udjela mangana i kroma na mikrostrukturu tj. vrstu, morfologiju i udio bainita te utjecaj mikrostrukture na vlačnu čvrstoću, udarnu žilavost i tvrdoću. Kod svih uzoraka postignuta je mješovita martenzitno-bainitna mikrostruktura. Obzirom na približno jednake temperature početka stvaranja bainita i martenzita nisu očekivane drastične razlike u morfologiji bainita. Rezultati su pokazali da uzorci hlađeni većom brzinom imaju strukturu u kojoj prevladava martenzit te je prisutan donji bainit u približno jednoj trećini. Kod oba kemijska sastava mikrostrukturne faze su u približno jednakim omjerima. Kod uzoraka hlađenih manjom brzinom nastao je pretežno gornji bainit i to većinom bez izlučenih karbida između feritnih zrna, morfologije degeneriranog gornjeg bainita. Vrsta i udio nastalog bainita utjecao je na mehanička svojstva pri čemu je vidljivo da

su uzorci s mješavinom martenzita i donjeg bainita imali značajno veću vlačnu čvrstoću te veću konvencionalnu granicu razvlačenja dok su uzorci s većinskim udjelom mekše faze tj bainita imali veću udarnu žilavost.

LITERATURA

[1] S. Zajac, V. Schwinn, KH. Tacke, Characterization and Quantification of Complex Bainitic Microstructures in High and Ultra-High Strength Linepipe Steels. Proceedings of the International Conference on Microalloying for New Steel Processes and Applications, Donostia-San Sebastian, Spain, 7–9 September, (2005) Trans Tech Publications Ltd, Zurich, Switzerland pp. 387–394.

[2] G. Krauss & SW. Thompson, Ferritic Microstructures in Continuously Cooled Low- and Ultralow-carbon Steels. ISIJ International 35(8) (1995) pp. 937–945.

[3] Y. Ohmori, H. Ohtani & T. Kunitake, Bainite in low carbon low alloy high strength steels. Transactions of ISIJ 11(4) (1971) pp. 250–259.

[4] BL. Bramfitt & JG. Speer, A Perspective on the Morphology of Bainite. Metallurgical and Materials Transactions A 21(4) (1990) pp. 817–829.

[5] A. Barbacki, The role of bainite in shaping mechanical properites of steels. Jorunal of Materials Processing Technology 53 (1995) pp. 57 - 63

[6] Hs. Fang, Yk. Zheng, Xu. Chen, et al. Novel Air-Cooled Bainitic Steels Journal of Metals, 1988, 40(3) pp. 51-58.

[7] Hs. Fang, Yk. Zheng, Xu. Chen, et al. A Series of New Type Air cooling Bainitic Steels [J]. SEAISI Qurrerly , 1991, 20(3) pp. 30-37.

[8] Hs. Fang, C. Feng, Yk. Zheng, Zg. Yang, Bz. Bai, Creation of Air-Cooled Mn series bainitic steels, Jorunal of Iron and Steel Research International, 2008, 15 (6), pp. 01-09.

[9] T. Kunitake, Y. Okada, The estimation of bainite transformation temperatures in steels by the empirical formulas. J. Iron Steel Inst. 84, (1998) pp. 137–141.

[10] K.W. Andrews, Empirical formulae for the calculation of some transformation temperatures. J. Iron Steel Inst. 203, (1965) pp. 721–727.

[11] H.K.D.H. Bhadeshia, E. Keenan, L. Karlsson, H.O. Andren, Coalesced Bainite, Transaction of the Indian Intstitute of Metals 59, (2006), pp. 689 – 694.

[12] H.K.D.H. Bhadeshia, Bainite in Steel, The Institute of Materials, London, (1992).

[13] K. Abbaszadeh, H. Saghafian, S. Kheirandish, Effect of Bainite Morphology on Mechanical Properties of the Mixed Bainite-martensite Microstructure in D6AC Steel, J. Mater. Sci. Technol. 28 (4), (2012), pp. 336 – 342.

15th INTERNATIONAL FOUNDRYMEN CONFERENCE

INNOVATION – The foundation of competitive casting production

Opatija, May 11th-13th, 2016

http://www.simet.hr/~foundry/

THERMAL ANALYSES AND PHASE CHARACTERISATION OF AlCu5.5Nd2.5

M. Vončina[1], D. Volšak[2] and J. Medved[1]

[1]University of Ljubljana Faculty of Natural Sciences and Engineering, Department for Materials and Metallurgy, Ljubljana, Slovenia
[2]IMPOL d.d., Slovenska Bistrica, Slovenia

Poster presentation
Original scientific paper

Abstract

In this paper, system Al-Cu-Nd was used where AlCu5.5Nd2.5 alloy was analysed, whereas this system is not known in detail yet. In order to analyse the path of the solidification and phase identification in alloy AlCu5.5Nd2.5, simple thermal analysis (ETA), differential scanning calorimetry (DSC) and electron microscopy were used. Nevertheless, the influence of grain refining element Ti was analysed.

Keywords: *Thermal analysis, AlCu5.5 alloy, DSC analysis, rare earth*

*Corresponding author (e-mail address): *maja.voncina@omm.ntf.uni-lj.si*

INTRODUCTION

The main reason for the addition of alloying elements is to improve the mechanical properties of aluminium alloys. Alloying has an effective impact on the alloy, since it achieve the desired material properties. The literature [1, 2, 3, 4, 5, 6] indicates that additions of rare earth elements such as Ce, La, Nd and Pr into aluminium alloys improve certain properties. It increases the mechanical properties, abrasion resistance and processability. Neodymium forms with aluminium and copper characteristic structures, which can be defined in the binary phase diagrams Cu - Nd and Al - Nd. [7, 8, 9, 10, 11, 12] Al-alloys are combined also with Ti, whereas the content of titanium in pure aluminium is up to 0.0001 wt. %. Titanium reduces conductivity of aluminium, but the effect can be reduced by the addition of boron with the formation of insoluble TiB_2 phase. Titanium is mainly used in order to reduce the grain size in casting ingots.

System Al-Cu

Alloys from system 2XXX, with the main alloying element of copper, is mainly used in the automotive, aerospace and military industries for the manufacture of forgings and hardware for further processing. [13, 14, 15] The copper content in aluminium alloys is between 2 and 10 wt. %. Hardening mechanism is the largest when there is 4 to 6 wt. % of Cu in the alloy, whereas it depends on other elements in the alloy.

Aging properties of binary alloys Al-Cu are explored in detail. The most widely used alloys are additionally provided with another alloying element such as: Si, Fe, Mn, Mg and Zn [16]. Figure 1 shows an isothermal cross section of the system Al-Cu-Nd at 500 °C. Rare earth elements are used as an alloying elements in aluminium alloys, their content is about 5 wt. %. These alloys show extremely high mechanical properties, about twice as the normal commercial alloys, they are ductile and due to the low density suitable for aerospace and aviation industry [17, 18, 19, 20, 21].

For the analysis of solidification and phase identification, literature data of binary systems Al - Nd and Cu-Nd were used [22, 23, 24, 25, 26, 27, 28, 29, 30]. Table 3 shows the phases in the system Al-Cu-Nd.

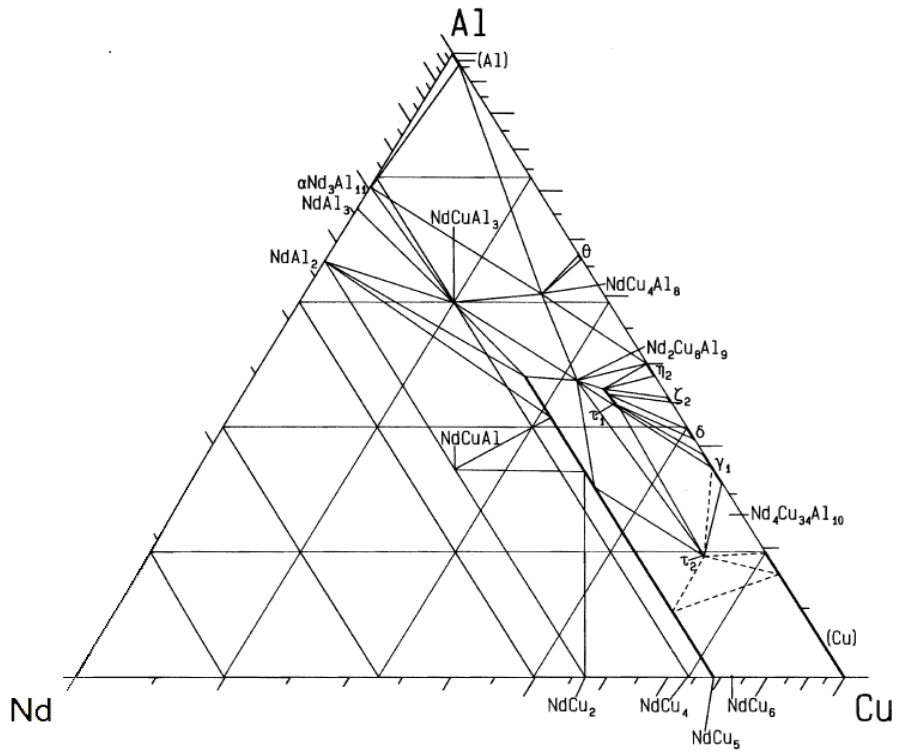

Figure 1. Partial isotherme cross section of alloy system Al-Cu-Nd at 500 °C, using more than 33.3 at. % Nd

Table 1. Phases in system Al–Cu–Nd

Phase no.	Stoichiometry
1	$(Al_xCu_{1-x})Nd$
2	AlCuNd
3	Al_3CuNd
4	Al_8Cu_4Nd
5	$Al_9Cu_8Nd_2$
6	$\tau_1(Al_6Cu_{6+x}Nd)$
7	$\tau_2(Al_{2.4}Cu_{8.6}Nd)$

In the aluminium corner of the presented system it is predicted to exist two ternary intermetallic phases, Al_3CuNd and Al_8Cu_4Nd, which begins to melt at 1030 °C and 1240 °C. In the case of alloys with a higher content of Nd, it is predicted the existence of binary phases $\alpha(Al_{11}Nd_3)$ Al_3Nd and Al_2Nd, that are specific for the binary alloying system Al-Nd [29]. In case of a higher contents of Cu and Nd, ternary intermetallic phases $\tau_1(Al_6Cu_6 + xNd)$, τ_2 $(Al_{2.4}Cu_{8.6}Nd)$, AlNdCu and $Al_9Cu_8Nd_2$ and two-component phase Cu_5Nd, characteristic for the system Cu-Nd, occur [31, 29]. The diagram also shows that a solid solution of α-Al does not soluble Nd and it depends on the solubility of Cu, which means that all the areas below the temperature of 650 °C can contain very low levels of $\alpha(Al_{11}Nd_3)$ phase [28].

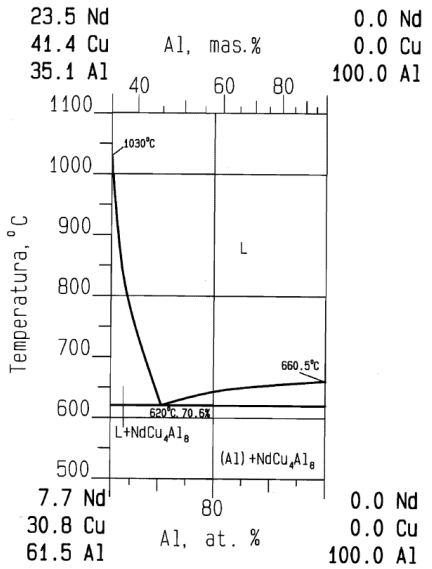

Figure 2. Vertical cross section of alloying system Al-Cu-Nd at Al – Al_8Cu_4Nd

EXPERIMENTAL WORK

Investigated alloys were made of pure 99.9 Cu and 99.9 Nd and grain refining master alloy AlTi5B1. Alloys were melted in an induction furnace and cast into Croning measuring cell, whereas cooling curves were recorded and the course of solidification was analysed.

Furthermore, samples were cut from ETA and prepared for DSC analysis and metallography. The apparatus STA 449 from NETZSCH Company was used to perform differential scanning calorimetry (DSC). DSC is a method of thermal analysis, wherein a single test during the heating above the melting temperature and then cooling to room temperature, examine the effects of the heat and the change in mass of the sample. In this way different types of materials such as metals and alloys, minerals, ceramics, polymers, ... can be characterized. In the case of the DSC analyses, the sensor is made of platinum, two corundum crucible are inserted, one for the investigated material and one for the inert/comparative material. The samples were heated in an argon atmosphere at a constant rate of 10 K/min until the temperature of 710 °C. The samples were set on constant temperature of 710 °C for 10 min. During the measurement, the time and temperature, and the temperature difference between the sample and the comparative sample were measured.

The samples for the microstructure analysis by scanning electron microscope (JEOL JSM5610) were cut from the castings after the ETA. EDS analysis was performed in order to identify the phases that occur during the solidification of investigated alloys.

RESULTS AND DISCUSSION

Figures 3 - 5 show the cooling curves of investigated alloys AlCu5.5, AlCu5.5Nd2.5 and AlCu5.5Nd2.5 + AlTi5B1. The transformation points and the course of solidification was characterized. An alloy containing only Al and Cu, the solidification course goes through two steps; first is the solidification of the primary α-Al at temperature 637.5 °C and recalescence 2.5 ° C, as a second is eutectic (α-Al + Al_2Cu) at T = 540.5 °C. Solidification is completed at a temperature of T_S = 537 ° C.
Figure 4 shows the cooling curve of the sample AlCu5.5 containing 2.5 wt. % Nd. Coagulation was initiated by the formation of crystals α-Al at T = 632.7 °C with recalescence 1.6 °C. Further, the eutectic using Nd solidifies at $T_{E/min}$ = 608.1 °C with recalescence 2.2 °C. Solidification ended at T_S = 596.6 ° C.
From the cooling curve (Figure 5) of alloy, which contains the addition of Nd and AlTi5B1 it can be seen that the solidification starts with the formation α-Al at T = 639.4 °C, and there was no recalescence. Eutectic solidification began at the $T_{E/min}$ = 607.6 °C, recalescence is 1.7 °C. Solidification ended at T_S = 597.2 ° C.

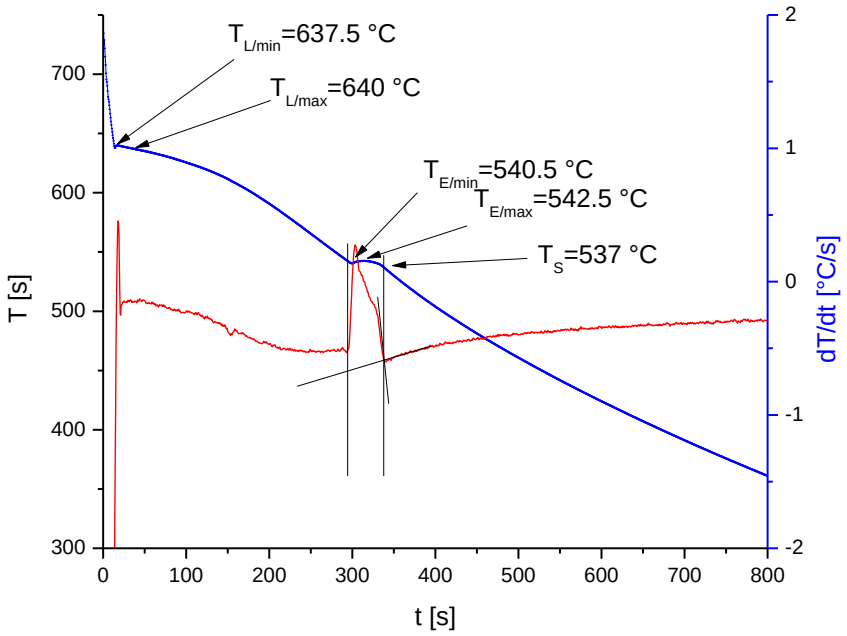

Figure 3. Cooling and differential cooling curve of alloy AlCu5.5

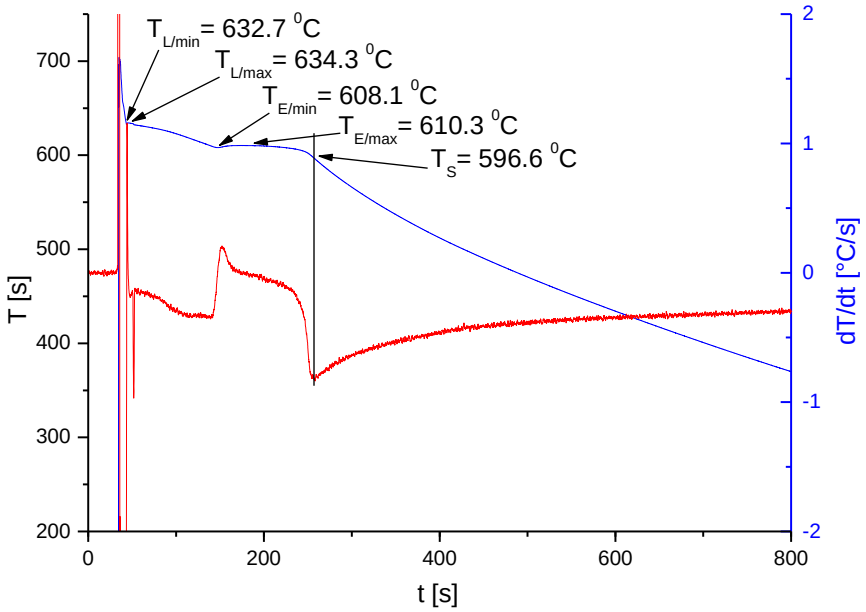

Figure 4. Cooling and differential cooling curve of alloy AlCu5.5Nd2.5

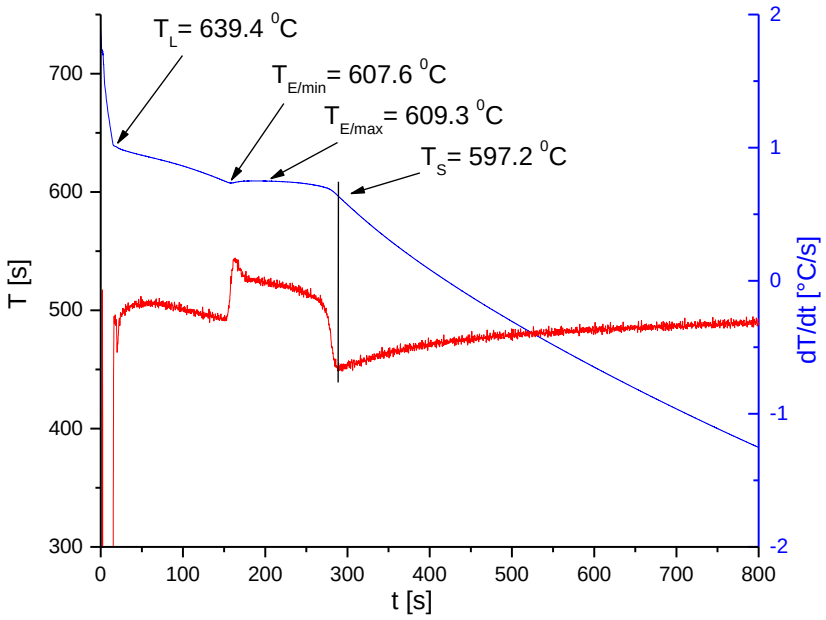

Figure 5. Cooling and differential cooling curve of alloy AlCu5.5Nd2.5 using Ti

The results indicate that the addition of Nd does not substantially effect on the liquidus temperature but it effected on the increase in the temperature of the eutectic solidification for about 65 °C and on the solidus temperature for about increasing 60 °C.

Furthermore, Figure 6 shows the heating DSC curves, while Figure 7 shows cooling DSC curves of the three investigated samples. For two-component alloy AlCu5.5 the precipitation was detected (Figure 6.a) at T_p = 191.9 °C with the precipitation enthalpy was H_p= 5.031 J/g. Melting of the binary eutectic (α-Al + Al_2Cu) started at T = 546.5 °C with enthalpy 5.271 J/g. Enthalpy of melting was 272.7 J/g. For alloy AlCu5.5 with addition of Nd heating DSC curve is shown in Figure 6.b. The melting of the eutectic with Nd was set to be at a temperature T = 611.8 °C, the primary melting starts at 638.4 ° C. The total enthalpy of melting was 346.9 J/g. At the sample AlCu5.5 alloyed with 2.5 wt. % Nd and AlTi5B1, eutectic melting started at T_E = 611.0 ° C. Primary melting α-Al started at 640.1 °C. The total enthalpy of melting was 313.5 J/g.

From the cooling DSC curve of the alloy with no Nd and Ti (Figure 7.a) can be seen that the solidification of α-Al started at T_L = 638.4 °C, and the solidification temperature of the binary eutectic was at T_E = 531 °C. Total solidification enthalpy was 331.1 J/g. Sample from AlCu5.5, alloyed by the addition of Nd, started to solidify (Figure 7.b) at temperature T_L = 632.0 °C and the two-phase eutectic solidification temperature was at T_E = 596.6 °C. Total solidification enthalpy was 359.5 J/g. Sample AlCu5.5 alloyed by the addition of Nd and AlTi5B1 showed

(Figure 7.c) the liquidus temperature at T_L = 634.3 °C and the two-phase eutectic solidification temperature at T_E = 592.8 °C. Solidification enthalpy was 336.6 J/g.

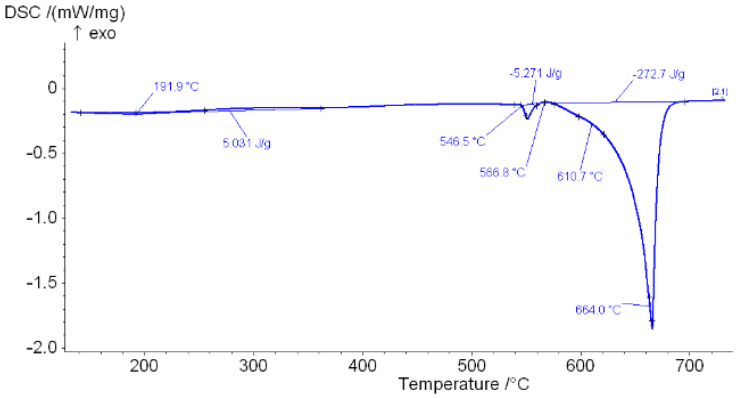

a)

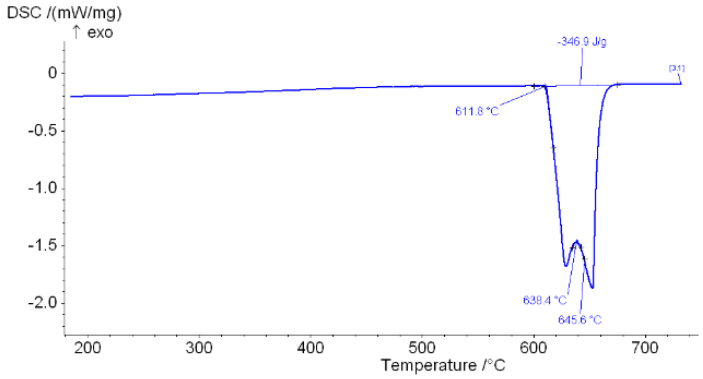

b)

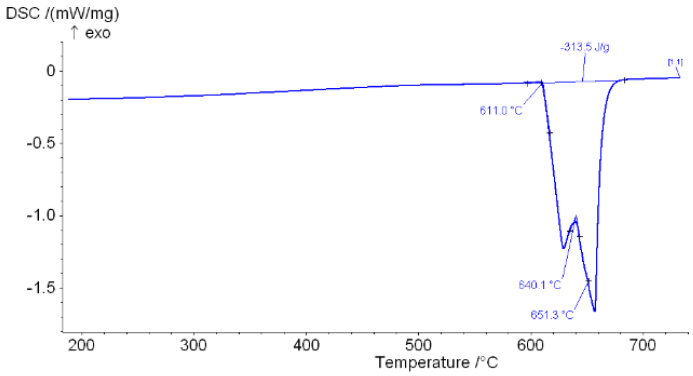

c)

Figure 6. Heating DSC curves of investigated samples: alloy AlCu5.5 (a), alloy AlCu5.5Nd5.5 (b) and alloy AlCu5.5Nd5.5+Ti (c)

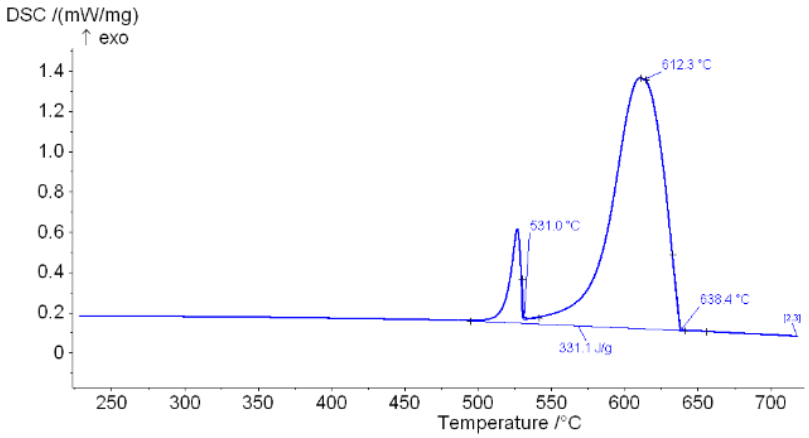

a)

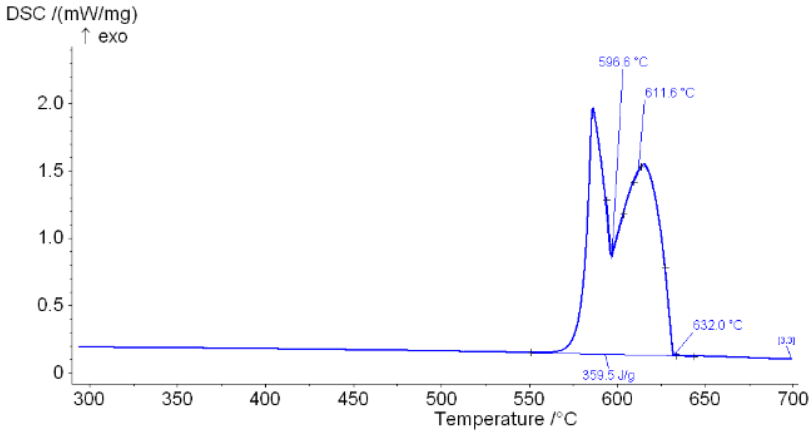

b)

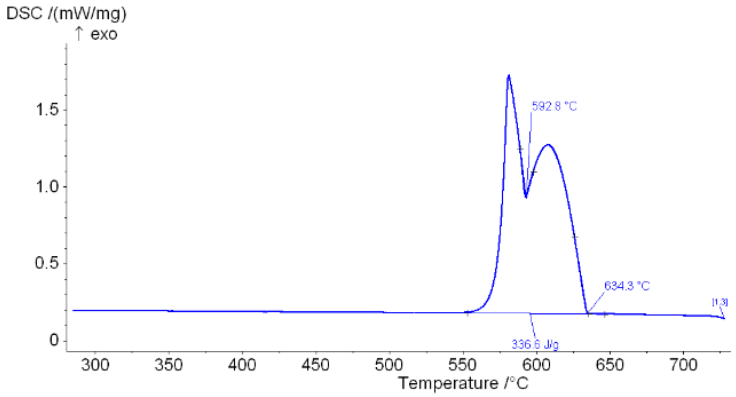

c)

Figure 7. Cooling DSC curves of investigated samples: alloy AlCu5.5 (a), alloy AlCu5.5Nd5.5 (b) and alloy AlCu5.5Nd5.5+Ti (c)

Using electron microscope and EDS analysis the surface chemical analysis of the investigated samples was made. Table 5 presents the results of chemical composition.

Table 2. Chemical composition of investigated samples, wt. %

Alloy	Al	Cu	Nd
AlCu5.5	rest	5.6	0
AlCu5.5Nd5.5	rest	5.1	3.1
AlCu5.5Nd5.5-Ti	rest	5.6	3.6

Furthermore, phases obtained in the microstructure of investigated samples were analysed. Figure 8 shows the SEM micro-shot, where in on Figure 8.b phases analysed by EDS analysis were marked.

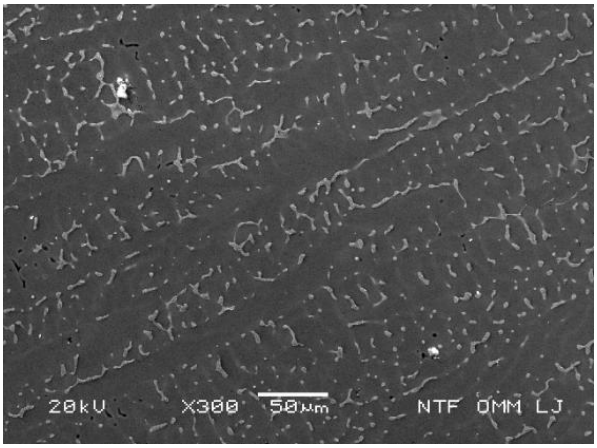

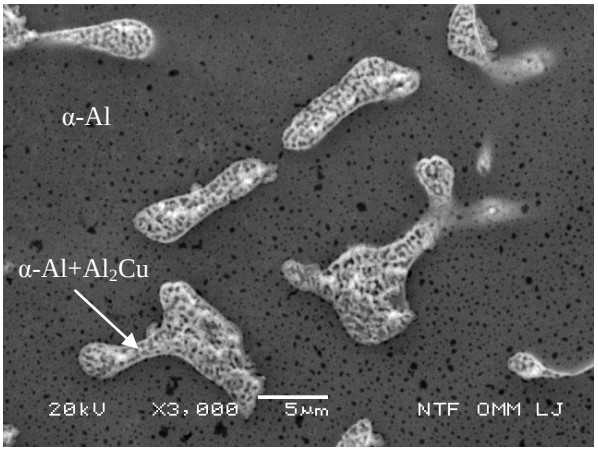

a) b)

Figure 8. SEM micro-shot of sample AlCu5.5: at 300 x magnification (a) and phases analysed with EDS analysis (b)

The sample with the Nd and Ti was also analysed using EDS, results are presented in Table 3. The results show that grains of α-Al are obtained in the microstructure. In paragraph 2, the interdendritic space was analysed and in field 3 eutectic with Nd was obtained, presumably (α-Al + Al_8Cu_4Nd).

Table 3. Results from EDS analysis of certain phases in sample with Nd and Ti

Analysis point	Al		Cu		Nd	
	wt. %	at. %	wt. %	at. %	wt. %	at. %
1	97.0	98.7	3.0	1.3	0	0
2	69.4	87.3	18.2	9.7	12.4	2.9
3	90.3	96.4	6.4	2.9	3.2	0.6

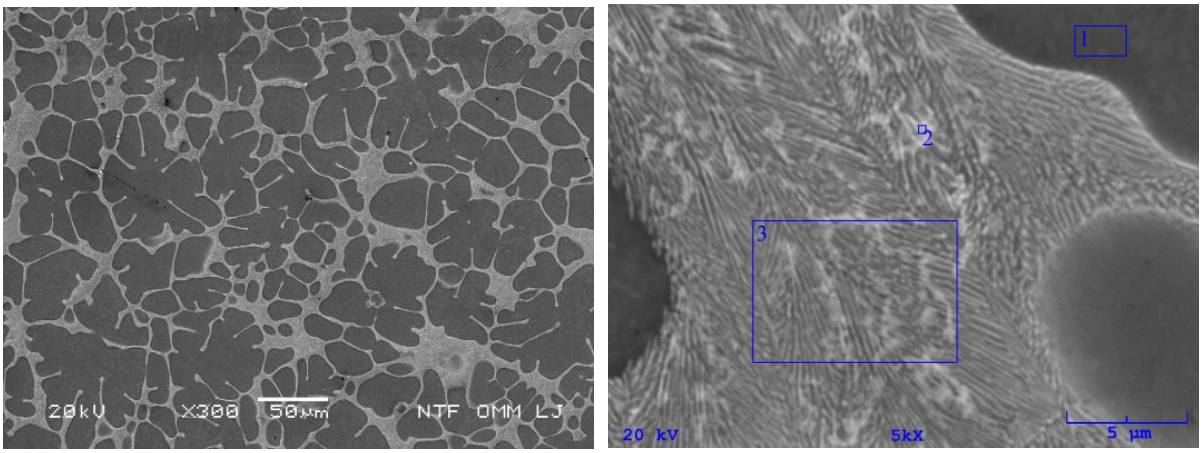

a) b)

Figure 9. SEM micro-shot of sample AlCu5.5Nd2.5+Ti: at 300 x magnification (a) and phases analysed with EDS analysis (b)

CONCLUSIONS

Used experimental methods lead us to following results:
1. Using ETA, it was found that the solidification of the binary eutectic (α-Al + Al_2Cu) starts at T = 540.5 C, at the alloy with the Nd at $T_{E/min}$ = 608.1 °C with recalescence 2.2 ° C and the alloy with addition of Nd and AlTi5B1 at $T_{E/min}$ = 607.6 °C with recalescence 1.7 ° C.
2. DSC analysis showed the precipitation of Al_2Cu at T_p = 191.9 ° C and an onset of melting of the binary eutectic (α-Al + Al_2Cu) in T_E = 546.5 at the alloy AlCu5.5. At the alloy AlCu5.5 with 2.5 wt. % Nd the melting of two-phases heterogeneous compound started at T_E = 611.8 °C. Alloy AlCu5.5Nd2.5 using grain-refiner AlTi5B1 the melting of the two-phase heterogeneous compound starts at T_E = 611.0 ° C.
3. EDS analysis of phase composition gave us one main conclusion; the microstructure of the alloys AlCu5.5Nd2.5 was composed only from α-Al and binary eutectic (α-Al + Al_8Cu_4Nd), whereby the whole Nd incorporated into eutectic phase.

REFERENCES

[1] N. Clavaguera, Y. Du, Thermodynamic Calculation of the Nd-Al System, Jurnal of Phase Equilibria, 17 (1996) 2, pp. 107–111.
[2] J. Wang, Thermodynamic Evaluation of Al-Nd System, Pergamon, Calphad, 20, (1996) 2, pp. 135–138.
[3] A. Hawksworth, W.M. Rainforth, H. Jones; Solidification microstructure selection in the Al-rich Al-La Al-Ce and Al-Nd systens, Journal of growth, 197 (1999), pp.286–296.
[4] G.S. Choi, Y. H. Kim, H. K. Cho, A. Inoue, T. Masumoto; Ultrahigh tensile strength of amorphous Al-Ni-(Nd,Gd)-Fe alloys containing nanocrystalline Al particles, Scripta Metallurgica et Materiala, 33 (1995) 8, pp. 1301–1306.
[5] G. Borzone, N. Parodi, R. Ferro, J.P. Bros, J.P. Dubes, M. Gambino; Heat capacity and phase equilibria in rare earth alloy systems. R-rich R-alloys (R = La, Pr and Nd), Journal of Alloys and Compounds, 320 (2001). pp.242–250.

[6] P. R. Subramanian; D. E. Laughlin;. The Cu-Nd (Copper – Neodymium) System; Bulletin of Alloy Phase Diagrams, 9 (1998) 3a, pp.362–369.
[7] P. Wang, L. Zhou, Y. Du, H. Xu, S. Liu, L. CHEN, Y. Ouyang; Thermodynamic optimization of the Cu-Nd system; Journal of Alloys and Compounds, 509 (2011), pp.2679–2683.
[8] N. Pierron, P. Sallamand, S. Matteï; Study of magnesium and aluminum alloys absorption coefficient during Nd:YAG laser interaction; Applied Surface Science, 253 (2007), pp.3208–3214.
[9] J. Y. Chang, G. H. Kim, I. G. Moon, S. Choi C, Rare earth concentration in the primary Si crystals in rare earth added Al-21 wt. % Si alloy. Scripta Materialia, 39 (1998) 3, pp. 307–314.
[10] B. J. Ye, C. R. JR. Loper, D. Y. Lu, et al. An assessment of the role of rare earth in the eutectic modification of cast aluminum-silicon alloy. AFS Transactions, 30 (1985) pp. 533–544.
[11] D. Volšak, M. Vončina, P. Mrvar, J. Medved; Thermodynamic characterization of an AlCu5.5BiSn alloy with various neodymium additions Mater. tehnol., 46 (2012) 6, pp.607–611.
[12] G. Vassilev, D. Kiradzhiyska, D. Volšak, M. Vončina, P. Mrvar, J. Medved, N. Milcheva, G. Patronov, V. Gandova, Microstructure and thermochemical characterization of Al-Cu-Nd alloys, 22 (2013) B1, pp.8–17.
[13] http://www.grupomecalbe.com/sites/default/files/foto_activ_sector/estampacion.jpg
[14] http://www.czub.cz/en/catalog/327-weapons-for-hobby-and-sport/AIRSH/CZ-75-P-07-DUTY.aspx.
[15] http://www.czub.cz/en/catalog/300-production-capabilities/NP-AUT/CZ-automobilova-vyroba-odmastovani.aspx.
[16] J.R. Davis. ASM Specialty Handbook, Aluminium and Aluminium Alloys. ASM International, 1993, p.60.
[17] B. Liu, M.Zhang, R. Wu; Effects of Nd on microstructure and mechanical properties of as-cast LA141 alloys, Materials Science and Engineering A, 487 (2008), pp.347–351.
[18] L. Zhilin, Z. Yichun, Z. Yinghong, C. Rongzhen, L. Jingqi, W. Xianyou; Phase relations in the Nd-Al-Si system at 500°C, Journal of Alloys and Compounds, 325 (2001), pp.190–193.
[19] H. Zou, X. Zeng, C. Zhai, W. Ding; Effects of Nd on the microstructure of ZA52 alloy, Materials Science and Engineering A, 392 (2005), pp.229–234.
[20] S. Kores, M. Vončina, B. Kosec, P. Mrvar, J. Medved; Effect of cerium additions on the AlSi17 casting alloy. Materials and Technology, 40 (2010) 3, pp. 137–140.
[21] B. Markoli, S. Spaić, Mikrostrukturna karakterizacija zlitine AlSi6CuMg z dodatki samarija. Kovine zlitine tehnologije, ISSN 1318-0010, 1995, letn. 29, št. 5/6, str. 455–457.
[22] http://www.czub.cz/en/catalog/327-weapons-for-hobby-and-sport/AIRSH/CZ-75-P-07-DUTY.aspx
[23] ASM Metals HandBook Volume 15 – Casting, published in 1988.
[24] L.F. Mondolfo, Aluminium Alloys: Structure and Properties, Butterworth Co. London 1962.
[25] J. Wang, J. Yang, Y. Wu, H. Zhang, L. Wang; Microstructures and mechanical properties of as-cast Mg-5Al-0,5Mn-xNd (x=0, 1, 2 and 4) alloys; Materials Science and Enginrrting A, 472 (2008), pp.332–337.

[26] L. LU, K. Raviprasad, M. O. LAI; Nanostructured Mg-5%Al-x%Nd alloys; Materials Science and Engineering A ,368 (2004) pp.117–125.
[27] B. Liu, M.Zhang, R. Wu; Effects of Nd on microstructure and mechanical properties of as-cast LA141 alloys, Materials Science and Engineering, A 487 (2008) 347–351.
[28] L.G. Zhang, Phase Diagrams and Microstructure Evolution of Al-Cu-RE (RE=Y, Nd, Gd, Dy, Er, Yb and Ti) Alloys, PhD thesis, Central South Univesity, 2010.
[29] G. Borzonea, N. Parodia, R. Ferroa, J.P. Brosb, J.P. Dube`sc, M. Gambinob, Heat capacity and phase equilibria in rare earth alloy systems. R-rich R-Al alloys, Journal of Alloys and Compounds, 320 (2001), pp.242–250.
[30] A. Hawksworth, W.M. Rainforth, H. Jones, Solidification microstructure selection in the Al-rich Alpha, AlCe and AlNd systems, Journal of Crystal Growth 197 (1999), pp.286-296.
[31] P. R. Subramanian; D. E. Laughlin, The Cu-Nd (Copper – Neodymium) System; Bulletin of Alloy Phase Diagrams, 9 (1998) 3a, pp.362–369.

15th INTERNATIONAL FOUNDRYMEN CONFERENCE
INNOVATION – The foundation of competitive casting production
Opatija, May 11th-13th, 2016
http://www.simet.hr/~foundry/

REFERENCES REVIEW IN THE FIELD OF COPPER-BASED CASTED ALLOYS FOR LAST FIFTEEN YEARS

D. Živković[1], N. Štrbac[1], N. Dolić[2], Z. Zovko Brodarac[2], D. Manasijević[1], Lj. Balanović[1], A. Mitovski[1], S. Mladenović[1], I. Marković[1]

[1]University of Belgrade Technical Faculty in Bor, Bor, Serbia
[2]University of Zagreb Faculty of Metallurgy, Sisak, Croatia

Poster presentation
Subject review

Abstract

References review in the field of copper-based casted alloys for last ten years is presented in this paper. Based on bibliometric analysis for the period 2000 to 2015, data including number of scientific papers per year, authors, countries, affiliations, subject areas and document types were obtained and analyzed using Scopus database as selected index database.

Keywords: *copper-based casted alloys, bibliometric analysis, scientometry*

*Corresponding author (e-mail address): *dzivkovic@tf.bor.ac.rs*

INTRODUCTION

Copper-based casted alloys have an extremely broad range of application - they are used in almost every industrial market category, from ordinary plumbing goods to precision electronic components and state-of-the-art marine and nuclear equipment [1]. Their favorable properties - the reason for their wide use - are excellent corrosion resistance, favorable mechanical properties, friction and wear properties, high electrical and thermal conductivity, good castability, excellent machinability and fabricability, reasonable cost, etc. [2].

Having in mind the importance of these alloys, the references review in the field of copper-based casted alloys for last fifteen years is presented in this paper. As one of the most effective tool of data-mining method [3], significant in technology development monitoring, knowledge management, and evaluation of global scientific production, the bibliometric analysis [4] was applied on this scientific area.

METHOD

The number of documents per year, as well as documents per year by source, author, affiliation, country, type and subject area, for a period from 2000 to 2015, has been investigated using SCOPUS database [5] (on date 24 March 2016).

Also, patent analysis for the same period was done using Patent Scope [6]. Obtained data represents an adequate indicator for scientific and technological performance analysis in development trend of copper-based casted alloys, and can be taken in further quantitative innovation research [7,8].

RESULTS AND DISCUSSION

According to the results obtained using SCOPUS database [5] (on date 24 March 2016), the number of documents per year, as well as documents per year by source, author, affiliation and country for period 2000-2015, has been obtained. Searching key-words used were "copper alloys" + "casting". During the analysis of the references review in the field of copper-based casted alloys for last fifteen years, different bibliometric parameters were determined, as presented in Figures 1-4 and Table 1.

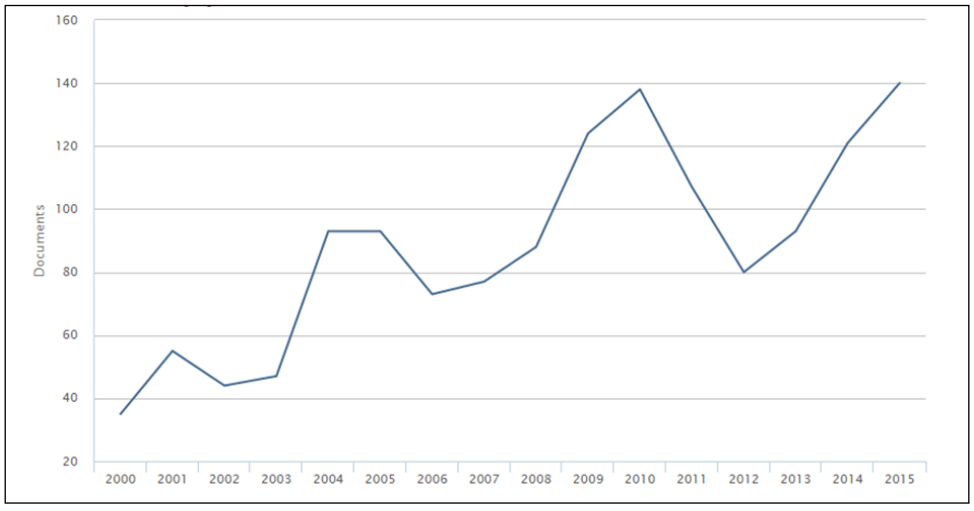

Figure 1. Review of the documents by year

Table 1. Review of the documents per year by source

Source	Documents
Materials Science Forum	90
Journal of Alloys and Compounds	62
Advanced Materials Research	57
Materials Transactions	45
Metallurgical and Materials Tran...	36
Materials and Design	29
Litejnoe Proizvodstvo	25
Zhongguo Youse Jinshu Xueba...	25
Solid State Phenomena	21
TMS Annual Meeting	20

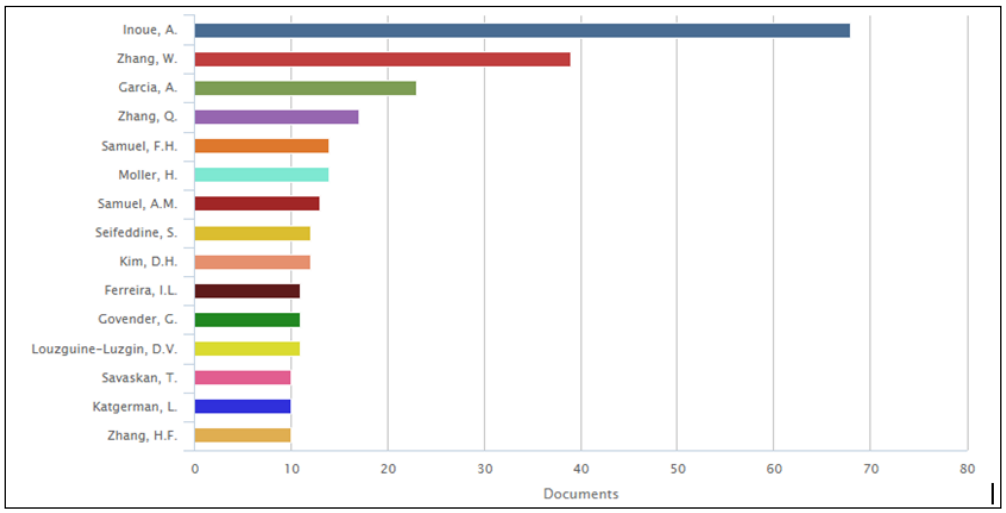

Figure 2. Review of the documents by author

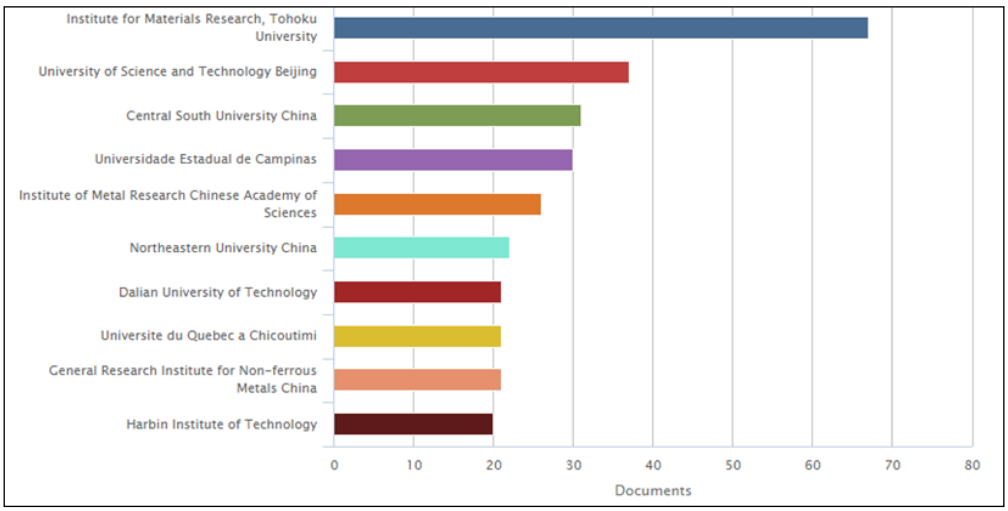

Figure 3. Review of the documents by affiliation

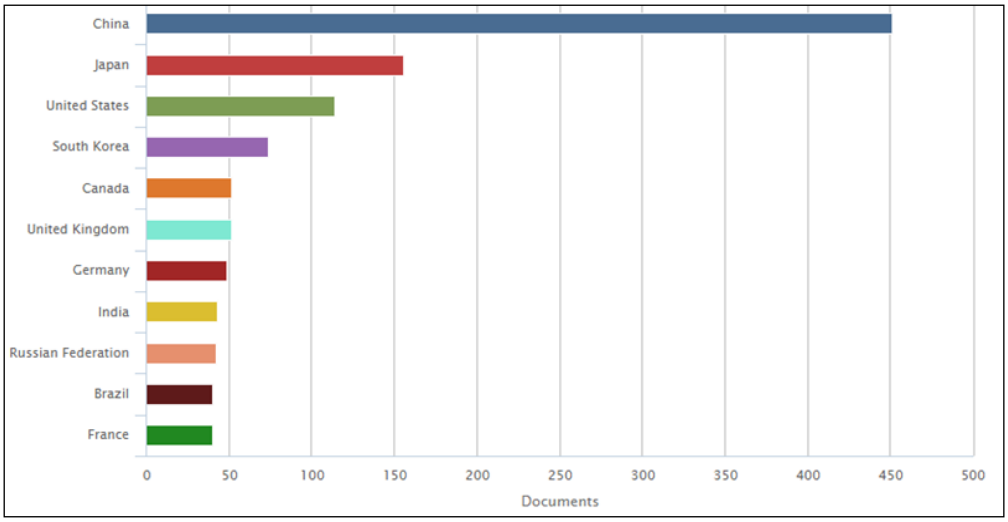

Figure 4. Review of the documents by country

As can be seen from previous Figs.1-4 and Table 1, applied bibliometric analysis done according to SCOPUS gave following results: 1408 documents were published in examined period of fifteen years; most of the publications were from following journals: Materials Science Forum (90 documents), Journal of Alloys and Compounds (62 documents) and Advanced Materials Research (57 documents); the authors who published the highest number of papers in the field of copper-based casted alloys were Inoue A. (68 documents), Zhang W. (39 documents) and Garcia A. (23 documents); the institutions whose authors published most of the documents (over 30) in examined field are Institute for Materials Research, Tohoku University (Japan), University of Science and Technology Beijing (China) and Central South University (China); in accordance with already given results, most of published documents on copper-based casted alloys were from China (451 documents), Japan (156 documents) and United States (114 documents); two document types were

mostly common – articles (972) and conference papers (381) in the most common subject areas – Materials Science (1084), Engineering (770) and Physics and Astronomy (472).

Beside given bibliometric analysis, patent analysis for the examined period of last ten years was done using Patentscope [6]. Totally 871 published international patents in the field of casted copper-based alloys was determined to be proposed since 2000 to 2015.

CONCLUSIONS

According to the bibliometric analysis in the field of copper-based casted alloys done for reporting period (2000-2015), the references review given in this paper shows that specific cycles in the publication trend are noticed: the peaks related to highest number of published references are defined for 2001, 2004, 2010 and 2015, while the lowest number of publications is typical for 2002, 2008 and 2012. Also, it is confirmed that the researchers and institutions from China, Japan and USA published the highest number of publications for examined period.

Presented data-mining analysis in the field of copper-based casted alloys may be useful for further technological forecasting and knowledge maps formations, which can be important for trend monitoring [9] in this scientific and technological field.

REFERENCES

[1] American Foundrymen' s Society - Casting Copper-Base Alloys, AFS, Des Plaines, lL, 1984.
[2] Copper casting alloys - Copper Development Association Inc., 1994.
[3] Hastie, T., Tibshirani, R.; Friedman, J. - The Elements of Statistical Learning: Data Mining, Inference, and Prediction, 2009.
[4] http://ip-science.thomsonreuters.com/m/pdfs/325133_thomson.pdf
[5] https://www.scopus.com/
[6] https://patentscope.wipo.int/search/en/search.jsf
[7] D. Živković, M. Niculović, D. Manasijević, D. Minić, V. Ćosov, M. Sibinović, Bibliometric trend and patent analysis in nano-alloys research for period 2000-2013, Recent Patents on Nanotechnology, 9 (2) (2015) pp.126-138.
[8] D. Živković, M. Niculović , Lj. Balanović , D. Manasijević , V. Ćosović , N. Talijan , I. Janković, Intelectual property importance in example of recent patents in the field of biomaterials, Accessible on Internet: http://www.tmt.unze.ba/zbornik/TMT2015/TMT_2015_022.pdf
[9] A.Pouris, Nanoscale research in South Africa: A mapping exercise based on scientometrics. Scientometrics, 70 (3) (2007) pp.541-553.

Acknowledgements

The authors from Technical faculty in Bor acknowledged support in the frame of Project OI172037 (MPNTRS).

COMMERCIAL PAGES

Elkem
A Bluestar Company

Representative office:
Elkem AS, J.J.Strossmayer 176, Sisak Croatia
Tel:+385/44/659-065; Fax:+385/44/659-067
gordana.gojsevic@elkem.no; zoran.kovacic@elkem.no

Business areas


Silicon Materials


Silicones


Foundry Products


Carbon

Elkem´s solution for...

Aluminium	Automotive	Building&construction	Chemical industry
Electric arc furnace	Electronic&Solar	Energy	Engineering
Oilfield	Polymer applications	R&D services	Refractories and ceramics

Elkem Carbon Fiskaa

Elkem Carbon Fiskaa was established after the invention of the Soderberg electrode in 1917. Since 1919 Elkem Carbon Fiskaa has produced and marked electrode paste all over the world.

Elkem Carbon

Elkem Carbon is a world leading supplier of carbon electrode materials, lining materials and specialty carbon products to metallurgical processes for the production of ferro-alloys, base metals and primary aluminium. Our facilities are located near all major markets.

Processes and products

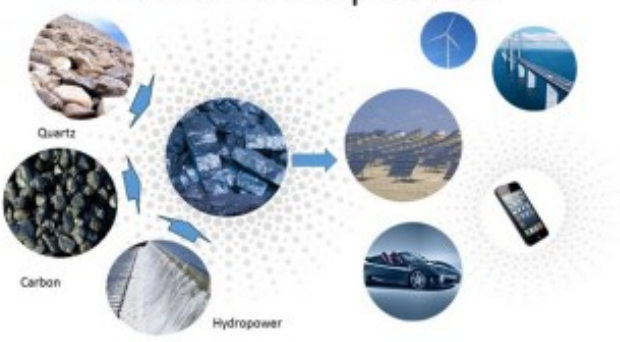

Elkem
A Bluestar Company

Representative office:
Elkem AS, J.J.Strossmayer 176, Sisak Croatia
Tel:+385/44/659-065; Fax:+385/44/659-067
gordana.gojsevic@elkem.no; zoran.kovacic@elkem.no

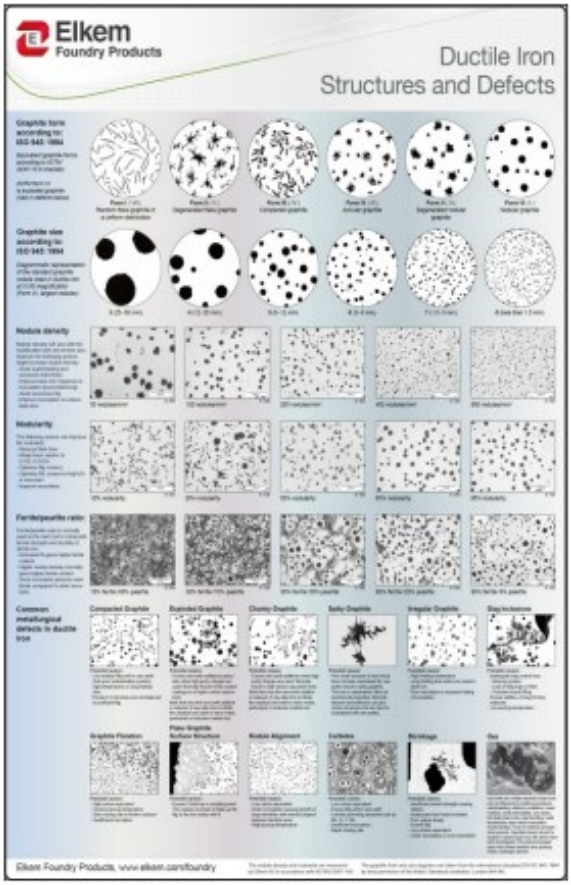

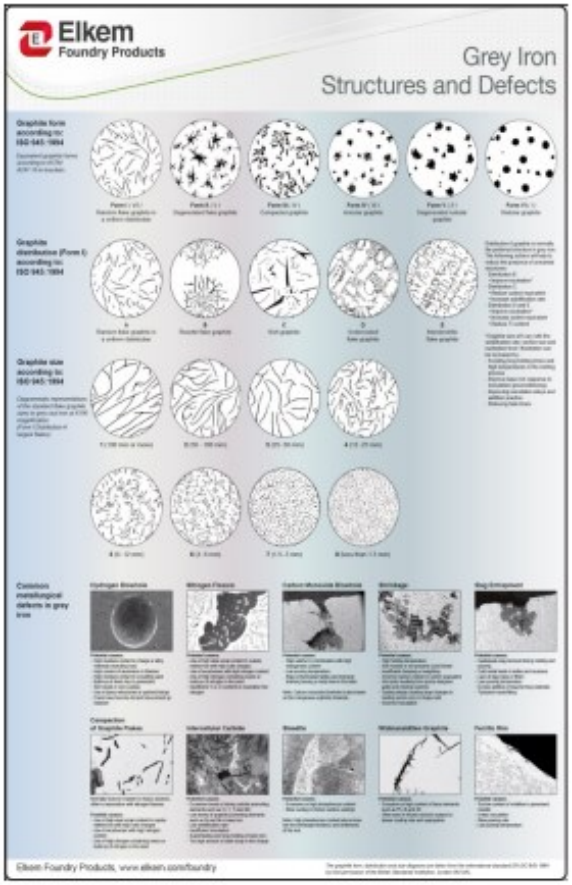

Our Partner: Ferrosad Low Carbon Steel Shot

METALLTECHNIK
SCHMIDT GMBH & CO. KG

COMET

Karnasch
PROFESSIONAL TOOLS

Visokokvalitetan alat za obradu metala

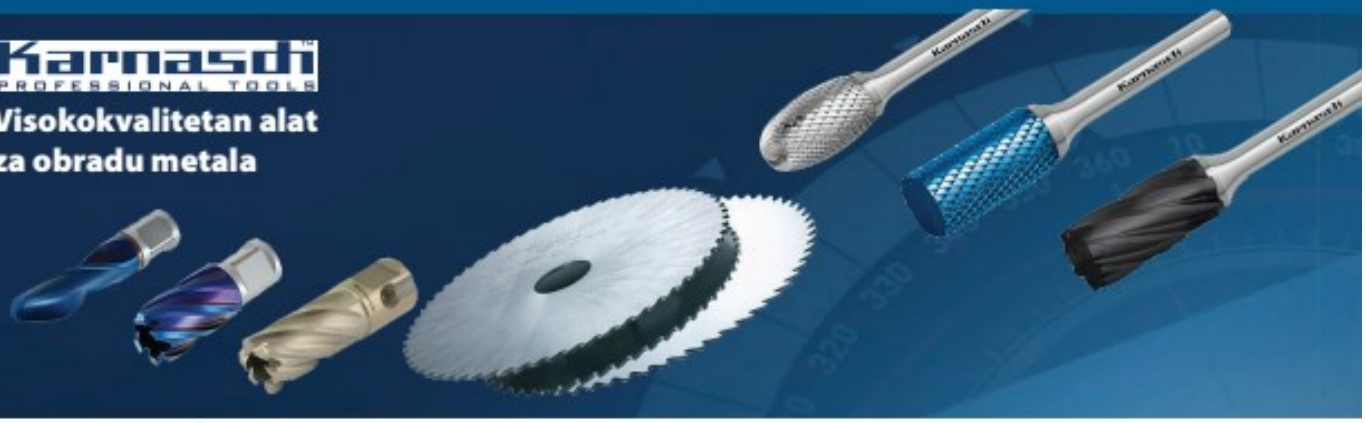

HELIOS · PREISSER

Profesionalni mjerni alati

Mikrometri

Mjerne ure

Pomična mjerila

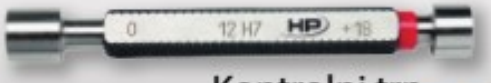

Kontrolni trn

Chicago Pneumatic

Industrijski pneumatski alati

COMET

Ekskluzivni uvoznik za Hrvatsku:
COMET d.o.o.
Varaždinska 40c, Novi Marof, Hrvatska
T:+385 (0)42 408 500
www.comet.hr

Thermo Scientific i BELEC - svjetski lideri u OES, XRF i XRD analizi

Ovlašteni zastupnik (prodaja, aplikacije, servis iz Zagreba i Beograda) :
Analysis DOO, Beograd, Srbija
+381 11 318 64 46, www.analysis.rs;

- OES spektrometri: ARL 4460, ARL 3460, ARL iSpark, BELEC Lab3000S
- XRF spektrometri:

WDX: Optim', Perform'X I ARL 9900
EDX: Quant'X, NITON XRF portabl

- XRD spektrometri: X'TRA
- XRF/XRD u jednom: ARL 9900 IP I WS

Thermo SCIENTIFIC

Thermo Scientific ARL iSpark Series
Optical Emission Spectrometers

ANALYSIS
LABORATORY EQUIPMENT

Innovative OES for reliable quality metals

High degree of functionality

Main features

- Improved PMT spectrometer
- High performance CCD spectrometer
- Advanced signal acquisition and processing for PMT and CCD
- New spark stand to facilitate maintenance and minimize argon consumption during analysis
- IntelliSource digital spark source with increased flexibility and efficiency
- Significant argon savings when instrument is idle with Smart Argon Management
- Reliable factory calibration
- Proven quality assurance
- Installation Qualification and Operational Qualification (IQ/OQ)
- Flexible OXSAS software
- Ultra-fast analysis of micro-inclusions
- Worldwide support

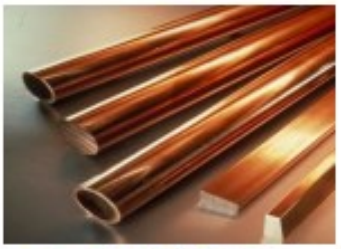

Speed • Precision • Accuracy • Repeatability • Stability • Reliability

www.thermoscientific.com/ispark

BENTO
PRODUCT

TRUE ALCHEMY

TRUE ALCHEMY TRUE ALCHEMY TRUE ALCHEMY

BENTOPRO-A je alkalno aktivirani bentonit vrhunskog kvaliteta koji se koristi kao vezivo za pripremu pješčanih kalupa za livenje sivog i nodularnog liva, čelika i nekih obojenih metala.

BENTOPROCARBO je kompozitno vezivo proizvedeno iz mješavine alkalno aktiviranog bentonita i različitog sadržaja prirodnih, mineralnih nosilaca sjajnog ugljenika, u skladu sa zahtjevima kupca.

BENTOPRODUCT DOO je regionalni lider u proizvodnji različitih proizvoda na bazi visokokvalitetnog bentonita. Trenutno, godišnji nivo prodaje iznosi 25-30.000 tona gotovih proizvoda za različite namjene:

- BENTOPRO-A i BENTOPROCARBO, za primjenu u livarstvu
- BENTOPRODRILL, za primjenu u bušaćim radovima
- BENTOPROSEAL, za primjenu u građevinarstvu
- BP GROUND, ispune za poboljšanje elektrovodljivosti kod uzemljenja
- BP FARMA, za primjenu u poljoprivredi (aditivi za stočnu hranu i tretman zemljišta)
- BP CLARIS, za primjenu u prehrambenoj industriji (sredstva za bistrenje vina i voćnih sokova)

BENTOPRODUCT DOO svoje proizvode prodaje u više od 10 zemalja, a preko 70% na teritoriji EU. 50% livačkog programa prodaje se livnicama u sektoru automobilske industrije.

Poslujemo u skladu sa Integrisanim menadžment sistemom koji uključuje ISO 9001, ISO 14001 i OHSAS 18001, a za proizvode za prehrambenu industriju posjedujemo sertifikate HALAL i KOSHER.

TRUE ALCHEMY TRUE ALCHEMY TRUE ALCHEMY

TÜV International Certification TÜV THÜRINGEN CERT ISO 9001 TIC
TÜV International Certification TÜV THÜRINGEN CERT ISO 14001 TIC
TÜV International Certification TÜV THÜRINGEN CERT OHSAS TIC

Bentoproduct d.o.o. | Bulevar vojvode Stepe Stepanovića 181c
78000 Banja Luka T: + 387 51 225 210 F: + 387 51 225 212
W: www.bentoproduct.ba E: contact@bentoproduct.ba

FERRO-PREIS

FOUNDRY

Dr. Tome Bratkovića 2, Čakovec, Croatia
Tel: +385 40 384 201, Fax: +385 40 384 209
e-mail: sales@ferro-preis.com

www.ferro-preis.com

+HAGI+ consulting+engineering+sales

Ingenieurbüro
für Giesserei- und Industriebedarf
DI Johann Hagenauer
Hauptstraße 14
A-3143 Pyhra

Tel.: +43 2745 24 172 - 0; Fax: - 30
Mobil: +43 664 22 47 128
johann.hagenauer@hagi.at • **www.hagi.at** • **www.giesserei.at**

+HAGI+ Giessereitechnik, technisches Büro für Giesserei- und Industriebedarf, ist auf den Märkten Österreich, Slowenien, Ungarn und dem ehemaligen Jugoslawien als Vertretung und Berater von namhaften Gießereianlagenherstellern tätig.

Das erstklassige, den größten Teil der Giessereianlagen abdeckende Vertretungsprogramm, ermöglicht zusammen mit der praxisorientierten Kompetenz von DI Johann Hagenauer optimale Betreuung bei allen Investitionsprojekten und Problemen in der Giesserei und Industrie.

+HAGI+ Giessereitechnik, technical office for foundry- and industrial demand, is a representative of the leading foundry equipment manufacturers. It operates as advisor in Austria, Slovenia, Hungary and the former Yugoslavia.

The high-standard +HAGI+ representation program includes nearly the whole range of foundry plant. Together with the practical skills of DI Johann Hagenauer, it guarantees an optimal support for all investment projects and problems in the foundry and industry.

StrikoWestofen Group — www.strikowestofen.com
HWS Heinrich Wagner Sinto — www.wagner-sinto.de
KÜTTNER — www.kuettner.de
INDUCTOTHERM EUROPE LIMITED — www.inductotherm.com
LAEMPE FORMING FUTURE — www.laempe.com
kurtz ersa — www.kurtz.de
wöhr — www.aagm.de
SAPP — www.sapp.it
ITALPRESSE — www.italpresse.it
INFRANORM — www.infranorm.at
ieci — www.iecionline.com
BOSELLO HIGH TECHNOLOGY — www.bosello.it
BRONDOLIN — www.omb-brondolin.com
NEOTECHNIK — www.neotechnik.com
Foundry-Planet.com — www.foundry-planet.com
JOST — www.joest.com
ELECTRONICS — www.electronics-gmbh.com
MTAG HIGH PERFORMERS — www.marti-tech.com

FAPROSID s.r.l
Sede legale e Stabilimento:
Via Zocco, 6 - 25030 ADRO (BS) - ITALY
Tel. 030.7450325 - Fax 030.7450367
www.faprosid.com
C.F. 01461680173 - P. IVA 00629030982
N. Identificativo IT 00629030982 - Cap. Soc. € 26.000 i.v.
C.C.I.A.A. BS Rea n. 289812 - N. Mecc. BS 035920 - Reg. Imp. BS n. 31688

CERTIFICAZIONE DI SISTEMA QUALITÀ
DNV·GL
ISO 9001

COMPANY HISTORY

The origin of Faprosid plant date back to 1965 thanks to the knowledge of its founder Mr. Piantoni Danilo and to his experience among the steel plants of the region.

The company is located in Brescia, city 90 km far from Milan, in an important district of the iron and steel production of the northern Italy.

It was born on an area of 1000 square meter, in a small workshop producing hot tops for steel plants. Its type of quality products turn out to be very appreciated from Italian Customers, so much to allows the company to carve out in a short time a significant share of the Italian market of steel plants which produces ingots, forcing Mr. Piantoni to move to a new industrial hub, doubling his production area.

Thanks to the knowledge acquired through the production of the hot tops, in 1992 Faprosid enters the field of foundries producing successfully sleeves suitable for the production of castings for cast iron and steel.

The growth of the company become almost compulsory taking into consideration the increase of products and the requests belongings from the Italian market, both in foundry and in steel plants industry. Therefore it is necessary to make new investments regarding the manufacturing lines and a further enlargement of the production area until 5000 Square Meters.

At the moment the company has a manufacturing area of 7000 Square Meters but this year, carrying on the positive trend, a further area of 5500 Square Meters have been acquired, thus arriving to a manufacturing hub of 12.500 Square Meters covered.

The continuous expansion and Customers acquisitions bring the company in year 2000 in getting the ISO 9001:2008 certification, necessary to cooperate with large organizations of the metallurgical system. Now it is working to implement the environmental management system according with regulations ISO 14001.

Plants have been realized thanks to the passion and the experience acquired and from to its technical staff, and this have allowed to build through the years unique plants with high productive and quality control efficiency.

With the experience, and thanks to the cooperation with Italian steel plants and foundries, company Faprosid have been able to develop mixtures which allows an high performance. According with the type of metal, it can supply insulating or exothermic products which besides ensuring an optimal shrinkage of the metal, helps improving the quality of the whole metal. It can satisfy Customers which casts various types of alloy steel, carbon, stainless steel, cast iron.

The structure of the laboratories adapts constantly to technological progress and to market needs. Over recent years investments have been made to increase efficiency and flexibility, in order to satisfy every need of innovation and competitiveness. The research and development are always aimed to research new solutions and new materials.

To ensure to the Customers an high quality of finished products, all raw material received are checked, and also the finished products are tested and approved with the issue of a certificate of conformity to the required parameters.

PLINOSERVIS KUZMAN

Projektiranje i izrada centralnih grijanja, plinovoda instalacija i kotlovnica za velike sustave. Ugradnja kondenzacijskih uređaja, razdjelnika topline i vodomjera. Ispitivanje ispravnosti plinskih instalacija i uređaja za M.T.U. Iznalaženje tehničkih rješenja kod negativnih nalaza dimnjaka i sanacija istih.

VI. Nenad Kuzman, 10040 ZAGREB, Mrzlopoljska 2 - HR

OIB: 53047211759 | tel/fax: +385 (1) 2859 294 | www.plin-grijanje-kuzman.hr
www.razdjelnici-kuzman.hr

RASTU VAM TROŠKOVI GRIJANJA I VODE ???
POŠTENO JE DA ONI KOJI TROŠE MANJE, MANJE I PLATE
NUDIMO VAM RJEŠENJA UGRADNJOM RAZDJELNIKA TOPLINE, KALORIMETARA I VODOMJERA
OBRATITE NAM SE SA PUNIM POVJERENJEM!!!

TOPOMATIKA

Industrijsko ispitivanje materijala

gom — Precizno industrijsko 3D mjeriteljstvo

Hegewald & Peschke Meß- und Prüftechnik GmbH — Ispitivanje mehaničkih svojstava

KB Prüftechnik — Ispitivanje tvrdoće površina

Vision ENGINEERING — Mjerni i metalurški mikroskopi

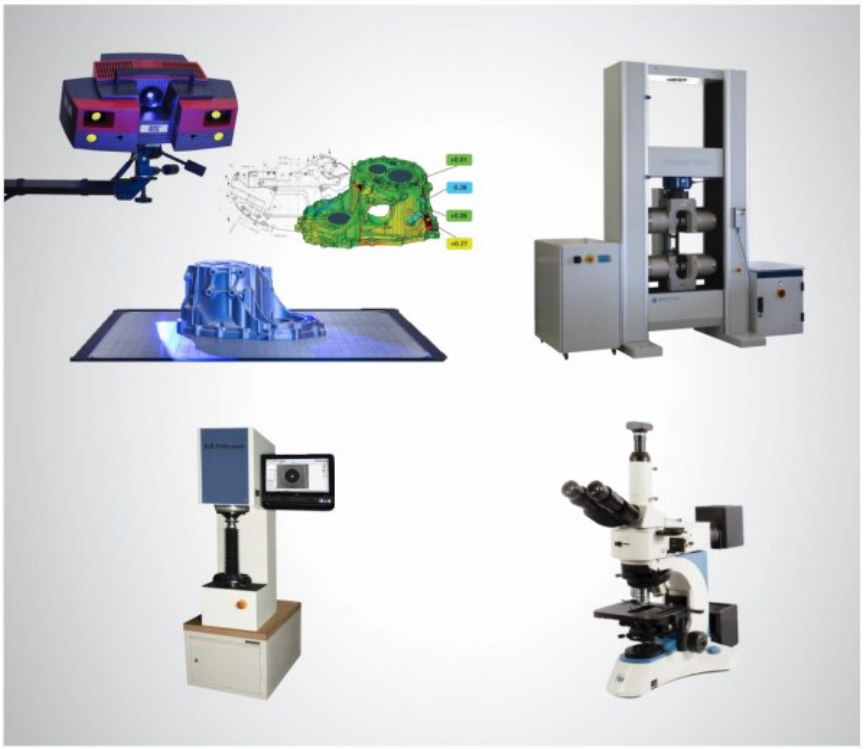

+385 1 349 60 10 • info@topomatika.hr • www.topomatika.hr

	WERNER METAL EXPORT-IMPORT d.o.o.
Name of company	**WERNER METAL-EXPORT IMPORT d.o.o.**
Address of company	Stjepana Radića 3, HR-49247 Zlatar Bistrica, Republic of Croatia
Contacts	Phone: 00 385 (0)49 462 555 Fax: 00 385 (0)49 461 971 Mail: werner-metal@kr.t-com.hr
Web page	http://www.wlw.hr
Materials of castings:	aluminum alloys, tin bronzes,aluminum bronzes
Capacity of production	150 tons per year
Production programm	Foundry: rings, rotors, machine parts, motor parts, transformer parts and other different types of sand castings Distributor and representative for Croatia and Bosnia and Herzegovina of: -MORGAN MOLTEN METAL SYSTEMS GmbH , Germany (crucibles and foundry equipment) -THERMAL CERAMICS (insulation materials) Distributor of: Vesuvius GmbH, Germany (Foseco); Lanik, Czech
Equipment in foundry	three oil furnaces
Quality	ISO 9001 certificate in progress
References	- KONČAR MJERNI TRANSFORMATORI DD,Croatia - KONČAR- MES DD, Croatia - TELEGRA d.o.o., Croatia - VENTILATOR-TVUS d.o.o., Croatia - DALEKOVOD DD, Croatia - WML, Germany - SCHLOSSEREI KRUTISCH, Austria - KAPRI D.O.O., Croatia - TEM d.o.o., Croatia - POINT-SPLIT,Croatia - MIV Varaždin, Croatia - INDUKO d.o.o., Croatia - TVIN d.o.o., Croatia - PODRAVKA DD, Croatia - TEKSTILSTROJ DD,Croatia - SAINT JEAN INDUSTRIES d.o.o., Croatia - JEDINSTVO DD, Croatia - STROJAR d.o.o., Croatia - HS PRODUKT d.o.o.,Croatia - STS d.o.o., Croatia - RS METALI d.o.o., Croatia - SLON- INŽENJERING d.o.o., Croatia - METAL PRODUCT d.o.o., Croatia - ALU LJevaonica umjetnina d.o.o., Croatia - LJEVAONICA UMJETNINA UJEVIĆ, Croatia - DUNI-LJevaonica obojenih metala, Croatia - DITRX D.O.O. , Bosna i Hercegovina - STANDARD MIO, Croatia